Studies Into the Structural Features of *C*-Linked Antifreeze Glycoprotein Analogues Responsible for Ice-Recrystallization Inhibition Activity

Roger Tam

B.Sc. (Tech.) Honours in Applied Pharmaceutical Chemistry (Co-op)- University of Guelph, 2005

Thesis submitted to the
Faculty of Graduate & Postdoctoral Studies
University of Ottawa
in partial fulfillment of the requirements for the
degree of Doctor of Philosophy in the
Ottawa-Carleton Chemistry Institute

Candidate	Supervisor
Roger Tam	Professor Robert N. Ben

This work is dedicated to my mother, father and all of my family

"Our greatest glory is not in never falling, but in getting up every time we do."

– 孔夫子 *(Confucius)*

Abstract

A major problem associated with cellular cryopreservation is the recovery of cellular viability upon thawing. Current cryopreservation techniques involve the use of additives such as dimethyl sulfoxide (DMSO), sucrose and fetal bovine/calf serum (FBS/FCS). However, each of these have their own respective cytotoxic issues. A significant contributing factor in cryotoxicity is the formation of large intra- and intercellular ice crystals which can damage cellular components and cause dehydration. This has significant impacts for applications such as food preservation, scientific research, and more importantly, tissue preservation.

To this end, our laboratory is interested in synthesizing biologically-relevant compounds which can act as cryoprotectants to decrease cryotoxicity by preventing the formation of large ice crystals in sub-zero temperatures. Our lab has previously synthesized structural analogues of native antifreeze glycoproteins (AFGPs, found in the blood of Antarctic cod *Trematomus borchgrevinki*), that possess the unique ability to inhibit ice-recrystallization. However, the mechanism by which biological antifreezes inhibit ice recrystallization is unclear.

This thesis focuses on efforts made to (1) understand this mechanism, and (2) synthesize molecules which are even more potent in ice recrystallization inhibition (IRI) activity compared to previously synthesized analogues.

By assessing the ice-recrystallization inhibition (IRI) activity of various reducing mono- and di-saccharides, we have shown that the density of water molecules which surround a carbohydrate (called the *Hydration Index*) is directly proportional to the ability of sugars to inhibit ice crystal growth.

In an effort to design functional AFGP analogues, various *C*-linked analogues were synthesized which contained different carbon linkers between the carbohydrate moiety and the

peptide backbone. Analysis of the solution conformation of these analogues has shown that IRI-active AFGP analogues contain a distinct conformation in which the carbohydrate is oriented to form a hydrophobic pocket with the side chain. We hypothesize that this subsequent change in hydration of the glycoconjugate is responsible for disturbing its surrounding waters, thereby preventing water from adding to the ice lattice required for ice growth.

Finally, previous structure-function relationship studies have shown that threonine-containing AFGP and antifreeze proteins (AFPs) are more potent in antifreeze activity than its serine-containing analogues. As the most potent AFGP analogue that has been previously synthesized by our lab contains a *C*-linked-α-galactosyl -serine residue, we hypothesized that the analogous glycopeptides containing a *C*-α-galactosyl-threonine residue will be even more potent in antifreeze activity. The final section describes efforts to synthesize a *C*-linked α-galactosyl-threonine glycoconjugate.

Acknowledgements

I would like to gratefully thank Professor Robert Ben for giving me the chance to join his research laboratory and continual funding throughout my degree. I highly appreciate his research guidance, and allowing me to contribute and pursue my ideas on various projects; also, for teaching 'big picture' research and life lessons.

I thank my parents for their love, encouragement, support and sacrifices that they have provided for me throughout my life. Without any of this, none of this work could have been done.

I thank those who helped me when I first arrived in Ottawa and in the lab: Dr. Vincent Bouvet and Frank Cease for teaching me chemistry and the ways of our lab, Ed 'line piece' Lin for his friendship and helping get me settled into Ottawa.

Also, those who taught me invaluable research and life skills towards the latter stages of my graduate studies : Dr. Pawel Czechura, Dr. Mike Souweha, Dr. Mathieu Leclère; also, for their help in adding to the bottle collection behind my desk. Jacqueline Tokarew for providing me with the necessary balance and support, and the following for their amazing and valued friendships: Taline Boghossian, Eggfoo Yung, Taz Cheema, Sandra Ferreira, Idralyn Alarcon, Dr. Benoît Liégault, Sophie Rousseaux and Chantelle Capiccotti.

I also acknowledge other lab members for helping me throughout my studies: John Trant, Dr. Jenn Chaytor, Wendy Campbell, Gloria Gong and Aleks Paliga; talented undergraduates that I have had the pleasure to work with, and who have helped me along the way: Ferenc Kontes, Caroline Proulx, Ivan Petrov, Elena Dimitrijevic, Nick Afagh.

I thank my fellow 'Accomadators' bandmates, past and present: Dr. Mathieu Lemay (for asking me to join their band), Dr. Joseph Moran, Matt Yorke, Charles Russell, Dr. Mathieu Frenette, Hasan Khan and Dr. Jessie Blake for an amazing experience. I never would have thought of actually being in a band, thanks for having me to tag along for the ride.

I would also like to thank the Professor Tom Woo, Dr. Chris Rowley and Mike Nohra for performing the computational studies on our work; Jacek at NRC for performing MALDI analysis on our glycopeptides, Dr. Glenn Facey for his help with the variable temperature NMR studies, Dr. Klemm Kazakoff for Mass spectroscopy analysis of our samples, and Ian Myers for re-designing and building our Peltier unit. Professsors Steve Withers, Christopher Boddy, Jeff Manthorpe and Roberto Chica for taking the time to read this thesis and provide useful suggestions and revisions.

Table of Contents

Chapter 2 Goals and Objectives

Chapter 3 Correlation between carbohydrate hydration and IRI activity

Chapter 4 : Effect of the side chain length of *C*-linked AFGP analogues on IRI activity

Chapter 5 : Effect of the side chain amide bond in C-linked AFGP analogues on IRI activity

Chapter 6 : Towards the synthesis of C-α-galactosyl-threonine glycoconjugate

List of Figures

List of Tables

List of Schemes

List of Abbreviations

α	alpha
β	beta
γ	gamma
δ	delta
ε	epsilon
^{1}H	proton
^{13}C	carbon
2D	two-dimensional
3D	three-dimensional
Ac	acetyl
Ac_2O	acetic anhydride
AFGP(s)	antifreeze glycoprotein (s)
AFGP8	antifreeze glycoprotein, fraction-8
AFP(s)	antifreeze protein(s)
AFP I	antifreeze protein type I
Ala	alanine
All	Allyl
Asn	Asparagine
Asp	Aspartate
Atm	atmospheres
BCl_3	boron trichloride
$BF_3•OEt_2$	boron trifluoride diethyl etherate
Bn	benzyl
Boc	*tert*-butyloxycarbonyl
Boc_2O	Di-*tert*-butyl dicarbonate
br	broad
brsm	based on recovered starting material
Bz	benzoyl
$CaCl_2$	Calcium chloride
Cat.	Catalytic
CD	circular dichroism
$CDCl_3$	deuterated chloroform
CDI	1,1-carbonyldiimidazole
CD_3OD	deuterated methanol
CH_2N_2	diazomethane
cm^{-1}	wavenumber
CN	nitrile
$CuBr·SMe_2$	copper bromide-dimethyl sulfide complex
d	doublet
D_2O	deuterium oxide
Dab	diaminobutanoate
dd	doublet of doublets
DCM	dichloromethane

DIBAL-H	diisobutylaluminum hydride
DIPEA	diisopropylethylamine
DIS	dynamic ice shaping
DMF	dimethyl formamide
DMSO	dimethyl sulfoxide
DSS	2,2-dimethyl-2-silapentane-5-sulfonic acid
Dpr	diaminopropanoate
dt	doublet of triplets
ESI	electrospray ionization
Et	ethyl
Et_2O	diethyl ether
EtOAc	ethyl acetate
EtOH	ethanol
Fmoc	9-fluorenylmethyloxycarbonyl
FmocOsuc	N-(9-Fluorenylmethoxycarbonyloxy) succinimide
Gal	galactose
GalNAc	*N*-acetyl-galactosamine
Glc	glucose
GlcNAc	*N*-acetyl glucosamine
Gln	glutamine
Glu	glutamate
Gly	glycine
HBTU	2-(1H-benzotriazole-1-yl)-1,1,3,3-tetramethylaminium hexafluorophosphate
HCl	hydrochloric acid
HCTU	2-(6-Chloro-1H-benzotriazole-1-yl)-1,1,3,3-tetramethylaminium hexafluorophosphate
HI	Hydration Index
HGlu	Homoglutamate
HOBT	*N*-hydroxyl benzotriazole
HPLC	high performance liquid chromatography
IR	Infrared
IR resin	Amberlite ion exchange resin
IRI	ice-recrystallization inhibition
Lac	lactose
LiBr	lithium bromide
kDa	kiloDaltons
m	multiplet
M	molar
M^+	parent molecular ion
MALDI-TOF	matrix-assisted laser desorption/ionization – time of flight
Man	mannose
MD	molecular dynamics
Me	methyl
MeOH	methanol
MGS	mean grain size

$MgSO_4$	magnesium sulate
MHz	mega Hertz
mM	millimolar
MS	mass spectrometry
MS	molecular sieves
NAc	*N*-acetyl
NaH	sodium hydride
Na_2SO_4	Sodium sulfate
$NaHCO_3$	sodium bicarbonate
NaOH	sodium hydroxide
NaOMe	sodium methoxide
NMM	N-methylmorpholine
NIS	N-iodosuccinimide
O_3	ozone
oDPPBA	*ortho*-diphenylphosphinobenzoic acid
OGG	ornithine-glycine-glycine
OMe	*O*-methoxy
O/N	overnight
OTf	trifluoromethane sulfonate
PIDA	phenyl iodine diacetate
PIFA	phenyl iodine di(trifluoroacetoxy)
PG	protecting group
PBS	phosphate-buffered saline
Pd/C	palladium on carbon
$Pd(OH)_2$	palladium hydroxide
pKa	acid dissociation constant
PMC	partial molar compressibility
PMV	partial molar volume
ppb	parts per billion
ppm	parts per million
q	quartet
Rf	Retention factor
RT	room temperature
s	singlet
Ser	serine
SM	starting material
Sm	samarium
SPPS	solid-phase peptide synthesis
t	triplet
Tal	talose
TBAF	*tert*-butylammonium fluoride
TBS	*tert*-butyldimethylsilyl
TEA	triethylamine
TEMPO	2,2,6,6-tetramethylpiperidine-1-oxyl
TFA	trifluoroacetic acid
TH	thermal hysteresis

THF	tetrahydrofuran
Thr	threonine
TIPS	triisopropylsilyl
TIS	triisopropylsilane
TMS	trimethylsilyl
TMSOTf	trimethylsilyl trifluoromethane sulfonate
VT-NMR	Variable temperature nuclear magnetic resonance

Chapter 1: Introduction to Biological Antifreezes

1.1 INTRODUCTION

The change in physical state from liquid water into ice at atmospheric pressure and sub-zero temperatures is an aggressive and powerful process, whereby ice growth is instantaneous upon nucleation. Due to the unique properties of water, the volume of its solid state (1.09 cm^3/g at 1 atm, between -5 ^oC to -10 ^oC) is actually larger than its liquid state (1.00 cm^3/g at 1 atm, +5 ^oC) due to the highly ordered ice lattice imposed by hydrogen bonding.[1] Taking into account these properties, it is not surprising that upon freezing, the formation of both intracellular and extracellular ice can damage cells.[2,3-7] For example, the presence of extracellular ice decreases the amount of extracellular bulk water, which consequently increases the solute concentration. This causes a large osmotic efflux that dehydrates the cell.[4] Similarly, intracellular ice can cause damage in cells during the formation[5], recrystallization[6] or melting[7] of ice. This has considerable implications on a macroscopic scale since this can lead to irreversible tissue damage and ultimately death in an organism.

Due to the significant consequences of in vivo ice formation, Nature has evolved small peptide-based compounds in certain types of fish, insects, and amphibians inhabiting sub-zero climates. The presence of these compounds, known as biological antifreezes, protects these organisms from cold-induced death by preventing cell damage, enzymatic loss of function and degradation in extremely cold environments.

There are two main classes of biological antifreezes – antifreeze proteins (AFPs) and antifreeze glycoproteins (AFGPs). AFPs are strictly peptide-based, and are typically found in species such as the winter flounder (*Pseudopleuronectus americanus*),[8] ocean pout (*Macrozoarces americanus*),[9] yellow mealworm beetle (*Telebrio molitor)*[10] and grass (*Lolium*

perenne).[11] They are generally divided into six classes (Table 1.1) . Unlike AFPs, AFGPs contain carbohydrates tethered to the peptide backbone, and are typically found in fish such as the Antarctic cod (*Eleginus gracilis*).[12] An interesting overall characteristic for biological antifreezes is the presence of repeating peptide residues. The following sections will illustrate in detail the structural features and antifreeze activity properties of AFPs and AFGPs.

1.1.1 ANTIFREEZE PROTEINS (AFPS)

Antifreeze proteins are found in a diverse number of organisms, ranging from fish to insects and plants. Although they consist only of amino acids and no carbohydrates, they vary greatly in their structure and function in antifreeze activity. For example, AFPs are classified into various types based on their amino acid sequences, Types I to VI, as shown in Table 1.1. Interestingly, these different types also possess different antifreeze properties such as *thermal hysteresis* (TH), and *ice-recrystallization inhibition* (IRI), which will be described in detail in subsequent Sections 1.3 and 1.4, respectively.

Table 1.1. Types of antifreeze proteins (AFPs) and important structural/activity characteristics.[10-17]

Type	Examples of Source	General Characteristics of Amino acid primary sequence	Notable characteristics about structure/ conformation	Antifreeze Characteristics
I[13]	Winter flounder *(Pseudopleuronectus americanus)*	Alanine rich (>60%) Threonines at every 11 residues	α- helices	TH and IRI
II[14]	Sea raven (*Hemitripterus americanus)* Smelt *(Osmerus mordax)* Atlantic herring (*Clupea harentus harengus)*	Cystine (S-S disulfide bond) rich Increased levels of asparagine, glutamine, threonine	Majority β-sheets and random coils	TH
III[15,16]	Ocean pout (*Macrozoarces Americanus)*	No sequence repeats	Globular with β-strands	TH
IV	longhorn sculpin *(Myoxocephalus octodecimspinosis)*	Rich in glutamine and alanine	α-helices	TH
V[10]	Yellow mealworm beetle (*Telebrio molitor)*	Thr-xaa-thr tripeptide repeat	β-sheet	Hyperactive TH
VI[11,17]	Perennial ryegrass (*Lolium perenne)*	Rich in asparagines, valine, serine, threonine, glycines, some aromatic/ hydrophobic residues xaa-xaa-asn-xaa-val-xaa-gly	Two flat ice-binding surfaces	Potent IRI, no TH

1.1.2 ANTIFREEZE GLYCOPROTEINS (AFGPS)

AFGPs (**1**) were originally isolated from the blood of Antarctic cod *Trematomus borchgrevinki* by DeVries and co-workers.[12] The crude extracts were separated by reversed-phase HPLC and examined for antifreeze activity. It was found that several fractions contained antifreeze activity. Interestingly, further examination of these fractions showed that they all contained similar molecular structures, but varied only in their polymeric size.[18]

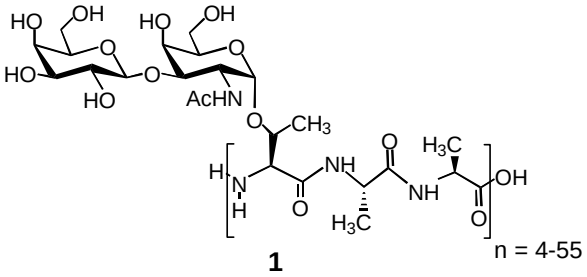

1

In general, AFGPs (**1**) contain a repeating tripeptide unit where one amino acid is glycosylated. The glycoconjugate consists of a D-galactosyl-β(1,3)-(*N*-acetyl-D-galactosamine) disaccharide linked via an anomeric oxygen atom in an α-configuration to a threonine residue,[19] which is adjacent to either alanine, proline, or arginine residues, although the latter two residues are less common.[20,21] The number of tripeptide units dictate their group classification. AFGP-1 contains 55 repeating tripeptide units, whereas AFGP-8 contains 4. It has been shown that the polypeptide length is proportional to thermal hysteretic activity.[22,23]

The overall conformation of AFGPs in solution has been investigated by numerous spectroscopic[24-30] and computational[24-31] techniques. Unfortunately, the definitive conformation of the glycopolymer has not been identified and the results of these studies are inconclusive. For example, vacuum ultraviolet circular dichroism (VUV-CD)[25] and ^{1}H-NMR[26] studies have shown that AFGP-8 primarily adopts a three-fold left-handed helix, whereas quasi-elastic light scattering (QELS)[27] studies suggest an extended coil; other dynamic light scattering (DLS),[28]

circular dichroism (CD),[28-29] ^{13}C-NMR,[30] and molecular dynamic (MD) simulation[31] studies suggest AFGP-8 predominantly exists as a random coil in solution. The largest factor contributing to this inconsistency is the lack of an available x-ray crystal structure.

1.1.3 General mechanism of action of biological antifreezes

There are two general properties of biological antifreezes: thermal hysteresis (TH) and ice-recrystallization inhibition (IRI). Until recently, it was thought that these two properties arose from the same fundamental physical basis, and that IRI activity was actually a phenomenon of TH activity. Thus, the majority of early antifreeze assays have assessed and quantified thermal hysteresis activity.

The following sections will describe TH and IRI in detail, and how biological antifreezes are responsible for these properties. Firstly, to gain an appreciation of the complexity of ice, a brief discussion into the physical properties of ice is necessary.

1.2 PHYSICAL PROPERTIES OF LIQUID AND SOLID H_2O

There exists many possible physical structures of ice, and these are a function of external forces such as temperature and pressure (Figure 1.1).[32-34]

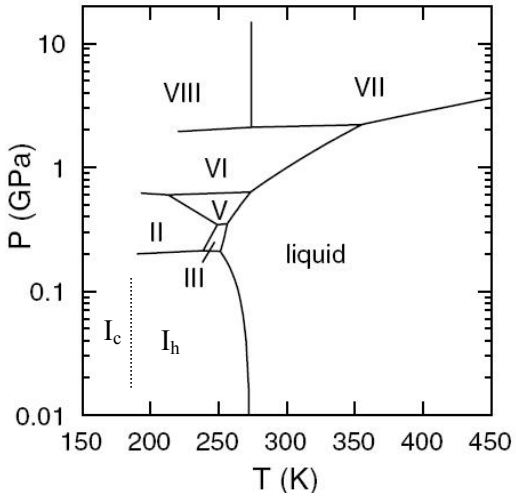

Figure 1.1 Physical properties of water at various pressures (Pa) and temperatures (K). Different types of ice are shown in red roman numerals (I-VIII)[34]

For example, at high elevations where the atmosphere is at a reduced pressure and reduced temperature, ice exists as cubic ice (I_c), where the symmetry of the ice lattice resembles that of a diamond (Figure 1.2).[35]

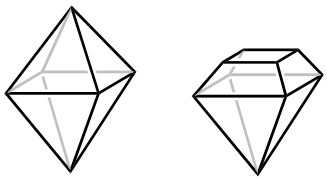

Figure 1.2 Schematic diagram of cubic ice (I_c) crystals.

Other types of ice lattice structures have been created in a controlled environment and are categorized from ice II to ice XV.[36]

Ice at standard atmospheric pressure and at temperatures above -80 ^oC is considered to be 'typical' ice and exists as hexagonal ice (I_h), as its lattice structure resembles a hexagonal prism (Figure 1.3).

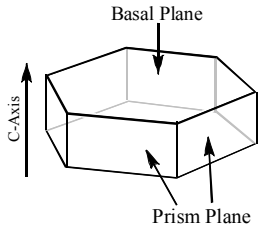

Figure 1.3 Schematic diagram of a hexagonal ice (I_h) crystal.

The orientation of water molecules in this structure can be viewed as two directional planes. First, a plane perpendicular to an arbitrarily labeled 'c-axis' contains molecules that are arranged in repeated 'chair' formations, held together by staggered hydrogen bonding (relative to neighboring hydrogen bonds), Figure 1.4. The plane of the ice lattice surface that is perpendicular to the c-axis is known as the *basal plane*.

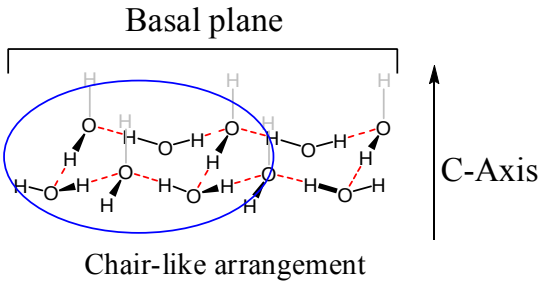

Figure 1.4 Schematic diagram of a basal plane of hexagonal ice (I_h). Chair-like arrangement of ordered water molecules is highlighted with blue circle.

Next, the plane that is parallel to the c-axis has eclipsed hydrogen bonding (relative to their neighboring hydrogen bonds); the arrangement of water molecules in this manner resembles that of repeated 'boat' formations, Figure 1.5. The surface of this plane is referred to as the *prism plane*.

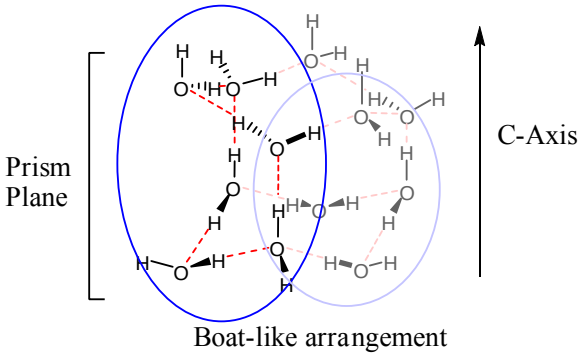

Figure 1.5 Schematic diagram of the prism plane of hexagonal ice (I_h). Boat-like arrangement of ordered water molecules are highlighted with blue circles.

Due to the difference in orientation and arrangement of water molecules in the ice lattice parallel and perpendicular to the c-axis, the addition rates of water molecules onto the prism and basal planes vary depending on the conditions. This property plays a significant role in the mechanism of action for antifreeze activity and subsequent ice crystal habits (or morphologies) that are observed.

In the liquid state, water is dynamic. Between water and solid ice is a semi-ordered glassy layer of water molecules, called the *quasi-liquid layer* (QLL).[37-39] It has been experimentally shown that the orientation and motion of water molecules in the QLL closely resembles that of ice more than of its liquid state. The thickness of the QLL is on the order of nanometers and its thickness is inversely proportional to the temperature.[37,38] For example, colder temperatures will decrease the thickness of the QLL. A schematic representation[40] of an ice-water interface is shown in Figure 1.6, illustrating the approximate relative degree of entropy in each physical state of water.

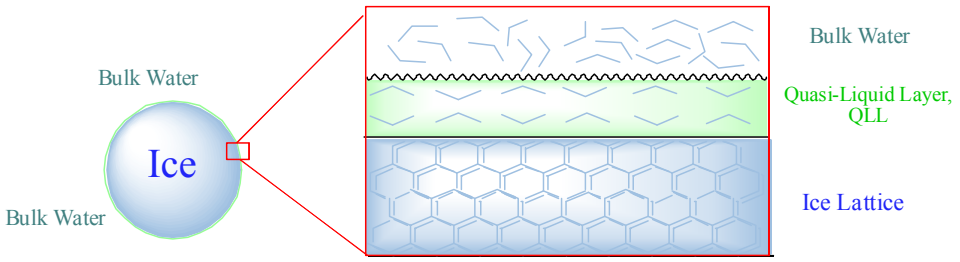

Figure 1.6 Schematic diagram of a liquid water-ice lattice interface of hexagonal ice (I_h), with a quasi-liquid layer (QLL) intermediate layer.

However, the exact nature and dynamics of this layer is still uncertain. Hence, the presence of such an amorphous layer significantly complicates any mechanism that involves the liquid-ice interface.

1.3 THERMAL HYSTERESIS (TH)

In an ideal solution of pure water, the melting point (MP) and freezing point (FP) are identical, and is at 0.0 ^{o}C. The introduction of electrolytes into this system will colligatively decrease both the MP and FP by the same amount, as solutes will hinder the gathering of water molecules into the proper orientation to form a lattice structure. Thus, a single ice crystal in this system will grow as temperature is decreased, or vice-versa, at the exact same MP and FP. As an ice crystal is allowed to grow, upon reaching a maximum size, it will act as a seeded nucleation site and cause a spontaneous freezing event of the surrounding water molecules. However, in the presence of certain biological antifreezes, interaction with the ice lattice alters the habit (or shape) of the ice crystal and causes a difference in temperatures between the MP and the FP. This difference in temperature is known as a thermal hysteretic gap and biological antifreezes that cause this effect are referred to as possessing thermal hysteretic activity.

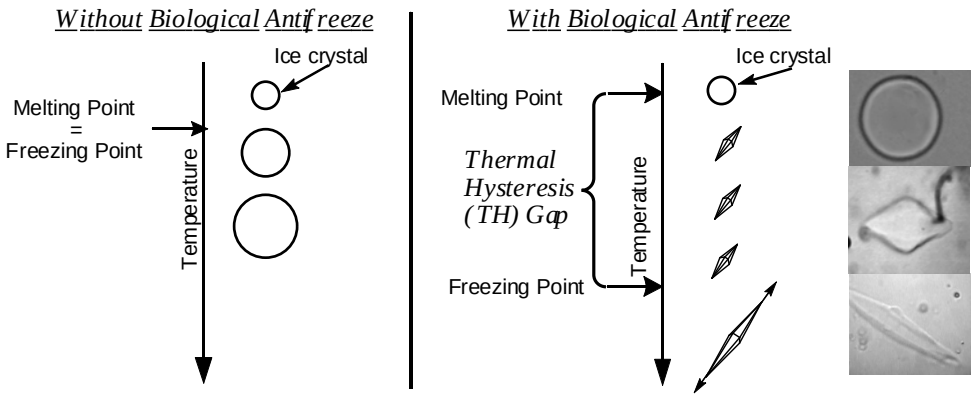

Figure 1.7 Representation of the change in ice crystal shape and size during Thermal Hysteresis (TH).

A typical assay for thermal hysteresis was described by Chakrabarrty and Hew.[41] A nanolitre drop of solution is inserted into a larger oil drop inside of a Peltier unit. The aqueous solution is flash frozen and gradually melted until only one small stable ice crystal is present. This temperature is the melting point. The solution is then slowly cooled (at approximately 0.001^{o}C / second) and in the absence of biological antifreeze, the ice crystal will grow as a circular disc. However, in the presence of an additive that possesses thermal hysteresis, cooling the solution will not result in the immediate growth of the ice crystal; instead, this will cause the additive to adsorb onto the ice crystal at the planes described in Section 1.2, causing a change in ice crystal morphology. As the temperature is sufficiently cooled, the ice crystal will grow as sharp hexagonal bipyramidal shapes, known as *spicules*, which will then cause mass freezing of the solution. This temperature is known as the freezing point.

The nature of this phenomenon is significant because at temperatures within this gap, ice crystals are neither growing nor melting. Thus, although ice is formed, it is unable to grow any larger. In terms of a mechanism for in vitro cryo-protection in cells, this is significant because as long as the temperature is within this TH gap, large amounts of ice will not form.

Early mechanistic considerations did not incorporate the effect of the QLL. For example, upon observation of formation of a hexagonal bipyramidal ice crystal by fish AFPs, it was first proposed that AFPs function by an irreversible binding mechanism of the antifreeze protein to the prism face of a single ice lattice.[42-44] As such, the binding of additional water molecules is disfavoured. This phenomenon is referred to as the Kelvin Effect (Figure 1.8).[42]

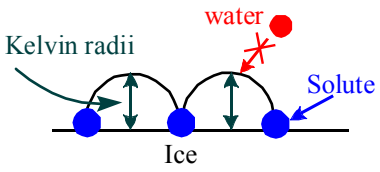

Figure 1.8 Schematic representation of the Kelvin Effect.

In this effect, the adsorption of solutes on an ice crystal surface hinders the addition of subsequent water molecules onto the same surface. The addition of water molecules onto an impure ice surface forms a curved ice surface between the solute adsorption sites. As the radius of curvature is increased through the addition of water molecules to the ice lattice, the associated increase in surface tension at the curved surface hinders the addition of other water molecules, resulting in a localized freezing point depression.[42] The radius threshold at which water can no longer add to the ice lattice is referred to as the Kelvin radius.

Therefore, as an AFP is bound to the prism plane, the addition of water to the ice lattice must occur on the basal plane, thereby increasing the distance along the c-axis. As water molecules are added in this direction, other water molecules and more AFPs continue to compete for adsorption to the new prism plane of the newly formed ice surface, with the addition of the latter being stronger than for water molecules, Figure 1.9. Therefore, this will result in a net increase of ice crystal length along the c-axis and decrease perpendicular to it, resulting in the characteristic hexagonal bipyramidal ice crystal morphology.[43]

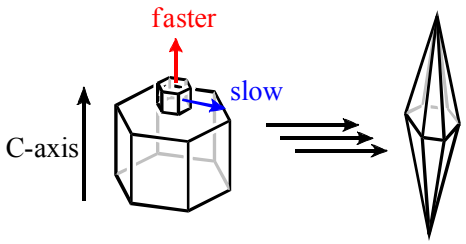

Figure 1.9 Spicule (needle shape) formation of an ice crystal in the presence of an antifreeze protein irreversibly bound to the prism plane.

There has been a wide range of experiments and theoretical work that supports the irreversibility in binding for antifreeze proteins and glycoproteins onto the prism plane.[43] Knight and co-workers showed this by adsorbing AFPs onto a large ice crystal, and upon sublimation of the ice, the orientation of AFPs is retained and showed that they adsorb on the prism plane.[45] Recent work[46] by Braslavsky and co-workers showed that type III AFP fused with a green fluorescent protein (GFP) adsorbs 'quasi-permanently' (more than seven days) onto the surface of an ice crystal. Figure 1.10 shows a fluorescent image of a characteristic hexagonal bipyramidal ice crystal which is coated with GFP-AFP III fused proteins. It is shown that the fluorescent proteins bind preferably to the ice crystal rather than remain in the bulk solution.

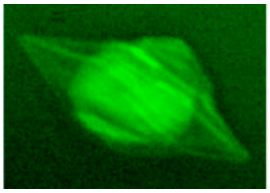

Figure 1.10 Spicule (needle shape) formation of an ice crystal in the presence of an antifreeze protein tagged with green fluorescent protein (GFP).[46]

Interestingly, recent work has shown that thermal hysteresis activity from AFPs of certain insects (*Telebrio molitor*[10,47] and spruce budworm *Choristoneura fumiferana*) is greater than that from fish AFPs. It is believed that these biological antifreezes, called *hyperactive* antifreezes, bind to all faces of a seeded ice crystal and consequently are more effective in preventing the

addition of water molecules to the nucleated ice crystal. By binding to all facets of an ice crystal (as opposed to an exclusive prism plane adsorption), a hexagonal bipyramidal ice crystal shape is not observed. This was elegantly shown by Braslavsky using AFP-GFP fusions.[48] Figure 1.11 shows how hyperactive AFPs bind to all faces of a seeded ice crystal.

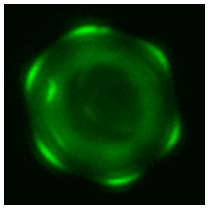

Figure 1.11 Formation of a hexagonal ice crystal in the presence of an antifreeze protein tagged with green fluorescent protein (GFP).[48]

While the general consensus is that fish AFPs bind irreversibly to the prism face and hyperactive insect AFPs bind to both prism and basal planes, the next question to address is which factors in the protein structures are responsible for ice binding.

1.3.1 Structural features of AFPs responsible for TH activity

Initial hypotheses of how AFPs were bound to ice were that each hydroxyl group of threonine residues in AFPs formed one hydrogen bond with the surface of the ice lattice.[49] However, subsequent studies suggested that this was insufficient to hold the protein onto the ice surface.[50]

By performing site-directed mutagenesis, Davies and co-workers demonstrated that substitution of threonine residues with more hydrophilic serine residues (removal of the β-methyl group) abolished TH activity. However, by interchanging threonine with isosteric valine residues, (thus replacing the polar hydroxyl group with a non-polar methyl group), the peptide still retained its TH activity comparable to that of the native system.[51] These results correlate

with work by Haymet and co-workers, where upon substitution of threonine residues with hydrophobic valine residues, TH activity was retained.[38] These results suggested that the binding of these proteins to ice involved a hydrophobic component, but did not exclude a hydrogen bonding hypothesis. Another factor that may contribute to the observed decrease in TH activity with the serine-containing peptides may be due to the increased flexibility of these peptides compared to the more conformationally-rigid β-branched amino acids threonine and valine.

Subsequent x-ray analyses show that AFP I and AFP III contain hydrophobic flat planes, and it was hypothesized that these planes are able to recognize the ice surface, much like the recognition of a receptor for its associated ligand.[43a,52,53] However, recent work has shown the importance of surrounding water molecules (in the hydration layer) on antifreeze protein ice recognition and binding.[38,54] This suggests that instead of the protein itself recognizing the ice lattice, the protein actually modulates its nearby water molecules to act as the 'receptor'. This is not a surprising phenomenon as it is well known that peptide hydration plays a significant role in other biological activities.[55]

1.3.2 Structural features of AFGPs responsible for TH activity

In AFGPs, it has been hypothesized that the hydroxyl groups of the carbohydrates play a vital role in binding to the ice lattice.[50] However, the exact manner in which this is done remains unclear. A major obstacle to conclusive mechanistic elucidation involving AFGPs is the lack of an x-ray crystal structure. Therefore, efforts to this end have involved the use of AFGP analogues, and various spectroscopic and computational techniques to probe ice-protein interactions and conformations.[24,31]

As a significant difference between AFPs and AFGPs is the glycosylation of the peptide, much effort has focused on the glycoconjugate moiety. Preliminary studies to assess the structural attributes responsible for thermal hysteresis activity focused on the effects of substitution of the carbohydrate moiety, Figure 1.12. Komatsu and co-workers showed that upon oxidation of the terminal galactose unit with sodium periodate to form (**2**), this AFGP derivative showed no TH activity.[12b] Similarly, formation of a boronic ester with C3 and C4 hydroxyls of the terminal carbohydrate (**3**) decreased TH activity.[56] This suggests that the C2, C3 and C4 hydroxyls of the terminal unit are essential for TH. Subsequent studies showed that upon selective oxidation of the C6 hydroxyls (**4**) with galactose oxidase, these analogues still retained TH activity, which signifies that these hydroxyls are not as important.[19] The disaccharide moiety (**5**) was also deemed important as elimination of the disaccharide under basic conditions abolished TH activity.[57]

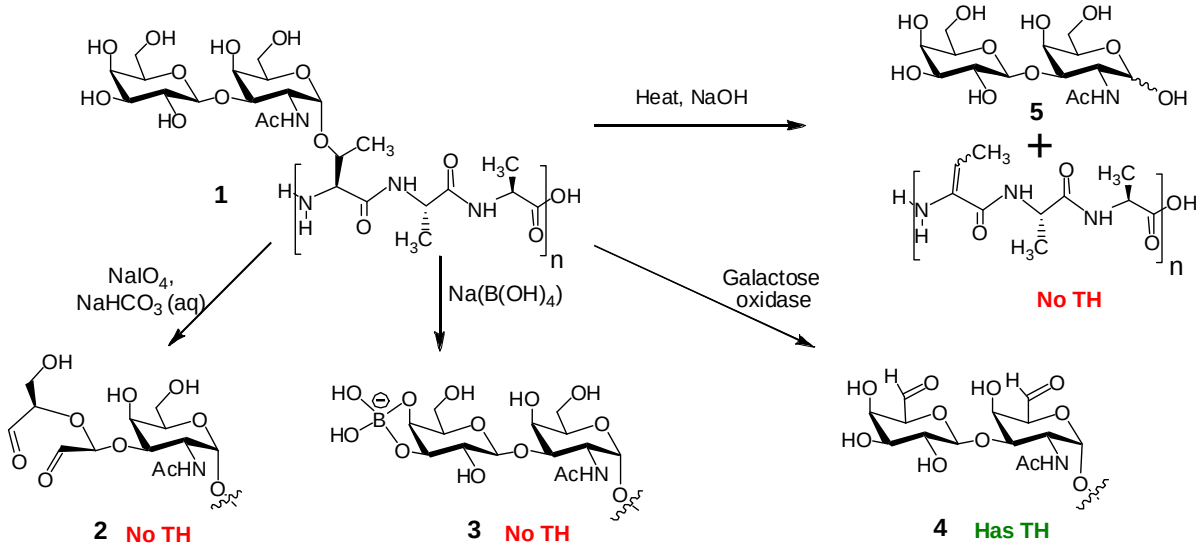

Figure 1.12 Effect of carbohydrate modifications of AFGP on thermal hysteresis activity.

Another key contribution in the determination of the factors responsible for TH in AFGP analogues was performed by Nishimura and co-workers.[31] His team synthesized 16 analogues

and assayed them all for TH activity. The key results from this extensive study were that the following parameters were important for TH activity: (i) presence of C2 N-acetyl group, (ii) stereochemistry of the anomeric linkage between the disaccharide and the peptide, (iii) the β-methyl group in the threonine residue linkage and (iv) the polypeptide length. Figure 1.13 shows that variation from the native AFGP system at these specified positions (with the exception of the variation in polypeptide length, *n*) completely eliminated TH activity. With respect to the polymer length, *n*, it was shown that the length is proportional to activity, corroborating with previously reported results,[22,23] and that shorter lengths still possessed a small degree of function.

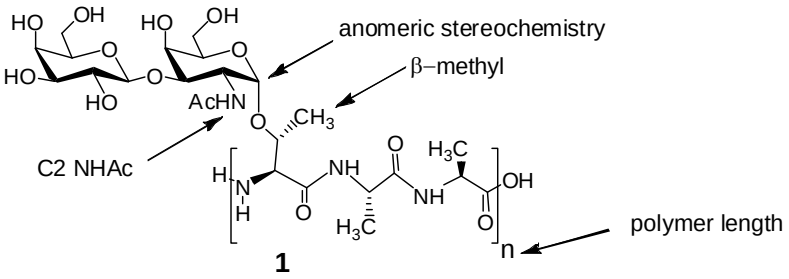

Figure 1.13 Structural features of AFGP-8 that were determined by Nishimura to be important for TH activity.[31]

The conformation of AFGP and its analogues have been investigated by techniques such as CD, NMR and MD simulations.[18,24-31] It was shown by CD that the presence of the β-methyl group of the threonine residue was important to maintain a random coil conformation; elimination of this group caused the glycoprotein to exist primarily as an α-helix.[31] With respect to the C2 acetamide, early NMR studies by Mimura on model systems of AFGP showed the presence of direct intramolecular hydrogen bonds involving the C2-NHAc group and the carbonyl of the peptide backbone, which was thought to be important for the localized conformation of the glycopeptides.[58] However, recent molecular dynamic simulation studies by

Corzana show that the conformation of the glycopeptide may be dictated by stabilizing water bridges.[59]

1.4 ICE-RECRYSTALLIZATION INHIBITION (IRI)

Recrystallization is the process of the formation of larger crystals by the combination of small crystals. Figure 1.14 shows two images of the same magnification of ice crystals which were identically prepared via the 'splat-cooling' assay which was first described by Knight and co-workers.[60]

A 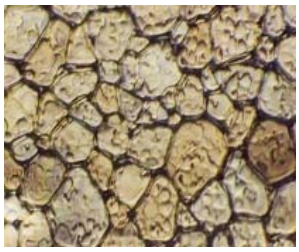 B 

Figure 1.14 Photographs of ice crystals in the presence of (A) phosphate buffer saline (PBS), negative control, and (B) AFGP-8 (10mg/mL), positive control, under the same magnification.

In this assay, a ten microlitre solution is dropped onto a pre-cooled plate, which causes instantaneous freezing of the solution as a thin wafer upon impact. Initial freezing of the solution forms many small ice crystals; the ice wafer is then warmed for a specific period of time (annealing period) to allow for small ice crystals to form into larger ones (recrystallization). The presence of small ice crystals after the specific annealing time indicates that there has been recrystallization inhibition, whereas large ice crystals show there was no inhibition of ice recrystallization. Figure 1.14A shows ice crystals in the presence of phosphate-buffered solution (PBS); Figure 1.14B contains ice crystals in the presence of a 5.5 μM solution of AFGP-8 in PBS buffer. It is clear that image Figure 1.14B contains much smaller ice crystals than Figure 1.14A.

Although this process has been extensively studied in the metallurgy field,[61] its analogous process with ice has not. One main difference with ice is the presence of the quasi-liquid layer of water molecules that exists at the ice-water interface, Section 1.2. The presence of this layer complicates the mechanism.

The notion that the mechanism of action for ice-recrystallization inhibition is different than for thermal hysteresis was first proposed as a result of the discovery of an antifreeze protein from the perennial ryegrass.[11] The proteins isolated from this plant possessed IRI activity, but no TH activity. It was thought that under extremely cold conditions, where the formation of intra- and extracellular ice crystals is inevitable, an antifreeze protein has evolved that enabled the tolerance of small ice crystals in vivo.[11,17]

However, a mechanism of action for compounds that possess exclusively IRI activity, and no TH activity is currently unclear. Our lab has been interested in studying this type of antifreeze activity because of its high potential in applications such as cryopreservation. The following will describe the current structure and function relationship studies underway to elucidate the IRI mechanism of action.

1.4.1 Structure and function relationships of AFP and AFGP on IRI

As mentioned, grass AFPs possess very different antifreeze characteristics than their fish and insect counterparts.[11] From a structural point of view, AFPs from perennial ryegrass were found to contain a repeat of seven residues of the following sequence: -Xaa-Xaa-Arg-Xaa-Val-Xaa-Gly-, where Xaa represents variable amino acid residues. Theoretical modeling analysis shows that the conformation of this protein contains two flat planes on opposite sides of the protein which are suitable for ice-surface binding to two different ice crystals.[17] However, the

question of whether these planes directly recognize the ice surface, or whether these planes re-organize their surrounding waters to recognize ice, is unclear.

Structure/function relationship studies of AFGP and its analogues have been investigated for about forty years.[12,18] However, a comprehensive study has been hampered by the difficulty in synthesis of these glycopolymers. In addition, the majority of these studies have focused on the property of thermal hysteresis (Section 1.3.2), while little has been done to probe the factors responsible for exclusive ice-recrystallization inhibition activity.

As the synthesis of compounds that possess IRI activity and no TH activity is an interest of our lab, three classes of analogues have been previously synthesized.[62-66] The classification of these analogues is dictated by the chemical structure of the glycoconjugate component. The first class of analogues resembles the native system in that the carbohydrate is covalently linked with an oxygen atom (*O*-linked) to the peptide backbone.[62] The second[62-65] and third[66] classes of analogues contain an anomeric carbon linkage (*C*-linked). The difference between these last two classes is that the former contains an amide bond in the side chain between the carbohydrate and the peptide backbone, whereas the latter contains a saturated alkyl chain in the side chain.

1.4.2 Structure and function relationships of *O*-Linked AFGP analogues on IRI activity

The common feature in this class of analogues that have been synthesized is the substitution of the disaccharide moiety in native AFGP-8 with a monosaccharide. Analogues of this type were designed and synthesized[62] containing structural variations at the stereochemistry of the anomeric position, the C2 acetamide group, the β-methyl group of the threonine linker, stereochemistry of C4 hydroxyl, and peptide backbones containing only alanine-alanine dipeptide, Figure 1.15.

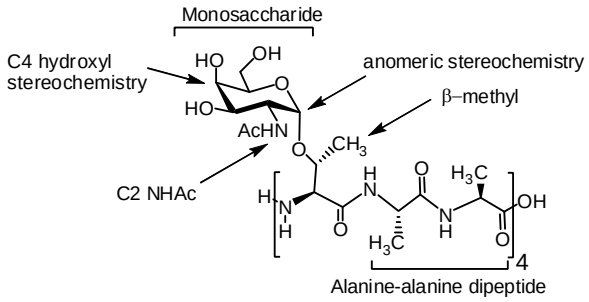

Figure 1.15 Structural features that were modified in synthetic AFGP analogues to assess their role in TH and IRI activity.[62]

Analogues with these modifications possessed no TH activity, and varying degrees of IRI activity. It was observed that an analogue retaining the C2 acetamide of the galactose moiety was slightly more potent in IRI activity than substitution with a C2 hydroxyl group. With respect to analogues that contain a galactose monosaccharide (C2 hydroxyl), it was observed that an α-anomeric linkage to the peptide backbone is higher in IRI activity than the β-anomer. In addition, the presence of an α-anomeric linkage to a threonine (with a β-methyl group) residue increased activity relative to linkage to a serine residue (lacking a β-methyl group). The stereochemistry of the carbohydrate was also found to be important, as inversion of the C4 hydroxyl group was detrimental to IRI activity.

The conformation of these analogues was examined by CD and it was shown that they adopt a random coil secondary structure.[62] This may be an important factor for IRI activity, as an element of flexibility may be necessary to interact with more than one ice crystal to prevent the fusion of two ice crystals into a larger one.

Unfortunately, analogues containing the disaccharide moiety have yet to be synthesized and tested completely in our lab. These analogues would provide a more direct comparison to the native AFGP system for mechanistic elucidation.

1.4.3 Structure and Function Relationships of *C*-Linked AFGP Analogues on IRI Activity

Although *O*-linked AFGP analogues and native AFGP possess antifreeze activity, the inherent instability of these compounds makes them less feasible for commercial applications. For example, carbohydrates linked to peptides by an oxygen atom can be cleaved in vitro by acidic, basic, and enzymatic conditions.[67] Therefore, the search for more stable analogues is essential.

The first *C*-linked AFGP analogue designed by our lab contained an anomeric carbon linkage (*C*-linked) between the carbohydrate and a peptide residue, and an amide bond in the side chain, Figure 1.16.[63,68]

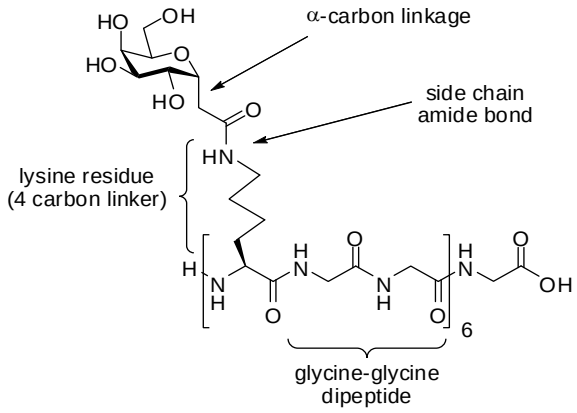

Figure 1.16 Chemical Structure of initial *C*-linked AFGP analogue possessing IRI activity.[63,68]

This compound contains a galactose monosaccharide, tethered via an amide bond to a lysine residue (which has a four carbon spacer between the amide bond and the peptide backbone). The glycoconjugate residue is adjacent to a glycine-glycine dipeptide residue. This tripeptide unit is repeated six times, and a decrease in the number of repeating tripeptide units from six to four decreased the IRI activity, which correlates to previous data.[22,23]

A decrease in length of the side chain tether by one carbon yielded the ornithine analogue (**6**), which was more potent in IRI activity.[64] Structural modifications of this analogue has included substitution of the glycine backbone with other amino acids such as prolines,[64] Freidinger lactams,[69] and β-alanines[70]. In addition, analogues have been synthesized that contain monosaccharides that differ in the C2 and C4 hydroxyl stereochemistry.[65] These structural modifications of the peptide backbone and the carbohydrate all resulted in a dramatic decrease in IRI activity compared to analogue (**6**).

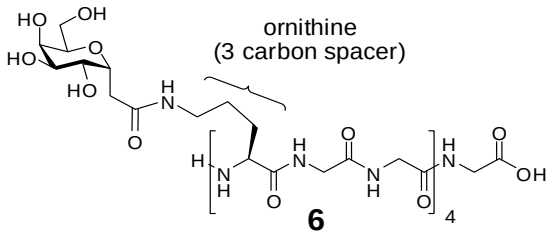

Figure 1.17 Chemical Structure of C-linked AFGP analogue **6** possessing potent IRI activity.[64]

The next generation of *C*-linked AFGP analogues contains a galactose monosaccharide which is carbon-linked at the anomeric position to the backbone via a saturated alkyl chain of various lengths, Figure 1.18A. As the glycoconjugate containing the shortest length (n=1) is a carbon isostere of an oxygen-linked galactosyl-serine linkage, Figure 1.18B, this set of analogues is referred to as *C*-Serine (*C*-Ser). Similar to the previous set of *C*-linked analogues containing a side chain amide bond, it was observed with *C*-Ser analogues that as the linker side chain is decreased, the IRI activity is increased. This suggests that a shorter carbohydrate tether decreases the carbohydrate's degrees of freedom, thereby enabling a favourable carbohydrate-peptide orientation necessary for interaction with the ice lattice.

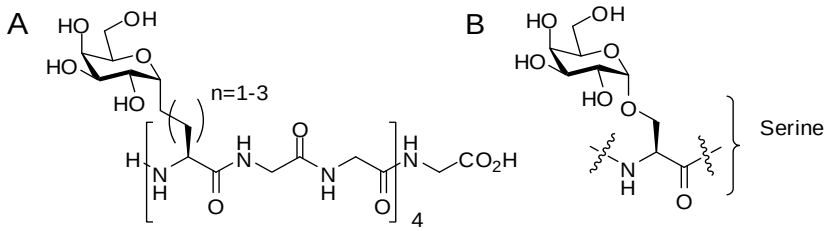

Figure 1.18 (A) Chemical Structure of *C*-linked AFGP analogues containing an alkyl chain glycosyl linkage.[66] (B) Structure of an *O*-linked galactosyl-serine isostere.

Interestingly, unlike the *O*-linked analogues (Section 1.4.2), it was observed that introduction of a C2 acetamide group significantly decreased IRI activity. It was speculated that the C2 acetamide may interact with the peptide backbone in a way that sets the orientation of the carbohydrate in an unfavourable manner.

As is the case with our *O*-linked set of analogues, a complete set of comparable *C*-linked disaccharide analogues have yet to be synthesized and analyzed. Obtaining these types of analogues will prove to be very valuable in the evaluation of the factors responsible for IRI activity.

REFERENCES:

1. Lide, D. R., ed. (2005), *CRC Handbook of Chemistry and Physics* (86th ed.), Boca Raton (FL): CRC Press

2. For examples of ice-induced damage on cells, see : (a) Heber, U.; Volger, H.; Overbeck, V.; Santarius, K. A. *"Proteins at Low Temperatures – Advances in Chemistry"* **1979**, 8, 158. (b) Franks, F.; Mathias, S.F.; Galfre, P.; Webster, S.D.; Brown, D. *Cryobiology*, **1983**, 20, 298-309. (c) Mathias, S.F.; Franks, F.; Trafford, K. *Cryobiology* **1984**, 21, 123-132.

3. Muldrew, K.; McGann, L. E. *Biophys. J*. **1990**, *57*, 525-532.

4. Mazur, P. *J. Gen. Physiol.* **1963,** *47*, 347-369.

5. Farrant, J.; Walter, C.; Lee, H.; McGann, L. *Cryobiology*, **1977,** *14*, 273-286.

6. (a) Mazur, P. *J. Bacteriol*. **1960**, *82*, 662 (b) Mazur, P.; Leibo, S. P.; Chu, E.H.Y. *Exp. Cell Res.* **1972**, *71*, 345-355.

7. Farrant, J.; Morris, G. J. *Cryobiology*, **1973**, *10*, 134-140.

8. (a) Duman, J.G.; DeVries. A.L. *Nature* **1974**, *247*, 237 (b) Hew C.L.; Yip, C. C. *Biochem. Biophys. Res. Commun.* **1976**, *71,* 845.

9. Hew, C.L.; Slaugher, D.; Joshi, S.B.; Fletcher, G.L. *J. Comp. Physiol.* **1984**, *155B,* 81.

10. Tomanchey, A.P.; Morris, J.P.; Kang, S.H.; Duman, J. G. *Biochemistry*, **1982**, *21*, 716-721.

11. Sidebottom, C.; Buckley, S.; Pudney, P.; Twigg, S.; Jarmann, C.; Holt, C.; Telford, J.; McArthur, A.; Worrall, D.; Hubbard, R.; Lillford, P. *Nature*, **2000**, *406*, 256.

12. (a) DeVries, A.L.; Komatsu, S.K.; Feeney, R.E. *J. Biol. Chem.* **1970**, *245*, 2901-2908. (b) Komatsu S.K.; DeVries, A.L.; Feeney, R.E. *J. Biol. Chem.* **1970**, *245*, 2909-2913. (c) DeVries, A.L.; Vandenheede, J.; Feeney, R. E. *J.Biol. Chem.* **1971**, *246*, 305-308.

13. Sicheri, F.; Yang, D.S. *Nature.* **1995**, *375*, 427– 431.

14. Gronwald, W.; Loewen, M.C.; Lix, B.; Daugulis, A.J.; Sönnichsen, F.D.; Davies, P.L.; Sykes. B.D. *Biochemistry* **1998**, *37,* 4712– 4721.

15. Jia, Z.; DeLuca, C.I.; Chao, H.; Davies, P.L. *Nature,* **1996**, *384,* 285–288.

16. Sönnichsen, F. D.; DeLuca, C.I.; Davies, P.L.; Sykes. B.D. *Structure.***1996,** *4*,1325–1337.

17. Kuiper, M.J.; Davies, P.L.; Walker, V.K. *Biophys. J.* **2001***, 81*, 3560-3565.

18. Feeney, R. E. *Am. Sci.* **1974**, *12*, 712.

19. Vandenheede, J. R.; Ahmed, A. I.; Feeney, R. E. *J. Biol. Chem.* **1972**, *247*, 7885.

20. (a) Feeney, R. E.; Burcham, T. S.; Yeh, Y. *Annu. Rev. Biophys. Biophys. Chem.* **1986**, *15*, 59. (b) Morris, H. R.; Thompson, M. R.; Osuga, D. T.; Ahmed, A. I.; Chan, S. M.; Vandenheede, J. R.; Feeney, R. E. *J. Biol. Chem.***1978**, *255*, 5155. (c) Hsiao, K. C.; Cheng, C. H. C.; Fernandes, I. E.; Detrich, H. W.; DeVries, A. L. *Proc. Natl. Acad. Sci. U.S.A.* **1990**, *87*, 9265.

21. (a) Burcham, T.S.; Osuga, D.T.; Rao, B.N.; Bush, C.A.; Feeney, R.E. *J. Biol. Chem.* **1986**, *261*, 6384-6389. (b) Burcham, T.S.; Osuga, D.T.; Yeh, Y.; Feeney, R.E. *J. Biol. Chem.* **1986**, *261*, 6390-6397.

22. Wilson, P. W.; Beaglehole, D.; DeVries, A. L. *Biophys. J.* **1993**, *64*, 1878-1884.

23. Rao, B. N.; Bush, C. A. *Biopolymers*, **1987**, *26*, 1227-1244.

24. (a) Lane, A. N.; Hays, L. M.; Feeney, R. E.; Crowe, L. M.; Crowe, J. H. *Protein Science* **1998**, *7*, 1555-1563. (b) Lane, A. N.; Hays, L. M.; Tsvetkova, N.; Feeney, R. E.; Crowe, L. M.; Crowe, J. H. *Biophys. J.* **2000**, *78*, 3195-3207. (c) Tsvetkova, N. M.; Phillips, B. L.; Krishnan, V. V.; Feeney, R. E.; Fink, W. H.; Crowe, J. H.; Risbud, S. H.; Tablin, F.; Yeh, Y. *Biophys. J.* **2002**, *82*, 464-473.

25. Bush, C. A.; Feeney, R. E.; Osuga, D. T.; Ralapati, S.; Yeh., Y. *Int. J. Peptide Protein Res.* **1981**, *17*, 125-129.

26. (a) Bush, C. A.; Feeney, R. E. *Int. J. Peptide Protein Res.* **1986**, *28*, 386-397. (b) Bush, C. A.; Ralapati, S.; Matson, G. M.; Yamasaki, R. B.; Osuga, D. T.; Yeh, Y.; Feeney, R. E. *Arch. Biochem. Biophys.* **1984**, *232*, 624-631.

27. Ahmed, A. I.; Feeney, R. E.; Osuga, D. T.; Yeh, Y. *J. Biol. Chem.* **1975**, *250*, 3344-3347.

28. Bouvet, V. R.; Lorello, G. R.; Ben, R. N. *Biomacromolecules* **2006**, *7*, 565-571.

29. (a)Filira, R.; Biondi, L.; Scolaro, B.; Foffani, M. T.; Mammi, S.; Peggion, E.; Rocchi, R. *Int. J. Biol. Macromol.* **1990**, *12*, 41-49. (b) Franks, F.; Morris, E. R. *Biochem. Biophys. Acta.* **1978**, *540*, 346-356. (c) Raymond, J. A.; Radding, W.; DeVries, A. L. *Biopolymers* **1977**, 16, 2575-2578.

30. Berman, E.; Allerhand, A.; DeVries, A. L. *J. Biol. Chem*. **1980**, *255*, 4407-4410.

31. Tachibana, Y.; Fletcher, G. L.; Fujitani, N.; Tsuda, S.; Monde, K.; Nishimura, S. *Angew. Chem. Int. Ed.* **2004**, *43*, 856-862.

32. For a recent review on the physical properties of ice, see : Malenkov, G. *J. Phys.: Condens. Matter* **2009**, *21*, 1-35 and references therein.

33. (a) Glasser, L. *J. Chem. Edu.* **2004**, *81*, 414. (b) Wagner, W.; Saul, A.; Pruss, A. *J. Phys. Chem. Ref. Data*, **1994**, *23*, 515. (c) *Handbook of Chemistry and Physics*, 82nd ed.; Lide, D. R., Ed.; CRC Press: Boca Raton, FL, 2001.

34. Sanz, E.; Vega, C.; Abascal, J. L. F.; MacDowell, L. B. *Phys. Rev. Lett.* **2004**, *92*, 255701-255704.

35. (a) Murray, B.J.; Knopf, D.A.; Bertram, A.K. *Nature* **2005**, *434*, 202-204. (b) Murray, B.J.; Bertram, A.K. *Phys. Chem. Chem. Phys.* **2006**, *8*, 186-192.

36. For examples of different types of ice in extreme temperatures and pressures, see (a) Salzmann, C.G.; Radaelli, P.G.; Hallbrucker, A.; Mayer, E.; Finney, J.L. *Science* **2006**, *311*, 1758–1761. (b) Londono, J.D.; Kuhs, W. F.; Finney, J.L. *J. Chem. Phys.* **1993**,*98*,4878-4888. (c) Salzmann, C.G.; Kohl, I.; Loerting, T.; Mayer, E.; Hallbrucker, A. *J. Phys. Chem.*

B **2003**, *107,* 2802-2807. (d) Kamb, B.; Davis, B.L. *Proc Natl Acad Sci U S A* **1964**, *52*, 1433-1439.

37. (a) Sadtchenko, V.; Ewing, G. E. *J. Chem. Phys.* **2002**, *116*, 4686-4697. (b) Golecki, I.; Jaccard, C. J. Phys. Chem. **1978**, *11*, 4229. (c) Döppenscmidt, A.; Butt, H.-J. *Langmuir* **2000**, *16*, 6709 . (d) Pittenger, G.; Fain, Jr. S.C.; Cochran, M.T.; Donev, J.M.K.; Robertson, B.E.; Szuchmacher, A.; Overney, T.M.;*Phys. Rev. B* **2001**, *63*, 134102.

38. (a) Beaglehole, D.; Wilson, P. *J. Phys. Chem.* **1993**, *97*, 11053-11055. (b) Wilson, P.W.; Arthur, J.W.; Haymet, A.D.J. *Biophys. J.* **1999**, *77*, 2850-2855.

39. Haymet, A.D.J.; Ward, L.G.; Harding, M.M. *J. Am. Chem. Soc.* **1999**, *121,* 941-948.

40. Adapted from Tam, R.Y.; Ferreira, S.S.; Czechura, P.; Chaytor, J.L.; Ben, R.N. *J. Am. Chem. Soc.* **2008**, *130,* 17494-17501.

41. Chakrabartty, A.; Hew, C. L. *Eur. J. Biochem.* **1991**, *202*, 1057–1063.

42. (a) Raymond, J. A.; DeVries, A.L. *Proc. Natl. Acad. Sci. USA.* **1977**, *77*, 2589-2593. (b) Wilson, P. *Cryoletters* **1993**, *14*, 31-36.

43. For examples of reviews on the binding of AF(G)Ps to ice surfaces, see (a) Jia, Z.; Davies, P.L. *Trends Biochem. Sci.* **2002**, *27*, 101-106. (b) Knight, C. A.; Wierzbicki, A. *Cryst. Growth Des.* **2001**, *1,* 429-438. (c) Knight, C. A.; Wierzbicki, A. *Cryst. Growth Des.* **2001**, *1,* 439-446.

44. Feeney, R. E.; Fink, W.H.; Hallet, J.; Osuga, D.T.; Vesenka, J.P.; Yeh, Y. *J. Cryst. Growth* **1991**, *113*, 417-429.

45. Knight, C.A.; Cheng, C.C.; DeVries, A.L. *Biophys. J.* **1991**, *59*, 409-418.

46. Pertaya, N.; Marshall, C.B.; DiPrinzio, C.L.; Wilen, L.; Thomson, E.S.; Wettlaufer, J.S.; Davies, P.L.; Braslavsky, I. *Biophys. J.* **2007**, 92, 3663-3673.

47. Graham, L.A., Liou, Y.C., Walker, V.K., Davies, P.L., Nature **1997**, *388*, 727–728.

48. Pertaya, N.; Marshall, C.B.; Celik, Y.; Davies, P.L.; Braslavsky,I. *Biophys. J.* **2008**, 95, 333-342.

49. a) DeVries, A. L. *Phil. Trans. R. Soc. Lond. B. BioL Sci*. **1984**, *B304,*575-588. (b) Chou, K.C. *J. Mol. Bio*.**1992**, *223*, 509-517.

50. Knight, C.A.; Driggers, E.; DeVries, A.L. *Biophys. J.* **1993**, *64*, 252-259.

51. Chao, H.; Houston, M. E.; Hodges, R.S.; Kay, C.M.; Sykes, B.D.; Loewen, M.C.; Davies, P.L; Sonnichsen, F.D. *Biochemistry*, **1997**, *36*, 14652-14660.

52. Graether, S. P., C. M. Slupsky, P. L. Davies, and B. D. Sykes. **2001**. Biophys. J. 81:1677–1683.

53. Jia, Z. *et al. Nature* **1996**, *384*, 285–288.

54. Nutt, D.R.; Smith, J.C. *J. Am. Chem. Soc.* **2008**, *130*, 13066-13073.

55. Frauenfelder, H.; Fenimore, P. W.; McMahon, B. H. *Biophys. Chem.* **2002**, *98*, 35–48.

56. Ahmed, I. A.; Yeh, Y.; Osuga, D.T.; Feeney, R.E. *J. Biol. Chem.* **1976**, *251*, 3033-3036.

57. Ahmed, I. A.; Yeh, Y.; Osuga, D.T.; Feeney, R.E *J. Biol. Chem.* **1973**, 248, 8524-8527.

58. Mimura, Y.; Yamamoto, Y.; Inoue, Y.; Chujo, R. *Int. J. Biol. Macromol.* **1992**, *14*, 242-248.

59. Corzana, F.; Busto, J. H.; Jiménez-Osés, G.; García de Luis, M.; Asensio, J. L.; Jiménez-Barbero, J.; Peregrina, J. M.; Avenoza, A. *J. Am. Chem. Soc.* **2007**, *129*, 9458-9467.

60. Knight, C. A.; Hallet, J.; DeVries, A. L. *Cryobiology* **1988**, *25*, 55–60.

61. (a) Pronk, P.; Infante Ferreira, C. A.; Witkamp, G. J. *J. Cryst. Growth* **2005**, *275*, e1355. (b) Huige, N. J. J.; Thijsenn, H. A. C. *J. Cryst. Growth* **1972**, 13/14, 483. (c) Inada, T.; Modak, P. R.; *Chem. Eng. Sci.* **2006**, 61, 3149. (d) Kingery, W. D. *J. Appl. Phys*. **1959**, *30*, 301.

62. Bouvet, V.R. Ph.D. Dissertation Thesis. University of Ottawa, Ottawa. 2006.

63. Eniade, A.; Purushotham, M.; Ben, R. N.; Wang, J. B.; Horwath, K. *Cell Biochem. Biophys.* **2003**, *38*, 115-124.

64. Murphy, A. Ph. D. Dissertation Thesis. University of Ottawa, 2004.

65. Czechura, P.; Tam, R.Y.; Murphy, A. V.; Dimitrijevic, E.; Ben, R. N. *J. Am. Chem. Soc.* **2008**, *130*, 2928–2929.

66. Liu, S.; Ben, R. N. *Org. Lett.* **2005**, *7*, 2385-2388.

67. Large, D.G.; Warren, C.D. *Glycopeptides and related compounds: synthesis, analysis, and applications*. CRC Press, 1997. New York, New York.

68. Ben, R. N.; Eniade, A.; Hauer, L. *Org. Lett.* **1999**, *11*, 1759–1762.

69. Kontes, F. B.Sc. Honours Thesis. University of Ottawa, 2006.

70. Thapa, I. M.Sc. Thesis. University of Ottawa, 2006.

Chapter 2: Goals and Objectives

2.1 FACTORS RESPONSIBLE FOR ICE-RECRYSTALLIZATION INHIBITION (IRI) ACTIVITY

Due to our group's interest in using antifreeze glycoprotein analogues as cryopreservants, our goal is to ultimately synthesize compounds that are not cyto- and cryotoxic, are structurally simple, and possess a high level of ice-recrystallization inhibition (IRI) activity. In addition, it is important that these compounds do not possess any thermal hysteretic (TH) activity, as this can lead to cell death.

The chemical synthesis of AFGP and previous AFGP analogues is a timely and labour-intensive task, and generally requires up to 15 synthetic steps.[1-7] As such, the development of a comprehensive library of analogues that can be screened for antifreeze activity is relatively nascent and will take a long time to develop. The lack of a large library has hampered the progress towards the determination of the structural factors of AFGP (and its analogues) that are responsible for IRI activity. This is clearly shown in the observed trends from previous structure-activity relationship studies, Sections 1.4.2 and 1.4.3. For example, a decrease in the side chain length between the carbohydrate and the polypeptide backbone showed an increase in IRI activity.[2,4,7] However, structural variations at C2 of the galactose residue and the type of anomeric linkage gave contradicting trends. For example, the presence of a C2 acetamide (NHAc) showed decreased IRI activity for the *C*-linked glycopeptide,[4] but not for the *O*-linked analogue, whereas substitution with a C2 hydroxyl group significantly increases the activity for the *C*-linked and not the *O*-linked analogue.[8] In addition, a change in carbohydrate stereochemistry was also shown to affect IRI activity.[7]

Therefore, the initial goal was to synthesize compounds that would provide further insight into these trends and also elucidate the structural features necessary for IRI activity.

2.1.1 *Objective 1*: Determination of the effect of carbohydrate stereochemistry on hydration and its relationship to IRI activity.

As mentioned in Section 1.2, the protein-ice binding event is complicated by the presence of an amorphous QLL layer. In addition to this, there remain questions regarding the exact role that AF(G)P hydration has on antifreeze activity.[9,10] For example, one notion proposes that the protein acts as a receptor and binds directly to the ice which acts as the ligand.[9] However, one problem with this hypothesis is that antifreeze proteins are surrounded by water molecules, and it is well precedented that water in the hydration layer has significant roles in a variety of protein functions.[11] Recent studies have suggested that the ice binding event is influenced by the orientation of water molecules that surround an antifreeze protein.[12] Thus, due to the dynamic nature of water molecules in both the QLL and the hydration layer of AFPs, probing the ice-protein interaction is a complicated issue.

One class of analogues previously synthesized in our group showing moderate IRI activity contains a galactose monosaccharide that is *C*-linked to the peptide backbone via an amide bond. Structure-activity relationship studies showed that stereochemical variation of the carbohydrate affected IRI activity, Figure 2.1.[5] The carbohydrate derivatives studied contained a systematic variation in the hydroxyl stereochemistry at the C2 and C4 position.

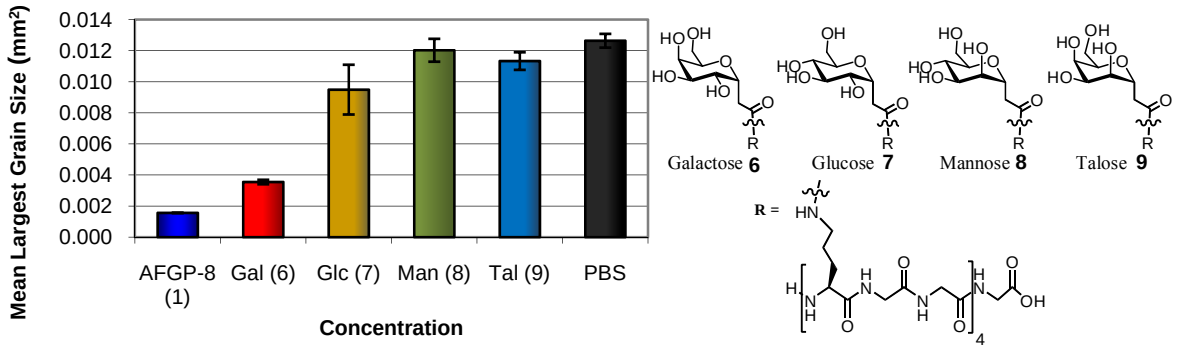

Figure 2.1 Ice-recrystallization inhibition (IRI) activity of *C*-linked AFGP analogues containing various monosaccharides (**6-9**). AFGP-8 (positive control) and PBS (negative control) are also shown for comparison.[5]

The IRI activity of these *C*-linked carbohydrate derivatives correlates to the *partial molar compressibility* (PMC) values[13] of their respective native reducing carbohydrates, Figure 2.2. Partial molar compressibility is a hydration parameter that measures the ability of a solvent in the hydration layer to compress, and will be described in detail in Section 3.1.

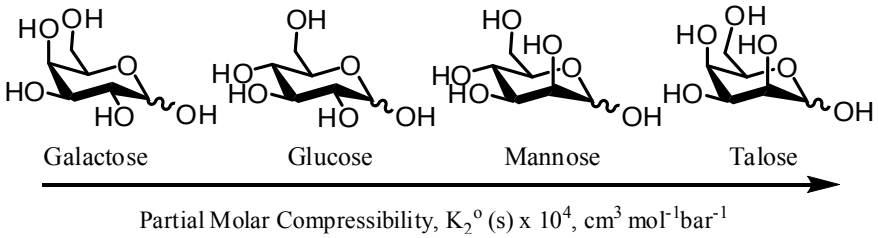

Figure 2.2 Literature values for partial molar compressibility (PMC), K_2^o (s) x 10^4 cm^3 $mol^{-1}bar^{-1}$, of native reducing monosaccharides.[13]

The significance of this correlation is that it demonstrated how a possible change in hydration of the carbohydrate component is able to affect IRI activity of these glycopeptides. The PMC values used in the aforementioned study were based on simple reducing saccharides, whereas our IRI results were obtained using *C*-linked glycopolymers, Figure 2.2. Thus, this prompted us to determine the IRI activity of simple reducing monosaccharides to ensure a more direct comparison between PMC and IRI activity. Assessing the IRI activity of these and other

simple sugars would also allow us to use this information as a carbohydrate screening parameter to rationally design potent AFGP analogues quickly.

To further confirm the trends observed between the IRI activity of *C*-linked AFGP analogues and the change in hydration of the carbohydrate component, we chose to synthesize simplified *C*-linked carbohydrate model systems (**10-13)** to mimic the nature of the anomeric position of their respective analogues, Figure 2.3. As with assaying reducing carbohydrates, screening these *C*-linked carbohydrate model systems for IRI activity will enable a predictive tool to incorporate the optimal carbohydrate component into synthetic glycoproteins for potent IRI activity.

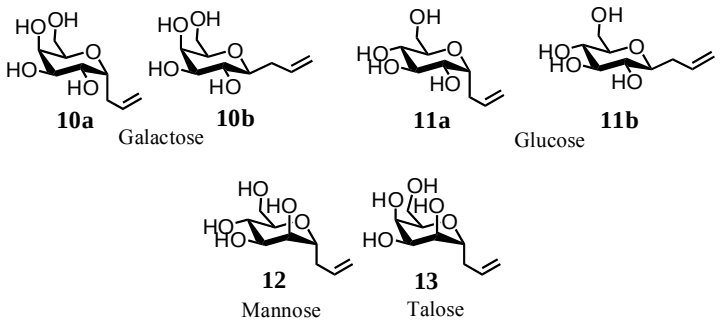

Figure 2.3 *C*-glycoside derivatives of monosaccharides, **10**-**13**.

2.1.2 *OBJECTIVE 2*: DETERMINATION OF THE EFFECT OF LENGTH AND ISOMERIC VARIATIONS IN THE AMIDE-CONTAINING CARBOHYDRATE LINKER OF *C*-LINKED AFGP ANALOGUES ON IRI ACTIVITY.

One observed trend in AFGP analogues that have been synthesized in our group involves the length of the linkage between the carbohydrate and the peptide backbone. Two classes of *C*-linked AFGP analogues have been synthesized, Section 1.4.3. In the case of the *C*-linked alkyl chain series (*C*-Serine),[4] an increase in the linker length diminished IRI activity; similarly with

the amide-linkage series, lysine analogue (**14**)[3] has less IRI activity than the ornithine analogue (**6**)[5] which has a shorter side chain length, Figure 2.4.

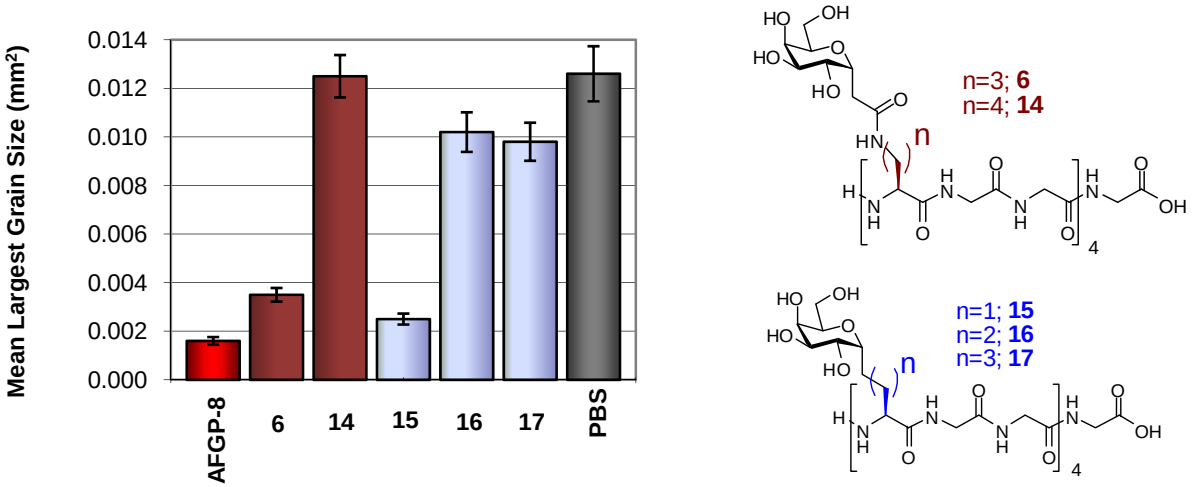

Figure 2.4 IRI Activity of *C*-linked AFGP analogues (at 5.5 μM) previously synthesized by the Ben lab.[3-5]

The correlation that a decreased length of the carbohydrate-backbone tether was proportional to increased IRI activity led to the initial hypothesis that a shortened tether decreases the degrees of freedom of the carbohydrate, thereby forcing the glycopeptide to adopt a specific orientation that is favourable for IRI activity. As one of our goals is to synthesize more potent analogues, we originally thought this would be achieved by decreasing the length of the side chain tether of analogue **6**. This led to the chemical synthesis of the diaminobutanoate (n=2) and diaminopropanoate (n=1) analogues, **18** and **19** respectively. The synthesis of these compounds would be achieved in a manner similar to that previously described.[2,5]

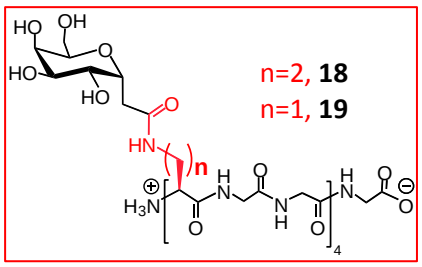

Figure 2.5 Target analogues **18** and **19**, containing a shortened linker between the carbohydrate and the peptide backbone.

As an extension of this project, we sought to further investigate the role of the amide bond in the side chain by designing isomers of this set of analogues. Amide bonds are important functional groups as they are able to impose structural rigidity, stereo- and electronic effects. Two approaches were sought to investigate its role in the side chain of AFGP analogues for antifreeze activity, Figure 2.6. The first was to change the location of the amide bond within the backbone for the active analogue (**6**), while maintaining the overall spacer length between the carbohydrate and the peptide (**20** and **21**); the second approach was to alter the orientation of the amide bond, as shown in analogue (**22**). Together, this would serve three purposes – (i) alter the intramolecular hydrogen bonding capabilities of the side chain amide bond, (ii) cause other localized conformational changes and (iii) probe the electronic properties of the side chain.

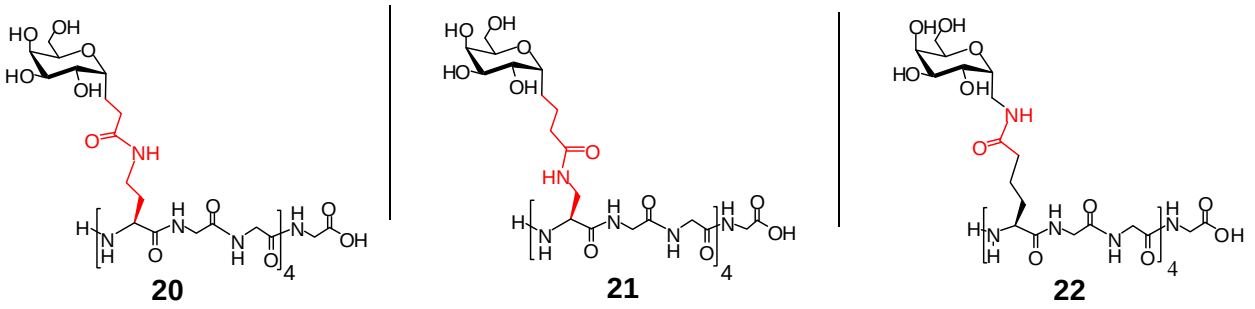

Figure 2.6 Target analogues **20- 22** which contain the same side chain linker length, but with varying locations and orientation of the side chain amide bond.

2.1.3 *Objective 3*: Determination of the effect of the β-methyl substituent in threonine residues on IRI activity and synthesis of *C*-linked α-galactosyl-threonine.

Results obtained from Section 2.1.2 on the effect of the side chain structure on IRI activity inspired the investigation of another important structural substituent in the side chain of native AFPs and AFGPs. Previous studies have indicated the significance of the threonine residue in functional AFPs[14] and AFGPs,[6,8] Table 2.1. In particular, the presence of the β-methyl

group in threonine plays an important role in activity, as there is a significant difference in antifreeze activities between native threonine and its serine analogues.

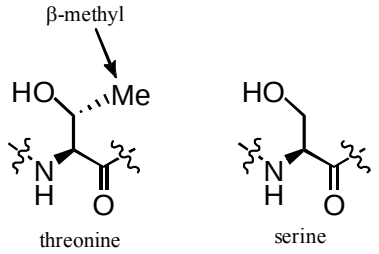

For example, early studies proposed that the increased hydrophobic nature of the threonine compared to serine was important for ice-binding of fish AFPs, Table 2.1A.[14]

Table 2.1 Comparison in antifreeze activities of antifreeze proteins and glycoproteins containing serine versus threonine residues. (A) Thermal hysteresis activity; (B) Ice-recrystallization inhibition activity.

(A)

Serine derivative	Thermal Hysteresis	Threonine derivative	Thermal Hysteresis
Ser-Ala-Ala	No	Thr-Ala-Ala	Yes
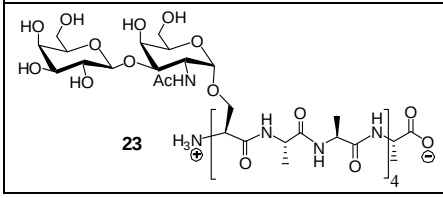 **23**	No	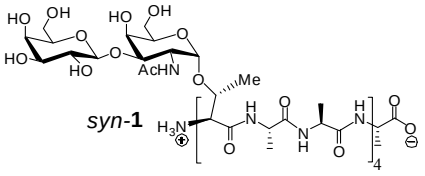 *syn*-**1**	Yes

(B)

Serine derivative	IRI Activity (Mean Grain Size mm^2)	Threonine derivative	IRI Activity (Mean Grain Size mm^2)
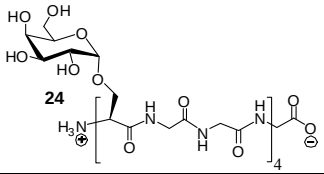 **24**	0.0064 ± 0.0004	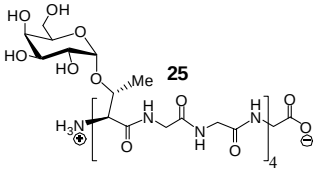 **25**	0.0056 ± 0.0002
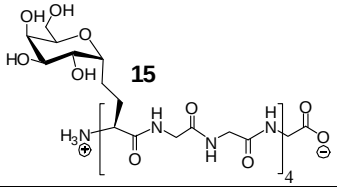 **15**	0.0025 ± 0.0002	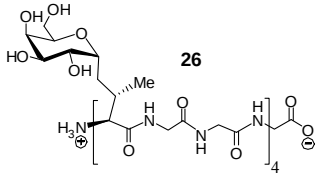 **26**	?

Similarly, Nishimura also showed that serine analogue (**23**) is not potent for thermal hysteresis activity compared to the threonine-containing synthetic AFGP analogues, *syn*-**1**, Table 2.1.[6] Similarly, studies from our lab showed slight increase in IRI activity of threonine (**25**), versus serine residues (**24**), in *O*-linked monosaccharide glycoprotein systems, Table 2.1B.[8]

With respect to the glycoprotein analogues, another factor may account for the change in activity (in addition to the hydrophobic rationale): recent NMR and MD simulations have shown a significant difference in glycoconjugate conformation as a result of substituting threonine and serine residues.[15,16] In threonine glycoconjugates, MD simulations show the carbohydrate is on a plane which is tilted towards one side of polypeptide backbone, whereas serine glycoconjugates have the carbohydrates on a parallel plane as the backbone.[15]

It is currently unclear whether the increased antifreeze activity of AFGPs upon introduction of the β-methyl group is due to hydrophobic, steric parameters, or whether it is based on a drastic change in localized carbohydrate-amino acid conformation. Regardless, it is evident that the presence of the β-methyl group is important for imparting antifreeze activity.

Given the potent activity of *C*-serine analogue (**15**), Figure 2.4, it was hypothesized that a *C*-threonine derivative (**26**) would be even more potent in IRI activity, Table 2.1B. Thus we sought to chemically synthesize *C*-linked α-galactosyl-threonine analogue (**26**), which would be achieved by synthesizing the appropriate target building block (**26a**) and subsequent application to solid phase peptide synthesis, Scheme 2.1.

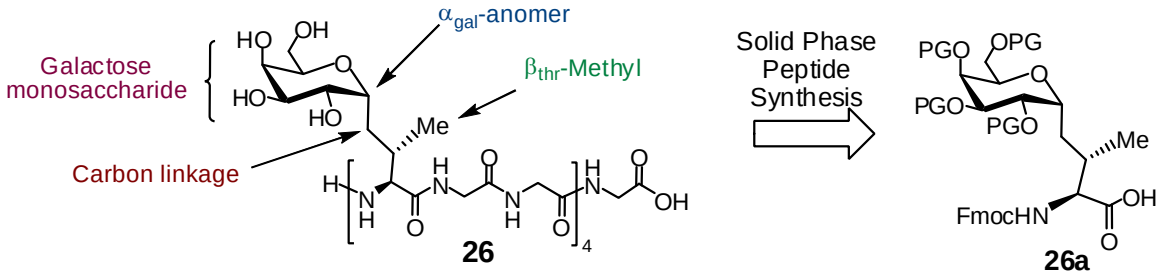

Scheme 2.1 Chemical structure and key features of *C*-linked α-galactosyl-threonine polymer (**26**), and its corresponding building block precursor (**26a)**.

Unfortunately, the synthesis of these compounds has not been previously reported. The distinctive features about this type of compound are the following : (i) α- anomeric carbon linkage (ii) cis (C1,C2) relative stereochemistry (iii) problematic galactose-based derivative (iv) stereochemistry of the threonine residue (at α- and β- amino acid positions).

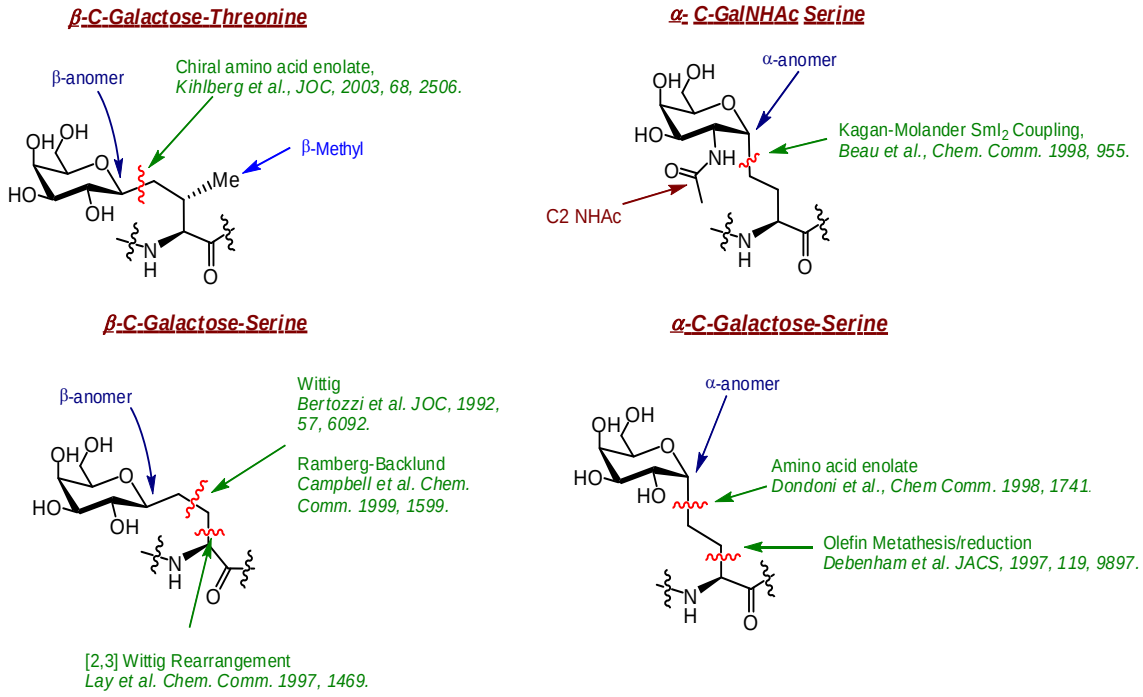

Figure 2.7 Chemical structures and brief overview of their synthetic disconnection/methodology of previously-synthesized *C*-linked glycoconjugates similar to *C*-α-galactosyl-threonine.[18]

Examples of similar compounds that have previously been synthesized are shown in Figure 2.7.[17,18] A detailed description will be described in Section 6.2.

While compounds in Figure 2.7 appear to be similar to our target core, they fail to address all of the synthetic difficulties associated with the α-C-galactosyl-threonine building block. These challenges include: (i) the formation of the anomeric C-C bond in a cis (1,2) fashion, (ii) introduction of the β-methyl group with the proper stereochemistry, and (iii) retention of the proper stereochemistry of the other natural stereocentres of the carbohydrate and α-carbon of the amino acid.

Inspired by work by Breit,[19] and Ichikawa,[20] we originally envisioned synthesis of the core of the target building block via a Reformatsky-type reductive coupling of the aldehyde of a threonine precursor (**27**), to a C2-keto galactopyranose derivative (**26c**), Scheme 2.2.

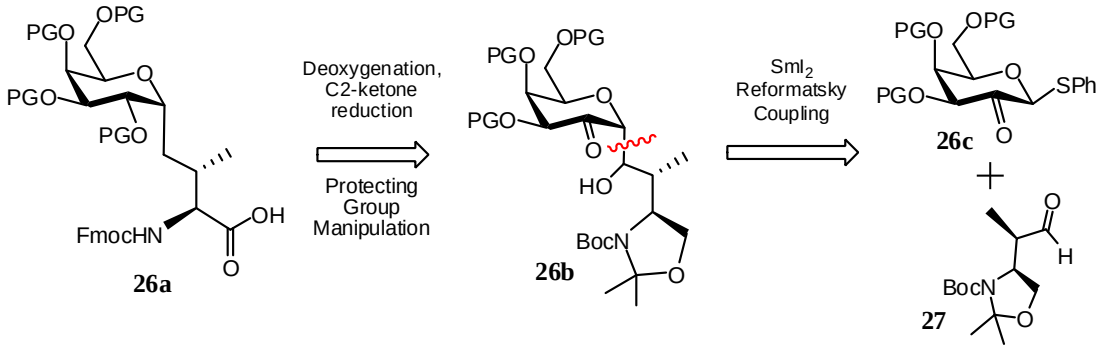

Scheme 2.2 Initial Retrosynthetic analysis to target **26a**

The synthesis of this building block will not only shed more light onto the structural factors responsible for IRI activity, but it will also provide the first synthesis of this type of synthetically-challenging structure.

2.2 SUMMARY OF GOALS AND OBJECTIVES:

(i) To determine the effect of hydration on simple monosaccharides and disaccharides on ice-recrystallization inhibition activity in an effort to elucidate the mechanism by which ice recrystallization is inhibited.

(ii) To probe the effect of the side chain length and role of the side chain amide bond *C*-linked AFGP analogues in an effort to ultimately synthesize more IRI-potent AFGP analogues.

(iii) To synthesize a *C*-linked α-galactosyl-threonine analogue and study the effect of the β-methyl group in the antifreeze activity.

REFERENCES:

1. Ben, R. N.; Eniade, A.; Hauer, L. *Org. Lett.* **1999**, *11*, 1759–1762.
2. Eniade, A.; Purushotham, M.; Ben, R. N.; Wang, J. B.; Horwath, K. *Cell Biochem. Biophys.* **2003**, *38*, 115-124.
3. Eniade, A.; Murphy, A.V.; Landreau, G.; Ben, R.N. *Bioconjugate Chem.* **2001**, *12*, 817-823
4. Liu, S.; Ben, R. N. *Org. Lett.* **2005**, *7*, 2385-2388.
5. Czechura, P.; Tam, R.Y.; Murphy, A. V.; Dimitrijevic, E.; Ben, R. N. *J. Am. Chem. Soc.* **2008**, *130*, 2928–2929.
6. Tachibana, Y.; Fletcher, G. L.; Fujitani, N.; Tsuda, S.; Monde, K.; Nishimura, S. *Angew. Chem. Int. Ed.* **2004**, *43*, 856-862.
7. Murphy, A. V. Ph. D. Dissertation Thesis. State University of New York, Binghamton, Binghamton, 2006.
8. Bouvet, V.R. Ph. D. Dissertation Thesis. University of Ottawa, 2006.

9. (a) Graether, S. P., C. M. Slupsky, P. L. Davies, and B. D. Sykes. **2001**. Biophys. J. 81:1677–1683. (b) Jia, Z.; Davies, P.L. *Trends Biochem. Sci.* **2002**, *27*, 101-106. (c) Jia, Z. *et al. Nature* **1996**, *384*, 285–288.

10. Madura, J. D.; Baran, K.; Wierzbicki, A. *J. Mol. Recognit.* **2000**, *13*, 101–113.

11. Frauenfelder, H.; Fenimore, P. W.; McMahon, B. H. *Biophys. Chem.* **2002**, *98*, 35–48.

12. Nutt, D. R.; Smith, J. C. *J. Am. Chem. Soc.* **2008**, *130*, 13066-13073.

13. Galema, S. A.; Høiland, H. *J. Phys. Chem.* **1991**, *95*, 5321

14. Chao, H.; Houston, M. E.; Hodges, R.S.; Kay, C.M.; Sykes, B.D.; Loewen, M.C.; Davies, P.L; Sonnichsen, F.D. *Biochemistry*, **1997**, *36*, 14652-14660.

15. (a) Corzana, F.; Busto, J. H.; Jiménez-Osés, G.; García de Luis, M.; Asensio, J. L.; Jiménez-Barbero, J.; Peregrina, J. M.; Avenoza, A. *J. Am. Chem. Soc.* **2007**, *129*, 9458-9467. (b) Corzana, F.; Busto, J. H.; Jiménez-Osés, G.; Asensio, J. L.; Jiménez-Barbero, J.; Peregrina, J. M.; Avenoza, A. *J. Am. Chem. Soc.* **2006**, *128*, 14640-14648.

16. Kindahl, L.; Kenne, L.; Sandström, C. *Can. J. Chem.* **2005**, *83*, 156-165.

17. (a) Dondoni, A.; Marra, A. *Chem. Rev.* **2000**, *100*, 4395-4421. (b) Marcaurelle, L. A.; Bertozzi, C. R. *Chem. Eur. J.* **1999**, *5*, 1384-1390. (c) von Moos, E.; Ben, R. N. *Curr. Topics Med. Chem.*. **2005**, *5*, 1351-1361.

18. (a) Gustafsson, T.; Saxin, M.; Kihlberg, J. *J. Org. Chem*. **2003**, *68*, 2506. (b) Urban, D.; Skrydstrup, T.; Beau, J.-M. *Chem. Commun.* **1998**, 955. (c) Bertozzi, C. R.; Hoeprich, P. D.; Bednarski, M. D. *J. Org. Chem.* **1992**, *57*, 6092. (d) Campbell, A. D.; Paterson, D. E.; Taylor, R. J. K.; Raynham, T. M. *Chem. Commun.* **1999**, *1599*. (d) Lay, L.; Meldal, M.; Nicotra, F.; Panza, L.; Russo, G. *Chem*. *Commun*. **1997**, 1469. (e) Dondoni, M.; Marra, A.; Massi, A. *Chem. Commun.* **1998**, 1741. (f) Debenham, S.D.; Debenham, J.S.; Burk, M.J.; Toone, E.J. *J. Am. Chem. Soc.* **1997**, *119*, 9897.

19. Spangenberg, T.; Schoenfelder, A.; Breit, B.; Mann, A. *Org. Lett*. **2007**, *9*, 3881-3884.

20. (a) Ichikawa, S.; Shuto, S.; Matsuda, A. *Tet. Lett.* **1998**, *39*, 4545-4528. (b) Ichikawa, S.; Shuto, S.; Matsuda, A. *J. Am. Chem. Soc.* **1999**, *121*, 10270-10280.

Chapter 3 *:* Correlation between carbohydrate hydration and IRI activity

3.1 INTRODUCTION TO HYDRATION PARAMETERS

Initial hypotheses on the mechanism of action for antifreeze activity has focused on direct ice-protein interactions.[1] However, because this interaction occurs in the presence of water, the dynamic nature of a pseudo-ordered intermediate layer encompassing ice[2] and protein[3] (known as the quasi-liquid layer and hydration layer, respectively) must be accounted for. It is well precedented in literature that the hydration layer of biologically-relevant compounds such as carbohydrates[4,5] and proteins[3,6] play a significant role in their function. For example, water is known to be able to form hydrogen bonds with protein to stabilize active conformations.[3]

In contrast, carbohydrates possess unique hydration characteristics because of the number and stereochemistry of their hydroxyl groups. This feature allows the ability to form intramolecular networks of hydrogen bonds and water bridges connecting the hydroxyl groups with each other.[7,8] Many hypotheses to address these characteristics have been made that focused only on certain parameters within a carbohydrate molecule such as: anomeric effect,[9] ratio of axial versus equatorial hydroxyl groups,[10] and compatibility with bulk water based upon the position of the next-nearest-neighbour hydroxyl groups.[11] The numerous aforementioned hypotheses are due to the inherent difficulty in studying such a dynamic system of water molecules.[12] In addition, these hypotheses focus only on certain factors within a carbohydrate molecule and do not the incorporate the overall hydration of the entire carbohydrate.

However, using molecular dynamics simulations, kinetic experiments and density and ultrasonic measurements, Galema and Engberts were able to determine three different parameters

that assessed hydration of carbohydrates.[13,14] These include, *hydration number*, *partial molar compressibility* and *partial molar volumes*.

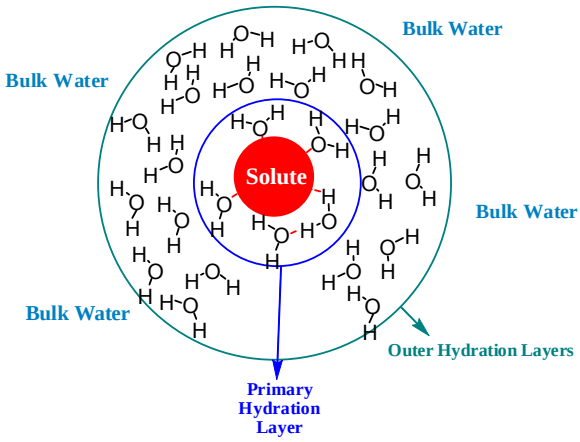

Figure 3.1 Schematic representation of water that surrounds a solute.

Hydration number represents the number of water molecules that are hydrogen bonded and tightly bound to the substrate.[13,15,16] These water molecules are also referred to as being in the primary hydration shell or layer, and for carbohydrates, are considered to be non-compressible.[16] As such, they are indicative of the number of water molecules that are interacting with the other hydration layers and the bulk solvent.

Partial molar compressibility (PMC) is a measure of the ability of the solvent in the outer hydration layers (Figure 3.1) to compress. For example, pure water has a value of +8.18 cm^3 $mol^{-1}bar^{-1}$.[13] However, for a hydrophobic compound in water, water in the hydration layer of the hydrophobic compound forms tighter hydrogen bonds with other nearby water molecules. Hence, the hydration layer is more dense and less compressible, thereby decreasing the partial molar compressibility value of the compound. It was initially hypothesized that as the hydration layer of a solute becomes less compressible (thereby having a lower PMC value), its

resemblance to the three-dimensional orientation of water molecules in the exterior bulk water is decreased.[13]

The total volume of a hydrated solute (or a solute and its surrounding hydration shells), that is able to displace a solution of bulk solvent is generally referred to as the *partial molar volume*. The boundary limit of the outer hydration layer (green circle of Figure 3.1) that is considered for partial molar volume occurs when the dynamics of the water in this hydration layer approaches the identity of the bulk water. Thus, this is a description of the overall interactions between the hydrated solute and the bulk solvent.[13]

While these three parameters are similar to each other with respect to the overall effect of solute-solvent interactions, their subtle differences are important for deduction into the mechanism of action for IRI activity, as will be described throughout this section.

3.2 PRECEDENCE FOR CORRELATION BETWEEN HYDRATION AND IRI ACTIVITY

With our objective to determine the factors required for IRI activity, it was observed that this activity was dependent upon the structure of the carbohydrate component in the *C*-linked AFGP analogue.[17]

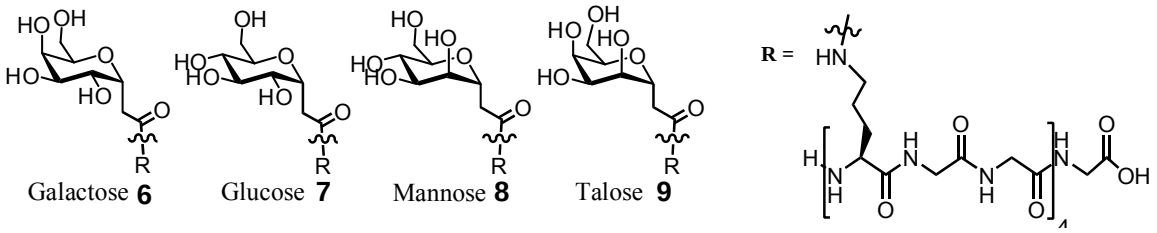

Figure 3.2 *C*-linked AFGP analogues (**6-9**) containing various monosaccharides.[17]

Analysis of the overall solution conformation of these analogues showed that each *C*-linked AFGP analogue was similar to each other and collectively, comparable to native AFGP-8. Based upon this it was concluded that the carbohydrate moiety did not significantly alter the

overall conformations of the glycopeptides which was consistent with a large percentage of random coil structure with varying degrees of more ordered secondary structure, Figure 3.3. This data correlates well with earlier conformational analyses of native AFGP-8 using CD spectroscopy.[18,19] Thus, the observed change in IRI activity can be attributed to the stereochemistry of the carbohydrate.

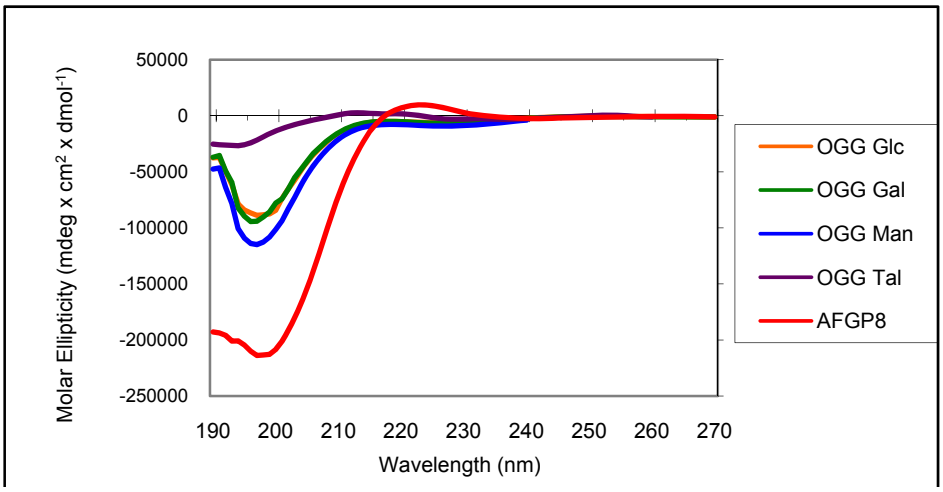

Figure 3.3 Circular dichroism (CD) spectra of analogues **6-9** and AFGP-8.[17]

A comparison between the IRI activities of *C*-linked AFGP analogues and the partial molar compressibility values of their respective free-reducing simple carbohydrates is shown in Figure 3.4. From Figure 3.4, two interesting aspects are observed.

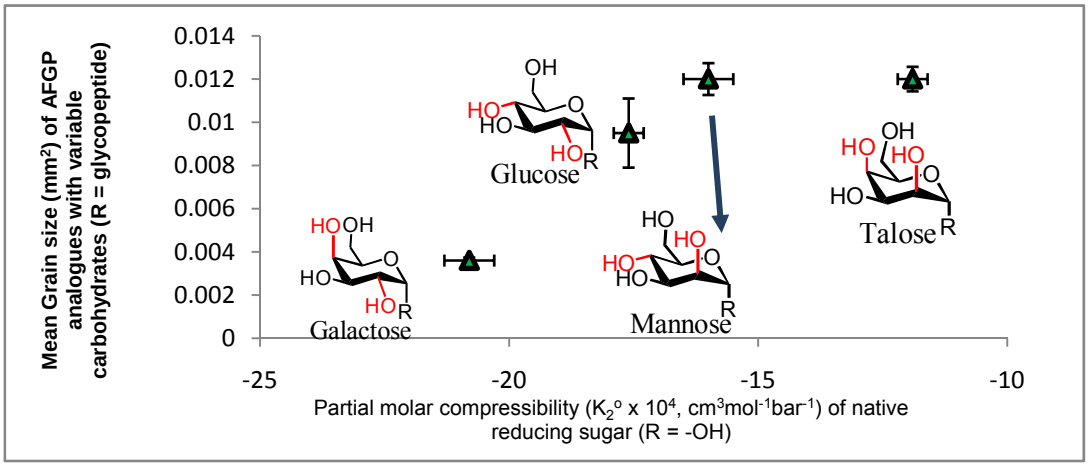

Figure 3.4 Plot of IRI activity and partial molar compressibility (PMC) values of *C*-linked AFGP analogues (**6-9**, R = glycopeptide), and their native free-reducing monosaccharides, (R = -OH), respectively.[13,17]

Firstly, the data plotted along the y-axis shows an interesting result where the stereochemical relationship of the pyranose ring is clearly important for IRI activity. The specific orientation between the OH groups at C2 and C4 appears to be crucial, such that when the C4-OH group is axial and the C2-OH group is equatorial, as in the galactose-containing AFGP analogue (**6**), the largest amount of IRI activity is observed. Variation in the stereochemistry of these two hydroxyl groups drastically decreases IRI activity.

Secondly, plotting the IRI activities of the *C*-linked AFGP analogues versus the PMC values of their respective native reducing carbohydrates (x-axis),[13] shows a correlation. As partial molar compressibility relates to the measure of the ability of a solute to 'fit' into, or disrupt the three-dimensional arrangement of bulk solvent molecules (Section 3.1), it was suggested that the compatibility of a hexose into the arrangement of water molecules is inversely proportional to its ability to inhibit ice-recrystallization. For example, galactose has the lowest PMC value, which correlates to it having the poorest fit (compared to the other monosaccharides) into the three dimensional ordered bulk water structure; this consequently causes a disturbance in the ordering of nearby waters, and hinders addition of water to the structured ice lattice, leading to the inhibited growth of ice crystals.

Furthermore, it was found that these analogues also did not possess any TH activity, although the galactose-containing analogue was observed to be able to cause a slight change in ice-crystal morphology. This suggests that the mechanism of action for IRI does not require an irreversible ice binding event, as it is postulated for the mechanism of TH (Section 1.3). As no TH was observed, it was hypothesized that the major factor for IRI activity is due to the substrate's disturbance of water molecules *near* the ice lattice and not by binding to it.

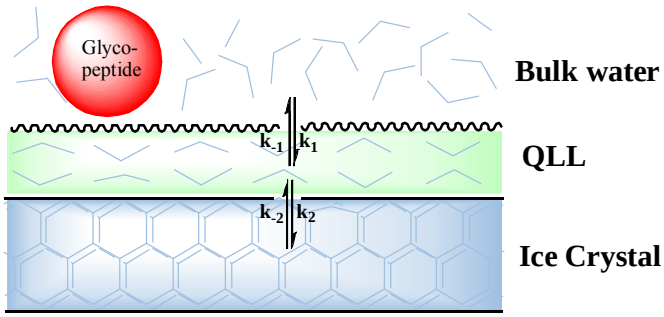

Figure 3.5. Schematic representation of proposed mechanism for inhibition of ice recrystallization. Water molecules surrounding a glycopeptides with potent IRI activity will be more disordered. Shaded red represents hydrated solute, QLL = Quasi-liquid layer.

Therefore, having a poor 'fit' into the three-dimensional hydrogen bonded network of water near the ice lattice consequently causes an increased overall disturbance (or increased entropy) of the surrounding water molecules, which makes the transfer of molecules from the bulk water into QLL, and subsequently the ice lattice, more difficult. As water is unable to add to the ice lattice, ice crystal growth is stopped.

These results show that IRI activity is dependent upon the stereochemistry of the carbohydrate hydroxyl groups; however, the fact that the carbohydrate is covalently bonded to a peptide presents an undesired experimental variable. While CD analysis shows similar conformation between the overall structure of the various peptides, other short-range conformational effects of the glycoconjugate moiety could be present which may affect the overall hydration of the peptides. Therefore it is important to screen the analogous simple reducing carbohydrates to confirm that IRI activity can directly be linked to the hydration properties of carbohydrates. In addition, as syntheses of AFGP analogues are laborious, screening simple carbohydrates for their IRI activity prior to glycopeptide synthesis will increase the efficiency in designing functional AFGP analogues.

3.3. ASSESSING THE CARBOHYDRATE-ICE INTERACTION

As previously mentioned in Section 3.2, the significance of the solute binding to ice for antifreeze mechanism elucidation is great as this indicates where the solute is having its greatest effect on antifreeze activity.

Recent reports have suggested that the antifreeze activity of simple mono- and disaccharides is based on complementarity of hydroxyl groups with the ice lattice. It has been proposed that the optimal distance between hydroxyl groups of a carbohydrate is 4.2 - 4.5 Ångstroms.[20] This distance allows the hydroxyl groups to favourably bind to the ice lattice, consequently stopping ice crystal growth. To investigate this possibility, we examined three monosaccharides (galactose, glucose, and talose) and three disaccharides (melibiose, trehalose, and sucrose) for antifreeze activity as a function of thermal hysteresis using nanoliter osmometry, Table 3.1.[21]

Table 3.1 Results of thermal hysteresis assay of various monosaccharides and disaccharides at 10 mg/mL in doubly-deionized water, determined using nanolitre osmometry. Ice crystal morphologies are shown in the photographs.

Carbohydrate	Melting Point (ºC)	Crystal Morphology	Carbohydrate	Melting Point (ºC)	Crystal Morphology
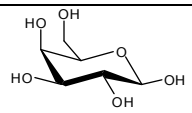 D-Galactose	-0.069	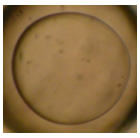	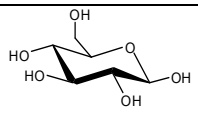 D-Glucose	-0.055	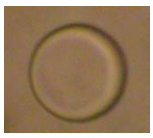
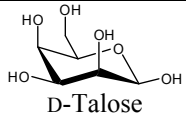 D-Talose	-0.22		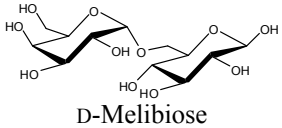 D-Melibiose	-0.17	
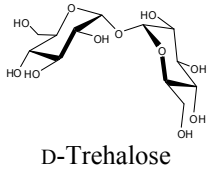 D-Trehalose	-0.015	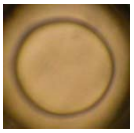	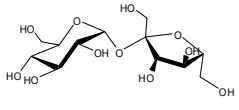 D-Sucrose	-0.12	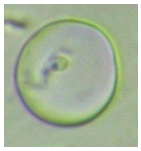

From Table 3.1, it is evident that these carbohydrates exhibit no dynamic ice shaping, and also do not have thermal hysteresis activity. The slight freezing point depressions are due to the colligative properties of each carbohydrate. More interesting is the fact that the ice crystal morphologies of the carbohydrate solutions are consistent with samples of distilled water.

This is significant as it indicates that no direct interaction with the ice lattice is occurring with carbohydrates as previously proposed[20] for both simple sugars and AFGPs, and that a specific distance between hydroxyls is not the only factor responsible for imparting antifreeze activity. This lack of ice binding also corroborates to results from our previous study with *C*-linked AFGP analogues containing various carbohydrates, Section 3.2. While it has been suggested that the protein-ice interaction has an element of surface complementary with antifreeze proteins,[22] recent molecular dynamics simulations have implied that the QLL plays an important role in the binding of biological antifreezes to ice.[23] However, it is still unclear how these biological antifreezes recognize the pseudo-ordered QLL. We propose that a key contributing factor for IRI activity is hydration of the carbohydrate residue. To explore this hypothesis, the IRI activities of various carbohydrates were examined as a function of their various hydration properties.

3.4. CORRELATION BETWEEN THE IRI ACTIVITY AND THE HYDRATION PROPERTIES OF SACCHARIDES

By correlating the IRI activity of simple monosaccharides and disaccharides to their previously determined hydration data, we envisioned this would serve to (1) understand the hydration factors responsible for IRI activity and (2) to select for the optimal carbohydrate to use for AFGP analogues. Using this information will ultimately speed up the process of rationally designing AFGP analogues with custom tailored antifreeze activity.

The partial molar compressibility values, hydration numbers and partial molar volumes of monosaccharides and disaccharides used in this investigation are shown in Table 3.2.[13,24]

Table 3.2 Literature values for isentropic partial molar compressibility ($10^4 K_2^o(s)$, $cm^3\ mol^{-1}\ bar^{-1}$), hydration number, and partial molar volume (cm^3) of various monosaccharides and disaccharides. Errors of molar compressibility values are shown in parentheses.[13,24]

Carbohydrate	Molar Compressibility ($K_2^o(s)x10^4$, $cm^3\ mol^{-1}\ bar^{-1}$)	Hydration Number[13]	Partial Molar Volume (cm^3)[13]	Carbohydrate	Molar Compressibility ($K_2^o(s)x10^4$, $cm^3\ mol^{-1}\ bar^{-1}$)	Hydration Number[13]	Partial Molar Volume (cm^3)[13]
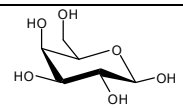 D-Galactose **(28)**	-20.8 (0.5)[24] -20.4 (0.4)[13]	8.7	110.2 (0.3)	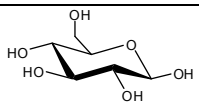 D-Glucose **(29)**	-17.6(0.3)[13]	8.4	111.7 (0.3)
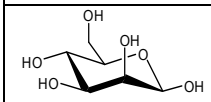 D-Mannose **(30)**	-16.0 (0.5)[24]	8.1	111.3 (0.3)	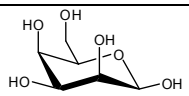 D-Talose **(31)**	-11.9(0.3)[13]	7.7	112.5 (0.1)
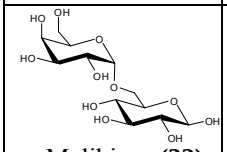 D-Melibiose **(32)**	-31.2 (1.0)[13]	15.5	204.0 (0.7)	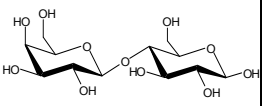 D-Lactose **(33)**	-31.1(0.2)[13] -30.4(1.0)[24]	15.3	209.1 (1.0)
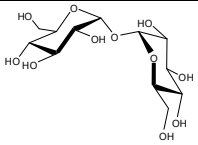 D-Trehalose **(34)**	-30.2 (0.3)[24]	15.3	206.9 (0.5)	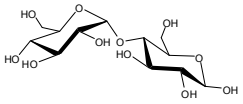 D-Maltose **(35)**	-23.7(1.0)[24]	14.5	208.8 (0.2)
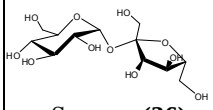 D-Sucrose **(36)**	-17.8 (0.5)[24]	13.9	211.6 (0.3)				

3.4.1. Effect of carbohydrate concentration on IRI activity

To determine the optimal working concentration for our IRI assay, a concentration scan was performed using galactose (**28**) (which is the monosaccharide present in *C*-linked AFGP analogue (**6**) that possesses potent IRI activity), Figure 3.6A.

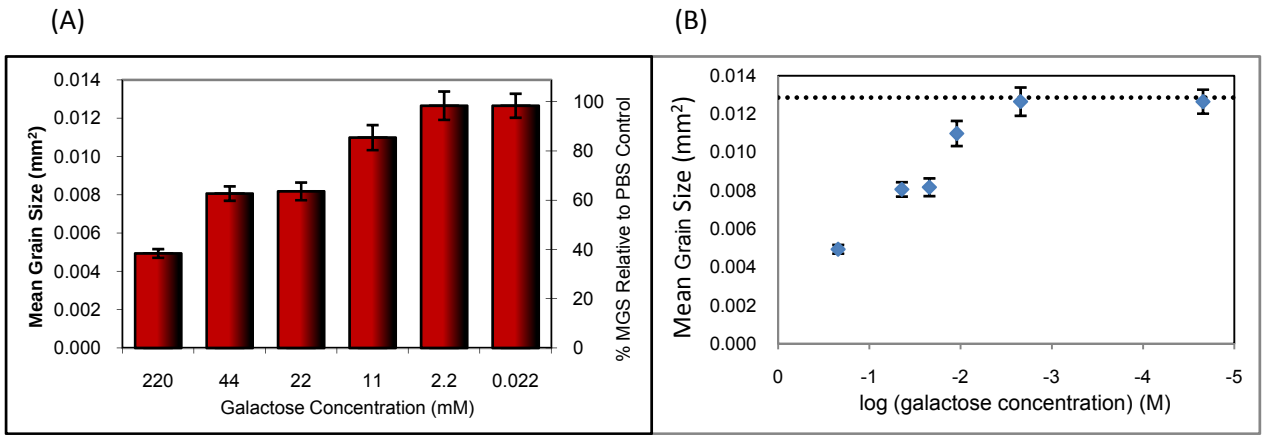

Figure 3.6. IRI activity of various concentrations of D-galactose in PBS. X-axis shows concentrations of D-galactose in (A) mM, and (B) in logarithmic scale.

Examining the activity-concentration profile for D-galactose, a 220 mM solution was significantly greater in activity than any other concentration, whereas a 22 mM solution showed nearly identical activity to a 44 mM solution. However, at 220mM, the high concentration of sugar posed technical difficulties that adversely affected assay performance due to the increased viscosity. Consequently, as we were interested in clearly distinguishing compounds that can effectively inhibit ice crystal growth, we chose to use the lowest concentration possible that showed modest IRI activity. Thus, a carbohydrate concentration of 22 mM was employed for all saccharides in subsequent assays.

The overall relationship between carbohydrate concentration and IRI activity appears to be a logarithmic relationship for the five highest concentrations tested, as shown in Figure 3.6B. At concentrations lower than 2.2 mM, there is a limiting effect whereby the size of the ice crystals in more-diluted galactose solutions approaches the size of ice crystals in PBS solution (dashed horizontal line in Figure 3.6B). This suggests that at higher concentrations, the IRI activity of galactose is non-colligative as has been observed for biological antifreezes.[18] This non-colligative relationship has also been reported by Uchida, who utilized field-emission type

transmission electron microscopy (FE-TEM) to study ice crystal size as a function of trehalose concentration.[25]

3.4.2. Effect of carbohydrate stereochemistry on IRI activity

Four monosaccharides (**28 – 31**), were assayed for their IRI activities at concentrations of 22 mM and 220 mM, Figure 3.7. At 220 mM, all of the sugar solutions show moderate activity, and at both concentrations, a comparable trend to Figure 3.4 is observed. These results are interesting because it shows at high enough concentrations (220 mM), even mannose and talose show IRI activity.

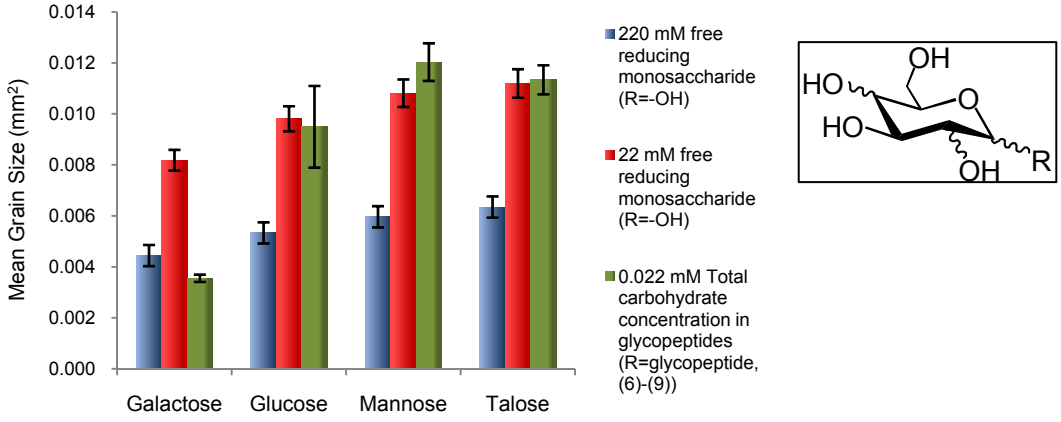

Figure 3.7 IRI activity of various free reducing monosaccharides (**28-31**) at 220 mM (blue bars) and 22 mM (red bars), and the total carbohydrate concentration (22 μM) of their respective *C*-linked AFGP analogues (**6-9**) at glycopeptide concentrations of 5.5 μM (green bars).

Also of note is the difference in concentration of the monosaccharides compared to their respective glycoprotein analogues. IRI activity analyses of glycoproteins are performed at 5.5 μM (Figure 2.4), and because each glycoprotein contains four carbohydrate moieties, the effective carbohydrate concentration is 22 μM. This is four to five orders of magnitude more diluted than the free reducing sugar. This emphasizes the additional importance of the protein on IRI activity, as will be discussed in Chapters 4 and 5.

Previous reports have suggested that the compatibility of a carbohydrate with the three-dimensional hydrogen-bonded network of water is governed by carbohydrate stereochemistry.[8,13,14] This observation correlates well with experimentally derived molar compressibility values[13] in that these also vary as a function of hydroxyl stereochemistry at C2 and C4 (Table 3.2).

Section 3.2 described how AFGP analogues containing carbohydrates with low partial molar compressibilities (such as galactose) fit poorly into the three dimensional hydrogen bonded network of bulk water and hence are effective inhibitors of recrystallization. This hypothesis was based upon isentropic molar compressibilities of the carbohydrates. Compressibility values were derived from isentropic compressibility coefficients, β_s, that were obtained from density ultrasound measurements, Eq. 1,

$$\beta_s = 1/u^2 d \qquad \text{(Eq. 1)}$$

where u is the speed of sound and d is the density of the solution. This technique is regarded as one of the best experimental methods in that it delineates subtle differences in solution structure,[15,16] such as water that is tightly bound to a solute versus water that is only loosely associated with a solute.[26]

Interestingly, using the experimentally derived β_s, hydration numbers, n_h, can be derived according to the Passynsky equation (Eq. 2),

$$n_h = (n_w/n_s)(1-\beta_s/\beta_{so}) \qquad \text{(Eq.2)}$$

where n_w/n_s are the mole fractions of water and carbohydrate, respectively, and β_{so} is the isentropic compressibility value of water. While both the hydration number and isentropic partial molar compressibility (PMC) are derived from the same coefficient β_s, the difference between the two is that hydration number accurately predicts the effective total number of water

molecules that immediately encompass sugars,[13,15,16] whereas the PMC describes the ability of the overall water molecules to compress under constant entropy.[13]

Therefore, to assess which of these parameters was more significant in contributing to the manner carbohydrates are able to inhibit ice crystal growth, the IRI activities of mono- and disaccharides with varying hydroxyl stereochemistry were plotted as a function of their partial molar compressibility values (Figure 3.8A), and hydration numbers, n_h (Figure 3.8B).

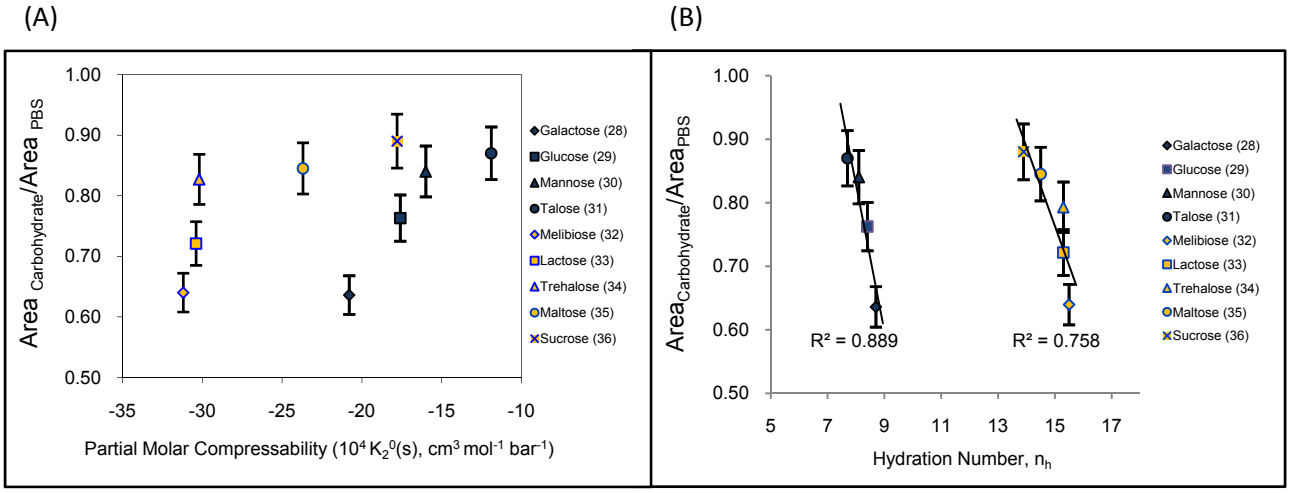

Figure 3.8 IRI activity of various monosaccharides (blue points) and disaccharides (yellow data points) at 22 mM in PBS, plotted against their respective (A) partial molar compressibility values, and (B) hydration number values.

Figure 3.8A shows that there is no overall correlation between the IRI activities of carbohydrates and their partial molar compressibility values. However, there is observed to be a correlation between these two parameters for the monosaccharides tested (blue data points, $R^2 = 0.87$), and also a weaker correlation for the disaccharides tested (yellow data points, $R^2 = 0.62$). Surprisingly, galactose (which has a more positive compressibility value than maltose (**35**), trehalose (**34**) or lactose(**33**)) possessed greater IRI activity than disaccharides (**33-35**).

Figure 3.8B illustrates the plotting the IRI activities of carbohydrates tested and their respective hydration numbers results in comparable correlations to Figure 3.8A. For example,

while there is no overall single correlation between the ability of these carbohydrates to inhibit ice recrystallization, there is again correlations between these parameters for each class of mono- and disaccharides. (R^2 = 0.89, 0.76 for mono- and di-saccharides, respectively), compared to their molar compressibility values, Figure 3.8A. However, the general increase in hydration number for disaccharides relative to the monosaccharides did not necessarily correlate to an increase in IRI activity for the former. For example, the IRI activity of galactose (**28**, n_h = 8.7), and melibiose (**32**, n_h = 15.5) are the same (Figure 3.8B), despite the large difference between their respective hydration numbers. More surprisingly, the increase in hydration numbers between galactose (**28**, n_h = 8.7) and sucrose (**36**, n_h = 13.9) resulted in a decrease in IRI activity for the latter.

We believe this discrepancy is due to the difference in steric volumes between monosaccharides and disaccharides, and that this parameter must be accounted for in correlating a carbohydrate's hydration state to its ability to inhibit ice recrystallization.

3.4.3 A NEW HYDRATION PARAMETER: *HYDRATION INDEX (HI).*

As disaccharides are approximately twice the size of monosaccharides, water molecules in the hydration shells of disaccharides occupy a larger surface area and volume. Therefore, a disaccharide that has the same hydration number as a smaller monosaccharide will result in the larger disaccharide having a lower number of water molecules in its hydration shell per unit volume. This difference in hydration numbers per unit volume is hypothesized to give rise to different interactions with bulk solvent. Thus, while the absolute number of water molecules surrounding a solute is important for predicting IRI activity,[17] the number of water molecules per unit volume of solute is also important.

Taking into account the effect of steric volume of each carbohydrate, the respective hydration numbers were divided by their partial molar volumes,[13,24] which results in a description of the effective number of tightly bound water molecules per molar volume of carbohydrate. We refer to this value as a *hydration index*.

Similar correlations have been reported by Parke et al. in relating the taste properties of solutes of various masses, volumes, and hydrophobicity to the hydration per volume of the solute.[27] Figure 3.9 shows that plotting the hydration index against IRI activity of carbohydrates (**28**-**36**) results in a single trend for all carbohydrates, compared to Figure 3.8 which had two distinct correlations.

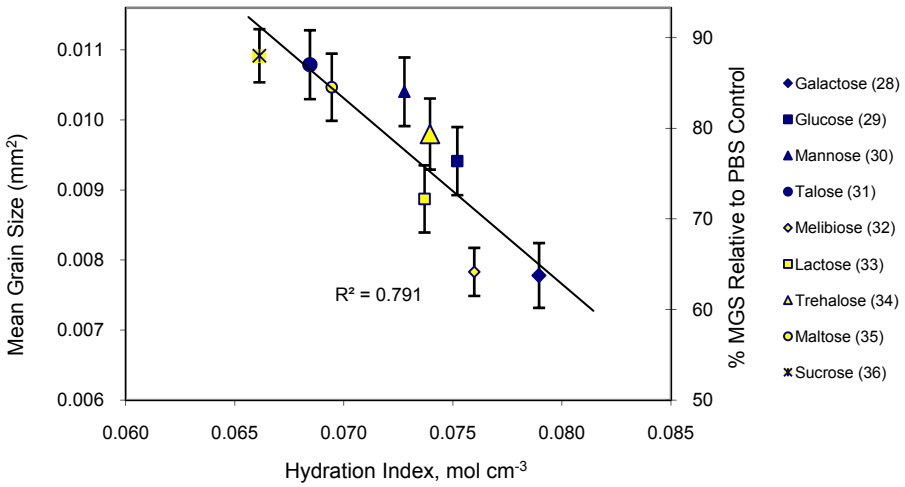

Figure 3.9 IRI activity of carbohydrates (**28**-**36**) at 22 mM, plotted against their respective hydration index (hydration number/partial molar volume, mol cm^{-3}).

A disaccharide that has a large absolute hydration number, but also a small hydration index such as sucrose (**36**) has little effect upon ice recrystallization inhibition. Conversely, carbohydrates with larger hydration indices, such as galactose (**28**) and melibiose (**32**) function as better ice recrystallization inhibitors. The ultimate significance of this relationship is that

there needs to be a highly concentrated number of water molecules around the solute for it to be an effective inhibitor of ice recrystallization.

3.5 PROPOSED ICE-RECRYSTALLIZATION INHIBITION MECHANISM OF ACTION

As thermal hysteresis experiments have shown that mono- and disaccharides do not bind irreversibly to the ice lattice (Section 3.3), these carbohydrates will therefore be concentrated at the interface between two adjacent ice crystals and their QLLs during the recrystallization process, Figure 3.10. This correlates to data by Uchida and co-workers, who studied the antifreeze activity of trehalose using TEM and proposed that trehalose functions at the bulk water-QLL interface.[25] However, the question of exactly where the carbohydrate localizes with respect to the QLL to have such a large effect on ice crystal growth is a difficult question to answer given current inabilities to study the QLL.[2]

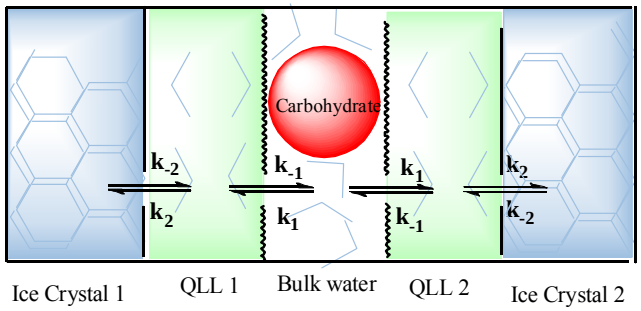

Figure 3.10. Schematic representation of proposed mechanism for inhibition of ice recrystallization. Carbohydrates reside at the QLL-bulk water interface between two adjacent ice crystals.

Recent work by Heyden and co-workers have suggested that the long-range motion of nearby water molecules of solvated carbohydrates is affected by the number of water-carbohydrate hydrogen bonds using terahertz absorption measurements.[28] Thus, we propose that at our working concentrations of 22 mM, an increased density of water molecules in the

hydration shell is important for ice-recrystallization inhibition as this causes a greater disruption (or increase in entropy) on the ordering of bulk water surrounding the hydration shell, Figure 3.11A. This leads to increased energies associated with the transfer of water molecules from (i) bulk water to the QLL and/or (ii) water in the QLL into ice lattice. As this system is very dynamic, the exact nature of these two scenarios is unclear. Regardless, the mechanism of action for transfer of water into the growing ice lattice is believed to involve the QLL. Given the small thickness of the QLL (only 3-10 Ångstroms under our testing conditions) and the entropic effect of a solute's first hydration shell extending out to its third hydration shell,[28] this energy difference in water phase-transfer in the presence of a solute with high hydration index is believed to be significant.

In contrast, if the number of water molecules in the immediate hydration shell is low and dispersed, it is hypothesized that surrounding water is not disturbed as much by the substrate, and thus, the transfer of water molecules into the ice lattice is not hindered, Figure 3.11B.

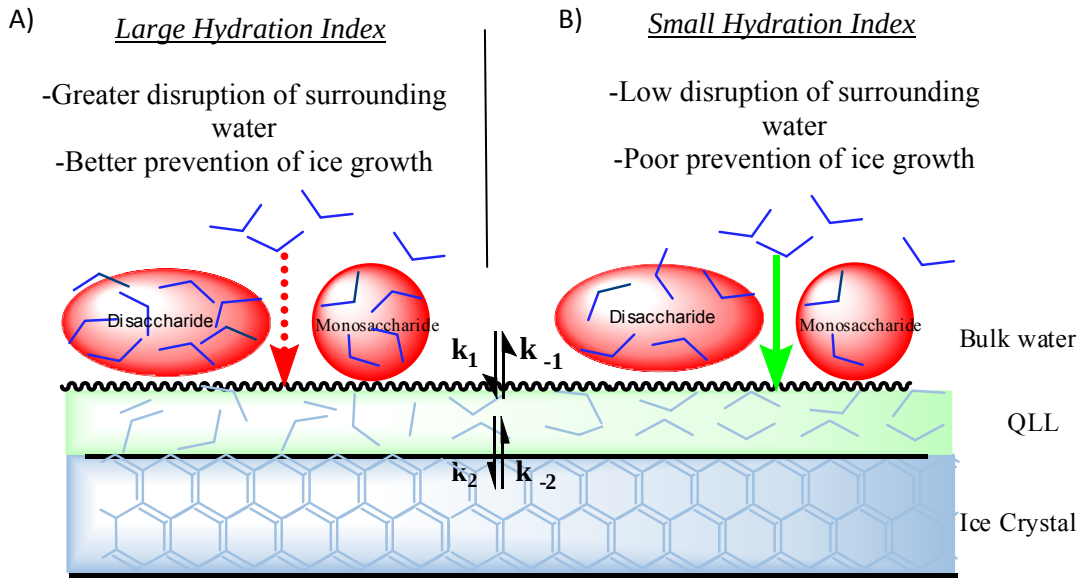

Figure 3.11 Schematic representation of the effects of varying hydration index (HI) on surrounding water and its effects on ice crystal growth.

Therefore, we hypothesize that the primary distinction between the mechanism of action for thermal hysteresis and ice-recrystallization inhibition is that for the latter to exclusively function, the solute must have the ability to (i) bind to the ice lattice reversibly, (ii) to associate with the QLL of more than one ice crystal and (iii) cause significant entropic change to distant bulk water molecules.

3.6 COMPARISON BETWEEN THE IRI ACTIVITIES OF C-GLYCOSIDES AND O-GLYCOSIDES

Having assessed the role of carbohydrate hydration parameters of free reducing carbohydrates (**28**-**36**) and their ability to inhibit ice recrystallization, we subsequently investigated the significance of the substituents at the anomeric position, as our previously synthesized AFGP analogues are *C*-linked in nature.[17] While it is well precedented that *C*-glycosides may be more conformationally flexible than native *O*-linked glycosides due to presence of the exo-anomeric effect for the latter,[29] *C*-linked carbohydrates are able to adopt key conformations *in vitro* ensuring they are just as active or in some instances more active than their *O*-linked counterparts. Furthermore, conformational analyses of *C*-linked and *O*-linked oligosaccharides suggest that the conformations between these two substrates are identical as intramolecular hydrogen bonds play a significant role in dictating conformation. Intramolecular hydrogen bonding cooperation also has an effect on the structuring of water, and has been studied extensively by Dashnau et al.[8] This study indicated that the stereochemistry of the C4-OH is crucial for forming intramolecular hydrogen bonds. In addition the stereochemistry at C4 and C2 serves to modulate the magnitude of the response for hydration. However, the effect of substituents and stereochemistry on hydration at the anomeric and C3 positions were unclear and required investigation.

While the conformation of *C*-linked carbohydrate analogues is generally accepted to be similar to *O*-linked systems, hydration numbers of *C*-linked carbohydrates have not been reported and the relationship between hydration and IRI activity has not been previously studied. Literature,[8,13,14,24] as well as our data presented in this section, suggests that hydration is largely dictated by substituents at C2 and C4 of the pyranose ring. Thus, we were interested to determine if the observed IRI activity trends with varying C2 and C4 substituents holds true with small anomeric carbon substituents. To test this, *C*-allylated derivatives of galactose, glucose, mannose and talose (**10-13**, Figure 3.12), were synthesized.

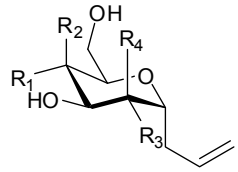

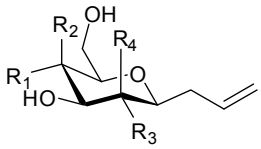

10a (Gal), R_1=H, R_2=OH; R_3=OH, R_4=H
11a (Glc), R_1=OH, R_2=H; R_3=OH, R_4=H
12 (Man), R_1 =OH, R_2=H; R_3=H, R_4=OH
13 (Tal), R_1 =H, R_2=OH; R_3=H, R_4=OH

10b (Gal), R_1=H, R_2=OH; R_3=OH, R_4=H
11b (Glc), R_1=OH, R_2=H; R_3=OH, R_4=H

Figure 3.12. *C*-allylated derivatives of D-galactose (**10a, 10b**), D-glucose (**11a**, **11b**), α-D-mannose (**12**), and α-D-talose (**13**).

3.5.1 SYNTHESIS OF *C*-LINKED CARBOHYDRATE MODEL SYSTEMS

The preparation of the β-D-galactopyranose (**10b**) and β-D-glucopyranose (**11b**) derivatives were synthesized by Dr. Jennifer Chaytor,[30] and peracetylated α-anomers of D-mannose (**37**) and D-glucose (**38**) precursors were previously synthesized by Dr. Pawel Czechura and Dr. Anastasia Murphy.[17,31] The acetylated monosaccharide derivatives were deprotected using sodium methoxide, and neutralized using ion-exchange resin in 90-95% yields, Scheme 3.1. The synthesis of the deprotected mannose derivative (**12**) was performed by Masters student Sandra Ferreira in our laboratory.

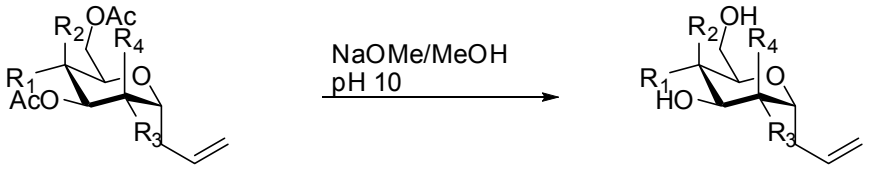

37 (Gal), R_1=H, R_2=OAc; R_3=OAc, R_4=H
38 (Glc), R_1=OAc, R_2=H; R_3=OAc, R_4=H
39 (Man), R_1 =OAc, R_2=H; R_3=H, R_4=OAc

10a (Gal), R_1=H, R_2=OH; R_3=OH, R_4=H
11a (Glc), R_1=OH, R_2=H; R_3=OH, R_4=H
12 (Man), R_1 =OH, R_2=H; R_3=H, R_4=OH

Scheme 3.1. Deprotection of per-acetylated *C*-α-glycosyl allyl compounds.

The synthesis of *C*-α-allyl talose derivative (**13**) was more complicated as talose is an expensive starting material.[32] Our synthesis of (**13**), Scheme 3.2, was inspired by the work of Lowary and Bundle, who have previously synthesized thiotalopyranosides by an oxidation-reduction pathway of the C2 hydroxyl group to invert the stereochemistry of the galactopyranose starting material.[33]

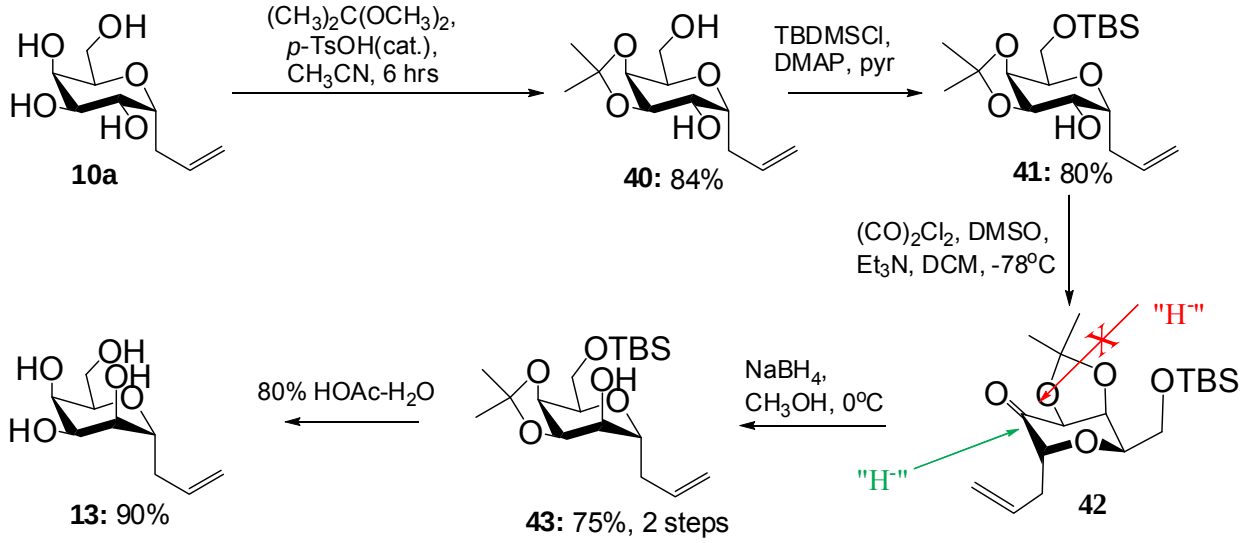

Scheme 3.2 Synthesis of *C*-linked D-talopyranoside derivative (**13**)

Starting from compound (**10a**), selective acetonide protection of C3 and C4 was achieved with catalytic p-toluene sulfonic acid and 2,2-dimethoxypropane, as this led to the

thermodynamically favoured ring product (**40**) in 84% yield. The primary C6 alcohol was then selectively protected over the sterically-hindered C2 alcohol using bulky tert-butyl dimethyl silyl chloride to yield (**41**) in 80% yield.

With the C2 alcohol selectively deprotected, the oxidation-reduction reaction sequence was performed to invert the C2 stereochemistry of (**41**). Swern oxidation furnished the C2 ketone (**42**), which was then immediately reduced by sodium borohydride to form exclusively talopyranoside derivative (**43**) in 75% yield over two steps. The protecting groups were subsequently cleaved using aqueous acidic conditions (80% acetic acid) to afford the *C*-α-allylated talose derivative (**13**) in 90% yield.

3.5.2 IRI ACTIVITY OF *C*-LINKED CARBOHYDRATE MODEL SYSTEMS

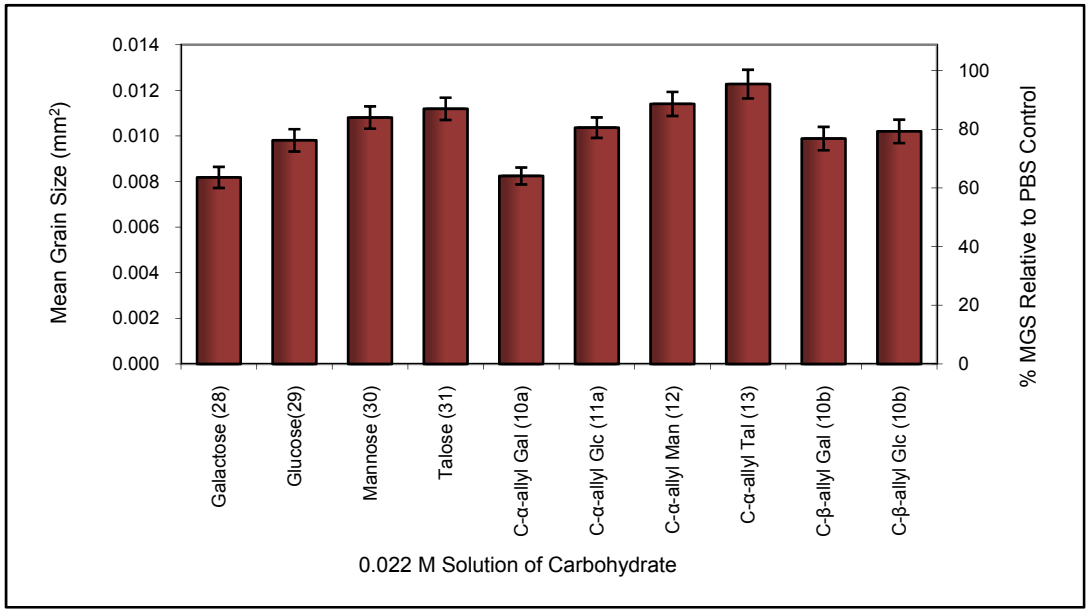

Figure 3.13 IRI activity of native *O*-linked monosaccharides (**28-31**) and their respective *C*-glycoside derivatives (**10-13**) at 22 mM in PBS.

Despite the absence of hydration numbers, the IRI activity of *C*-linked analogues was assayed and shown in Figure 3.13, along with the IRI activity of their respective *O*-linked

monosaccharides. Of the *C*-α-allyl pyranoses (**10a**, **11a**, **12**, **13**), galactose derivative **10a** possesses more potent IRI activity with mean grain sizes statistically identical to native D-galactose. In addition, the IRI activity trend of these *C*-α-linked analogues is identical to their corresponding native monosaccharides (**28-31**). This was consistent with the hypothesis that the nature of the small substituent at C1 may have less influence on hydration and hence IRI activity. In contrast, the β-anomer of *C*-allyl galactopyranose (**10b**) exhibits a marked decrease in IRI activity relative to native *O*-linked galactose and *C*-α-linked derivative (**10a**), suggesting that the anomeric configuration of *C*-linked carbohydrates may play a larger role in hydration (and therefore IRI activity) than previously thought. Comparatively, *C*-β-allyl glucose (**11b**), displayed the same amount of IRI activity as its *C*-α-anomer (**11a**), with no statistically significant difference in mean grain size.

To gain further insight into the effect of anomeric substituents and stereochemistry on IRI activity, the syntheses and IRI analyses of the *C*-β-linked derivatives of mannose and talose should be achieved. In addition, because a solution of native reducing carbohydrates contains an equilibrium mixture of α and β anomers (due to mutarotation), a solution containing a similar proportion of *C*-α/β-linked glycosides should be assayed to allow for a direct correlation between IRI activities and the nature of the anomeric substituent.

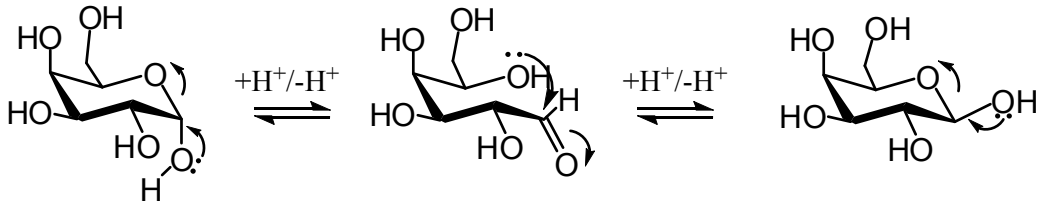

Figure 3.14. Mutarotation of reducing carbohydrates.

As it is clear that further studies are required to ascertain the exact effect of the anomeric configuration on IRI activity and its subsequent relationship to hydration, these issues are currently being addressed in our laboratory.

3.6. CHAPTER SUMMARY

In summary, this chapter has described the correlation between the ice-recrystallization inhibition (IRI) activities of mono- and disaccharides and their hydration properties at 22 mM. Specifically, it was shown that at these concentrations, the hydration numbers and partial molar compressibility values of monosaccharides correlated well with their respective IRI activities. A similar trend was observed between various disaccharides. However, such a correlation could not be made when comparing the hydration properties of both mono- and disaccharides to their IRI activities. We believed this is due to the significant volume difference between mono- and disaccharides, and led us to introduce a new hydration parameter, the *Hydration Index* (HI), which is the hydration number per unit volume and describes the concentration of water that surrounds the substrate. It was determined that an increase in HI results in an increase in IRI activity.

A comparison between *C*- and *O*-linked glycosides were also performed, and showed that *C*-α-galactopyranose possessed similar IRI activities to the native *O*-linked system, whereas *C*-β-galactopyranose did not. This discrepancy in IRI activity between the α and β *C*-galactopyranosides is contrary to previous reports which indicate that the C1 position does not play a significant role in carbohydrate hydration.

REFERENCES:

1. For a review on early hypotheses of AFP-ice interactions, see: Yeh, Y.; Feeney, R.E. *Chem. Rev*. **1996**, *96*, 601-618.

2. (a) Sadtchenko, V.; Ewing, G.E. *J. Chem. Phys.* **2002**, 116, 4686.(b) Karim, O.A.; Haymet, A.D.J. *J. Chem. Phys.* **1988**, 89, 6889.

3. For examples of discussion about the hydration layer surrounding proteins, see (a) Teixera, J. *Gen. Physiol. Biophys.* **2009**, *28*, 168-173 and references cited therein (b) Bagchi, B. *Chem. Rev.* **2005**, *105*, 3197-3219.

4. Franks, F. *Pure Appl. Chem.* **1987,** 59, 1189.

5. Quiocho, F. A. *Ann. Rev. Biochem.* **1986**, *55*, 287-315. (b) Lemieux, R. U. *Chem. Soc. Rev.* **1989**, *18*, 347-374.

6. Frauenfelder, H.; Fenimore, P.W.; McMahon, B.H. *Biophys. Chem.* **2002,** *98*, 35-48.

7. Carcabal, P.; Jockusch, R.A.; Hunig, I.; Snoek, L.C.; Kroemer, R.T.; Davis, B.G.; Gamblin, D.P.; Compagnon, I.; Oomens, J.; Simons, J.P. *J. Am. Chem. Soc.*, **2005**, *127*, 11414-11425.

8. Dashnau, J; Sharp, K. A.; Vanderkooi, J. M. *J. Phys. Chem. B* **2005**, *109*, 24152-24159.

9. Kabayama, M. A.; Patterson, D.; Piche, L. *Can. J. Chem.* **1958,** *36*, 557-562.

10. (a) Franks, F. *Cryobiology* **1983,** *20*, 335-345. (b) Suggett, A., *J. Solution Chem.* **1976**, *5*, 33-46.

11. (a) Danford, M. D.; Levy, H.A. *J. Am. Chem. Soc.* **1962**, *84*, 3965-3966. (b) Warner, D. T. *Nature* **1962**, *196*, 1055-1058.

12. (a) Quiocho, F. A. *Ann. Rev. Biochem.* **1986**, *55*, 287-315. (b) Lemieux, R. U. *Chem. Soc. Rev.* **1989**, *18*, 347-374.

13. Galema, S.A.; Høiland, H. *J. Phys. Chem.* **1991**, *95*, 5321-5326.

14. (a) Galema, S.A.; Eduardo, H.; Engberts, J.B.F.N.; Raul Grigera, J. *Carbohydr. Res.* **1994**, *265*, 215-225. (b) Galema, S.A.; Engberts, J.B.F.N.; Høiland, H.; Førland, G.M. *J. Phys.Chem.* **1993**, *97*, 6885-6889.

15. Gliński, J.; Burakowski, A. *Eur. Phys. J. Special Topics* **2008**, *154*, 275-279.

16. Moulik, S. P.; Gupta, S.; Das, A.R. *Can. J. Chem.* **1989**, *67*, 356-364.

17. Czechura, P.; Tam, R.Y.; Murphy, A.V.; Dimitrijevic, E.; Ben, R.N. *J. Am. Chem. Soc.* **2008**, *130*, 2928-2929.

18. Bouvet, V.; Lorello, G.; Ben, R.N. *Biomacromolecules* **2006**, *7*, 565-571.

19. (a) Filira, R.; Biondi, L.; Scolaro, B.; Foffani, M. T.; Mammi, S.; Peggion, E.; Rocchi, R. *Int. J. Biol. Macromol.* **1990**, *12*, 41-49. (b) Franks, F.; Morris, E. R. *Biochem. Biophys. Acta.* **1978**, *540*, 346-356. (c) Raymond, J. A.; Radding, W.; DeVries, A. L. *Biopolymers* **1977**, 16, 2575-2578.(d) Tachibana, Y.; Fletcher, G. L.; Fujitani, N.; Tsuda, S.; Monde, K.; Nishimura, S. *Angew.Chem. Int. Ed.* **2004**, *43*, 856-862. (e) Berman, E.; Allerhand, A.; DeVries, A. L. *J. Biol. Chem*. **1980**, *255*, 4407-4410

20. Baruch, E.; Belostotskii, A.M.; Mastai, Y. *J. Mol. Struct.* **2008**, *874*, 170-177.

21. Chakrabartty, A.; Hew, C. L. *Eur. J. Biochem.* **1991**, *202*, 1057–1063.

22. (a) Leinala, E. K.; Davies, P. L.; Jia, Z. *Structure* **2002**, *10*, 619-627. (b) Baardsnes, J.; Davies, P.L. *Biochim. Biophys. Acta*, **2002**, *1601*, 49-54

23. Madura, J.D.; Baran, K.; Wierzbicki, A. *J. Mol. Recognit.* **2000**, *13*, 101-113.

24. (a) Høiland, H.; Holvik, H. *J. Solution Chem.* **1978**, *7*, 587-596. (b) Shahidi, F.; Farrell, P.G.; Edward, J. T. *J. Solution Chem.* **1976**, *5*, 807-816.

25. Uchida, T.; Nagayama, M.; Shibayama, T.; Gohara, K. *J. Crys. Growth* **2007**, *299*, 125-135.

26. Gharsallaous, A.; Roge, B.; Genotelle, J.; Mathlouthi, M. *Food Chem.* **2008,** *106*¸1443-1453.

27. Parke, S.A.; Birch, G.G.; Dijk, R. *Chem. Senses* **1999**, *24*, 271-279.

28. Heyden, M.; Bründermann, E.; Heugen, U.; Niehues, G.; Leitner, D.M.; Havenith, M. *J. Am. Chem. Soc.* **2008**, *130*, 5773-5779.

29. (a) Espinosa, J. F.; Montero, E.; Vian, A.; Garcı´a, J. L.; Dietrich, H.; Schmidt, R. R.; Martín-Lomas, M.; Imberty, A.; Cañada, F. J.; Jiménez-Barbero, J. *J. Am. Chem. Soc.* **1998**, *120*, 1309-1318. (b) Wang, J.; Kováč, P.; Sinaÿ, P.; Glaudemans, C. P. J. *Carbohydr. Res*.**1998**, 308, 191. (c) Wang, Y.; Barbirad, S. A.; Kishi, Y. *J. Org. Chem.* **1992**, *57*, 468-481. (d) Ravishankar, R.; Surolia, A.; Vijayan, M.; Lim, S.; Kishi, Y. *J. Am. Chem. Soc.* **1998**, *120*, 11297-11303. (e) Ma, B.; Schaefer, H. F., III; Allinger, N. L. *J. Am. Chem. Soc.* **1998**, *120*, 3411.

30. Chaytor, J.L. Ph.D. Dissertation, University of Ottawa, 2010.

31. Pontén, F.; Magnusson, G. *J. Org. Chem.* **1996**, *61*, 7463-7466.

32. $207.50 / 250mg from Sigma-Aldrich

33. Lowary, T.L.; Eichler, E.; Bundle, D. *Can. J. Chem.* **2002**, *80*, 1112-1130.

Chapter 4 : Effect of the side chain length of AFGP analogues on IRI activity

4.1 STRUCTURE-FUNCTION RELATIONSHIP OF PREVIOUS C-LINKED AFGP ANALOGUES – EFFECT OF THE SIDE CHAIN LENGTH

Previous work in our laboratory has shown that various *C*-linked AFGP analogues at 5.5 μM possess a wide range of ice-recrystallization inhibition (IRI) activity Figure 4.1.[1-3] It has been previously shown that a sample concentration of 5.5 μM is optimal within the dynamic range for this IRI assay.[1-3]

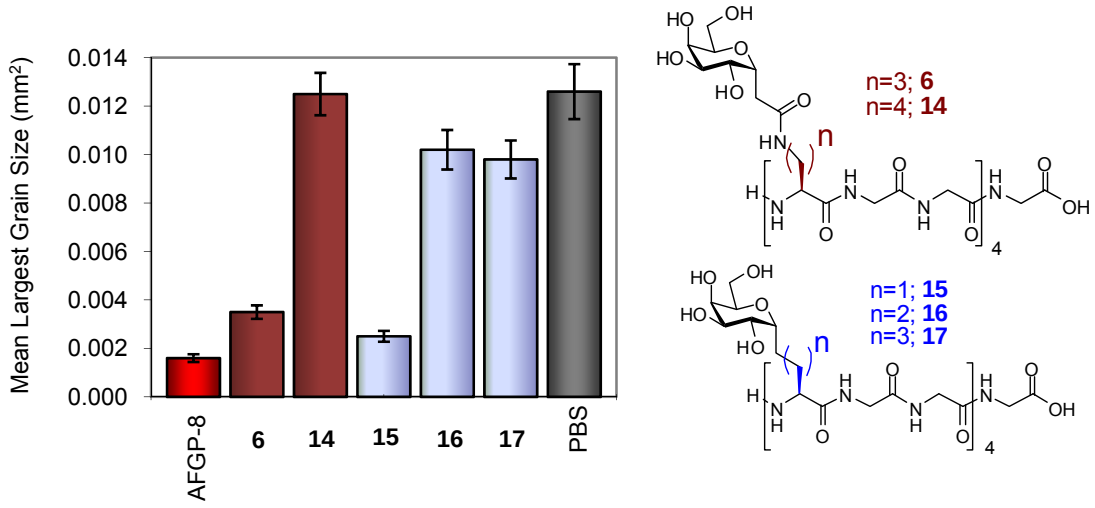

Figure 4.1 IRI activity of *C*-linked AFGP analogues (at 5.5 μM) with varying linkages between the carbohydrate and the peptide backbone.[2,3]

Of these, one interesting trend was observed. Firstly, analogue (**6**), which contains an amide bond in the glycoconjugate tether, showed potent ice-recrystallization inhibition (IRI) activity. However, extension of the carbon spacer by one carbon atom (**14**), dramatically decreased the ability of these analogues to inhibit ice recrystallization.[1,3] A second class of *C*-linked AFGPs contains a saturated aliphatic linker between the carbohydrate and the peptide backbone (referred to as the *C*-Serine class), **15-17**.[2] In this class, the analogue with the shortest linker (**15**), has the highest ability to inhibit ice-recrystallization. Similarly to analogues (**6**) and

(**14**), an increase by even one carbon atom in the side chain of analogue (**15**) abolished IRI activity. This is interesting because although potent analogue (**6**) has the shortest length of the amide-containing class, the number of atoms in the tether between the carbohydrate and the peptide of (**6**) is two more than the longest *C*-serine analogue (**17**), which is not potent in activity. Therefore, this data suggests that the amide bond in the side chain of (**6**) may be an important structural feature in this type of ice recrystallization-inhibitors. With our lab's ultimate goals to (1) synthesize compounds which are potent in IRI activity for the purpose of cryopreservation, and (2) to understand the factors responsible for IRI, structural analogues of (**6**) were prepared and assessed for antifreeze activity to achieve this end.

Specifically, as the length of the side chain is inversely proportional to the IRI activity with both classes of analogues, we initially hypothesized that a decrease in the number of carbons in the side chain of the amide-containing analogues (**18** and **19**) would yield analogues with even higher IRI activity. In addition, these shortened, amide-containing analogues would also help to better understand how the spatial relationship between the carbohydrate moiety and polypeptide backbone affects IRI activity.[2]

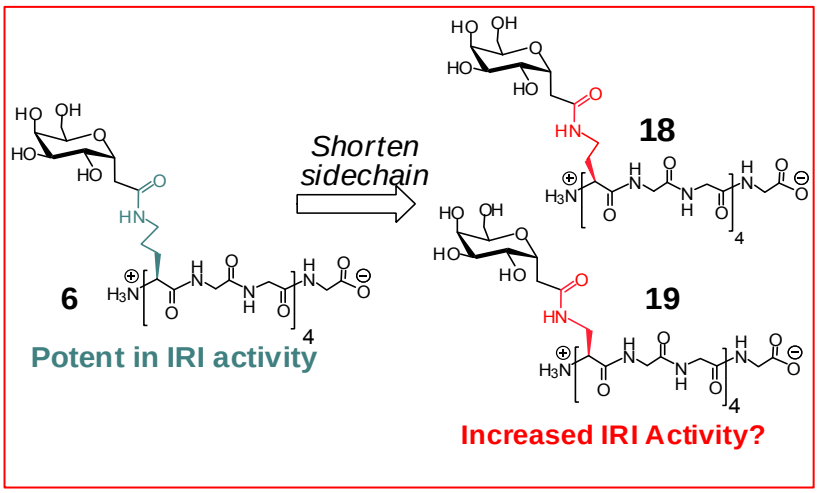

Figure 4.2 Target analogues (**18** and **19**) that contain a shortened side chain linker between the carbohydrate and the peptide backbone compared to IRI-active analogue **6.**

The current section explores how a decrease in the length of the amide-containing side chain in analogues of (**6**) influences IRI activity and how this activity is modulated by subtle localized changes in conformation of the glycoconjugate.

4.2 SYNTHESIS OF C-LINKED ANTIFREEZE GLYCOPROTEIN ANALOGUES (**18**,**19**)

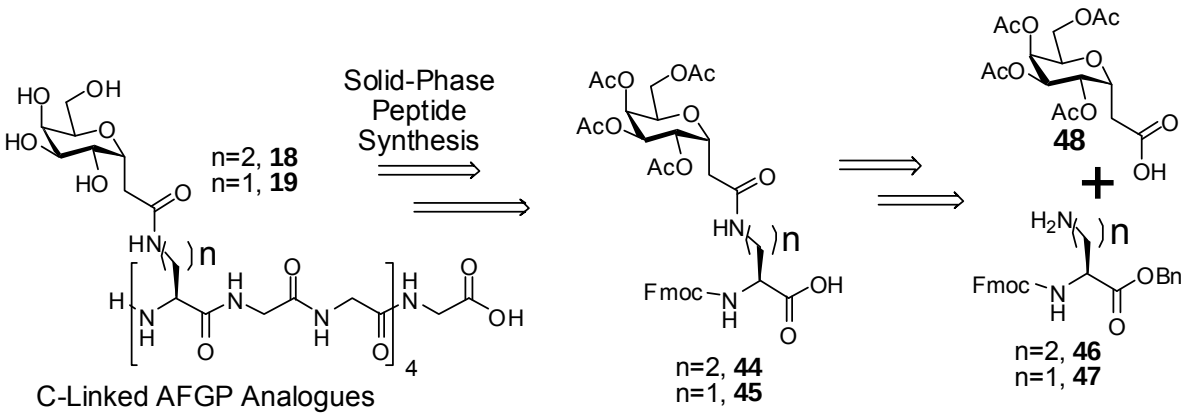

Scheme 4.1 Retrosynthetic analysis of analogues **18** and **19**.

C-Linked AFGP analogues (**18**) and (**19**) were prepared using standard Fmoc-based solid-phase peptide synthesis protocols (Scheme 4.1),[1,3,4] whereby the glycoconjugate monomers

(building blocks **44** and **45**) were assembled prior to solid phase synthesis. Building blocks (**44** and **45**) were synthesized by coupling the respective orthogonally-protected unnatural amino acid derivatives of L-diaminobutanoic acid (**46**) and L-diaminopropanoic acid (**47**), with *C*-linked pyranose derivative (**48**).[3,5] The unnatural amino acids were prepared via a modified Hofmann rearrangement[6] with orthogonally protected L-glutamine and L-asparagine, respectively (Scheme 4.2).

4.2.1 DIAMINOPROPYL AND DIAMINOBUTL AMINO ACID DERIVATIVE SYNTHESIS

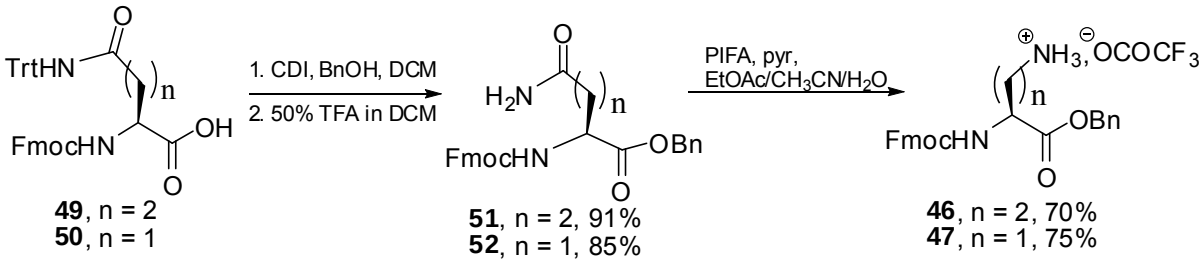

49, n = 2
50, n = 1

51, n = 2, 91%
52, n = 1, 85%

46, n = 2, 70%
47, n = 1, 75%

Scheme 4.2 Synthesis of unnatural amino acids **46** and **47**.

To prepare unnatural amino acids (**46** and **47**), commercially available trityl-protected glutamine (**49**) and asparagine (**50**) were reacted with 1,1-carbonyldiimidazole (CDI) in the presence of benzyl alcohol to afford the corresponding benzyl esters in 91 and 85% yields, respectively. Deprotection of the trityl protecting group using trifluoroacetic acid (TFA) furnished primary amides (**51** and **52**) in quantitative yields.

A modified Hofmann reaction using bis(trifluoroacetoxyiodo)benzene (PIFA) produced the diaminobutanoic and diaminopropanoic amino acid derivatives (**46**) and (**47**) in 70 and 75% yields, respectively. This method was used instead of the conventional Hofmann rearrangement conditions[7] (NaOH, Br_2) due to the presence of the base-labile Fmoc and hydrolysis-labile

benzyl protecting groups. However, the formation of the resulting primary amine was problematic.

For both glutamate and aspartate derivatives (**51** and **52**, respectively), the reactions were sluggish in the absence of a weak base. This may be due to the low pH of the reaction mixture as PIFA dissolution in water liberates trifluoroacetic acid (Scheme 4.3). This decrease in pH decreases the nucleophilicity of the primary amide towards the electrophilic iodobenzene moiety. Therefore to optimize reaction conditions, glutamate derivative (**51**) was used as a model system, Table 4.1.

Table 4.1 Optimization of Hofmann Rearrangement reaction of glutamine and asparagine.

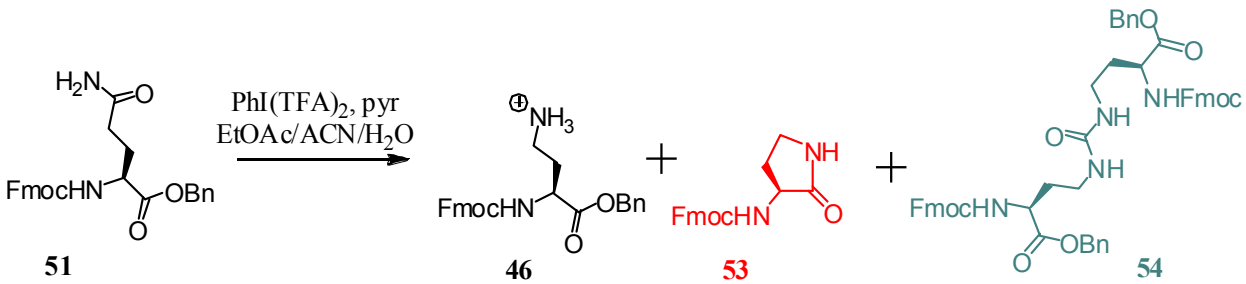

51 **46** **53** **54**

	Oxidizing agent (1.1 Equiv.)	Base (2.2 Equiv.)	% Desired amine (46)	% Lactam (53)	%Dimer (54)
1	PIFA	TEA	20	30	50
2	PIFA	DIPEA	25	25	50
3	PIFA	Pyr, overnight	40	40	0
4	PIFA	Pyr, 5 hrs	70	trace	0

Various bases were screened, and pyridine provided the best results. Under these conditions, the glutamate derivative was consumed in 5 hrs, whereas the aspartate derivative required 9 hrs. However, the use of more basic triethylamine or di-isopropylethylamine, while speeding up the consumption of the primary amide, also resulted in two major byproducts by increasing the nucleophilicity of the resulting primary amine. The byproducts formed were

lactam (**53**) (via intramolecular cyclization on the benzyl ester), and dimerized product (**54**) (via the reaction of a primary amine product and an isocyanate intermediate of another molecule).

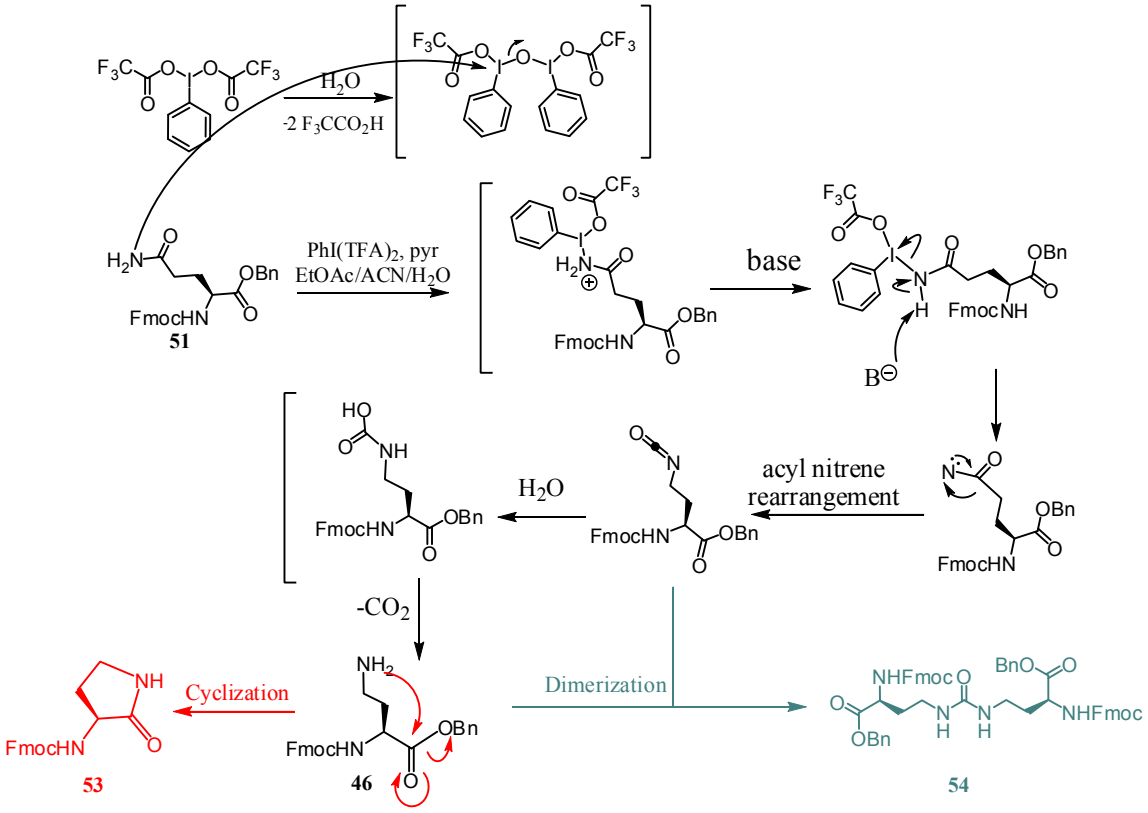

Scheme 4.3 Mechanism of Hofmann Rearrangement of glutamine (**51**) , yielding desired amine **46** and undesired byproducts **53** and **54**.

The latter can be rationalized by the fact that this reaction was performed in a biphasic mixture, and as such, amines which are formed in the organic layer will react with isocyanates in the same organic layer faster than the reaction of isocyanates with the aqueous phase to form carbamic acid. In addition, the formation of the lactam byproduct (**53**) was readily formed in noticeable quantities if: (1) the reaction was left stirring overnight, and (2) the compound solution was heated and evaporated prior to acidification (following workup or column chromatography). Reaction conditions using various concentrations (ranging from 0.0075 M to

0.050 M) were also used, but these did not yield significantly different results. The use of the appropriate base and aforementioned reaction/workup protocol was significantly more influential in dictating the formation of the desired amine.

As prolonged storage of these primary amines resulted in degradation, they were immediately purified and coupled to pyranose derivative (**48**) to furnish the respective glycoconjugates, Section 4.2.2.

4.2.2 *C*-LINKED GLYCOCONJUGATE SYNTHESIS

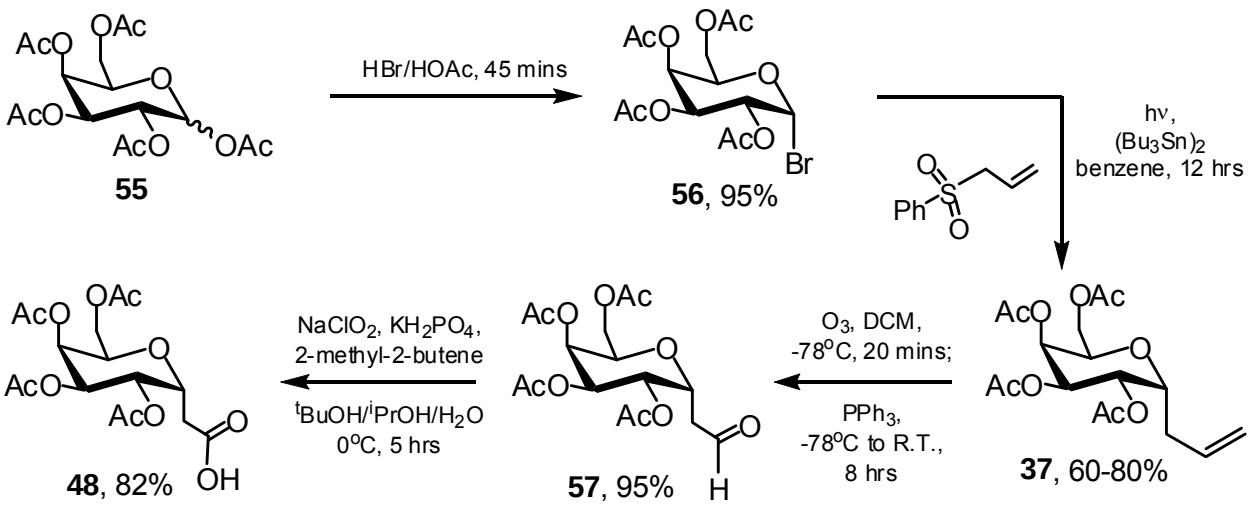

Scheme 4.4 Synthesis of *C*-α-linked galactopyranose derivative **48**.

The synthesis of the *C*-α-pyranose derivative (**48**) was performed according to previous methodology extensively used in our lab, Scheme 4.4.[1,3,5] Starting with commercially available D-galactose pentacetate (**55**), bromination with hydrobromic acid, followed by stereoselective photochemical allylation with bis(tributyl)tin and phenyl allyl sulfone, gave the α-allylated galactose derivative (**37**).[8] Ozonolysis of the terminal alkene, followed by Pinnick oxidation afforded carboxylic acid (**48**).[1,3,5]

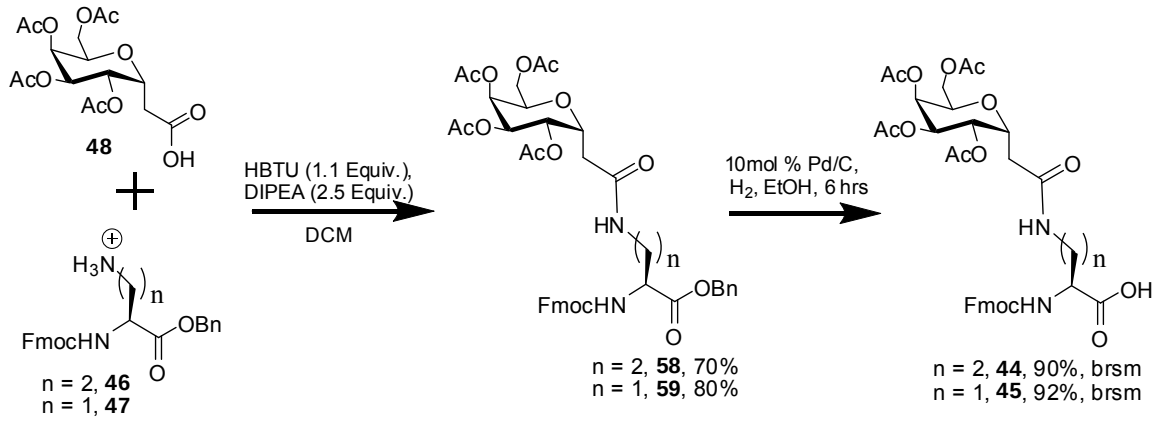

Scheme 4.5 Synthesis of *C*-α-glycoconjugate building blocks **44** and **45**.

Carboxylic acid (**48**) was then coupled to the unnatural amino acid (**46** or **47**) using 2-(1H-benzotriazole-1-yl)-1,1,3,3-tetramethylaminium hexafluorophosphate (HBTU), and diisopropylethylamine (DIPEA) in dichloromethane to afford (**58**) and (**59**) in 70 and 80 % yields, respectively. Selective deprotection of the benzyl ester was accomplished by hydrogenolysis under atmospheric pressure and 10% wt Pd/C in 4 hrs to furnish building blocks (**44** and **45**) in 90 and 92% yields, respectively (based on recovered starting materials).

4.2.3 SOLID-PHASE SYNTHESIS OF GLYCOPEPTIDE POLYMERS (**18**, **19**)

All glycoconjugates were synthesized using conventional Fmoc solid-phase synthesis, Scheme 4.6, on an APEX 396 using acid labile Wang resin.[4] Glycopeptide purification was performed via HPLC using reverse phase chromatography (Polaris C-18 RP column; mobile phase: 100% water to 15 : 85 (v/v) acetonitrile : water gradient over 30 minutes).

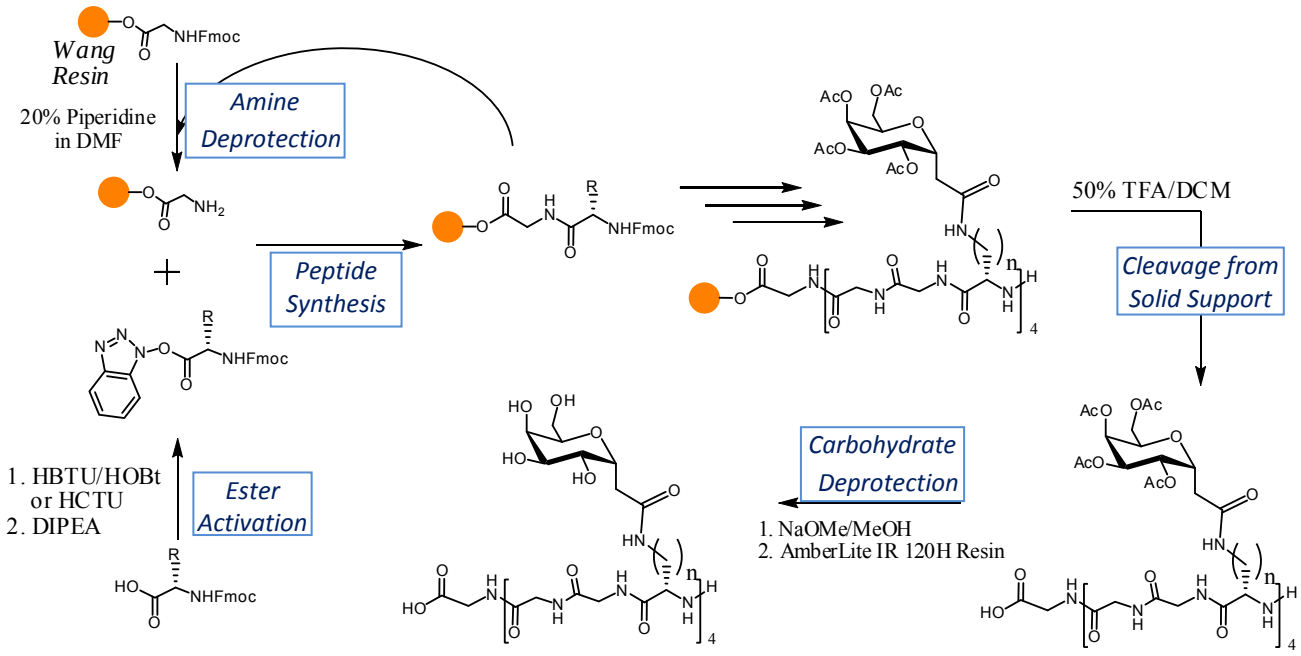

Scheme 4.6 General scheme for solid-phase peptide synthesis of *C*-linked AFGP analogues

4.3. ASSAY FOR ANTIFREEZE ACTIVITY

4.3.1 ASSESSING THE INTERACTION OF AFGP ANALOGUES WITH THE ICE LATTICE

C-Linked AFGP analogues (**6** and **14**) were previously assessed[9] for thermal hysteresis (TH) activity with a Clifton nanoliter osmometer[10] and showed no TH activity. Analogues (**18** and **19**), which contain a shortened linkage between the carbohydrate and the peptide backbone, were also assessed for TH activity and were also inactive, Figure 4.3.

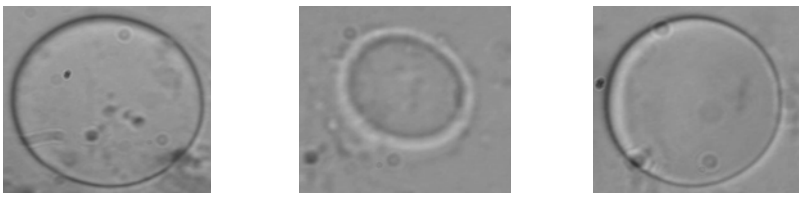

Figure 4.3 Ice crystals of analogues of distilled water (left), (**18**, middle) and (**19**, right), at 10mg/mL of glycoprotein, as determined by nanolitre osmometry.

Interestingly, under these assay conditions, analogue (**6**) (possessing a three carbon side chain between the polypeptide backbone and the side chain amide bond) was previously shown to produced hexagonally-shaped ice crystals, which indicates a weak interaction with the ice surface.[11] Analogues (**18** and **19**) did not show any change in ice crystal morphology compared to a water standard solution, suggesting that there is no strong interaction with the ice lattice.

4.3.2 Ice Recrystallization Inhibition (IRI) Activity

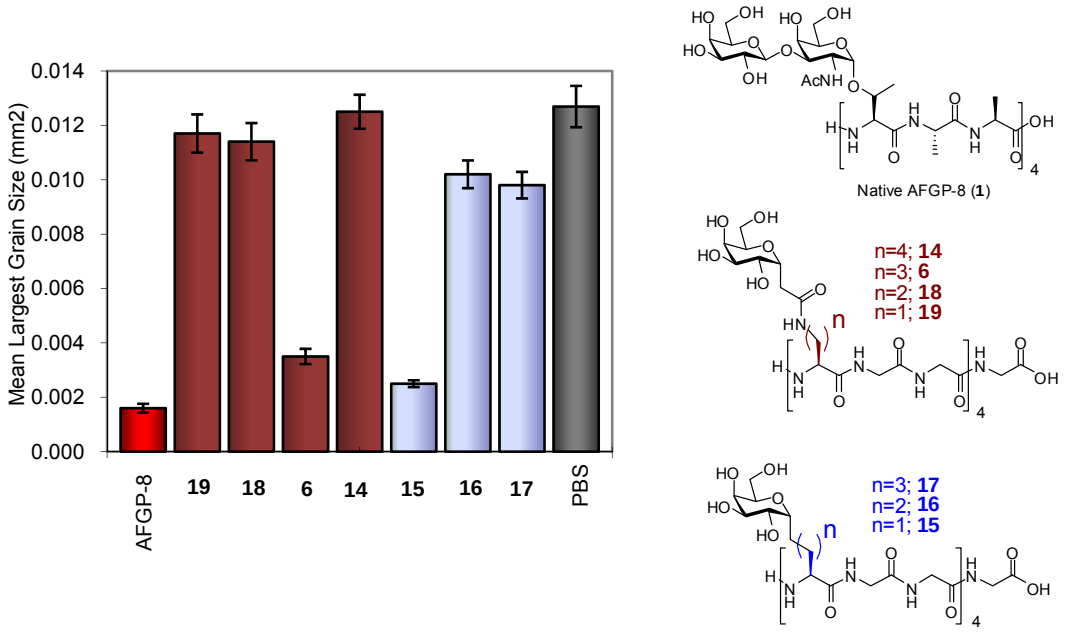

Figure 4.4 Ice Recrystallization Inhibition results for AFGP-8 (1) and *C*-linked AFGP analogues (**6**, **14**-**19**) at 5.5 μM in PBS, and PBS buffer as negative control.

Glycoconjugates (**18** and **19**) were assessed for the ability to inhibit ice recrystallization, Figure 4.4. Our initial hypothesis (Section 4.1) was that a decrease in the length of the side chain of (**6**) would increase IRI activity because a shortened linker may constrain the orientation of the carbohydrate moiety in the glycopeptide to interact favourably with the ice lattice. However, we were surprised that a decrease in side chain length (**18** and **19**) resulted in no IRI activity, despite having apparent closer proximities to the polypeptide backbone. We subsequently hypothesized

that the increased IRI activity of (**6**) may be the result of a dramatic change in solution conformation compared to the inactive analogues. Consequently, the solution conformations of analogues (**6**, **14**, **18**, **19**) were studied using circular dichroism (CD), variable-temperature nuclear magnetic resonance (VT-NMR), and molecular dynamics (MD) simulations.

The solution conformation of native AFGP has been extensively studied using a variety of spectroscopic[12-18] and computational[12,19,20] techniques. Previous spectroscopic studies have shown inconsistent results. Vacuum ultraviolet circular dichroism[13] and ^{1}H-NMR[14] experiments have shown the dominant conformation to be a three-fold left-handed helix, whereas quasi-elastic light scattering (QELS) studies[15] suggest an extended coil; other dynamic light scattering (DLS),[16] circular dichroism (CD),[16,17] and ^{13}C-NMR studies[18] suggest AFGP-8 adopts predominantly a random coil in solution.

4.4 CONFORMATIONAL ANALYSIS BY CIRCULAR DICHROISM (CD)

The solution conformations of AFGP-8, *C*-linked AFGP analogues (**6**, **15-19**) were analyzed using CD spectroscopy (Table 4.2).[9,16,21]

Table 4.2 Circular dichroism deconvolution data for native AFGP-8, and *C*-linked analogues (**6**, **15-19**), dissolved in doubly de-ionized water. Solution conformations were estimated using IBASIS 5. Potent IRI-active compounds are highlighted in red boxes.

Compound	**α-Helix**	**β – Sheet**	**β – Turn**	**Polyproline II**	**Random Coil**	**Sum**
AFGP-8	0.146	0.189	0.152	0.122	*0.432*	1.041
6	0.162	0.175	0.071	0.055	*0.573*	1.036
18	0.031	0.326	0.097	0.113	*0.406*	0.973
19	0.159	-0.017	0.157	0.197	*0.544*	1.040
15	0.101	0.212	0.136	0.108	*0.434*	0.991
16	-0.028	0.358	0.100	0.127	*0.441*	0.998
17	0.163	0.246	0.122	0.081	*0.393*	1.005

Previous studies have demonstrated that the long range solution conformation of native AFGP does not change as a function of temperature.[16] Consequently, all CD measurements were performed at 22°C. The results presented in Table 4.2 suggest that the predominant solution conformations of all glycopeptides on the timescale of CD are random coil. This finding is consistent with recent NMR studies of AFGP,[16-18] indicating that the long range conformation of these synthesized *C*-linked AFGP analogues is not very different than native AFGP-8. More importantly, no significant trends are observed between the solution conformations of IRI-active analogues (AFGP-8, **6**, **15**, red boxes in Table 4.2) and the other IRI-inactive analogues, which suggests that the apparent loss in IRI activity observed in (**16-19**) is not due to a dramatic change in long-range solution conformation.

However, while CD spectroscopy can provide useful insight into the overall solution structure of proteins, it does not provide information about the spatial relationship between the carbohydrate residue and the polypeptide backbone or verify the existence of non-bonding

interactions between the carbohydrate moiety and the polypeptide backbone in glycoproteins. Such interactions could be important for antifreeze activity as it has been suggested that they may orient the disaccharide of native AFGP-8 relative to the backbone.[14,19,22] For example, variable-temperature (VT) ^{1}H-NMR studies by Mimura[22] suggested the existence of intramolecular hydrogen bonds between the amide proton of N-acetylgalactosamine (GalNHAc) and the carbonyl oxygen of threonine in model systems of native AFGP-8, Figure 4.5A. It was suggested this hydrogen bonding interaction significantly restricted orientation of the carbohydrate moiety relative to the polypeptide backbone and facilitated interaction with the ice lattice. While *C*-linked AFGP analogues (**6**, **14**, **18** and **19**) do not possess a C2 acetamide residue in the carbohydrate, we hypothesized that a similar interaction might exist between the side chain amide and the polypeptide backbone in *C*-linked analogue (**6**), Figure 4.5B. If so, the carbohydrate might be ideally positioned to interact with the ice lattice and this favourable interaction may not be present in the other analogues.

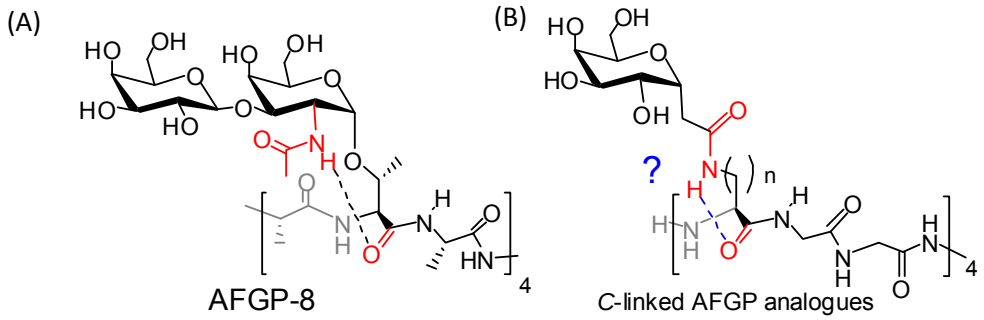

Figure 4.5 Speculated intramolecular hydrogen bonding interactions between the peptide backbone and the (a) C2-GalNHAc in AFGP-8,[22] and (b) side chain amide bond in *C*-linked AFGP analogues.

To investigate this possibility, variable temperature (VT) ^{1}H-NMR studies were performed on truncated model systems (**60-62**) of the *C*-linked AFGP analogues (**18**, **19** and **6**), respectively.

4.5 INTRAMOLECULAR HYDROGEN BONDING ANALYSIS BY VARIABLE-TEMPERATURE ^{1}H-NMR (VT-NMR)

In this technique, the strength of intramolecular hydrogen bonding between amide protons and carbonyl oxygens can be determined by calculating the change in chemical shit (dδ) in the ^{1}H-NMR spectra of the amide protons with respect to the change in temperature (dT) of the NMR experiment.[23-25] This temperature-dependent change in chemical shifts is known as the temperature coefficient (dδ/dT, where δ is the chemical shift and T is the temperature in ^{o}C or K). An amide proton that is involved in an intramolecular hydrogen bond with a carbonyl (sp^2) oxygen will be more deshielded (or downfield) compared to an amide proton that is not involved in an intramolecular hydrogen bond. This is due to anisotropy of the π-electrons of the carbonyl group.[25] Therefore, an increase in the temperature of a molecule will rupture weak intramolecular hydrogen bonds, thereby causing a change in chemical shift of the amide proton. To quantitatively correlate the strength of intramolecular hydrogen bonds with temperature coefficients, Cierpicki and Otlewski examined the temperature coefficients of 793 amide bonds from 14 proteins in H_2O/D_2O and by comparison with existing X-ray and NMR data, determined that values greater than -4.6 ppb/°C is indicative of the amide proton being involved in an intramolecular hydrogen bond 70-98% of the time.[24]

Variable-temperature (VT) ^{1}H-NMR studies were performed on truncated glycopolymers[22] (**60**-**62**), Figure 4.6, on a Varian Inova 500 MHz spectrometer at temperatures ranging from 0°C to 50°C in 5-degree increments at a concentration of 5 mM[24], with a mixture of H_2O and D_2O (95:5) as solvent. An appropriate water suppression program was run and 2,2-dimethyl-2-silapentane-5-sulfonic acid (DSS) at a concentration of 20 μg/mL was used as a chemical shift internal standard.[26]

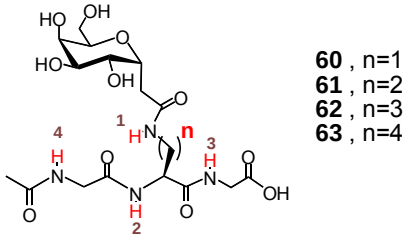

Figure 4.6 Truncated tripeptide glycopeptides model systems **60-63**. Amide protons are highlighted in red and labeled.

Truncated monomeric tripeptide model systems (**60-62**) were used in our analysis since it has previously been suggested that AFGPs are structurally segmented into semi-rigid tripeptide units.[19] Furthermore, the use of such model systems in similar experiments is precedented and greatly simplifies the analysis.[22] These model systems were synthesized using solid phase synthesis in a manner similar to their full polymer (Scheme 4.6), with the exception that the terminal amine was acetylated in these model systems. While (**60** and **61**) were synthesized using building blocks (**45** and **44**) respectively, (**62**) was synthesized using (**65**), which was synthesized in the same manner as previously reported, Scheme 4.5.[3]

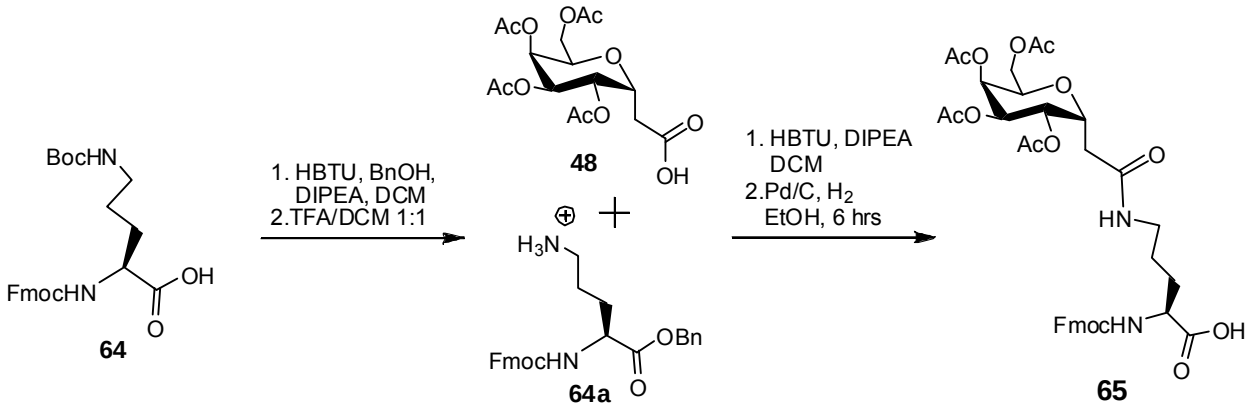

Scheme 4.7 Synthesis of building block **65**.[3]

4.5.1 AMIDE-PROTON (-N-H) ASSIGNMENTS FOR VARIABLE-TEMPERATURE ^{1}H-NMR STUDIES

Assignment of the appropriate amide protons for truncated model systems (**60-62**) was achieved using 2-D homonuclear (COSY) spectra, Figures 4.7 - 4.9 respectively.

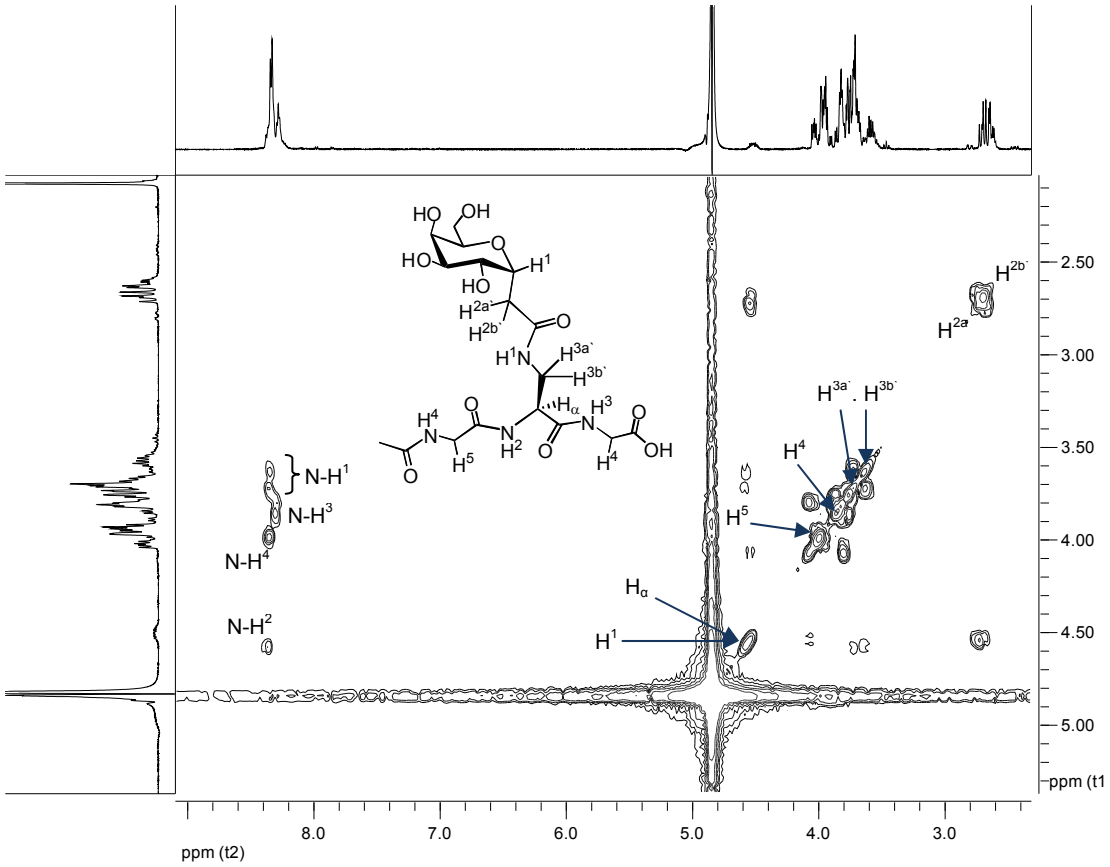

Figure 4.7 2-D COSY NMR analysis for amide proton assignment of (**60**)

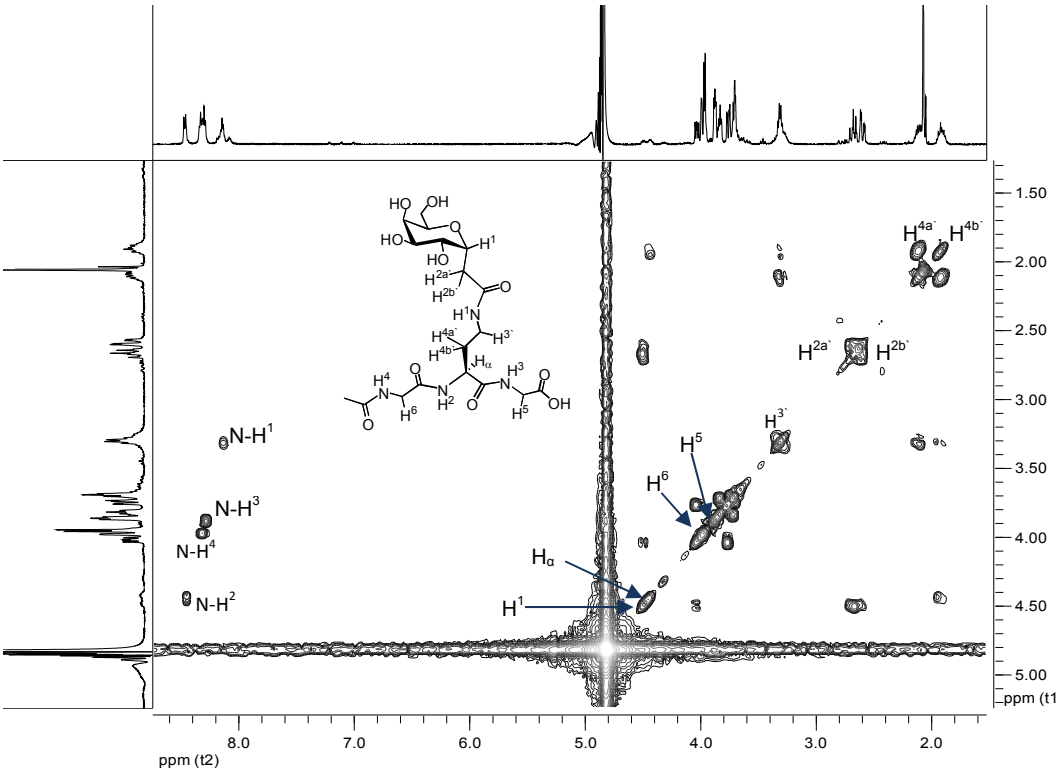

Figure 4.8 2-D COSY NMR analysis for amide proton assignment of (**61**)

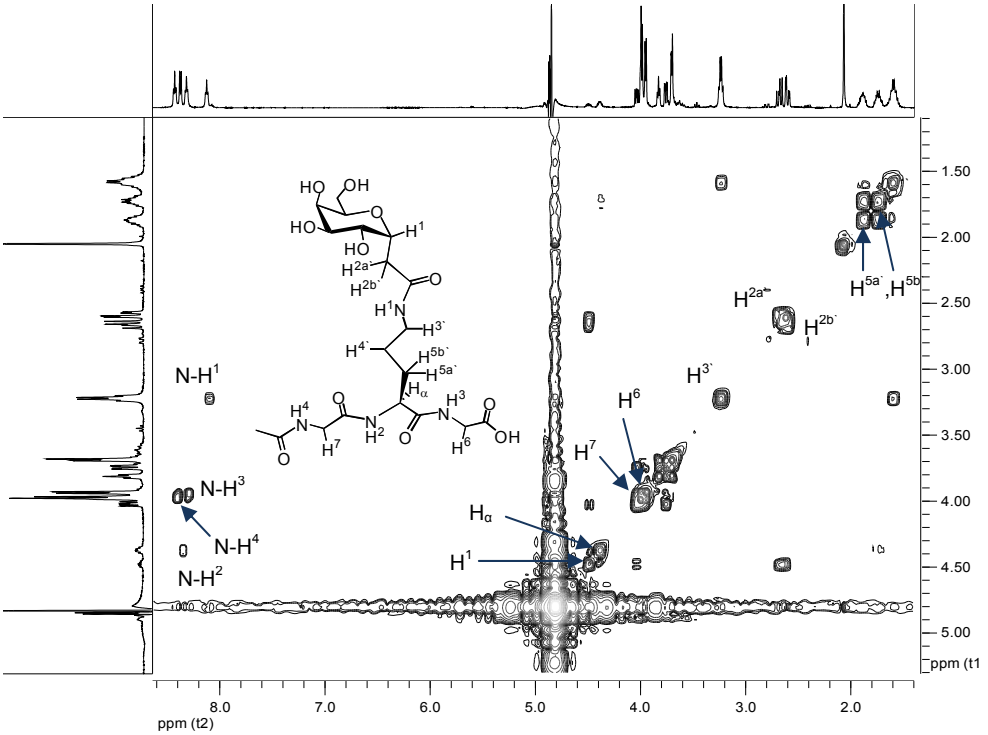

Figure 4.9 2-D COSY NMR analysis for amide proton assignment of (**62**)

4.5.2 Analysis of variable-temperature ^{1}H-NMR spectra

As a positive control, the variable temperature ^{1}H-NMR spectra of native AFGP-8 was also analyzed (Figure 4.10).[27] Proton assignments of AFGP-8 have previously been established by Lane.[12a] Temperature coefficients of the C2 N-acetylgalactosamine N-H proton ranged from -4.6 to -5.5 ppb/°C for glycoconjugate residues that are bracketed by two alanines, which are slightly more negative than the temperature coefficient threshold of -4.6 ppb/^{o}C for strong intramolecular hydrogen bonding;[12a,22] this suggests that there is the presence of some (although not very strong) intramolecular hydrogen bonding between the C2 NHAc group with the peptide backbone, which agrees with the observations previously reported by Mimura on truncated model systems of AFGP.[22]

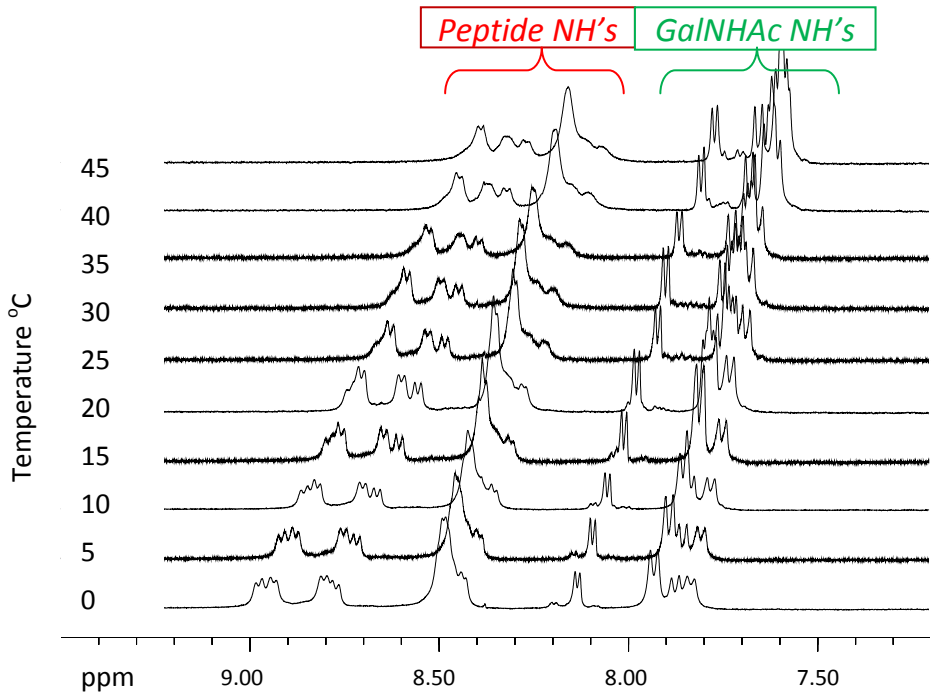

Figure 4.10 Variable temperature ^{1}H-NMR profile of AFGP-8 ranging from 0^{o}C to 45 ^{o}C

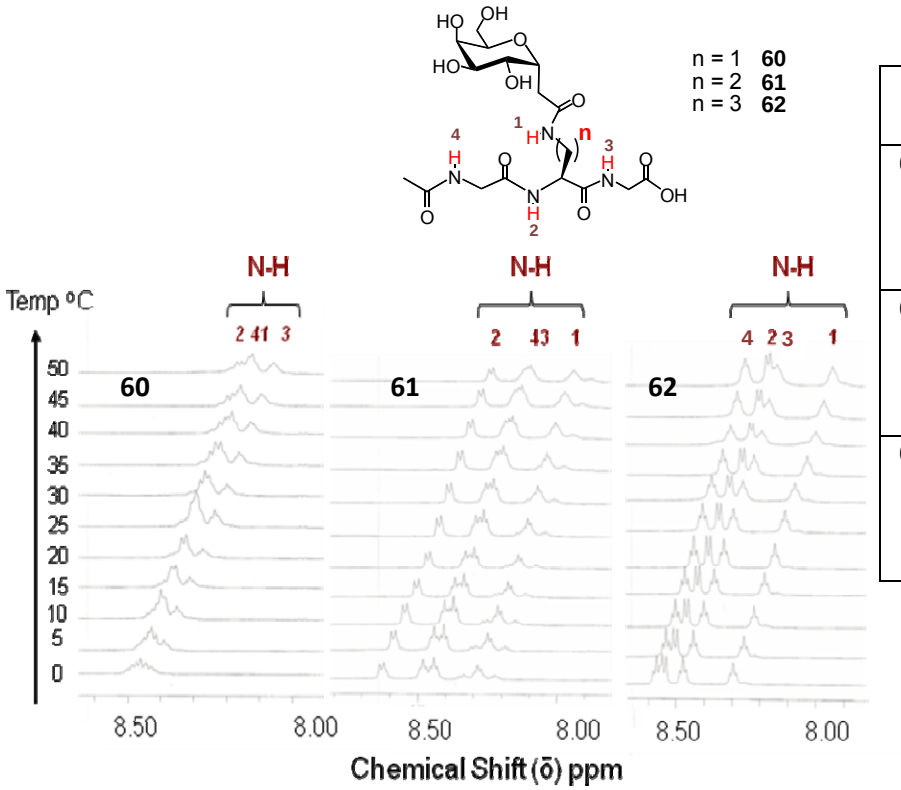

	Amide proton	mean dδ/dT (ppb/°C)
60	1	-6.58 (±0.94)
	2	-6.34 (±0.63)
	3	-7.42 (±0.35)
	4	-6.58 (±0.94)
61	1	-6.92 (±0.30)
	2	-7.75 (±0.37)
	3	-6.98 (±0.36)
	4	-7.30 (±0.47)
62	1	-7.52 (±0.84)
	2	-7.89 (±0.86)
	3	-7.12 (±1.01)
	4	-6.64 (±0.88)

Figure 4.11. Variable-temperature ^{1}H-NMR (500MHz) spectra and temperature coefficients (ppb/°C) of amide protons of truncated monomer model systems for (**60**)-(**62**), in 95:5 (H_2O:D_2O) with DSS as an internal standard.

The temperature coefficients for all three monomers (**60-62**) ranged from -6.3±0.6 ppb/°C to -7.9±0.9 ppb/°C, which is significantly more negative than the threshold of -4.6 ppb/°C, suggesting no strong intramolecular hydrogen bonds persist between the side chains and peptide backbone on the NMR timescale, Figure 4.15. Furthermore, these results do not show any significant trends between temperature coefficients of each monomer and the IRI activity of the respective polymer. This implies that the change in IRI activity as a function of side chain length in (**6**, **18** and **19**) is not due to strong intramolecular hydrogen bonds between the side chain and polypeptide backbone as previously hypothesized. However, this result does not rule

out the possibility that the carbohydrate moiety of (**6**) adopts a unique spatial orientation relative to the polypeptide backbone. Consequently, we modeled the aqueous-phase conformational dynamics of *C*-linked AFGP tripeptide model systems (**60-63**) using molecular dynamic simulations.

4.6 MOLECULAR DYNAMIC SIMULATIONS

Simulations of localized solution conformations of the truncated glycopeptides **60-63** and native AFGP-8 were performed in water using the AMBER 9 program[28] by Dr. Christopher Rowley and Professor Tom Woo.[29]

4.6.1 ANALYSIS OF MD SIMULATIONS OF *C*-LINKED AFGP ANALOGUES (**60-63**)

Monomeric tripeptides (**60-63**) were modeled in the presence of water to corroborate the variable temperature ^{1}H-NMR studies and to determine whether key conformational differences between IRI-active (**6**) and inactive *C*-linked AFGP analogues (**14**, **18**, **19**) existed. The presence of intramolecular hydrogen bonding was examined using AMBER's ptraj program and failed to identify any persistent intramolecular hydrogen bonds between the amide protons and other hydrogen bond acceptors.[29] This result correlates to the results of the VT ^{1}H-NMR studies previously described in Section 4.5.2. While weak intramolecular hydrogen bonds between the galactose residue and the backbone were detected, the occupancy of these interactions was too transient to account for any significant structural differences between the conformations adopted by (**60-62**). It should be noted that Corzana and co-workers[30] recently reported that a direct intramolecular hydrogen bond between the N-H donor of a N-acetylgalactosamine and the threonine peptide backbone carbonyl acceptor in an AFGP analogue was minimal in the solution conformation and that the unique conformation of the N-acetylgalactosamine-threonine

glycoconjugate was strongly influenced by the formation of water bridges between the carbohydrate and the amino acid.

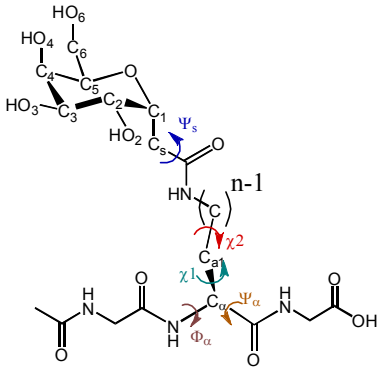

Figure 4.12 Atom and torsional angle definitions used for MD simulations of model AFGP analogue tripeptides (**60-63**)

Table 4.3 Summary of statistical analysis of MD simulations showing % intramolecular hydrogen-bonding occupancy, average C_α-C_1 distance (Å), and free energy of isomerization from chair ($^4C_1$) to skew boat ($^1S_3$) conformations of tripeptides (**60-63**) and native AFGP-8. Those representing IRI-active compounds are highlighted in red boxes.

		Summary of key results of MD simulations			
Compound	n =	Intramolecular Hydrogen Bonding (%)		C_α-C_1 distance (Å)	$\Delta G_{C\rightarrow S}$ (kcal mol^{-1})
		O_4 --- H-O_6	O_4-H ---O_6		
63	4	15.66	2.27	8.03 (1.45)	-0.76
62	3	4.55	1.37	5.81 (1.09)	0.81
61	2	8.51	1.14	6.15 (0.82)	0.40
60	1	6.92	1.86	5.59 (0.38)	0.44
AFGP 8 (GalNHAc)		0.69	2.36	3.49 (0.26)	--
AFGP 8 (Galactose)		2.35	3.48	6.67 (0.59)	--

Our MD simulations did reveal intramolecular hydrogen bond interactions existed between the O4 and H-O6 hydroxyls of galactose, and that the amount of hydrogen bonding varied as a function of side chain length in *C*-linked AFGP analogues (**60-63**), Table 4.3. An increase in intramolecular hydrogen bonds existed between O4 and H-O6 for analogues (**60**, **61** and **63**, all of which are model systems for compounds that do not possess IRI activity). However, a lower percentage of hydrogen bonding was observed between O4 and H-O6 for (**62**)

which is the model system for analogue (**6**), a potent inhibitor of ice recrystallization. A decrease in hydrogen bonding at these positions was also observed when we examined both carbohydrate residues of the native AFGP-8 system. This result implies that the interaction of O4 and H-O6 with water molecules adjacent to the glycoprotein (as opposed to interaction with each other) may be an important requirement for IRI activity. Furthermore, the relative stereochemistry of the O4 hydroxyl has previously been shown[31,32] to be an important factor in modulating the hydration environment of the carbohydrate and our laboratory has verified that the degree of hydration is directly related to IRI activity.[3,33]

The Φ_α/Ψ_α torsional distributions for (**60-63**) were calculated, and suggested these four peptides adopt similar polypeptide backbone conformations.[29] As such, we investigated the relationship between orientation of the carbohydrate moiety and the backbone as a function of IRI activity. This was done by examining the torsion angles in the side chain (χ^1 - χ^n and ψ_s) and the average distance from the C_α of the glycosylated amino acid residue to C1 of the carbohydrate (Table 4.3, Figure 4.13).

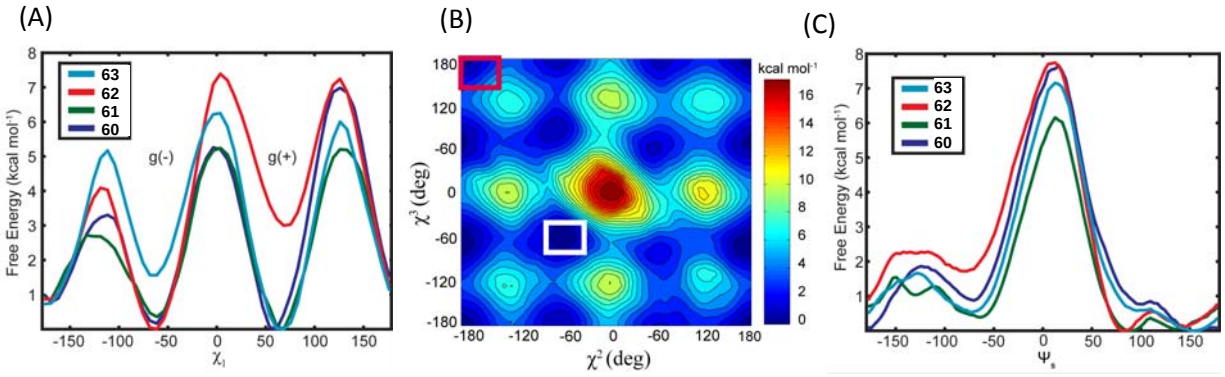

Figure 4.13 (A) Free energy profile of the χ^1 torsional angle for (**60-63**) in kcal mol^{-1}. (B) Free energy profile for χ^2 and χ^3 torsional angles in **62**. Global minima (white box) and the higher energy trans conformation (red box) are indicated. (C) Free energy profile of the Ψ_s torsional angle for (**60-63**) in kcal mol^{-1}.

The orientation of the side chain relative to the backbone depends on the rotation of the χ^1 torsion. To quantify this interaction, the free energy profile around the χ^1 torsional angle for (**60-63**) was calculated (Figure 4.13A). The energy barrier of rotation at $\chi^1$is greater for (**62)** than for (**60**, **61** and **63**), indicating that the χ^1 torsional angle of (**62**) is more restricted in its rotation, and favours the gauche (**-**) conformation. In addition, it is observed that in the gauche (+) conformation, IRI active analogue model (**62**) is less favoured compared to the other IRI-inactive analogue model systems. Therefore, analogues that are in the gauche (+) conformation may be unable to interact with adjacent water molecules in a way to disturb the surrounding network of water to hinder the transfer of water to the ice lattice and thereby inhibiting ice growth. As model compound (**62**) does not favourably attain this gauche (+) conformation, it may be prevented from being in an undesired conformation that is detrimental for ice-recrystallization inhibition.

Analysis of MD trajectories revealed the tendency of the χ^2 and χ^3 angles in the alkyl chain of (**62**) to adopt a (gauche (-), gauche (-)) conformation (Figure 4.13B). The (g(-),g(-)) torsion angles for χ^2 and χ^3 of (**62**) causes the carbohydrate to be oriented almost parallel to the backbone, forming a hydrophobic pocket with the alkyl chain and peptide backbone. Water molecules appear to be excluded from this pocket, increasing the conformational stability. This is consistent with the increased rotational energy barrier around χ^1 in (**62**). This hydrophobic pocket is not observed in (**60**, **61** and **63**) and consequently, the alkyl side chain of these analogues extends in a *trans*- fashion into solution resulting in greater freedom of rotation around the χ^1 torsional angle and less conformational stability. Restraining the χ^3 and χ^4 torsional angles of the lengthier (**63**) to (g(-), g(-)) allows this analogue to adopt a conformation in which a

hydrophobic pocket is formed similar to that of (**62**), but at an increase of 1-2 kcal mol^{-1} in free energy.

The orientation of the carbohydrate residue relative to the backbone was determined based on the Ψ_s torsional angle in the *C*-glycosidic bond (Figure 4.13C). Rotation of Ψ_s affects the orientation of the carbohydrate relative to the side chain. The hydrophobic contact formed in (**62**) favours a Ψ_s in the range of 60° to 180°. For Ψ_s in the range of -180° to 0°, the free energy of (**62**) is between 0.5-2.0 kcal mol^{-1} higher than for (**60**, **61**, and **63**). Thus, as a result of the different side chain conformations attributed to their varying lengths, the orientation of the carbohydrate relative to the peptide backbone in IRI-active analogue (**62**) is significantly different than the other three analogues. Therefore, we believe that IRI activity of this analogue is due to the fact that the side chain conformation permits formation of a hydrophobic pocket and the side chain is consequently "folded back" on itself. Representative "snapshots" of these model analogues are shown in Figure 4.14.

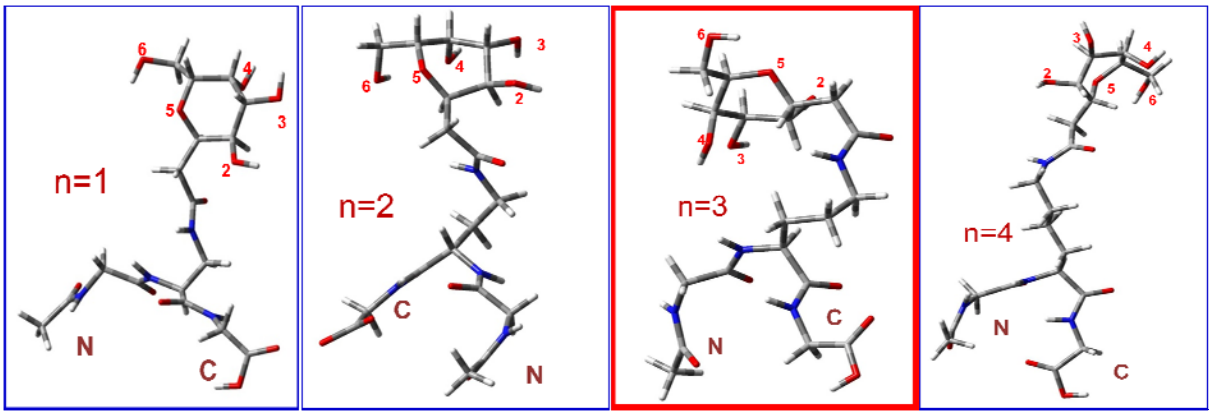

Figure 4.14. Snapshots from unrestrained MD simulations of minimum energy conformations of **60**-**63**. Truncated model system (**62**) of ice recrystallization-inhibition potent analogue (**6**) is highlighted by the red box.

The free energy profiles of the various torsional angles of the carbohydrate ring were examined using the Weighted Histogram Analysis Method (WHAM).[34] While the lowest energy

conformation of (**60-62**) was a skew-boat ($^1S_3$), the conformation of (**63**) was calculated to be a $^4C_1$ chair (Table 4.3). The importance of skew-boat conformations with respect to carbohydrate isomerization has been studied in a series of recent papers.[35,36] In many carbohydrates, the skew-boat conformation has been found to be up to 4 kcal mol^{-1} less stable than the more stable chair conformation.[36] It is highly likely that the lack of an electronegative anomeric oxygen and the presence of an anomeric methylene group in these *C*-linked carbohydrates derivatives may cause the skew-boat and chair conformations to be closer in energy. If the energy difference is small enough, as seen in our simulations, the two conformations may readily interconvert. Hence, it is not clear whether the observed increase in IRI activity of (**62**) is also attributed to a subtle difference in the conformation of the carbohydrate residue.

4.7 EFFECT OF GLYCOCONJUGATE CONFORMATION ON IRI ACTIVITY

The overall lowest energy conformation of the various analogues takes into account the contributions from the various torsion angles, C_α-C1 distances, and inter-/intramolecular hydrophobic/hydrophilic interactions, and is shown in Figure 4.14. From this Figure, it is evident that there is a drastic conformational change between model system **62** (representing IRI-active analogue **6**), and **60**, **61** and **63** (representing IRI-inactive analogues **18**, **19** and **14** respectively). The latter compounds have an extended alkyl side chain, which subsequently leads to a carbohydrate that has both of its faces exposed freely to the bulk solvent. This may be due to: 1) the increased geometric constraints imposed by the shorter analogues (**60** and **61**) such that the carbohydrate is unable to 'fold back' on its own backbone and 2) the increased flexibility of the longer analogue (**63**). In contrast, (**62**) is able to adopt a unique conformation that

positions the more hydrophilic face of the carbohydrate toward the peptide backbone and away from the bulk solvent, Figure 4.15.

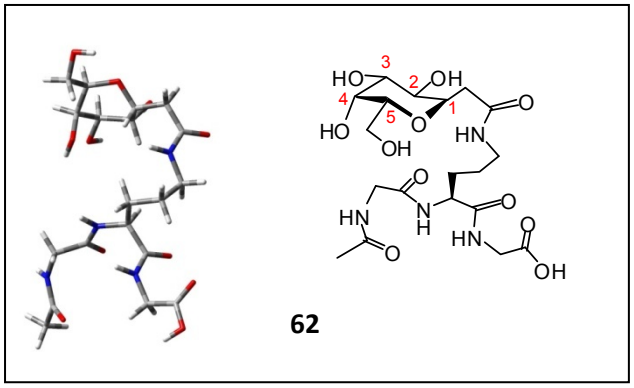

Figure 4.15 Molecular dynamic simulations of the lowest energy conformation of model system **62**, and a schematic representation of this conformation.

We hypothesize this is important as it may drastically alter the hydration shell of the overall glycoconjugate and hence peptide. While the conformation of the carbohydrate moiety may also influence hydration, it is likely that carbohydrate stereochemistry (Section 3.3) and exposure to bulk solvent are the predominant factors. The influence of carbohydrate stereochemistry on peptide hydration is unknown at this point. However, the importance of peptide hydration has recently been examined by Davidovic and co-workers, who report that upon cold-induced peptide denaturation, peptides are able to maintain their hydration state.[37] This is relevant to our work as our IRI assays are performed at sub-zero temperatures so any contribution of carbohydrate hydration to hydration of the peptide at temperature above zero degrees should be consistent at temperature below zero degrees. In addition, it is worth remembering that the difference in concentration between the free reducing carbohydrate and the glycopeptides is roughly a thousand fold different, meaning that the effect of the peptide is tremendous.

4.8 CHAPTER SUMMARY

Previous work in our laboratory had led to the hypothesis that the IRI activity of *C*-linked analogues was indirectly proportional to the length of their respective side chains, Figure 4.1. To corroborate this, the synthesis of analogues with shortened amide-containing side chains was achieved and then were tested for IRI activity. Surprisingly, it was observed that these analogues did not possess the expected IRI activity. To investigate this further, the solution conformations were analyzed via circular dichroism, variable temperature ^{1}H-NMR, and molecular dynamic simulations. It was observed that monomer (**62**, a model for *C*-linked AFGP analogue **6**) adopted a unique conformation in solution where the carbohydrate moiety did not extend fully away from the polypeptide backbone into the surrounding bulk solution, but rather, the side chain folded back upon itself forming a hydrophobic "pocket" between the carbohydrate and the backbone. This appears to be a highly favourable carbohydrate orientation for interaction with the quasi-liquid layer of the ice lattice resulting in potent IRI activity. The other *C*-linked AFGP analogues examined in this study did not adopt such conformations in solution and failed to exhibit IRI activity. We further speculate that formation of this hydrophobic pocket may influence the hydration shell of the carbohydrate (and subsequently the whole glycopeptide), and this may also contribute to the observed IRI activity.

REFERENCES:

1. Eniade, A.; Purushotham, M.; Ben, R. N.; Wang, J. B.; Horwath, K. *Cell Biochem. Biophys.* **2003**, *38*, 115-124.

2. Liu, S.; Ben, R. N. *Org. Lett.* **2005**, *7*, 2385-2388.

3. Czechura, P.; Tam, R.Y.; Murphy, A. V.; Dimitrijevic, E.; Ben, R. N. *J. Am. Chem. Soc.* **2008**, *130*, 2928–2929.

4. Fields, G. B.; Fields, C. G. *J. Am. Chem. Soc.* **1991**, *113*, 4202-4207.

5. Eniade, A.; Murphy, A. V.; Landreau, G.; Ben, R. N. *Bioconjugate Chem.* **2001**, *12*, 817-823.

6. (a) Loudon, G. M.; Radhakrishna, A. S.; Almound, M. R.; Blodgett, J.K.; Boutin, R. H. *J. Org. Chem.,* **1984**, *49*, 4272-4276. (b) Zhang, L.; Kaufmann, G. S.; Pesti, J. A.; Yin, J. *J. Org. Chem,* **1997**, *62*, 6918-6920. (c) Schmuck, C.; Geiger, L. *Chem. Comm.* **2005**, 772-774.

7. (a) Hofmann, A. W. Chem. Ber. **1881**, *14*, 2725-2736. (b) Shioiri, T. *Comp. Org. Syn.* **1991**, *6*, 800-806.

8. Pontén, F.; Magnusson, G. *J. Org. Chem.* **1996**, *61*, 7463-7466.

9. Murphy, A. V. Ph.D. Dissertation, State University of New York Binghamton, New York, 2004.

10. Chakrabartty, A.; Hew, C. L. *Eur. J. Biochem.* **1991**, *202*, 1057–1063.

11. (a) Knight, C. A., Cheng, C. C., DeVries, A. L. *Biophys. J.* **1991**, *59*, 409-418. (b) Knight, C. A.; Driggers, E.; DeVries, A. L. *Biophys. J.* **1993**, *64*, 252-259. (c) Pertaya, N.; Marshall, C. B.; DiPrinzio, C.L.; Wilen, L.; Thomson, E.S.; Wettlaufer, J.S.; Davies, P.L.; Braslavsky, I. *Biophys. J.* **2007**, 92, 3663-3673.

12. (a) Lane, A. N.; Hays, L. M.; Feeney, R. E.; Crowe, L. M.; Crowe, J. H. *Protein Science* **1998**, *7*, 1555-1563. (b) Lane, A. N.; Hays, L. M.; Tsvetkova, N.; Feeney, R. E.; Crowe, L. M.; Crowe, J. H. *Biophys. J.* **2000**, *78*, 3195-3207. (c) Tsvetkova, N. M.; Phillips, B. L.; Krishnan, V. V.; Feeney, R. E.; Fink, W. H.; Crowe, J. H.; Risbud, S. H.; Tablin, F.; Yeh, Y. *Biophys. J.* **2002**, *82*, 464-473.

13. Bush, C. A.; Feeney, R. E.; Osuga, D. T.; Ralapati, S.; Yeh., Y. *Int. J. Peptide Protein Res.* **1981**, *17*, 125-129.

14. (a)Bush, C. A.; Feeney, R. E. *Int. J. Peptide Protein Res.* **1986**, *28*, 386-397. (b) Bush, C. A.; Ralapati, S.; Matson, G. M.; Yamasaki, R. B.; Osuga, D. T.; Yeh, Y.; Feeney, R. E. *Arch. Biochem. Biophys.* **1984**, *232*, 624-631.

15. Ahmed, A. I.; Feeney, R. E.; Osuga, D. T.; Yeh, Y. *J. Biol. Chem.* **1975**, *250*, 3344-3347.

16. Bouvet, V. R.; Lorello, G. R.; Ben, R. N. *Biomacromolecules* **2006**, *7*, 565-571.

17. (a) Filira, R.; Biondi, L.; Scolaro, B.; Foffani, M. T.; Mammi, S.; Peggion, E.; Rocchi, R. *Int. J. Biol. Macromol.* **1990**, *12*, 41-49. (b) Franks, F.; Morris, E. R. *Biochem. Biophys. Acta.* **1978**, *540*, 346-356. (c) Raymond, J. A.; Radding, W.; DeVries, A. L. *Biopolymers* **1977**, 16, 2575-2578.

18. Berman, E.; Allerhand, A.; DeVries, A. L. *J. Biol. Chem*. **1980**, *255*, 4407-4410

19. Nguyen, D. H.; Colvin, M. E.; Yeh, Y.; Feeney, R. E.; Fink, W. H. *Biophys. J.* **2002**, *82*, 2892-2905.

20. Tachibana, Y.; Fletcher, G. L.; Fujitani, N.; Tsuda, S.; Monde, K.; Nishimura, S. *Angew. Chem. Int. Ed.* **2004**, *43*, 856-862.

21. Compounds **15-17** were previously analyzed by S. L. Liu. Liu, S. L. PhD dissertation, University of Ottawa, Ottawa, 2005.

22. Mimura, Y.; Yamamoto, Y.; Inoue, Y.; Chujo, R. *Int. J. Biol. Macromol.* **1992**, *14*, 242-248.

23. Ohnishi, M. and Urry, D.W. (1969) *Biochem. Biophys. Res. Commun.*, **36**, 194–202

24. Baxter, N. J.; Williamson, M. P. *J. Biomolecular NMR*. **1997**, *9*, 359-369.

25. Hoffman, R.E.; Davies, D.B. *Mag. Res.Chem.* **1988**, *26*, 523-535.

26. Native AFGP-8 was generously donated by AquaBounty Farms Inc. and has the amino acid sequence as described in reference 12a.

27. (a) Case, D. A. et al. *AMBER 9*; University of California: San Francisco, 2006. (b) Case, D. A.; Cheatham, T. E.; Darden, T.; Gohlke, H.; Luo, R.; Merz, K. M.; Onufriev, A.; Simmerling, C.; Wang, B.; Woods, R. J. *J. Comput. Chem.* **2005**, *26*, 1668–1688.

28. For more MD parameters and free energy profiles of Φ_α/Ψ_α , see Experimental Methods and Data Section.

29. (a) Corzana, F.; Busto, J. H.; Jiménez-Osés, G.; Asensio, J. L.; Jiménez-Barbero, J.; Peregrina, J. M.; Avenoza, A. *J. Am. Chem. Soc.* **2006**, *128*, 14640-14648. (b) Corzana, F.; Busto, J. H.; Jiménez-Osés, G.; García de Luis, M.; Asensio, J. L.; Jiménez-Barbero, J.; Peregrina, J. M.; Avenoza, A. *J. Am. Chem. Soc.* **2007**, *129*, 9458-9467.

30. Galema, S. A.; Høiland, H. *J. Phys. Chem.* **1991**, *95*, 5321-5326.

31. Dashnau, J. L.; Sharp, K. A.; Vanderkooi, J. M. *J. Phys. Chem. B* **2005**, *109*, 24152-24159.

32. Tam, R.Y.; Ferreira, S.S.; Czechura, P.; Chaytor, J.L. *J. Am. Chem. Soc.* **2008**, 130, 17494 – 17501.

33. Kumar, S.; Rosenberg, J. M.; Bouzida, D.; Swendsen, R. H.; Kollman, P. A. *J. Comput. Chem.* **1995**, *16*, 1339-1350.

34. (a) Biarnes, X.; Ardevol, A.; Planas, A.; Rovira, C.; Laio, A.; Parrinello, M. *J. Am. Chem. Soc.* **2007**, *129*, 10686-10693. (b) Ionescu, A. R.; Berces, A.; Zgierski, M. Z.; Whitfield, D. M.; Nukada, T. *J. Phys. Chem. A* **2005**, *109*, 8096-8105.

35. Kräutler, V.; Müeller, M.; Hünenberger, P. H. *Carbohydr. Res.* **2007**, *342*, 2097-2124.

36. Davidovic, M.; Mattea, C.; Qvist, J.; Halle, B. *J. Am. Chem. Soc.* **2009**, *131,* 1025-1036.

Chapter 5 : Effect of the side chain amide bond in *C*-linked AFGP analogues on IRI activity

5.1 ROLE OF THE SIDE CHAIN AMIDE BOND IN C-LINKED AFGP ANALOGUES

The previous chapter showed that a change in the side chain length of *C*-linked AFGP analogues has significant effects on glycoconjugate conformation, Figure 4.14. This is believed to be responsible for the dramatic change in IRI activity between these analogues, Figure 4.4. Thus, we hypothesized that the relationship between glycoconjugate conformation and IRI activity may be that specific orientations of the hydrated carbohydrate are able to affect the overall hydration of the glycopeptide to prevent bulk water from adding to the ice lattice, thereby inhibiting ice growth. In an effort to further investigate how the nature of the side chain affects glycoconjugate conformation and IRI activity, we subsequently focused on the role of the orientation and location of the amide bond in the side chain.

Amide bonds are abundant and important in Nature as they are able to impart structural rigidity, act as hydrogen acceptors or donors, and possess stereo- and electronic effects.[1] To account for these factors in studying the side chain amide bond of IRI-active *C*-linked AFGP analogue (**6**), two classes of analogues were designed, Figure 5.1: (1) a variation in the relative location of the side chain amide bond, while maintaining the same number of carbon atoms in the side chain, (**20** and **21**), and (2) a change in orientation of the side-chain amide bond (**22**).

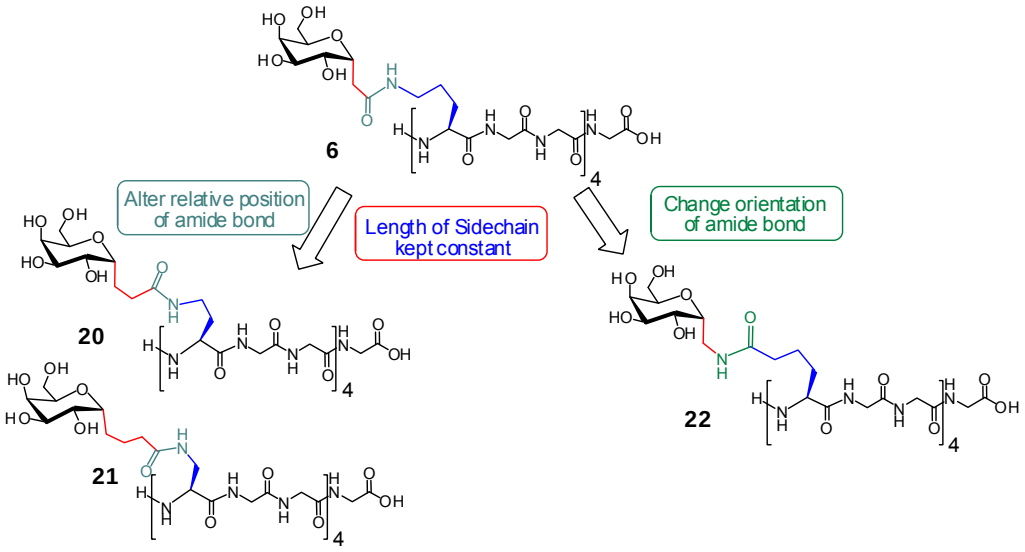

Figure 5.1 Target *C*-linked AFGP analogues with varying linkages between the carbohydrate and the peptide backbone.

*5.2 SYNTHESIS OF C-LINKED AFGP ANALOGUES **20** AND **21** – VARIATION IN THE LOCATION OF AMIDE BOND IN SIDE CHAIN.*

The syntheses of glycopolymers (**20** and **21**) were performed similarly to previously synthesized *C*-linked AFGP analogues using solid phase peptide synthesis (Scheme 4.6) from the corresponding glycoconjugate building blocks (**66** and **67**), Scheme 5.1. These glycoconjugates were synthesized by coupling the appropriate unnatural amino acids (**46** and **47**) to *C*-linked carbohydrate derivatives (**68** and **69**), respectively. Both *C*-linked carbohydrate derivatives were synthesized from aldehyde (**57**), which is an intermediate in the syntheses of analogues (**18** and **19**), Scheme 4.4.

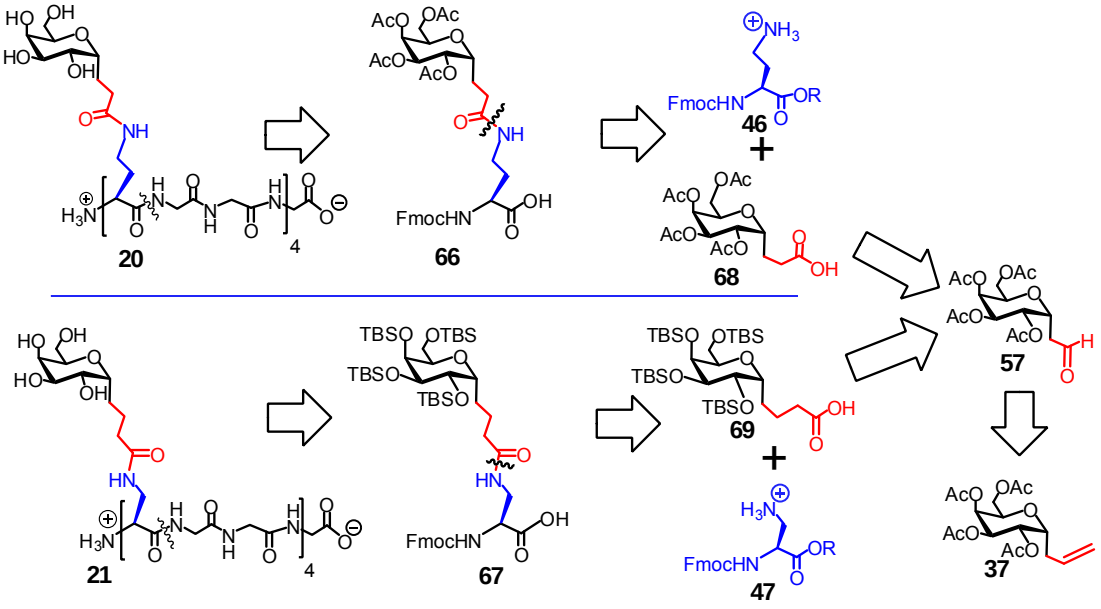

Scheme 5.1 Retrosynthetic analysis of analogues **20** and **21**.

5.2.1 Synthesis of *C*-linked AFGP Analogue (**20**)

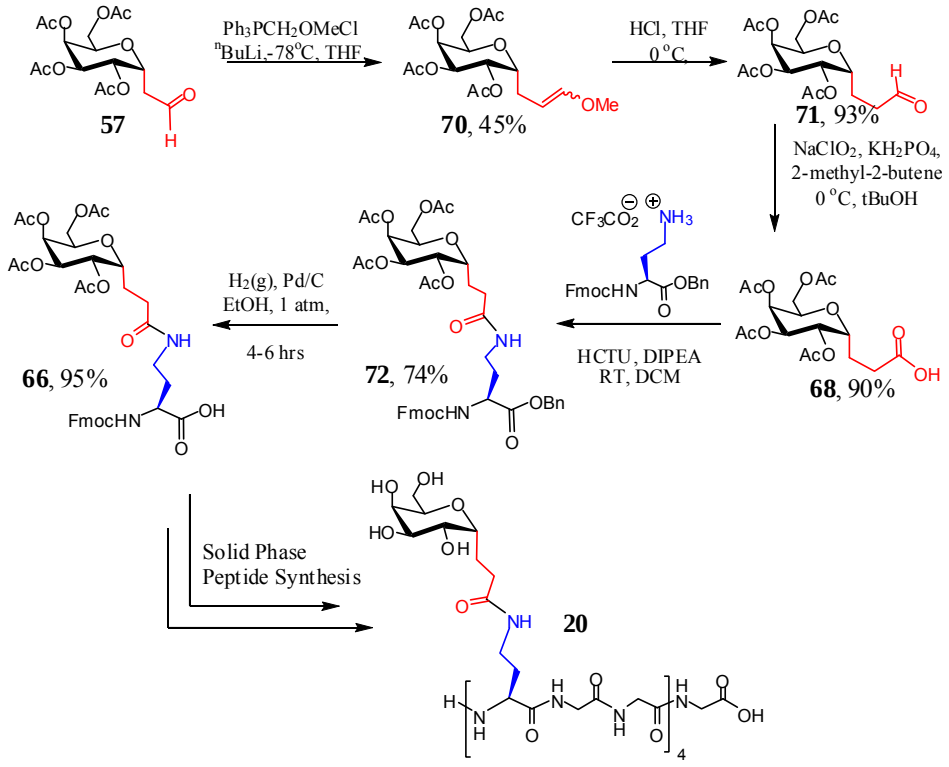

Scheme 5.2 Synthesis of *C*-linked AFGP analogue **20**.

Analogue (**20**) was synthesized via carbohydrate derivative (**68**), Scheme 5.2. Homologation of aldehyde (**57**) was achieved by a Wittig reaction using methoxymethyl(triphenyl)phosphonium chloride in the presence of a strong base.[2-5] Under acidic conditions, the resulting enol ether (**70**) was converted into the homologated aldehyde (**68**).[6]

However, an interesting side reaction was observed in the Wittig reaction as a result of the structure of the starting material (**57**). Initial attempts to use potassium *tert*-butoxide as the base (pKa 29.0 in DMSO)[2] resulted in epimerization of the starting material. ^{1}H-NMR of the recovered starting material (Figure 5.2A) shows a change in chemical shift and coupling constants of H2 and H3 of the epimerized aldehydes (**57** and **57b**). The large H2 coupling constants ($J_{1,2}$ and $J_{2,3}$ = 10.2, 9.8 Hz) of (**57b**) show that H2 is in a diaxial relationship between the H1 and H3, thus confirming the β-configuration of the anomeric substituent. By comparison, a ^{1}H-NMR spectrum of the α-anomer (**57**) is shown in Figure 5.2B.

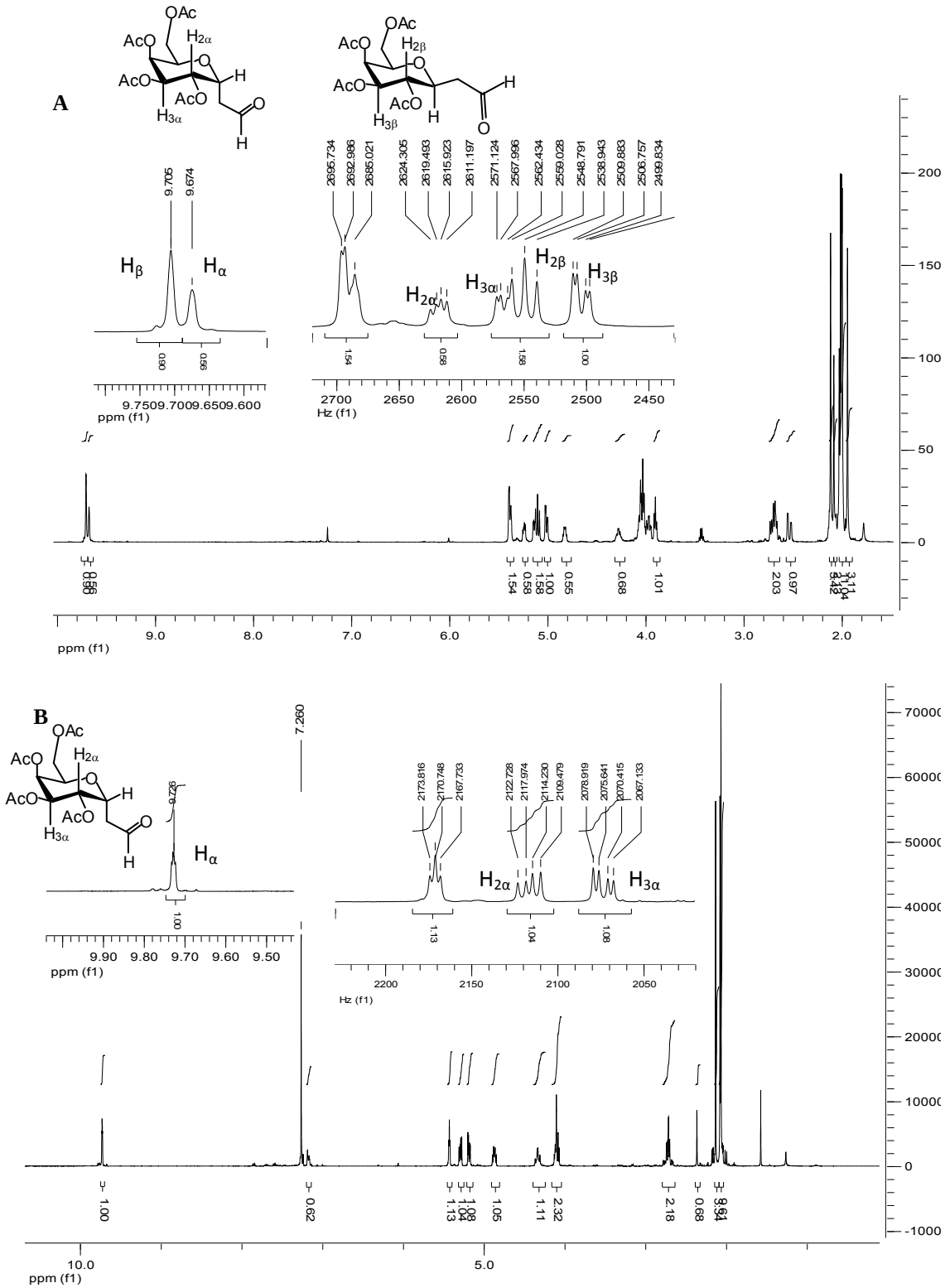

Figure 5.2 [1]H-NMR spectra of (A) recovered epimerized starting material **57** and **57b**, and (B) starting material **57**

Epimerization of (**57**) may be attributed to the incomplete deprotonation of the non-stabilized phosphonium reagent by *tert*-butoxide, resulting in residual strong base in the reaction solution. Even in a large excess of phosphonium salt, epimerization of recovered starting material was observed.

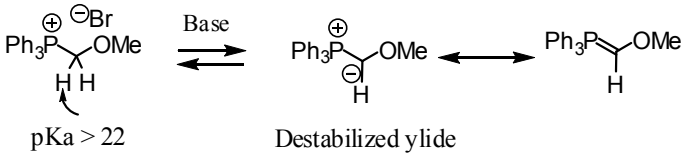

Figure 5.3 Formation of phosphonium ylide for Wittig reaction.

It is hypothesized that the presence of a strong base with aldehyde (**57**) results in deprotonation of the α-proton adjacent to the starting aldehyde to form the acyclic enone (**73**), Scheme 5.3. Due to 1,3-diaxial interactions between the anomeric methyl and the C3 and C5 protons, the orientation of the enone to adopt an equatorial position is favoured. Ring closure of the pyranose ring forms the epimerized starting material (**57b**). Similar results have been observed of anomeric *C*-linked esters in the presence of basic conditions.[7]

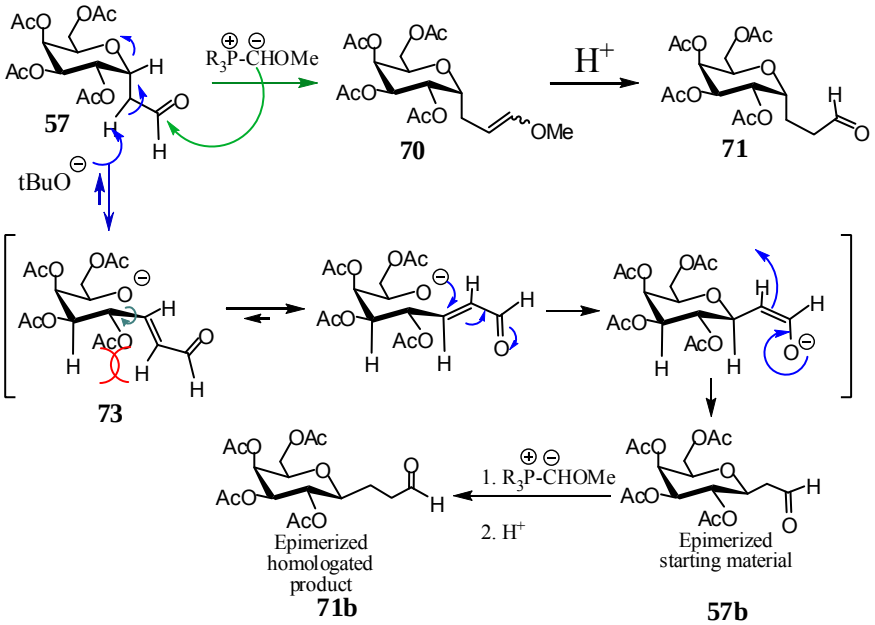

Scheme 5.3 Undesired epimerization of starting aldehyde **57** in the presence of strong base.

This problem was overcome with the use of a stronger base. In the presence of *n*-butyl lithium (pKa ~53), no epimerization was observed, and enol ether (**70**) was obtained in 45% yield. A minor byproduct that was obtained was the addition of a butyl chain to aldehyde (**57**). Such a byproduct has been reported in literature, and is the result of the nucleophilicity of *n*-butyl lithium.[4] In addition, the yield was quite low due to some acetate cleavage by the nucleophilic *n*-butyl lithium.

The desired aldehyde (**71**) was then oxidized to the corresponding carboxylic acid (**68**) in 90% yield via a Pinnick oxidation protocol. Compound (**68**) was then coupled to the desired diaminobutanoate derivative (**46**) to afford glycoconjugate (**72**). Upon debenzylation with hydrogen gas and palladium on carbon, building block (**66**) was obtained in 95% yield and was subjected to solid phase peptide synthesis as in Scheme 4.6.

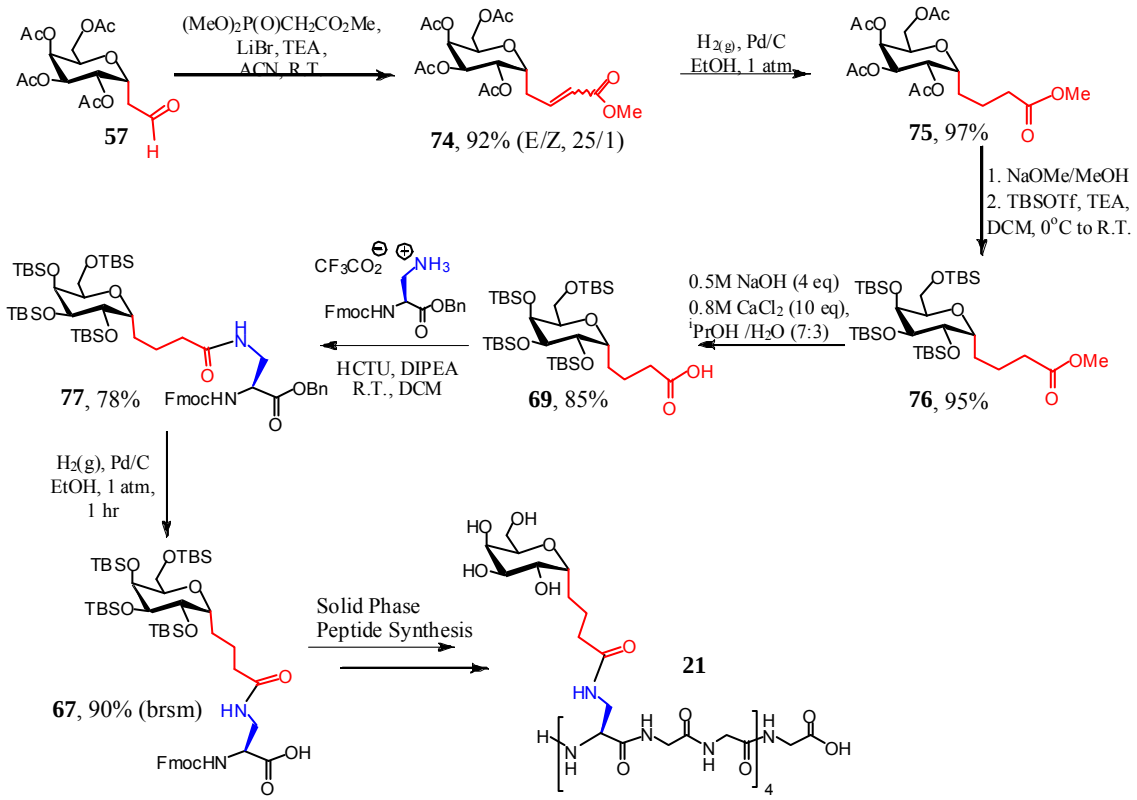

Scheme 5.4 Synthesis of *C*-linked AFGP analogue **21.**

5.2.2 SYNTHESIS OF *C*-LINKED AFGP ANALOGUE **21**

The synthesis of carbohydrate derivative (**69**) was achieved using a Horner-Wadsworth-Emmons procedure using methyl(dimethoxyphosphoryl) acetate, triethylamine and lithium bromide.[8] Although the pKa of the phosphonate methylene is ~19 in DMSO, the use of lithium bromide drastically decreases this pKa to enable deprotonation by the weak base triethylamine (pKa = 9 in DMSO) to form the corresponding ylide (Figure 5.4).

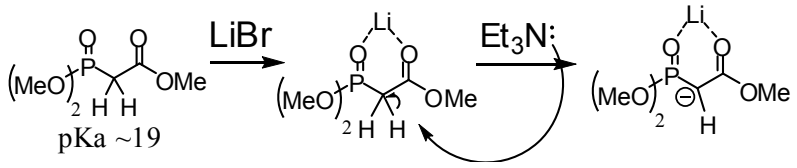

Figure 5.4 Effects of lithium bromide on trimethoxyphosphonium acetate.

An E/Z mixture (E/Z, 25/1) of the corresponding enone (**74**) was formed. The next transformation required the saponification of the terminal methyl ester while preserving the protecting groups of the carbohydrate hydroxyls for subsequent transformations. This was achieved by substitution of the pyranose acetates with *tert*-butyl dimethyl silyl ethers using 1.0 M sodium methoxide in methanol, followed by treatment with *tert*-butyldimethylsilyl-triflate.[9] As silyl ethers are slightly sensitive to strongly basic conditions,[10] mild hydrolysis conditions were used. This was achieved using sodium hydroxide in the presence of excess calcium chloride in isopropanol and water.[11] The resulting silyl-protected carboxylic acid was then coupled to the unnatural amino acid derivative to form the glycoconjugate derivative (**77**).

Glycoconjugate (**77**) was then debenzylated using hydrogen gas and palladium on carbon to form building block (**67**) which formed the desired glycopolymer (**21**) by solid phase peptide synthesis.

*5.3 SYNTHESIS OF C-LINKED AFGP ANALOGUE (**22**) – VARIATION IN THE ORIENTATION OF SIDE CHAIN AMIDE BOND*

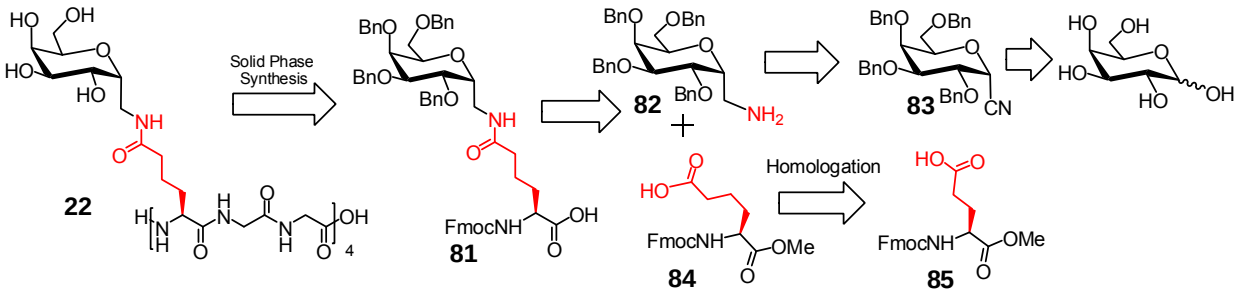

Scheme 5.5 Retrosynthetic analysis of *C*-linked AFGP analogue (**22**).

The synthesis of analogue (**22**), possessing an amide bond in the side chain with a different orientation relative to IRI-active analogue (**6**), was achieved by solid phase peptide synthesis of the appropriate glycoconjugate building block (**81**). Building block (**81**) was synthesized by coupling of *C*-α-methylamino-D-galactopyranose (**82**) with unnatural homoglutamic acid (**84**). Carbohydrate derivative (**82**) was synthesized from reduction of the starting anomeric nitrile (**83**),[12] whereas homoglutamic acid (**84**) was synthesized from an Arndt-Eistert homologation[13] strategy from orthogonally-protected glutamate derivative (**85**).

5.3.1 SYNTHESIS OF *C*-GALACTOPYRANOSYL METHYLAMINE **82**

As it was desired to obtain the anomeric galactopyranose-methylamine (**82**) from reduction of the corresponding nitrile (**83**), the first key step was to install the anomeric *C*-linked nitrile group with the proper stereochemistry.

To enhance the stereoselectivity of glycosylation, the choice of protecting groups for non-anomeric hydroxyl groups is important. It is known that C2-ester protecting groups such as acetates significantly favour the formation of 1,2-trans-glycosylations via a neighbouring-group

effect, Scheme 5.6.[14,15] Therefore, the protecting groups of choice were benzyl ethers, as these do not favour the formation of the undesired β-glycosylation product.

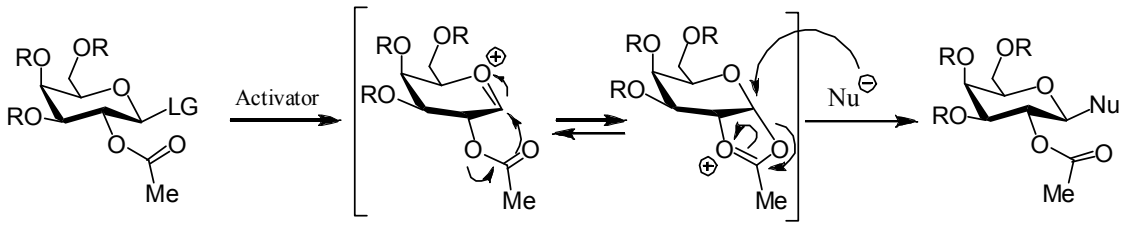

Scheme 5.6 Neighbouring-group effect of C2 ester on stereochemistry of anomeric nucleophilic addition.

Various glycosylation procedures using various donors (Scheme 5.7) were attempted in an effort to install the nitrile functionality in the α-configuration, Table 5.1. Of the various glycosyl donors used, anomeric acetate (**88**) proved to be the most effective, as use of donors (**86**) and (**87**) primarily resulted in no reaction, undesired side reactions, or decomposition, Table 5.1.

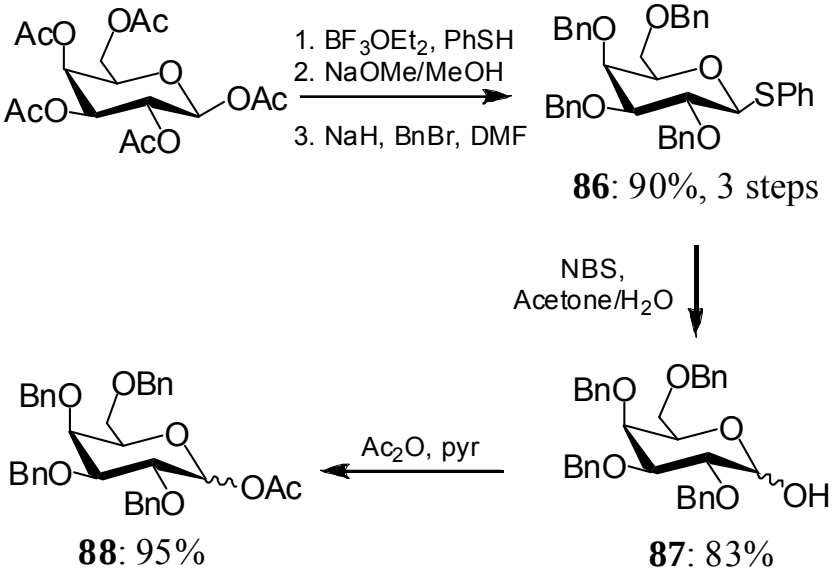

Scheme 5.7 Synthesis of various galactopyranose donors **86-88**.

Table 5.1 Conditions attempted to form anomeric nitrile **83**

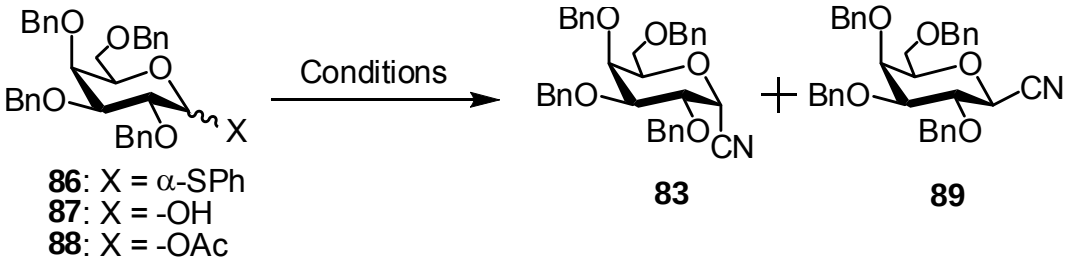

86: X = α-SPh
87: X = -OH
88: X = -OAc

83 **89**

Entry	Donor	Nitrile source	Conditions	Results
1	**86**	TMS-CN (2.0 eq)	AgOTf (cat.) NIS (1.3 eq) Et_2O, MS 4Å, 22°C	Decomposition, hydrolysis **87**, No desired product
2			TMS-OTf (0.4 eq) NIS (1.5 eq) Et_2O or DCM, MS 4Å -40°C to -20°C overnight	Mostly starting material **86** Epimerization of **86** No desired product
3			TMS-OTf (0.4 eq) NIS (1.5 eq) DCM, 22°C	Mostly starting material **86** Epimerization of **86** No desired product
4			TMS-OTf (0.4 eq) NIS (1.5 eq) DCM, 22°C, sonicate	Hydrolysis **87** Some dimerization No desired product
5	**87**	TMS-CN (1.2 eq)	TMS-OTf (1.1 eq), DMF, 22°C	Starting material **87** No desired product
6		KCN (1.2 eq)	TMS-OTf (1.1 eq), DMF, 22°C	Starting material **87** No desired product
7		TMS-CN (1.2 eq) KCN (1.2 eq)	DMF, Sonicate overnight	Starting material **87** No desired product
8		TMS-CN (1.2 eq) KCN (1.2 eq)	DMF, 70°C	Starting material **87** No desired product
9	**88**	TMS-CN (5 eq)	BF_3OEt_2, Et_2O, 30 mins, 0°C	30% (3:1) **83** : **89** (α/β) Significant decomposition
10			BF_3OEt_2, CH_3CN, 0°C, 5 hrs	No Reaction
11			BF_3OEt_2, CH_3CN, 15 minutes, 22°C, immediate workup and purification	80%, (1:1) **83** : **89** (α/β)

The use of anomeric acetate (**88**) in the presence of trimethylsilylcyanide and boron trifluoride was successful in formation of the desired product (**83**). Despite also forming the undesired *C*-β-nitrile anomer (**89**), these two anomers were easily separated by silica gel column chromatography.[12]

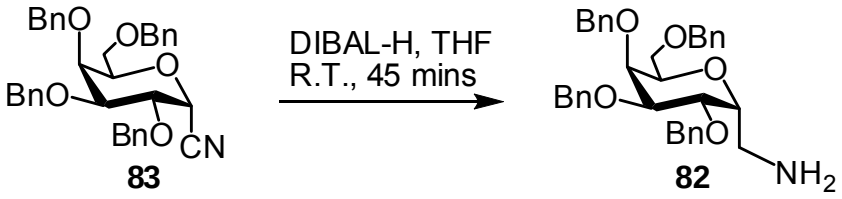

Scheme 5.8 Synthesis of α-galactopyranosyl methylamine **82** from reduction of nitrile **83**.

Anomeric nitrile (**83**) was reduced using di-isobutylaluminum hydride (DIBAL-H). The use of a stronger reducing agent (lithium aluminum hydride) resulted in the additional cleavage of one of the benzyl groups, as was determined by electrospray ionization mass spectrometry analysis. As the primary amine is unstable,[12] it was immediately coupled to the amino acid without purification to give the desired glycoconjugate, Section 5.3.3.

5.3.2 HOMOGLUTAMIC ACID (**84**) SYNTHESIS

To obtain unnatural amino acid homoglutamate (**84**), an Arndt-Eistert homologation procedure of natural glutamate derivative (**85**) was used. Homologation occurs as a result via the formation of α-diazoketone intermediate (**90**) from the corresponding activated carboxylic acid (**85**).[13,16] Upon thermal or acidic decomposition, a Wolff rearrangement occurs, whereby the resulting ketene is trapped with water to form a homologated carboxylic acid.[16]

The success of the synthesis of (**90**) from (**85**) proved to be dependent upon the type of activating agent that was used, Table 5.2

.

Table 5.2 Optimization of α-diazoketone intermediate **90** synthesis.

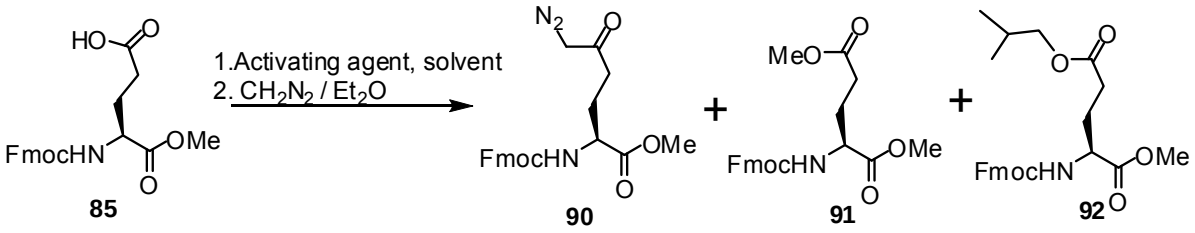

Entry	Activating Agent, solvent	Conditions	Results
1	Isobutyl chloroformate (1.2 Equiv.), NMM (2.5 Equiv.), THF	-20°C (30 mins) to -5°C, then add CH_2N_2/Et_2O	(~1:5) **90 : 92**
2	HBTU (1.1 Equiv.), DIPEA (2.5 Equiv.), DCM	22°C (30 mins), then add CH_2N_2/Et_2O	(~1:1) **90 : 91**
3	HCTU (1.1 Equiv.), DIPEA (2.5 Equiv.), DCM	22°C (30 mins), then add CH_2N_2/Et_2O	82% **90**, trace byproducts

The use of isobutyl chloroformate and N-methyl morpholine (NMM) as activating agents[17] (Table 5.2, entry 1) yielded little desired product (**90**). However, significant amounts of isobutyl ester (**92**) were also formed as a result of competing nucleophilicities between residual isobutanol (from the isobutyl chloroformate reagent) and diazomethane towards the activated ester. The use of another carboxylic acid activating reagent,[18] HBTU (Table 5.2, entry 2), formed more of the desired product, but a significant amount of acid methylation product (**91**) was also formed as a result of incomplete activation of the carboxylic acid starting material (**85**). The use of HCTU, which is a better activating agent than HBTU,[19] afforded the α-diazoketone intermediate **90** in 76% yield, with minimal formation of byproducts.

α-Diazoketone (**90**) was converted into the homologated carboxylic acid (**84**) in 87% yield using catalytic amounts of silver benzoate in dioxane and water under sonication conditions for 30 minutes (Scheme 5.9).[20] Compared to conventional decomposition procedures of heating

at 70°C, it was observed that sonication yielded significantly less byproducts as determined by thin-layered chromatography analysis.

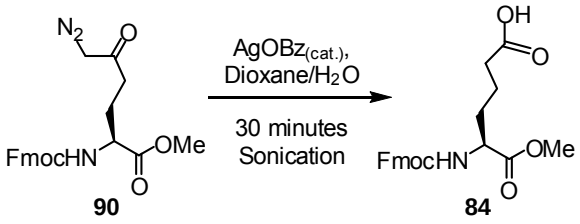

Scheme 5.9 Wolff rearrangement of **90** to form homoglutamate derivative **84**.

5.3.3 GLYCOCONJUGATE SYNTHESIS OF (**93**) AND (**94**)

As a model system to synthesize *C*-linked glycoconjugate (**93**), synthesis of glycoconjugate (**94**) was first achieved to optimize coupling conditions to the amino carbohydrate derivative (**82**), Scheme 5.10. In addition to being a representative synthetic model, the synthesis of glycoconjugate (**94**) would also allow for the subsequent synthesis of the corresponding analogue. *C*-glycoconjugates (**93** and **94**) were synthesized in 66 and 63% yields respectively (for both reduction and coupling steps).

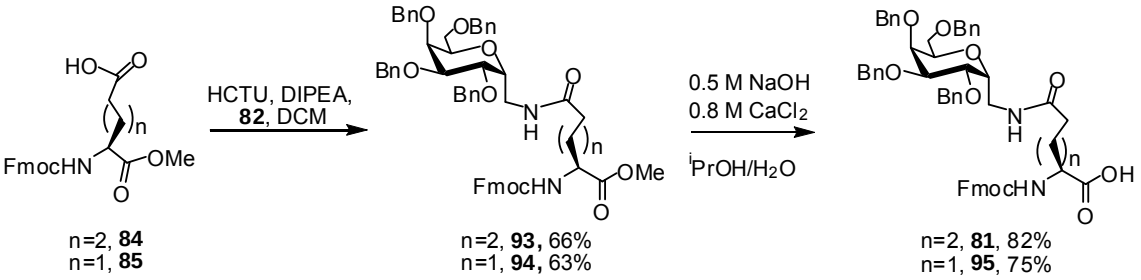

Scheme 5.10 Glycoconjugate synthesis of (**93** and **94**) from coupling of (**82**) to (**84** and **85**) respectively, followed by saponification to form building blocks (**81** and **95**).

However, as carbohydrate derivative (**82**) was unstable and required immediate coupling to the corresponding amino acid precursor,[12] the stereochemistry of the anomeric carbon linkage of the glycoconjugates must be confirmed to ensure epimerization of the anomeric center did not occur during the reduction and coupling procedures. To achieve this, β-galactosyl-nitrile (**89**) was also reduced and conjugated to glutamic acid derivative (**85**) (Scheme 5.11) in the same

manner as for the α-anomer. The NMR spectra of (**94**) and (**97**) were then compared to confirm the stereochemistry at the anomeric centre.

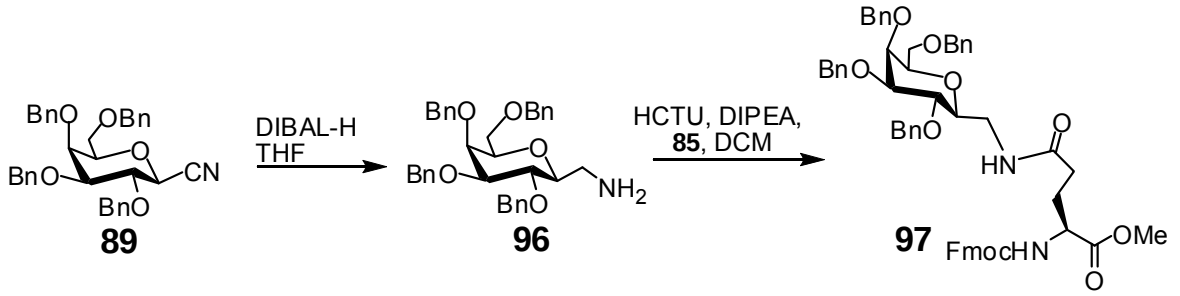

Scheme 5.11 Synthesis of *C*-β-galactosyl-nitrile (**96**) and the corresponding *C*-β- glycoconjugate (**97**)

Figures 5.5 and 5.6 show partial ^{1}H- and 2D-COSY NMR spectra of the α- and β-glycoconjugates (**94**) and (**97**), respectively. While the coupling constants of the anomeric protons are complex and overlap with other peaks, the drastic difference in chemical shifts shows that the two reaction pathways yielded two different products. In addition, electrospray ionization mass spectroscopy analysis showed that these compounds (**94** and **97**) had the same molecular ion (see experimental data). This shows that epimerization at the anomeric centre did not occur during the nitrile reduction and amino-acid coupling steps.

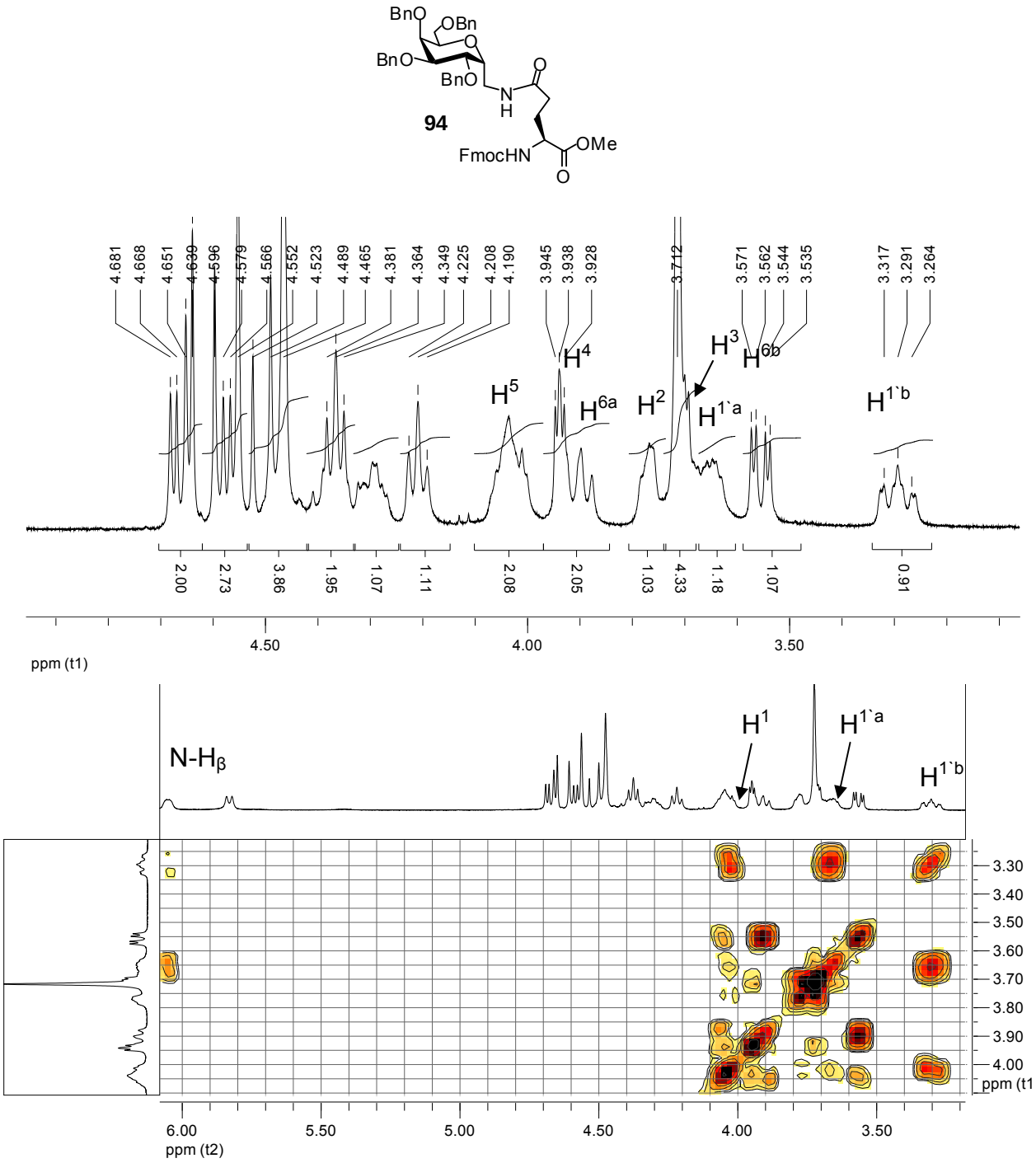

Figure 5.5 Partial ^{1}H- and 2D-COSY NMR spectra of the α-glycoconjugate (**94**)

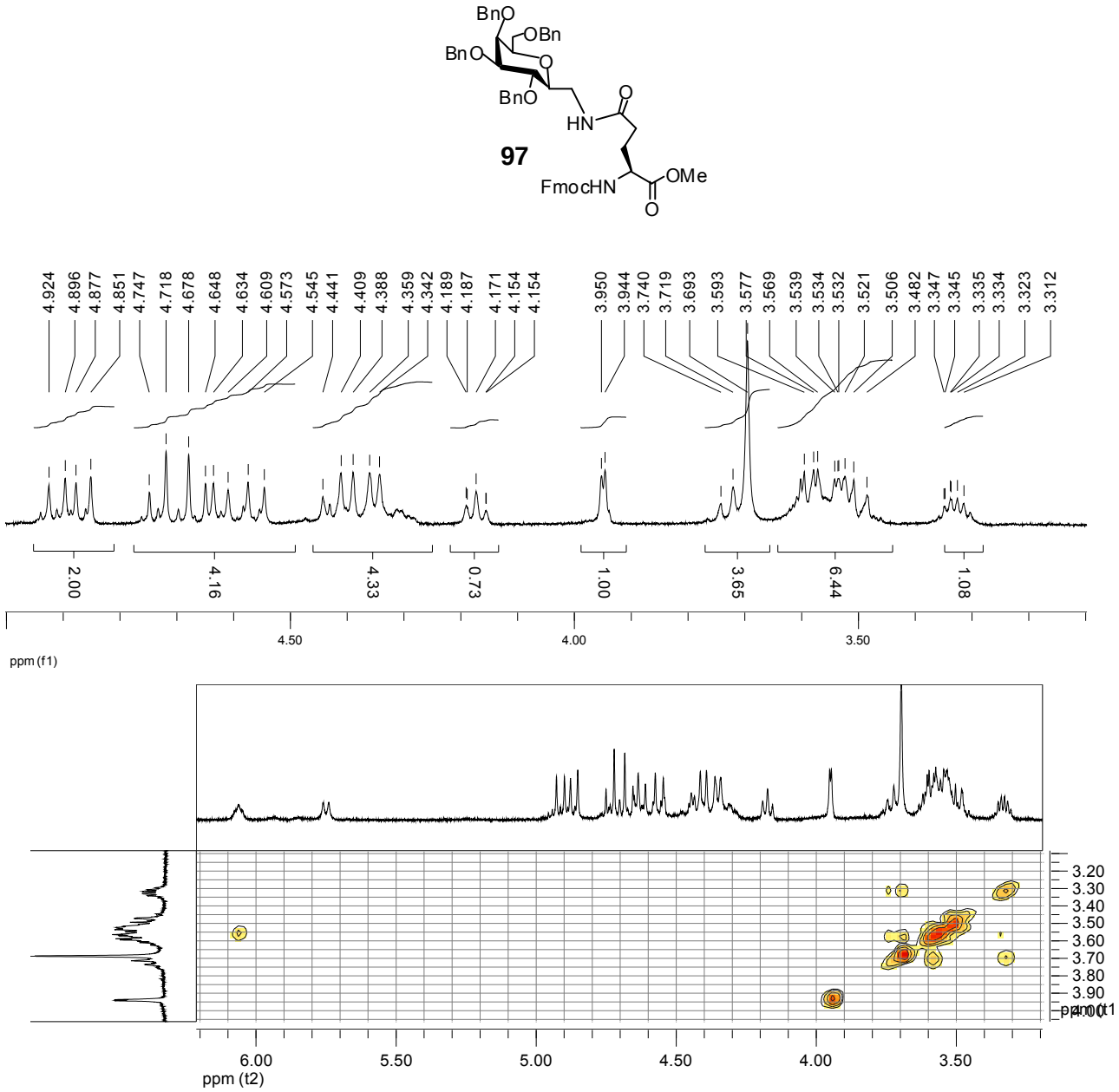

Figure 5.6 Partial ^{1}H- and 2D-COSY NMR spectra of the β-glycoconjugate (**97**)

Deprotection of the methyl esters of (**93** and **94**) to form building blocks (**81** and **95**) for solid-phase peptide synthesis was achieved (82 and 75% yields, respectively) using a mixture of sodium hydroxide and excess calcium chloride in isopropanol and water (Scheme 5.10).[11]

As a test case, building block (**95**) was subjected to solid phase peptide synthesis in a similar manner as before, Scheme 4.6. Unfortunately, after cleavage of the benzylated glycopeptide from the bead, attempts to fully deprotect the numerous benzyl protecting groups (Table 5.3) were unsuccessful as determined by HPLC and subsequent MALDI-TOF analysis.

Table 5.3 Solid phase peptide synthesis of benzylated glycopeptides (**95**) and attempts for debenzylation

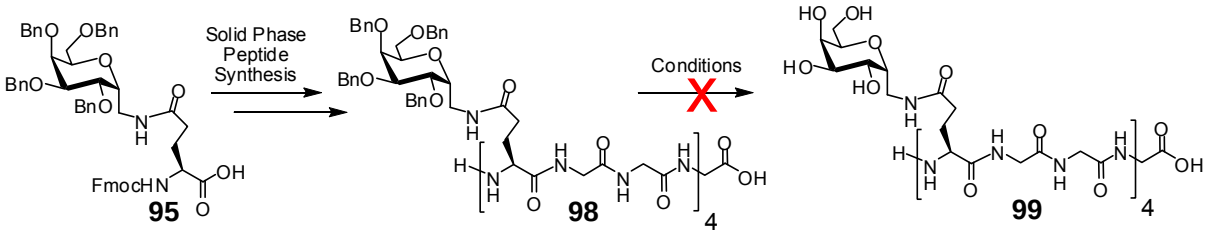

Entry	Conditions	Result
1	H_2, 10 wt% Pd/C, 1 atm, EtOH/EtOAc	No desired product
2	H_2, 10 wt% $Pd(OH)_2$, EtOH/EtOAc	No desired product
3	H_2, 20 wt% Pd/C, TFA, EtOH/EtOAc	
4	(5:3:1) TFA : Me_2S : m-cresol, TMSOTf/H_2O	No desired product
5	1. O_3/EtOH/DCM 2. NaOMe/MeOH	No desired product
6	BCl_3, CH_2Cl_2	No desired product

5.4 ANTIFREEZE ACTIVITY OF C-LINKED AFGP ANALOGUES (**20**, **21**)

Analogues (**20**) and (**21**) were assessed for their thermal hysteresis and ice-recrystallization inhibition activity. Similar to the previous *C*-linked AFGP analogues, no thermal hysteresis was observed, Figure 5.7.

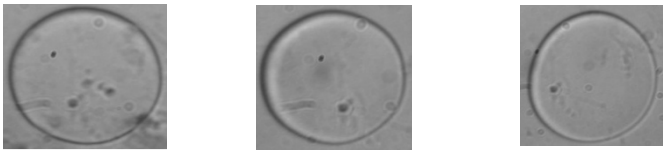

Figure 5.7 Ice crystals of analogues of distilled water (left), **20** (middle) and **21** (right), at 10 mg/mL, as determined by nanolitre osmometry.

Assay for the IRI activity of analogues (**20** and **21**) showed that they are better inhibitors of ice recrystallization compared to PBS (the negative control), and analogues (**18** and **19**), Figure 5.8. However, compared to analogue (**6**), the activities of (**20** and **21**) are significantly lower.

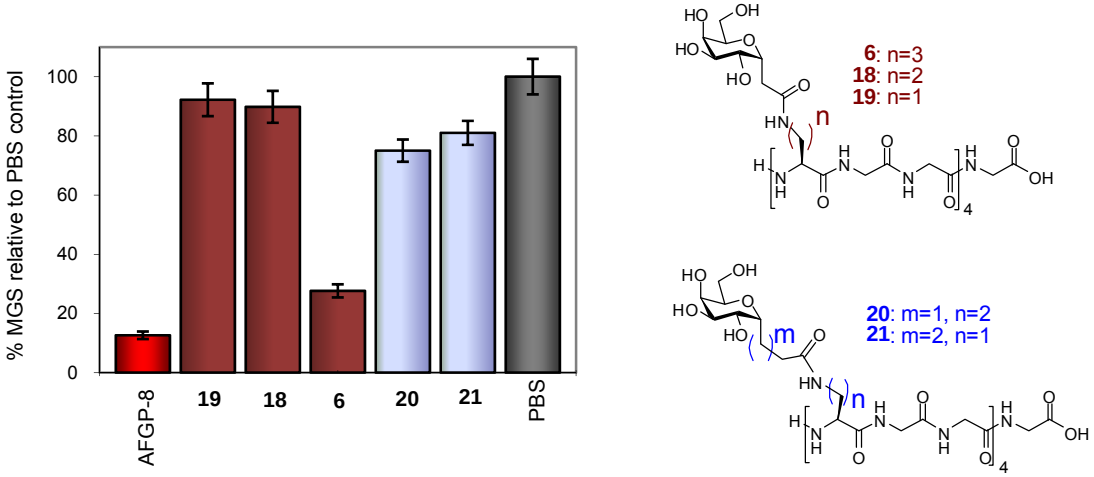

Figure 5.8 Ice recrystallization inhibition results for AFGP-8 (1) and *C*-linked AFGP analogues (**6**, **18**-**21**) at 5.5 μM in PBS, and PBS buffer as negative control.

These results demonstrate the importance of the amide bond location in the side chain of *C*-linked AFGP analogue (**6**). Altering the relative location of this amide bond along the length of the side chain drastically affects the IRI activity of these compounds. However, this effect was not as significant as altering the length of the side chain, as with analogues (**18** and **19**).

5.5 RELATIONSHIP BETWEEN THE SOLUTION CONFORMATIONS OF TRUNCATED MODEL SYSTEMS OF AFGP ANALOGUES AND THEIR IRI ACTIVITY

In an effort to understand the factors responsible for the IRI activity of these *C*-linked analogues, we assessed the solution conformation of the model systems (**100** and **101**) of analogues (**20** and **21** respectively), by molecular dynamics simulations. These were performed using the same parameters as was previously mentioned in Section 4.6, by Michael Nohra and Professor Tom Woo.

From Figure 4.14, the solution conformation of the model system (**62**) of IRI-active analogue (**6**) was shown to be unique compared to the model system of inactive analogues (**60**, **61**, **63**). In (**62**), the carbohydrate is 'folded back' on itself with the β-face oriented towards the side chain and peptide backbone, Figure 5.9.

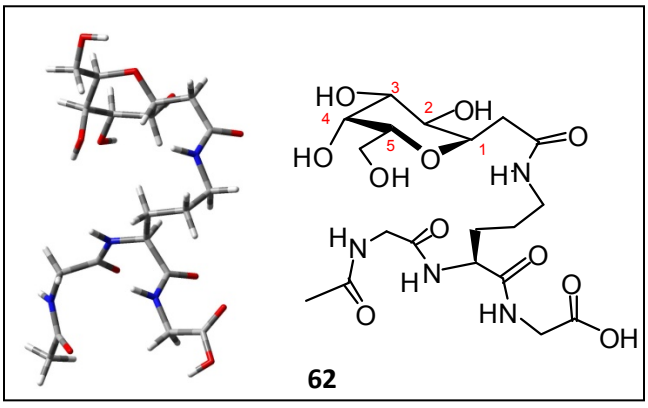

Figure 5.9 Lowest energy conformation of model system (**62**) obtained by molecular dynamic simulations, and a schematic representation of its conformation.

From this data, we hypothesized that there is a change in the overall hydration of this analogue, possibly due to a co-operative effect between the hydrated carbohydrate and the hydrophobic peptide backbone. This possible change in hydration is believed to be responsible for the observed differences in IRI activities between *C*-linked AFGP analogues.

Figure 5.10 shows the MD simulation snapshots of the lowest energy solution conformation of the model systems (**100**) and (**101**).

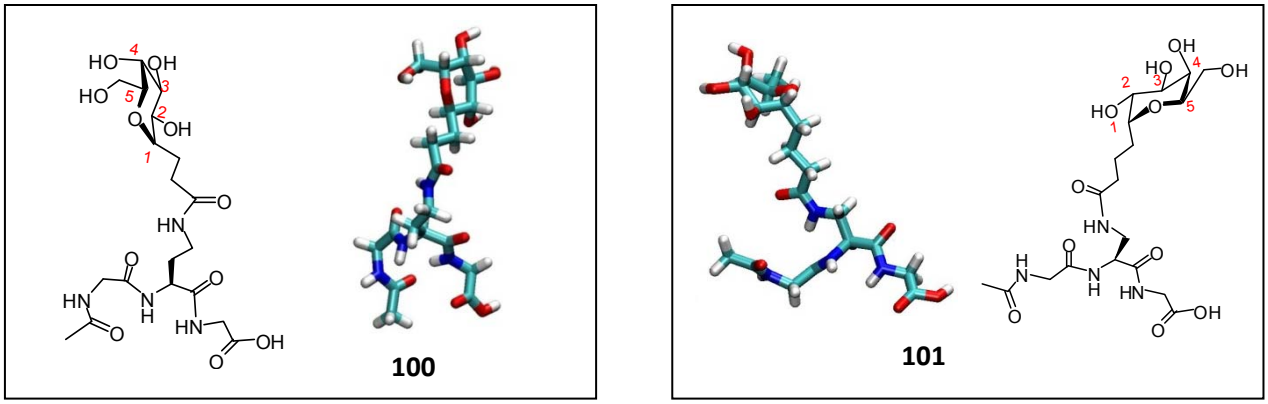

Figure 5.10 Lowest energy conformation of model systems (**100**) and (**101**) obtained by molecular dynamic simulations, and a schematic representation of their conformations.

These results indicate that despite containing the same number of atoms in the side chain, a change in the location of the amide bond within the side chain in analogues (**100**), (**101**) and (**62**) results in significant differences in their side chain conformation and carbohydrate presentation. Unlike the solution conformation of IRI-active analogue (**62**), glycoconjugates (**100**) and (**101**) have the carbohydrate extended into the solution away from the polypeptide backbone exposing both faces of the carbohydrate to the bulk solvent, similar to that observed for model systems (**61** and **60**), which have shorter side chains and are unable to inhibit ice recrystallization, Figure 4.14. These results are in agreement with our hypothesis that exposure of both faces of the galactose moiety to the bulk solvent may be responsible for the dramatic decrease in IRI activity of *C*-linked AFGP analogues under our assay concentrations of 5.5 μM.

Unfortunately, these results do not explain why the orientation of the carbohydrate is so important for IRI activity. Based upon our results, one plausible explanation centres on the interaction between the carbohydrate moiety with nearby water molecules. We had previously hypothesized that the intramolecular hydrogen bonding that occurs between the C4-oxygen (H-acceptor) of galactose with the C6 hydroxyl (H-donor) of galactopyranose (Tables 4.3 and 5.4) is detrimental to IRI activity because as these atoms are involved in intramolecular hydrogen bonding, they become unable to interact with nearby waters of hydration, Section 4.6.1. For example, IRI-inactive analogues (**60**, **61**, **63**) have a higher percentage of this hydrogen bonding (6.9 %, 8.5 % and 15.7 %, respectively), compared to IRI-active analogue **62** (4.6 %) and each carbohydrate of the native AFGP disaccharide (0.7 and 2.4) Consequently, water molecules in the bulk water are not disturbed by the hydrated carbohydrate, and can easily add to the growing ice lattice, thereby rendering the glycoprotein as poor ice recrystallization inhibitors.

Analysis of intramolecular hydrogen bonding of analogues (**100**) and (**101**) shows that there is no persistent hydrogen bonding at the O4--HO6 position, Table 5.4. This result may account for their weak ability to act as ice-recrystallization inhibitors (Figure 5.8), compared to analogues (**60**, **61** and **63**) that have a higher percentage of intramolecular (O4-HO6) hydrogen bonding and are IRI-inactive, Table 4.3 and Figure 4.4.

Table 5.4. Summary of statistical analysis of MD simulations showing % intramolecular hydrogen-bonding occupancy of **100**, **101**, **60**-**63** and native AFGP-8.

Compound		Intramolecular Hydrogen Bonding (%)
		O_4 --- H-O_6
100		0.0
101		0.0
63		15.7
62		4.6
61		8.5
60		6.9
AFGP 8	(GalNHAc)	0.7
	(Galactose)	2.4

Another factor that may contribute to the slight increase in IRI activity of (**20** and **21**) compared to (**18** and **19**) may be the number of methylene groups between the carbohydrate and the side chain amide bond (*m*, Figure 5.8). Analysis of the lowest energy conformations of the model systems of analogues (**18**-**21**) using appropriately truncated model peptides suggests that the number of these methylene groups affects the orientation of the amide bond in the side chain. For example, this is observed in a comparison between the conformations of analogues (**61**) and (**100**), which have the same number of methylene groups between the side chain amide bond and the polypeptide backbone, but varying number of methylene groups between the carbohydrate and the side chain amide bond, and are structural analogues of (**18**) and (**20**) respectively; the carbonyl of the amide bond in the side chain of (**61**) is directed towards the N-terminus (Figure 4.14), whereas the side chain carbonyl of (**100**) is directed towards the C-terminus (Figure 5.10), similar to that of IRI-active analogue (**62**). Thus, it is hypothesized that the orientation of the carbonyl in this manner may facilitate the formation of different water bridges between the side chain and backbone amide bonds of these analogues (**61**) and (**100**). Similar results have been reported by Corzana,[21] who hypothesized that an important factor in the difference in antifreeze activity between threonine- and serine-containing glycopeptides is the water-bridging pattern of these glycoconjugates, Chapter 6.1. Further studies are required to test this hypothesis.

By correlating the results of conformational analyses and IRI activities of *C*-linked AFGP analogues (**100**) and (**101**), we have provided further evidence that the potent IRI activity of (**62**) may be attributed to its unique conformation, whereby the carbohydrate folds back towards the hydrophobic side chain and peptide backbone. The presence of intramolecular hydrogen bonding at the O4-HO6 position and orientation of the side chain ketone may also be factors (albeit minor) in modulating IRI activity.

5.6 CHAPTER SUMMARY

The synthesis of *C*-linked AFGP analogues that contain an amide bond at various positions in the side chain (**20** and **21**) have been described. In addition, efforts towards the synthesis of *C*-linked AFGP analogues with the side chain amide bond in different orientations were also described.

The ice recrystallization inhibition activities of analogues (**20**) and (**21**) were performed and show weak IRI activity (75-80% mean ice-grain size relative to PBS negative control). Molecular dynamics simulations of (**100**) and (**101**) showed that their conformations are different than that of IRI-active (**62**), supporting the notion that the potent IRI activity of (**62**) may be attributed to its unique conformation. With this information, we may be able to use computational simulations to rationally design glycoconjugates that have specific conformations desired for IRI activity.

REFERENCES:

1. (a) Pauling, L. *The Nature of the Chemical Bond*; Cornell University Press: Ithaca, NY, 1960. (b) Wheland, G. W. *Resonance in Organic Chemistry*; Wiley: New York, 1955. (c) Carey, F. A. *Organic Chemistry,* 6th ed.; McGraw Hill: New York, 2006. (d) Wade, L. G. *Organic Chemistry,* 6th ed.; Pearson Prentice Hall: Upper Saddle River, NJ, 2006. (e) McMurry, J. *Organic Chemistry,* 6th ed.; Brooks/Cole-Thomson Learning: Belmont, CA, 2004.

2. (a) Jiao, L.; Yuan, C.; Yu, Z.-X. *J. Am. Chem. Soc.* **2008**, *130*, 4421-4430. (b) Poschalko, A.; Welzig, S.; Treu, M.; Nerdinger, S.; Mereiter, K.; Jordis, U. *Tetrahedron*, **2002**, *58*, 1513-1518.

3. Thompson, A.; Canella, K. A.; Lever, J. R.; Miura, K.; Posner, G.H.; Seliger, H.H. *J. Am. Chem. Soc.* **1986**, *108*, 4498-4504.

4. Anderson, C.L.; Soderquist, J. A. *Tet. Lett.* **1992**, *33*, 6915-6918.

5. For recent examples of Wittig reactions using methoxymethyl(triphenyl)phosphonium salts and various strong bases, see: (a) Trost, B.M.; Pang, W.; Toste, D. F. *J. Am. Chem. Soc.*

2005, *127*, 14785-17803. (b) Owen, R. M.; Gestwicki, J.E.; Young, T.; Kiessling, L.L. *Org. Lett.* **2002**, *4*, 2293-2296. (c) Seganish, W.M.; DeShong, P. *Org. Lett.* **2006**, *8*,3951-3954. (d) Nicolau, K. C.; Wang, J; Tang, Y. *Angew. Chemie. Int. Ed.* **2008**, *47*, 1432-1435.

6. Stork, S.; Yamashita, A.; Adams, A.; Schulte, G.R.; Chesworth, R.; Miyazaki, Y.; Farmer, J. J. *J. Am. Chem. Soc.* **2009**, *131*, 11402-11406.

7. (a) Giannis, A.; Munster, P.; Sandhoff, K.; Steglich, W. *Tetrahedron* **1988**, *44*, 7177. (b) Allevi, P.; Anastasia, M.; Ciuffreda, P.; Fiecchi, A.; Scala, A. *J. Chem.Soc., Perkin Trans. 1* **1989**, 1275-1280.

8. Rathke, M.W.; Nowak, M. *J. Org. Chem.* **1985**, *50*, 2624-2626.

9. Mander, L.N.; Sethi, S.P. *Tetrahedron Lett.,* **1984**, *25*, 5953.

10. Shimizu, N.; Takesue, N.; Yasuhara, S.; Inazu, T. *Chem. Lett.* **1993**, *22*, 1807.

11. Pascal, R.; Sola, R. *Tetrahedron Lett.* **1998**, *39*, 5031-5034.

12. Garcia Lopez, M.-T.; De las Heras, F. G.; San Felix, A. *J. Carbohydrate Chemistry.* **1987**, *6*, 273-279.

13. (a) Arndt, F.; Eistert, B. *Ber. Dtsch. Chem. Ges* **1935**, *1,* 200–208. (b) Arndt, F.; Eistert, B. Patale, W. *Ber. Dtsch. Chem. Ges* **1927**, *60B,* 1364.

14. Demchenko, A.V. *Handbook of Chemical Glycosylation*; Wiley: Morlenbach, Germany, 2008.

15. Levy, D.E.; Tang, C. *The Chemistry of C-glycosides,* Vol. 13; Pergamon: Oxford, 1995.

16. Ye, T.; McKervey, M.A. *Chem. Rev.* **1994**, *94*, 1091-1160.

17. Stachowiak, K. ; Khosla, M.C.; Plucinska, K.; Khairallah, P.A.; Bumpus, F.M. *J. Med. Chem.* **1979**, *22,* 1128-1130.

18. Vasanthakumar, G.-R.; Babu, V.V.S. *J. Peptide Res.* **2003**, *61*, 230-236.

19. Hood, C. A.; Fuentes, G.; Patel, H.; Page, K.; Menakuru, M.; Park, J. H. *J. Pept. Sci.* **2008**, *14*, 97-101.

20. Müller, A.; Vogt, C.; Sewald, N. *Synlett*, **2006**, 837-841.

21. (a)Corzana, F.; Busto, J. H.; Jiménez-Osés, G.; Asensio, J. L.; Jiménez-Barbero, J.; Peregrina, J. M.; Avenoza, A. *J. Am. Chem. Soc.* **2006**, *128*, 14640-14648. (b) Corzana, F.; Busto, J. H.; Jiménez-Osés, G.; García de Luis, M.; Asensio, J. L.; Jiménez-Barbero, J.; Peregrina, J. M.; Avenoza, A. *J. Am. Chem. Soc.* **2007**, *129*, 9458-946.

Chapter 6 : Towards the synthesis of *C*-α-galactosyl-threonine glycoconjugate

6.1 ROLE OF ALIPHATIC LINKER IN THE FUNCTION OF IRI-POTENT C-LINKED AFGP (**15**)

The relationship between a glycoprotein's hydration and its ability to inhibit ice recrystallization has been described by structure-function correlation studies of *C*-linked AFGP analogues containing various carbohydrates and linkages to the peptide backbone. By altering the side chain length and position of the amide bond in the side chain of *C*-linked AFGP analogues (**6**,**14**, **18-21**), the orientation of the carbohydrate was shown to change relative to the peptide backbone. This is believed to affect how water molecules orient around the carbohydrate moiety (and subsequently the entire glycopeptide) which is an important factor required for these glycoproteins to inhibit ice recrystallization.

Interestingly, results by Liu and Ben[1] showed that a *C*-linked AFGP analogue (**15**), which contains a shortened side chain linkage and lacks an amide bond in the side chain, is more potent in IRI activity than those which contain an amide bond in the side chain.

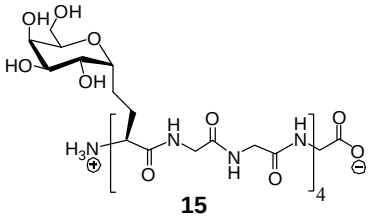

15

As the results described in the previous chapters suggests that the IRI activity of *C*-AFGP analogues is affected by the hydration of the carbohydrate and the side chain, we were interested in synthesizing analogues of (**15**) that have varying hydration properties in an attempt to (1) synthesize an analogue with increased IRI potency, and (2) to further understand the effect of hydration on glycopeptides. To this end, we subsequently focused on the effect of varying the linkage between the carbohydrate and polypeptide of analogue (**15**).

6.2 EFFECT OF SERINE AND THREONINE LINKAGES ON GLYCOCONJUGATE CONFORMATION

Recent molecular dynamic simulation studies by Corzana[2-4] and NMR analysis of contulakin-G by Kindahl and Sandström[5] have shown that there are distinct differences in glycoconjugate conformations between oxygen-linked serine- and threonine-containing glycoconjugates.

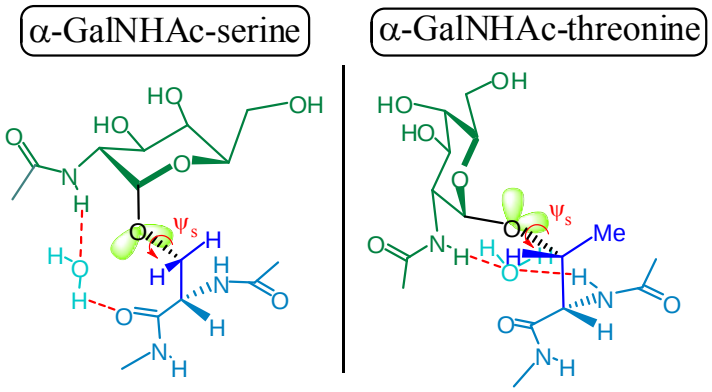

Figure 6.1 Lowest energy conformations of *O*-α-GalNHAc-serine and *O*-α-GalNHAc-threonine glycoconjugates and the presence of an intramolecular water bridge.

This change in glycoconjugate conformation is significant because this causes a drastic change in the hydration between the carbohydrate and the peptide backbone. For example, Corzana has shown that there are different water bridges between the carbohydrate and the peptide backbones of these two types of glycoconjugate residues.[2,3] In the *O*-serine glycoconjugate, a water bridge is formed between the *C*2-N-Acetyl group and the carbonyl of the serine residue.[2] However, in the threonine derivative, it is found that this water bridge consists of a common water oxygen atom bound to the NH protons of the *C*2-NHAc and threonine residue backbone, Figure 6.1.[3]

Thus, as structure-function relationship studies[6,7] have shown that threonine-containing glycoproteins possess increased antifreeze activity compared to their serine analogues (Entries 2

and 3, Table 2.1), it is possible that the hydration around the threonine-containing glycoconjugate is favourable for antifreeze activity compared to its serine-containing analogues.

Given the potent IRI activity of *C*-linked serine AFGP analogue **15**, we hypothesized that a *C*-threonine AFGP analogue (**26)** will possess even greater IRI activity, and that it will also provide insight into the factors responsible for IRI activity in *C*-linked AFGP analogues. The synthesis of (**26**) would be achieved by solid-phase peptide synthesis of the corresponding *C*-α-galactosyl-threonine building block (**26a**), Figure 6.2

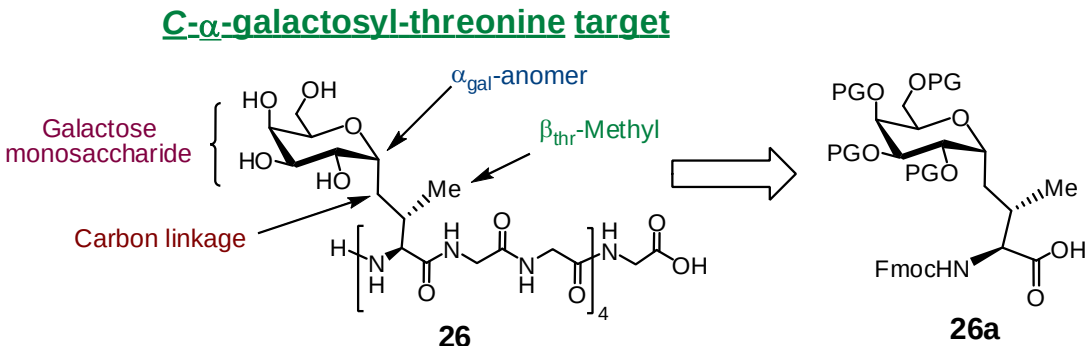

Figure 6.2 Chemical structure and key features of *C*-α-galactyl-threonine polymer (**26**), and glyconconjugate target (**26a**).

6.3 PRECEDENCE FOR C-GALACTOPYRANOSE-AMINO ACID GLYCOCONJUGATES

While similar *C*-glycosyl amino acids have previously been synthesized by other groups using various methodologies (Figure 6.3),[1,8-12] our desired *C*-α-galactose threonine target has not.

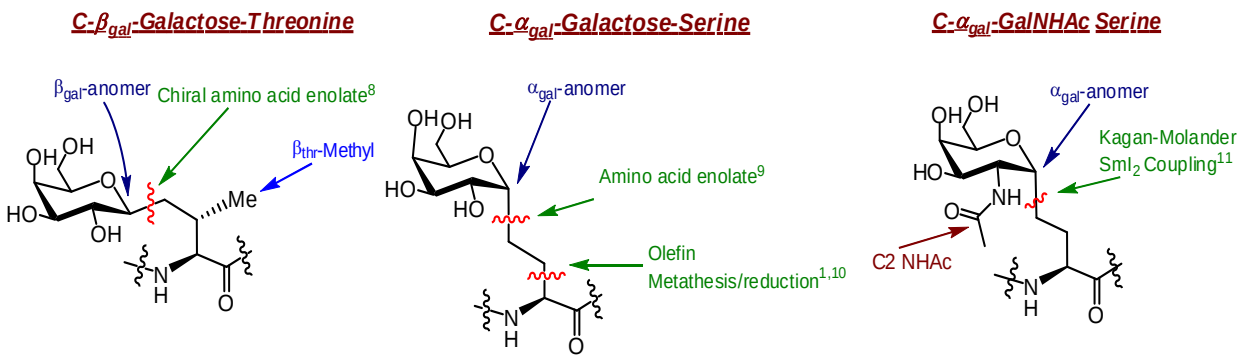

Figure 6.3 Previous syntheses of similar *C*-α-glycosyl-amino acid glyconconjugates to target, **26a**.[1,8-11]

The formation of the β_{gal}-anomer of our target has previously been reported Kihlberg,[8] who used a chiral auxiliary to install the β_{thr}-methyl group of the threonine residue, Scheme 6.1. This lengthy synthesis was achieved in 20 steps and less than 12% yield. The 1,2-trans-anomeric *C*-linkage was achieved using a Grignard reaction between a homoallylic Grignard reagent and a galactopyrano-lactone, which favours nucleophilic addition from the β-face due to steric interactions with the *C*2 benzyl group and the diaxial protons at the *C*3 and *C*5 positions.

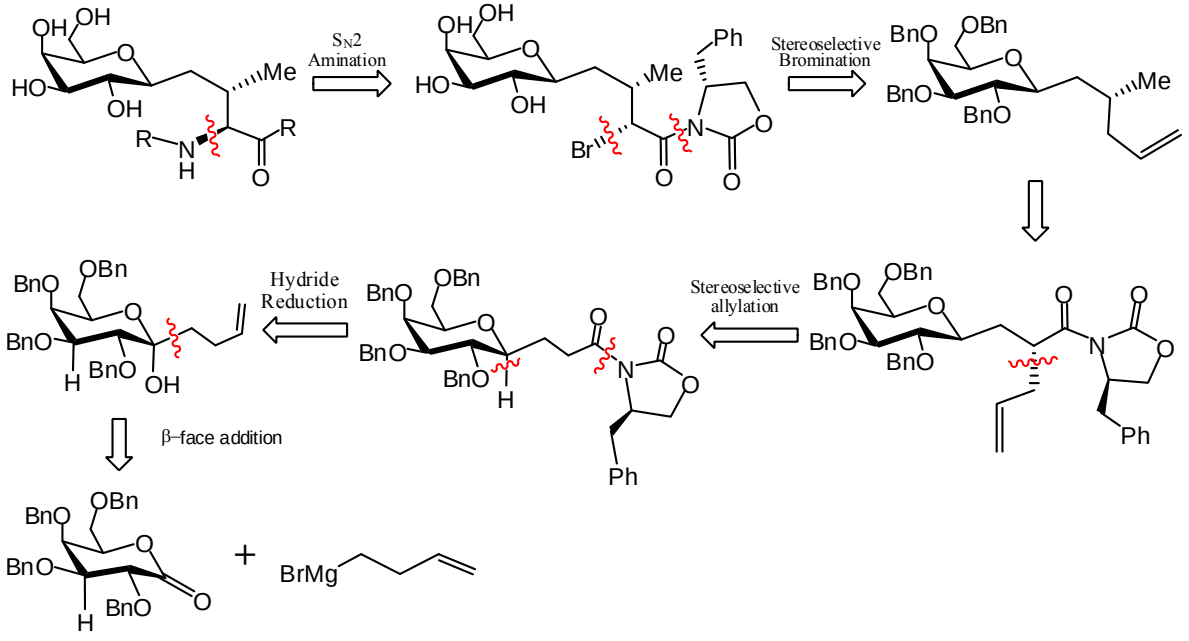

Scheme 6.1 Previous synthesis of *C*-β-linked galacto-threonine by Kihlberg.[8]

Subsequent reductive dehydroxylation of the anomeric alcohol to give the β_{gal}-anomer was achieved using boron trifluoride and triethylsilane, Scheme 6.2.[13] The undesired β_{gal}-product is favoured due to the formation of an oxocarbenium formation upon the addition of the Lewis acid; nucleophilic attack of the silane in the α-face is favoured due to the interaction of the O n→C-H σ* orbitals.[13] In addition, approach of the silane onto the β_{gal}-face would force the anomeric C-H_2 to be in the axial position, which would be disfavoued due to the *syn*-pentane interactions between the anomeric methylene group with H3 and H5.

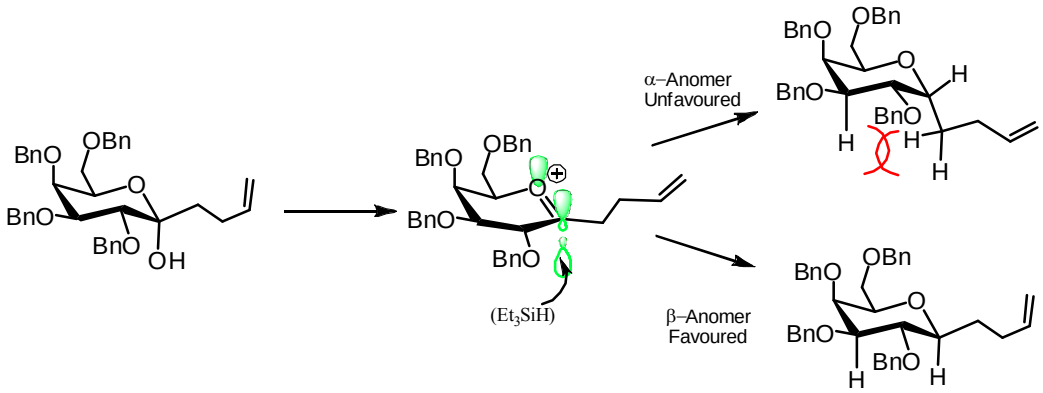

Scheme 6.2 Stereoselective hydride addition to anomeric oxocarbenium.[13]

Formation of our desired 1,2-cis-anomeric *C*-linkage has been reported for the syntheses of *C*-α_{gal}-galactopyranose-serine glycoconjugates.[9,10] Dondoni has reported the use of a silylated enolate amino acid precursor to covalently bond directly to the carbohydrate donor in an α_{gal}-configuration, Scheme 6.3.[9]

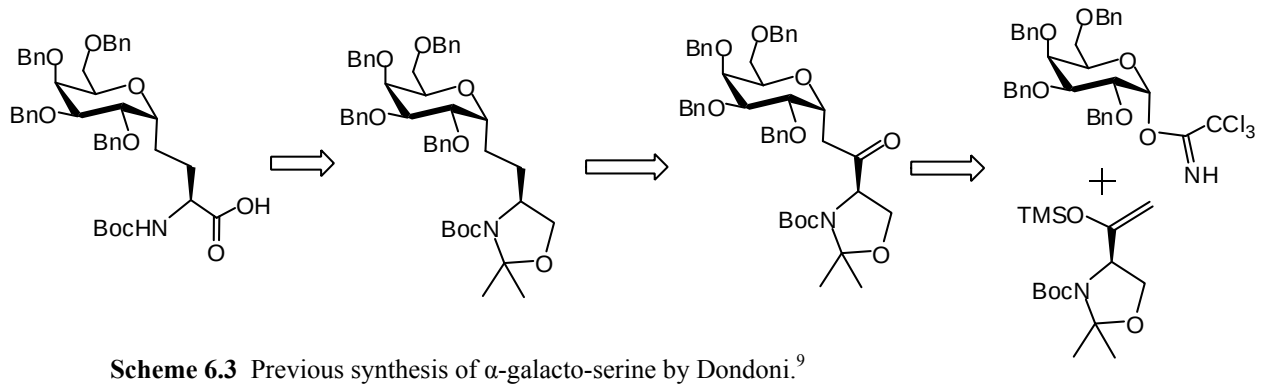

Scheme 6.3 Previous synthesis of α-galacto-serine by Dondoni.[9]

Liu[1] and Toone[10] have reported syntheses of the same *C*-α-galactosyl-serine glycoconjugate by olefination between an amino ester phosphonate and a *C*-α-galactopyranose derivative, Scheme 6.4. The glycoconjugate alkene was subsequently reduced by asymmetric reduction to afford the glycoconjugate with the proper stereochemistry.

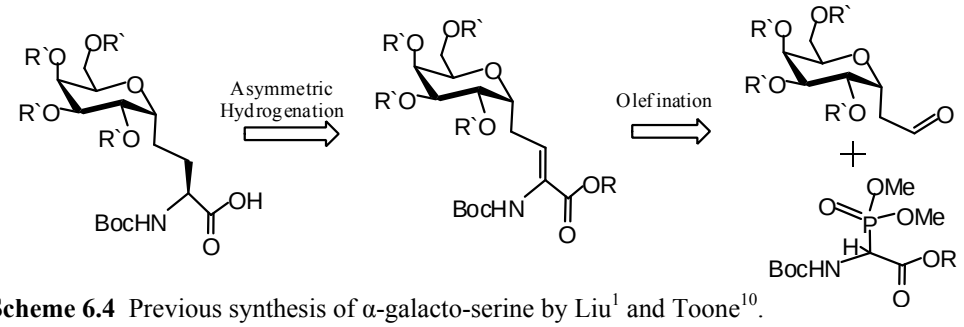

Scheme 6.4 Previous synthesis of α-galacto-serine by Liu[1] and Toone[10].

Another method to form a 1,2-cis-anomeric *C*-linkage of a galactopyranose derivative was reported by Beau and co-workers,[11] who formed a C-C bond between the anomeric position of an N-acetyl-galactosamine and the appropriate amino acid aldehyde precursor.

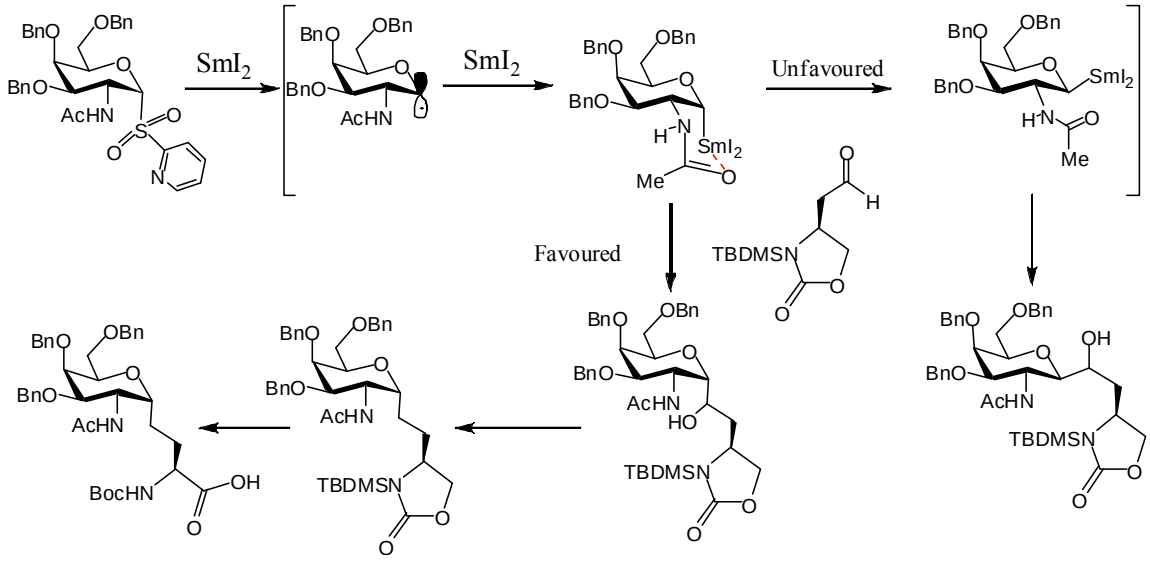

Scheme 6.5 Previous synthesis of *C*-α-N-acetylgalactosamine-serine by Beau.[11]

The stereoselectivity in the key *C*-glycosylation step was proposed to be favoured by a C2-assisted stabilization of the organo-samarium intermediate.[11,14]

6.4 RETROSYNTHESIS OF C-α-GALACTOSYL-THREONINE GLYCOCONJUGATE (**26a**)

While the aforementioned approaches elegantly show the syntheses of similar *C*-linked glycoconjugates to our desired target, they do not meet both of our desired requirements of (i) formation of a 1,2-cis anomeric *C*-linkage, and (ii) introduction of the β_{thr}-methyl group with the proper stereochemistry. However, Beau's aforementioned samarium diiodide reductive coupling approach is an attractive methodology to use for our system as the synthesis of the glycoconjugate using this method is independent of the β-position of the amino acid precursor.

Unfortunately, it has been reported that upon subjecting C2-hydroxy galacto-and gluco-pyranose derivatives to samarium diiodide reductive coupling conditions, two byproducts are

observed, Scheme 6.6. First, *syn*-elimination of the C2 group occurs readily, or secondly, the α-organosamarium species equilibrates to form the stabler trans-β-organosamarium intermediate.[15]

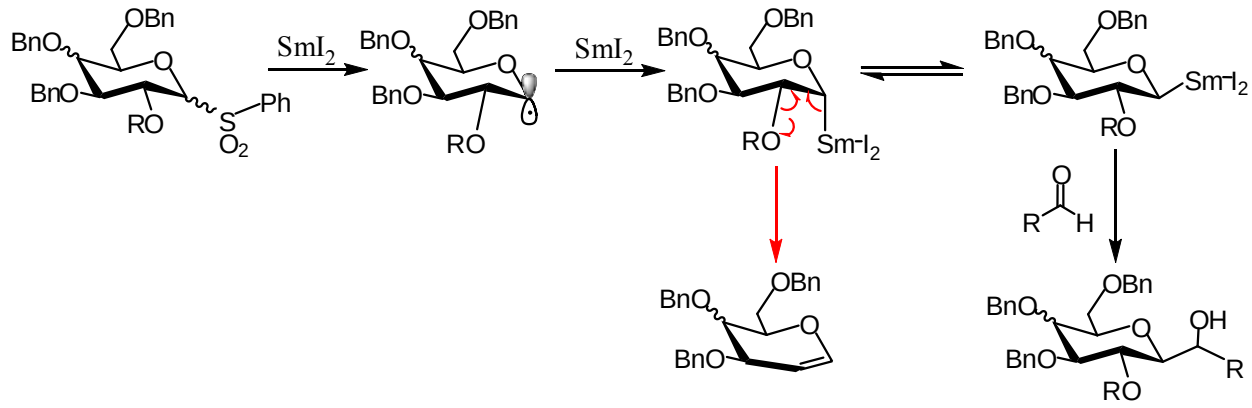

Scheme 6.6 Samarium diiodide reductive coupling of galacto- and glucopyranose.[15]

To overcome these issues, Ichikawa and coworkers reported the use of a C2 keto-glucopyranose derivative (D-*arabino*-hexopyranoside-2-ulose, **102**), which can undergo a samarium diiodide-mediated Reformatsky-type reaction to form the desired *C*-α-glycosyl linkage, Scheme 6.7.[16] The stereoselectivity of the favoured α-product is rationalized to occur due to the formation of a favourable chair-like transition state upon addition of the aldehyde to the anomeric position of the favoured twist-boat pyranose intermediate. In addition, formation of the chair-like transition state in the unfavoured twist-boat intermediate is also unfavourable due to the steric effects of the C5 axial functionality.[17]

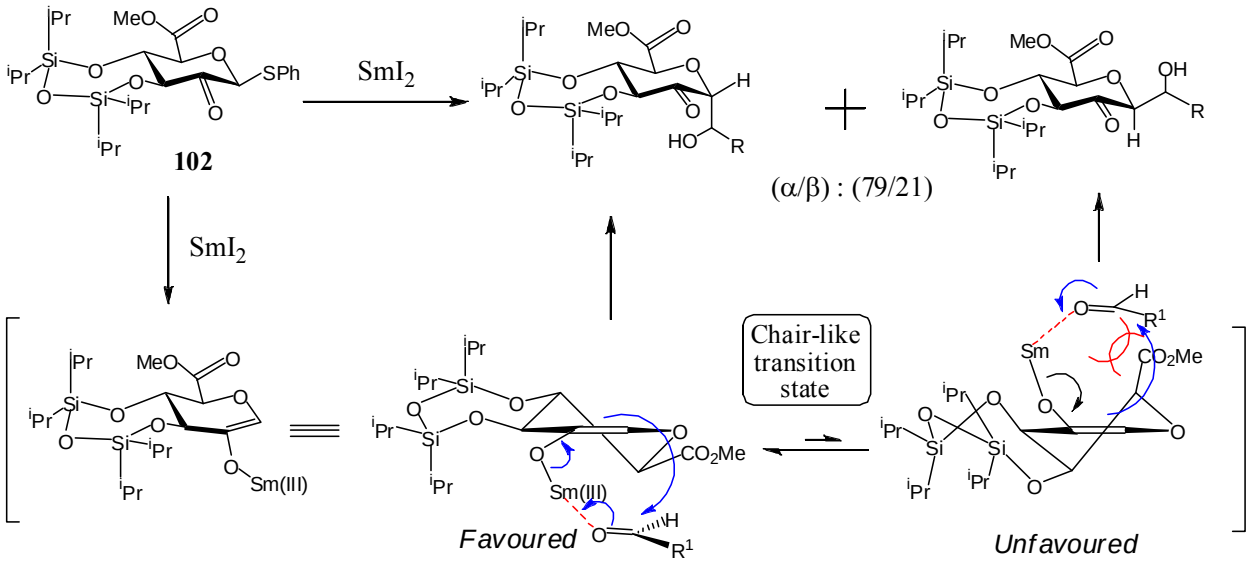

Scheme 6.7 Diastereoselective SmI_2- Reformatsky-type reductive coupling of glucopyranose.[16,17]

Therefore, it was envisioned that application of this methodology to a C2 keto-galactopyranose derivative (**103**) would result in higher α-selectivity due to increased steric effects of the C4 hydroxyl group and silylated C5 hydroxymethyl group of the C2-keto-galactopyranose, Scheme 6.8.

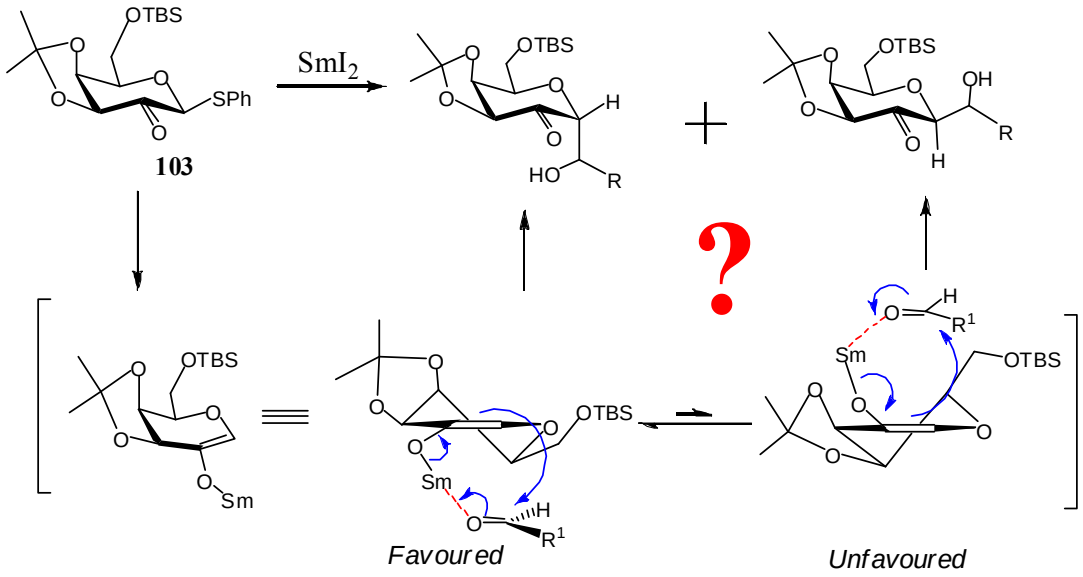

Scheme 6.8 Proposed diastereoselective SmI_2- Reformatsky reductive coupling of C2-ketogalactopyranose and aldehyde.

Therefore, retrosynthetic analysis of our desired target is shown in Scheme 6.9, and is based upon the strategy of using a C2-keto-galactopyranose, **103**, to set the anomeric *C*-linkage between the carbohydrate and the amino acid precursor.

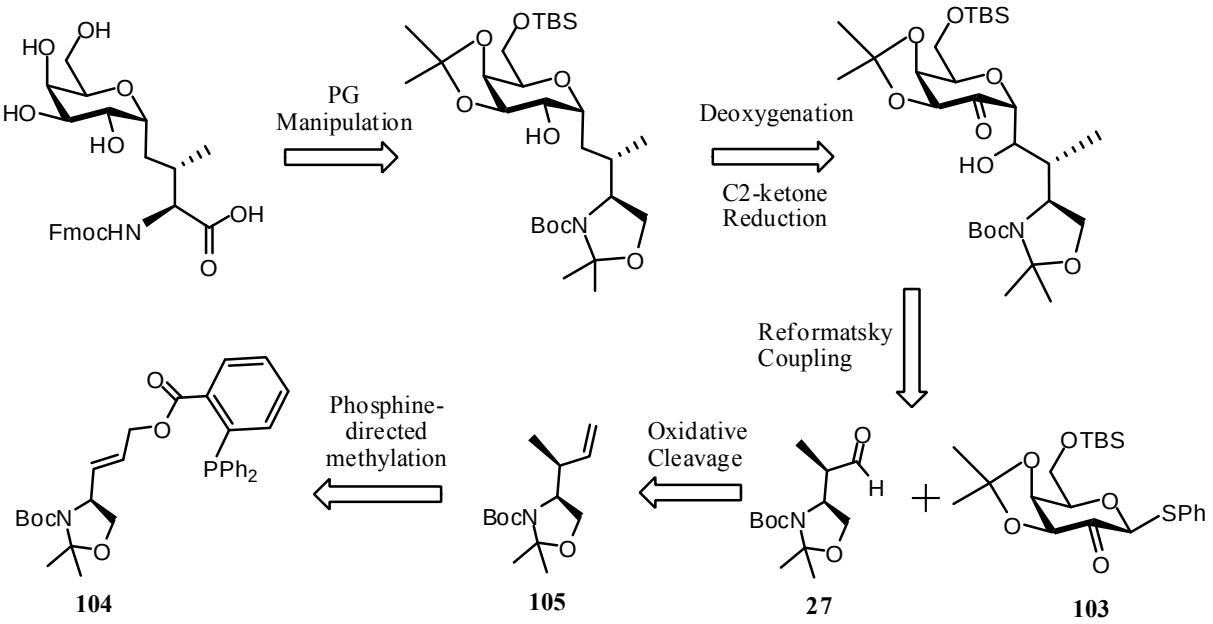

Scheme 6.9 Retrosynthesis of target building block **26a**.

Thus, final target building block (**26a**) would be synthesized by using the appropriate protecting group manipulation of the glycoconjugate precursor. The stereochemistry of the C2 hydroxyl of galactopyranose was envisioned to be set from the C2 ketone precursor by a stereoselective reduction to yield the thermodynamic equatorial hydroxyl product.[18] This C1` hydroxyl group of the precursor was envisioned to be deoxygenated using modified McCrombie-Barton procedures.[11] The key *C*-glycosylation step would be achieved using samarium diiodide of a C2 keto-galactopyranose and a threonine aldehyde precursor. The stereochemistry of the β_{thr}-methyl group would be achieved by using an organocuprate phosphine-directed S_N2` methylation as has been reported by Breit, Scheme 6.10.[19] While there are other possible methods to install the β_{thr}-methyl group with high stereoselectivity, the phosphine-directed

approach was employed due to the ability to vary the substitution at the β-position. Variation of alkyl substituents at this position would be beneficial to gain further insight into the role of hydration of *C*-linked glycoconjugates on IRI activity.

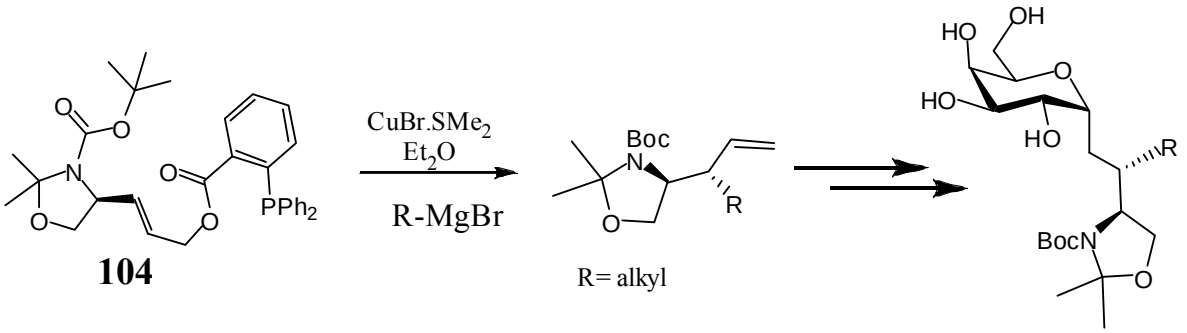

Scheme 6.10 Synthesis of threonine derivative precursor.

6.5 SYNTHESIS OF THREONINE-ALDEHYDE PRECURSOR (**27**)

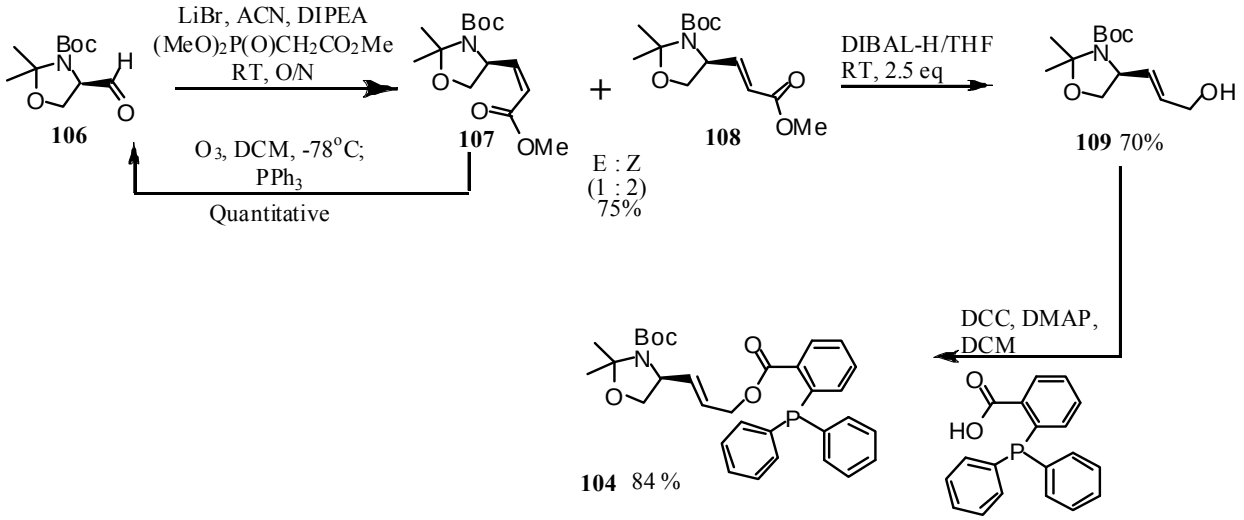

Scheme 6.11 Synthesis of threonine precursor.

Commercially available Garner's aldehyde (**106**) was subjected to homologation using a modified Horner-Wadsworth-Emmons procedure.[20] A mixture of *E*/*Z* conjugated enone was formed in a 2:1 ratio. As the desired β_{thr}-methyl group requires the use of *E*-isomer (**108**), the *Z*-isomer was oxidatively cleaved using ozonolysis to regenerate starting material (**106**). The ester

of the conjugated methyl ester was reduced using di-isobutylaluminum hydride (DIBAL-H)[21] and esterified to form the *ortho*-diphenylphosphino-phenylbenzoate (o-DPPB).[19]

Studies by Breit on allylic o-DPPB systems has shown that stereoselective allylic substitution can achieved by a phosphine-directed organocuprate addition, and is due to the presence of 1,3-allylic strain between the alkene and the phosphino-ester (Scheme 6.12).[19,22]

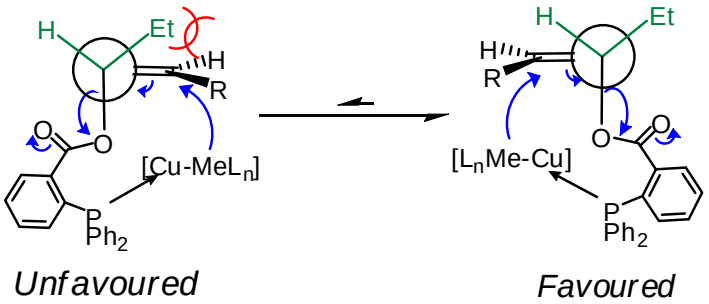

Scheme 6.12 Proposed mechanism for stereoselective phosphine-directed organocuprate $S_N2`$ allylic displacement by Breit.[19,22]

However, in our system, this explanation is insufficient due to the lack of substitution at the allylic position in (**104**), Scheme 6.13. Instead, it is proposed that the presence of the N-Boc group acts to : (1) direct the *anti*-addition of the methyl cuprate, and (2) hinder *syn*-addition of the methyl cuprate.

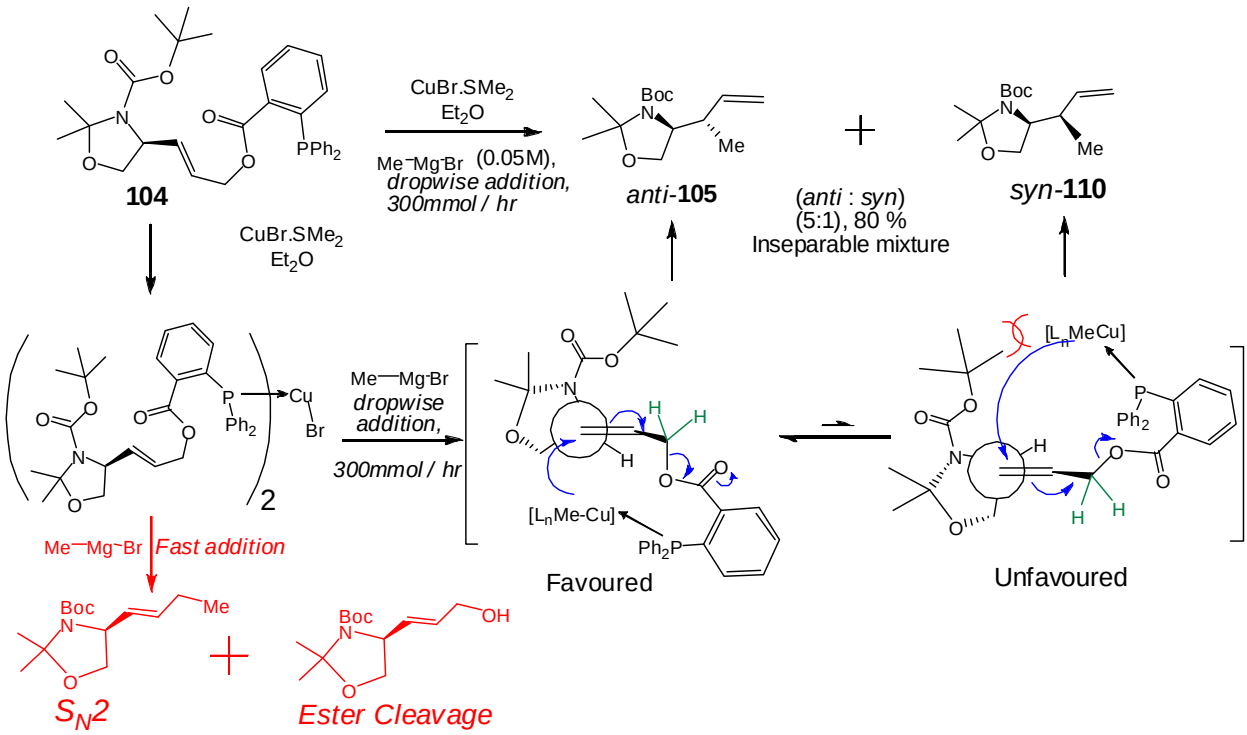

Scheme 6.13 Stereoselective phosphine-directed organocuprate $S_N2`$ allylic methylation.

Therefore, to install the proper stereochemistry of the β_{thr}-methyl group, the allylic phosphine (**104**) was pre-complexed with copper bromide dimethyl sulfide to form diphosphino-copper complex, as was previously determined by X-Ray crystallography.[22] A diluted methyl Grignard solution (0.05M) was subsequently added dropwise by syringe pump at 300 µmol per minute. This slow addition of the Grignard reagent was crucial for the success of this reaction, as faster addition rates resulted in side reactions such as ester cleavage and S_N2 displacement of the aryl ester (Scheme 6.13, shown in red). Slow addition permits transmetallation of methyl magnesium bromide with copper bromide to form methyl cuprate in situ. As the copper is chelated to the phosphine, the bound methyl group is able to stereoselectively displace the aryl ester via a $S_N2`$ allylic reaction. Under these conditions, an inseparable mixture of *anti*/*syn* (**105**/**110**) was obtained in 80% yield. Using GC/MS analysis, Breit reported approximately a

5.7:1 (*anti/syn*) ratio.[19] Unfortunately, in our hands, we were unable to quantify this diastereomeric ratio using GC/MS due to unsufficient peak resolution. However, comparison of the obtained ^{13}C-NMR spectra (Figure 6.4) with literature values[19] shows that the major product is the *anti* diastereomer.

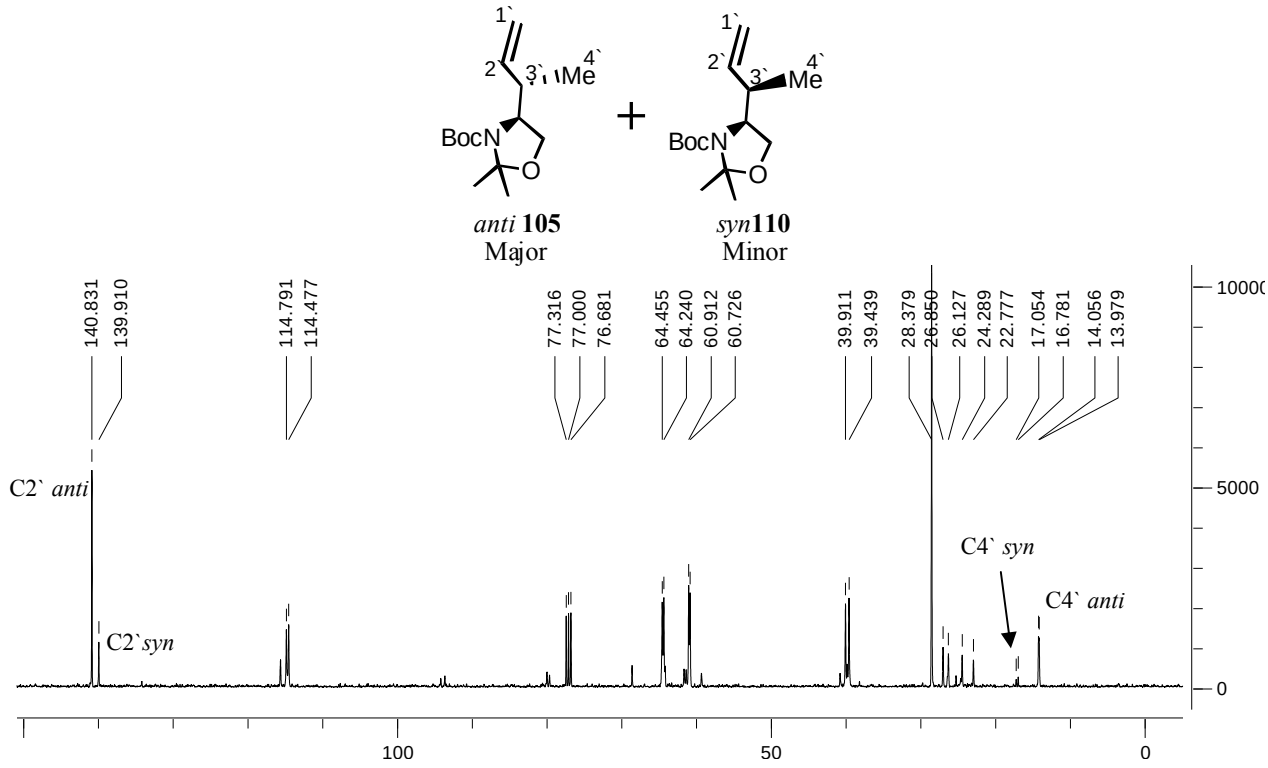

Figure 6.4 ^{13}C-NMR spectrum of mixture of alkenes *anti*-**105** (major) and *syn*-**110** (minor).

The mixture was then oxidatively cleaved using ozonolysis to form aldehydes (**27**) and (**111**). Fortunately, these compounds were separable by silica gel chromatography.

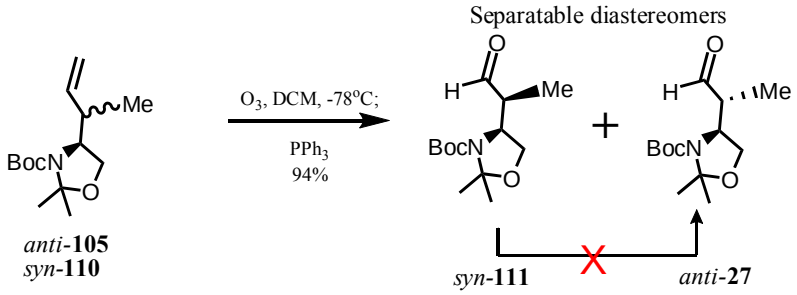

Scheme 6.14 Ozonolysis of terminal alkenes **105** and **110**.

To confirm that (**111** and **27**) were indeed diastereomers, aldehyde (**111**) was synthesized by using a different starting material. Breit reported the use of *Z*-alkenes for the $S_N2`$ reactions resulted in significant diastereoselectivity for the *syn* diastereomer (*syn* : *anti* = 32.3 : 1) due to an increase in (1,3)- allylic strain.[19] Thus, subjecting *Z*-enone (**107**) to the aformementioned synthetic pathway (Schemes 6.11 and 6.13), will yield mostly aldehyde (**111**) compared to its diastereomer (**27**), Scheme 6.15.

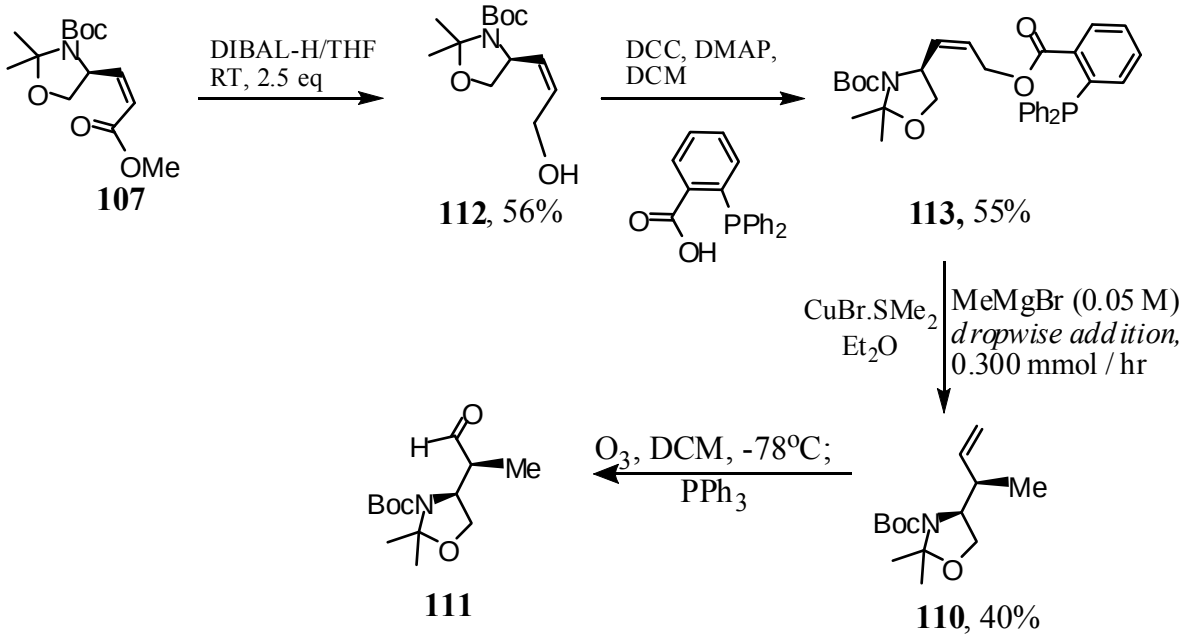

Scheme 6.15 Synthesis of aldehyde *syn*-(**111)** from Z-enone (**107)**.

Methylation of (**113**) yielded (**110**) in 40% yield, and examination of the ^{13}C-NMR spectrum of this product (Figure 6.5) matched literature values for (**110**)[19] and the minor diastereomer previously shown in Scheme 6.13 and Figure 6.4. Ozonolysis of (**110**) produced the corresponding aldehyde (**111**). Thin layer chromatography, infrared, and mass spectroscopy analysis showed that the product formed from Scheme 6.15 yielded a product that matched (**111**) as previously made in Scheme 6.13. Consequently, it was concluded that the two compounds isolated in Scheme 6.13 were indeed diastereomers.

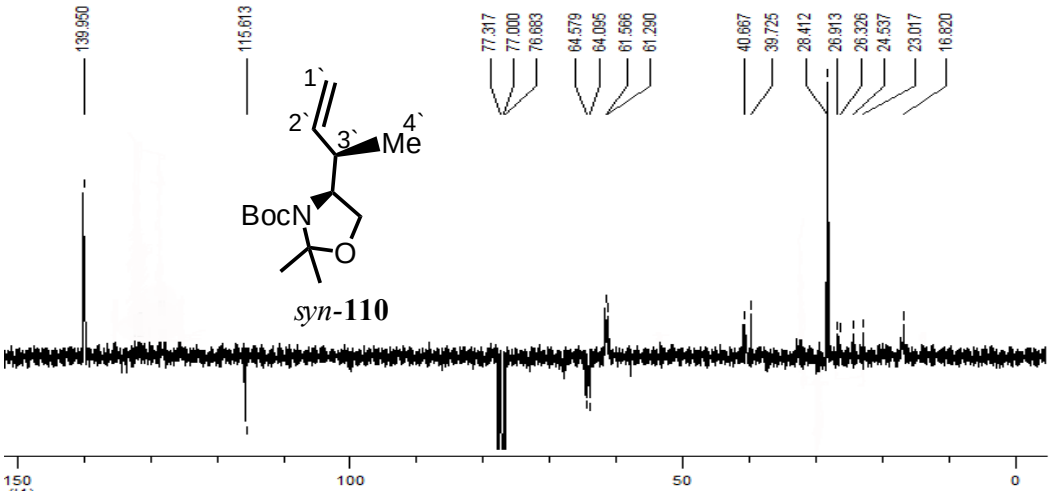

Figure 6.5 ^{13}C DEPT-135 NMR (101 MHz) spectrum of *syn*-**110** .

Attempts to epimerize the undesired *syn* diastereoisomer into the desired *anti* isomer are shown in Table 6.1. However, the aldehydes were prone to decomposition rather than epimerization.

Table 6.1 Attempts at epimerization of aldehyde (**111)** to (**27)**.

	Epimerization Conditions	Result
1	HOAc, (Room Temp, 40^{o}C or sonication)	No Reaction or decomposition
2	PivOH, (Room Temp, 40^{o}C or sonication)	No Reaction or decomposition
3	TsOH,	Decomposition
4	^{t}BuOK/^{t}BuOH	Decomposition

6.6 SYNTHESIS OF (C2-KETO-GALACTOPYRANOSE) PRECURSOR

To form the desired C2 keto-galactopyranose precursor (**103**) to be used for the Reformatsky coupling procedure, a suitable anomeric functional group that could be reductively cleaved by samarium diiodide was required. Since Ichikawa has reported the use of an anomeric thiophenyl group in their C2 keto-glucopyranose derivative for Reformatsky coupling,[16] we decided to use a similar C2 keto-galactopyranose as our starting material.

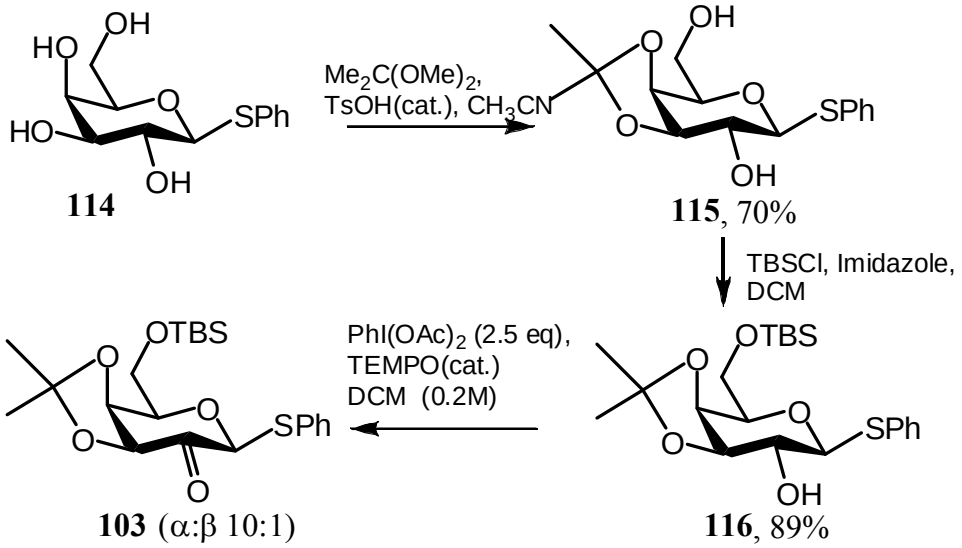

Scheme 6.16 Synthesis of C2-keto-galactopyranoside

Synthesis of (**103**) started with the selective protection of thiophenyl-β-D-galactopyranoside (**114)** to yield the protected C3 and C4 positions using dimethoxypropane and catalytic *para*-toluene sulfonic acid.[23] The primary C6 hydroxyl group was then selectively protected with the sterically-demanding tert-butyldimethyl silyl group. The C2 hydroxyl was then oxidized using TEMPO and iodobenzene di-acetate.[24] To increase the rate of oxidation, increased reaction concentrations (>0.15 M) were required. Diluted concentrations resulted in product decomposition prior to full consumption of the starting material. Unfortunately, this

product was very unstable and immediate reaction with SmI_2 and amino acid aldehyde precursor (**27**) was required.

6.7 SYNTHESIS OF C-GALACTOSYL-THREONINE GLYCONJUGATE CORE

Samarium diiodide-mediated Reformatsky-type reductive coupling between *C*-glycoside (**103**) and threonine precursor (**27**) was attempted using a variety of methods, Table 6.2.

Table 6.2 Attempts at *C*-glycosylation using SmI_2. Method A: To 3.0 equiv. 0.1M SmI_2 solution, dropwise add **103** and stir. Bubble in a solution of O_2(g) until blue colour turns to yellow. Then dropwise addition of a solution of **27.** Method B: To 3.0 equiv. 0.1M SmI_2 solution, dropwise add **103** and stir. Transfer to a solution of **27**. Method C: Barbier Conditions - Premix **103** + **27**, dropwise add 2.2 equiv. 0.1M SmI_2 /THF solution.

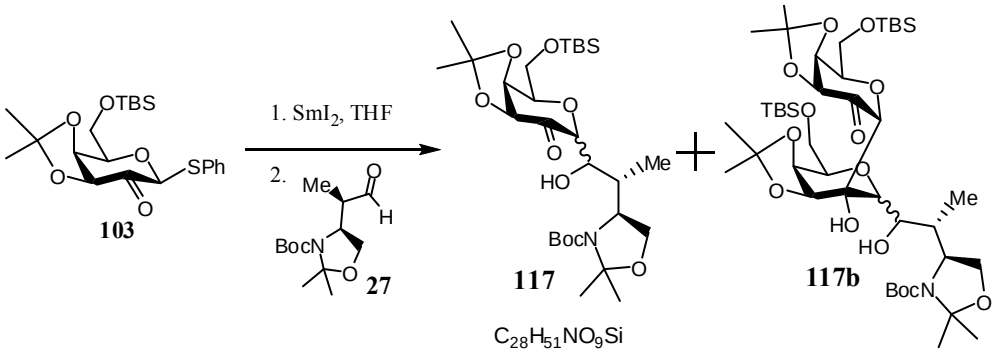

Procedure	Reaction Temp (^oC)	% Yield 117	% Yield 117b
Method A	-78	30	30
Method B	-78	30	10
Method C	-78	0	0
	-10	50	0
	0	32	0
	22	34	0

Of the various compounds that were formed in these reaction attempts, Barbier conditions[25] provided the least amount of byproducts in the reaction. The desired *C*-linked glycoconjugate (**117**) was isolated by column chromatography, and was confirmed by analysis of the electrospray ionization mass spectra (calculated for $[C_{28}H_{51}NO_9Si\ [M+H]^+$ = 574.341; $[M+Na]^+$ = 596.323; found 574.288, 596.270). Unfortunately, unambiguous characterization of

this *C*-glycoconjugate by NMR was not possible due an unseparable mixture of speculated α and β isomers, C_{1}` hydroxyl group diastereomers, and also the presence of rotamers of the Boc-protected oxazoline.

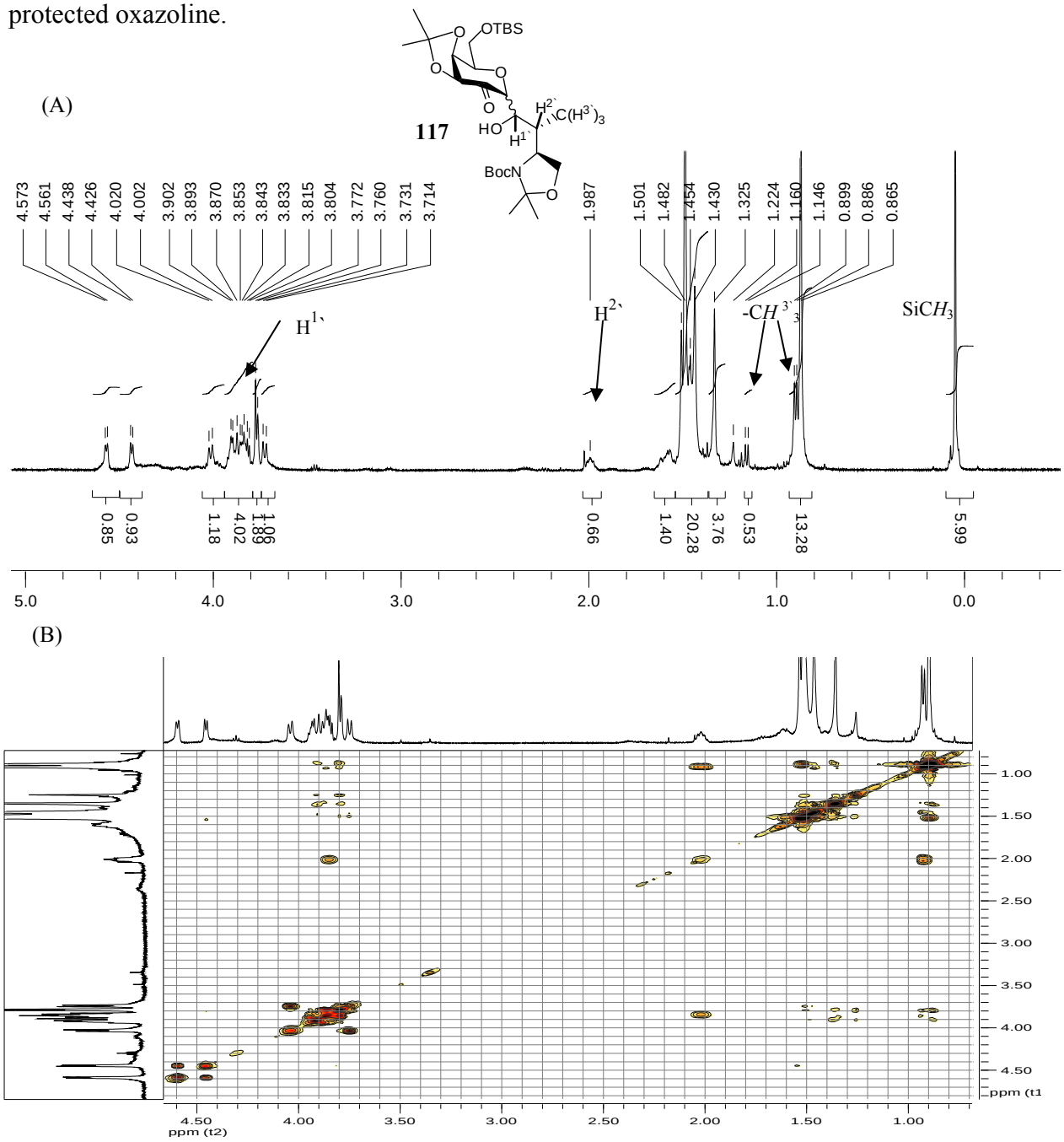

Figure 6.6 (A) Partial ^{1}H NMR spectra (500 MHz), and (B) Partial 2D-COSY NMR spectra of a diastereomeric mixture of *C*-linked glycoconjugate core (**117**).

Figure 6.6A shows an example of the ^{1}H NMR (500 MHz) of the inseparable diastereomeric mixture. Partial proton assignments were achieved using 2D-COSY NMR (Figure 6.6B). As compound (**117**) does not have a C2-galactopyranose proton (H2), determination of the anomeric configuration via coupling constant determination is not possible. Thus to assign the configuration of the anomeric position, NOESY experiments are necessary to determine the anomeric configuration.[16] However, due to the number of compounds isolated, this was not possible. Therefore, the actual anomeric stereochemistry could not be confirmed at this step.

Consequently, the mixture of products was subjected to deoxygenation conditions because the outcome of this reaction would eliminate 4 of the possible products (the two C_1` hydroxyl diastereomers of both the α- and β-*C*-glycosides). Variations of the Barton-McCombie deoxygenation procedures were used in an attempt to remove the $C_1$` hydroxyl groups, Table 6.3.

However, manipulation of the C1` hydroxyl group proved to be difficult, as this functional group was not very reactive, possibly due to it being sterically hindered by the large adjacent carbohydrate and the N-Boc-protected oxazoline. As reaction conditions were altered to increase reaction rates, increased amounts of elimination product (**118**),[16] or other degradation products were also formed.

Table 6.3 Attempts at deoxygenation of *C*-linked glycoconjugate **117**.

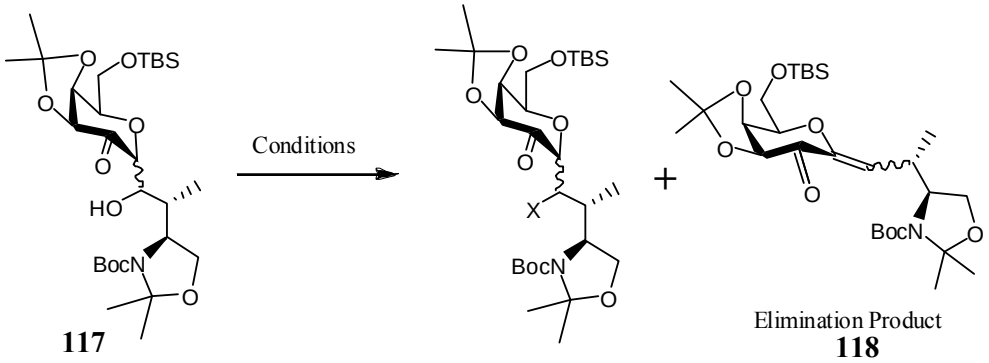

117 **118**

	X =	Conditions	Result
1	Im-C(S)-O -	90 °C, 10 eq. Im_2CS, Toluene	Decomposition
2	Im-C(S)-O -	75 °C, 5.0 eq. Im_2CS, THF	No Reaction
3	Im-C(S)-O -	60 °C, 10.0 eq. Im_2CS, THF	StartingMaterial or Elimination Product (**118**)
4	PhO-C(S)-O-	3.0 eq. PhO-C(S)-Cl, 1.4 eq DMAP, CH_3CN	No Reaction
5	I	1.0 eq. PPh_3, 1.2 eq. I_2, 1.0 eq. imidazole, CH_2Cl_2	C6 TBS cleavage
6	Br	1.3 eq. PPh_3, 1.3 eq. CBr_4, Et_2O	Decomposition
7	Br	3.0 eq. PPh_3, 4.5 eq. CBr_4, Et_2O, 4.5 eq. pyr	Decomposition
8	H_3C-$S(O)_2$-O-	1.5 eq. $H_3CS(O)_2Cl$, 1.5 eq. NEt_3, DCM , 0°C	Elimination (**118**)

Elimination byproduct (**118**) may occur via an E1cB mechanism of (**117**) by deprotonation of the anomeric centre to form a stabilized enolate anion (Scheme 6.17); movement of electrons from the resulting enolate anion is then able to displace the leaving group in the β-keto position to form the α,β-unsaturated enone.

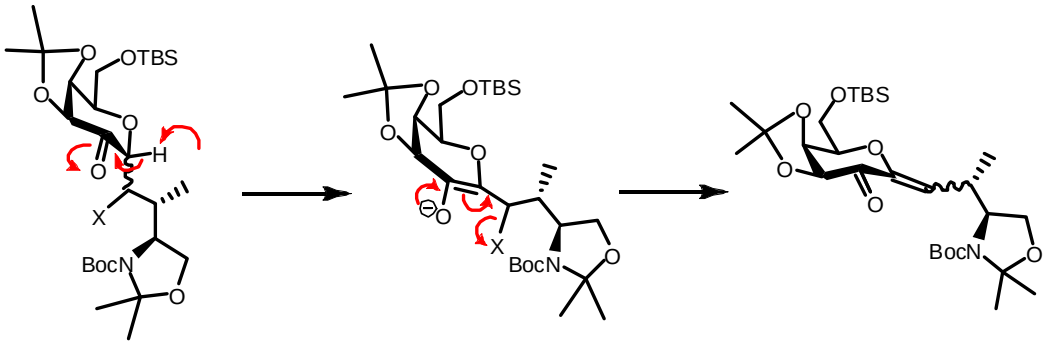

Scheme 6.17 E1cB elimination of *C*-linked glycoconjugate to produce

While the alkene of conjugated enones can generally be reduced using typical conditions such as heterogeneous hydrogenation and conjugate nucleophilic addition/selective protonation, in our system, it is likely that reduction will result in the formation of the least-sterically hindered undesired *C*-β-linked anomer, as has been previously reported by Ichikawa on the C2-keto glucose derivative.[16]

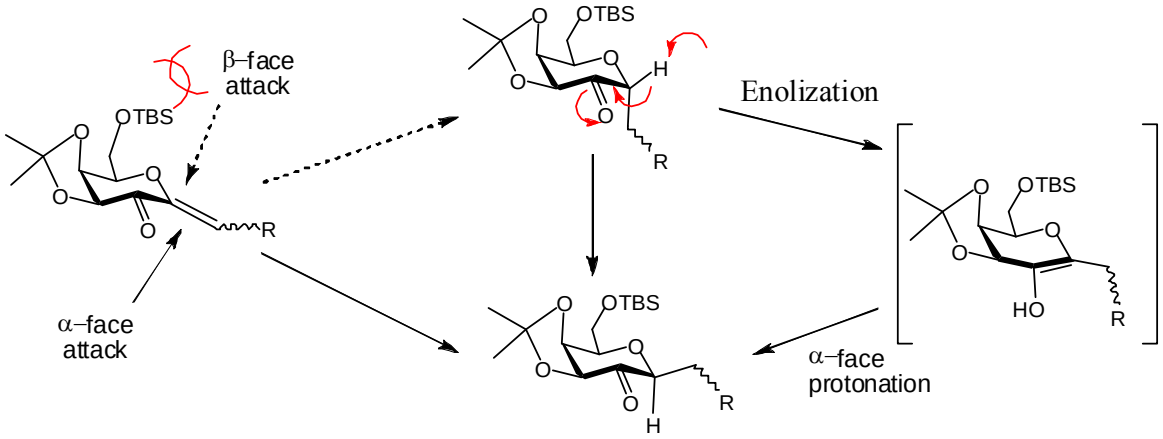

Scheme 6.18 Proposed formation of β-anomer by reduction of enone **118**.

The presence of the C2 ketone proved to be a difficult challenge in accessing the desired *C*-glycoconjugate due to the increased acidity of the anomeric proton. This increases the formation of undesired side reactions such as epimerization and eliminations. Therefore, a

revision of the synthetic route was required in which the C2 ketone is reduced earlier in the synthetic sequence.

6.8 REVISED SYNTHETIC ROUTE

Upon revision of the synthetic route, increased stability of the carbohydrate moiety was desired. Thus, the protecting group at the C6 position of glycosyl donor (**103**) was substituted for a more stable triisopropylsilyl (TIPS) protecting group (**119**).

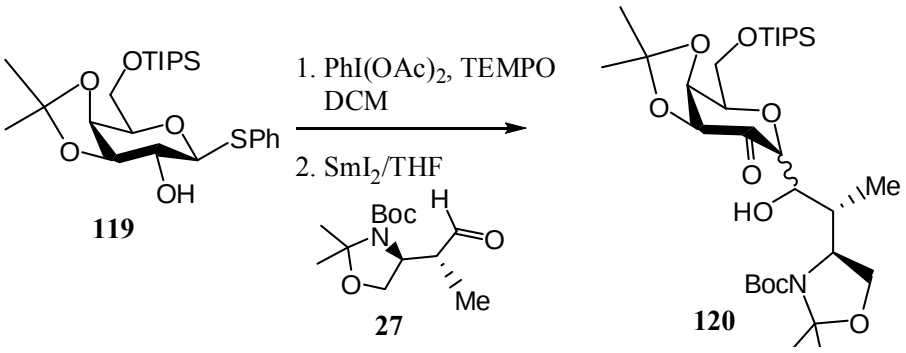

Scheme 6.19 Formation of *C*-linked glycoconjugate **120** from **119**.

C2-oxidation and *C*-glycosylation was performed in a similar fashion as previously described, Scheme 6.19. The next revision in the synthetic route was to reduce the C2 ketone prior to selective deoxygenation of the C1` position, Scheme 6.20. The two free hydroxyl groups are envisioned to be selectively protected using the sterically demanding pivaloyl chloride (Route A or B).[26] Subsequent deoxygenation reactions[11,27] would then enable the formation of the core of the *C*-galactosyl threonine target.

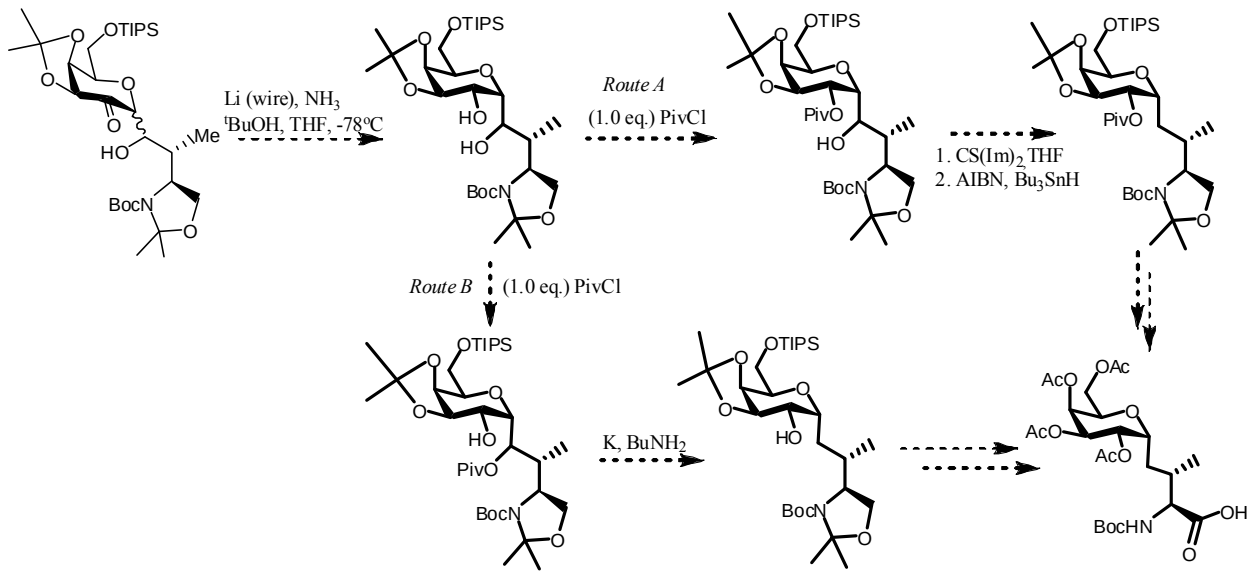

Scheme 6.20 Revised synthetic route for synthesis of C-α-galactosyl threonine target

6.9 CHAPTER SUMMARY

This chapter describes attempts to synthesize a *C*-α-galactosyl-threonine glycoconjugate. To set the stereochemistry of the threonine methyl group, a phosphine-directed organocuprate S_N2`approach was used. This approach was used due to the ease in substitution at the β-threonine position for other alkyl groups. This was envisioned to be useful to allow for the synthesis of various *C*-α-galactosyl-threonine derivatives. To obtain the *C*-α-glycoconjugate, SmI_2-mediated reductive coupling was used via a C2 keto-galactopyranose derivative. Unfortunately, the numerous diastereomers and rotamers present in the isolated product prevented unambiguous structural determination. Although attempts to proceed with the synthesis were performed, the subsequent deoxygenation and further reduction of the C2 ketone was unsuccessful.

REFERENCES:

1. Liu, S.; Ben, R. N. *Org. Lett.* **2005**, *7*, 2385-2388.

2. Corzana, F.; Busto, J. H.; Jiménez-Osés, G.; Asensio, J. L.; Jiménez-Barbero, J.; Peregrina, J. M.; Avenoza, A. *J. Am. Chem. Soc.* **2006**, *128*, 14640-14648.

3. Corzana, F.; Busto, J. H.; Jiménez-Osés, G.; García de Luis, M.; Asensio, J. L.; Jiménez-Barbero, J.; Peregrina, J. M.; Avenoza, A. *J. Am. Chem. Soc.* **2007**, *129*, 9458-9467.

4. Corzana, F.; Busto, J. H.; García de Luis, M.; Fernandez-Tejada, A.; Rodriguez, F.; Jiménez-Barbero, J.; Avenoza, A.; Peregrina, J. M. *Eur. J. Org. Chem.* **2010**, 3525-3532.

5. (a) Kindahl, L.; Sandström, C.; Craig, A.G.; Norberg, T.; Kenne, L. *Can. J. Chem.* **2002**, *80*, 1022-1031. (b) Kindahl, L.; Kenne, L.; Sandström, C. *Can. J. Chem.* **2005**, *83*, 156-165.

6. (a) Frauenfelder, H.; Fenimore, P. W.; McMahon, B. H. *Biophys. Chem.* **2002**, *98*, 35–48. (b) Bouvet, V.R. Ph. D. Dissertation Thesis. University of Ottawa, 2006. (c) Chao, H.; Houston, M. E.; Hodges, R.S.; Kay, C.M.; Sykes, B.D.; Loewen, M.C.; Davies, P.L; Sonnichsen, F.D. *Biochemistry*, **1997**, *36*, 14652-14660.

7. Tachibana, Y.; Fletcher, G. L.; Fujitani, N.; Tsuda, S.; Monde, K.; Nishimura, S. *Angew. Chem. Int. Ed.* **2004**, *43*, 856-862.

8. Gustafsson, T.; Saxin, M.; Kihlberg, J. *J. Org. Chem.* **2003**, *68*, 2506-2509.

9. (a) Dondoni, M.; Marra, A.; Massi, A. *Chem. Commun.* **1998**, 1741. (b) Dondoni, M.; Marra, A.; Massi, A.; *J. Org. Chem.* **1999**, *64*, 933.

10. Debenham, S.D.; Debenham, J.S.; Burk, M.J.; Toone, E.J. *J. Am. Chem. Soc.* **1997**, *119*, 9897.

11. Urban, D.; Skrydstrup, T.; Beau, J.-M. *Chem. Commun.* **1998**, 955.

12. For Recent Reviews on *C*-Glycosylation, see: (a) Levy, D.E.; Tang, C. *The Chemistry of C-glycosides,* Vol. 13; Pergamon: Oxford, 1995 (b) Beau, J.-M.; Gollagher, T. *Topics Curr. Chem.* **1997**, *187*, 1-54. (c) Sinaÿ, P. *Pure & Appl. Chem.* **1997**, *69*, 459-463. (d) Nicotra, F. *Topics Curr. Chem.* **1997***, 187*, 55-83. (d) Du, Y.; Linhardt, R.J. *Tetrahedron*, **1998**, *54*, 9913-9959.

13. Terauchi, M.; Abe, H.; Matsuda, A.; Shuto, S. *Org. Lett.* **2004**, *6*, 3751-3754.

14. (a) Urban, D.; Skrydstrup, T.; Beau, J.-M. *J. Org. Chem.* **1998**, *63*, 2507. (b) Urban, D.; Skrydstrup, T.; Riche, C.; Chiaroni, A.; Beau, J.-M. *Chem. Commun.* **1996**, 1883-1884.

15. Miquels, N.; Doisneau, G.; Beau, J.-M. *Angew. Chem. Int. Ed.* **2000**, *39*, 4111-4114.

16. (a) Ichikawa, S.; Shuto, S.; Matsuda, A. *Tet. Lett.* **1998**, *39,* 4545-4528. (b) Ichikawa, S.; Shuto, S.; Matsuda, A. *J. Am. Chem. Soc.* **1999**, *121,* 10270-10280.

17. Kodama, T.; Shuto, S.; Ichikawa, S.; Matsuda, A. *J. Org. Chem.* **2002**, *67*, 7706-7715.

18. (a) House, H. O. *Modern Synthetic Reactions*, 2nd Ed., W. A. Benjamin, 1972. Menlo Park, Californiap. pp152-158. (b) Nasipuri, D. *Stereochemistry of Organic Compounds - Principles and Applications*, 2nd Ed. New Age International Ltd., 1994. Daryaganj, New Delhi. pp395-397. (c) Huffman, J. W.; McWhorter, W. W. *J. Org. Chem.* **1979**, *44,* 594-599. (d) Pradhan, S. K. *Tetrahedron* **1986**, *42*, 6351-6388.

19. Spangenberg, T.; Schoenfelder, A.; Breit, B.; Mann, A. *Org. Lett*. **2007**, *9*, 3881-3884.

20. Rathke, M.W.; Nowak, M. *J. Org. Chem.* **1985***, 50*, 2624-2626.

21. Devel, L.; Hamon, L.; Becker, H.; Thellend, A.; Vidal-Cros, A. *Carbohydrate Res.* **2003**, *338*, 1591-1601.

22. Demel, P.; Keller, M.; Breit, B. *Chem. Eur. J.* **2006**, *12*, 6669-6683.

23. (a) Kitamura, M.; Isobe, M.; Ichikawa, Y.; Goto, T. *J. Am. Chem. Soc.* **1984***, 106*, 3252. (b) Mori, K.; Maemoto, S. *Liebigs Ann. Chem.* **1987**, 863.

24. De Mico, A.; Margarita, R.; Parlanti, L.; Vescovi, A.; Piancatelli, G. *J. Org. Chem.* **1997**, *62*, 6974-6977.

25. For a detailed SmI_2 procedure, see experimental methods and Data Section.

26. Grove, J.J.C.; van Heerden, P.S.; Ferreira, D.; Bezuidenhoudt, B.C.B. *Tetrahedron Letters* **2010**, *51*, 57-59.

27. Barrett, A. G.; Godfrey, C. R. A.; Hollinshead, D.M.; Prokopiou, P.A.; Barton, D. H. R.; Boar, R. B.; Joukhadar, L.; McGhie, J. F.; Misra, S. C. *J. Chem. Soc., Perkin Trans.1*. **1981**, 1501-1509.

CONCLUSIONS AND FUTURE WORKS

The overall aims of this work were to (1) determine the factors of a solute that are responsible for inhibiting ice recrystallization, and (2) synthesize AFGP analogues that are potent ice recrystallization inhibitors. These goals are important to achieve because of their high potential for various applications such as food and organ cryo-preservation.

To achieve the first goal, we initially assayed a variety of commercially available mono- and disaccharides for their ability to prevent ice recrystallization; it was observed that the carbohydrates possessed different levels of ice recrystallization inhibition (IRI) activity. Correlation of this data to the respective hydration properties of the carbohydrates led to the hypothesis that the ability of a carbohydrate to disturb its nearby water molecules is important to hinder the transfer of bulk water molecules to the QLL and subsequently the ice lattice. We believe a significant contributing factor that influences the ordering of bulk water molecules is the relative density of water molecules in the hydration layer of the carbohydrate. We refer to this term as the *Hydration Index* (*HI*), and it is directly proportional to the IRI activity of a carbohydrate. The significance of this parameter is that it provides further evidence that the mechanism of action for ice recrystallization is different than that of thermal hysteresis.

An important aspect that still needs to be examined further is the effect of the anomeric stereochemistry and substituents on IRI activity. The work described in Section 3.6 has shown inconsistent results with the *C*-linked glycosyl allyl derivatives (**10** and **11**). Synthesis of the β-anomers of *C*-allyl manno- and talopyranosides, along with other anomeric substituents would provide further insight into the influence of the anomeric position on IRI activity.

For the second goal, we rationally designed and synthesized various *C*-linked AFGP analogues that contain an amide bond in the sidechain (between carbohydrate and the peptide backbone). We initially hypothesized that a decrease in the sidechain length would be beneficial for IRI activity because this would restrict the conformational flexibility of the carbohydrate, which may enable optimal interactions with its nearby waters to prevent ice growth. However, IRI assay analysis of *C*-linked analogues (**18** and **19**, containing a shortened sidechain) showed that these analogues did not possess any activity. Molecular dynamic (MD) simulations revealed that IRI-active analogue (**6**) attains a unique lowest energy conformation, such that the carbohydrate is 'folded back' onto its hydrophobic side chain and backbone. In contrast, IRI-inactive analogues were unable to attain this conformation, and the carbohydrates in these analogues were fully exposed to the bulk solvent. Next, we explored the significance of the amide bond in the sidechain and its role in affecting the ability of an analogue to inhibit ice recrystallization. To this end, we designed and synthesized analogues (**20** and **21**) that contain an amide bond at various positions in the side chain. The IRI activities of these analogues were performed and show weak activity. MD simulations showed that in model systems of these analogues, their conformations are different than that of IRI-active (**6**), supporting the notion that the potent IRI activity of (**6**) may be attributed to its unique glycoconjugate conformation.

To confirm this hypothesis, it is necessary to determine the overall solution conformation of the entire glycopolymer. In addition, an accurate calculation of the numbers and nature of the nearby water molecules (in the hydration shell and nearby in solution) will be important to determine the exact role that hydration of a glycopeptide has on IRI activity.

To further investigate and determine what structural features of the sidechain in *C*-linked AFGP analogues are important for IRI activity, we targeted the synthesis of a *C*-α-galactosyl-threonine glycoconjugate as threonine residues in AFPs and AFGPs are known to be important for imparting antifreeze activity. It was believed the bulky β_{thr}-methyl group can favour certain conformations of the carbohydrate. The synthetic challenge of this compound is to install the appropriate stereocentres in the *C*-α-galactosyl-threonine residue. To set the key *C*-anomeric stereochemistry, SmI_2-mediated Reformatsky reductive coupling was used to couple the carbohydrate to the threonine aldehyde precursor (**27**). Unfortunately, the produced diastereomers were inseparable, and thus unambiguous structure determination was not possible. Despite attempting to proceed with the synthetic pathway, time constraints did not permit completion of the revised synthesis (Scheme 6.20). Therefore, work that remains to be done is the completion of this synthesis, and also to synthesize *C*-α-galactosyl-threonine derivatives by varying the alkyl substituents at the β_{thr} position. To synthesize these derivatives, the only change in the syntheses is simply to use a different desired Grignard reagent in the phosphine-directed cuprate addition step (Scheme 6.13).

By understanding the factors that are responsible for IRI activity, a future goal will be to use MD simulations to rationally design compounds that have specific conformations and hydration properties desired for IRI activity. As the syntheses of AFGP analogues are expensive, difficult and timely, the syntheses of simpler compounds will be desired. This will enable the use of these compounds as cryoprotectants for applications such as long-term storage of cells, tissues, and organs.

EXPERIMENTAL METHODS AND DATA

1. PROCEDURE FOR THERMAL HYSTERESIS ASSAY

Nanoliter osmometry was performed using a nanoliter osmometer (Clifton Technical Physics, Hartford, NY) as described by Chakrabartty and Hew.[1] All measurements were made in doubly distilled water. Ice crystal morphology was observed through a Leitz compound microscope equipped with an Olympus 20X (infinity corrected) objective, Leitz Periplan 32X photo eyepiece and a Hitachi KP-M2U CCD camera connected to a Toshiba MV13K1 TV/VCR system. Still images were captured directly using a Nikon CoolPix digital camera.

2. PROCEDURE FOR ICE-RECRYSTALLIZATION INHIBITION ASSAY

Samples for the IRI assay were prepared by dissolving the sample (either carbohydrate or glycopeptide) in phosphate buffer saline (PBS, pH 7.4) solution at the desired concentrations. The samples were then analyzed for IRI activity was performed using the "splat cooling" method as described previously.[2] A 10 μL drop of the sample solution was dropped from a micropipette through a two metre high plastic tube (10 cm in diametre) onto a block of polished aluminum pre-cooled to approximately -80 ºC. The droplet froze instantly on the polished aluminum block and was approximately 1 cm in diameter and 20 μm thick. This wafer was then carefully removed from the surface of the block and transferred to a cryostage held at -6.4 ºC for annealing. After a period of 30 minutes, the wafer was photographed between crossed polarizing filters using a digital camera (Nikon CoolPix 5000) fitted to the microscope. A total of three images were taken from each wafer. During flash freezing, ice crystals spontaneously nucleated from the super-cooled solution. These initial crystals were relatively homogenous in size and quite small. During the annealing cycle recrystallization occurred, resulting in a dramatic increase in ice crystal size. A quantitative measure of the difference in recrystallization inhibition of two compounds X and Y is the difference in the dynamics of the ice crystal size distribution. Image analysis of the ice wafers was performed using a novel domain recognition software (DRS)[3] program that was developed at the Steacie Institute for Molecular Sciences (SIMS) of the National Research Council of Canada (NRCC). This processing employed the Microsoft Windows Graphical User Interface to allow a user to visually demarcate and store the vertices of ice domains in a digital micrograph. These data were then used to calculate the domain areas. To eliminate the need to fully process each micrograph, an algorithm was developed to randomly display a number of x/y locations. The algorithm made use of a built-in pseudo random number generator (rand(x)) and was written so that no two locations were closer than 1/10th the field of view of the micrograph. The formula for the area of a polygon that is not self-intersecting and contains no holes is then given by Eq.1,

---

[1] Chakrabartty, A.; Hew, C. L. *Eur. J. Biochem.* **1991**, *202*, 1057–1063.
[2] Knight, C.A.; Hallet, J.; DeVries, A.L. *Cryobiology*, **1988**, *25*, 55-60
[3] Jackman, J.; Noestheden, M.; Moffat, D.; Pezacki, J. P.; Findlay, S.; Ben, R. N. *Biochem. Biophys. Res. Commun.* **2007**, *354*, 340-344.

$$A = \frac{1}{2}\sum_{i=0}^{N-1}\left(x_i y_{i+1} - x_{i+1} y_i\right) \qquad \text{(Eq.1)}$$

where N is the number of vertices, and x_0, y_0 to x_{N-1}, y_{N-1} are the vertices circumventing the polygon in a clockwise direction. The point x_0, y_0 is assumed to be equivalent to the point x_N, y_N. The software was written in C using Microsoft Visual Studio 6.0 on a Pentium class personal computer running Microsoft Windows 2000 or XP. All data was plotted and analyzed using Microsoft Excel.

3. GENERAL EXPERIMENTAL CONDITIONS FOR CHEMICAL REACTIONS

All anhydrous reactions were performed in flame-dried or oven-dried glassware under a positive pressure of dry argon or nitrogen. Air or moisture-sensitive reagents and anhydrous solvents were transferred with oven-dried syringes or cannulae. All flash chromatography was performed with E. Merck silica gel 60 (230-400 mesh). All solution phase reactions were monitored using analytical thin layer chromatography (TLC) with 0.2mm pre-coated silica gel aluminum plates 60 F254 (E. Merck). Components were visualized by illumination with a short-wavelength (254 nm) ultra-violet light and/or staining (ceric ammonium molybdate, potassium permanganate, or phosphomolybdate stain solution). All solvents used for anhydrous reactions were distilled. Tetrahydrofuran (THF) and diethyl ether were distilled from sodium/benzophenone under nitrogen. Dichloromethane, acetonitrile, triethylamine, benzene and diisopropylethylamine (DIPEA) were distilled from calcium hydride. Methanol was distilled from calcium sulfate. *N,N*-dimethylformamide (DMF) was stored over activated molecular sieves 4Å under argon.

^{1}H (300, 400 or 500 MHz) and ^{13}C NMR (75, 101 or 126 MHz) spectra were recorded at ambient temperature on a Bruker Avance (300, 400, 500), or Varian Inova 500 spectrometer, unless otherwise stated. Deuterated chloroform ($CDCl_3$), methanol (CD_3OD), or water (D_2O) were used as NMR solvents, unless otherwise stated. Chemical shifts are reported in ppm downfield from trimethylsilane (TMS) or 2,2-dimethyl-2-silapentane-5-sulfonic acid (DSS) and corrected using the solvent residual peak, TMS, or DSS as an internal standard. Splitting patterns are designated as follows: s, singlet; d, doublet; t, triplet; q, quartet; m, multiplet and br, broad. Low resolution mass spectrometry was performed on a Micromass Quatro-LC Electrospray spectrometer with a pump rate of 20 μL/min using electrospray ionization (ESI) or a Voyager DE-Pro matrix-assisted desorption ionization-time of flight (MALDI-TOF), (Applied Biosystem, Foster City, CA) mass spectrometer operated in the reflectron/positive-ion mode with DHB in 20% EtOH/H_2O as the MALDI matrix. Analytical and preparatory scale RP-HPLC were carried out with C-18 columns on a Varian Dynomax HPLC system equipped with a variable wavelength detector (ProStar 330 PDA) or a Waters Delta 600E HPLC system equipped with a variable wavelength detector. Automated solid phase peptide synthesis (SPPS) was performed on APEX 396 (Advanced ChemTech) equipped with a 40 well reaction vessel.

4. EXPERIMENTAL PROCEDURES AND DATA

General Protocol for deacetylation of (3`-((2,3,4,6-tetra-O-acetyl)-α-D-pyranosyl)-propene)

3`(2,3,4,6-tetra-*O*-acetyl-glycopyranosyl) propene (100 mg, 0.27 mmol) was dissolved in a NaOMe/MeOH (pH 10) solution (4 mL) and stirred at room temperature overnight. The solution was then neutralized with Amberlite® IR-120H ion-exchange resin, filtered and concentrated under reduced pressure. The product recrystallized using a system comprising of MeOH/EtOAc/Et_2O. Typical yields obtained ranged between 90-95%.

3`-(α-D-Galactopyran-1-yl)-prop-1`-ene (10a)[4]

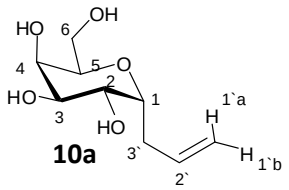

10a

^{1}H NMR (400 MHz, MeOD) δ 5.90-5.83 (1H, dddd, *J* = 7.0, 7.0, 10.2, 17.1 Hz, H2`), 5.10 (1H, dd, *J* = 1.9, 17.2 Hz, H1a`), 5.04-4.99 (1H, m, H1b`), 4.01-3.93 (1H, m, H1), 3.94-3.91 (1H, m, H5), 3.88 (1H, dd, *J* = 5.3, 8.8 Hz, H2), 3.76-3.61 (4H, m, H4, H6, H3), 2.49-2.31 (2H, m, H3`); ^{13}C NMR (100 MHz, MeOD) δ 136.7, 116.9, 75.7, 74.1, 71.9, 70.2, 70.0, 62.0, 31.1. HRMS calcd for $(M+Na)^+$ 227.0895, found 227.0879.

3`-(α-D-Glucopyran-1yl)-prop-1`-ene (11a)

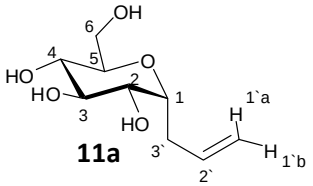

11a

^{1}H NMR (400 MHz, D_2O) δ 5.84 (1H, dddd, *J* = 6.9, 7.0, 10.2, 17.1 Hz, H2`), 5.20 (1H, dd, *J* = 1.2, 17.2 Hz, H1a`), 5.14 (1H, d, *J* = 10.2 Hz, H1b`), 4.08 (1H, ddd, *J* = 4.1, 5.7, 11.3 Hz, H1), 3.79 (1H, dd, *J* = 2.3, 12.3 Hz), 3.76-3.64 (3H, m), 3.58 (1H, ddd, *J* = 2.3, 5.3, 10.0 Hz), 3.37 (1H, dd, *J* = 8.8, 9.9 Hz), 2.50-2.37 (2H, m, H3`); ^{13}C NMR (100 MHz, D_2O) δ 134.6, 117.5, 75.3, 73.2, 72.4, 71.1, 70.2 60.9, 28.8; HRMS calcd for $(M+Na)^+$ 227.0895, found 227.0879.

[4] Mari, S.; Cañada, F. J.; Jiménez-Barbero, J.; Bernardi, A.; Marcou, G.; Motto, I.; Velter, I.; Nicotra, F.; La Ferla, B. *Eur. J. Org. Chem*. **2006**, 2925.

3`-(α-D-Talopyran-1-yl)-prop-1`-ene (13)

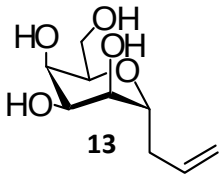

13

O-protected talopyranoside **43** (50 mg, 0.13 mmol) was dissolved in 80% acetic acid (4mL) and heated for 1 hr at 80 °C. The reaction mixture was cooled and the solvent was evaporated by co-evaporation with toluene. The desired deprotected alkene was crystallized as a white solid using a solvent system comprising of MeOH/EtOAc/Et_2O, (27 mg, 80% yield). ^{1}H NMR (400 MHz, MeOD) δ 5.89 (1H, dddd, *J* = 7.0, 7.0, 10.2, 17.1 Hz, H2`), 5.13 (1H, ddd, *J* = 1.4, 3.3, 17.1 Hz, H1a`), 5.07 (1H, d, *J* = 10.2 Hz, H1b`), 3.95 (1H, ddd, *J* = 3.7, 6.2, 8.2 Hz), 3.85-3.77 (3H, m), 3.75-3.68 (2H, m), 3.60-3.58 (1H, m), 2.43-2.34 (2H, m, H3`); ^{13}C NMR (100 MHz, MeOD) δ 136.0, 117.5, 77.5, 75.2, 72.6, 71.2, 68.6, 62.2, 35.1; HRMS calcd for $(M+Na)^+$ 227.0895, found 227.0908.

General Procedure for Solid Phase Synthesis of C-Linked Glycopeptide Polymers and Monomeric Model Systems

All glycoconjugates were synthesized using conventional Fmoc solid-phase synthesis on an APEX 396 using acid labile Wang resin. A typical procedure[5,6] started from Fmoc-glycine Wang resin with loading capacities of ~0.066 mmol/g. The resin was swollen in DMF for 30 minutes in the reaction vessel. The solvent was then drained and 20% piperidine solution in DMF was added. The solution was allowed to stir for 1 hour, drained, and the resin was then washed with three aliquots of DMF. Kaiser and TNBS tests for free amine were then performed. The next successive building block (5 equivalents) to be coupled (commercially available amino acid) was premixed with 5 equivalents of HBTU and 10 equivalents of DIPEA in DMF for 20 minutes. The reaction solution was then transferred to the resin, and the reaction mixture was allowed to stir for 4 hours. Kaiser and TNBS tests were performed to verify the coupling had reached completion (negative test outcome). The reaction vessel was drained and the resin was rinsed three times with DMF. The resin was treated with 20% piperdine in DMF solution for 1 hour, the flask was drained and the resin was washed thoroughly with DMF. Kaiser and TNBS tests were performed to ensure the presence of free amine. The glycoconjugate building block (1.5 equivalents) was premixed with 1.6 equivalents of HBTU in DMF, followed by the addition of 3.0 equivalents of DIPEA in DMF. The reaction was stirred for 30 minutes, transferred to the reaction vessel and stirred for 36 hours. The Fmoc deprotection and coupling steps were repeated until the desired number of amino acid residues were coupled to the resin. To cleave the glycopeptide from the resin, the resin was successively rinsed with DMF, EtOH, and CH_2Cl_2,

[5] Czechura, P.; Tam, R. Y.; Dimitrijevic, E.; Murphy, A.V. *J. Am. Chem. Soc.* **2008**, *130,* 2928.
[6] Fields, G. B.; Fields, C. G. *J. Am. Chem. Soc.* **1991**, 113, 4202.

and stirred for 2 hours in 92.5 : 5 : 2.5 (v:v:v) trifluoroacetic acid/triisopropylsilane/water. The solution was filtered and concentrated, and the product precipitated from diethyl ether to produce a white powder.

General Procedure for deacetylation of C-linked glycopeptides

The crude glycopolymer was dissolved in a sodium methoxide (pH=10) solution (4:1 sodium methoxide/water) and stirred for 5 hours. The solution was neutralized with IR-120 ion exchange resin, filtered, concentrated to remove MeOH and lyophilized to give the product as a white powder. Purification via HPLC using reverse phase chromatography (Polaris C-18 RP column; mobile phase: 100% water to 15 : 85 (v:v) acetonitrile/water gradient over 30 minutes) was then performed to obtain the desired glycopeptides as a white powder.

[[(S)-*N*γ-[2`-(α-D-galactopyranosyl)-ethan-1`-amido]-α,γ-diaminobutyric-1-amido]-glycinamido-glycinamido]$_4$-glycine (18)

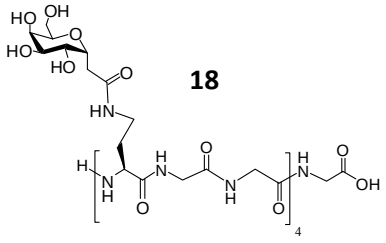

Glycopeptide **18** was synthesized from building block **44**, according to "General procedures for solid-phase synthesis" and "General Procedure for deacetylation of *C*-linked glycopeptides". ^{1}H NMR (500 MHz, D_2O) δ 4.36-4.28 (4H, m), 4.26-4.18 (4H, m), 3.90-3.75 (25H, m), 3.75- 3.62 (7H, m), 3.59-3.48 (12H, m), 3.30-3.09 (8H, m), 2.50 (4H, dd, *J* = 10.9, 14.8 Hz), 2.41 (4H, dd, *J* = 4.1, 15.0 Hz), 2.00-1.85 (4H, m), 1.80-1.68 (4H, m); ^{13}C NMR (126 MHz, D_2O) δ 174.4, 174.1, 173.7, 173.6, 172.0, 171.9, 171.7, 72.9, 72.8, 72.5, 69.6, 68.8, 68.8, 67.5, 61.1, 60.9, 51.5, 51.4, 51.0, 42.6, 42.5, 42.4, 42.4, 42.3, 42.3, 35.7, 32.3, 30.7, 30.2, 30.1, 30.0. MALDI-TOF calcd. for $C_{66}H_{109}N_{17}O_{38}$ $[M+H]^+$: 1748.7; $[M+Na]^+$: 1770.7. Found 1748.8, 1771.0.

[[(S)-*Nβ*-[2`-(α-D-galactopyranosyl)-ethan-1`-amido]-α,β-diaminopropanoic-1-amido]-glycinamido-glycinamido]$_4$-glycine (19)

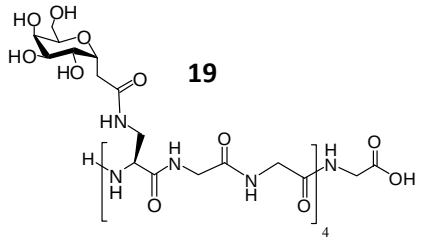

Glycopeptide **19** was synthesized from building block **45**, according to "General procedures for solid-phase synthesis" and "General Procedure for deacetylation of *C*-linked glycopeptides". ^{1}H NMR (500 MHz, D_2O) δ 4.40-4.26 (8H, m), 3.94-3.70 (31H, m), 3.70-3.62 (5H, m), 3.60-3.43 (18H, m), 3.42-3.34 (4H, m), 2.52 (4H, dd, *J* = 11.0, 15.0 Hz), 2.44 (4H, dd, *J* = 3.9, 15.2 Hz); ^{13}C NMR (126 MHz, D_2O) δ 174.7, 174.4, 172.1, 172.1, 171.9, 171.9, 171.8, 171.6, 171.5, 72.9, 72.7, 72.5, 69.5, 68.8, 67.4, 61.2, 61.1, 53.6, 42.6, 42.4, 42.3, 42.3, 40.0, 32.2; MALDI-TOF calcd. for $C_{62}H_{101}N_{17}O_{38}$ $[M+H]^+$: 1692.7. Found 1692.7.

[[(S)-*N*γ-[3`-(α-D-galactopyran-1-yl)-propan-1`-amido]-α,γ-diaminobutyric-1-amido]-glycinamido-glycinamido]$_4$-glycine (20)

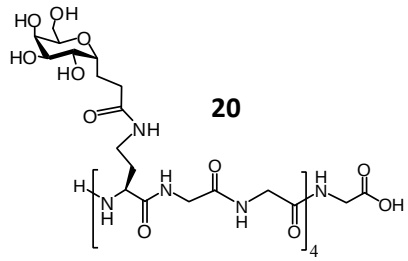

Glycopeptide **20** was synthesized from building block **66**, according to "General procedures for solid-phase synthesis" and "General Procedure for deacetylation of *C*-linked glycopeptides". ^{1}H NMR(500 MHz, D_2O) δ 8.60-8.55(m, NH), 8.54-8.46 (m, NH), 8.45-8.42 (d, *J*=6.9 Hz, NH), 8.40-8.35 (d, *J*=6.3 Hz, NH), 8.31-8.24 (m, NH), 4.39-4.32 (4H, m), 4.00-3.90 (34H, m), 3.88-3.83 (3H, m), 3.77-3.69 (9H, m), 3.69-3.64 (8H, m), 3.30-3.18 (8H, m), 2.37-2.29 (4H, m), 2.28-2.19 (4H, m), 2.11-2.00 (4H, m), 2.00-1.80 (12H, m). ^{13}C NMR (101 MHz, D_2O) δ 170.1, 174.2, 173.4, 171.9, 171.8, 171.7, 171.7, 74.7, 71.7, 69.5, 68.9, 68.0, 61.1, 51.4, 42.5, 42.4, 42.2, 41.1, 35.5, 31.9, 30.0, 20.2. MALDI-TOF calcd. For $C_{70}H_{117}N_{17}O_{38}$ [M+H]:1804.8. Found 1805.0.

[[(S)-*Nβ*-[4`-(α-D-galactopyran-1-yl)-butan-1`-amido]-α,β-diaminopropanoic-1-amido]-glycinamido-glycinamido]$_4$-glycine (21)

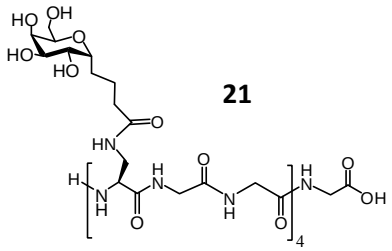

21

Glycopeptide **21** was synthesized from building block **67**, according to "General procedures for solid-phase synthesis". Deprotection of the carbohydrate was achieved simultaneously during acid-mediated glycopeptide cleavage from the Wang resin. ^{1}H NMR(500 MHz, D_2O) δ 4.43-4.32 (4H, m), 4.00-3.90 (38H, m), 3.90-3.74 (29H, m), 3.62-3.42(m), 3.40-3.30 (m), 2.20-2.05(8H, m), 1.60-1.45 (8H, m), 1.45-1.30 (8H, m). ^{13}C NMR (126 MHz, D_2O) δ 177.8, 177.3, 172.0, 171.9, 171.7, 171.6, 171.5, 75.0, 71.6, 69.6, 69.0, 68.2, 61.1, 53.6, 53.5, 52.9, 42.5, 42.4, 42.3, 40.0, 39.9, 39.9, 35.1, 34.9, 22.9, 22.8, 21.4, 21.2. MALDI-TOF calcd. For $C_{70}H_{117}N_{17}O_{38}$ $[M+H]^+$:1804.8.; $[M+Na]^+$: 1826.8; Found 1805.0, 1827.0.

***tert*-Butyl-4-(S)-[2`-(R)-1`-oxopropan-2`-yl]-2,2-dimethyl-1,3-oxazolidine-3-carboxylate (27)**

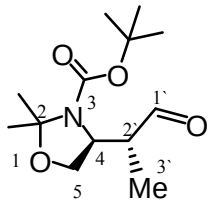

27

Alkene **105** (150 mg, 0.588 mmol) was dissolved in dichloromethane (20 mL), purged with nitrogen, and cooled to -78 ^{o}C. A steady stream of ozone gas was then bubbled into the solution until a royal blue colour persisted. The ozone gas was then removed from the solution by bubbling nitrogen gas into the solution until it became colourless. Triphenylphosphine (0.62 g, 2.35 mmol) was then added and the solution was stirred for 6 hrs, while gradually warming up to room temperature. The solvent was removed under reduced pressure, and purified by column chromatography to afford the desired aldehyde **27** as an oil (116 mg, 77% yield). ^{1}H NMR (500 MHz, 20 °C, $CDCl_3$) δ major rotamer 9.60 (1H, m, H1`), 4.20 (1H, t, *J* = 5.9 Hz, H4), 3.94-3.81 (1H, m, H5a), 3.77-3.71 (1H, m, H5b), 2.91-2.81 (1H, m, H2`), 1.56 (3H, s, C2-Me), 1.44 (9H, s, *t*Bu), 1.42 (3H, s, C2 Me), 1.17 (3H, d, *J* = 7.1 Hz, C3`); minor rotamer 9.64 (1H, m, H7),4.10-4.04 (1H, m, H4), 3.94-3.81 (1H, m, H5a), 3.77-3.71 (1H, m, H5b), 2.80-2.73 (1H, m, H6), 1.62 (3H, s, C2-Me), 1.49 (3H, s, C2-Me), 1.44 (9H, s, *t*Bu), 1.17 (3H, d, *J* = 7.1 Hz, C6-Me); $^1$H NMR (500 MHz, 50 °C, $CDCl_3$) δ 9.63 (1H, s, H1`), 4.30-4.00 (1H, m, H4), 3.98 (1H, dd, *J* = 6.2, 9.4 Hz, H5a), 3.74 (1H, dd, *J* = 1.2, 9.3 Hz, H5b), 2.95-2.70 (1H, m, H2`), 1.59 (3H, s, C2-Me), 1.47 (3H, s, C2-Me), 1.45 (9H, s, C(C*H*$_3$)$_3$), 1.11 (3H, d, *J* = 7.1 Hz, H3`).^{13}C NMR (126 MHz, 20 °C, $CDCl_3$) δ major rotamer 202.6 (C1`), 151.4(CO), 93.4 (*C*(Me)$_3$), 80.5 (C2), 64.8(C5), 57.5(C4), 49.2(C2`), 28.2(C(*C*H$_3$)$_3$), 26.9 (C2-*C*H$_3$), 24.0(C2-*C*H$_3$), 9.6(C6-*C*H$_3$);

minor rotamer 202.7(C1`), 152.3(CO), 94.0 (*C*(Me)$_3$), 80.5(C2), 65.4(C5), 57.3(C4), 49.2(C2`), 28.2 (C(*C*H$_3$)$_3$), 26.3 (C2-*C*H$_3$), 22.6 (C2-*C*H$_3$), 9.6 (C6-*C*H$_3$). (126MHz, 50^{o}C, $CDCl_3$) δ 202.4, 80.5, 64.9, 57.5, 28.2, 26.8, 24.0, 9.4. ESI-MS calcd for $C_{13}H_{24}N_1O_4$ $[M+Na]^+$: 280.1525; Found 280.193. IR(film): 2979.8, 2937.4, 2875.7, 1689.5,1652.9, 1456.2, 1386.7, 1365.5, 1255.6, 1205.4, 1170.7, 1083.9, 1053.1, 846.7, 767.6. Rf = 0.42 (4:1 Hexane: EtOAc)

3`-(2,3,4,6-Tetra-*O*-acetyl-α-D-galactopyran-1-yl)-prop-1`-ene (37)[7]

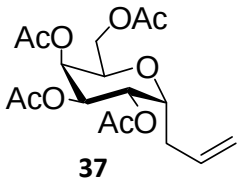

37

To a solution of 2,3,4,6-tetra-*O*-acetyl-α-D-pyranosyl bromide (1.24 g, 3.01 mmol) in benzene (15 mL), allyl phenyl sulfone (1.418 mL, 7.52 mmol), and bis-tributyl tin (2.19 mL, 4.21 mmol) were added. The solution was degassed and sonicated for 30 minutes under argon. The flask was then sealed, and irradiated for 9 hours under a 450W mercury arc lamp. The reaction was monitored using TLC at time intervals of 2, 6 and 8 hours. The reaction mixture was loaded directly onto a silica gel column packed with hexanes. The organostannanes were flushed with 3 void volumes of hexanes, after which the solvent system was changed to 5:1 hexanes/EtOAc to remove the unreacted allyl phenyl sulfone. The product was eluted with 3:1 hexanes/EtOAc and concentrated to afford the allylated derivative as colorless oil (0.67 – 0.90g, 60-80 % yield). ^{1}H NMR (360 MHz, $CDCl_3$) δ 5.76 (1H, dddd, *J* = 6.5, 7.1, 10.0, 16.6 Hz, H2`), 5.42 (1H, dd, *J* = 2.4, 3.1 Hz, H4), 5.28 (1H, dd, *J* = 4.8, 9.3 Hz, H2), 5.22 (1H, dd, *J* = 3.1, 9.3 Hz, H3), 5.13 (1H, ddd, *J* = 1.6, 3.0, 16.6 Hz, H1a`), 5.12 (1H, ddd, *J* = 1.4, 3.0, 10.0 Hz, H1b`), 4.30 (1H, ddd, *J* = 4.7, 5.2, 10.3 Hz, H1), 4.21 (1H, dd, *J* = 8.9, 12.5 Hz, H6a), 4.09 (2H, m, H5, H6b), 2.46 (1H, m, H3`a), 2.29 (1H, m, H3`b), 2.12 (1H, s, $CH_3$), 2.07 (1H, s, $CH_3$), 2.04 (1H, s, $CH_3$), 2.03 (1H, s, $CH_3$); $^{13}$C NMR (90 MHz, $CDCl_3$) δ 170.5, 170.1, 169.9, 169.8, 133.3(C2`), 117.6(C1`), 71.4, 68.2, 67.9, 61.4, 30.9(C3`), 20.8(CH_3), 20.7(CH_3), 20.6(CH_3). ESI-MS calcd for $C_{17}H_{25}O_9$ $[M+H]^+$ 373.1, found 373.1. Rf = 0.25 (3:1 Hexane: EtOAc)

[7] Ponten, F.; Magnusson, G. *J. Org. Chem.* **1996**, *61*, 7463-7466.

3`-(3,4-*O*-isopropylidene-α-D-galactopyran-1-yl)-prop-1`-ene (40)

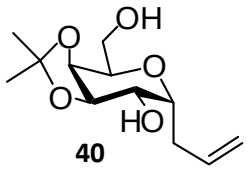

40

To a solution of *C*-allylglycoside **10a** (0.81 g, 3.97 mmol) and dimethoxypropane (2.44 mL, 19.85 mmol) in dry acetonitrile (15 mL), p-TsOH (40 mg) was added and the reaction mixture was stirred for 2h. Water (3 mL) was then added and after 30 min the reaction was neutralized with triethylamine and evaporated. Flash column chromatography (10% CH_2Cl_2 in EtOAc) afforded **40** (0.82 g, 84% yield) as white crystalline solid. ^{1}H NMR (400 MHz, $CDCl_3$) δ 5.86 (1H, dddd, *J*=7.1, 7.1, 10.2, 17.2 Hz, H2`), 5.15 (1H, dd, *J*=1.8, 17.2 Hz, H1a`), 5.09 (1H, dddd, *J*=1.5, 10.2 Hz, H1b`), 4.33-4.25 (2H, m), 4.08-4.02 (2H, m), 3.87-3.77 (3H, m), 2.45-2.30 (2H, m, H3`), 2.20 (1H, dd, *J*=3.2, 9.3 Hz, O6H), 2.00 (1H, d, *J*=4.5 Hz, O2H), 1.47 (3H, s, CH_3), 1.32 (3H, s, CH_3); ^{13}C NMR (100 MHz, $CDCl_3$) δ 134.3 (C2`), 117.7 (C3`), 109.7($(Me)_2C(O_2)$), 74.8, 73.1, 70.6, 69.6, 69.1, 63.6, 34.9(C3`), 26.8(CH_3), 24.6(CH_3). HRMS (ESI): Calcd for $C_{12}H_{21}O_5$ $[M+H]^+$ 245.1388, found 245.1377. Rf = 0.50 (100% EtOAc)

3`-(3,4-*O*-isopropylidene-6-*O*-*tert*-butyldimethylsilyl-α-D-galactopyran-1-yl)-prop-1`-ene (41)

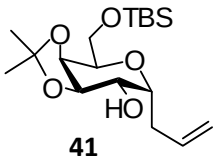

41

To a solution of diol **40** (0.30 g, 1.21 mmol) in dry pyridine/CH_2Cl_2 (5/5 mL), tert-butyldimethylsilyl chloride (0.22 g, 1.45 mmol) and DMAP (7 mg) were added sequentially. The reaction mixture was stirred overnight, diluted with CH_2Cl_2 and washed successively with 0.5 N HCl, water and brine. The organic extract was dried over $MgSO_4$ and concentrated *in vacuo*. Flash column chromatography (25% EtOAc/hexanes) gave the product **41** in 80% yield (0.35 g). ^{1}H NMR (400 MHz, $CDCl_3$) δ 5.82 (1H, dddd, *J* = 7.0, 7.0, 10.2, 17.1 Hz, H2`), 5.16-5.10 (1H, m, H1`a), 5.08-5.04 (1H, m, H1`b), 4.34 (1H, dd, *J* = 1.8, 7.1 Hz), 4.17 (1H, dd, *J* = 3.4, 7.1 Hz), 3.99-3.93 (2H, m), 3.76-3.64 (3H, m), 2.50-2.40 (1H, br, OH), 2.35-2.28 (2H, m, H3`), 1.43 (3H, s, CH_3), 1.28 (3H, s, CH_3), 0.84 (9H, s, ($C(CH_3)$), 0.02 (3H, s, ($SiCH_3$)), 0.02 (3H, s, ($SiCH_3$)); ^{13}C NMR (100 MHz, $CDCl_3$) δ 134.4 (C2`), 117.5(C1`), 109.0 ($(Me)_2C(O_2)$), 74.6, 71.7, 70.4, 69.9, 69.7, 62.6, 34.9 (C3`), 27.0 (CH_3), 25.9 ($C(CH_3)_3$), 24.5 (CH_3), 18.3 (($SiC(Me)_3$), -5.3 ($SiCH_3$),-5.4 ($SiCH_3$). HRMS (ESI): Calcd for $C_{18}H_{35}O_5Si$ $[M+H]^+$ 359.2253, found 359.2257. Rf = 0.65 (2:1 Hexane: EtOAc)

3`-(3,4-*O*-isopropylidene-6-*O*-*tert*-butyldimethylsilyl-α-D-talopyran-1-yl)-prop-1`-ene (43)

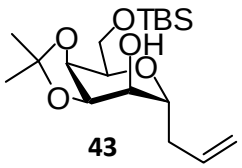

43

To a solution of oxalyl chloride (0.13 mL, 1.51 mmol) in CH_2Cl_2 (10 mL) at -78°C, DMSO (0.23 mL, 3.31 mmol) was added dropwise and the reaction mixture was stirred for 30 min. Then, **41** (0.27 g, 0.75 mmol) in CH_2Cl_2 (10 mL) was added over 10 min. After an additional 30 min of stirring, triethylamine (0.73 mL, 5.27 mmol) was added at -60°C and the reaction mixture was brought to room temperature. After 1 hr, the reaction mixture was diluted with CH_2Cl_2 and water was added. The layers were separated and the organic extract was washed with water, brine, dried over $MgSO_4$, and concentrated. The crude product was immediately dissolved in MeOH (20 mL) and $NaBH_4$ (0.06 g, 1.51 mmol) was added. After stirring for 30 min, the reaction mixture was quenched with acetic acid and the solvent was evaporated. The residue was dissolved in CH_2Cl_2, washed with water, brine and then dried over $MgSO_4$. The organic phase was evaporated under reduced pressure and purified by silica gel column chromatography (3:1, Hexane : EtOAc). Compound **43** was obtained as a colourless oil (0.41 g, 75%). ^{1}H NMR (400 MHz, $CDCl_3$) δ 5.93 (1H, dddd, *J* = 6.7, 7.4, 10.2, 17.1 Hz, H2`), 5.19-5.07 (2H, m, H1`), 4.50 (1H, dd, *J* = 3.6, 8.0 Hz), 4.42 (1H, dd, *J* = 1.5, 8.0 Hz), 3.77 (1H, ddd, *J* = 4.2, 6.5, 9.7 Hz), 3.74-3.57 (4H, m), 2.52-2.27 (2H, m, H3`), 1.99 (1H, br, OH), 1.51 (3H, s, $CH_3$), 1.36 (3H, s, $CH_3$), 0.89 (9H, s, C(C*H*$_3$)$_3$), 0.06 (3H, s, SiC*H*$_3$), 0.06 (3H, s, SiC*H*$_3$); $^{13}$C NMR (100 MHz, $CDCl_3$) δ 134.4(C2`), 117.6(C1`), 109.8((CH$_3$)$_2$*C*(O)$_2$-), 73.4, 73.1, 72.5, 70.5, 68.2, 62.3, 36.9(CH_2), 26.2(CH_3), 25.9(C(*C*H$_3$)), 24.7(CH_3), 18.7 (Si*C*(CH$_3$)), -5.3(Si*C*H$_3$), -5.5(Si*C*H$_3$). HRMS (ESI): Calcd for $C_{18}H_{38}NO_5Si$ $[M+NH_4]^+$ 376.2519, found 376.2508. Rf = 0.65 (2:1 Hexane: EtOAc)

General procedure for synthesis of C-linked glycoconjugate building blocks **44** *and* **45**

Benzylated glycoconjugate (**58** or **59**) was dissolved in EtOH, and Pd/C (5 % wt) was added. The flask was degassed in vacuo and filled with a H_2(g) balloon. The reaction was stirred until the Fmoc protecting group was seen to be cleaved by TLC (typical times ranged from 4-6 hrs). The reaction was then purged with N_2, gravity filtered and washed with EtOH. The solvent was removed by evaporation, and the residue was purified by column chromatography (7% MeOH in dichloromethane) to afford an amorphous white solid in 90 and 92% yield for **44** and **45**, respectively.

***Nα*-(S)-[(9H-fluoren-9-ylmethoxy)carbonyl]-*Nγ*-[2`-(2,3,4,6-tetra-*O*-acetyl-α-D-galactopyran-1-yl) ethan-1`-amido]-α,γ-diaminobutyric acid (44)**

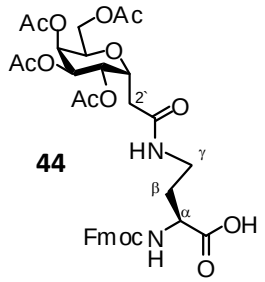

44

^{1}H NMR (500 MHz, CD_3OD) δ 7.79 (2H, d, *J* = 7.5 Hz), 7.68 (2H, t, *J* = 7.1 Hz), 7.38 (2H, t, *J*=7.5 Hz), 7.33-7.28 (2H, m), 5.39 (1H, m, H4), 5.26 (1H, dd, *J* = 5.0, 9.5 Hz, H2), 5.22 (1H, dd, *J*= 3.1, 9.5 Hz, H3), 4.69-4.63 (1H, m, H1), 4.38-4.30 (2H, m, FmocCH_2), 4.25-4.08 (5H, m, Hα, FmocCH, H5, H6), 3.39-3.32 (1H, m, Hγa), 3.25-3.17 (1H, m, Hγb), 2.65 (1H, dd, *J*=9.4, 14.7 Hz, H2`a), 2.50 (1H, dd, *J*= 5.2, 14.8 Hz, H2`b), 2.08 (3H, s, CH_3), 2.02 (3H, s, CH_3), 2.00-1.95 (1H, m, Hβa), 1.98 (3H, s, CH_3), 1.98 (3H, s, CH_3), 1.90-1.80 (1H, m, Hβb); ^{13}C NMR (101 MHz, $CDCl_3$) δ 169.9, 169.8, 169.7, 156.1, 143.8, 141.3, 141.3, 127.8, 127.1, 125.1, 120.0, 70.0(C1), 68.4(C5), 68.2(C2), 67.8(C3), 67.2(C4), 66.7(FmocCH_2), 61.0 (C6), 51.4 (Cα), 47.1(FmocCH), 36.0(Cγ), 34.7(C2`), 33.3(Cβ), 20.7(CH_3), 20.6 (CH_3); ESI-MS calcd for $C_{35}H_{40}N_2O_{14}$ $[M+H]^+$: 713.255; $[M+Na]^+$: 735.237; $[M+K]^+$: 751.211. Found 713.328, 735.312, 751.286. Rf = 0.10 (1:9, methanol : dichloromethane)

***Nα*-(S)-[(9H-fluoren-9-ylmethoxy)carbonyl]-*Nβ*-[2`-(2,3,4,6-tetra-*O*-acetyl-α-D-galactopyran-1-yl) ethan-1`-amido]-α,β-diaminopropanoic acid (45)**

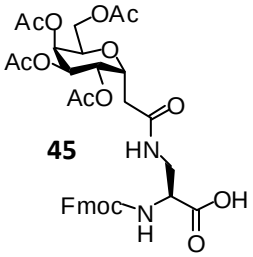

45

^{1}H NMR (500 MHz, CD_3OD) δ 7.81 (2H, d, *J*=7.5 Hz), 7.69 (2H, dd, *J*=7.6, 10.5 Hz), 7.39 (2H, ddd, *J*=1.9, 7.4, 7.5 Hz), 7.36-7.28 (2H, m), 5.36 (1H, dd, *J* = 2.6, 2.6 Hz, H4), 5.26 (1H, dd, *J* = 5.2, 9.5 Hz, H2), 5.17 (1H, dd, *J* = 3.2, 9.5 Hz, H3), 4.69-4.62 (1H, m, H1), 4.38-4.29 (3H, m, Hα, FmocCH_2), 4.26-4.21 (1H, t, *J*=7.0 Hz, FmocCH), 4.21-4.09 (3H, m, H5, H6), 3.77 (1H, dd, *J*=4.6, 13.8 Hz, Hβa), 3.46 (1H, dd, *J*= 7.9, 13.7 Hz, Hβb), 2.67 (1H, dd, *J*=9.5, 14.8 Hz, H2`a), 2.49 (1H, dd, *J*= 4.9, 14.8 Hz, H2`b), 2.06 (3H, s, CH_3), 2.02 (3H, s, CH_3), 1.98 (3H, s, CH_3), 1.95 (3H, s, CH_3); ^{13}C NMR (101 MHz, $CDOD_3$) δ 171.9, 170.0, 170.0, 169.9, 169.9, 169.8, 156.5, 143.7, 143.6, 141.3, 127.8, 127.1,125.1, 120.0, 69.7(C1), 68.5(C5), 68.0(C2), 67.8 (C3), 67.4(C4), 66.7(Fmoc*C*H_2), 60.9(C6), 54.8(Cα), 47.0(FmocCH), 41.7(Cβ), 34.4(C2`), 20.7(CH_3),

20.6(CH_3). ESI-MS calcd for $C_{34}H_{38}N_2O_{14}$ $[M+H]^+$: 699.240; $[M+Na]^+$: 721.222. $[M+K]^+$: 737.196. Found 699.306, 721.288, 737.264. Rf = 0.15 (1:9, methanol : dichloromethane)

General procedure for Hofmann rearrangement of primary amide[8]

Phenyliodo-bis(trifluoroacetate) (530 mg, 1.24 mmol) was dissolved in acetonitrile (15 mL) and water (15 mL). Primary amide (**51** or **52**) (500 mg, 1.13 mmol) was dissolved in warm ethyl acetate (30 mL) and the two mixtures were combined. The pH of the mixture was adjusted to 4.0 with pyridine and was stirred vigorously until the disappearance of starting material. The mixture was evaporated under reduced pressure, saturated sodium bicarbonate solution was added, and then extracted with ethyl acetate. The organic layers were combined and acidified with trifluoroacetic acid and then evaporated in vacuo. The residue was purified with silica column chromatography (0.1: 5: 94.9, TFA:MeOH:DCM) to obtain the primary amine as an amorphous white solid in 70% and 74% yields for **46** and **47**, respectively.

Benzyl-*Nα*-(S)-[(9H-fluoren-9-ylmethoxy)carbonyl]-α-γ-diaminobutanoate (46)

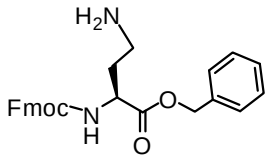

46

^{1}H NMR (500 MHz, CD_3OD) δ 7.77 (1 H, d, *J* = 7.6 Hz), 7.62 (1 H, dd, *J* = 7.2, 4.5 Hz), 7.37 (1 H, t, *J* = 7.4, 7.4 Hz), 7.33 (1 H, d, *J* = 6.3 Hz),7.30-7.24 (5H, m), 5.21-5.12 (2H, m, OC*H*$_2$Ph), 5.08-5.00 (3H, m, NH), 4.42-4.29 (3H, m, FmocC*H*$_2$, Hα), 4.16 (1H, t, *J* = 6.8 Hz, FmocC*H*), 2.99 (2H, t, *J* = 7.7 Hz, Hγ), 2.30-2.19 (1H, m, Hβa), 2.10-1.98 (1H, m, Hβb);^{13}C NMR (126 MHz, CD_3OD) δ172.4,158.8, 145.2, 145.1, 142.6, 136.9, 129.6, 129.4, 129.3, 128.8,128.2, 126.2, 126.2, 121.0, 68.4(O*C*H$_2$Ph), 68.1(Fmoc*C*H$_2$), 53.1(Cα), 48.3(FmocCH), 37.8(Cγ), 30.4(Cβ); R_f = 0.09 (9:1, DCM : MeOH); ESI-MS calcd for $C_{26}H_{26}N_2O_4$ $[M+H]^+$: 431.197; $[M+Na]^+$: 453.179. Found 431.176, 453.197. $[\alpha_D]^{20}$ = -10.7 (c=2.92, MeOH). IR (film) : 3055, 2927, 1681, 1674, 1642, 1525, 1454 ,1203, 1180, 1134 cm^{-1}. Rf = 0.15 (1:9, methanol : dichloromethane)

[8] (a) Loudon, G. M.; Radhakrishna, A. S.; Almound, M. R.; Blodgett, J.K.; Boutin, R. H. *J. Org. Chem.,* **1984**, *49*, 4272-4276. (b) Zhang, L.; Kaufmann, G. S.; Pesti, J. A.; Yin, J. *J. Org. Chem,* **1997**, *62*, 6918-6920. (c) Schmuck, C.; Geiger, L. *Chem. Comm.* **2005**, 772-774.

Benzyl-*Nα*-(S)-[(9H-fluoren-9-ylmethoxy)carbonyl]-α,β-diaminopropionate (47)

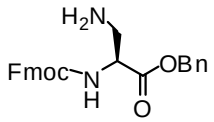

47

^{1}H NMR (500 MHz, $CDCl_3$) δ 7.77 (2H, d, *J*= 7.5Hz), 7.61 (2H, d, *J*= 7.3 Hz), 7.41 (2H, t, *J*=7.5 Hz), 7.38-7.28 (9H, m), 5.23 (1H, d, *J* = 7.7 Hz, NH), 5.27-5.15 (2H, m, -CH_2Ph), 4.46-4.36 (3H, m, FmocCH_2, Hα), 4.06 (1H, t, *J* = 6.9 Hz, FmocCH), 3.12 (1H, dd, *J*= 4.3, 13.3 Hz, Hβa), 3.08 (1H, dd, *J*= 4.3, 13.3 Hz, Hβb); ^{13}C NMR (126 MHz, $CDCl_3$) δ 168.8, 157.0, 143.6, 143.3, 141.2, 134.3, 128.6, 128.6, 128.3, 127.7, 127.1, 125.1, 125.0, 119.9, 68.3 (O*C*H_2Ph), 67.8(FmocCH_2), 51.9(Cα), 46.7(FmocCH), 41.4(Cβ); R_f = 0.39 (9:1 DCM:MeOH); ESI-MS calcd for $C_{25}H_{24}N_2O_4$ $[M+H]^+$: 417.181; $[M+Na]^+$: 439.1628. Found 417.167, 439.156. $[\alpha_D]^{20}$ = -10.0 (c=1.00, MeOH). IR (film) : 3065, 2953, 1670, 1632, 1516, 1450, 1437, 1420, 1398, 1386, 1387, 1339, 1265, 1250 cm^{-1}. Rf = 0.30 (1:9, methanol : dichloromethane)

2`-(2,3,4,6-Tetra-*O*-acetyl-α-D-galactopyran-1-yl)-ethan-1`-oic acid (48) [5]

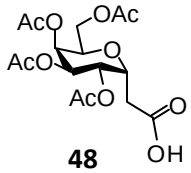

48

Aldehyde **57** (1.36 g, 3.48 mmol) was dissolved in *tert*-butanol (15 mL). 2-methyl-2-butene (4.8 mL, 45 mmol) was added, stirred, and cooled to 0 ^oC. In another flask, potassium phosphate (5.3 g, 30.5 mmol) and sodium chlorite (2.7 g, 30.5 mmol) were dissolved in water (20 mL), and then added to the aldehyde solution and vigorously stirred at 0 ^oC until starting material disappeared (5 hrs). Upon completion, the reaction was extracted with ethyl acetate. The organic layer was then dried with $MgSO_4$ and evaporated in vacuo. The desired carboxylic acid was purified using (1:1, acetone:toluene) to afford an amorphous white solid (1.15 g, 85% yield). ^{1}H NMR (400 MHz, $CDC1_3$) δ 5.43 (t, *J* = 3.20 Hz, 1H), 5.33 (dd, *J* = 9.21, 5.21 Hz, 1H), 5.17 (dd, *J* = 8.81, 3.20, Hz, 1H), 4.71 (dt, *J* = 9.2, 3.6 Hz, 1H), 4.25 (q, *J* = 6.4, 9.6 Hz, 1H), 4.18-4.05 (m, 3H), 2.75-2.61 (m, 2H), 2.13 (s, 3H), 2.07 (s, 3H), 2.04 (s, 6H). ^{13}C NMR (101 MHz, $CDCl_3$) δ 175.5, 170.8, 170.1, 170.0, 169.7, 69.4, 68.9, 67.8, 67.6, 67.1, 61.2, 33.1(C2`), 20.7(CH_3). Rf = 0.47 (10% MeOH/CH_2Cl_2).

General procedure for benzylation of FmocNH-Gln(Trt)-OH (**49**) *and FmocNH-Asn(Trt)-OH* (**50**)

Under argon, Fmoc-protected carboxylic acid (**49** or **50** 1.0 eq) was dissolved in distilled dichloromethane and a minimal amount of dried N,N-dimethylformamide. 1,1`-Carbonyldiimidazole (1.1 eq) was added and the mixture was stirred for 30 minutes. Benzyl

alcohol (1.05 eq) was then added and the reaction was stirred for 16 hours. The reaction was diluted with dichloromethane and quenched with an aqueous solution of saturated ammonium chloride. The organic layer was washed several times with NH_4Cl_{aq} and brine, dried with $MgSO_4$, and evaporated in vacuo. The benzyl ester was purified using silica column chromatography (10:1, toluene : acetone) to obtain an amorphous white solid. 91% and 85% yields for **49a** and **50a**, respectively.

***Nα*-(S)-[(9H-fluoren-9-ylmethoxy)carbonyl]-*Nδ*-(triphenylmethyl)-glutamine benzyl ester (49a)**

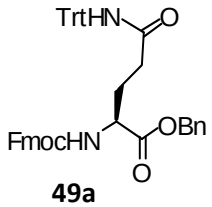

49a

^{1}H NMR (400 MHz, $CDCl_3$) δ 7.75 (2H, d, *J*=7.2Hz), 7.57 (2H, d, *J*=6.7Hz), 7.42-7.36 (2H, m), 7.36-7.12 (22H, m), 6.79 (1H, br, NHβ), 5.55 (1H, d, *J* = 7.3Hz, NHα), 5.15 (2H, m, -C*H*$_2$Ph), 4.50-4.30 (3H, m, FmocC*H*$_2$, Hα), 4.20 (1H, t, *J* = 6.6Hz, FmocC*H*), 2.40-2.10 (3H, m, Hγ, Hβa), 2.00-1.85 (1H, m, Hβb); ^{13}C NMR (126 MHz, $CDCl_3$) δ 171.8, 170.7, 156.3, 144.5, 143.8, 143.6, 141.3, 141.2, 135.2, 128.6, 128.6, 128.5, 128.4, 127.9, 127.7, 127.1, 127.0, 127.0, 126.9, 125.1, 125.1, 119.9, 70.6 (O*C*H$_2$Ph), 67.3(Fmoc*C*H$_2$), 67.0, 53.6 (Cα), 47.1 (FmocCH), 33.2 (Cγ), 28.3 (Cβ); ESI-MS calcd for $C_{46}H_{40}N_2O_5$ $[M+H]^+$: 701.301; $[M+Na]^+$:723.283; $[M+K]^+$:739.257. Found 701.361, 723.342, 739.316. Rf = 0.50 (5:1, toluene:acetone)

***Nα*-(S)-[(9H-fluoren-9-ylmethoxy)carbonyl]-*Nγ*-(triphenylmethyl)-asparagine benzyl ester (50a)**

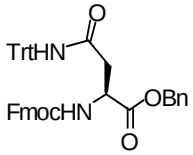

50a

^{1}H NMR (400 MHz, $CDCl_3$) δ 7.73 (2H, dd, *J*=3.9, 7.3Hz), 7.54 (2H, dd, *J*=3.5, 7.2Hz), 7.37 (2H, t, *J* = 7.4Hz), 7.28-7.21 (15H, m), 7.15-7.10 (7H, m), 6.64 (1H, br, NHβ), 6.11(1H, d, *J*=8.7Hz, NHα), 5.10 (2H, m, -CH$_2$Ph), 4.64 (1H, m), 4.39 (1H, dd, *J*=7.2, 10.2 Hz), 4.24 (1H, dd, *J*= 7.6, 10.5Hz), 4.16 (1H, t, *J*=7.3 Hz), 3.11 (1 H, dd, *J*=4.3, 15.8Hz), 2.82 (1H, dd, *J*=4.0, 15.7Hz); ^{13}C NMR (101 MHz, $CDCl_3$) δ 170.8, 169.2, 156.3, 144.2, 143.9, 143.7, 141.2, 141.2, 135.3, 128.6, 128.5, 128.4, 128.2, 128.0, 127.6, 127.2, 127.1, 125.2, 125.2, 119.9, 70.1(-O*C*H$_2$Ph), 67.4(Fmoc*C*H$_2$), 67.2, 51.1(Cα), 47.1(Fmoc*C*H), 38.6(Cβ); ESI-MS calcd for $C_{45}H_{38}N_2O_5$ $[M+H]^+$: 687.285; $[M+Na]^+$:709.267; $[M+K]^+$:725.241. Found 687.343, 709.316, 725.289. Rf = 0.60 (5:1, toluene:acetone)

General procedure for detritylation of FmocNH-Gln(Trt)-OBn (**50a**) *and FmocNH-Asn(Trt)-OBn* (**51a**)

N-trityl protected amino acid (**49a** or **50a**) was dissolved in a 1:1 mixture of dichloromethane : trifluoroacetic acid (20 mL solvent /g amino acid), and stirred until the disappearance of starting material as indicated by TLC. The mixture was evaporated and the desired product was precipitated with diethyl ether to yield a white amorphous solid in quantitative yields.

N*α*-(S)-[(9H-fluoren-9-ylmethoxy)carbonyl]-glutamine benzyl ester (51)

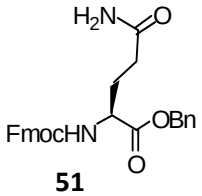

51

^{1}H NMR (400 MHz, $CDCl_3$) δ 7.89-7.64 (2H, m), 7.59 (2H, dd, *J*=7.2, 3.3 Hz), 7.41 (2H, t, *J*=7.5Hz), 7.37- 7.28 (7H, m), 5.74 (1H, br, NHβa), 5.65 (1H, d, *J* = 8.0Hz, NHα), 5.28 (1H, br, NHβb), 5.19 (1H, d, *J*= 5.1, -OCH_{2a}Ph, 5.14 (1H, d, *J* = 12.2Hz, -OCH_{2b}Ph), 4.48-4.38 (3H, m, FmocCH_2, NHα), 4.21 (1H, t, *J*= 6.9Hz, FmocCH), 2.32-2.16 (3H, m, Hγ, Hβa), 2.06 – 1.90 (1H, m, Hβb); ^{13}C NMR (101 MHz, $CDCl_3$) δ 174.1, 171.7, 156.3, 143.8, 143.6, 141.3, 135.1, 128.6, 128.6, 128.4, 127.7, 127.1, 125.1, 120.0, 67.4 (O*C*H$_2$Ph), 67.0(Fmoc*C*H$_2$), 53.5(Cα), 47.1(FmocCH), 31.5(Cγ), 28.3(Cβ); ESI-MS calcd for $C_{27}H_{26}N_2O_5$ $[M+H]^+$: 459.192; $[M+Na]^+$: 481.173; $[M+K]^+$:497.147. Found 459.230, 481.203, 497.181. Rf = 0.50 (1:9, methanol : dichloromethane)

N*α*-(S)-[(9H-fluoren-9-ylmethoxy)carbonyl]-asparagine benzyl ester (52)

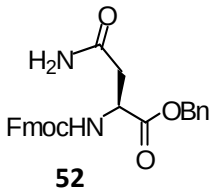

52

^{1}H NMR (400 MHz, $CDCl_3$) δ 7.87-7.67 (2H, m), 7.59 (2H, d, *J*=7.37 Hz), 7.40 (2H, t, *J*= 7.45Hz), 7.37-7.26 (7H, m), 6.07 (1H, d, *J*=8.4Hz, NHα), 5.45 (1H, br, NH, NHβa), 5.32 (1H, br, NHβb), 5.21 (2H, s, -CH_2Ph), 4.69-4.62 (1H, m, Hα), 4.42 (1H, dd, *J* = 7.2, 10.2Hz, FmocCH_2a), 4.33 (1H, dd, *J*= 7.6, 10.4Hz, FmocCH_2b), 4.21 (1H, t, *J*=7.2 Hz, FmocC*H*), 3.01 (1H, dd, *J*= 4.2, 16.3Hz, Hβa), 2.80 (1H, dd, *J*=3.9, 16.2Hz, Hβb); ^{13}C NMR (101 MHz, $CDCl_3$) δ 171.9, 171.8, 156.2, 143.8, 143.7, 141.3, 128.6, 128.4, 128.2, 127.7, 127.1, 125.2, 120.0, 67.5, 67.2, 50.7(Cα), 47.1(Fmoc*C*H), 37.1(Cβ); ESI-MS calcd for $C_{26}H_{24}N_2O_5$ $[M+H]^+$: 445.176; $[M+Na]^+$: 467.158; $[M+K]^+$:483.132. Found 445.167, 467.144, 483.120. Rf = 0.55 (1:9, methanol : dichloromethane)

2`-(2,3,4,6-Tetra-*O*-acetyl-α-D-galactopyran-1-yl)-ethan-1`-al (57)[5]

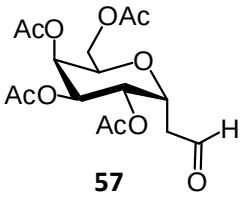

57

Ozonolysis of alkene **37** to yield aldehyde **57** was performed in a similar manner as for the synthesis of aldehyde **27**. **57** was obtained as a colourless oil in 95% yield. ^{1}H NMR (400 MHz, $CDCl_3$) δ 9.73 (1H, dd, *J* = 2.4, 1.4 Hz, H1`), 5.42 (1H, dd, *J* = 3.1, 3.1 Hz, H4), 5.29 (1H, dd, *J* = 8.5, 4.8 Hz, H2), 5.18, (1H, dd, *J* = 8.5, 3.3 Hz, H3), 4.87 (1H, dt, *J* = 8.0, 5.5 Hz, H1), 4.36–4.30 (1H, m, H6a), 4.12–4.06 (2H, m, H5, H6b), 2.77–2.65 (2H, m, H2`), 2.12 (3H, s, CH_3), 2.07 (3H, s, CH_3), 2.06 (3H, s, 2 x CH_3); ESI-MS calcd for $C_{16}H_{22}O_{10}$ $[M+H]^+$ = 375.1. Found 375.1. Rf = 0.42 (4:1 toluene:acetone)

General procedure for synthesis of C-linked glycoconjugate

To a flame-dried flask, 2`-(2,3,4,6-tetra-*O*-acetyl-α-D-galactopyran-1-yl)-ethan-1`-oic acid (**48**) (400 mg, 1.0 mmol) was dissolved in distilled CH_2Cl_2, and HBTU (448 mg, 1.1 mmol) was added, and the mixture was stirred for 15 minutes. The amino acid (**46** or **47**) was then added (1.2 mmol), followed by DIPEA (0.52 mL, 3.0 mmol) and the solution was stirred overnight. Upon consumption of starting material, the solution was diluted with CH_2Cl_2 and then washed three times with saturated NH_4Cl (aq). The organic phase was then dried with $MgSO_4$, filtered, and dried in vacuo. The glycoconjugate was then purified using 2:1 Hexanes : EtOAc, in 70 and 80% yields for **58** and **59**, respectively.

Benzyl-*Nα*-(S)-[(9H-fluoren-9-ylmethoxy)carbonyl]-*Nγ*-[2`-(2,3,4,6-tetra-*O*-acetyl-α-D-galactopyran-1-yl) ethan-1`-amido]-α,γ-diaminobutanoate (58)

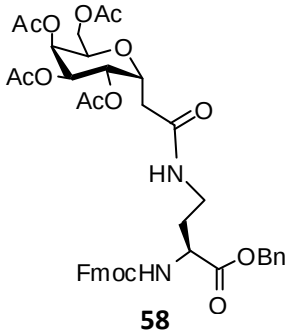

58

^{1}H NMR (500 MHz, $CDCl_3$) δ 7.77 (1H, dd, *J* = 7.5, 2.1 Hz), 7.60 (1H, dd, *J* = 7.3, 2.7 Hz), 7.40 (1H, dt, *J* = 7.5, 7.4, 5.1 Hz), 6.61 (1H, t, *J* = *5.7* Hz, NHβ), 5.66 (1H, d, *J* = 8.1 Hz, NHα), 5.40 (1H, dd, *J* = 2.9, 2.9 Hz, H4), 5.28 (1 H, dd, *J* = 8.4, 4.7 Hz, H2), 5.18 (2H, s, -C*H*$_2$Ph), 5.14 (1 H, dd, *J* = 8.7, 3.2 Hz, H3), 4.69 (1 H, td, *J* = 9.1, 4.7, 4.7 Hz, H1), 4.48-4.38(3H, m, FmocCH$_2$, Hα), 4.27-4.19 (2H, m, FmocC*H*, H6a), 4.15-4.09 (2H, m, H5, H6b), 3.72-3.62 (1H, m, Hγa), 2.94-2.84 (1H, m, Hγb), 2.52 (1H, dd, *J* = 15.2, 9.2 Hz, H2`a), 2.41 (1H, dd, *J* = 15.3, 4.6 Hz, H2`b), 2.17-2.08 (1H, m, Hβa), 2.10 (3H, s, CH_3), 2.04 (3H, s, CH_3), 2.03 (3H, s, CH_3), 1.97 (3H, s, CH_3), 1.74-1.64 (1H, m, Hβb); ^{13}C NMR (101 MHz, $CDCl_3$) δ 171.9, 170.5, 170.0, 169.8, 169.6, 169.3, 156.6, 143.7, 143.5, 141.3, 141.3, 135.0, 128.7, 128.6, 128.3, 127.8, 127.1, 127.0, 125.0, 125.0, 120.0, 120.0, 69.3, 67.8, 67.5, 67.2, 66.9, 60.9(C6), 51.5, 47.1(Fmoc*C*H), 35.4(Cγ), 34.6(C2`), 32.9(Cβ), 20.7(CH_3), 20.7(CH_3), 20.6(CH_3); ESI-MS calcd for $C_{42}H_{46}N_2O_{14}$ $[M+H]^+$: 803.302; $[M+Na]^+$: 825.284; $[M+K]^+$:841.258. Found 803.342, 825.324, 841.303.

Benzyl-*Nα*-(S)-[(9H-fluoren-9-ylmethoxy)carbonyl]-*Nβ*-[2`-(2,3,4,6-tetra-*O*-acetyl-α-D-galactopyran-1-yl) ethan-1`-amido]-α,β-diaminopropanoate (59)

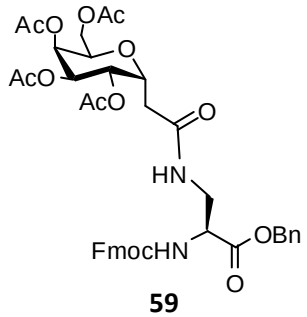

59

^{1}H NMR (500 MHz, $CDCl_3$) δ 7.77 (2H, d, *J*=7.6 Hz), 7.60 (2H, t, *J*=7.6 Hz), 7.43-7.28 (9H, m), 6.36 (1H, t, *J*=5.4 Hz, NHβ), 5.99 (1H, d, *J*=5.4 Hz, NHα), 5.39 (1H, t, *J* = 3.3 Hz, H4), 5.23 (1H, dd, *J*=4.5, 8.1 Hz, H2), 5.19 (2H, s, -OCH$_2$Ph), 5.12 (1H, dd, *J*=3.2, 8.2 Hz, H3), 4.61-4.53 (1H, m, H1), 4.52-4.32 (3H, m), 4.30-4.18 (2H, m), 4.13 (1H, dd, *J*= 4.8, 11.9 Hz, H6b), 4.09-4.03 (1H, m, H5), 3.70 (2H, t, *J*=5.2 Hz, Hβ), 2.47 (1H, dd, *J*=9.9, 15.3 Hz, H2`a), 2.33 (1H, dd, *J*=3.7, 15.6 Hz, H2`b), 2.09 (3H, s, CH_3), 2.07 (3H, s, CH_3), 2.04 (3H, s, CH_3), 1.99 (3H, s, CH_3); ^{13}C NMR (101 MHz, $CDCl_3$) δ 170.6, 170.2, 170.0, 169.8, 169.7, 169.5, 156.1, 143.8, 143.7, 141.3, 135.1, 128.7, 128.6, 127.7, 127.1, 125.1, 125.1, 120.0, 69.7, 68.4, 67.9, 67.7, 67.2, 66.7(Fmoc*C*H$_2$), 60.9(C6), 54.5(Cα), 47.1(Fmoc*C*H), 41.4(Cβ), 34.4(C2`), 20.7(CH_3), 20.6(CH_3); ESI-MS calcd for $C_{41}H_{44}N_2O_{14}$ $[M+H]^+$: 789.287; $[M+Na]^+$:811.269. Found 789.332, 811.312.

General procedure for synthesis of glycoconjugate tripeptides **60-62**

Glycoconjugate tripeptides were synthesized using solid-phase peptide synthesis as previously described for glycopolymers **18-21**. However, prior to cleavage from the Wang resin, the

solution was stirred with acetic anhydride and pyridine for 1 hr to acetylate the terminal amine. The excess solutions were then drained, and the resin was washed successively with DMF, EtOH and then CH_2Cl_2. The desired glycopeptides were then cleaved from the resin and de-acetylated in the manner previously described.

_N_-Acetyl-glycinamido-[(S)-_Nβ_-[2`-(α-D-galactopyran-1-yl)-ethan-1`-amido]-α,β-diaminopropanoic-1-amido]-glycine (60)

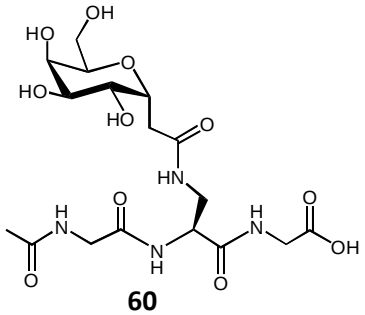

60

^{1}H NMR (500 MHz, 95:5 H_2O:D_2O) δ: 8.33 (1H, d, *J*=7.0Hz,), 8.30 (2H, t, *J*=7.5Hz), 8.23(1H, t, *J*=4.0Hz), 4.57-4.45 (2H, m, Hα, H1), 4.04-4.01 (1H, m, H2), 3.98-3.94 (3H, m), 3.82-7.70 (7H, m, Hβa, H3), 3.60-3.54 (1H, m, Hβb), 2.71-2.60(2H, m, H2`), 2.08 (3H, s, NHAc) ; $^{13}$C NMR (101 MHz, 95:5 $H_2O$:$D_2O$) δ 175.1, 174.5, 171.9, 171.2, 73.0(C1), 72.6, 69.8, 69.1, 67.8 (C2), 61.3(C6), 53.8 (Cα), 43.4($C\alpha_{Gly1}$), 42.7($C\alpha_{Gly2}$), 40.3(Cβ), 32.4 (C2`), 21.9(CH_3). ESI-MS calcd for $C_{17}H_{28}N_4O_{11}$ $[M+Na]^+$: 487.165. Found 487.197.

_N_-Acetyl-glycinamido-[(S)-_Nγ_-[2`-(α-D-galactopyran-1-yl)-ethan-1`-amido]-α,γ-diaminobutyric-1-amido]-glycine (61)

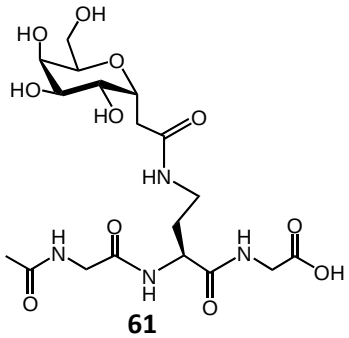

61

^{1}H NMR (500 MHz, 95:5 H_2O:D_2O) δ: 8.63 (1H, d, *J* = 7.5Hz), 8.48 (1H, t, *J* = 5.0Hz), 8.44(1H, t, *J* = 6.0Hz), 8.29 (1H, t, *J* = 6.0Hz), 4.51-4.41 (2H, m, H1, Hα), 4.03 (1H, dd, *J* = 6.5, 10.0 Hz, H2), 3.90-3.80 (3H, m), 3.68-3.50 (7H, m), 3.35-3.26 (2H, m, Hγ), 2.71-2.64 (1H, m, H2`a), 2.58

(1H, dd, *J* = 4.0, 15.0 Hz, H2`b), 2.15-2.08 (1H, m, Hβa), 2.06 (3H, s, $CH_3$), 1.94-1.88 (1H, m, Hβb); $^{13}$C NMR (126 MHz, 95:5 $H_2O$:$D_2O$) δ 175.0, 173.8, 173.7, 173.5, 171.9, 72.9(C1), 72.5, 69.7, 68.9, 67.7, 61.0(C6), 51.4(Cα), 42.7($CH_2$), 42.5($CH_2$), 35.9(Cγ), 32.4 (C2`), 30.3(Cβ), 21.7(CH_3); ESI-MS calcd for $C_{18}H_{30}N_4O_{11}$ $[M+Na]^+$: 501.180. Found 501.210.

_N_-Acetyl-glycinamido-[(S)-_Nδ_-[2`-(α-D-galactopyran-1-yl)-ethan-1`-amido]-ornithinamido-glycine (62)

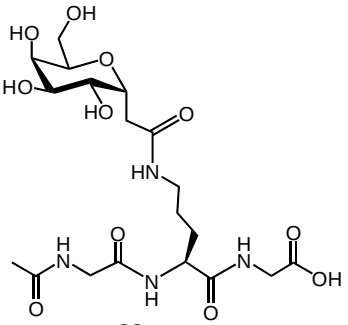

62

^{1}H NMR (500 MHz, 95:5 H_2O:D_2O) δ 8.57 (1H, t, *J* = 7.0Hz), 8.54 (1H, d, *J* = 6.0Hz), 8.46 (1H, t, *J* = 6.0Hz), 8.28 (1H, t, *J* = 5.5Hz), 4.55-4.47 (1H, m, H1), 4.39-4.35 (1H, m, Hα), 4.03 (1H, dd, *J* = 6.0, 10.0Hz, H2), 4.01-3.99 (1H, m, H4), 3.97(2H, d, *J* = 6.0Hz), 3.94 (2H, d, *J* = 6.0Hz), 3.82 (1H, t, *J* = 6.0Hz, H5), 3.75 (1H, dd, *J* = 3.0, 10.5Hz, H3), 3.72-3.66(2H, m, H6), 3.23(2H, dt, *J* = 6.5, 6.5Hz, Hδ), 2.70-2.57 (2H, m, H2`), 2.05 (3H, s, $CH_3$), 1.92-1.86 (1H, m, Hβa), 1.77-1.69 (1H, m, Hβb), 1.63-1.55 (2H, m, Hγ); $^{13}$C NMR (126 MHz, 95:5 $H_2O$:$D_2O$) δ174.9, 174.3, 173.6, 173.4, 171.7, 72.9(C1), 72.5(C5), 69.7(C3), 68.8(C4), 67.7(C2), 60.9(C6), 53.4(Cα), 42.6(CαGly), 41.4(CαGly), 38.9(Cδ), 32.4(C2`), 28.3(Cβ), 24.7(Cγ), 21.7(CH_3); ESI-MS calcd for $C_{19}H_{32}N_4O_{11}$ $[M+Na]^+$: 515.196. Found $[M+Na]^+$ 515.222.

_Nα_-(S)-[(9H-fluoren-9-ylmethoxy)carbonyl]-_Nγ_-[3`-(2,3,4,6-tetra-_O_-acetyl-α-D-galactopyran-1-yl) propan-1`-amido]-α,γ-diaminobutyric acid (66)

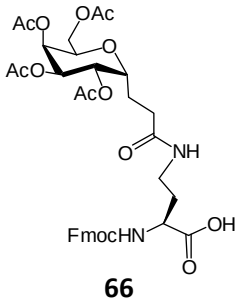

66

Glycoconjugate building block **66** was prepared using the same procedures as previously described for **44**. **66** was obtained as an amorphous white solid in 95% yield (based on recovered starting material). ^{1}H NMR(500 MHz, CD_3OD) δ 7.80 (2H, d, *J* = 7.5 Hz), 7.69 (2H, dd, *J* = 5.7, 6.7 Hz), 7.39 (2H, dd, *J* = 7.4, 7.5 Hz), 7.31 (2H, dd, *J* = 7.4, 7.4 Hz), 5.40-5.38 (1H, m, H4), 5.27 (1H, dd, *J* = 3.2, 9.7 Hz, H2), 5.22 (1H, dd, *J* = 5.1, 9.6 Hz, H3), 4.36 (2H, d, *J* = 7.0 Hz, FmocCH_2), 4.27-4.22 (2H, m), 4.21-4.13 (2H, m), 4.12-4.06 (1H, m, H6b), 3.36-3.28 (1H, m, Hγa), 3.26-3.19 (1H, m, Hγb), 2.35-2.27 (1H, m, H2`a), 2.25-2.16 (1H, m, H2`b), 2.13-2.04 (2H, m, H3`a, Hβa), 2.06 (3H, s, $CH_3$), 2.04(3H, s, $CH_3$), 1.99 (3H, s, $CH_3$), 1.97 (3H, s, $CH_3$), 1.89-1.76 (2H, m, H3`b, Hβb); ^{13}C NMR (101 MHz,$CDCl_3$) δ 173.8, 173.4, 171.0, 170.2, 170.1, 169.9, 156.3, 143.8, 143.5, 141.3, 141.2, 127.8, 127.1, 125.1, 120.0, 71.4(C1), 68.3, 68.2, 67.9, 67.4, 67.2(Fmoc*C*H_2), 61.4 (C6), 51.3 (Cα) , 47.1(Fmoc*C*H), 35.9 (Cγ), 33.1, 32.1 (C2`), 21.7, 20.8(CH_3), 20.8(CH_3), 20.7(CH_3), 20.6 (CH_3). ESI-MS calcd for $C_{36}H_{42}N_2O_{14}$ $[M+H]^+$: 727.2714; $[M+Na]^+$:749.2534. Found 727.243, 749.229. Rf = 0.15 (1:9 MeOH : CH_2Cl_2)

_Nα_-(S)-[(9H-fluoren-9-ylmethoxy)carbonyl]-_Nβ_-[2`-(2,3,4,6-tetra-_O-tert_-butyldimethylsilyl-α-D-galactopyran-1-yl) butan-1`-amido]-α,β-diaminopropanoic acid (67)

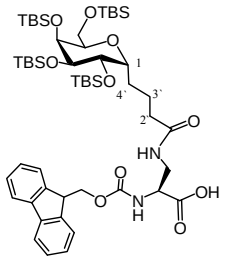

67

Glycoconjugate building block **67** was prepared using the same procedures as previously described for **44**. **67** was obtained as an amorphous white solid in 93% yield (based on recovered starting material). ^{1}H NMR(500 MHz, CD_3OD) δ 7.79 (2H, d, *J*= 7.5 Hz), 7.67 (2H, dd, *J*= 6.3, 6.3 Hz), 7.39 (2H, d, *J*=7.4 Hz), 7.31 (2H, d, *J*= 7.4 Hz), 4.38-4.20 (6H, m, FmocCH_2, Hα, H6a,H4, FmocCH), 3.90-3.84 (1H, m, H5), 3.84-3.76 (3H, m, H2,H1,H6b), 3.66 (1H, dd, *J*= 4.1, 13.6 Hz, Hβa), 3.54-3.51(1H, m, H3), 3.50 (1H, dd, *J* = 8.2, 14.0 Hz, Hβb), 2.30-2.15 (2H, m, H2`), 1.79-1.69 (1H, m, H3`a), 1.69-1.52 (2H, m, H3`b, H4`a), 1.48-1.37 (1H, m, H4`b), 0.93 (18H, s, C(C*H*$_3$)$_3$), 0.91 (9H, s, C(C*H*$_3$)$_3$), 0.89 (9H, s, C(C*H*$_3$)$_3$), 0.08 (6H, s, 2 x SiC*H*$_3$), 0.06 (9H, s, 3 x SiC*H*$_3$), 0.04 (9H,s, 3 x SiC*H*$_3$) ; ^{13}C NMR (101 MHz,$CDCl_3$) δ 174.6, 170.2, 156.1, 143.9, 143.7, 141.3, 141.2, 135.2, 128.6, 128.5, 128.4, 127.7, 127.1, 125.2, 119.9, 79.2(C5), 74.3(C3), 73.6(C2), 67.4(Fmoc*C*H_2), 67.2 (C4), 66.6(C1), 58.6(C6), 55.3(Cα), 47.1(FmocCH), 41.2(Cβ), 35.8(C2`), 30.0 (C4`), 26.0 (C(*C*H_3)$_3$), 26.0(C(*C*H_3)$_3$), 25.8(C(*C*H_3)$_3$), 25.7(C(*C*H_3)$_3$), 23.1 (C3`), 18.3(*C*(Me)$_3$), 18.1(*C*(Me)$_3$), 18.0(*C*(Me)$_3$), 17.9 (*C*(Me)$_3$), -4.4(Si*C*H_3), -4.6(Si*C*H_3), -4.9(Si*C*H_3), -4.9(Si*C*H_3), -4.9(Si*C*H_3), -5.2(Si*C*H_3), -5.3(Si*C*H_3). ESI-MS calcd for

$C_{52}H_{90}N_2O_{10}Si_4$ $[M+H]^+$: 1015.575; $[M+Na]^+$: 1037.5570. Found 1015.983, 1037.956. Rf = 0.5 (7:1:1:1 ethyl acetate : water : acetonitrile : methanol).

3`-(2,3,4,6-Tetra-*O*-acetyl-α-D-galactopyran-1-yl)-propan-1`-oic acid (68)

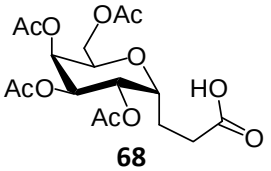

68

68 was synthesized using **71** (300 mg, 0.70 mmol) as the starting material. Oxidation was performed in the same manner as for the conversion of aldehyde **57** into carboxylic acid **48**. **48** was obtained as an amorphous white solid in 90 % yield (253 mg). ^{1}H NMR(500 MHz, $CDCl_3$) δ 5.39 (1H, dd, *J* = 2.7, 2.7 Hz, H4), 5.26 (1H, dd, *J* = 5.2, 9.4 Hz, H2), 5.18 (1H, dd, *J*= 3.3, 9.4 Hz, H3), 4.26-4.19 (2H, m, H6a,H1), 4.07-3.99 (2H, m, H5,6b), 2.51-2.37 (2H, m, H2`), 2.10 (3H, s, $CH_3$), 2.07 (3H, s, $CH_3$), 2.04 (3H, s, $CH_3$), 2.00 (3H, s, $CH_3$), 2.05-1.95 (1H, m, H3`a), 1.83-1.75 (1H, m, H3`b); $^{13}$C NMR (101 MHz,$CDCl_3$) δ 177.3, 170.6, 170.1, 169.9, 169.8, 71.3(C1), 68.3(C5), 68.2(C3), 67.8(C2), 67.4(C4), 61.3(C6), 29.6 (C2`), 21.0(CH_3), 20.8(CH_3), 20.7(CH_3), 20.7(CH_3), 18.6(C3`). ESI-MS calcd for $C_{17}H_{24}O_{11}$ $[M+Na]^+$: 427.1216. Found 427.153. Rf = 0.37 (1:1 toluene:acetone)

4`-(2,3,4,6-Tetra-*O-tert*-butyldimethylsilyl-α-D-galactopyran-1-yl)-butan-1`-oic acid (69)

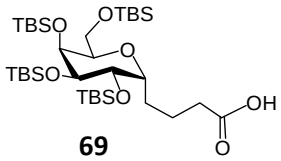

69

To the starting methyl ester **76** (0.44 g, 0.61 mmol), was added 10 equivalents of a 0.8 M solution of $CaCl_2$ (dissolved in 7:3 isopropanol:water), and vigorously stirred at room temperature. 3 equivalents of a 0.5M solution of NaOH (dissolved in 7:3 isopropanol:water) was then added dropwise, and the mixture was stirred until disappearance of the starting material. The carboxylic acid was extracted from the aqueous layer using 5 portions of ethyl acetate. The ethyl acetate layers were combined, washed with brine, dried with $MgSO_4$, evaporated, and purified using silica gel column chromatography (10:1, hexane : diethyl ether) to obtain an amorphous white solid (350 mg, 85% yield) ^{1}H NMR(400 MHz, $CDCl_3$) δ 4.25-4.16 (2H, m, H6a, H4), 3.91 (1H, dd, *J*=7.4, 7.4 Hz, H5), 3.79 (1H, dd, *J*=3.1, 8.8 Hz, H1), 3.73-3.67 (2H, m, H6b, H2), 3.45- 3.39 (1H, m, H3), 2.49-2.36 (2H, m, C2`), 1.88-1.72 (1H, m, C3`a), 1.78-1.62 (2H, m, C3`b, C4`a), 1.44-1.33 (1H, m, C4`b), 0.90 (9H, s, C(CH_3)$_3$), 0.90 (9H, s, C(CH_3)$_3$), 0.89

(9H, s, C(CH_3)$_3$), 0.87 (9H, s, C(CH_3)$_3$), 0.08 (3H, s, SiCH_3), 0.07 (3H, s, SiCH_3), 0.06 (6H, s, SiCH_3), 0.06 (3H, s, SiCH_3), 0.05 (3H, s, SiCH_3), 0.03 (3H, s, SiCH_3), 0.02 (3H, s, SiCH_3) ; ^{13}C NMR (101 MHz,$CDCl_3$) δ 179.2, 79.2(C5), 74.1(C3), 73.7(C2), 67.4(C4), 66.0(C1), 58.5(C6), 33.8 (C2`), 30.0 (C3`), 26.0(C(CH_3)$_3$), 25.9(C(CH_3)$_3$), 25.8(C(CH_3)$_3$), 25.7(C(CH_3)$_3$), 21.7(C4`), 18.3(C(Me)$_3$), 18.1(C(Me)$_3$), 18.0(C(Me)$_3$), 18.0(C(Me)$_3$), -4.4(SiCH_3), -4.5(SiCH_3), -4.6(SiCH_3), -4.9(SiCH_3), -4.9(SiCH_3), -5.4(SiCH_3). ESI-MS calcd for $C_{34}H_{74}O_7Si_4$ $[M+H]^+$: 707.4590; $[M+Na]^+$: 729.4409. Found 707.517, 729.510. Rf = 0.30 (3:1 hexane: diethyl ether)

3`-(2,3,4,6-Tetra-*O*-acetyl-α-D-galactopyran-1-yl)-1`-methoxyprop-1`-ene (70)

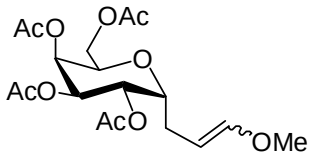

70

To a flame dried flask under argon, 30 mL distilled THF was added to (4.43 g, 12.9 mmol) dried (methoxymethyl)triphenylphosphonium chloride, stirred and cooled to -78 ^{o}C. A pre-cooled solution of n-butyl lithium (4.3 mL of 1.0 M in THF) was then added and the mixture was stirred for 40 minutes. A pre-cooled solution of the starting aldehyde **57** (1.62 g, 4.3 mmol), 0.21 M in THF, was then slowly cannulated into the mixture and stirred for 1.5 hrs at -78^{o}C, and then allowed to warm up to room temperature and stirred overnight. The reaction was then quenched with dropwise addition of a saturated aqueous solution of ammonium chloride. Diethyl ether was then added to the mixture, and then transferred to a separatory funnel. The aqueous phase was extracted three times with diethyl ether. The organic layers were combined and washed with brine, concentrated under reduced pressure, and purified by column chromatography (8:1 toluene:acetone) to afford an amorphous white solid (0.753 g, 45% yield). E:Z isomeric ratio, 5.9:1. ^{1}H NMR(500 MHz, $CDCl_3$) E-isomer: δ 6.34 (1H, d, J=12.7 Hz, H1`), 5.39 (1H, dd, $J$=2.8, 2.8 Hz, H4), 5.24 (1H, dd, $J$=4.9, 9.0 Hz, H2), 5.19 (1H, dd, $J$= 3.2, 9.1 Hz, H3), 4.62 (1H, td, $J$=7.3, 12.8Hz, H2`), 4.26-4.19 (1H, dd, J=9.2, 12.6 Hz, H6a), 4.17-4.11(1H, m, H1), 4.08-4.03 (2H, m, H5,6b), 3.50 (3H, s, OCH_3), 2.35-2.25 (1H, m, H3`a) 2.16-2.09 (1H, m, H3`b), 2.10 (3H, s), 2.06, (3H, s), 2.03 (3H, s), 2.01 (3H, s); Z-isomer δ 5.98 (1H, d, J=6.2 Hz, H1`), 5.39 (1H, dd, $J$=2.8, 2.8 Hz, H4), 5.27-5.22 (2H, m, H2, H3), 4.29 (1H, td, $J$ = 6.8, 6.8, 7.2 Hz, H2`), 4.26-4.19 (1H, m, H6a), 4.17-4.11(1H, m, H1), 4.08-4.03 (2H, m, H5,6b), 3.57 (3H, s, OCH_3), 2.58-2.49 (1H, m, H3`a), 2.24-2.17 (1H, m, H3`b), 2.10 (3H, s, CH_3), 2.06, (3H, s, CH_3), 2.03 (3H, s, CH_3), 2.01 (3H, s, CH_3). ^{13}C NMR (101 MHz,$CDCl_3$) E-isomer δ 170.1, 170.0, 169.8, 169.8, 149.0 (C1`), 97.1 (C2`), 72.1(C1), 68.3(C5), 67.9(C2), 67.9 (C3), 67.6 (C4), 61.4(C6), 55.8(OCH_3), 25.0(C3`), 20.7 ($CH_3$), 20.7($CH_3$), 20.6($CH_3$); Z-isomer δ 170.1, 170.0, 169.8, 169.8, 148.3(C1`), 100.4 (C2`), 71.9(C1), 68.2 (C5), 68.0(C2), 67.8 (C3), 67.7(C4), 61.5(C6), 59.5 ($OCH_3$), 21.0 (C3`), 20.7(CH_3), 20.7(CH_3), 20.6(CH_3). ESI-MS calcd for $C_{18}H_{26}O_{10}$ $[M+H]^+$: 403.1604; $[M+NH_4]^+$:420.1870. Found 403.147, 420.172. Rf = 0.55 (4:1 toluene:acetone)

3`-(2,3,4,6-Tetra-*O*-acetyl-α-D-galactopyran-1-yl)-propan-1`-al (71)

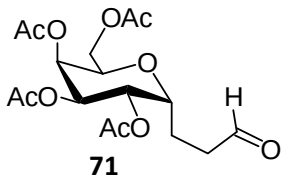

71

Vinyl methoxy ether (**70**, 0.73 g, 1.8 mmol) was dissolved in 5mL of THF, and cooled to 0 ^{o}C. Concentrated HCl (3.4 mL) was added dropwise and the reaction was stirred for 45 minutes. The reaction was quenched and neutralized using an aqueous solution of saturated sodium bicarbonate. The aqueous layer was extracted three times with dichloromethane, and the organic layer was concentrated in vacuo to afford the resulting aldehyde in 93% yield (0.66 g) as an amorphous white solid. ^{1}H NMR (500 MHz, $CDCl_3$) δ 9.78 (1H, s, CHO), 5.37 (1H, dd, *J*= 2.7, 2.7 Hz, H4), 5.23 (1H, dd, *J*= 4.9, 9.1 Hz, H2), 5.17 (1H, dd, *J*= 3.2, 9.1 Hz, H3), 4.23 (1H, dd, *J* = 9.6, 13.4 Hz, H6a), 4.16 (1H, ddd, *J*= 3.5, 4.6, 11.6 Hz, H1), 4.04-3.98 (2H, m, H5,6b), 2.61-2.47 (2H, m, H2`), 2.09 (3H, s, $CH_3$), 2.07 (3H, s, $CH_3$), 2.04 (3H, s, $CH_3$), 2.00 (3H, s, $CH_3$), 2.01-1.93 (1H, m, H3`a), 1.82-1.73 (1H, m, H3`b) $^{13}$C NMR (101 MHz,$CDCl_3$) δ 200.8(CO), 170.5, 169.9, 169.7, 71.2(C1), 68.5(C5), 68.2(C2), 67.7(C3), 67.3(C4), 61.1(C5), 39.7(C2`), 20.7 (CH_3), 20.7(CH_3), 20.6(CH_3), 20.6(CH_3), 18.6(C3`). ESI-MS calcd for $C_{17}H_{24}O_{10}$ $[M+Na]^+$:411.1267. Found 411.156. Rf = 0.42 (4:1 toluene:acetone)

Benzyl *Nα*-(S)-[(9H-fluoren-9-ylmethoxy)carbonyl]-*Nγ*-[3`-(2,3,4,6-tetra-*O*-acetyl-α-D-galactopyran-1-yl) propan-1`-amido]-α,γ-diaminobutanoate (72)

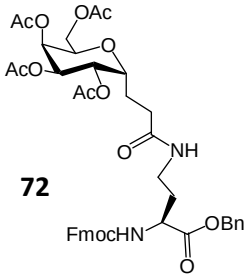

72

Glycoconjugate **66** was prepared using the same procedure as for **58** by coupling amino acid **46** (365 mg, 0.85 mmol) with *C*-α-glycoside **68** (245 mg, 0.61 mmol) to afford an amorphous white solid (74% yield). ^{1}H NMR(500 MHz, $CDCl_3$) δ 7.77 (2H, dd, *J*= 2.3, 7.5 Hz), 7.59 (2H, dd, *J*= 6.1, 6.1 Hz), 7.44-7.28 (9 H, m), 6.41 (1H, t, *J*= 5.4 Hz, NHβ), 5.63 (1H, d, *J*= 8.3 Hz, NHα), 5.42-5.39 (1H, m, H4), 5.29 (1H, dd, *J*= 5.4, 9.5 Hz, H2), 5.23-5.16 (3H, m, H3, -C*H*$_2$Ph), 4.47-4.37 (3H, m, Hα, FmocCH_2), 4.25-4.13 (3H, m, FmocC*H*, H1, H6a), 4.07-4.01 (2H, m, H5,

H6b), 3.75-3.66 (1H, m, Hγa), 2.89-2.81 (1H, m, Hγb), 2.30-2.22 (1H, m, H2`a ), 2.21-2.15 (1H, m, H2`b), 2.15-2.08 (1H, m, Hβa), 2.11 (3H, s, CH_3), 2.05 (3H, s, CH_3), 2.08-2.00 (1H, m, H3`a), 2.01 (6H, s, 2 x $CH_3$), 1.90-1.80 (1H, m, H3`b), 1.71-1.62 (1H, m, Hβb); ^{13}C NMR (101 MHz,$CDCl_3$) δ 172.1, 172.0, 170.6, 170.1, 169.9, 156.6, 143.7, 143.4, 141.3, 141.3, 135.0, 128.7, 128.6, 128.4, 127.8, 127.1, 127.0, 125.0, 120.0, 71.9 (C1), 68.1, 68.0, 67.9, 67.6(C4), 67.5(*C*H_2Ph), 67.1(Fmoc*C*H_2), 61.5(C6), 51.4(Cα), 47.1(Fmoc*C*H), 35.2, 33.1, 32.2, 21.4(Cβ), 20.8 (CH_3), 20.7 (CH_3), 20.6 (CH_3). ESI-MS calcd for $C_{43}H_{48}N_2O_{14}$ $[M+H]^+$: 817.3184; $[M+Na]^+$: 839.3003. Found 817.365, 839.348. Rf = 0.29 (2:1 hexane : EtOAc).

Methyl-4`-(2,3,4,6-tetra-*O*-acetyl-α-D-galactopyran-1-yl)-but-2`-en-1`-oate (74)

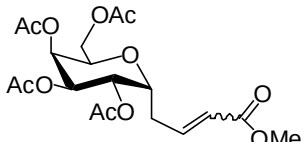

74

To a flamed dried flask was added dried lithium bromide (2.5g, 2.9 mmol) and distilled acetonitrile under argon. Methyl(dimethoxyphosphoryl) acetate (0.79 g, 2.1 mmol) was added and the solution was stirred for 15 minutes. Triethylamine (0.41 mL, 2.9 mmol) was then added and the solution was stirred for another 30 minutes. Aldehyde **57** (0.73 g, 1.95 mmol) was dissolved in distilled acetonitrile in another flamed-dried flask and slowly cannulated to the phosphonate-containing flask and stirred overnight. The reaction was diluted with diethyl ether, and quenched with a saturated aqueous solution of ammonium chloride. The resulting conjugated ester was extracted using diethyl ether, dried with $MgSO_4$, and evaporated. The desired products were purified using silica gel column chromatography (8:1 toluene:acetone), and obtained as an oil (0.84 g, 92% yield) (E/Z : 25/1). ^{1}H NMR (500 MHz, $CDCl_3$) *Z*-isomer δ 6.86 (1H, td, *J* = 7.0, 15.6 Hz, H3`), 5.90 (1H, d, *J* = 15.7 Hz, H2`), 5.37 (1H, dd, *J*= 2.9, 2.9 Hz, H4), 5.22 (1H, dd, *J*= 4.9, 9.0 Hz, H2), 5.16, (1H, dd, *J*= 3.3, 9.0 Hz, H3), 4.35-4.30 (1H, m, H1), 4.23 (1H, dd, *J*= 7.6, 10.8 Hz, H6a), 4.07-4.02 (1H, m, H5), 4.01 (1H, dd, *J*=4.6, 11.0 Hz, H6b), 4.00 (3H, s, OCH_3), 2.61-2.53 (1H, m, H4`a), 2.40-2.33 (1H, m, H4`b), 2.07 (3H, s, CH_3), 2.04 (3H, s, CH_3), 2.00 (3H, s, CH_3), 1.99 (3H, s, CH_3); ^{13}C NMR (101 MHz,$CDCl_3$) δ 170.5, 169.8, 169.7, 169.6, 166.2(C1`), 143.6(C3`), 123.5(C2`), 70.4(C1), 68.6(C5), 68.0, 67.6, 67.2(C4), 61.2(C6), 51.4(O*C*$H_3$), 29.4(C4`), 20.7(CH_3). ESI-MS calcd for $C_{19}H_{26}O_{11}$ $[M+Na]^+$: 453.1317 Found 453.166. Rf = 0.50 (4:1 toluene : acetone).

Methyl-4`-(2,3,4,6-tetra-*O*-acetyl-α-D-galactopyran-1-yl)-butan-1`-oate (75)

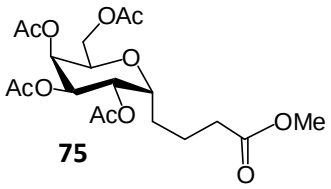

75

Conjugated ester **74**, 800 mg, 0.186 mmol) was dissolved in ethanol, and 10% w/w Pd/C was added. The flask was degassed under vacuum, and hydrogen gas was added via a balloon. After consumption of the starting material by TLC, the solution was purged with nitrogen, and gravity filtered to remove Pd/C. The resulting ester was evaporated in vacuo and purified by silica column chromatography (5:1, Et_2O : CH_2Cl_2) to obtain a colourless oil (780mg, 97% yield) ^{1}H NMR(500 MHz, $CDCl_3$) δ 5.40 (1H, dd, *J*= 2.8, 2.8 Hz, H4), 5.26 (1H, dd, *J*= 5.3, 9.5 Hz, H2), 5.17 (1H, dd, *J*= 3.4, 9.5 Hz, H3), 4.25-4.17 (1H, m, H6a,H1), 4.11-4.03 (1H, m, H5, H6b), 3.76 (3H, s, OCH_3), 2.43-2.30 (2H, m, H2`), 2.12 (3H, s, $CH_3$), 2.07 (3H, s, $CH_3$), 2.06 (3H, s, $CH_3$), 2.02 (3H, s, $CH_3$), 1.85-1.69 (2H, m, H3`), 1.65-1.56 (1H, m, H4`a), 1.50-1.42 (1H, m, H4`b); ^{13}C NMR (101 MHz,$CDCl_3$) δ 173.5, 170.6, 170.1, 169.9, 169.8, 71.9(C1), 68.3(C5), 68.0(C2), 67.9(C3), 67.6(C4), 61.5(C6), 51.6(O*C*H_3), 33.3 (C2`), 24.9(C3`), 20.8(C4`), 20.7(CH_3), 20.7(CH_3), 20.7(CH_3). ESI-MS calcd for $C_{19}H_{28}O_{11}$ $[M+H]^+$: 433.1710; $[M+NH_4]^+$: 450.1975. Found 433.181, 450.196. Rf = 0.50 (4:1 toluene: acetone)

Methyl-4`-(2,3,4,6-tetra-*O-tert*-butyldimethylsilyl-α-D-galactopyran-1-yl)-butan-1`-oate (76)

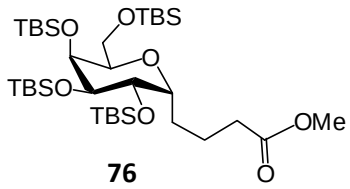

76

Peracetylated *C*-glycoside **75** (750 mg, 0.174 mmol) was dissolved in methanol. 9 mL of a 1.0 M solution of sodium methoxide in methanol was added and stirred until TLC showed only the fully de-acetylated product. Pre-washed sulfonic acid IR-resin was then added to neutralize the solution. The mixture was then filtered and rinsed with methanol and evaporated in vacuo to afford a white solid. The deprotected carbohydrate derivative was dried overnight over phosphorus pentoxide in vacuo. The mixture placed under argon, distilled dichloromethane (20 mL) was added, and cooled to 0 ^{o}C. 2,6-lutidine (0.12 mL, 1.04 mmol) was added, followed by dropwise addition of tertbutyldimethylsilyl trifluoromethanesulfonate (TBS-OTf, 0.20mL, 0.87 mmol). The reaction was stirred for 2 hrs at 0^{o}C, and was subsequently quenched with a saturated aqueous solution of ammonium chloride. The silylated carbohydrate derivative was extracted using dichloromethane, dried with $MgSO_4$, evaporated, and purified using silica

column chromatography (30:1, hexane : diethyl ether) to afford a white solid (1.19 g, 95% yield). ^{1}H NMR(500 MHz, $CDCl_3$) δ 4.18 (1H, dd, *J* = 2.4, 6.5 Hz, H4), 4.17-4.13 (1H, m, H6a), 3.87 (1H, dd, *J* = 7.3, 7.3 Hz, H5), 3.75 (1H, dd, *J* = 3.6, 9.1 Hz, H1), 3.69 (1H, dd, *J* = 3.2, 3.2 Hz, H2), 3.67 (1H, dd, *J* = 1.7, 12.0 Hz, H6b), 3.62 (3H, s, OCH_3), 3.39 (1H, br s, H3), 2.43-2.35 (1H, m, H2`a ), 2.34-2.26 (1H, m, H2`b), 1.84-1.73 (1H, m, H3`a), 1.71-1.57 (2H, m, H3`b, H4`a ), 1.38-1.28 (1H, m, H4`b), 0.89 (9H, s, $C(CH_3)_3$), 0.88 (9H, s, $C(CH_3)_3$), 0.87 (9H, s, $C(CH_3)_3$), 0.85 (9H, s, $C(CH_3)_3$), 0.06 (3H, s, $SiCH_3$), 0.05 (3H, s, $SiCH_3$), 0.04 (9H, br, 3 x $SiCH_3$), 0.03 (3H, s, $SiCH_3$), 0.00 (3H, s, $SiCH_3$), 0.00 (3H, s, $SiCH_3$); ^{13}C NMR (101 MHz,$CDCl_3$) δ 174.1(C1`), 79.2(C5), 74.1(C3), 73.6(C2), 67.4(C4), 65.7(C1), 58.4(C6), 51.2($OCH_3$), 33.8(C2`), 30.3 (C4`), 25.9($C(CH_3)_3$), 25.9($C(CH_3)_3$), 25.7($C(CH_3)_3$), 25.7($C(CH_3)_3$), 21.8(C3`), 18.2($C(Me)_3$), 18.1($C(Me)_3$), 18.0($C(Me)_3$), 17.9($C(Me)_3$), -4.4($SiCH_3$), -4.5($SiCH_3$), -4.6($SiCH_3$), -4.9($SiCH_3$), -5.0($SiCH_3$), -5.0($SiCH_3$), -5.4($SiCH_3$), -5.5($SiCH_3$). ESI-MS calcd for $C_{35}H_{76}O_7Si_4$ $[M+H]^+$: 721.4746; $[M+NH_4]^+$: 738.5012. Found 721.482, 738.505. Rf = 0.25 (10:1 hexane : diethyl ether)

Benzyl *Nα*-(S)-[(9H-fluoren-9-ylmethoxy)carbonyl]-*Nβ*-[4`-(2,3,4,6-tetra-*O-tert*-butyl-dimethylsilyl)-α-D-galactopyran-1-yl)-butan-1`-amido)-α,β-diaminopropanoate (77)

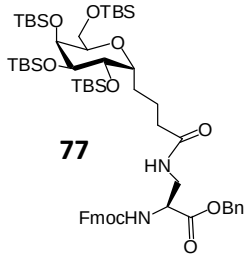

77

Glycoconjugate **77** was prepared using the same procedure as for **58** by coupling amino acid **47** (247 mg, 0.59 mmol) with *C*-α-glycoside **69** (300 mg, 0.42 mmol), and obtained as an amorphous white solid (362 mg, 78% yield). ^{1}H NMR(500 MHz, $CDCl_3$) δ 7.76 (2H, d, *J* = 7.5 Hz), 7.61 (2H, d, *J* = 6.3 Hz), 7.42-7.28 (9H, m), 6.16 (1H, d, *J*= 6.9 Hz, NHα), 6.07 (1H, m, NHβ), 5.23-5.15 (2H, m, -CH_2Ph), 4.48-4.42 (1H, m, Hα), 4.40 (1H, dd, *J*= 7.4, 10.3 Hz, FmocCH_2a), 4.32 (1H, dd, *J*= 7.3, 10.5 Hz, FmocCH_2b), 4.27-4.17 (3H, m, FmocC*H*, H6b, H4), 3.94-3.86 (1H, m, H5), 3.80-3.68 (4H, m, H2, H1, H6b, Hβa), 3.66-3.59 (1H, m, Hβb), 3.45-3.38 (1H, m, H3), 2.30-2.15 (2H, m, H2`), 1.80-1.65 (2H, m, H3`), 1.65-1.54 (1H, m, H4`a), 1.42-1.32 (1H, m, H4`b), 0.90 (27H, s, 3 x $C(CH_3)_3$), 0.80 (9H, s, $C(CH_3)_3$), 0.08 (6H, s, 2 x $SiCH_3$), 0.06 (9H, s, 3 x $SiCH_3$), 0.04 (9H,s, 3 x $SiCH_3$) ; ^{13}C NMR (101 MHz, $CDCl_3$) δ 174.6, 170.2, 156.1, 143.9, 143.7, 141.3, 141.2, 135.2, 128.6, 128.5, 128.4, 127.7, 127.1, 125.2, 119.9, 79.2 (C5), 74.3(C3), 73.6(C2), 67.5(CH_2Ph), 67.3(C4), 67.3(FmocCH_2), 66.5(C1), 58.6(C6), 55.3(Cα), 47.1(Fmoc*C*H), 41.2(Cβ), 35.8(C2`), 30.0(C4`), 26.0($C(CH_3)_3$), 25.8($C(CH_3)_3$), 25.7($C(CH_3)_3$), 23.1(C3`), 18.3($C(Me)_3$), 18.1($C(Me)_3$), 18.0($C(Me)_3$), 17.9($C(Me)_3$), -4.4

(Si*C*H_3), -4.6(Si*C*H_3), -4.9(Si*C*H_3), -4.9(Si*C*H_3), -4.9(Si*C*H_3), -5.2(Si*C*H_3), -5.3(Si*C*H_3). ESI-MS calcd for $C_{59}H_{96}N_2O_{10}Si_4$ $[M+H]^+$: 1105.6220; $[M+Na]^+$: 1127.6040 Found 1105.695, 1127.679. Rf = 0.30 (4:1 CH_2Cl_2: diethyl ether).

_Nα_-(S)-[(9H-fluoren-9-ylmethoxy)carbonyl]- _Nε_-[1`-( 2,3,4,6-tetra-_O_-benzyl-α-D-galactopyran-1-yl)-methyl-1`-amino]- homoglutamine (81)

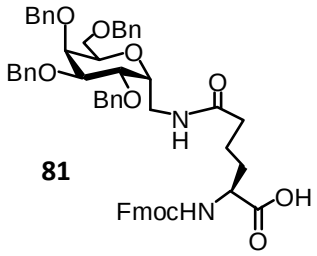

81

Methyl ester (300 mg, 0.32 mmol) was dissolved in 5 mL of 7:3 isopropanol:water and stirred vigorously. Aqueous solutions of 0.8M $CaCl_2$ (3.2 mL) and 0.5M NaOH (1.3 mL) were sequentially added and stirring was continued until starting material was consumed by TLC. The reaction was quenched by cooling the mixture to 0°C, followed by addition of a saturated solution of NH_4Cl. The desired compound was extracted several times with EtOAc and concentrated under vacuum. Glycoconjugate building block was purified by silica gel column chromatography to obtain an amorphous white solid (220 mg, 75% yield). ^{1}H NMR(400 MHz, MeOD) δ 7.77 (2H, m, *J* = 7.6 Hz), 7.58 (2H, dd, *J* = 4.1, 7.3 Hz), 7.39 (2H, t, *J* = 7.5 Hz), 7.30 (2H, t, *J* = 7.4 Hz), 7.39-7.22 (20H, m), 4.68-4.42 (8H, m, 4 x -C*H*$_2$Ph), 4.31 (2H, m, FmocC*H*$_2$), 4.19 (1H, t, *J* = 7.0 Hz, FmocC*H*), 4.16-4.10 (1H, m, Hα), 4.09-4.01 (2H, m, H5, H1), 3.94 (1H, dd, *J* = 3.0, 3.8 Hz, H4), 3.87-3.76 (3H, m, H6a, H2, H3), 3.59 (1H, dd, *J* = 4.1, 10.7 Hz, H6b), 3.52 (1H, dd, *J* = 3.8, 14.2 Hz, H1`a), 3.36 (1H, dd, *J* = 9.9, 14.2 Hz, H1`b), 2.06-1.98 (2H, m, Hδ), 1.82-1.70 (1H, m, Hβa), 1.68-1.50 (3H, m, Hβb, Hγ). ^{13}C NMR(101 MHz, $CDCl_3$) δ 172.7, 172.2, 155.9, 143.8, 143.8, 141.2, 138.2, 138.2, 138.1, 137.7, 128.4, 128.4, 128.3, 128.0, 127.9, 127.8, 127.7, 127.7, 127.7, 127.6, 127.6, 127.0, 125.1, 119.9, 76.0(C2), 75.8(C3), 75.8(C4), 73.9(*C*H$_2$Ph), 73.2(*C*H$_2$Ph), 73.1(*C*H$_2$Ph), 72.9(*C*H$_2$Ph), 72.8 (C5), 69.1(C1), 67.4(C6), 67.0(Fmoc*C*H$_2$), 53.5(O*C*H$_3$), 52.4(Cα), 47.1(Fmoc*C*H), 37.9 (C1`), 35.4(Cδ), 31.7(Cβ), 21.2(Cγ). ESI-MS calcd for $C_{56}H_{58}N_2O_{10}$ $[M+H]^+$: 919.4170; $[M+NH_4]^+$: 936.4435. Found 919.392, 919.419. Rf = 0.36 (10% MeOH /CH_2Cl_2).

General procedure for synthesis of C-nitrile galactopyranoside

To a flamed dried flask under argon, 1-acetoxy-2,3,4,6-tetra-*O*-benzyl-D-galactopyranose (**88**) (1.3 g, 2.2 mmol) was added, and dissolved in distilled acetonitrile (10 mL). Trimethylsilyl cyanide (1.4 mL, 11.2 mmol) was added, and the solution was cooled to 0 ^{o}C. 3 drops of a solution of distilled boron trifluoride dietherate was then added dropwise. The reaction was completed in 10-15 minutes as monitored by TLC, and resulted in the formation of both α and β anomers. The reaction was immediately quenched upon consumption of starting material with a saturated solution of $NaHCO_3$. The reaction was then diluted and extracted with diethyl ether. The organic phases were combined, evaporated under reduced pressure and immediately purified on silica gel column chromatography (α-anomer (**83**): 483 mg, 40% yield. β-anomer (**89**): 480 mg, 40 % yield).

2,3,4,6-Tetra-*O*-benzyl-α-D-galactopyranosyl cyanide (83)[9]

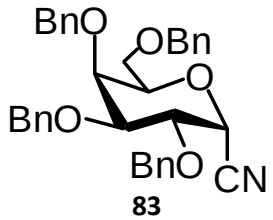

83

^{1}H NMR (400 MHz, $CDCl_3$) δ 7.39-7.22 (20H, m), 4.90 (1H, d, *J* = 11.3 Hz, -C*H*$_2$Ph), 4.84 (1H, d, *J* = 11.5 Hz, -C*H*$_2$Ph), 4.82 (1H, d, *J* = 10.3 Hz, -C*H*$_2$Ph), 4.75 (1H, d, *J* = 11.6 Hz, -C*H*$_2$Ph), 4.69-4.63 (2H, m, -C*H*$_2$Ph, H1), 4.53 (1H, d, *J*= 11.3 Hz, -C*H*$_2$Ph), 4.46 (1H, d, *J*= 11.8 Hz-C*H*$_2$Ph), 4.39 (1H, d, *J*= 11.8 Hz-C*H*$_2$Ph), 4.09 (1H, dd, *J* = 6.1, 9.8 Hz, H2), 3.99-3.95 (2H, m, H4, H5), 3.80 (1H, dd, *J*= 2.2, 9.8 Hz, H3), 3.51 (1H, dd, *J*= 5.9, 9.3 Hz, H6a), 3.47 (1H, dd, *J*= 7.0, 9.3 Hz, H6b). ^{13}C NMR(126 MHz, $CDCl_3$) δ 138.1, 138.1, 137.5, 137.5, 128.8, 128.6, 128.5, 125.4, 128.3, 128.2, 128.2, 128.0, 128.0, 127.9, 127.8, 127.7, 127.5, 115.8(*C*N), 80.3, 75.0, 75.0, 74.0, 73.9, 73.5, 73.5, 73.4, 67.9, 67.6. ESI-MS calcd for $C_{35}H_{35}N_1O_5$ $[M+Na]^+$: 572.6; Found 572.5. Rf = 0.55 (3:1 Hexane:EtOAc)

2,3,4,6-Tetra-*O*-benzyl-β-D-galactopyranosyl cyanide (89)[9]

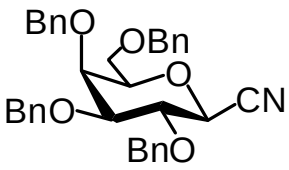

[9] Garcia Lopez, M.-T.; De las Heras, F.G.; San Felix, A.S. *J. Carbohydrate Chem.* **1987,** *6*, 273-279.

^{1}H NMR(500 MHz, $CDCl_3$) δ 7.42-7.24 (20H, m), 4.95 (1H, d, *J* = 11.5 Hz, -C*H*$_2$Ph), 4.92-4.90 (2H, m, -C*H*$_2$Ph), 4.75 (1H, d, *J* = 11.8 Hz, -C*H*$_2$Ph), 4.72 (1H, d, *J* = 11.8 Hz, -C*H*$_2$Ph), 4.59 (1H, d, *J* = 11.5 Hz, -C*H*$_2$Ph), 4.47 (1H, d, *J*= 11.8 Hz, -C*H*$_2$Ph),4.41 (1H, d, *J*= 11.8 Hz, -C*H*$_2$Ph), 4.18 (1H, dd, *J*= 9.7, 9.7 Hz, H2), 4.03 (1H, d, *J*= 10.0 Hz, H1), 3.94 (1H, d, *J*= 2.6 Hz), 3.58 (1H, dd, *J*= 3.7, 6.7 Hz), 3.56-3.48 (3H, m). ^{13}C NMR(126 MHz, $CDCl_3$) δ 138.1, 137.7, 137.4, 137.1, 128.6, 128.5, 125.4, 128.3, 128.2, 128.1, 128.1, 128.0, 127.9, 127.9, 127.8, 127.5, 116.8(*C*N), 82.9, 78.2, 76.2, 76.1, 74.8, 73.6, 73.2, 72.7, 68.3, 67.9. ESI-MS calcd for $C_{35}H_{35}N_1O_5$ $[M+Na]^+$: 572.6; Found 572.5. Rf = 0.48 (3:1 Hexane:EtOAc)

N*α*-(S)-[(9H-fluoren-9-ylmethoxy)carbonyl]-homoglutam-1-yl methyl ester (84)

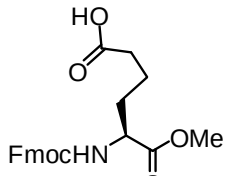

84

α-Diazoketone **90** (400 mg, 0.98 mmol) was dissolved in acetone/water, and catalytic amounts of silver benzoate was added. The solution was sonicated for 30 minutes and the starting material was consumed. The mixture was then filtered, evaporated under reduced pressure, and purified by column chromatography (5% MeOH/CH_2Cl_2) to obtain a white solid (340 mg, 87 % yield) . ^{1}H NMR(500 MHz, CD_3OD) δ 7.77 (2H, m, *J* = 7.6 Hz), 7.58 (2H, dd, *J* = 6.4, 6.4 Hz), 7.39 (2H, t, *J* = 7.5 Hz), 7.30 (2H, t, *J* = 7.4 Hz), 4.43-4.30 (2H, d, *J* = 7.2 Hz, FmocCH_2), 4.23 (2H, m, Hα, FmocC*H*), 3.71 (3H, s, OCH_3), 2.35-2.25 (2H, m, Hδ), 1.93-1.83 (1H, m, Hβa), 1.70-1.60 (3H, m, Hβb, Hγ); ^{13}C NMR(101 MHz, CD_3OD) δ 177.1, 174.5, 158.7, 145.4, 145.2, 142.7, 128.8,128.2, 126.3, 121.0, 121.0, 119.5, 68.0 (Fmoc*C*H_2), 55.3(OCH_3), 52.7(Cα), 48.5 (Fmoc*C*H), 34.3(δ), 31.9(γ), 22.5(Cβ). ESI-MS calcd for $C_{22}H_{23}N_1O_6$ $[M+H]^+$: 398.1604$^+$; $[M+Na]^+$: 420.1423 Found 398.145, 420.126. Rf = 0.20 (10% MeOH / CH_2Cl_2)

***Nα*-(S)-[(9H-fluoren-9-ylmethoxy)carbonyl]-glutam-1-yl methyl ester (85)**[10]

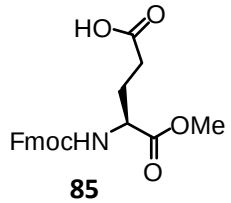

85

To a flame dried flask, was added glutamic acid (3.0 g, 8.1 mmol) under argon, and dissolved in diethyl ether. A diluted solution of diazomethane (in diethyl ether[11]) was added until the colour of the solution remained yellow, and stirred for another 30 minutes. Complete methylation of the ester was determined by TLC analysis. The reaction was then exposed to atmospheric conditions for 30 minutes, and then 10% HCl was added dropwise until the solution became colourless. The remaining solvent was evaporated under a stream of air. 8 mL of a (1:1) solution of dichloromethane : trifluoroacetic acid was then added and stirred for 1 hr until the starting material was consumed. The excess solvents/reagents were then evaporated under reduced pressure, and the product was recrystallized using methanol/diethyl ether (2.95 g, 95% yield). ^{1}H NMR (500 MHz, CD_3OD) δ 7.77 (2H, m, *J* = 7.5 Hz), 7.64 (2H, dd, *J* = 6.6, 6.6 Hz), 7.40 (2H, t, *J* = 7.5 Hz), 7.32 (2H, t, *J* = 7.5 Hz), 4.37-4.29 (2H, m, FmocCH_2), 4.26-4.19 (1H, m, Hα), 4.19 (1H, t, *J* = 7.1 Hz, FmocCH), 3.70 (3H, s, CH_3), 2.38 (2H, t, *J* = 7.4 Hz, Hγ), 2.18-2.09 (1H, m, Hβa), 1.95-1.85 (1H, m, Hβb). ^{13}C NMR(101 MHz, CD_3OD) δ 176.3, 174.2, 158.7, 145.3, 145.2, 142.6, 128.8, 128.2, 126.3, 120.9, 68.0(FmocCH_2), 54.8(Cα), 52.8 (O*C*H_3), 48.4(Fmoc*C*H), 31.1(Cγ), 27.8(Cβ). ESI-MS calcd for $C_{21}H_{21}NO_6$ $[M+H]^+$: 384.147; $[M+NH_4]^+$: 401.1713. Found 384.128, 401.154. Rf = 0.20 (10% MeOH in CH_2Cl_2)

[10] Mandal, P.K.; McMurray, J.S. et al. *J. Med. Chem.* **2009**, *52*, 2429-2442.

[11] Using *all unscratched* glassware and behind a blastshield, CH_2N_2/Et_2O solution was prepared by *SLOWLY* adding small portions of N-nitrosourea to a 2:1 (v/v) solution of Et_2O : 50%$KOH_{(aq)}$ in an ice bath (with slow gentle swirling between addition), until a yellow colour persisted in the Et_2O layer. The Et_2O layer was then carefully transferred into an Erlenmeyer flask containing KOH(s) in an ice bath, and kept in the freezer overnight to dry.

1-Acetoxy-2,3,4,6-tetra-*O*-benzyl-D-galactopyranose (88)[12,13]

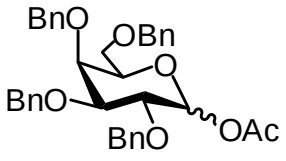

88

2,3,4,6-Tetra-*O*-benzyl-D-galactopyranose **87** (1.5 g, 2.8 mmol) was dissolved in 20 mL of distilled dichloromethane. Pyridine (7 mL), acetic anhydride (7 mL), then catalytic N,N-dimethylaminopyridine (DMAP) were sequentially added, and stirred at room temperature until starting material was consumed by TLC. The mixture was then diluted with dichloromethane and washed repeatedly with 10% HCl solution until pyridine was removed from the organic phase. The organic phase was then evaporated under reduced pressure and purified on silica gel column chromatography to yield an α/β mixture of the anomeric acetate as a viscous colourless oil. ^{1}H NMR(400 MHz, $CDCl_3$) δ α-anomer: 7.40-7.20 (20H, m), 6.36 (1H, d, *J* = 3.7 Hz, H1α), 4.94 (1H, d, *J* = 11.3 Hz, -C*H*$_2$Ph), 4.81 (1H, d, *J* = 11.7 Hz, -C*H*$_2$Ph), 4.73 (1H, d, *J* = 11.8 Hz, 1H, -C*H*$_2$Ph), 4.70 (2H, s, -C*H*$_2$Ph), 4.56 (1H, d, *J* = 11.4 Hz, -C*H*$_2$Ph), 4.44 (1H, d, *J* = 11.6 Hz, -C*H*$_2$Ph), 4.38 (1H, d, *J* = 11.7 Hz, -C*H*$_2$Ph), 4.15 (1H, dd, *J* = 3.7, 10.1 Hz, H2), 4.04-3.97 (2H, m), 3.87 (1H, dd, *J* = 2.7, 10.1 Hz, H3), 3.62-3.58 (1H, m), 3.50 (1H, dd, *J* = 5.5, 9.2 Hz, H6b) 2.10 (3H, s, CH_3). β-anomer 7.40-7.20 (20H, m), 5.56 (1H, d, *J* = 8.0 Hz, H1), 4.92 (1H, d, *J* = 11.6 Hz, -C*H*$_2$Ph), 4.83 (1H, d, *J* = 11.2 Hz, -C*H*$_2$Ph), 4.71 (1H, d, *J* = 11.2 Hz, 1H, -C*H*$_2$Ph), 4.70 (2H, s, -C*H*$_2$Ph), 4.61 (1H, d, *J* = 11.6 Hz, -C*H*$_2$Ph), 4.42 (1H, d, *J* = 11.6 Hz, -C*H*$_2$Ph), 4.39 (1H, d, *J* = 11.7 Hz, -C*H*$_2$Ph), 3.97 (1H, d, *J* = 2.5 Hz, H4), 3.94 (1H, dd, *J* = 8.2, 9.7 Hz, H2), 3.72-3.65 (1H, m), 3.60-3.45 (3H, m, H3, H6), 2.00 (3H, s, CH_3);.^{13}C NMR(101 MHz, $CDCl_3$) δ 169.5,169.3,138.5,138.4,138.3, 138.1, 137.9, 137.7, 137.4, 128.4, 128.4, 128.3, 128.2, 128.1, 128.0, 127.9, 127.9, 127.8, 127.7,127.6, 127.5, 127.3, 94.2, 90.7, 82.3, 80.0, 78.5, 78.1, 77.3, 77.0, 76.7, 75.3, 75.2, 74.8, 74.7, 74.6, 74.4, 73.9, 73.5, 73.4, 73.3, 73.0, 72.9, 72.7, 72.7, 72.4, 71.7, 68.3, 67.8, 67.4, 21.1, 21.0. ESI-MS calcd for $C_{36}H_{38}O_7$ $[M+NH_4]^+$:600.3 $[M+Na]^+$: 605.3. Found 600.5, 605.4. Rf = 0.48 (3:1 Hexane:EtOAc)

[12] Kulkarni, S.S.; Gervay-Hague, J. *Org. Lett.* **2006**, *8*, 5765-5768.
[13] Ren, C. -T.; Tsai Y.-H.; Yang, Y.- L.; Zou, W.; Wu, S. –H. *J. Org. Chem.* **2007**, *72*, 5427-5430.

Methyl *Nα*-(S)-[(9H-fluoren-9-ylmethoxy)carbonyl]-*Cδ*-oxo-*C*ε-diazo-α-aminohexan-1-oate (90)

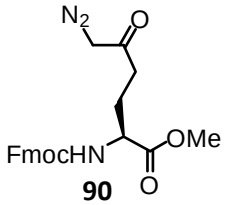

90

To a flame-dried flask under argon was added amino acid **85** (500 mg, 1.31 mmol) and dissolved in distilled DCM (13mL). HCTU (590 mg, 1.44 mmol) and distilled DIPEA (0.58mL, 0.328mmol) were sequentially added, and the reaction was stirred for 30 minutes. A diluted solution of diazomethane in diethyl ether was then added dropwise until the solution remained yellow. Upon completion of the reaction as monitored by TLC, 10% acetic acid was added to quench the reaction. The mixture was washed three times with saturated solution of ammonium chloride, and then brine. The organic layer was evaporated under pressure and then purified on column chromatography (4:1 Hexane : EtOAc) to obtain a white solid (464 mg, 82% yield).^{1}H NMR(500 MHz, $CDCl_3$) δ 7.77 (2H, m, *J* = 7.6 Hz), 7.58 (2H, dd, *J* = 6.4, 6.4 Hz), 7.39 (2H, t, *J* = 7.5 Hz), 7.30 (2H, t, *J* = 7.4 Hz), 5.55 (1H, d, *J* = 7.7 Hz, NH), 5.30-5.15 (1H, br s, C*H*N_2), 4.43-4.30, (3H, m, FmocCH_2, Hα), 4.20 (1H, t, *J* = 7.0 Hz, FmocCH), 3.74 (3H, s, OCH_3), 2.52-2.28 (2H, m, Hγ), 2.28-2.14 (1H, m, Hβa), 2.08-1.93 (1H, m, Hβb). ^{13}C NMR(101 MHz, $CDCl_3$) δ 172.3(*C*O_2Me), 156.0(NH*C*(O)O), 143.8, 143.6, 141.3, 127.7,127.1, 125.1, 121.1, 120.0, 67.1(Fmoc*C*H2), 54.8(*C*HN_2), 53.4(Cα), 52.6(OCH_3), 47.1(FmocCH), 36.4(Cγ), 27.4(Cβ). ESI-MS calcd for $C_{22}H_{21}N_3O_5$ [M+H]: 408.1559; $[M+Na]^+$: 430.1379. Found 408.140, 430.122. IR(film): 3300.0, 2950.9, 2106.1, 1716.5, 1631.7, 1517.9, 1450.4, 1380.9, 1350.1, 1321.2, 1255.6, 1217.0. Rf = 0.34 (2:1 Hexane: EtOAc)

General Procedure for Synthesis of Glycoconjugates **93** *and* **94**

To a flame dried flask was added *C*-glycosyl nitrile **83** (300 mg, 0.55 mmol) under argon and dissolved in distilled 7 mL of THF at room temperature. A 1.5 M solution of Di-isobutylaluminum hydride (DIBAL-H) in toluene (2.6 mL) was added at room temperature and the reaction was stirred for 45 minutes. The reaction was then cooled to 0^{o}C, and quenched by dropwise addition of methanol until bubbling stopped, followed by addition of 20 mL of a saturated solution of sodium potassium tartrate). 30 mL of EtOAc was then added and the solution was stirred for 45 minutes. The desired amine was then extracted using several portions of EtOAc. The organic layers were combined and evaporated under reduced pressure at 30 ^{o}C to afford the desired *C*-glycosyl methylamine **82**. The crude mixture was then co-evaporated with

several portions (5 x 5mL) of distilled toluene, and dried on a high vacuum for 2 hrs. In another flame dried flask under argon, amino acids **84** or **85** (0.77 mmol) was dissolved in 15mL dichloromethane and HCTU (0.89mmol) was added and stirred for 20 minutes. The crude mixture of *C*-glycosyl methylamine was then dissolved in 5mL distilled DCM and cannulated into the flask containing the activated ester. Distilled DIPEA (1.8mmol) was then added and the reaction was stirred overnight. Upon consumption of starting material, the solution was diluted with CH_2Cl_2 and then washed three times with saturated NH_4Cl (aq). The organic phase was then dried with $MgSO_4$, filtered, and dried in vacuo. The glycoconjugate was then purified using 2:1 Hexanes : EtOAc to obtain an amorphous white solid (66 and 63% for **93** and **94**, respectively)

Methyl *Nα*-(S)-[(9H-fluoren-9-ylmethoxy)carbonyl]- *Nε*-[1`-( 2,3,4,6-tetra-*O*-benzyl-α-D-galactopyran-1-yl)-methyl-1`-amino]- homoglutam-ε-amido-1-ate (93)

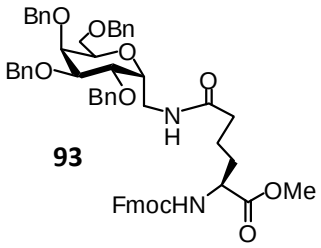

93

^{1}H NMR(500 MHz, $CDCl_3$) δ 7.77 (2H, m, *J* = 7.6 Hz), 7.58 (2H, dd, *J* = 6.4, 6.4 Hz), 7.39 (2H, t, *J* = 7.5 Hz), 7.30 (2H, t, *J* = 7.4 Hz), 7.39-7.22 (20H, m), 5.82 (1H, m, NH2), 5.47 (1H, d, *J* = 8.1 Hz, NH1), 4.66 (2H, dd, *J* = 4.3, 11.9 Hz, -C*H*$_2$Ph), 4.62-4.52 (3H, m, -C*H*$_2$Ph), 4.50-4.45 (3H, m, -C*H*$_2$Ph), 4.37 (2H, t, *J*= 6.5 Hz, FmocCH_2), 4.34-4.27 (1H, m, Hα), 4.21 (1H, t, *J* = 7.1 Hz, FmocCH), 4.08-3.97 (2H, m, H5, H1), 3.94 (1H, dd, *J* = 3.0, 3.8 Hz, H4), 3.93-3.86 (1H, m, H6a), 3.80-3.73 (1H, m, H2), 3.73-3.69 (1H, m, H3), 3.71 (3H, s, OCH_3), 3.63 (1H, ddd, *J*= 4.0, 7.2, 14.0 Hz, H1`a), 3.56 (1H, dd, *J* = 3.6, 10.7 Hz, H6b), 3.28 (1H, ddd, *J* = 3.4, 10.4, 13.8 Hz, H1`b), 2.06-1.98 (2H, m, Hδ), 1.82-1.70 (1H, m, Hβa), 1.68-1.50 (3H, m, Hβb, Hγ). ^{13}C NMR(101 MHz, $CDCl_3$) δ 172.7, 172.2, 155.9, 143.8, 143.8, 141.2, 138.2, 138.2, 138.1, 137.7, 128.4, 128.4, 128.3, 128.0, 127.9, 127.8, 127.7, 127.7, 127.7, 127.6, 127.6, 127.0, 125.1, 119.9, 76.0(C2), 75.8(C3), 75.8(C4), 73.9(*C*H$_2$Ph), 73.2(*C*H$_2$Ph), 73.1(*C*H$_2$Ph), 72.9(*C*H$_2$Ph), 72.8 (C5), 69.1(C1), 67.4(C6), 67.0(Fmoc*C*H$_2$), 53.5(OCH_3), 52.4(Cα), 47.1(Fmoc*C*H), 37.9 (C1`), 35.4(Cδ), 31.7(Cβ), 21.2(Cγ). Rf = 0.28 (1:1 Hexane:EtOAc)

Methyl *Nα*-(S)-[(9H-fluoren-9-ylmethoxy)carbonyl]- *Nδ*-[1`-( 2,3,4,6-tetra-*O*-benzyl-α-D-galactopyran-1-yl)-methyl-1`-amino]- glutam-δ-amido-1-ate (94)

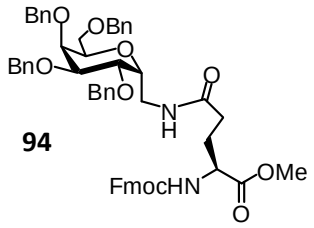

94

^{1}H NMR(400 MHz, $CDCl_3$) δ 7.76 (2H, m, *J* = 7.3 Hz), 7.60 (2H, d, *J* = 6.7 Hz), 7.39 (2H, t, *J* = 7.4 Hz), 7.36 (22H, m), 6.10-6.01 (1H, br, NHβ), 5.83 (1H, d, *J* = 7.8 Hz, NHα), 4.67 (2H, dd, *J* = 5.0, 11.8 Hz, -C*H*$_2$Ph), 4.61-4.46 (6H, m, -C*H*$_2$Ph), 4.37 (2H, t, *J*= 6.5 Hz, FmocCH_2), 4.34-4.25 (1H, m, Hα), 4.22 (1H, t, *J* = 7.0 Hz, Fmoc CH), 4.10-3.98 (2H, m, H5, H1), 3.94 (1H, dd, *J* = 3.0, 3.8 Hz, H4), 3.94-3.86 (1H, m, H6a), 3.80-3.75 (1H, m, H2), 3.73-3.69 (1H, m, H3), 3.71 (3H, s, OCH_3), 3.69-3.62 (1H, m, H1`a ), 3.56 (1H, dd, *J*= 3.7, 10.8 Hz, H6b), 3.30 (1H, ddd, *J* = 3.3, 10.2, 13.5 Hz, H1`b), 2.29-2.06 (2H, m, Hγ), 2.14-2.00 (1H, m, Hβa), 2.00-1.90 (1H, m, Hβb). ^{13}C NMR(101 MHz, $CDCl_3$) δ 172.7, 172.2, 155.9, 143.8, 143.8, 141.2, 138.2, 138.2, 138.1, 137.7, 128.4, 128.4, 128.3, 128.0, 127.9, 127.8, 127.7, 127.7, 127.7, 127.6, 127.6, 127.0, 125.1, 119.9, 76.0(C2), 75.8(C3), 75.8(C4), 73.9(*C*H_2Ph), 73.2(*C*H_2Ph), 73.1(*C*H_2Ph), 72.9(*C*H_2Ph), 72.8 (C5), 69.1(C1), 67.4(C6), 67.0(Fmoc*C*H_2), 53.5(OCH_3), 52.4(Cα), 47.1(Fmoc*C*H), 37.9 (C1`), 35.4(Cγ), 31.7(Cβ). ESI-MS calcd for $C_{56}H_{58}N_2O_{10}$ $[M+H]^+$: 919.4411; $[M+NH_4]^+$: 936.4435;$[M+Na]^+$: 941.3989. Found 919.385, 936.399, 941.365. Rf = 0.24 (1:1 Hexane : EtOAc)

***Nα*-(S)-[(9H-fluoren-9-ylmethoxy)carbonyl]- *Nδ*-[1`-( 2,3,4,6-tetra-*O*-benzyl-α-D-galactopyran-1-yl)-methyl-1`-amino]- glutamine (95)**

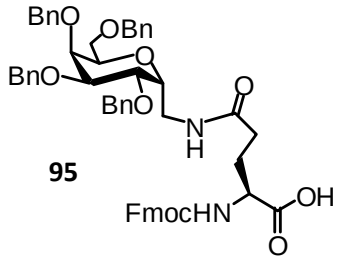

95

Building block **95** (275 mg, 0.300 mmol) was prepared using the same procedure as for **81**, and obtained an amorphous white solid (200 mg, 75% yield).^{1}H NMR(500 MHz, $CDCl_3$) δ 7.77 (2H, m, *J* = 7.6 Hz), 7.58 (2H, dd, *J* = 6.4, 6.4 Hz), 7.39 (2H, t, *J* = 7.5 Hz), 7.30 (2H, t, *J* = 7.4 Hz), 7.39-7.22 (20H, m), 5.82 (1H, m, NHδ), 5.47 (1H, d, *J* = 6.5 Hz, NHα), 4.90 (1H, d, *J* = 11.3 Hz, -C*H*$_2$Ph), 4.84 (1H, d, *J* = 11.5 Hz, -C*H*$_2$Ph), 4.82 (1H, d, *J* = 10.3 Hz, -C*H*$_2$Ph), 4.75 (1H, d, *J* = 11.6 Hz, -C*H*$_2$Ph), 4.69-4.63 (2H, m, -C*H*$_2$Ph), 4.53 (1H, d, *J*= 11.3 Hz, -C*H*$_2$Ph), 4.46 (1H, d, *J*= 11.8 Hz, -C*H*$_2$Ph), 4.43-4.30, (2H, m), 4.39 (1H, d, *J*= 11.8 Hz), 4.23 (2H, m), 4.09 (1H, dd, *J*= 6.1, 9.8 Hz), 3.99-3.95 (2H, m), 3.80 (1H, dd, *J*= 2.2, 9.8 Hz), 3.71 (3H, s), 3.51 (1H, dd, *J*= 5.9, 9.3 Hz), 3.47 (1H, dd, *J*= 7.0, 9.3 Hz), 2.35-2.25 (2H, m), 1.93-1.83 (1H, m), 1.70-1.60 (3H, m). ^{13}C NMR(101 MHz, CD_3OD) δ 172.3, 156.0, 143.8, 143.6, 141.3, 138.1, 138.1, 137.5, 137.5, 128.8, 128.6, 128.5, 128.4, 128.3, 128.2, 128.2, 128.0, 128.0, 127.9, 127.8, 127.7, 127.5, 127.4,126.8, 124.9, 119.5, 80.3, 75.0, 75.0, 74.0, 73.9, 73.5, 73.5, 73.4, 67.9, 67.6, 66.5, 53.8, 47.3, 32.8, 30.5, 21.0. ESI-MS calcd for $C_{55}H_{56}N_2O_{10}$ $[M+H]^+$: 905.4013; $[M+Na]^+$: 927.3833. Found 905.381, 927.356. Rf = 0.15 (10% MeOH in CH_2Cl_2)

***Nα*-(S)-[(9H-fluoren-9-ylmethoxy)carbonyl]- *Nδ*-[1`-( 2,3,4,6-tetra-*O*-benzyl-β-D-galactopyran-1-yl)-methyl-1`-amino]- glutamine (97)**

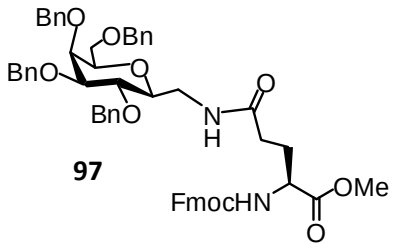

97

C-β-glycoconjugate **97** was synthesized using *C*-β-glycosyl nitrile **89** and amino acid **85** in the same manner as glycoconjugates **93** and **94**. ^{1}H NMR(500 MHz, $CDCl_3$) δ 7.75 (2H, m, *J* = 7.4 Hz), 7.60 (2H, t, *J* = 7.4 Hz), 7.41-7.21 (24H, m), 6.06-6.01 (1H, br, NHβ), 5.83 (1H, d, *J* = 7.7 Hz, NHα), 4.97-4.84 (2H, m, -C*H*$_2$Ph), 4.78-4.55 (5H, m, -C*H*$_2$Ph), 4.49-4.29 (5H, m), 4.19 (1H, t, *J* = 6.9 Hz, Fmoc CH), 3.97-3.95 (1H, m, H5), 3.76-3.69 (1H, m), 3.71 (3H, s, OCH_3), 3.65-3.46, 3.38-3.30 (1H,m), 2.24-2.10 (2H, m, Hγ), 2.24-2.10 (1H, m, Hβa), 2.03-1.94 (1H, m, Hβb).

^{13}C NMR(126 MHz, $CDCl_3$) δ 172.4, 171.7, 156.1, 143.7, 141.3, 141.3, 138.5, 138.1, 138.0, 137.7, 128.5, 128.4, 128.3, 128.2, 128.1, 127.9, 127.8, 127.7, 127.7, 127.5, 127.1, 125.2, 119.9, 84.4, 75.9, 74.5, 73.5, 73.5(*C*H_2Ph), 72.2, 68.8, 67.0, 53.6(OCH_3), 52.5(Cα), 47.1(Fmoc*C*H), 40.3 (C1`), 32.3(Cγ), 28.1(Cβ). ESI-MS calcd for $C_{56}H_{58}N_2O_{10}$ $[M+H]^+$: 919.4411; $[M+NH_4]^+$: 936.4435;$[M+Na]^+$: 941.3989. Found 919.449, 936.472, 941.427. Rf = 0.24 (1:1 Hexane : EtOAc)

Thiophenyl 3,4-*O*-isopropylidene-6-*O*-*tert*-butyldimethylsilyl-β-D–*lyxo*-hex-2-ulose (103)

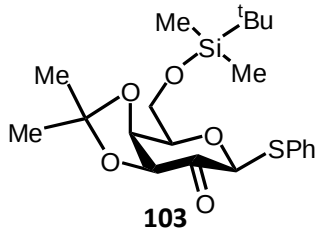

103

Alcohol **103** (300 mg, 0.70 mmol) was dissolved in 4.5 mL dichloromethane and PIDA (500 mg, 1.54 mmol) was added. Catalytic amounts of TEMPO was then added (until a deep orange colour persisted) and the reaction was stirred at room temperature until starting material was consumed by TLC. The reaction was immediately diluted with 20mL DCM and washed with several portions of brine and water. The resulting mixture was then purified by column chromatography and immediately concentrated under reduced pressure at 25 ^{o}C. ^{1}H NMR(400 MHz, $CDCl_3$) δ 7.56-7.51 (2H, m), 7.35-7.28 (3H, m), 5.64 (1H, s, H1α), 5.31 (1H, s, H1β), 4.18 (1H, dd, *J* = 2.2, 5.5 Hz, H4), 4.11 (1H, dd, *J* = 5.6, 6.8 Hz, H3), 3.98 (1H, dd, *J* = 7.2, 11.5 Hz, H6a), 3.90-3.85 (1H, m, H5), 3.81 (1H, dd, *J* = 4.0, 11.6 Hz, H6b), 1.42 (3H, s), 1.33 (3H, s). ^{13}C NMR(75 MHz, $CDCl_3$) δ 200.0, 199.6, 133.6, 133.3, 132.6, 132.3, 129.7, 129.4, 128.9, 128.3, 112.2, 111.5, 90.0, 89.8, 76.4, 77.0, 76.5, 75.8, 70.4, 62.2, 27.5, 26.4, 26.3, 18.7, -4.9, -5.0. ESI-MS calcd for $C_{21}H_{32}O_5SSi$ $[M+H]^+$: 425.1819; $[M+NH_4]^+$: 442.2083. Found 425.190, 442.215. Rf = 0.50 (4:1 Hexane:EtOAc)

***tert*-Butyl-4-(S)-[2`-(*E*)-1`-[(2-diphenylphosphino)-benzoyl]-oxy-prop-2`-en-3`-yl]-2,2-dimethyl-1,3-oxazolidine-3-carboxylate (104)**[14]

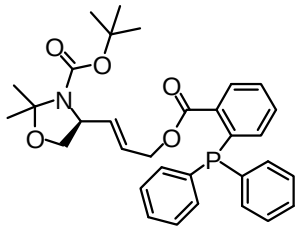

104

In a flame-dried flask under argon, alcohol **109** (285 mg, 1.11 mmol), was dissolved in distilled CH_2Cl_2 (5.6 mL, 0.2 M). *ortho*-diphenylphosphinobenzoic acid (oDPPBA) (340 mg, 1.11 mmol), DMAP (136 mg, 1.11 mmol) and DCC (229 mg, 1.11 mmol) were then added in succession, resulting in a cloudy mixture, which was stirred overnight at room temperature. To quench, brine was added and the mixture was extracted with dichloromethane. The organic layer was dried over $MgSO_4$, filtrated and evaporated under reduced pressure. The residue was purified by flash chromatography (9:1, Hexane/EtOAc) to afford an amorphous off-white solid (510 mg, 84% yield). ^{1}H NMR(300 MHz, $CDCl_3$) δ major rotamer 8.08 (1H, m), 7.44-7.25 (12H, m), 6.93 (1H, m), 5.85-5.60 (2H, m), 4.65 (2H, d, J = 4.8 Hz), 4.28-4.21 (1H, m), 4.03 (1H, m), 3.72 (1H, dd, J = 2.6, 8.8 Hz), 1.61 (3H, s), 1.51 (3H, s), 1.40 (9H, s); δ minor rotamer 5.82-5.55 (1H, m), 5.60 (1H, dd, J = 7.0, 15.4 Hz), 4.30-4.17 (1H, m), 4.10-4.02 (2H, m), 3.97 (1H, dd, J = 6.2, 8.9 Hz), 3.67 (1H, dd, J = 2.3, 8.9 Hz), 2.53 (1H, br, OH), 1.52 (3H, s), 1.44 (3H, s), 1.37 (9H, s); ^{13}C NMR (100 MHz, $CDCl_3$) δ 166.3, 151.8, 140.5 (d, $J_{C,P}$ = 26.0 Hz), 137.8 (d, $J_{C,P}$ =11.0 Hz), 134.3, 133.8 (d, $J_{C,P}$ = 20.7 Hz), 132.0, 130.6, 128.6, 128.5 (d, $J_{C,P}$ = 7.0 Hz), 128.1, 94.0, 79.7, 67.9, 64.8, 58.5, 28.4, 26.6, 23.7;. ESI-MS calcd for $C_{32}H_{36}NO_5P$ $[M+H]^+$ = 546.6; $[M+Na]^+$ = 568.6. Found 546.5, 568.5. Rf = 0.58 (2:1 Hexane : EtOAc)

***tert*-Butyl-4(S)-[3`-(*S*)-but-1`-en-3`-yl]-2,2-dimethyl-1,3-oxazolidine-3-carboxylate (major diastereomer) (105)**[14]

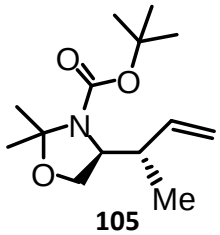

105

Into a flame-dried flask under argon, was added phosphinobenzoate ester **104** (80 mg, 0.146 mmol) in distilled Et_2O (14.6 mL, 0.01 M) followed by CuBr-Me_2S (15 mg, 0.073 mmol). The mixture was stirred at until the copper salt was completely dissolved to yield a clear light yellow solution. A 0.05M solution of methylmagnesium bromide in distilled diethyl ether (10.2 mL, 0.511 mmol) was added via a syringe pump (0.30 mmol/hr) at room temperature. The mixture was stirred for an additional 3 hours and quenched with a saturated aqueous solution of

[14] Spangenberg, T.; Schoenfelder, A.; Breit, B.; Mann, A. *Org. Lett*. **2007**, *9*, 3881-3884.

ammonium chloride. The aqueous phase was extracted several times with diethyl ether. The organic layers were combined, dried over $MgSO_4$, filtered and evaporated under reduced pressure. The residue was purified by flash chromatography (10:1 Hexane/Et_2O) to afford an unseparable mixture of *syn*- and *anti*- diastereomers (1:5 *syn/anti*, 30 mg, 80%). (Major diastereomer): ^{1}H-NMR (500 MHz, 50 °C, $CDCl_3$): δ 5.80-5.68 (1H, m, H2`), 5.04-4.92 (2H, m, H1`), 3.86-3.71 (3H, m, H5, H4), 2.82-2.58 (1H, br, H3`), 1.56 (3H, br s, $CH_3$), 1.49 (9H, s, $C(CH_3)_3$), 1.46 (3H, s, $CH_3$), 0.96 (3H, d, $J$ = 6.9 Hz, H4`). ^{13}C-NMR (101 MHz, 20 °C, $CDCl_3$): δ 152.7, 140.9 (C2`), 114.8/114.5 (rotamers, C1`), 94.2/93.6(rotamers, C2), 79.6(rotamers, CMe_3), 64.5/64.3 (rotamers, C5), 60.9/60.8(rotamers, C4), 39.9/39.5 (rotamers, C3`), 28.4 ($C(CH_3)_3$), 26.9/26.2 (rotamers, $CH_3$), 24.3/22.8 (rotamers, $CH_3$), 14.1/14.0 (rotamers, C4`). Rf = 0.48 (4:1 Hexane : Et_2O)

General Procedure for Horner-Wadsworth-Emmons olefination of aldehyde **106**

To a flame dried flask under argon, methyl(dimethoxyphosphotyl) acetate (4.9 g, 13.1 mmol) was added and dissolved in 15 mL distilled acetonitrile. Dried lithium bromide (15.6 g, 18.1 mmol) was added and stirred for 30 minutes until it was dissolved. Distilled triethylamine (1.8 mL, 13.1 mmol) was then added and stirred for 15 minutes. Aldehyde (*R*)-**106** (2.5 g, 10.9 mmol) was then added dropwise and the reaction was stirred until the aldehyde was consumed, as indicated by TLC analysis. To quench the reaction, a saturated solution of ammonium chloride was added. The desired product was extracted with several portions of diethyl ether. The organic layers were dried over $MgSO_4$, filtered and evaporated under reduced pressure. The residue was purified by flash chromatography (10:1 Hexane/Et_2O).

***tert*-Butyl-4(S)-[2`-(Z)-1`-methoxy-1`-oxoprop-2`-en-3`-yl]-2,2-dimethyl-1,3-oxazolidine-3-carboxylate (107)**[15,16]

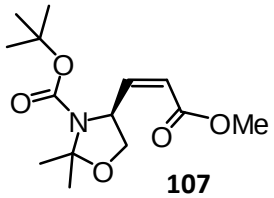

107

Obtained as a white solid (780 mg, 25% yield) ^{1}H NMR(300 MHz, 20 ^{o}C, $CDCl_3$) δ major rotamer 6.19 (1H, dd, J = 8.8, 10.9 Hz, H3`), 5.85-5.73 (1H, m, H2`), 5.38-5.36 (1H, m, H4), 4.28-4.14 (1H, m, H5a), 3.71 (1H, m, H5b), 3.65 (3H, s, OCH_3), 1.62-1.28 (15H, m); δ minor rotamer 6.29 (1H, dd, J = 8.1, 10.5, H3`), 5.85-5.73 (1H, m, H2`), 5.38-5.36 (1H, m, H4), 4.28-

[15] Devel, L.; Hamon, L.; Becker, H.; Thellend, A.; Vidal-Cros, A. *Carbohydrate Research*, **2003**, *338*, 1591-1601

[16] Drew, M. G. B.; Harrison, R. J.; Mann, J.; Tench, A. J.; Young, R. J. *Tetrahedron*, **1999**, *55*, 1163-1172.

4.14 (1H, m, H5a), 3.71 (1H, m, H5b), 3.65 (3H, s, OCH_3), 1.62-1.28 (15H, m) ^{13}C NMR (75 MHz, $CDCl_3$) δ major rotamer 166.1(*C*O_2Me), 152.2(CO), 151.1(C3`), 119.0(C2`), 94.3(C2), 80.4(*C*Me_3), 68.7(C5), 55.4, (C4) 51.3(OCH_3), 28.3(C(*C*H_3)$_3$), 26.5(CH_3), 23.6(CH_3). δ minor rotamer 166.1(CO_2Me), 152.2 (CO), 151.7(C3`), 119.6(C2`), 93.7 (C2), 79.8 (*C*Me_3), 68.9 (C5), 56.5(C4), 51.3(OCH_3), 28.3(C(*C*H_3)$_3$), 27.2(CH_3), 24.8(CH_3).

***tert*-Butyl-4(S)-[2`-(E)-1`-methoxy-1`-oxoprop-2`-en-3`-yl]-2,2-dimethyl-1,3-oxazolidine-3-carboxylate (108)**[16,17]

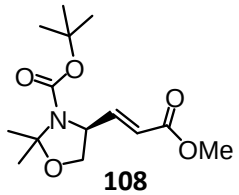

108

Colourless oil (1.56 g, 50% yield). ^{1}H NMR(300 MHz, 20 ^{o}C, $CDCl_3$) δ major rotamer 6.85-6.59 (1H, m, H3`), 5.81 (1H, d, *J* = 15.6 Hz, H2`), 4.38-4.27 (1H, m, H4), 4.05-3.96 (1H, m, H5a), 3.74-3.61 (1H, m, H5b), 3.65 (3H, s, OCH_3), 1.57-1.28 (15H, m); δ minor rotamer 6.85-6.59 (1H, m, H3`), 5.81 (1H, d, *J* = 15.6 Hz, H2`), 4.52-4.41 (1H, m, H4), 4.05-3.96 (1H, m, H5a), 3.74-3.61 (1H, m, H5b), 3.65 (3H, s, OCH_3), 1.57-1.28 (15H, m)^{13}C NMR (75 MHz, $CDCl_3$) δ major rotamer 166.3(*C*O_2Me), 151.3(CO), 146.1(C3`), 121.6(C2`), 94.3(C2), 80.0(*C*Me_3), 67.1(C5), 57.8, (C4) 51.4(OCH_3), 28.2(C(*C*H_3)$_3$), 26.2(CH_3), 23.3(CH_3). δ minor rotamer 166.3(*C*O_2Me), 151.3(CO), 145.9(C3`), 121.6(C2`), 93.8(C2), 80.5(*C*Me_3), 66.9(C5), 57.8, (C4) 51.4(OCH_3), 28.2(C(*C*H_3)$_3$), 27.1(CH_3), 24.4(CH_3)

***tert*-Butyl-4-(S)-[2`-(*E*)-1`-hydroxy-prop-2`-en-3`-yl]-2,2-dimethyl-1,3-oxazolidine-3-carboxylate (109)**[15]

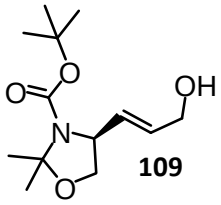

109

Unsaturated ester **108** (460 mg, 1.60 mmol) was dissolved in dry THF in a flame-dried flask. The reaction mixture was cooled to 0^{o}C and DIBAL-H (2.6 mL, 4.00 mmol, 1.5 M in toluene) was added dropwise. The reaction was then warmed to room temperature and stirred until comsumption of the starting material. The reaction was then cooled to 0 ^{o}C, and cold methanol was added dropwise until gas evolution stops. 25 mL of saturated solution of sodium potassium

[17] Dondoni, A., Merino, P., Perrone, D. *Tetrahedron* **1993**, *49*, 2939

tartrate, water (40 mL) and EtOAc (50 mL) were successively added and stirred overnight. The aqueous layer was then extracted with EtOAc. The organic phases were combined, washed with brine, dried over $MgSO_4$ and concentrated under reduced pressure. The desired product was purified by chromatography (2:1 Hexane: EtOAc) to afford a colourless oil (288 mg, 70% yield). ^{1}H NMR (300 MHz, $CDCl_3$) δ major rotamer 5.82-5.55 (1H, m, H2`), 5.60 (1H, dd, *J* = 7.0, 15.4 Hz, H3`), 4.40-4.25 (1H, m, H4), 4.10-4.02 (2H, m, H1`), 3.97 (1H, dd, *J* = 6.2, 8.9 Hz, H5a), 3.67 (1H, dd, *J* = 2.3, 8.9 Hz, H5b), 2.70 (1H, br, OH), 1.52 (3H, s, $CH_3$), 1.44 (3H, s, $CH_3$), 1.40 (9H, s, 3 x $CH_3$); minor rotamer 5.82-5.55 (1H, m, H2`), 5.60 (1H, dd, *J* = 7.0, 15.4 Hz, H3`), 4.30-4.17 (1H, m, H4), 4.10-4.02 (2H, m, H1`), 3.97 (1H, dd, *J* = 6.2, 8.9 Hz, H5a), 3.67 (1H, dd, *J* = 2.3, 8.9 Hz, H5b), 2.53 (1H, br, OH), 1.52 (3H, s, CH_3), 1.44 (3H, s, CH_3), 1.37 (9H, s, 3 x CH_3); ^{13}C NMR (75 MHz, $CDCl_3$) δ major rotamer 152.1(CO), 131.2(C2), 129.6(C3`), 93.6(C2`), 80.3(*C*Me_3), 68.0(C5), 62.4(C1`) , 58.6(C4), 28.3(C(*C*$H_3$)$_3$), 27.0($CH_3$), 24.7($CH_3$); minor rotamer 151.8(CO), 131.2(C2`), 129.6(C3`), 93.7(C2`), 79.5(*C*Me_3), 68.0(C5), 62.4(C1`), 58.6(C4), 28.3(C(*C*H_3)$_3$), 26.4(CH_3), 23.5(CH_3).

***tert*-Butyl-4(S)-[3`-(*R*)-but-1`-en-3`-yl]-2,2-dimethyl-1,3-oxazolidine-3-carboxylate (110)** [14]

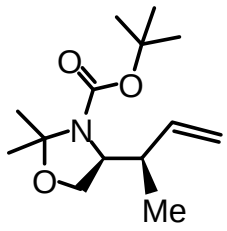

110

Synthesis of **110** (13 mg, 40% yield) was performed using phosphino-benzoate ester **113** as the starting material (70 mg, 0.128 mmol), according to the same procedure as described for **105**. ^{1}H-NMR (500 MHz, 20 °C, $CDCl_3$): δ 5.83-5.73 (1H, m, H2`), 5.09-5.02 (2H, m, H1`), 3.86-3.71 (3H, m, H5, H4), 2.81-2.57 (1H, br, H3`), 1.56 (3H, br s, $CH_3$), 1.49 (9H, s, C($CH_3$)$_3$), 1.46 (3H, s, $CH_3$), 0.96 (3H, d, *J* = 6.9 Hz, H4`). ^{13}C-NMR (101 MHz, 20 °C, $CDCl_3$): δ 152.7, 140.0 (C2`), 115.6 (C1`), 94.2/93.6 (rotamers, C2), 64.6/64.1 (rotamers, C5), 61.5/61.3 (rotamers, C4), 40.7/39.7 (rotamers, C3`), 28.4 (C(*C*$H_3$)$_3$), 26.9/26.3 (rotamers, $CH_3$), 24.3/23.0 (rotamers, $CH_3$), 17.1/16.8 (rotamers, C4`). Rf = 0.48 (4:1 Hexane : Et_2O)

***tert*-Butyl-4-(S)-[2`-(*Z*)-1`-hydroxy-prop-2`-en-3`-yl]-2,2-dimethyl-1,3-oxazolidine-3-carboxylate (112)**[14]

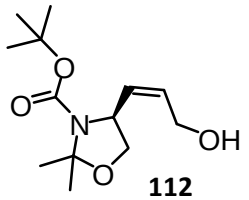

112

Synthesis of **112** (75.1 mg, 56% yield), was performed using *Z*-alkenone **107** (150 mg, 0.52 mmol) as the starting material, according to the same procedure as described for **109**. ^{1}H NMR (300 MHz, $CDCl_3$) δ major rotamer 5.81 (1H, ddd, *J* = 6.4, 8.6, 10.4 Hz, H2`), 5.48 (1H, dd, *J* = 10.7, 10.7 Hz, H3`), 4.86 (1H, m), 4.42-4.34 (1H, m), 4.22-4.13 (1H, m), 4.01 (1H, dd, *J* = 5.9, 9.0 Hz, H5`a), 3.86 (1H, m), 3.69 (1H, dd, *J* = 1.0, 8.9 Hz, H5`b), 1.52 (3H, s, CH_3), 1.44 (3H, s, CH_3), 1.42 (9H, s, CH_3); δ minor rotamer 5.66-5.56 (1H, m), 5.48 (1H, dd, *J* = 10.7, 10.7 Hz), 4.61-4.52 (1H, m), 4.22-4.12 (2H, m), 4.04-3.98 (1H, m), 4.01 (1H, dd, *J* = 5.9, 9.0 Hz), 3.69 (1H, dd, *J* = 1.0, 8.9 Hz), 1.56 (3H, s), 1.44 (3H, s), 1.39 (9H, s) ^{13}C NMR (101 MHz, $CDCl_3$) δ 152.1, 130.6 (C2`), 130.0(C3`), 93.3(C2), 80.9(*C*Me_3), 67.8, 57.5, 53.4, 28.3(C(*C*H_3)$_3$), 27.5(CH_3), 24.6(CH_3).

***tert*-Butyl-4-(S)-[2`-(Z)-1`-[(2-diphenylphosphino)-benzoyl]-oxy-prop-2`-en-3`-yl]-2,2-dimethyl-1,3-oxazolidine-3-carboxylate (113)**[14]

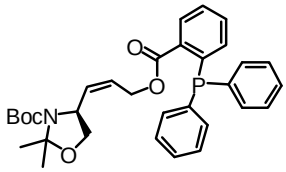

113

Synthesis of **113** (81mg, 55% yield) was performed using *Z*-alkenol **112** as the starting material (70 mg, 0.27mmol), according to the same procedure as described for **104**. ^{1}H NMR (500 MHz, CDCl3) δ major rotamer 8.07-8.01 (1H, m), 7.40-7.24 (12H, m), 6.93-6.88 (1H, m), 5.60-5.53 (2H, m, H2`), 4.93-4.85 (1H, m, H3`), 4.64-4.56 (2H, m, H1`), 3.99-3.91 (1H, m), 3.58-3.47 (1H, m), 1.62-1.35 (15H, 5 x $CH_3$). δ minor rotamer 8.07-8.01 (1H, m), 7.40-7.24 (12H, m), 6.93-6.88 (1H, m), 5.58-5.47 (2H, m, H2`), 5.09-4.98 (1H, m, H3`), 4.76-4.65 (2H, m, H1`), 3.99-3.91 (1H, m), 3.58-3.47 (1H, m), 1.62-1.35 (15H, 5 x CH_3). ^{13}C NMR (100 MHz, CDCl3) δ 166.5, 151.8, 140.6 (d, $J_{C,P}$ = 25.8 Hz), 138.0 (d, $J_{C,P}$ = 11.8 Hz), 134.4, 134.0 (d, $J_{C,P}$ = 20.7 Hz), 133.8 (d, $J_{C,P}$ = 20.4 Hz), 132.1, 130.7, 128.7 (d, $J_{C,P}$ = 3.6 Hz), 128.5 (d, $J_{C,P}$ = 7.2 Hz), 128.5 (d, $J_{C,P}$ = 7.2 Hz), 128.2, 123.6, 79.8, 68.5, 60.6, 54.3, 28.4, 26.5, 23.8. ESI-MS calcd for $C_{32}H_{36}NO_5P$ $[M+H]^+$ = 546.6; $[M+Na]^+$ = 568.6. Found 546.5, 568.5. Rf = 0.58 (2:1 Hexane : EtOAc)

Thiophenyl 3,4-*O*-isopropylidene-β-D-galactopyranoside (115)[18]

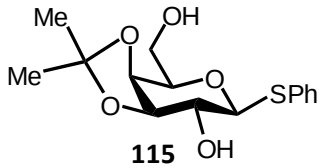

115

Starting material thiophenyl-β-D-galactopyranose **114** (1.3 g, 4.77 mmol)was dissolved in 15 mL acetonitrile, and 2,2 dimethoxypropane (7 mL) was added, followed by catalytic amount of para-toluene sulfonic acid. The reaction was stirred overnight at room temperature. The reaction was quenched by neutralization with triethylamine, evaporated under reduced pressure. The compound was then purified by column chromatography (20 : 10 : 0.3, Hexane : EtOAc : triethylamine, 1.05 g, 71%yield) . ^{1}H NMR(400 MHz, $CDCl_3$) δ 7.56-7.51 (2H, m), 7.35-7.28 (3H, m), 4.47 (1H, d, *J* = 10.2 Hz, H1), 4.18 (1H, dd, *J* = 2.2, 5.5 Hz, H4), 4.11 (1H, dd, *J* = 5.6, 6.8 Hz, H3), 3.98 (1H, dd, *J* = 7.2, 11.5 Hz, H6a), 3.90-3.85 (1H, m, H5), 3.81 (1H, dd, *J* = 4.0, 11.6 Hz, H6b), 3.56 (1H, dd, *J* = 7.0, 10.2 Hz, H2), 1.42 (3H, s), 1.33 (3H, s).

Thiophenyl 3,4-*O*-isopropylidene-6-*O*-*tert*-butyldimethylsilyl-β-D-galactopyranoside (116)[19]

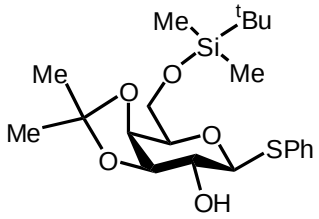

116

To a flame-dried flask, diol **115** (500 mg, 1.60 mmol) was added and stirred with distilled dichloromethane (75 mL). Distilled triethylamine (0.28 mL, 0.206 mmol) was added, followed by *tert*-butyldimethylsilyl chloride (277 mg, 1.84 mmol). The reaction was stirred until the starting material was consumed. The reaction was quenched by adding a saturated solution of ammonium chloride, and the product was extracted with dichloromethane. The organic layers were combined, washed with a saturated solution of sodium bicarbonate, brine, then dried over $MgSO_4$ and evaporated under reduced pressure. The product was purified by column

[18] Janczuk, A. D.; Zhang, W.; Andreana, P.R.; Warrick, J.; Wang, P.G. Carbohydr. Res. **2002**, *337*, 1247-1259.
[19] Branderhorst, H.M.; Liskamp, R. M. J.; Pieters, R. J. *Tetrahedron* **2007**, *63*, 4290-4296.

chromatography (4:1 Hexane/ EtOAc) and obtained as a white solid (607 mg, 89% yield) ^{1}H NMR(400 MHz, $CDCl_3$) δ 7.58-7.51 (2H, m), 7.35-7.22 (3H, m), 4.45 (1H, d, *J* = 10.3 Hz, H1), 4.23 (1H, dd, *J* = 1.9, 5.4 Hz, H4), 4.07 (1H, dd, *J* = 5.6, 6.8 Hz, H3), 3.93- 3.81 (3H, m, H5, H6), 3.57 (1H, dd, *J* = 7.0, 10.3 Hz, H2), 2.50-2.30 (1H, br, OH), 1.44 (3H, s, CH_3), 1.33 (3H, s, CH_3), 0.91 (9H, s, $C(CH_3)_3$), 0.09 (6H, s, $Si(CH_3)_2$). ESI/MS calcd for $C_{21}H_{34}O_5SSi$ $[M+H]^+$: 427.2. Found 427.2. Rf = 0.25 (4:1 Hexane: EtOAc)

Thiophenyl 3,4-*O*-isopropylidene-6-*O*-triisopropylsilyl-β-D-galactopyranose (119)

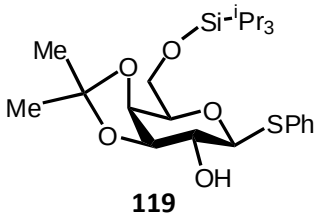

119

To a flame-dried flask, diol **115** (300 mg, 0.96 mmol) was added and stirred with distilled dichloromethane (40 mL). Distilled triethylamine (0.17 mL, 0.124 mmol) was added, followed by triisopropylsilyl chloride (212 mg, 1.10 mmol). The reaction was stirred until the starting material was consumed. The reaction was quenched by adding a saturated solution of ammonium chloride, and the product was extracted with dichloromethane. The organic layers were combined, washed with a saturated solution of sodium bicarbonate, brine, then dried over $MgSO_4$ and evaporated under reduced pressure. The product was purified by column chromatography(4:1 Hexane/ EtOAc) to afford a white gel-like oil (414 mg, 92% yield). ^{1}H NMR(400 MHz, $CDCl_3$) δ 7.57-7.52 (2H, m), 7.33-7.27 (3H, m), 4.45 (1H, d, *J* = 10.3 Hz, H1), 4.23 (1H, dd, *J* = 2.1, 5.4 Hz, H4), 4.07 (1H, dd, *J* = 5.4, 6.9 Hz, H3), 3.99- 3.96 (2H, m, H5, H6a), 3.88-3.83 (1H, m, H6b), 3.57 (1H, ddd, *J* = 2.3, 7.0, 10.1 Hz, H2), 2.46 (1H, d, *J* = 2.3 Hz, OH), 1.43 (3H, s, CH_3), 1.33 (3H, s, CH_3), 1.15-1.05 (3H, m, $SiCH(Me)_2$), 1.09-1.06 (18H, m, 6 x CH_3). ^{13}C NMR (101 MHz, $CDCl_3$) δ 132.4, 132.3, 128.9, 127.9, 110.0($C(Me)_2$), 88.4(C1), 78.9(C3), 77.5(C6), 73.1(C4), 71.6(C2), 62.4(C5), 28.1(CH_3), 26.3(CH_3), 17.9($SiCH(CH_3)_2$), 17.9($SiCH(CH_3)_2$), 11.9($SiCH(Me)_2$). ESI/MS calcd for $C_{24}H_{40}O_5SSi$ $[M+H]^+$: 469.2444; $[M+NH_4]^+$: 486.2709 $[M+Na]^+$:491.2633. Found 469.176, 486.197, 491.141. Rf = 0.30 (4:1 Hexane: EtOAc).

General Procedure for SmI_2-mediated C-glycosylation (Barbier conditions)

To a flamed dried flask, thiogalactoside **116** or **119** and aldehyde **27** were added and dissolved in minimal amounts of distilled THF. The solvent was evaporated by passing argon through the flask, and placed in a brine ice bath to reach -10 °C. In another flask, a freshly prepared solution of 0.1M SmI_2 in THF (182 mg samarium metal and 282 mg of diiodoethane in 10mL of distilled

THF, stirred vigorously until a dark teal colour is persistent) was also cooled to -10 ^{o}C. The SmI_2 solution was then added dropwise to the sugar/aldehyde mixture and stirred at -10^{o}C. The reaction was quenched by addition of a saturated solution of ammonium chloride, and the product was extracted using several portions of ethyl acetate, dried over $MgSO_4$ and evaporated under reduced pressure. The product was chromatographed using 4:1 (Hexane : EtOAc).

<u>*tert*-Butyl-4(S)-[2`-(*S*)-1`-hydroxy-1`-(3,4-*O*-isopropylidene-6-*O*-triisopropylsilyl-D–*lyxo*-hexa-2-ulos-1-yl)-prop-2`-yl]-2,2-dimethyl-1,3-oxazolidine-3-carboxylate (120)</u>

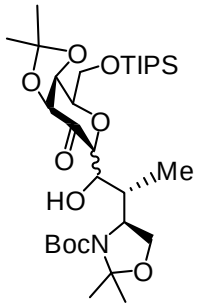

^{1}H NMR (500 MHz, $CDCl_3$)δ 4.95 (1H, d, *J* = 4.1 Hz), 4.57-4.51 (1H, m), 4.18-4.12 (1H, m), 4.09-3.98 (3H, m), 4.00-3.90 (3H, m), 3.76 (1H, d, *J* = 9.0 Hz), 3.72 (1H, d, *J* = 8.5 Hz), 3.66-3.58 (2H, m), 2.35-2.25 (1H, m), 1.58-1.48 (9H, m), 1.46-1.39 (15H, m), 1.18-1.00 (33H, m) ^{13}C NMR (126 MHz, $CDCl_3$) δ 207.0, 203.0, 154.6, 111.0, 93.6, 90.0, 81.4, 80.7, 79.5, 78.4, 78.3, 78.2, 77.9, 72.3, 66.8, 66.3, 62.3, 62.2, 61.2, 59.7, 36.8, 33.4, 30.9, 28.4, 28.4, 28.3, 27.5, 27.0, 26.0, 26.0, 25.8, 24.4, 24.0, 17.9, 17.9, 11.9, 10.2. ESI/MS calcd for $C_{31}H_{57}NO_9Si$ $[M+H]^+$: 616.3881; $[M+Na]^+$:638.3700. Found 616.462, 638.444. Rf = 0.33 (2:1 Hexane: EtOAc).

5. *MOLECULAR DYNAMICS PARAMETERS AND DATA*

Computational Simulation Data - Intramolecular Hydrogen Bonding Analysis for monomers **60-63**

Hydrogen bonding analysis using AMBER's ptraj program.[20] Distance cutoff was set at 3.00 Å, and angle cutoff at 120.0 degrees. Intramolecular bonding populations were examined for 10 ns trajectories.

Computational Simulation Data - Φ_α/Ψ_α Torsional Angle Analysis

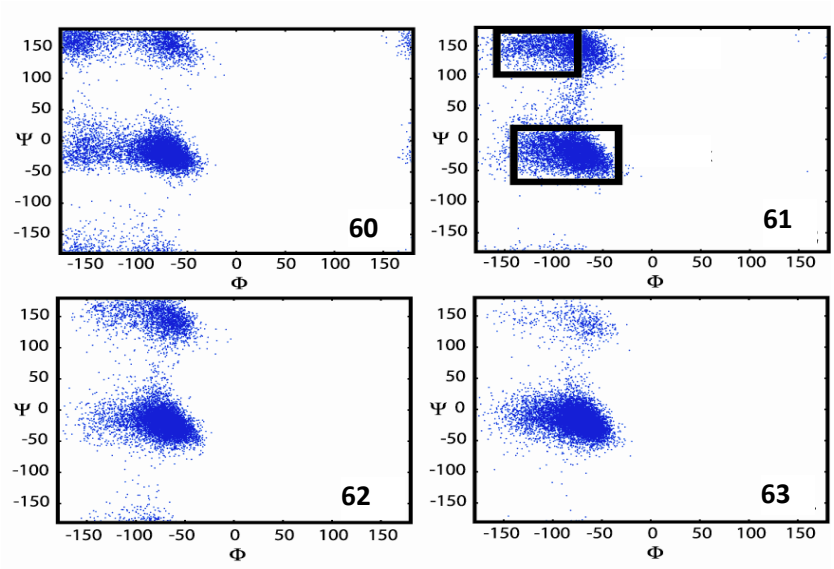

Figure S-1. Free energy profiles for Φ_α/Ψ_α torsional distributions for glycosylated residues of **60-63**.

[20] Case, D. A.; Darden, T. A.; Cheatham III, T.E.; Simmerling, C. J.; Wang, J.; Duke, R.E.; Luo, R.; Merz, K. M.; Pearlman, D. A.; Crowley, M.; Walker, R. C.; Zhang, W.; Wang, B.; Hayik, S.; Roitberg, A.; Seabra, G.; Wong, K. F.; Paesani, F.; Wu, X.; Brozell, S.; Tsui, V.; Gohlke, H.; Yang, L.; Tan, C.; Mongan, J.; Hornak, V.; Cui, G.; Beroza, P.; Mathews, D. H.; Schafmeister, C.; Ross, W.S.; Kollman P. A. *AMBER 9*; University of California: San Francisco, 2006.

CLAIMS TO ORIGINAL RESEARCH

1. Analysis of reducing mono-and disaccharides for ice-recrystallization inhibition (IRI) activity and correlation to their respective hydration parameters (including the development of the *Hydration Index*).

2. Synthesis of novel *C*-linked AFGP analogues (**18**-**21**) containing various sidechain linkers between the carbohydrate and the peptide backbone, and the IRI activity analysis thereof.

3. Investigated the significance of the sidechain length and the sidechain amide bond by analysis of the solution conformation of the model systems for analogues **18**-**21**, and correlation to their respective IRI activity.

PUBLICATIONS

1. **Tam, R.Y.**; Rowley, C.N.; Petrov, I.; Zhang, T.; Afagh, N.A.; Woo, T.; Ben, R.N. "Solution Conformation of C-Linked Antifreeze Glycoprotein analogues and Modulation of Ice Recrystallization." *Journal of American Chemical Society*. **2009**, *131*, 15745-15753.

2. **Tam, R.Y.**; Ferreira, S.S.; Czechura, P.; Chaytor, J.L.; Ben, R.N. "Hydration Index – A Better Parameter for Explaining Small Molecule Hydration in Inhibition of Ice Recrystallization." *Journal of American Chemical Society*. **2008**, *130*, 17494-17501.

3. Czechura, P.; **Tam, R.Y.**; Dimitrijevic, E.; Murphy, A.; Ben, R.N. "The Importance of Hydration for Inhibiting Ice Recrystallization with Novel C-Linked Antifreeze Glycoproteins." *Journal of the American Chemical Society*. **2008**, *130*, 2928-2929.

PATENTS

1. Ben, R.N.; Tam. R. Y.; Czechura, P.; **Tam R.Y.** Antifreeze Glycoprotein Analogues and Uses Thereof". Publication Date: March 18, 2010. U.S. Patent and Trademark Office. Application Publication No. US-2010-0068692-A1.

2. Czechura, P.; Ben, R.N.; **Tam, R.** "Antifreeze Glycoprotein Analogues and Uses Thereof". Filing Date: February 9, 2009. Canadian Intellectual Property Office. Application Serial Number: CA 2653153.

APPENDIX –

SELECTED NMR SPECTRA

3`-(α-D-galactopyran-1-yl)-prop-1`-ene (10a)

^{1}H NMR (400 MHz, CD_3OD)

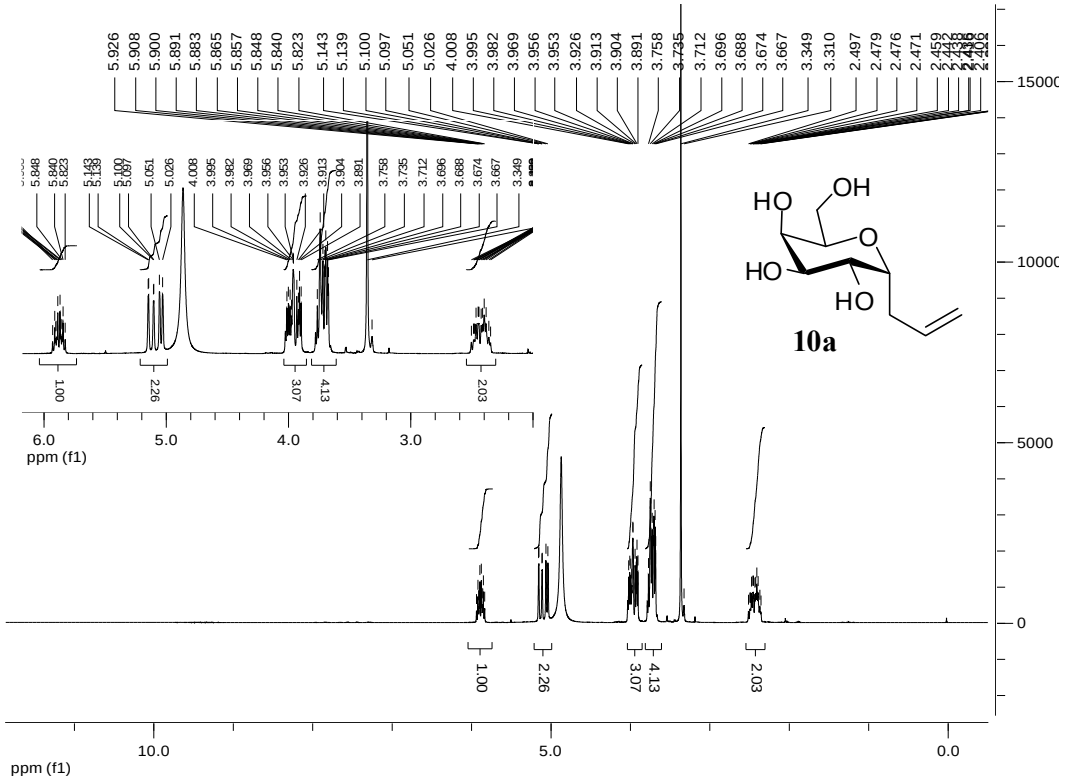

^{13}C NMR (100 MHz, CD_3OD)

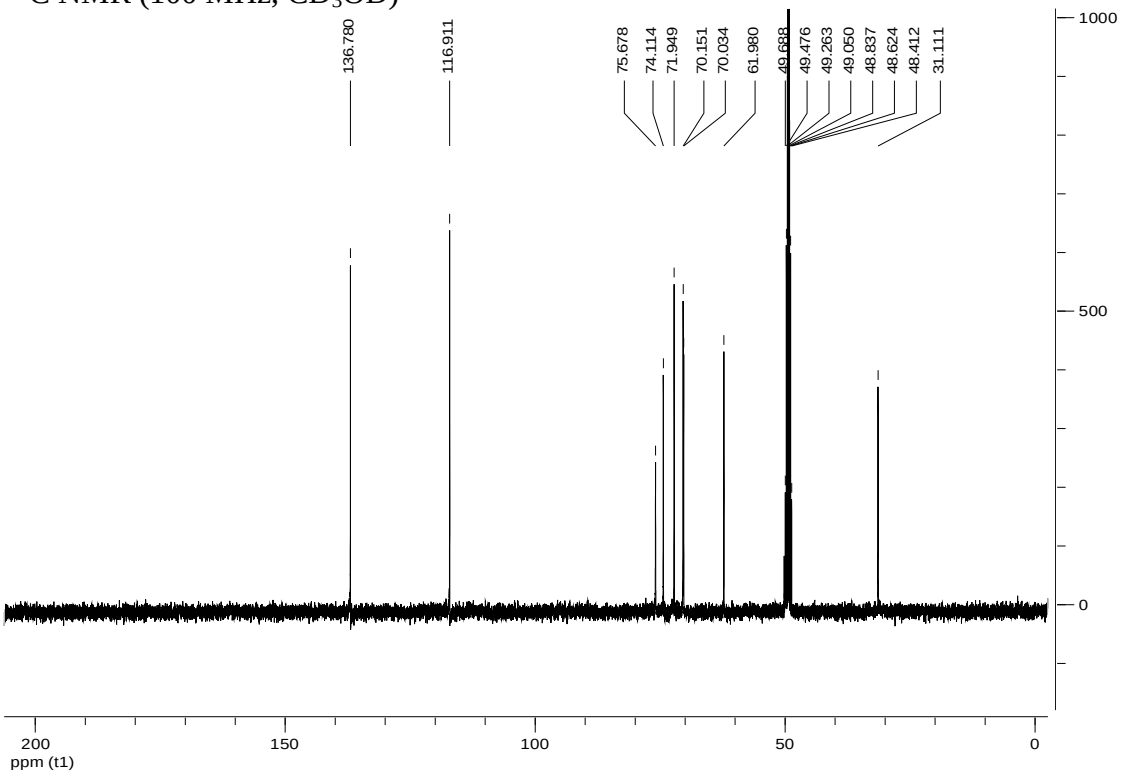

3`-(α-D-glucopyran-1-yl)-prop-1`-ene (11a),

^{1}H NMR (400 MHz, D_2O)

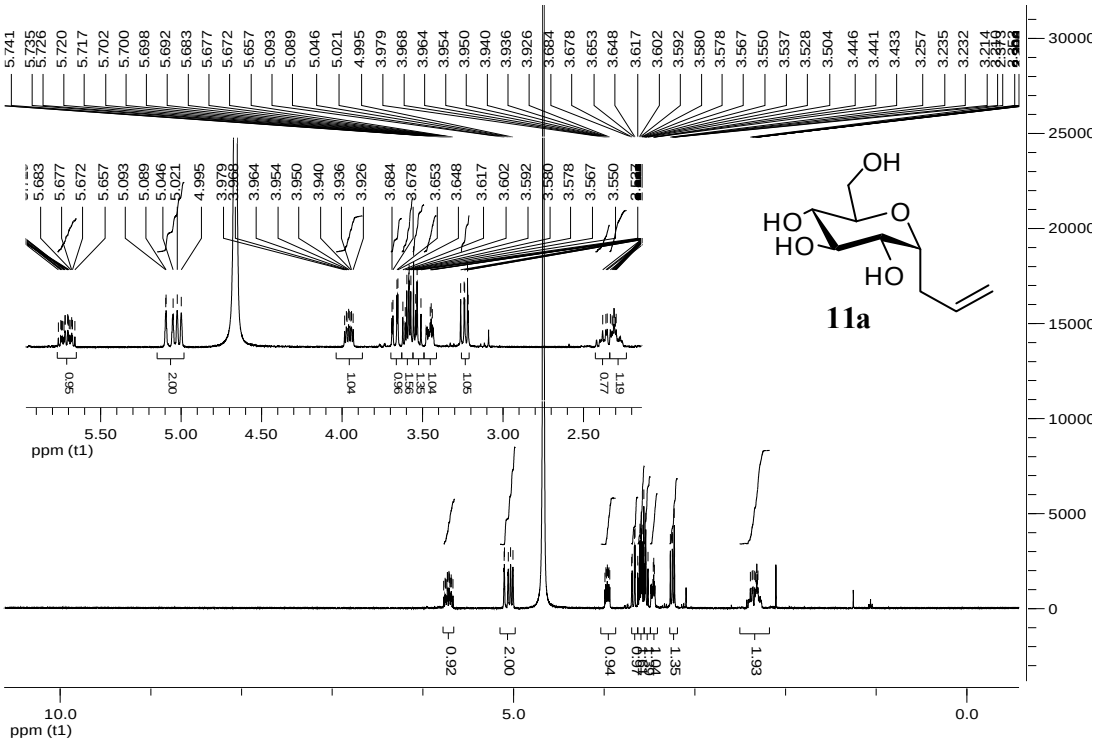

^{13}C NMR (100 MHz, D_2O)

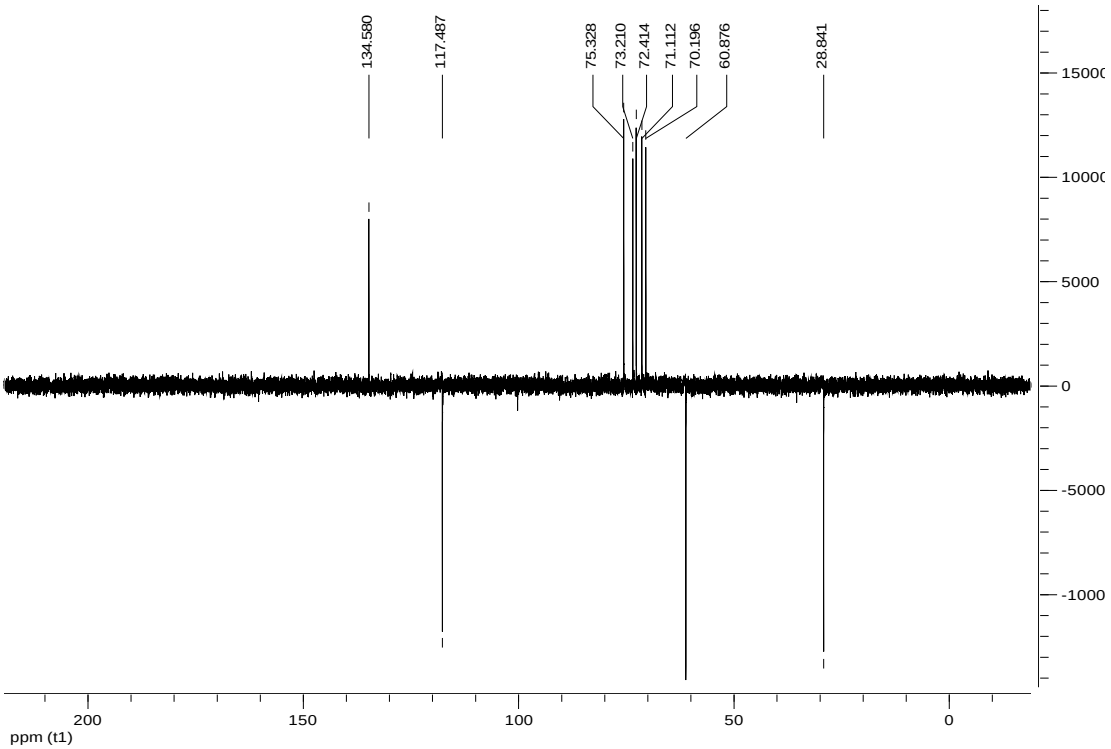

3`-(α-D-talopyran-1-yl)-prop-1`-ene (13),

^{1}H NMR (400 MHz, MeOD)

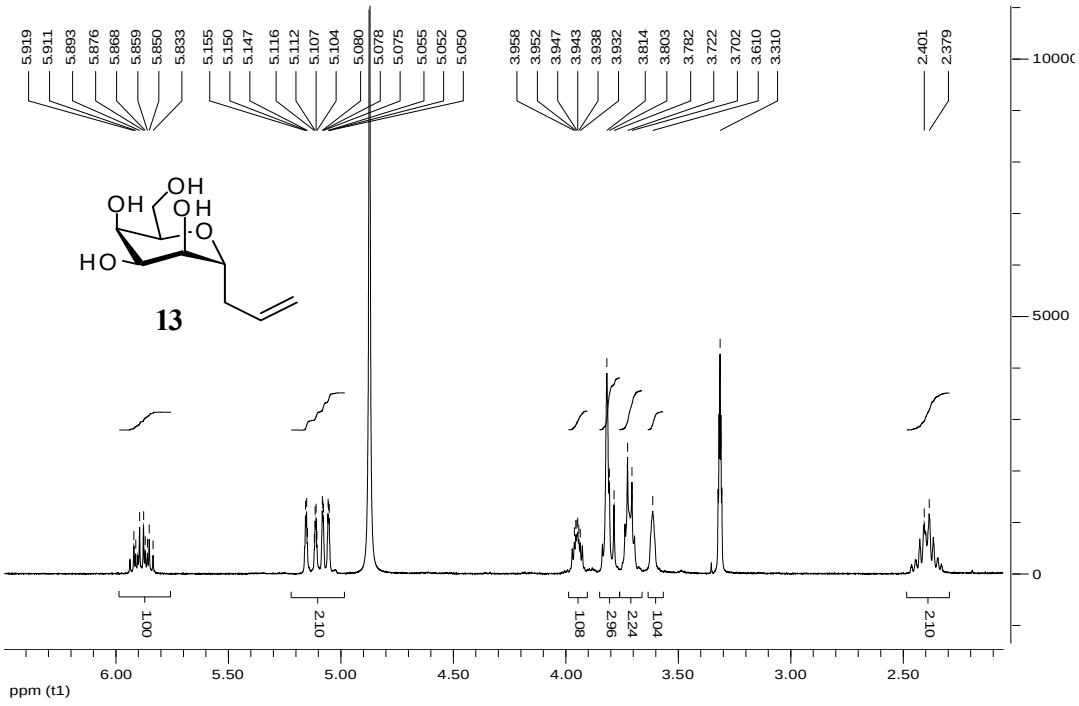

^{13}C NMR (100 MHz, MeOD)

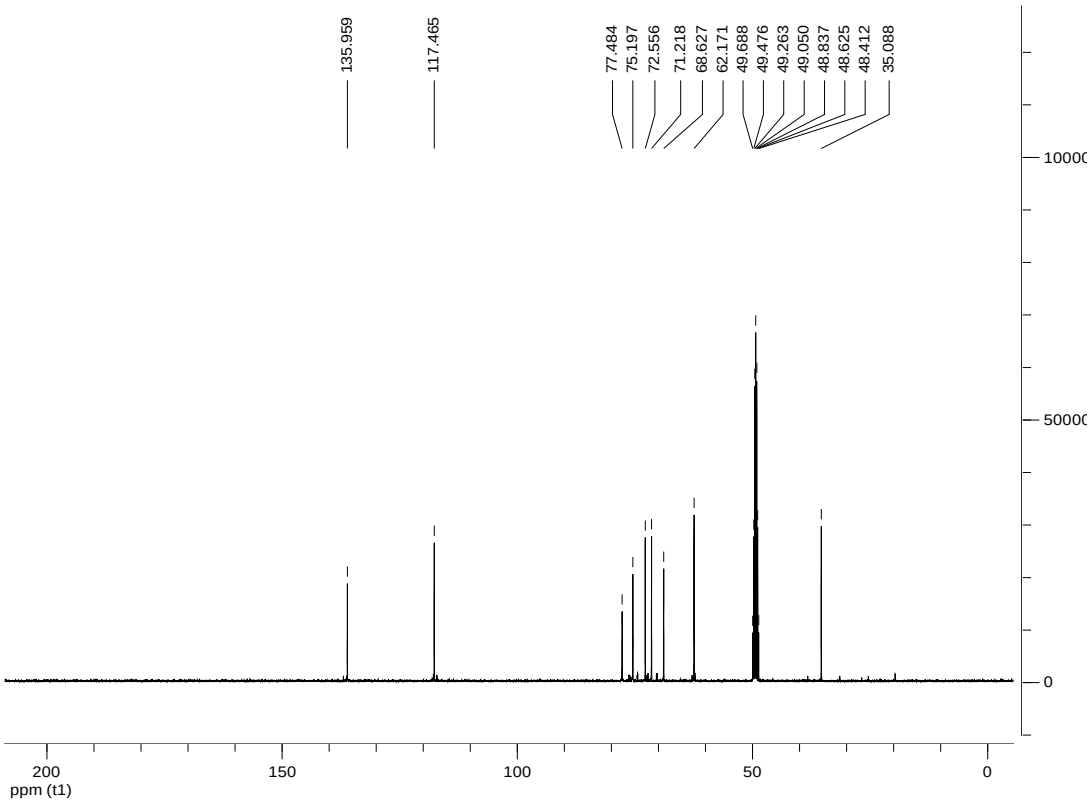

[[(S)-*N*γ-[2`-(α-D-galactopyranosyl)-ethan-1`-amido]-α,γ-diaminobutyric-1-amido]-glycinamido-glycinamido]$_4$-glycine (18), ^{1}H NMR (500 MHz, D_2O)

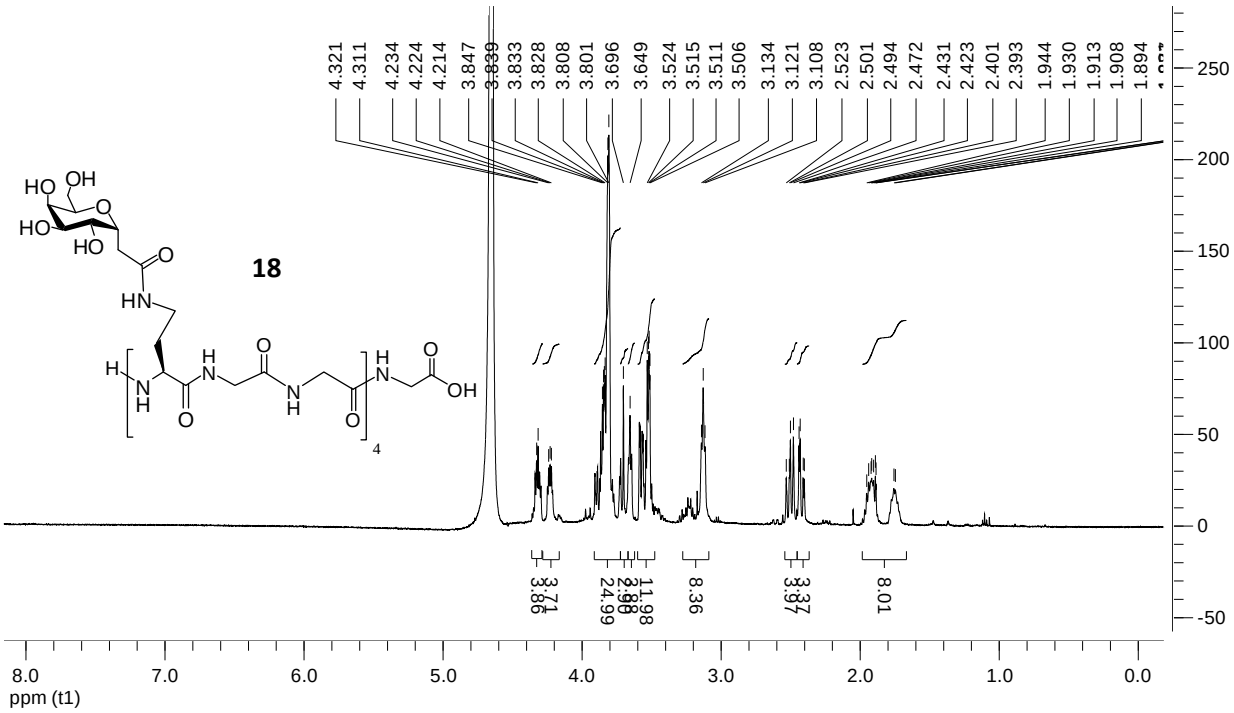

^{13}C NMR (126 MHz, D_2O)

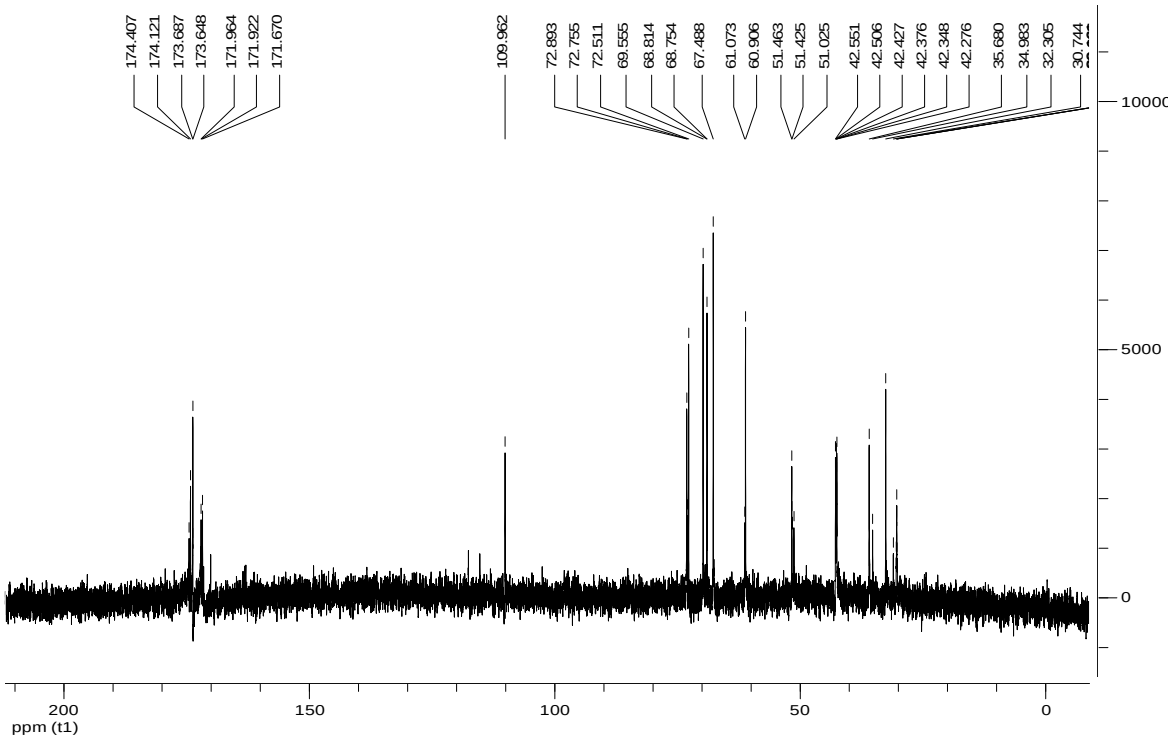

[[(S)-*N*γ-[2`-(α-D-glucopyranosyl)-ethan-1`-amido]-α,γ-diaminobutyric-1-amido]-glycinamido-glycinamido]$_4$-glycine (19), ^{1}H NMR (500 MHz, D_2O)

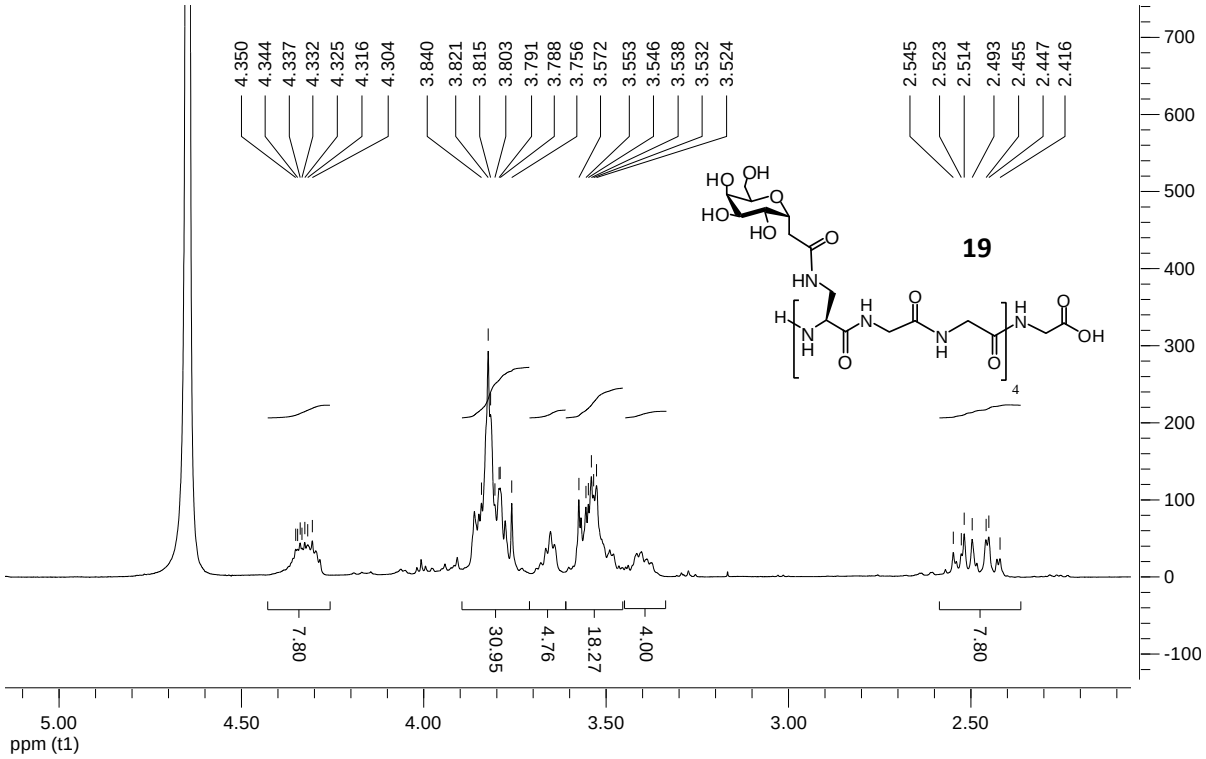

^{13}C NMR (126 MHz, D_2O)

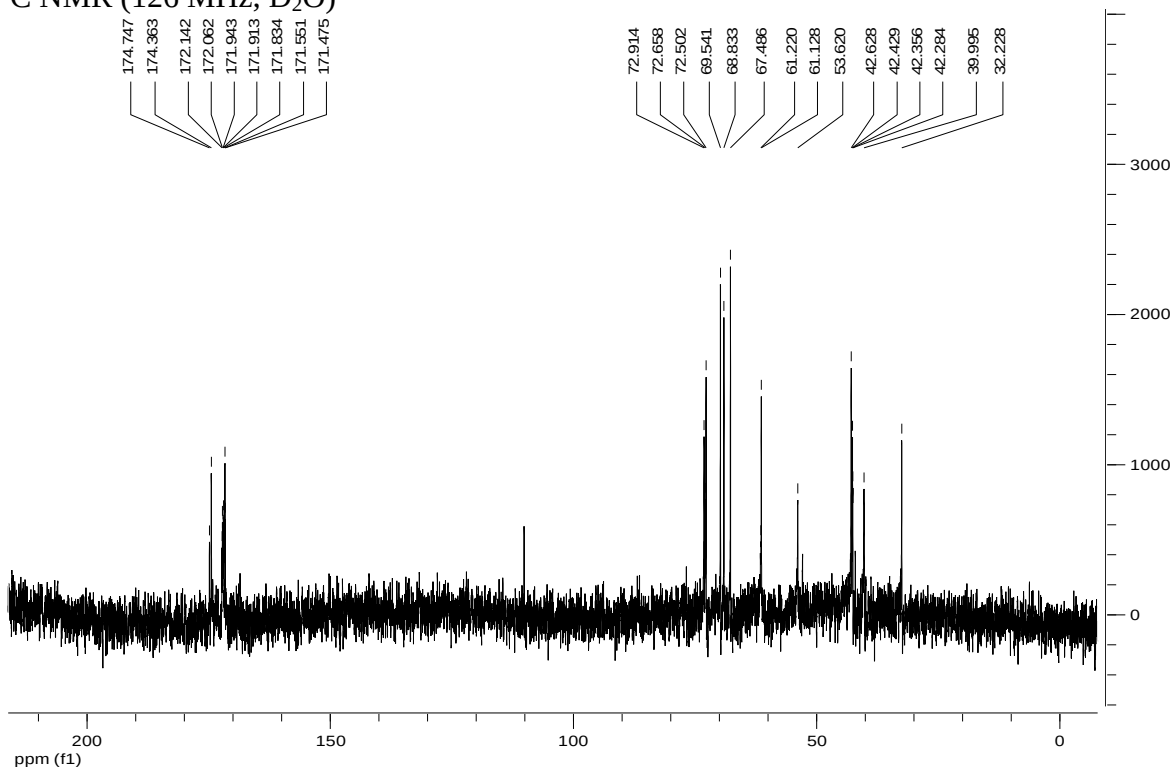

[[(S)-*N*γ-[2`-(α-D-galactopyranosyl)-propan-1`-amido]-α,γ-diaminobutyric-1-amido]-glycinamido-glycinamido]$_4$-glycine (20), ^{1}H NMR (500 MHz, D_2O)

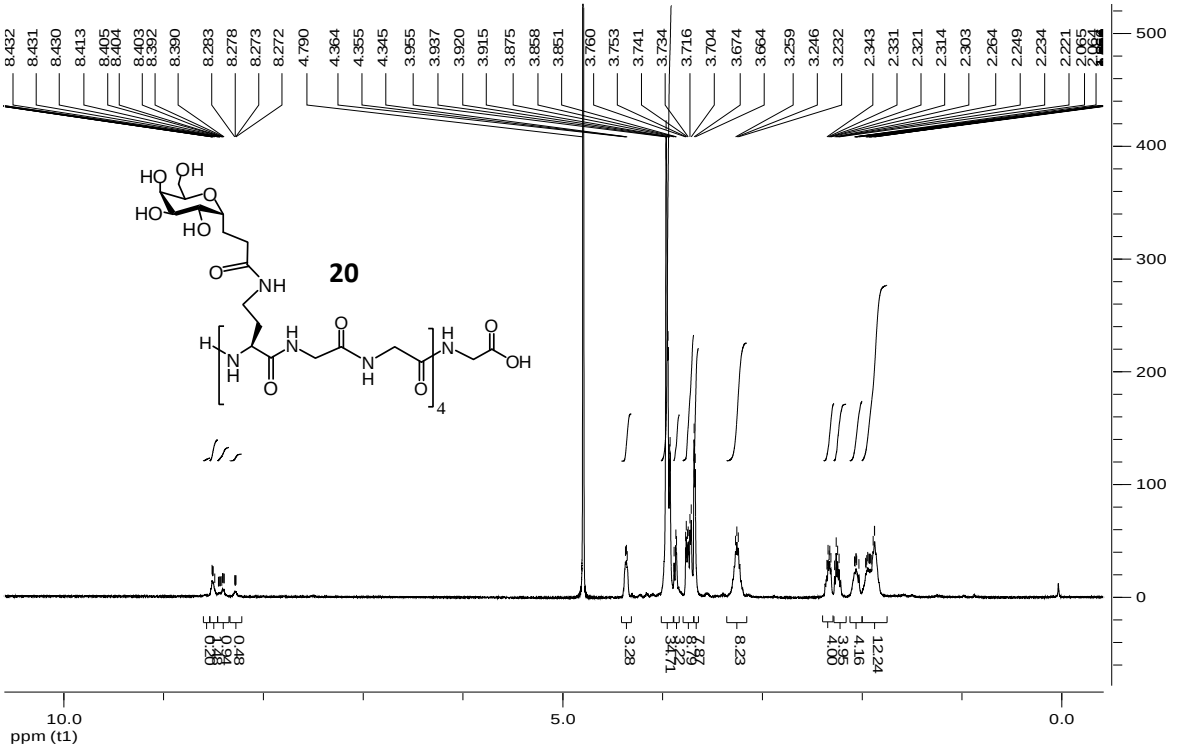

^{13}C NMR (126 MHz, D_2O)

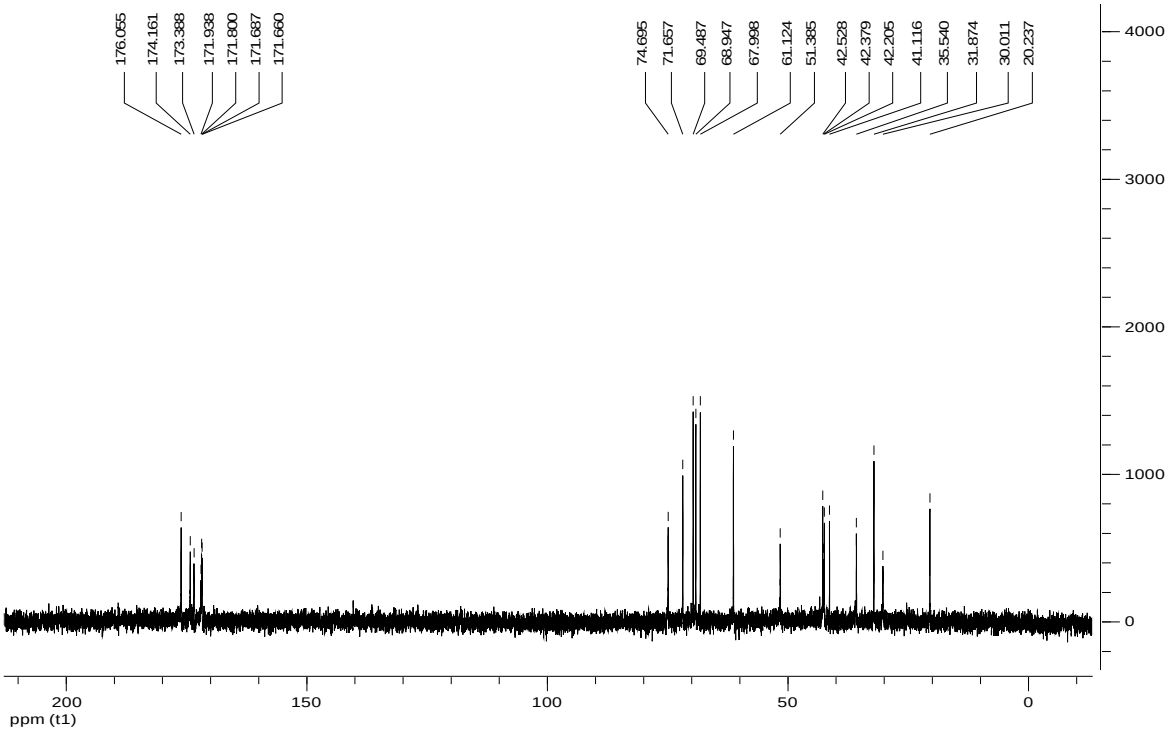

[[(S)-*Nβ*-[4`-(α-D-galactopyran-1-yl)-butan-1`-amido]-α,β-diaminopropanoic-1-amido]-glycinamido-glycinamido]$_4$-glycine (21), ^{1}H NMR (500 MHz, D_2O)

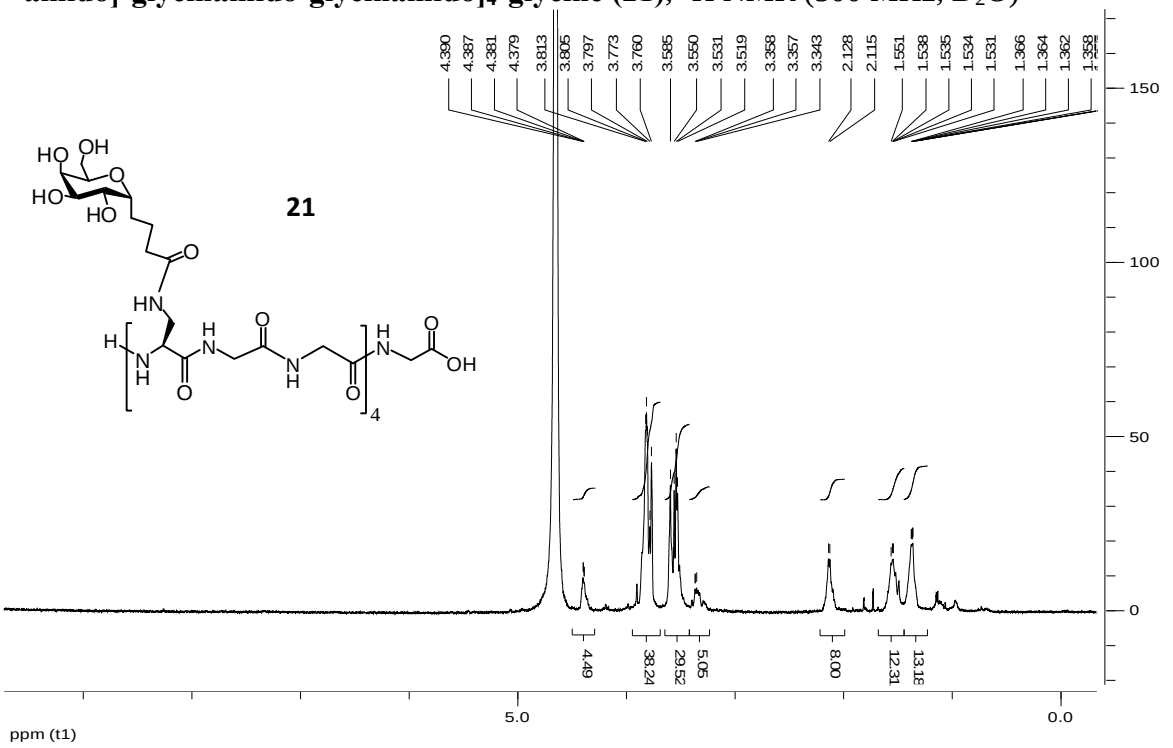

^{13}C NMR (126 MHz, D_2O)

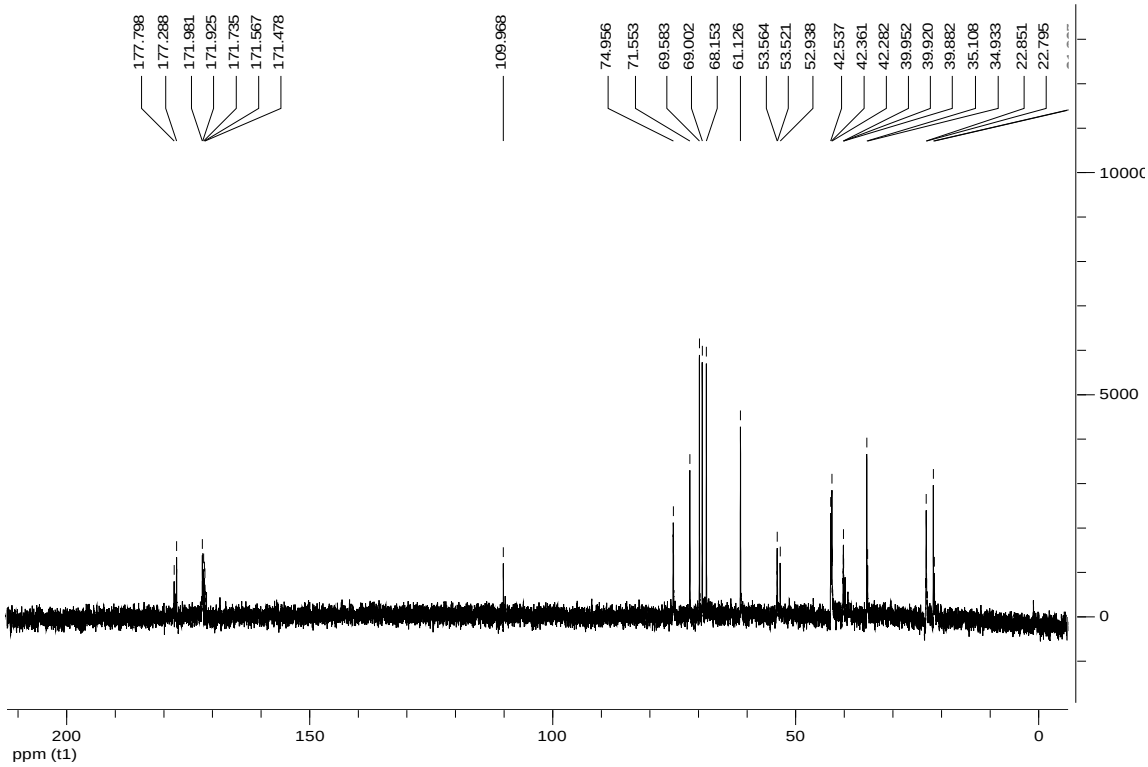

***tert*-butyl-4-(S)-[2`-(R)-1`-oxopropan-2`-yl]-2,2-dimethyl-1,3-oxazolidine-3-carboxylate (27)**, ^{1}H NMR (500 MHz, 20^{o}C, $CDCl_3$)

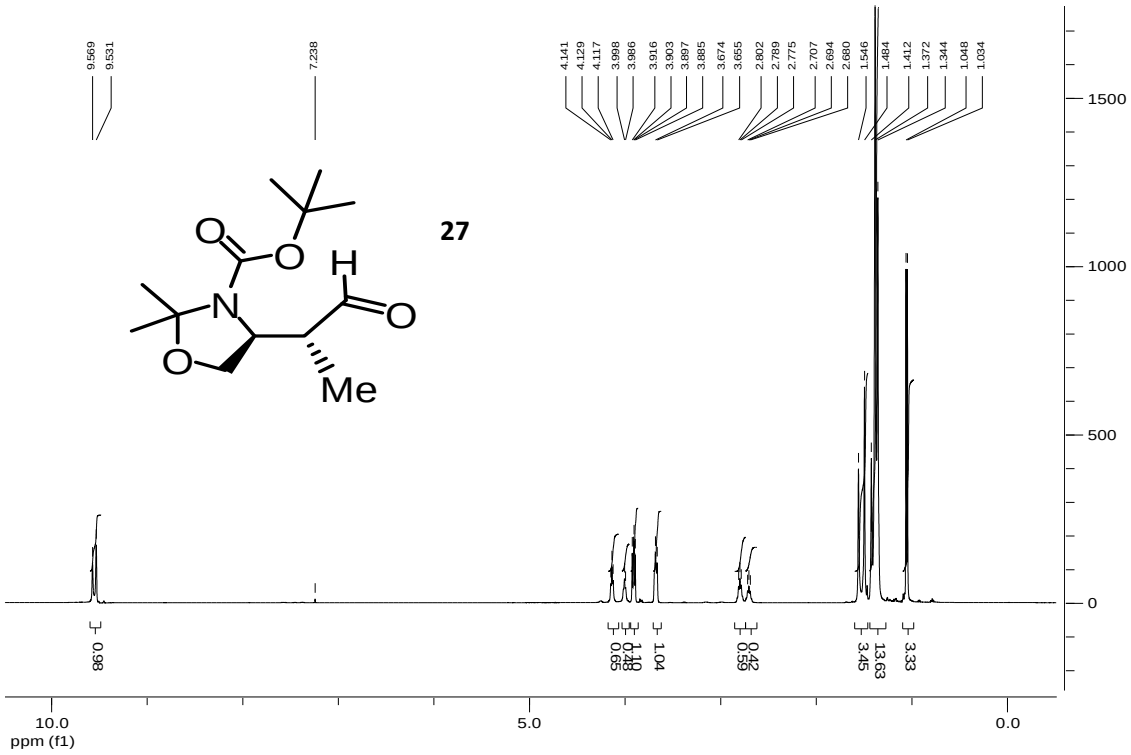

^{1}H NMR (500 MHz, 50^{o}C, $CDCl_3$)

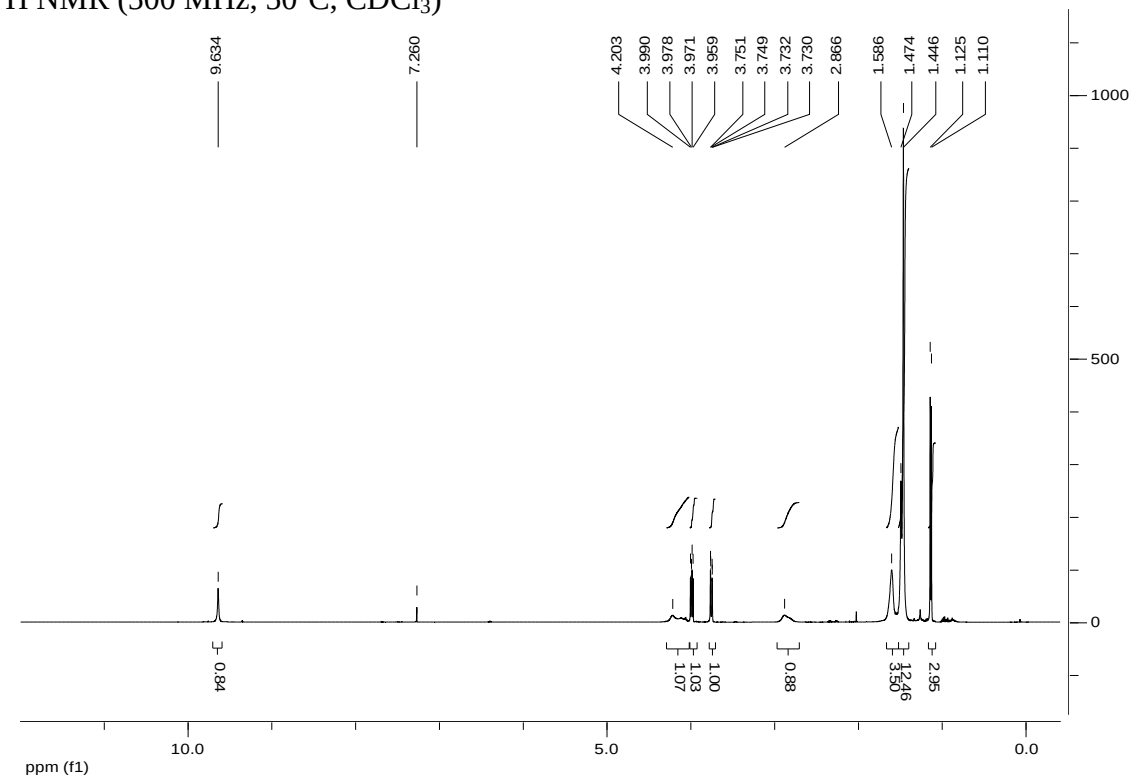

***tert*-butyl-4-(S)-[2`-(R)-1`-oxopropan-2`-yl]-2,2-dimethyl-1,3-oxazolidine-3-carboxylate (27)**, ^{13} C NMR (126 MHz, 20^{o}C, $CDCl_3$)

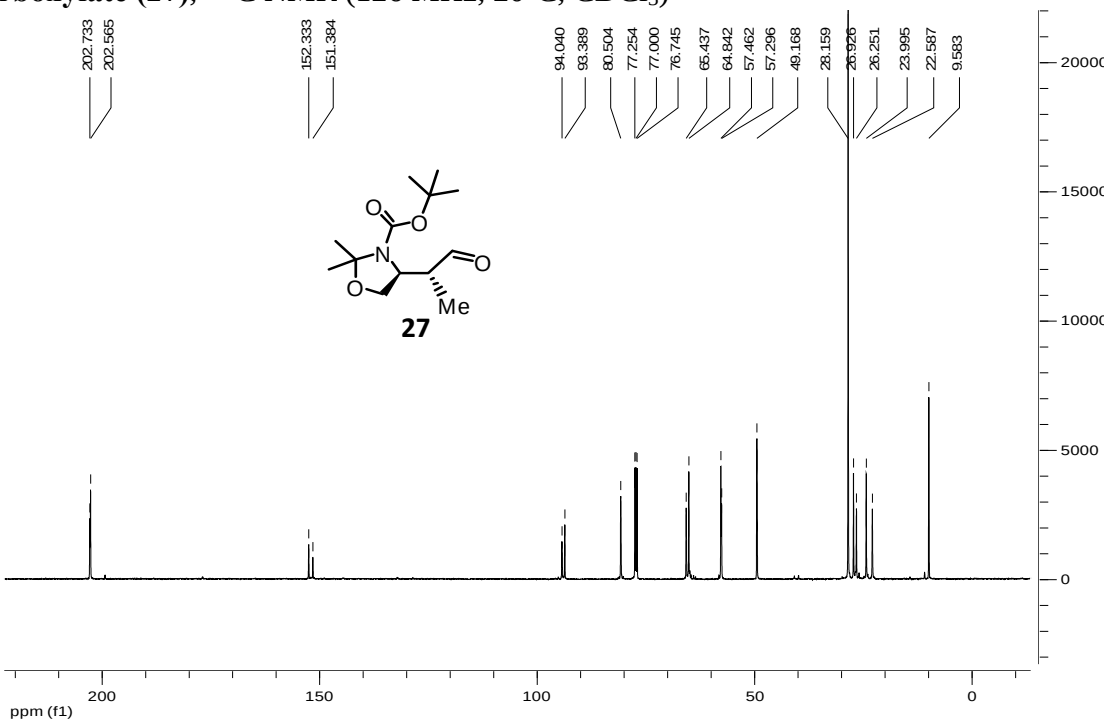

^{13} C NMR (126 MHz, 50^{o}C, $CDCl_3$)

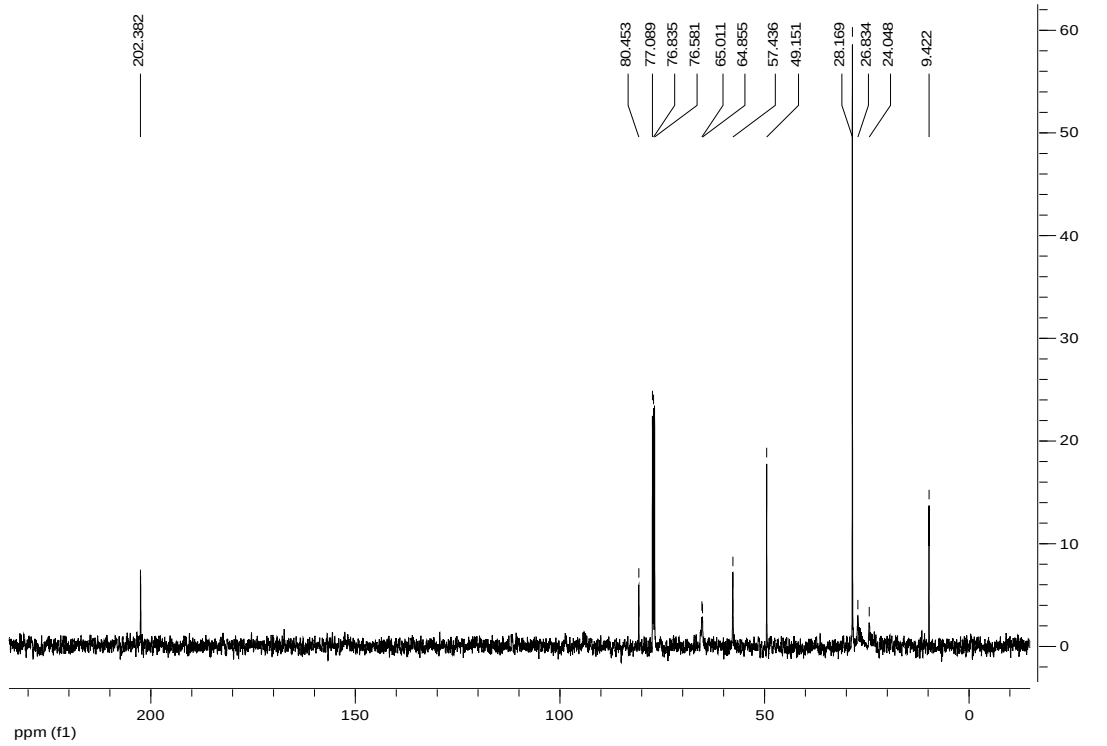

3`-(2,3,4,6-tetra-*O*-acetyl-α-D-galactopyran-1-yl)-prop-1`-ene (37) ,

^{1}H NMR (500 MHz, $CDCl_3$)

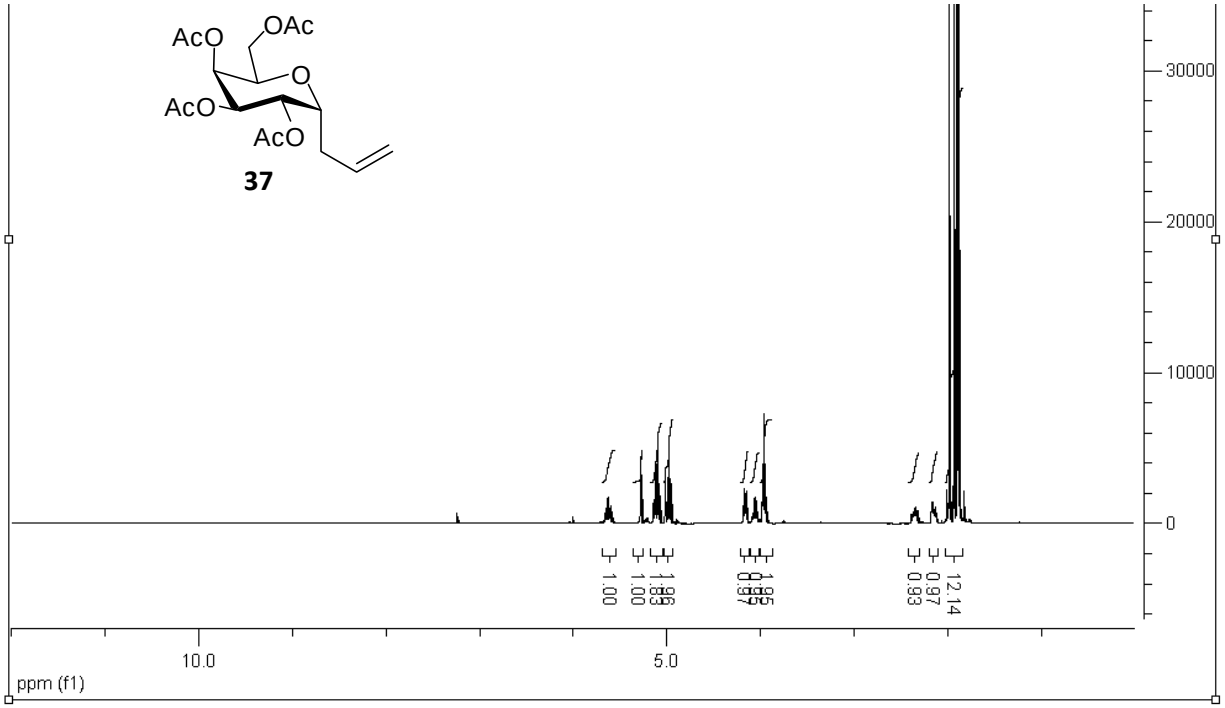

^{13}C NMR (101 MHz, $CDCl_3$)

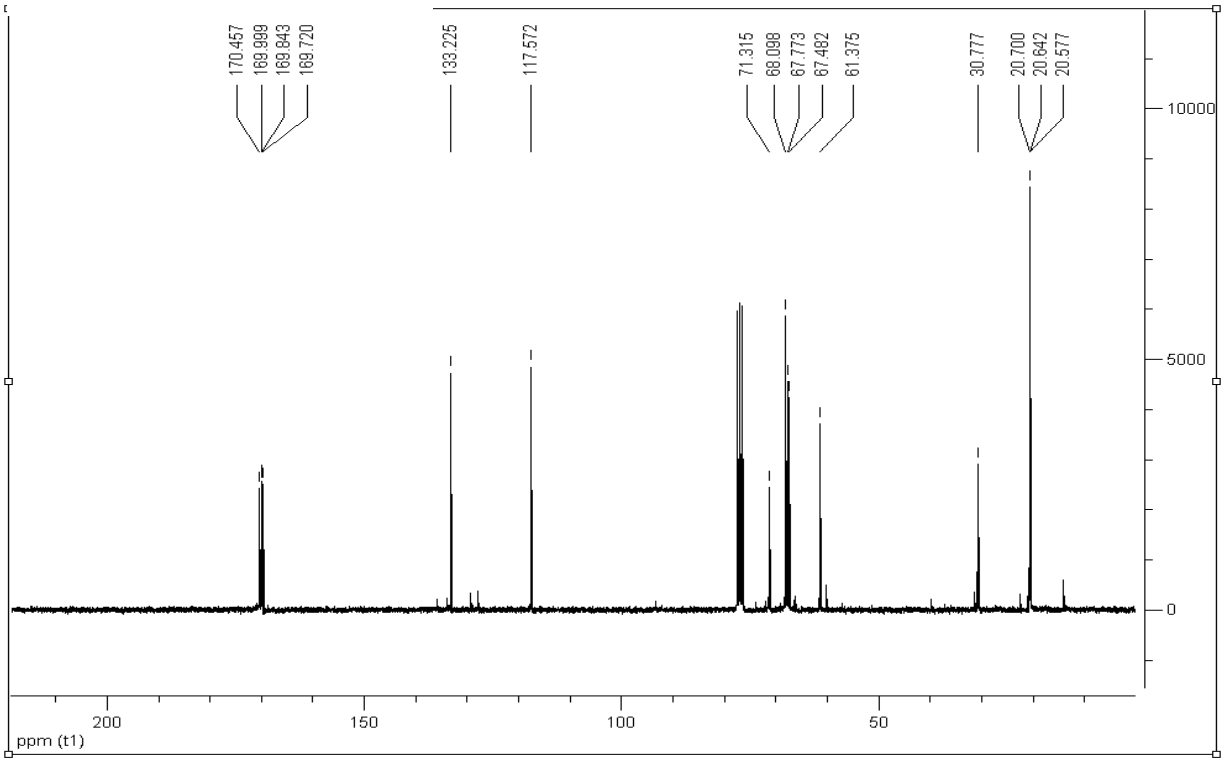

3`-(3,4-*O*-isopropylidene-α-D-galactopyran-1-yl)-prop-1`-ene (40),
^{1}H NMR (400 MHz, $CDCl_3$)

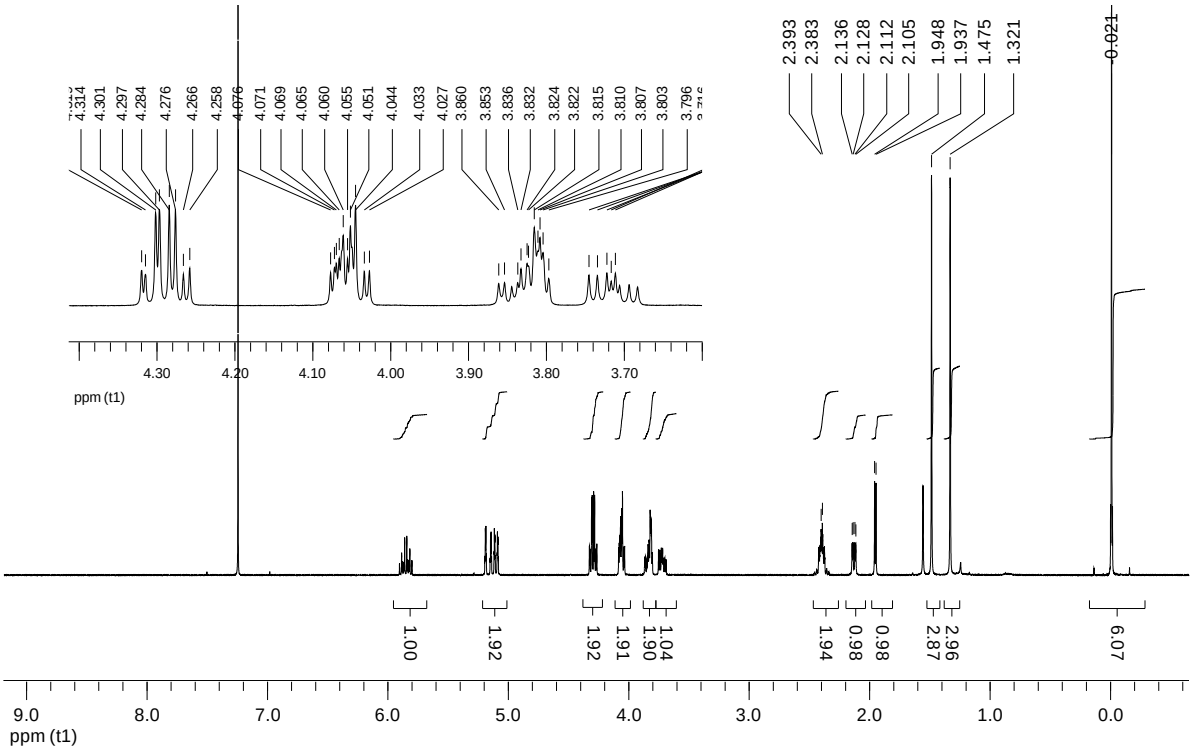

^{13}C NMR (101 MHz, $CDCl_3$)

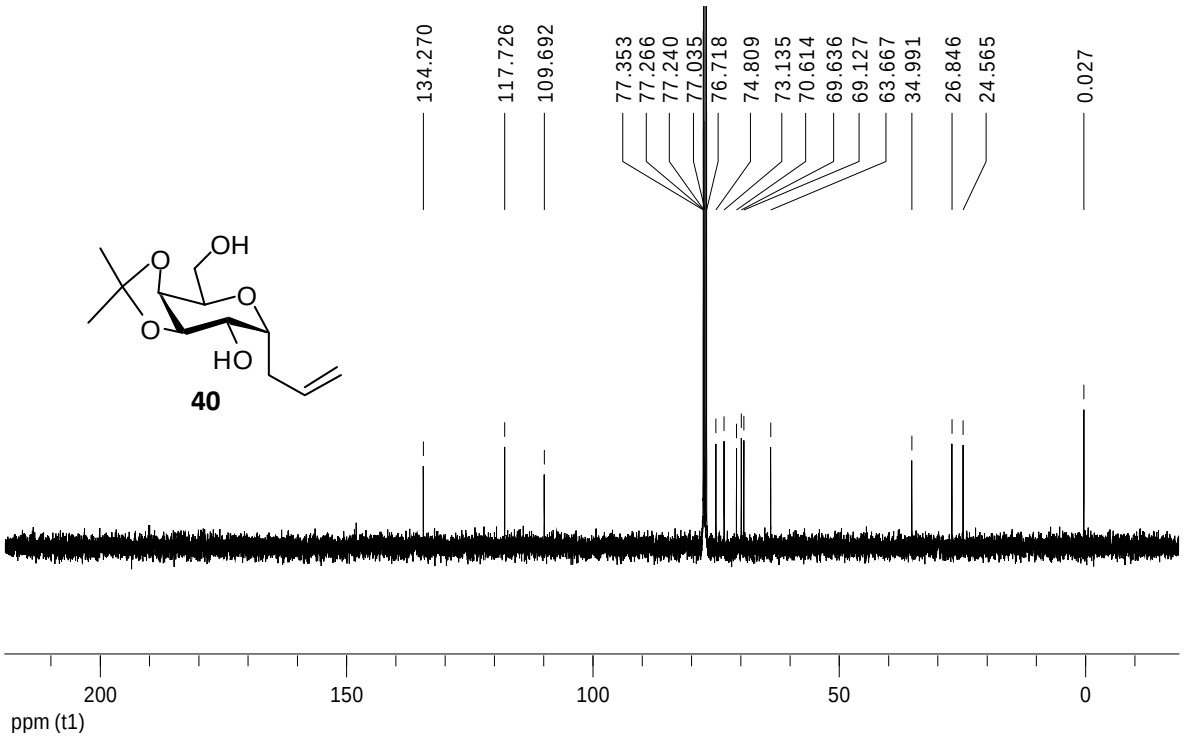

3`-(3,4-*O*-isopropylidene-6-*O*-*tert*-butyldimethylsilyl-α-D-galactopyran-1-yl)-prop-1`-ene (41), ^{1}H NMR (400 MHz, $CDCl_3$)

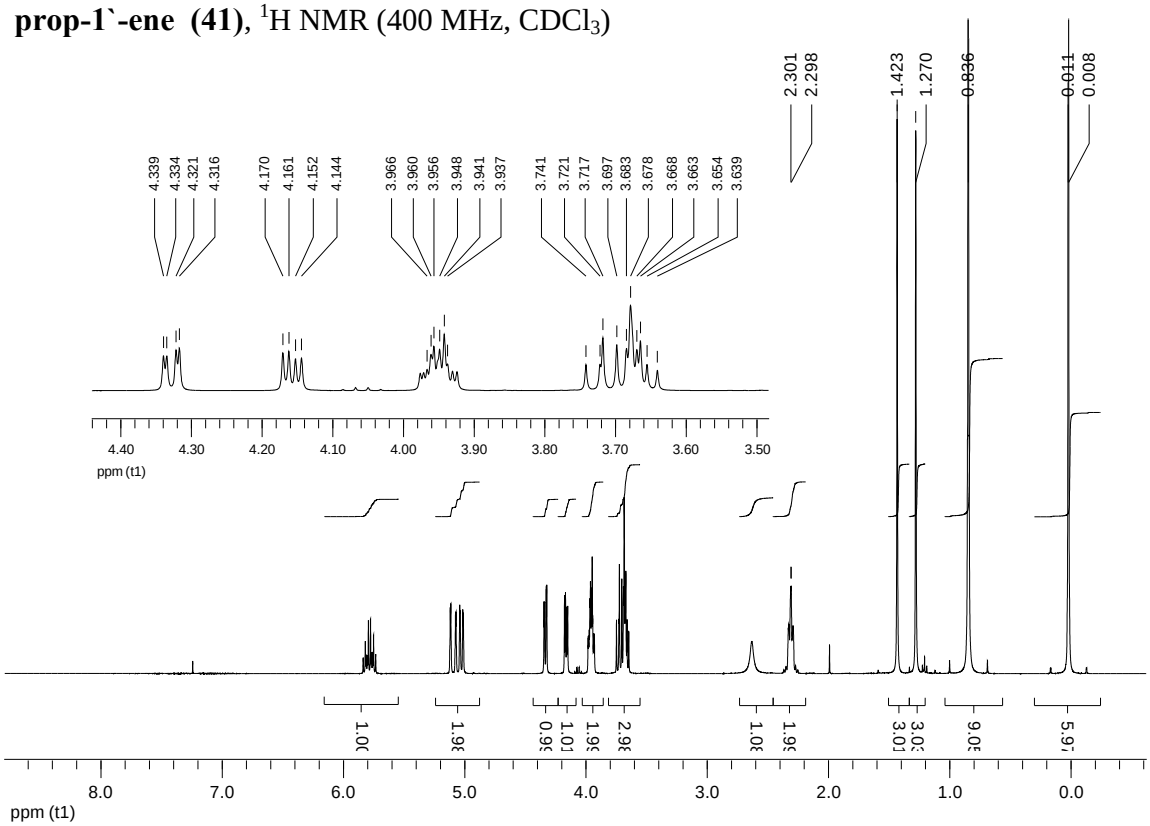

^{13}C NMR (101 MHz, $CDCl_3$)

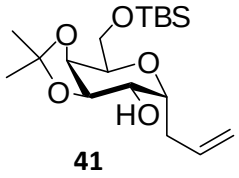

41

3`-(3,4-*O*-isopropylidene-6-*O-tert*-butyldimethylsilyl-α-D-galactopyran-1-yl)-prop-1`-ene (43), ^{1}H NMR (400 MHz, $CDCl_3$)

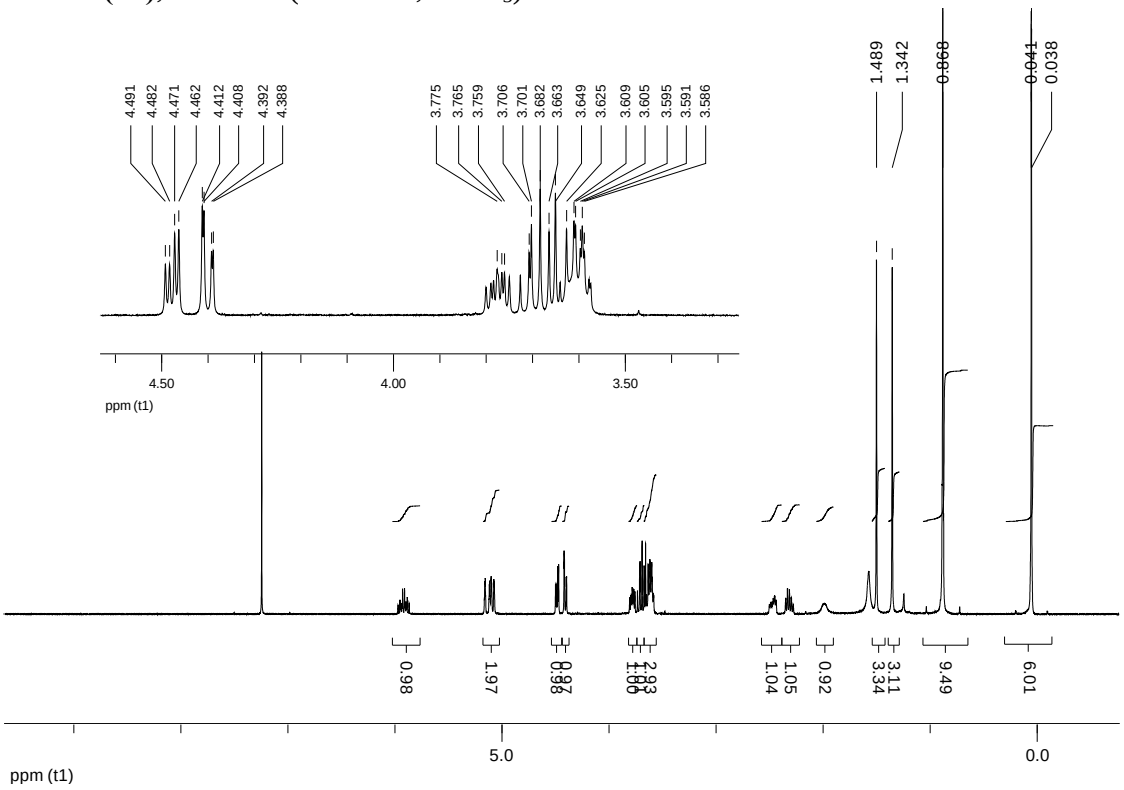

^{13}C NMR (101 MHz, $CDCl_3$)

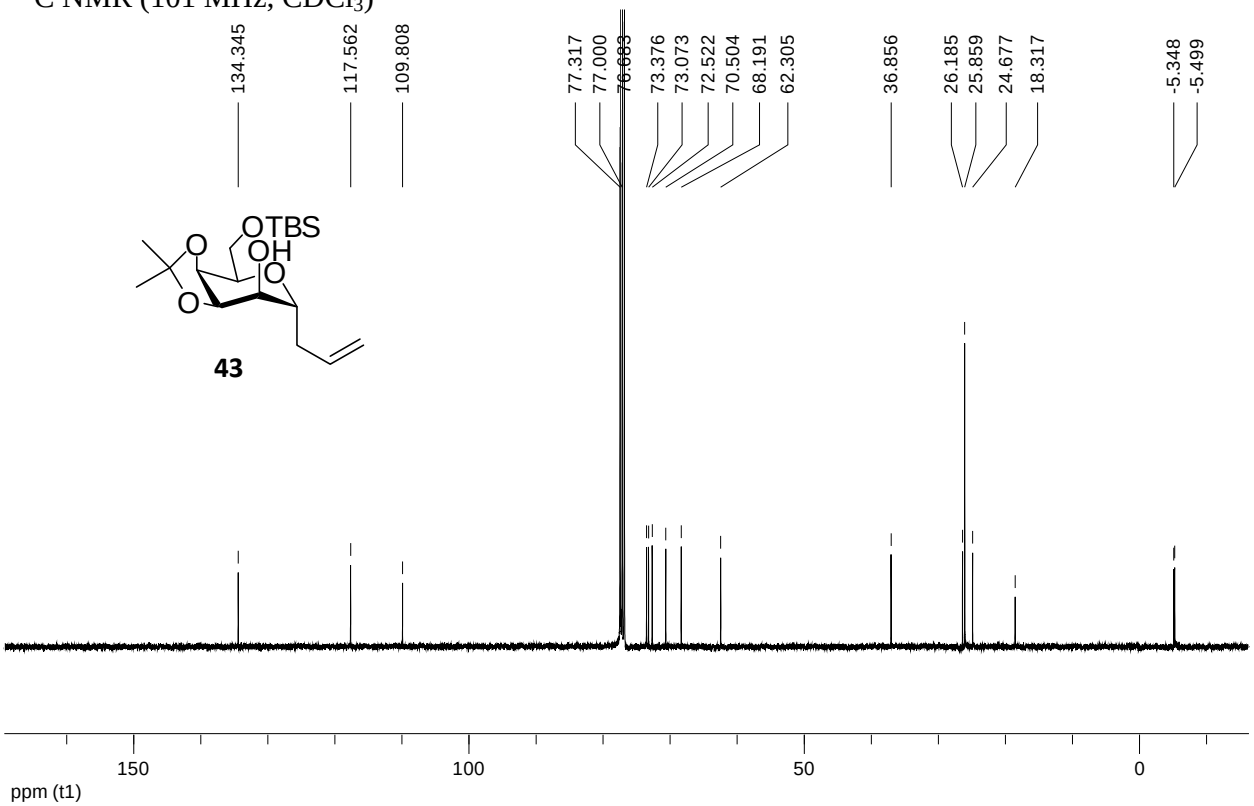

***Nα*-(S)-[(9H-fluoren-9-ylmethoxy)carbonyl]-*Nγ*-[2`-(2,3,4,6-tetra-*O*-acetyl-α-D-galactopyran-1-yl) ethan-1`-amido]-α,γ-diaminobutyric acid (44)**, ^{1}H NMR (500 MHz, CD_3OD)

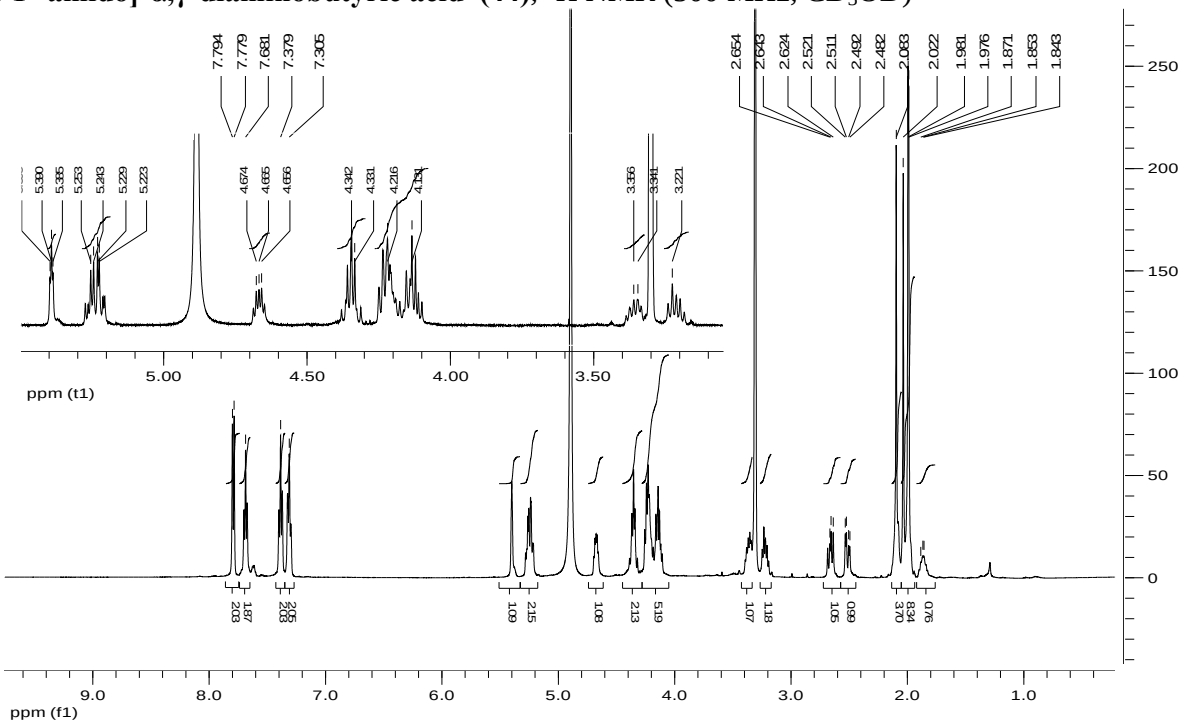

^{13}C NMR (101 MHz, $CDCl_3$)

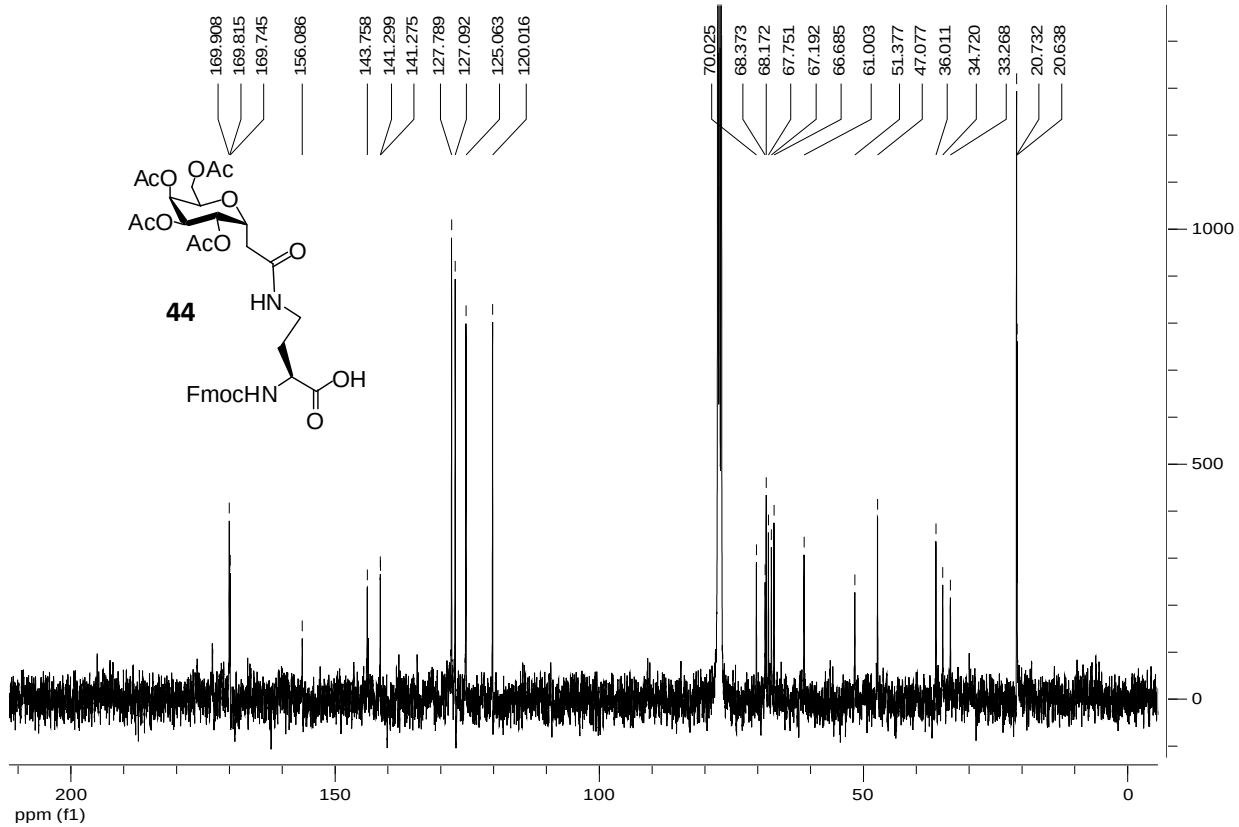

***Nα*-(S)-[(9H-fluoren-9-ylmethoxy)carbonyl]-*Nβ*-[2`-(2,3,4,6-tetra-*O*-acetyl-α-D-galactopyran-1-yl) ethan-1`-amido]-α,β-diaminopropanoic acid (45)**, ^{1}H NMR (500 MHz, CD_3OD)

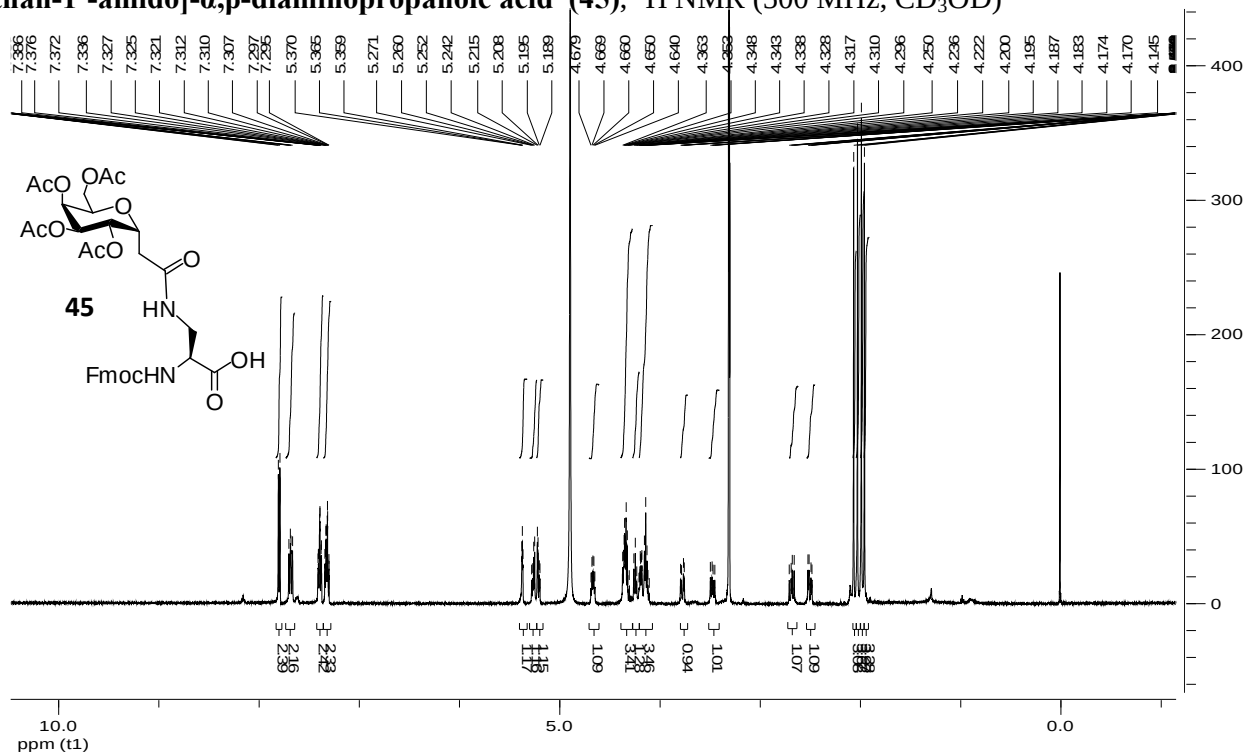

^{13}C NMR (101 MHz, $CDCl_3$)

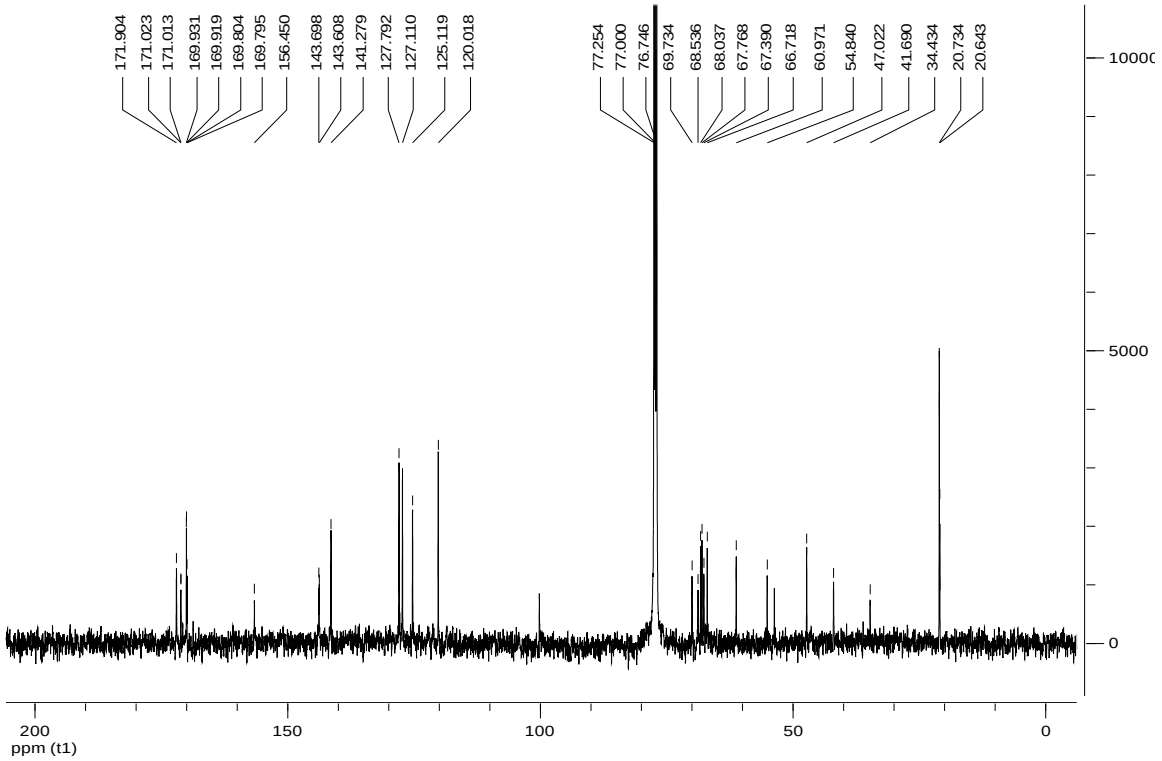

Benzyl-*Nα*-(S)-[(9H-fluoren-9-ylmethoxy)carbonyl]-α-γ-diaminobutanoate (46), ^{1}H NMR (500 MHz, CD_3OD)

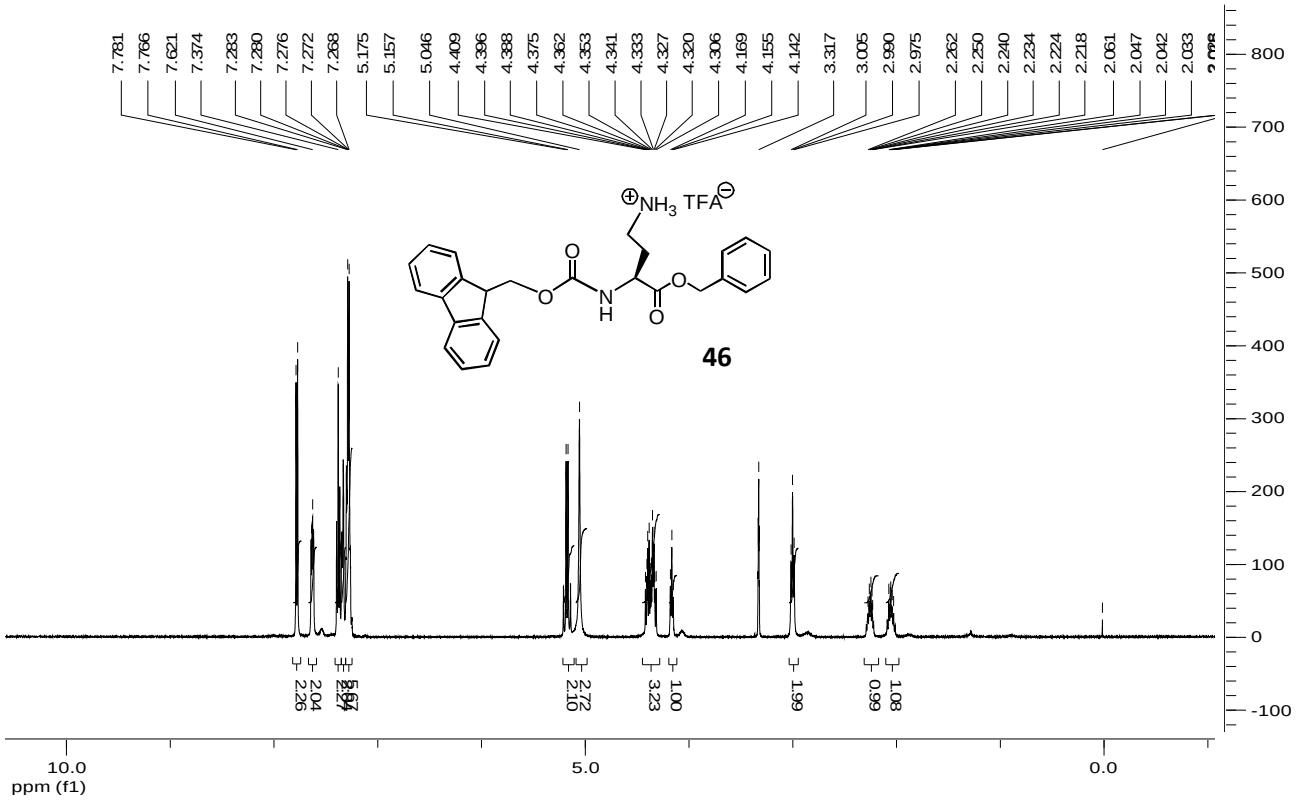

^{13}C NMR (101 MHz, CD_3OD)

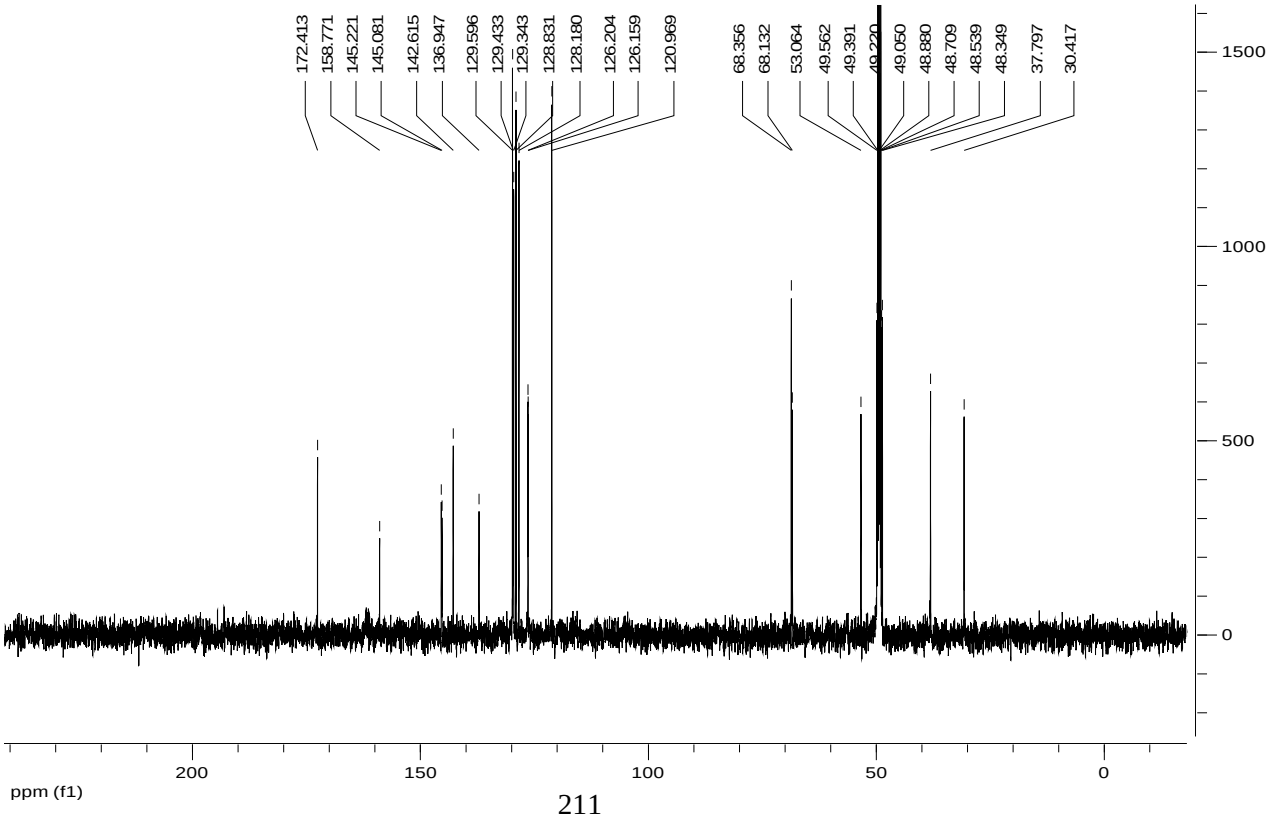

Benzyl-*Nα*-(S)-[(9H-fluoren-9-ylmethoxy)carbonyl]-α,β-diaminopropanoate (47),
^{1}H NMR (500 MHz, $CDCl_3$)

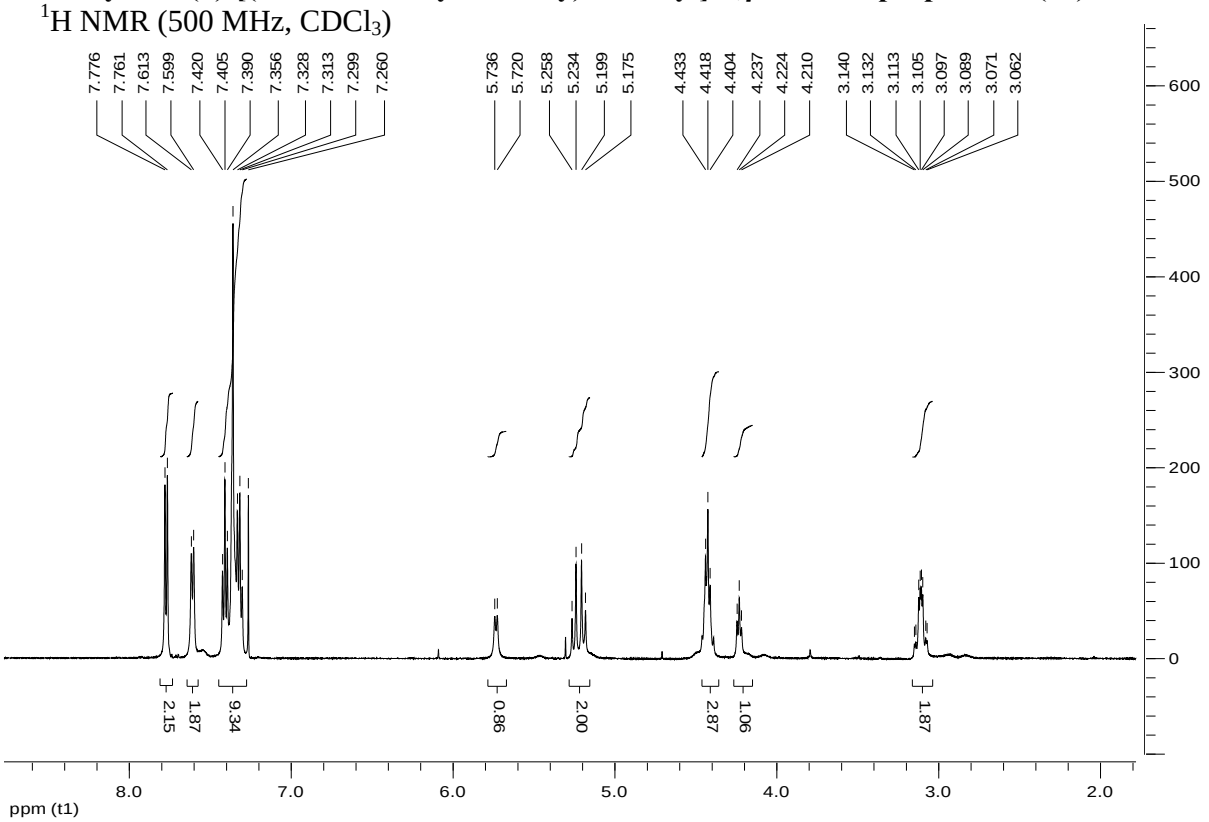

^{13}C NMR (126 MHz, $CDCl_3$)

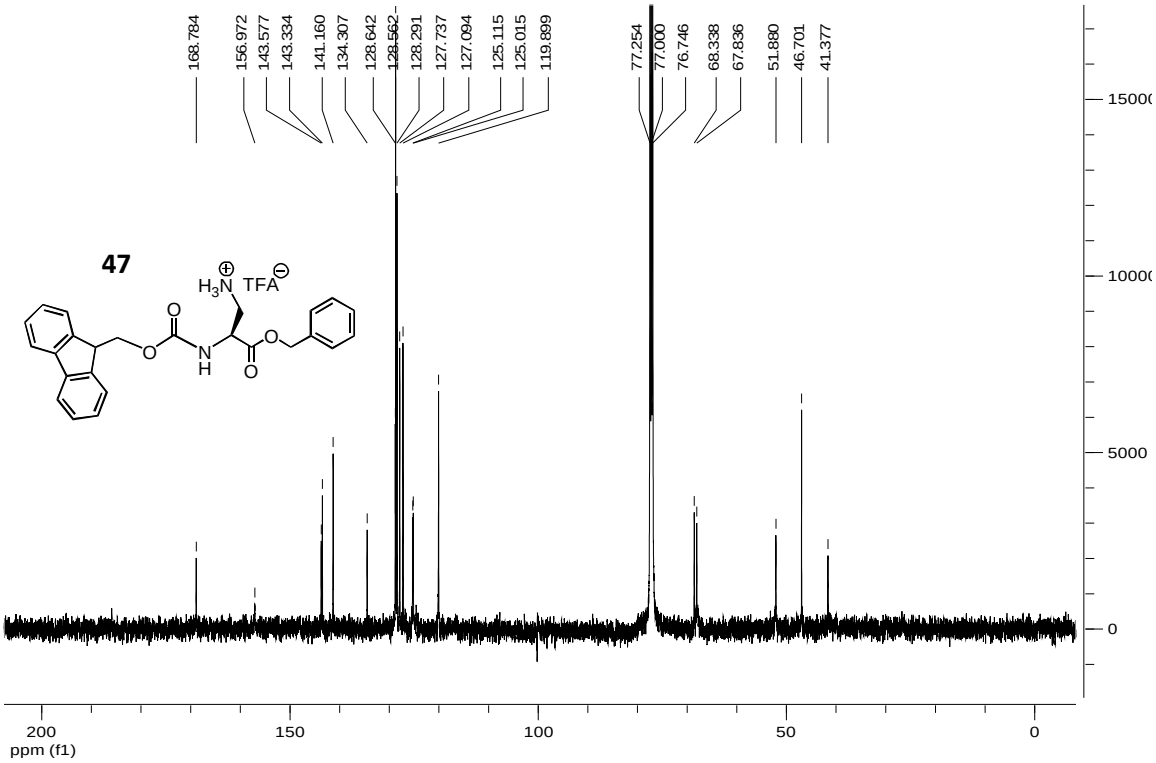

2`-(2,3,4,6-tetra-*O*-acetyl-α-D-galactopyran-1-yl)-ethan-1`-oic acid (48),

^{1}H NMR (400 MHz, $CDCl_3$)

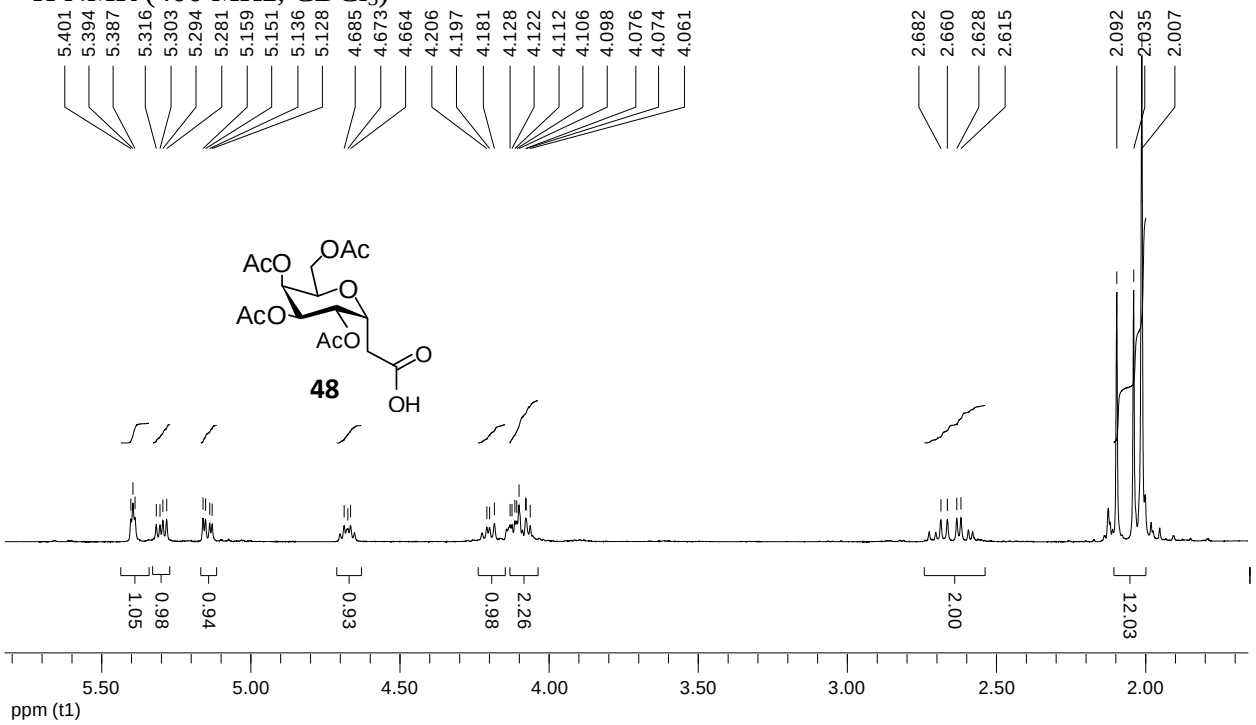

^{13}C NMR (101 MHz, $CDCl_3$)

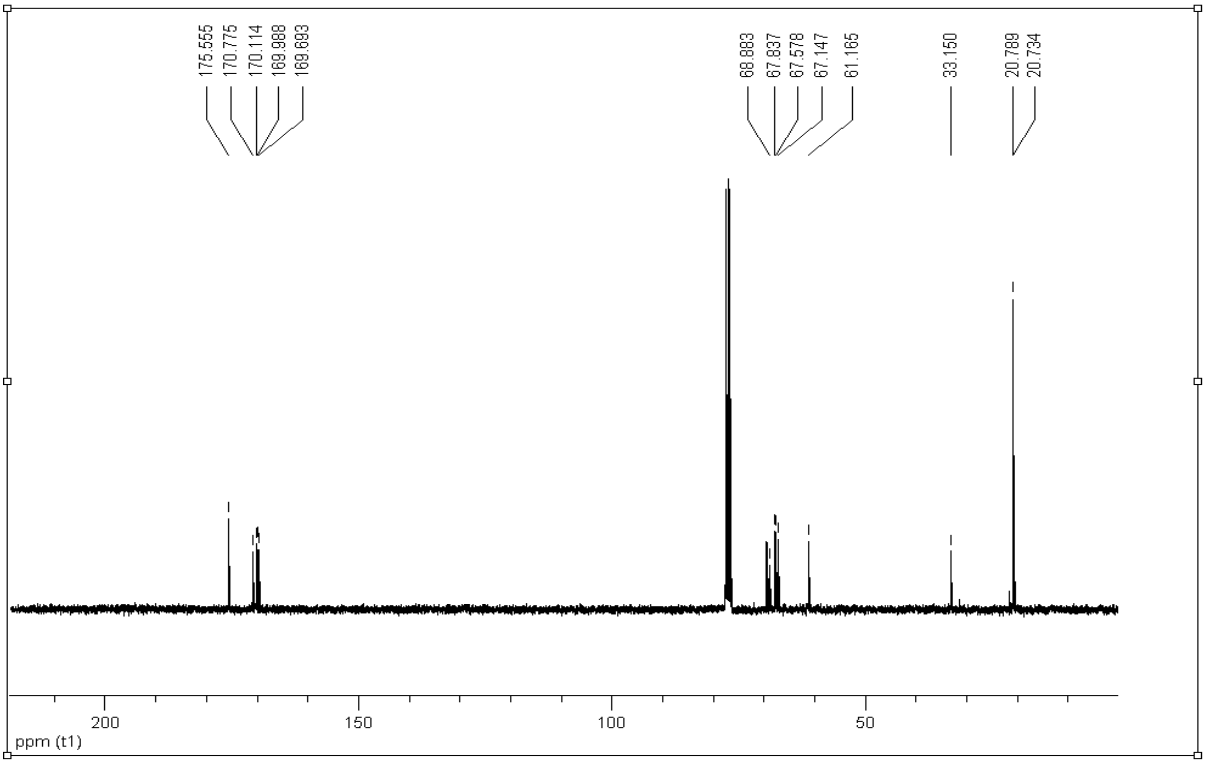

***Nα*-(S)-[(9H-fluoren-9-ylmethoxy)carbonyl]-*Nδ*-(triphenylmethyl)-glutamine benzyl ester (49a)** ^{1}H NMR (400 MHz, $CDCl_3$)

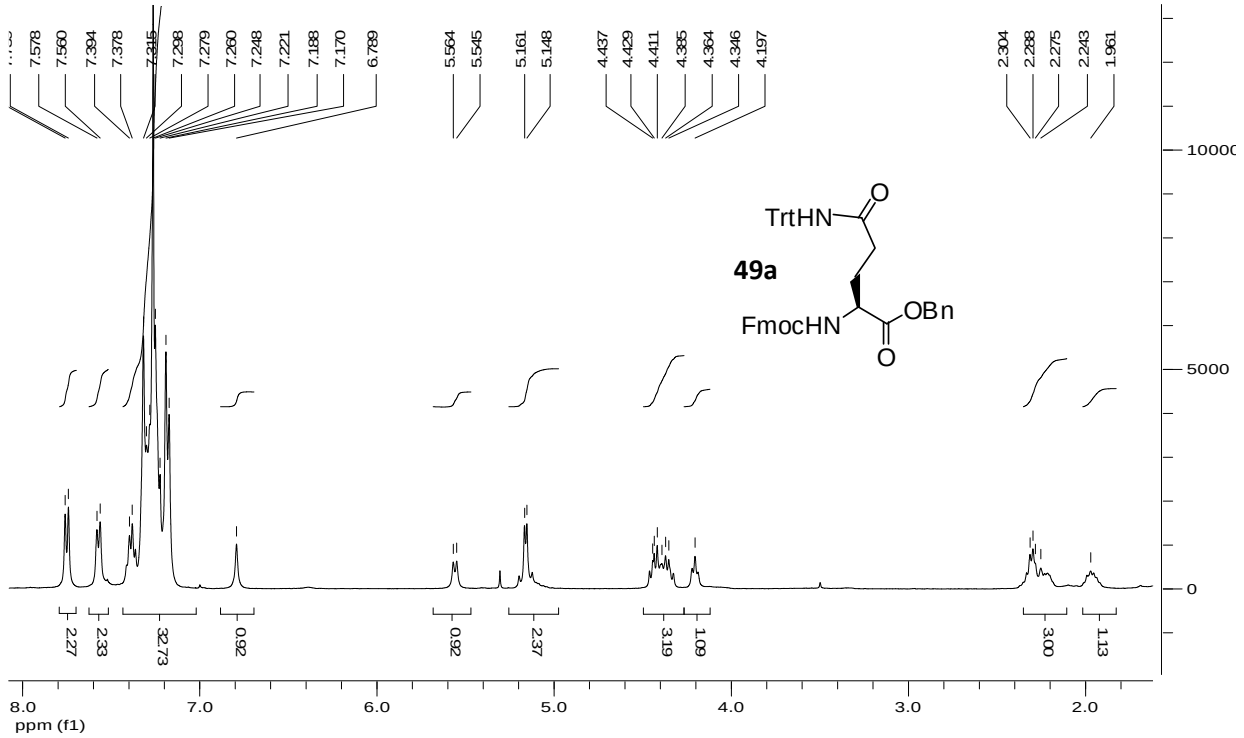

^{13}C NMR (101 MHz, $CDCl_3$)

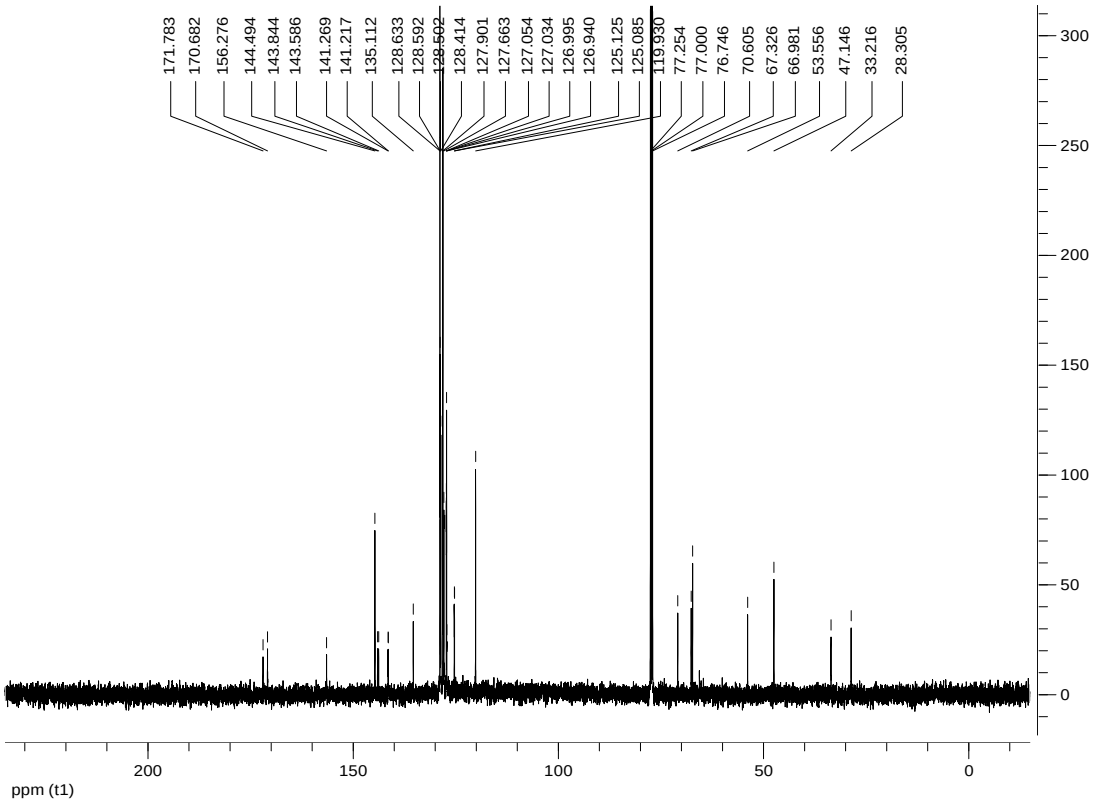

***Nα*-(S)-[(9H-fluoren-9-ylmethoxy)carbonyl]-*Nγ*-(triphenylmethyl)-asparagine benzyl ester (50a)**, ^{1}H NMR (400 MHz, $CDCl_3$)

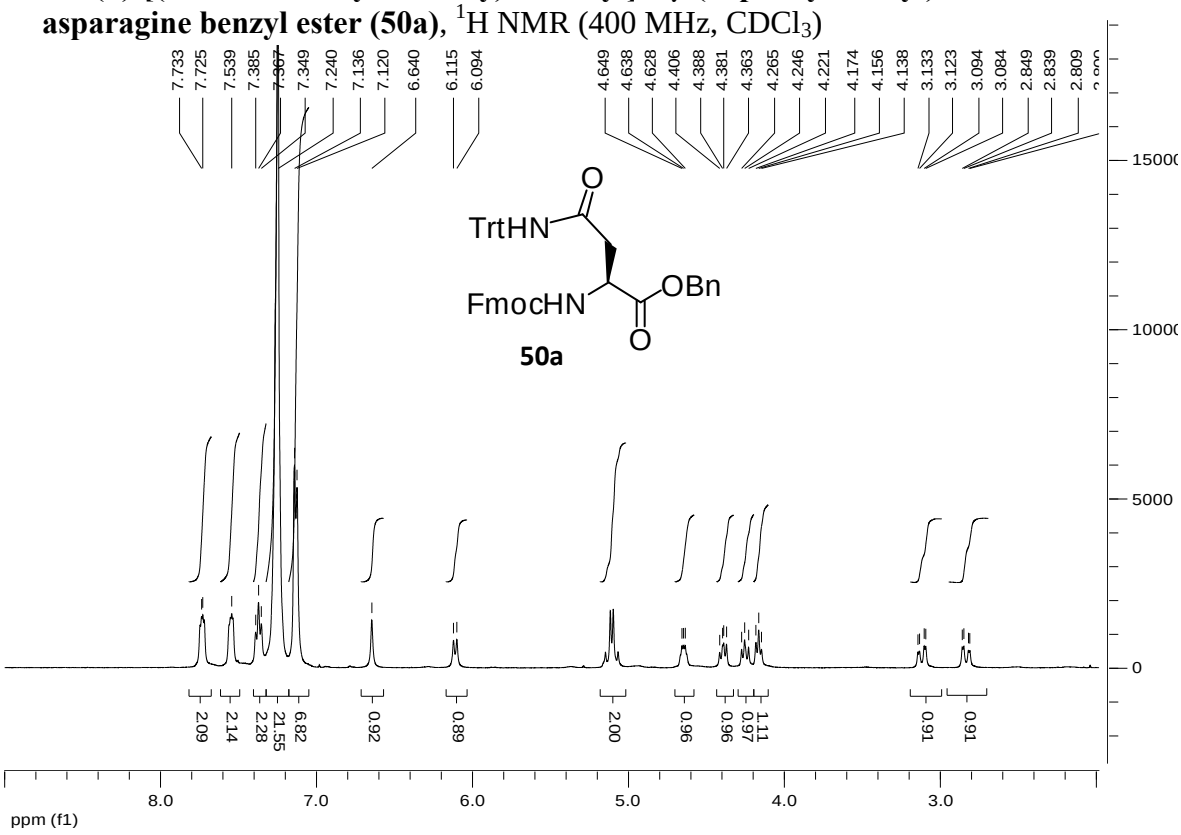

^{13}C NMR (101 MHz, $CDCl_3$)

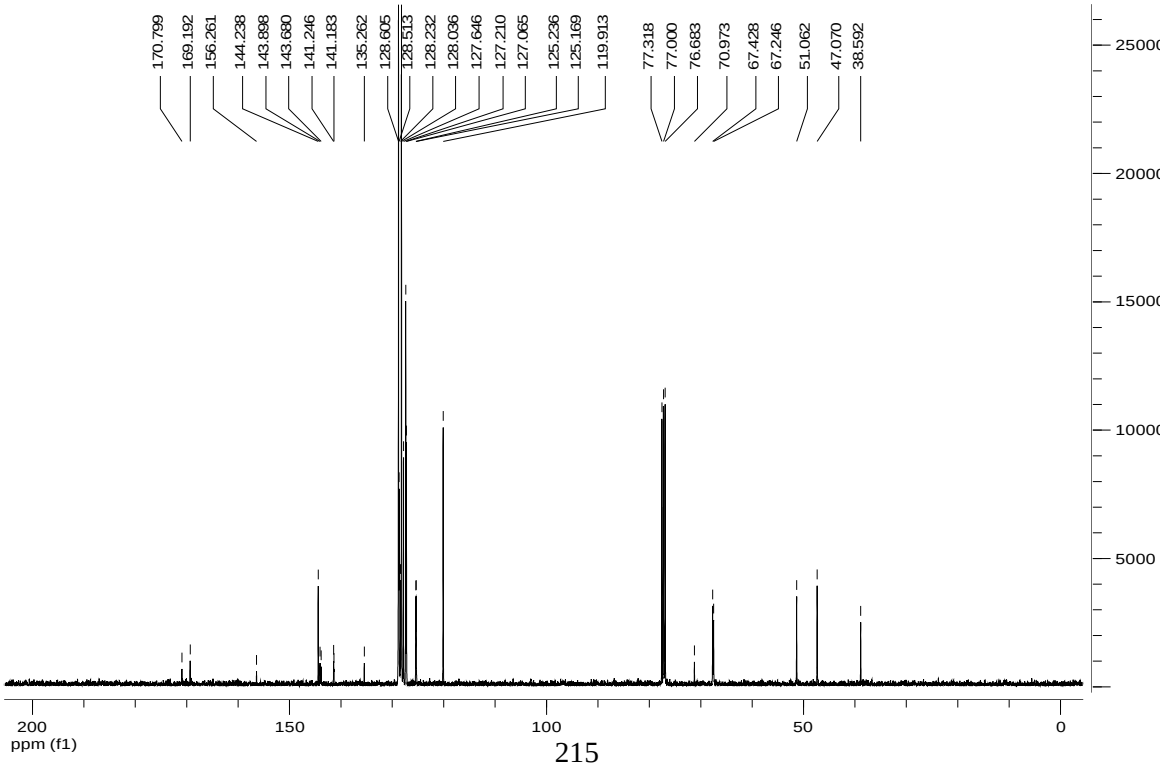

***Nα*-(S)-[(9H-fluoren-9-ylmethoxy)carbonyl]-glutamine benzyl ester (51)**,
^{1}H NMR (400 MHz, $CDCl_3$)

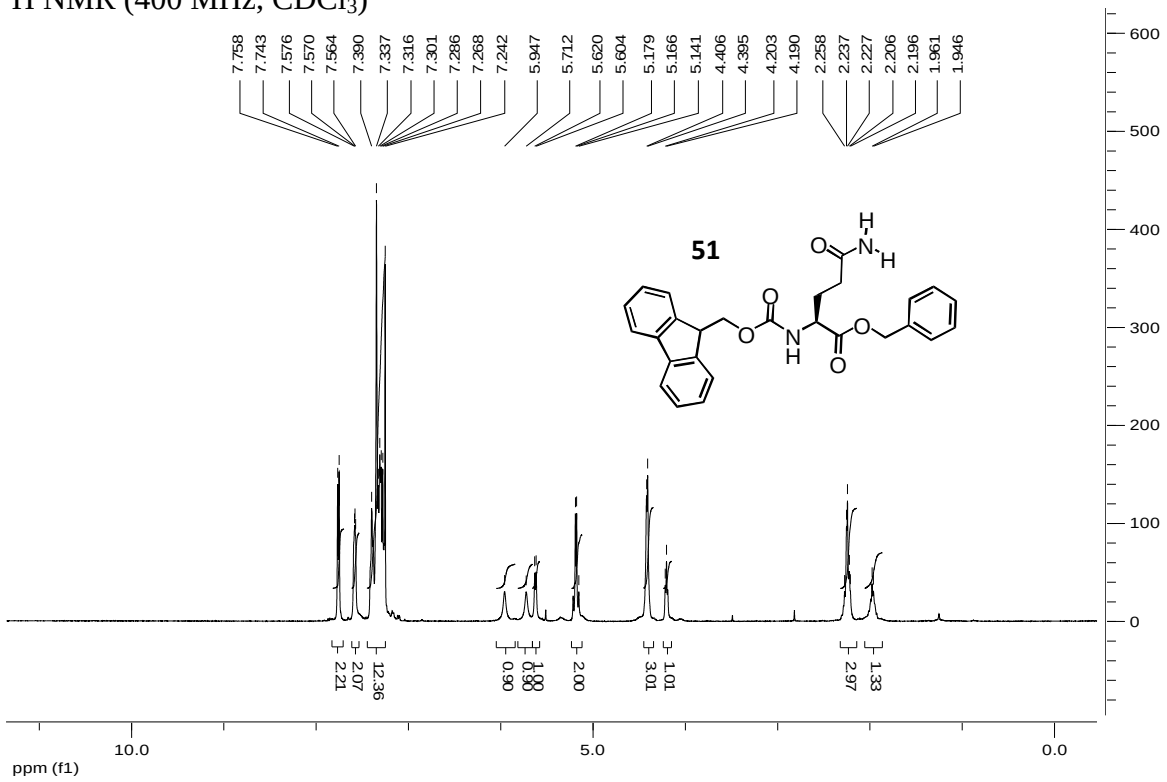

^{13}C NMR (101 MHz, $CDCl_3$)

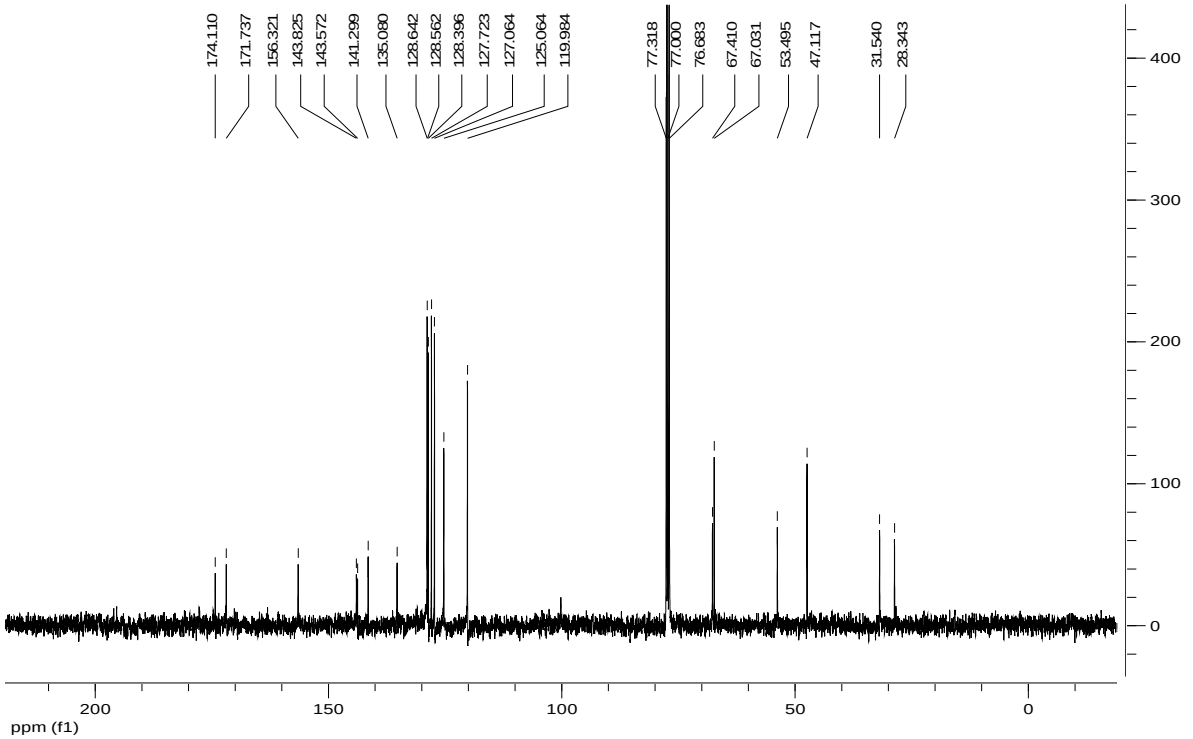

$N\alpha$-(S)-[(9H-fluoren-9-ylmethoxy)carbonyl]-asparagine benzyl ester (52),

^{1}H NMR (400 MHz, $CDCl_3$)

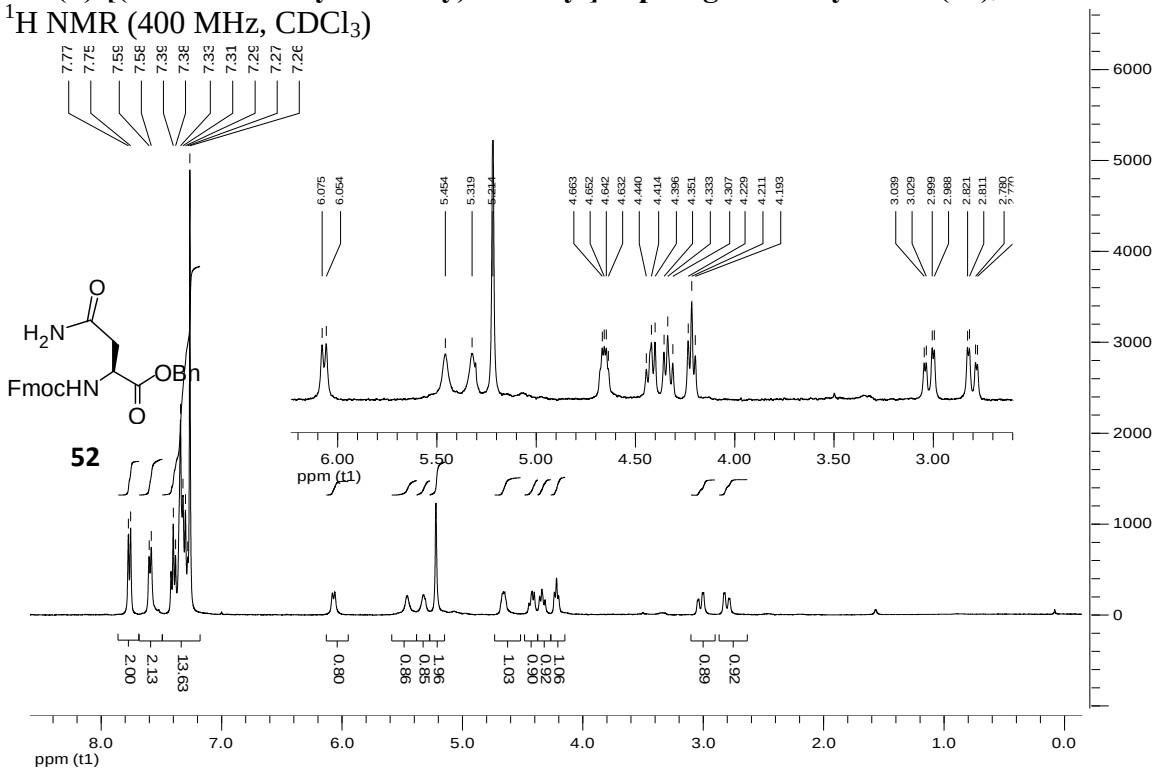

^{13}C NMR (101 MHz, $CDCl_3$)

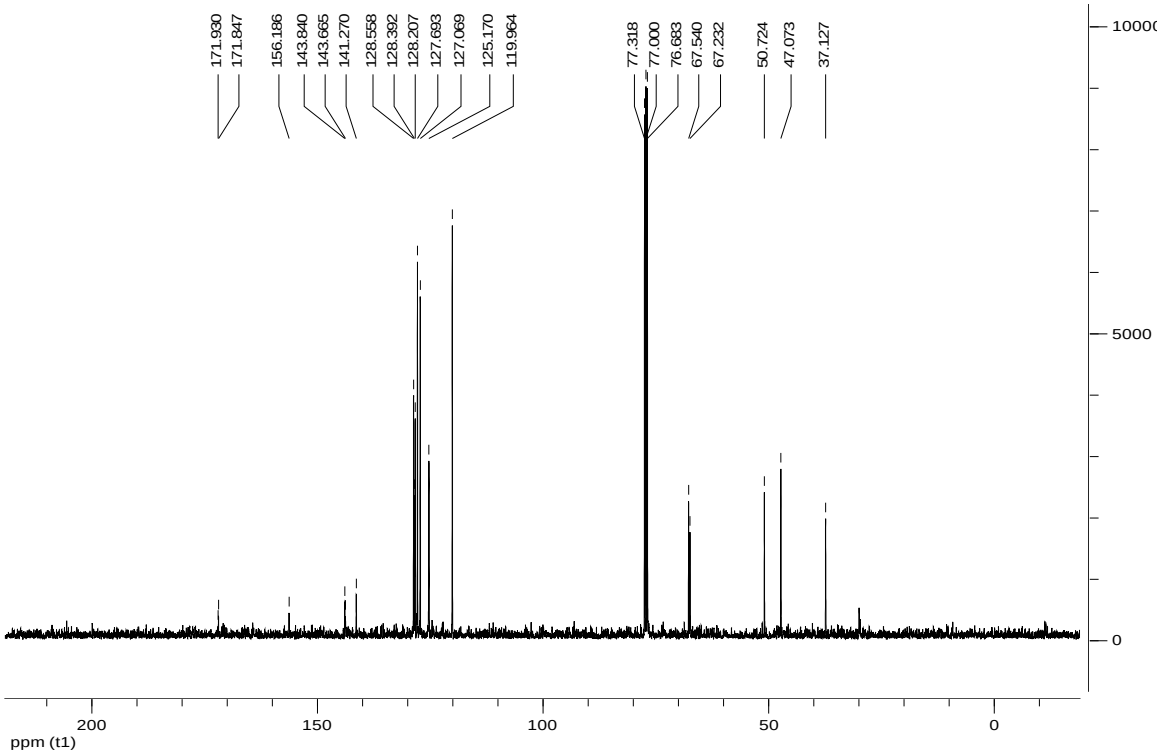

2`-(2,3,4,6-tetra-*O*-acetyl-α-D-galactopyran-1-yl)-ethan-1`-al (57),
^{1}H NMR (400 MHz, $CDCl_3$)

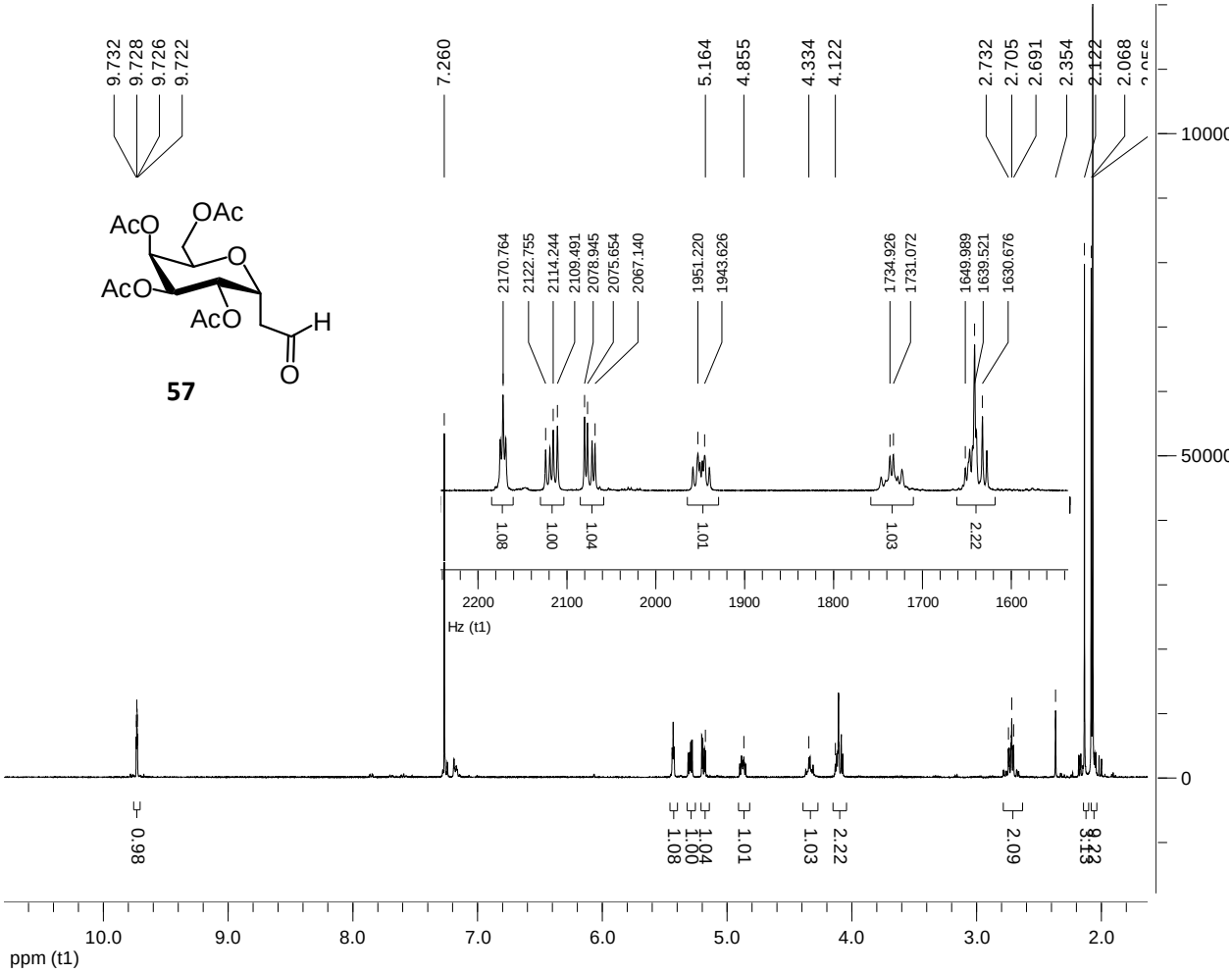

Benzyl-*Nα*-(S)-[(9H-fluoren-9-ylmethoxy)carbonyl]-*Nγ*-[2`-(2,3,4,6-tetra-*O*-acetyl-α-D-galactopyran-1-yl) ethan-1`-amido]-α,γ-diaminobutanoate (58),

^{1}H NMR (500 MHz, $CDCl_3$)

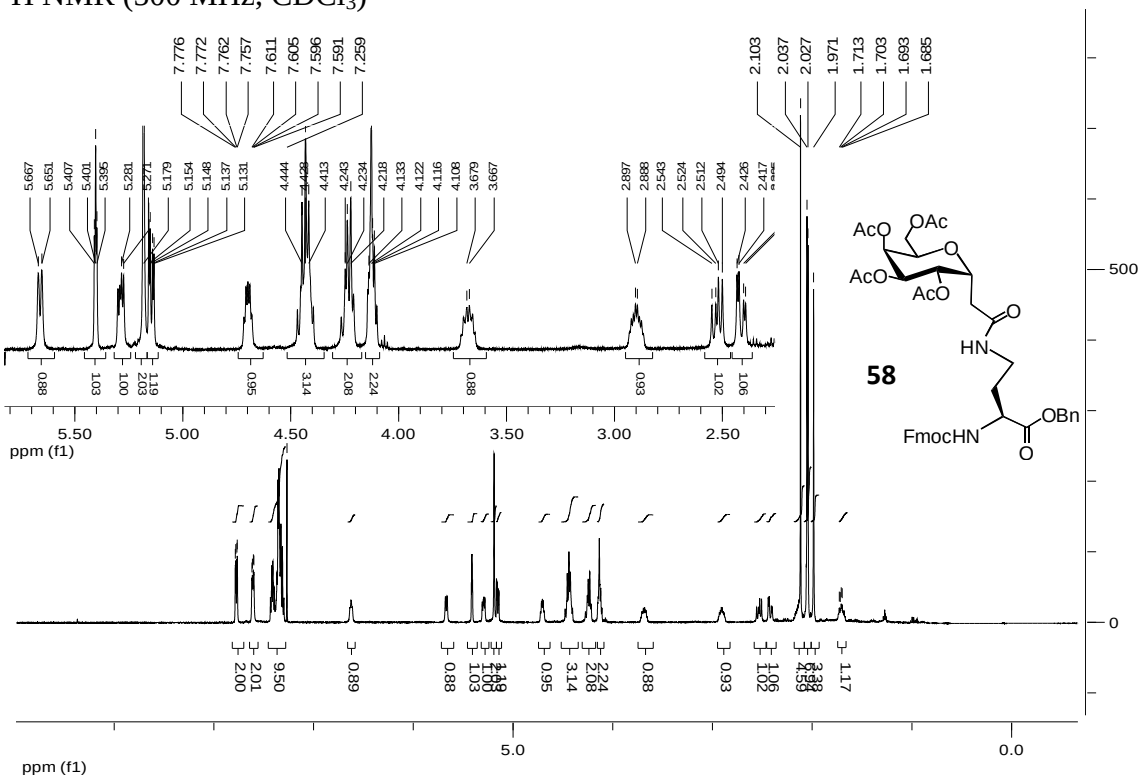

^{13}C NMR (101 MHz, $CDCl_3$)

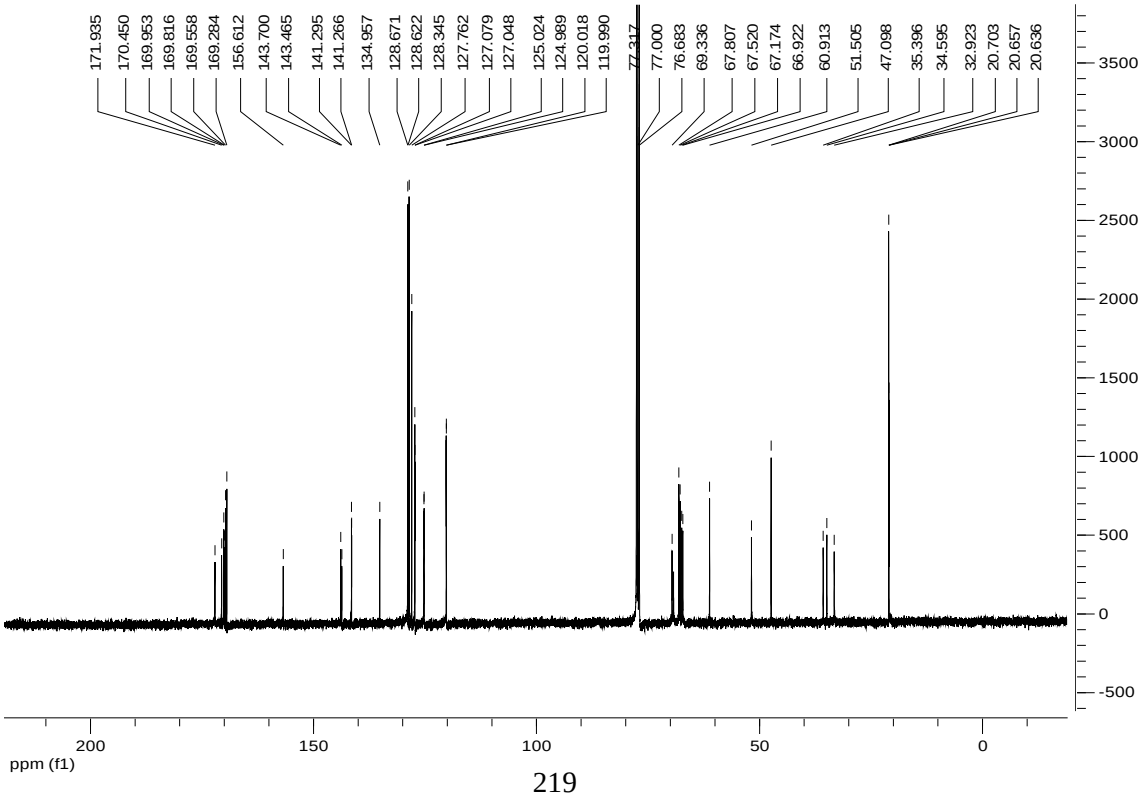

Benzyl-*Nα*-(S)-[(9H-fluoren-9-ylmethoxy)carbonyl]-*Nγ*-[2`-(2,3,4,6-tetra-*O*-acetyl-α-D-galactopyran-1-yl) ethan-1`-amido]-α,β-diaminopropanoate (59),

^{1}H NMR (500 MHz, $CDCl_3$)

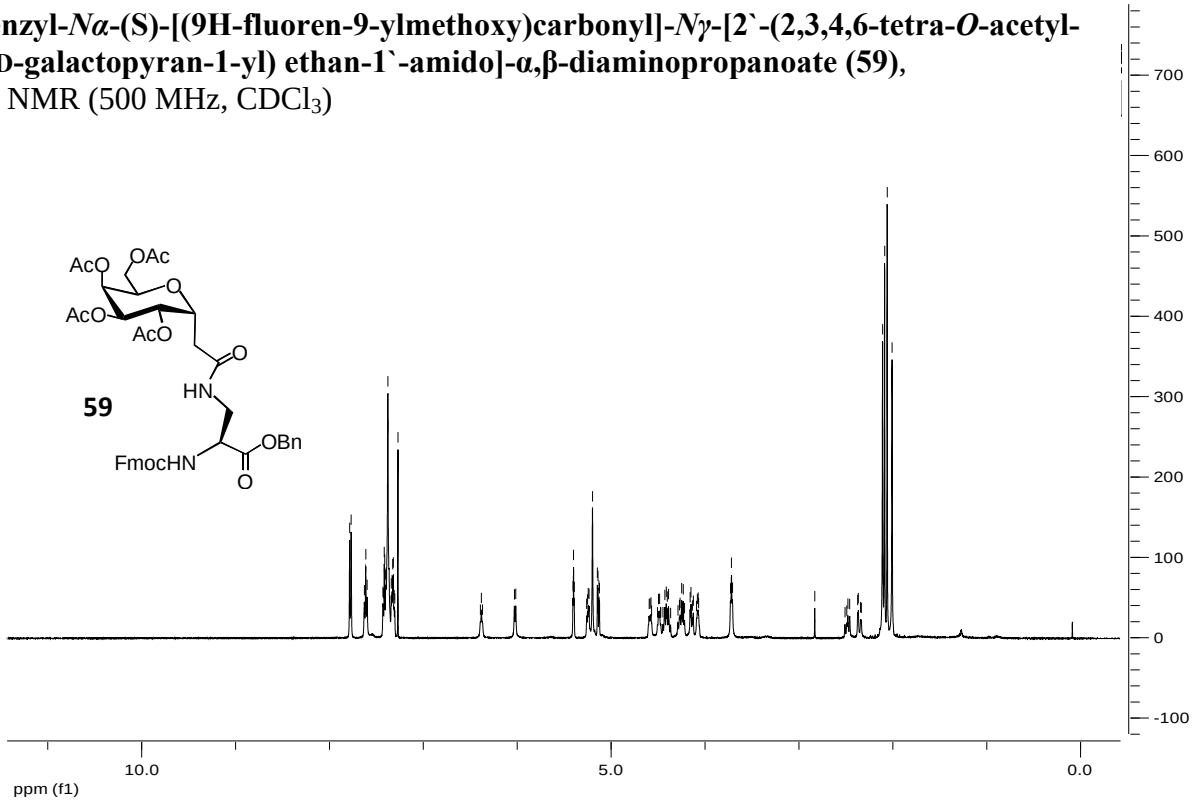

^{13}C NMR (101 MHz, $CDCl_3$)

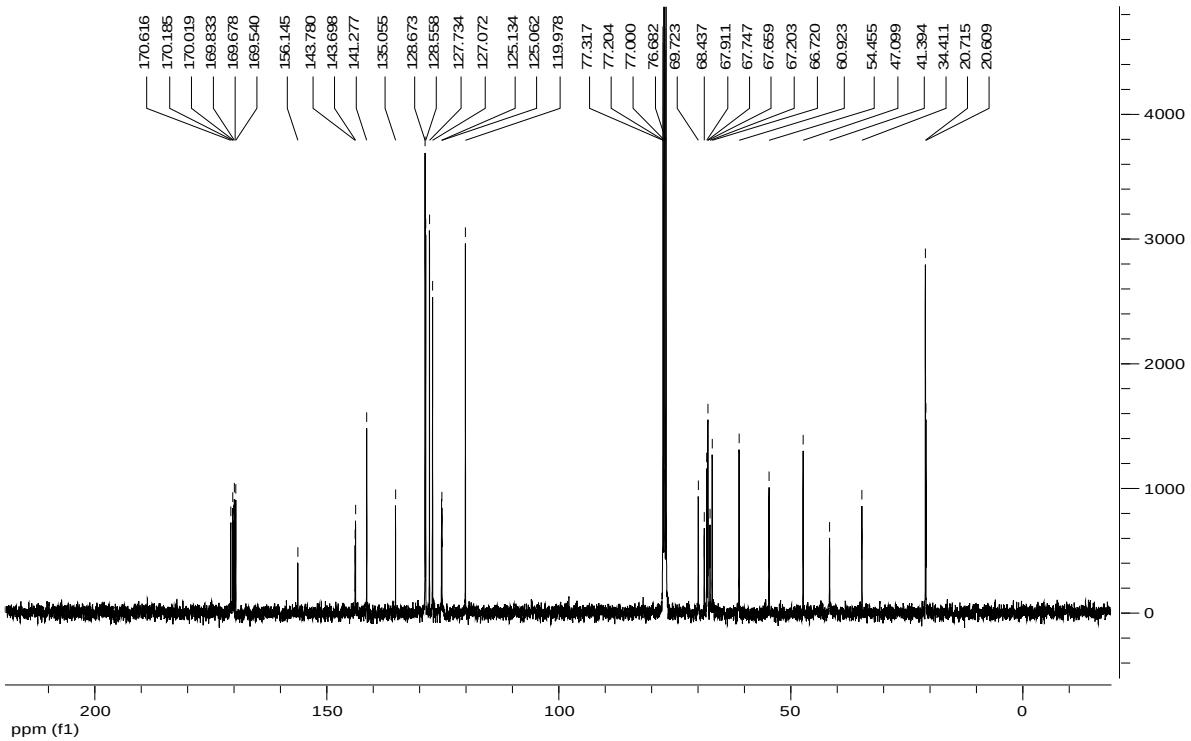

***N*-acetyl-glycinamido-[(S)-*Nβ*-[2`-(α-D-galactopyran-1-yl)-ethan-1`-amido]-α,β-diaminopropanoic-1-amido]-glycine (60)**,

^{1}H NMR (500 MHz, 95:5 H_2O:D_2O)

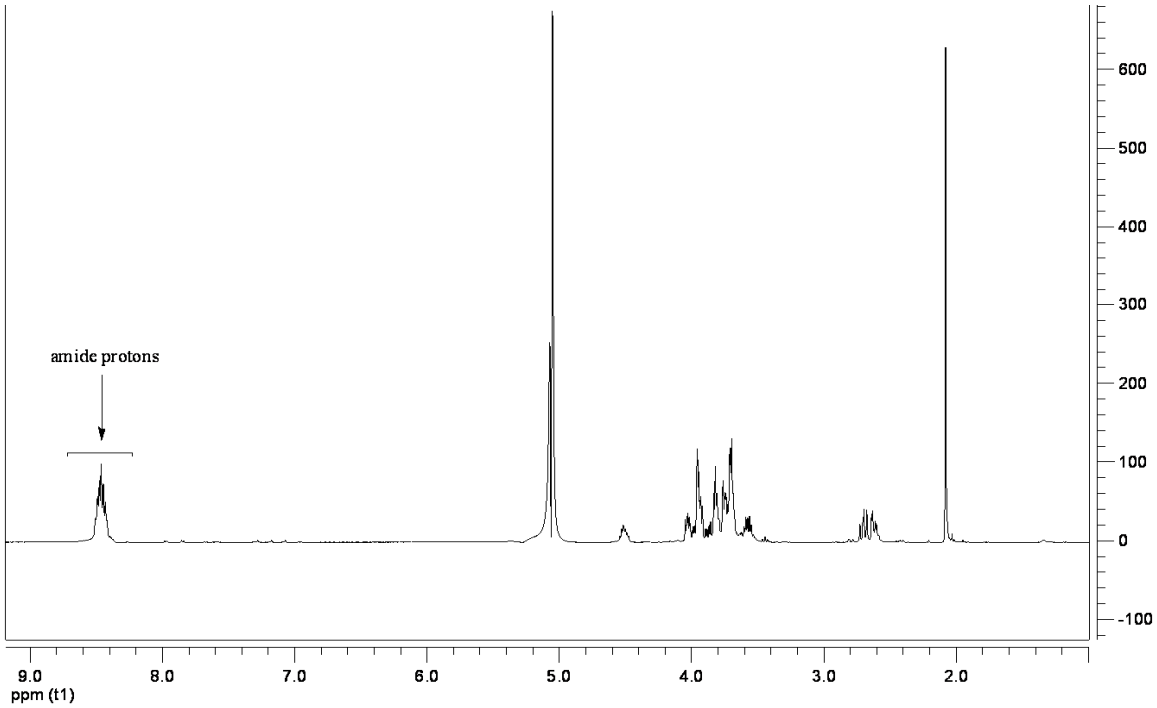

^{13}C NMR (101 MHz, 95:5 H_2O:D_2O)

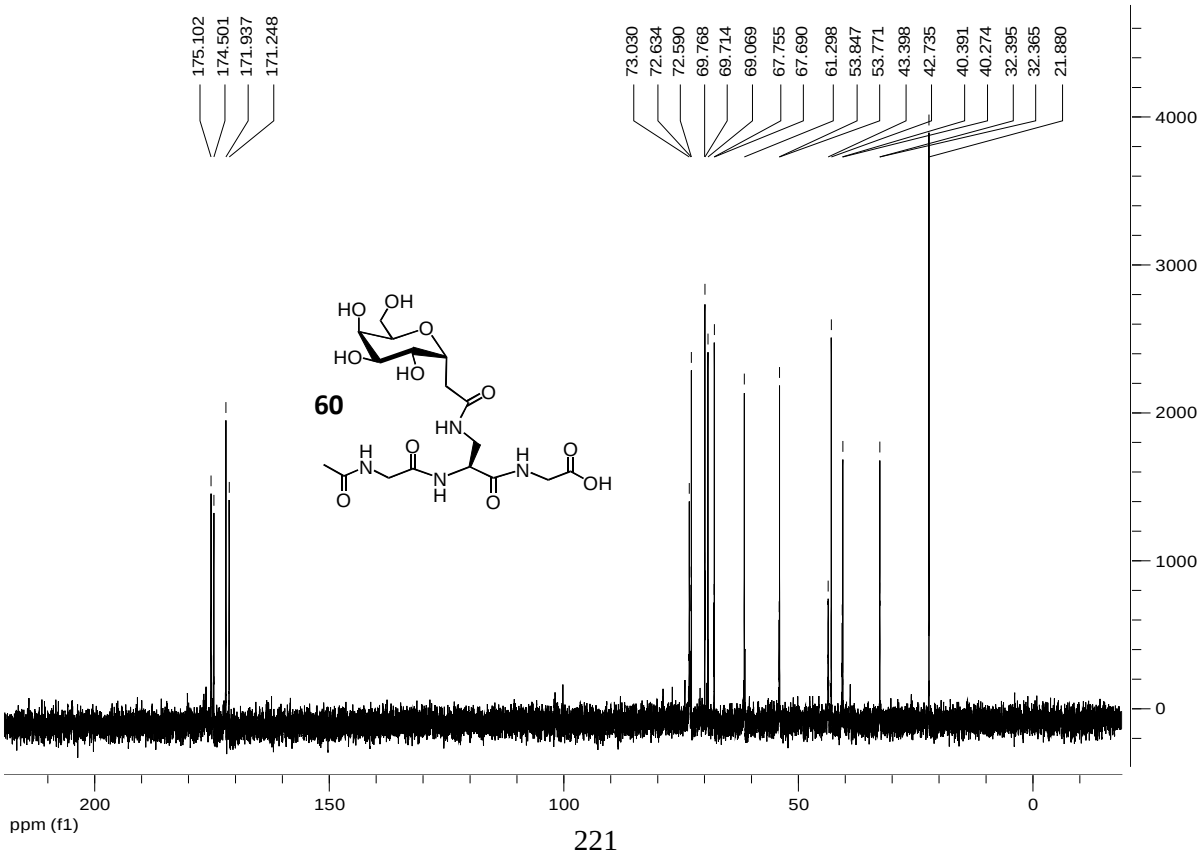

***N*-acetyl-glycinamido-[(S)-*Nγ*-[2`-(α-D-galactopyran-1-yl)-ethan-1`-amido]-α,γ-diaminobutyric-1-amido]-glycine (61),**

^{1}H NMR (500 MHz, 95:5 H_2O:D_2O)

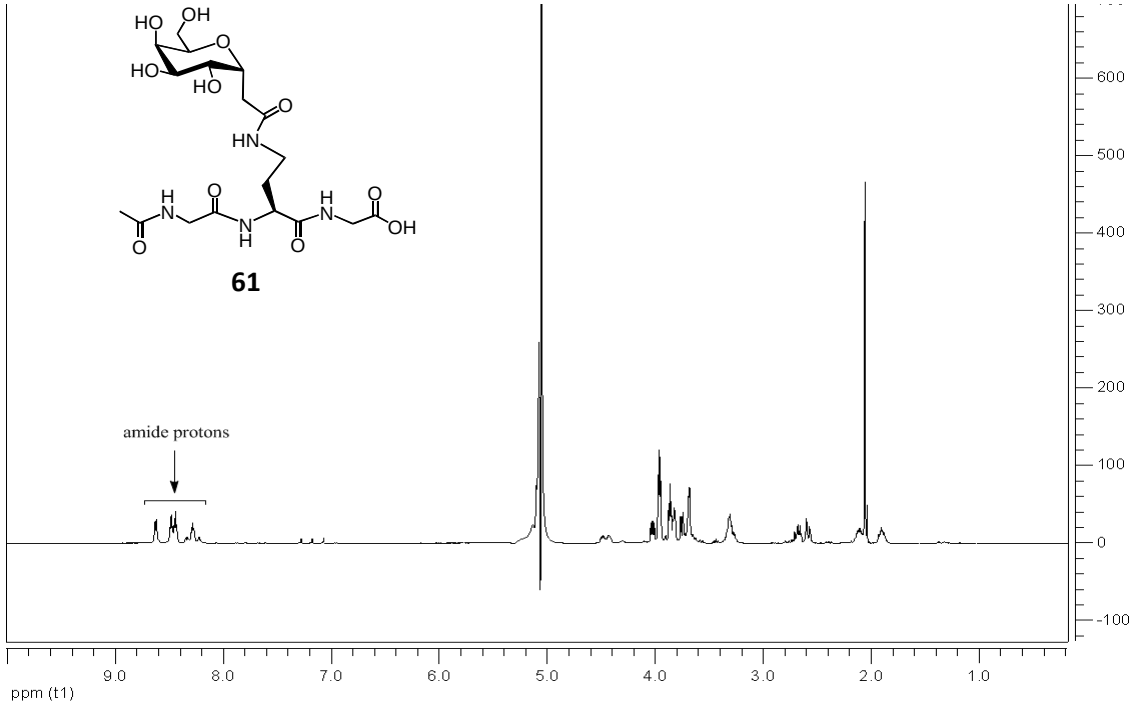

^{13}C NMR (101 MHz, 95:5 H_2O:D_2O)

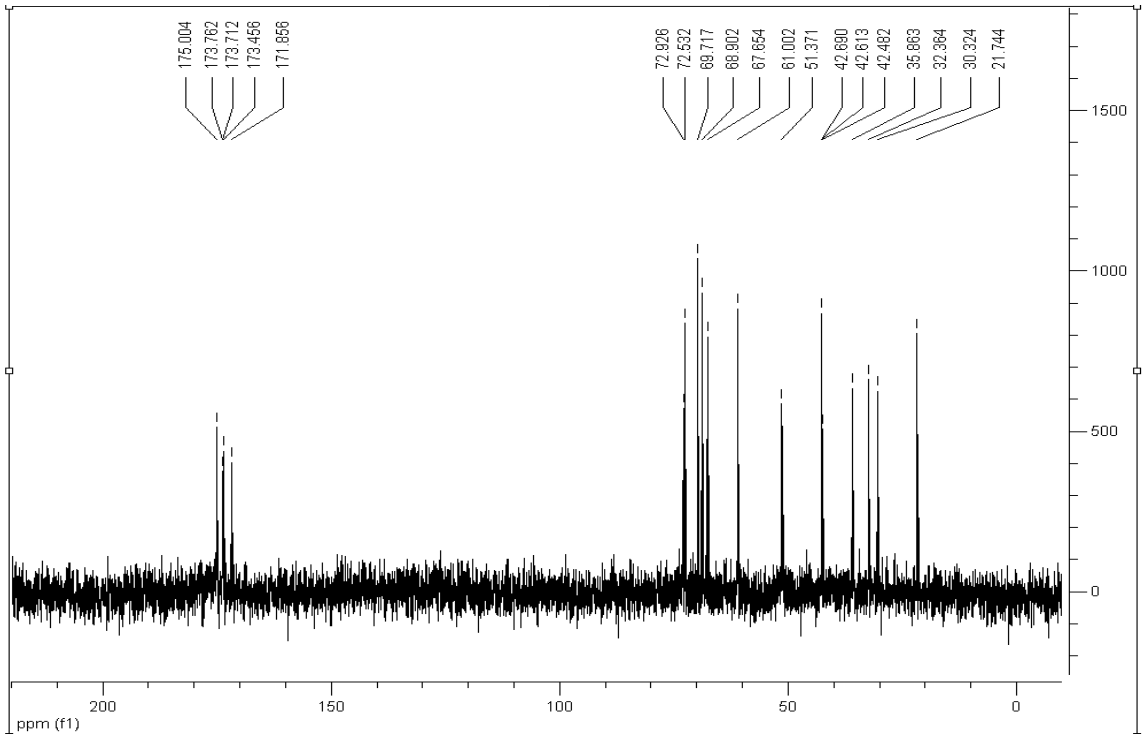

***N*-acetyl-glycinamido-[(S)-*Nδ*-[2`-(α-D-galactopyran-1-yl)-ethan-1`-amido]-ornithinamido-glycine (62)**,

^{1}H NMR (500 MHz, 95:5 H_2O:D_2O)

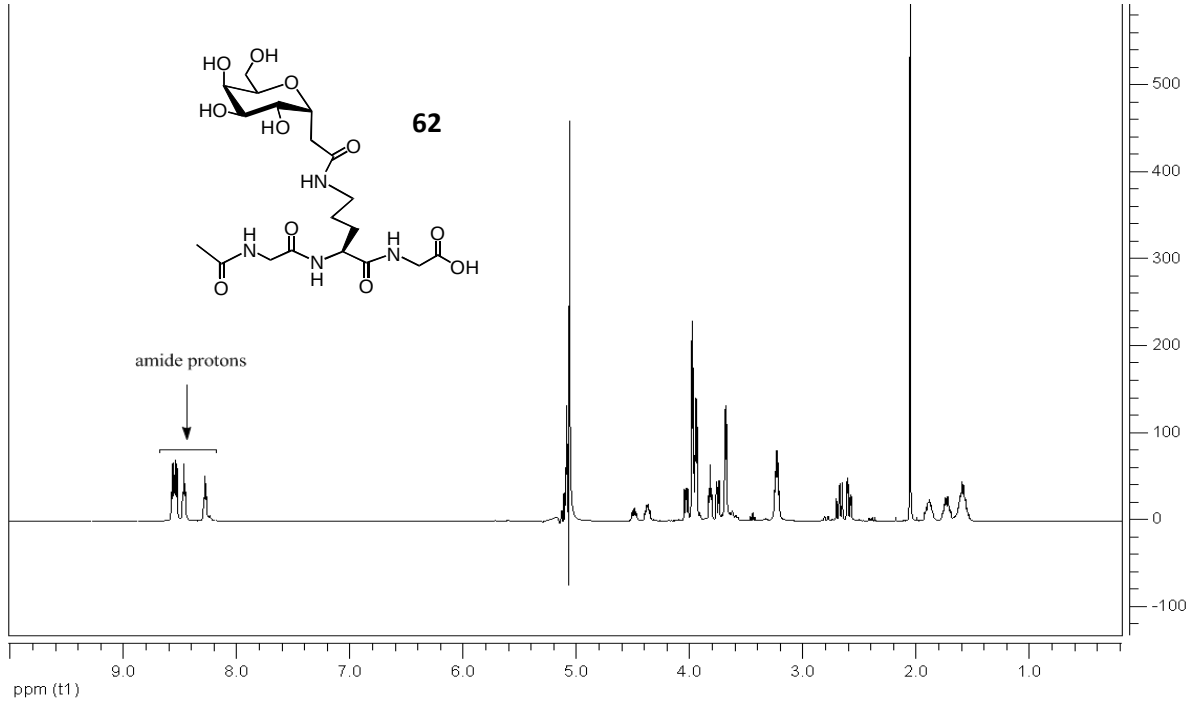

^{13}C NMR (101 MHz, 95:5 H_2O:D_2O)

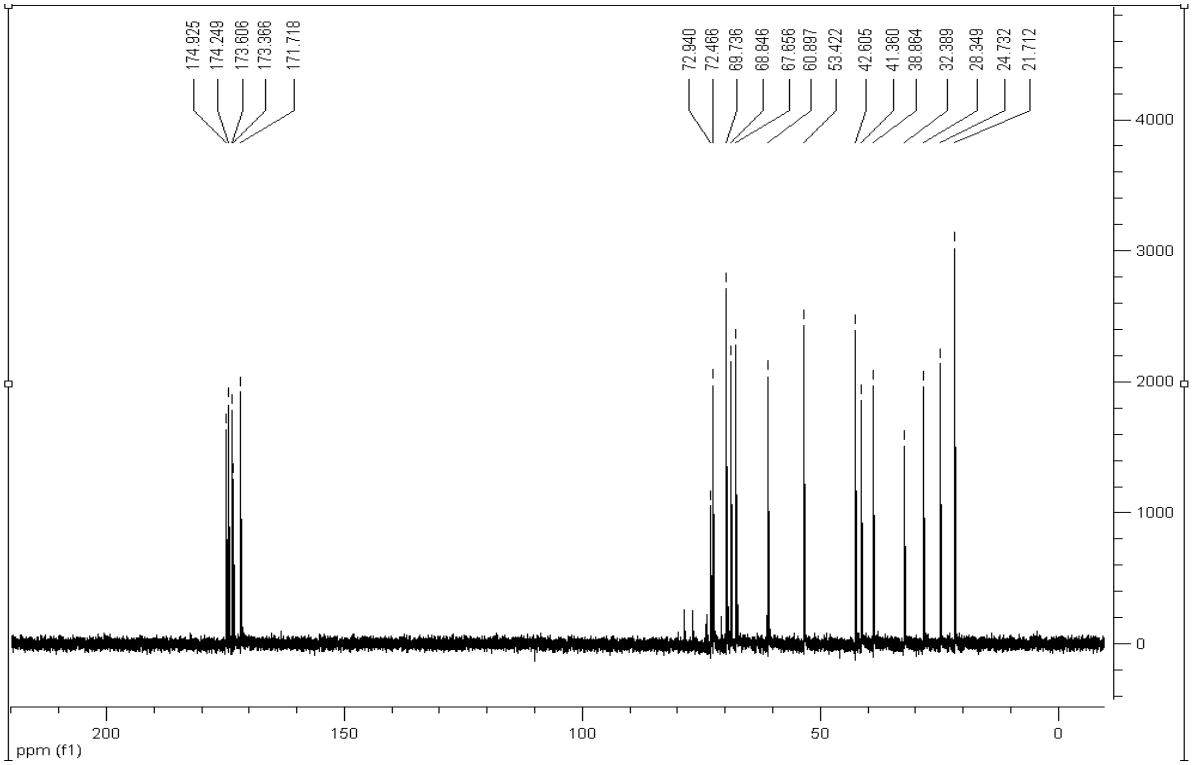

***Nα*-(S)-[(9H-fluoren-9-ylmethoxy)carbonyl]-*Nγ*-[3`-(2,3,4,6-tetra-*O*-acetyl-α-D-galactopyran-1-yl) propan-1`-amido]-α,γ-diaminobutyric acid (66)**,
^{1}H NMR (500 MHz, $CDCl_3$)

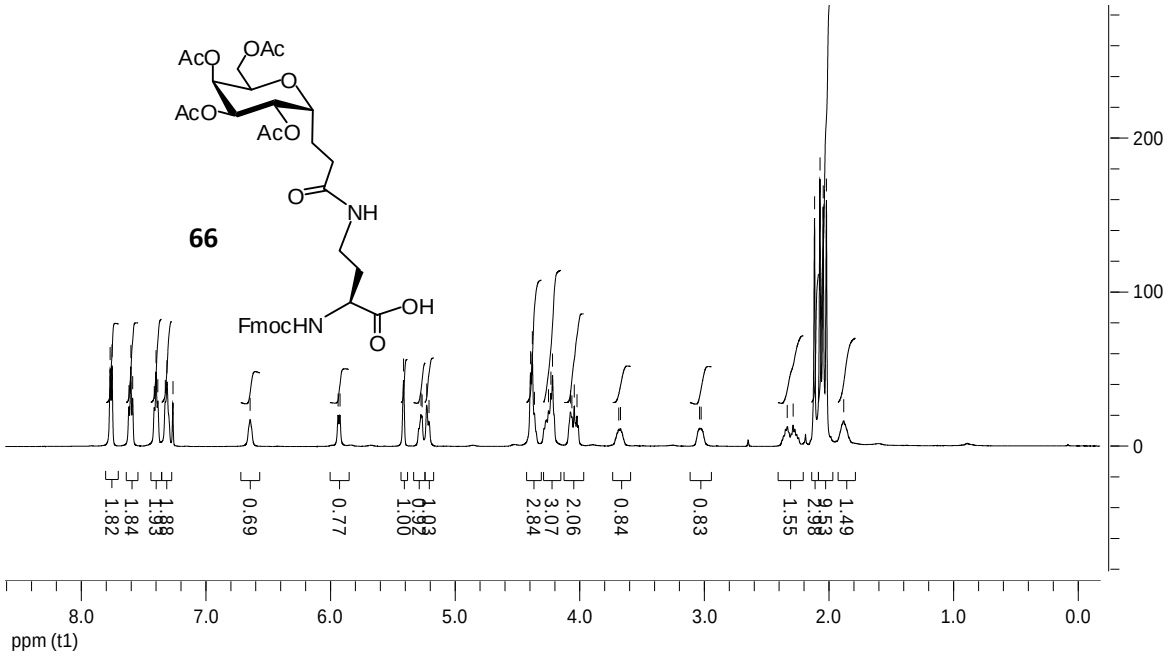

^{1}H NMR (500 MHz, CD_3OD)

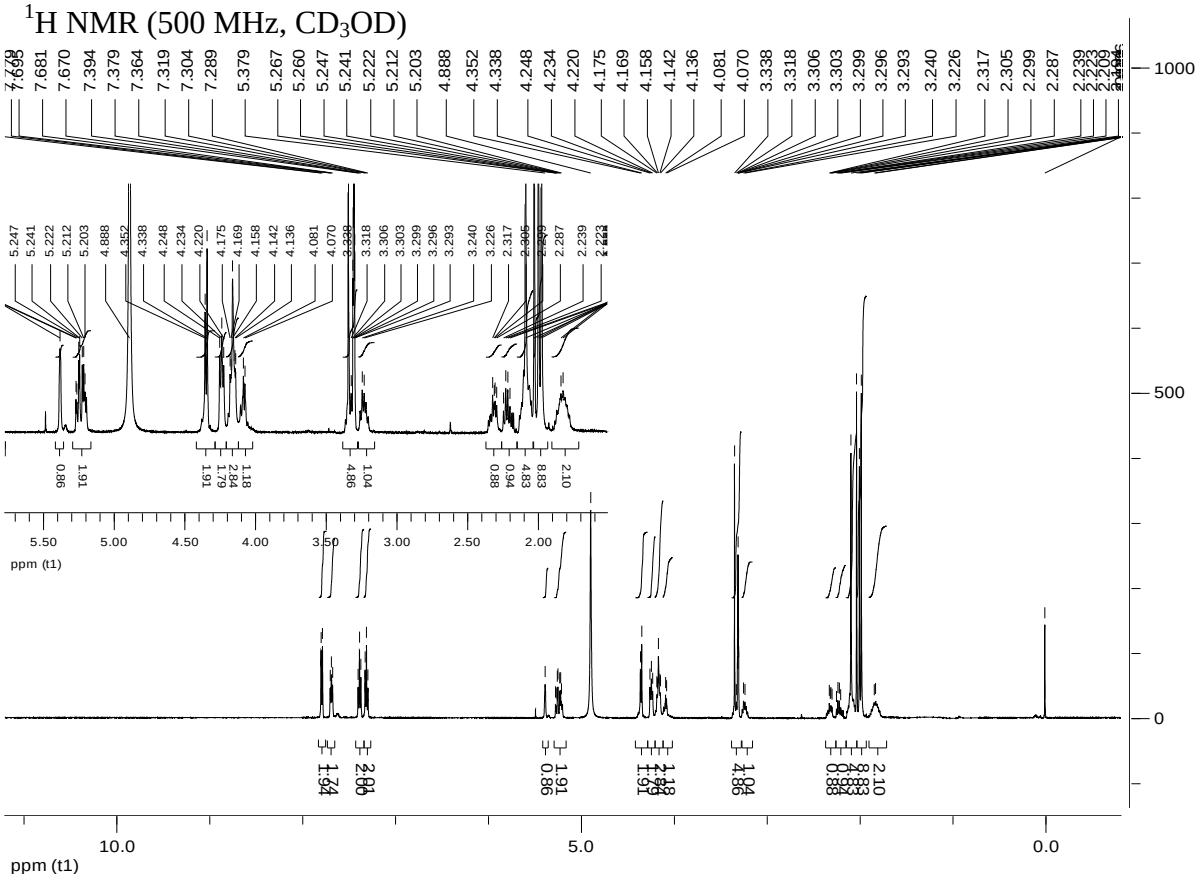

***Nα*-(S)-[(9H-fluoren-9-ylmethoxy)carbonyl]-*Nγ*-[3`-(2,3,4,6-tetra-*O*-acetyl-α-D-galactopyran-1-yl) propan-1`-amido]-α,γ-diaminobutyric acid (66)**,
^{13}C –DEPTQ135 NMR (101 MHz, $CDCl_3$)

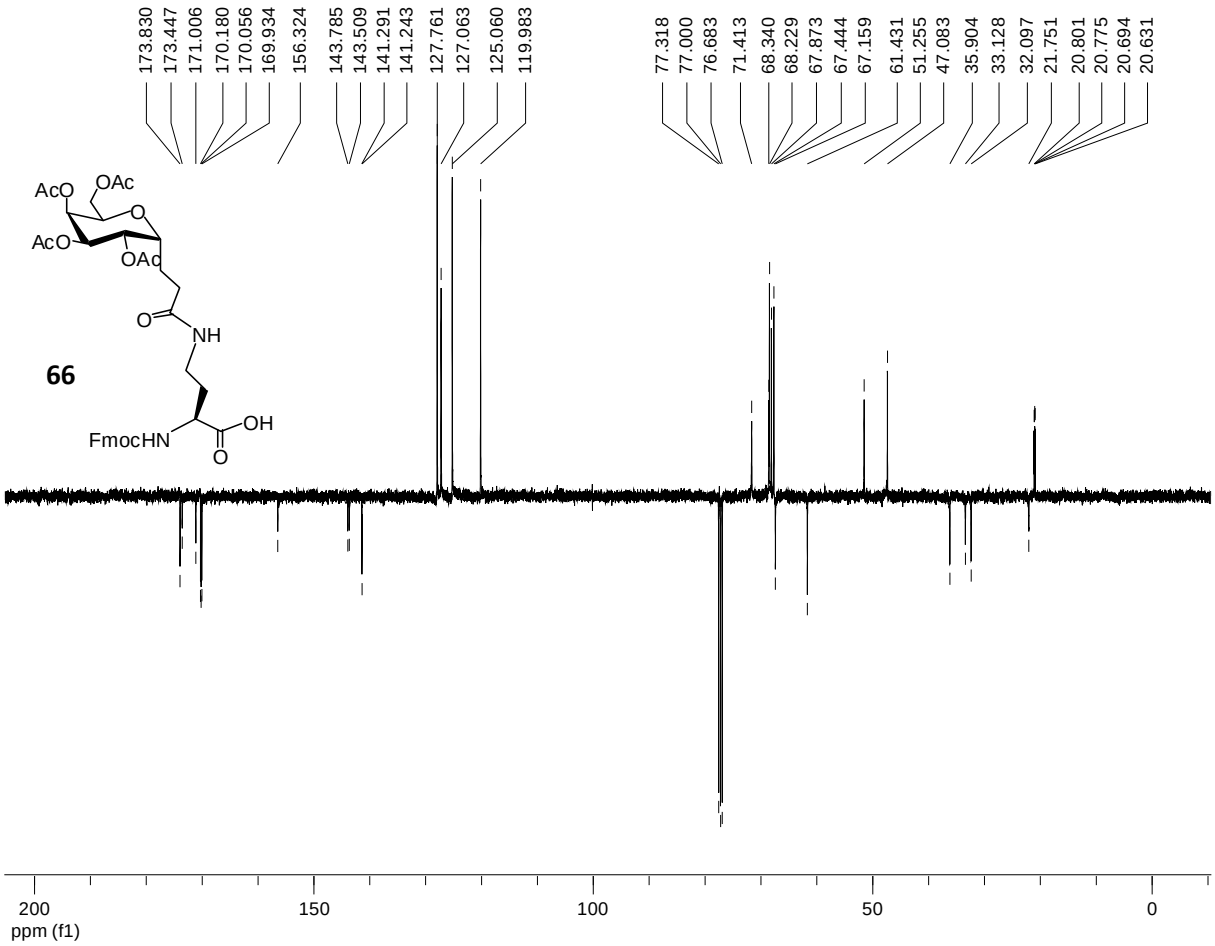

***Nα*-(S)-[(9H-fluoren-9-ylmethoxy)carbonyl]-*Nβ*-[2`-(2,3,4,6-tetra-*O*-*tert*-butyldimethylsilyl-α-D-galactopyran-1-yl) butan-1`-amido]-α,β-diaminopropanoic acid (67)**,

^{1}H NMR (500 MHz, CD_3OD)

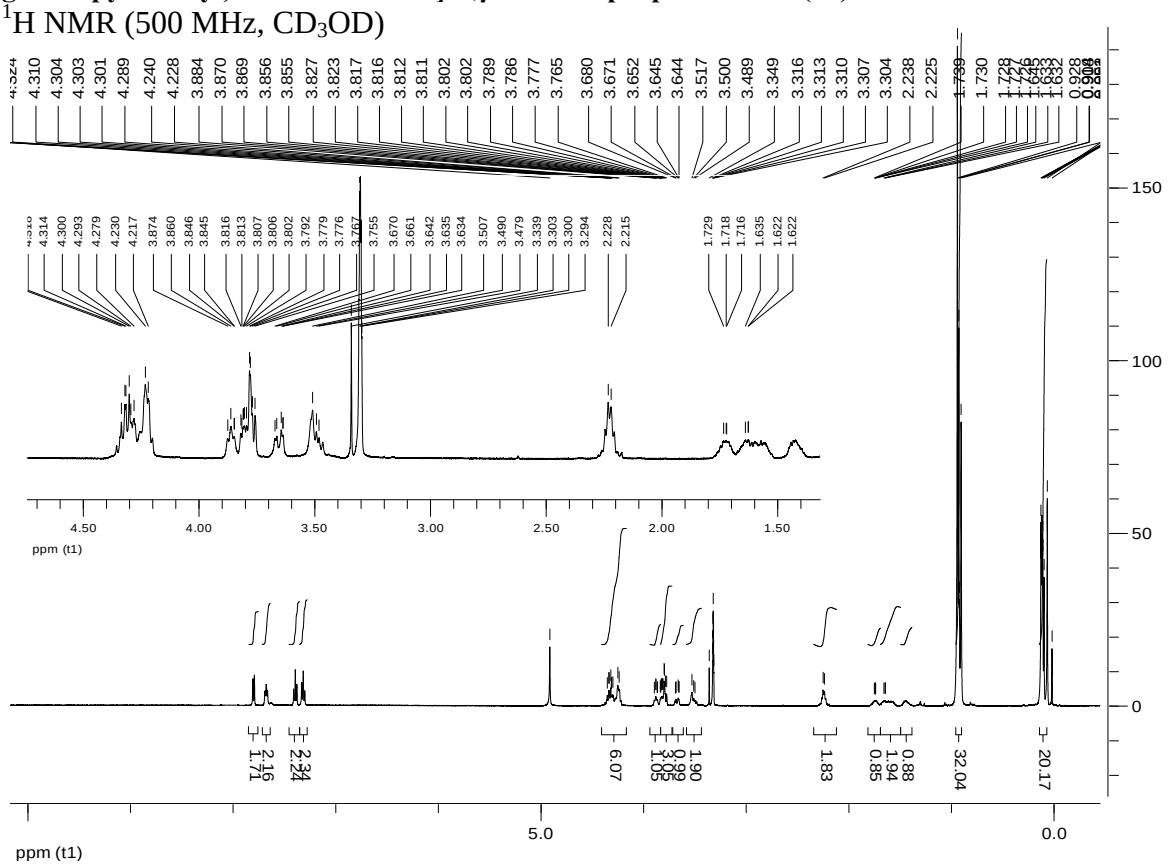

^{1}H NMR (500 MHz, $CDCl_3$)

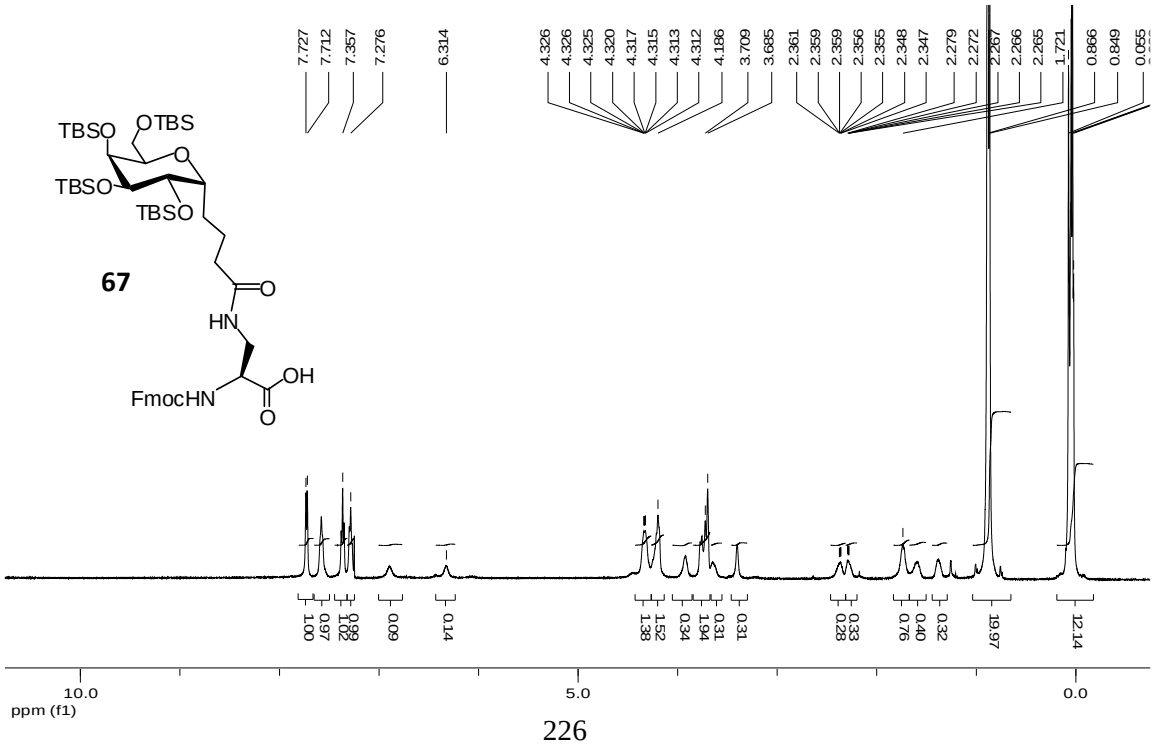

***Nα*-(S)-[(9H-fluoren-9-ylmethoxy)carbonyl]-*Nβ*-[2`-(2,3,4,6-tetra-*O-tert*-butyldimethylsilyl-α-D-galactopyran-1-yl) butan-1`-amido]-α,β-diaminopropanoic acid (67)**,

^{13}C NMR (101 MHz, $CDCl_3$)

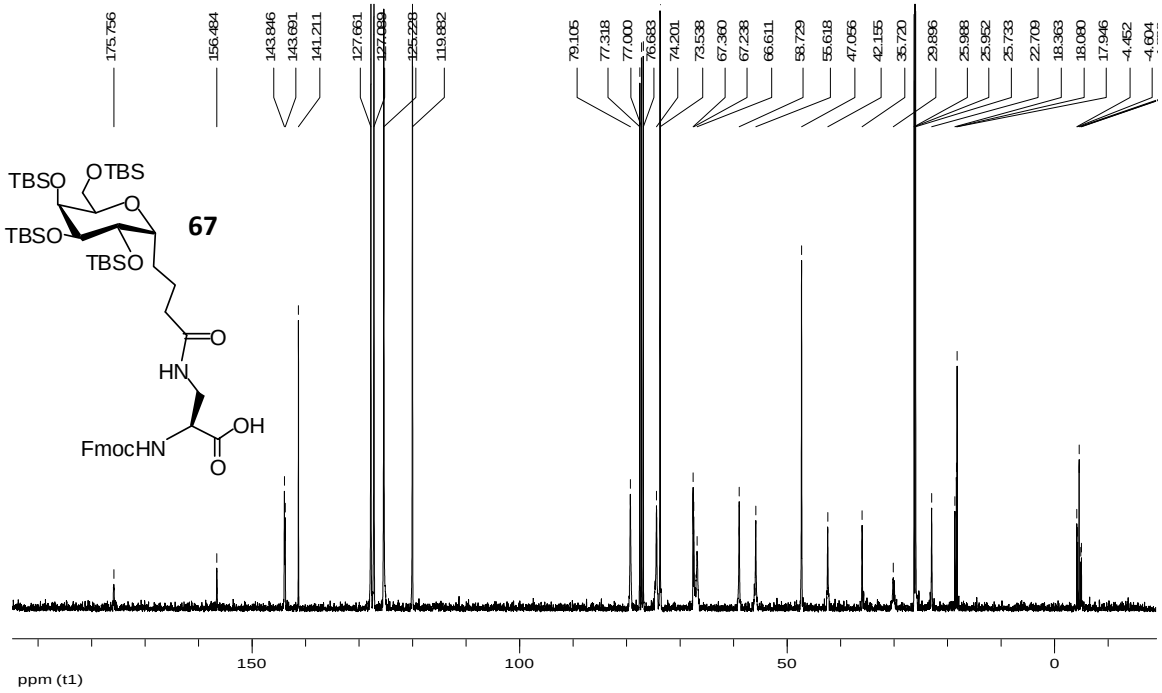

^{13}C DEPTQ 135 NMR (101 MHz, $CDCl_3$)

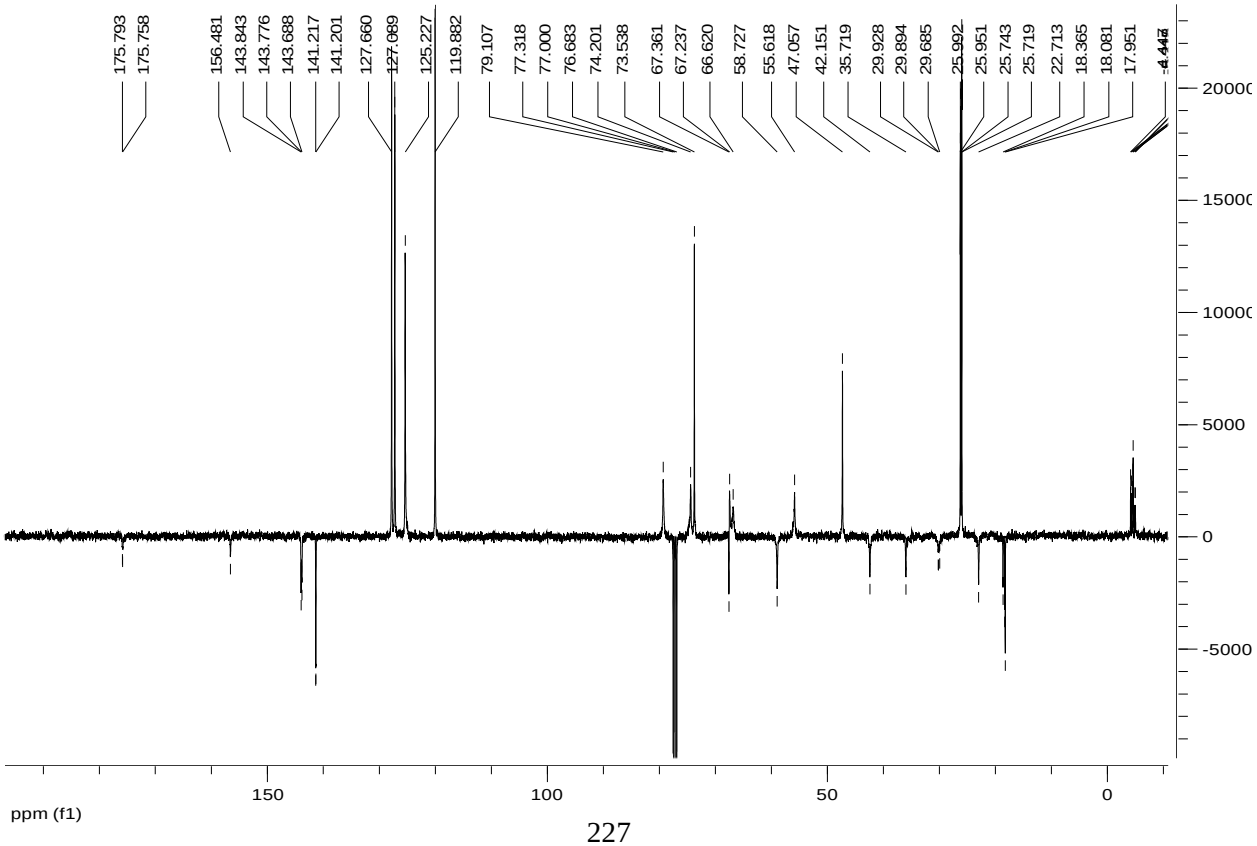

3`-(2,3,4,6-tetra-*O*-acetyl-α-D-galactopyran-1-yl)-propan-1`-oic acid (68),

^{1}H NMR (500 MHz, $CDCl_3$)

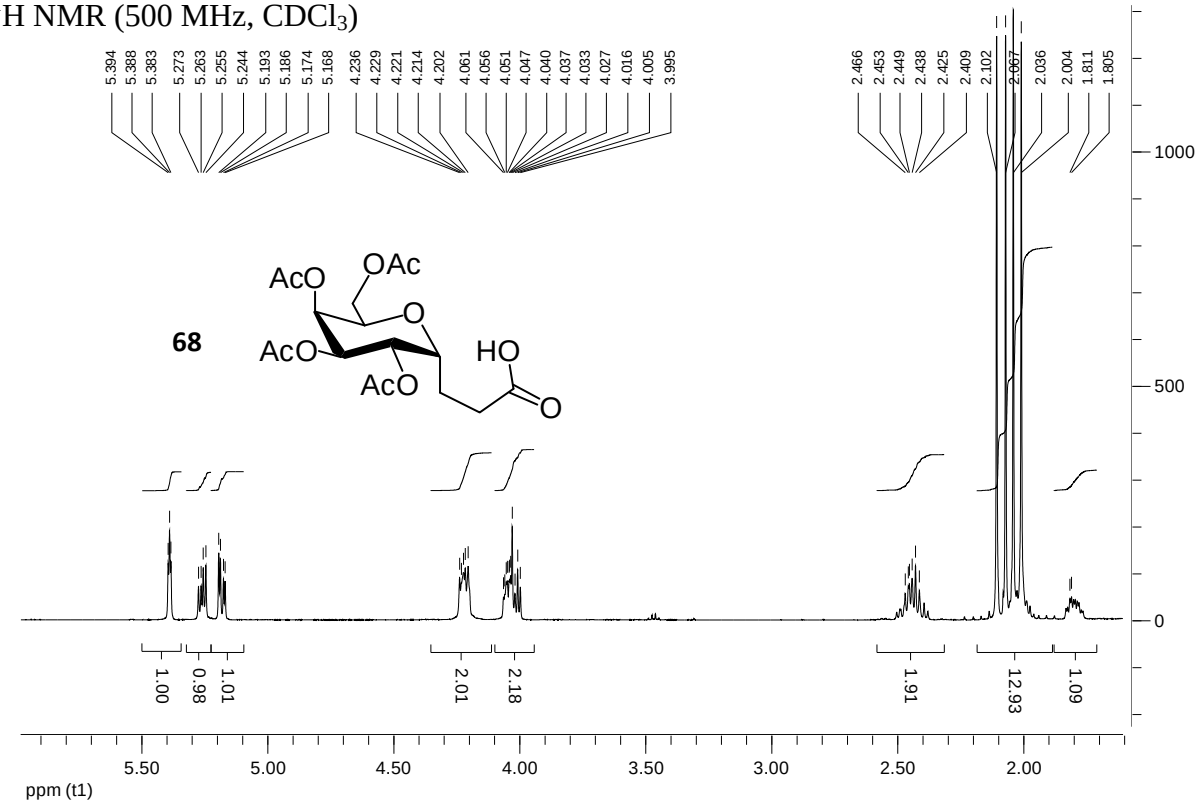

^{13}C NMR (101 MHz, $CDCl_3$)

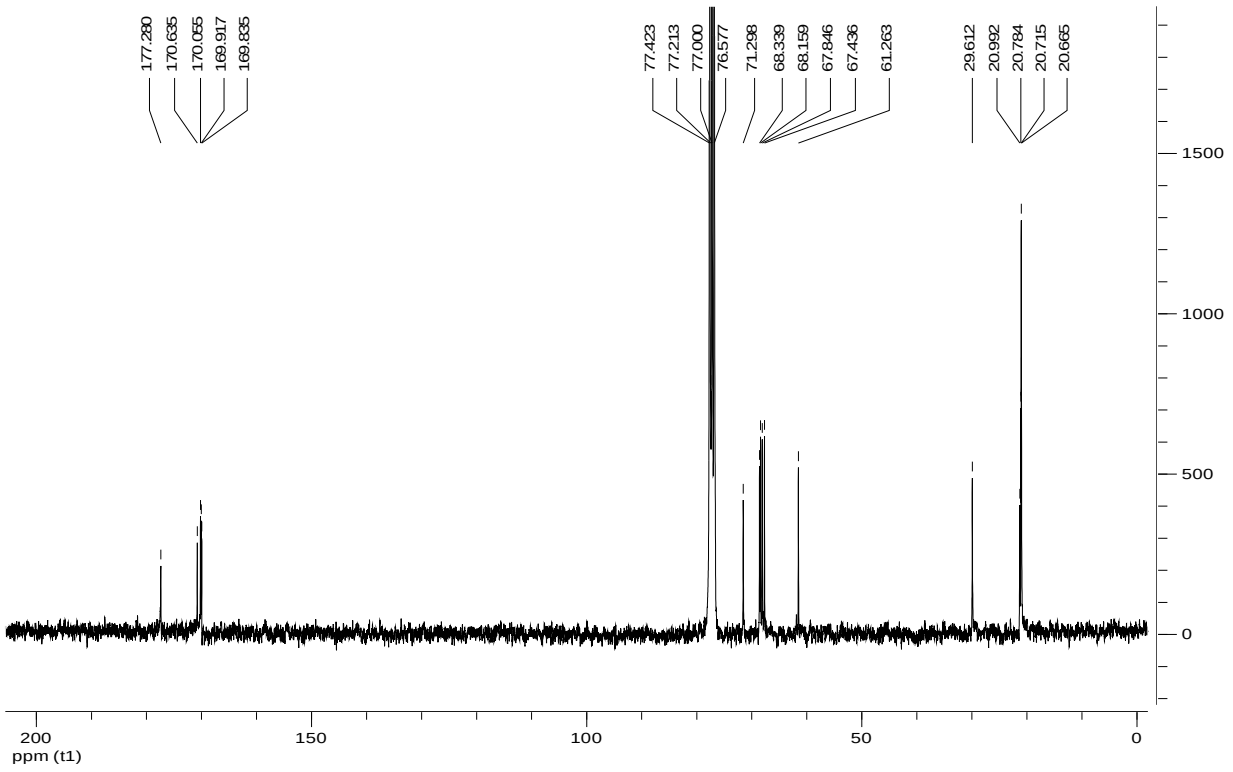

4`-(2,3,4,6-tetra-*O-tert*-butyldimethylsilyl-*α*-D-galactopyran-1-yl)-butan-1`-oic acid (69), ^{1}H NMR (500 MHz, $CDCl_3$)

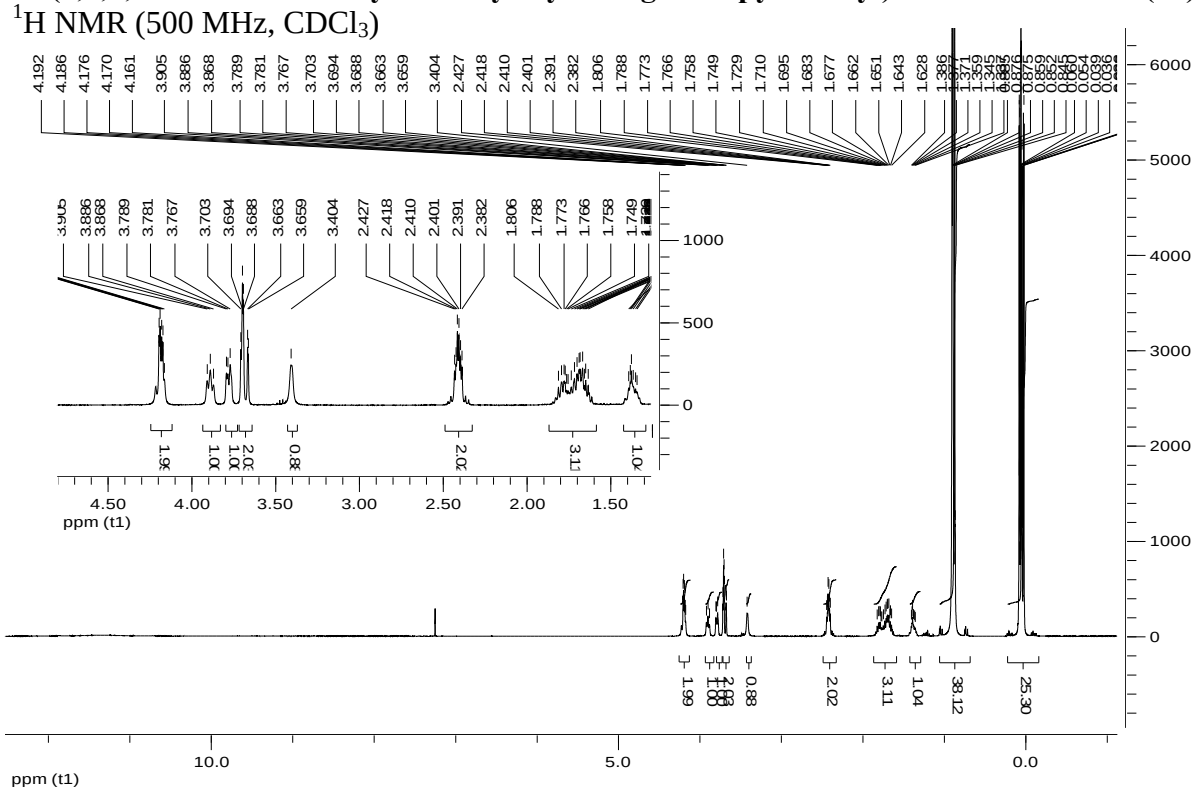

^{13}C DEPTQ 135 NMR (101 MHz, $CDCl_3$)

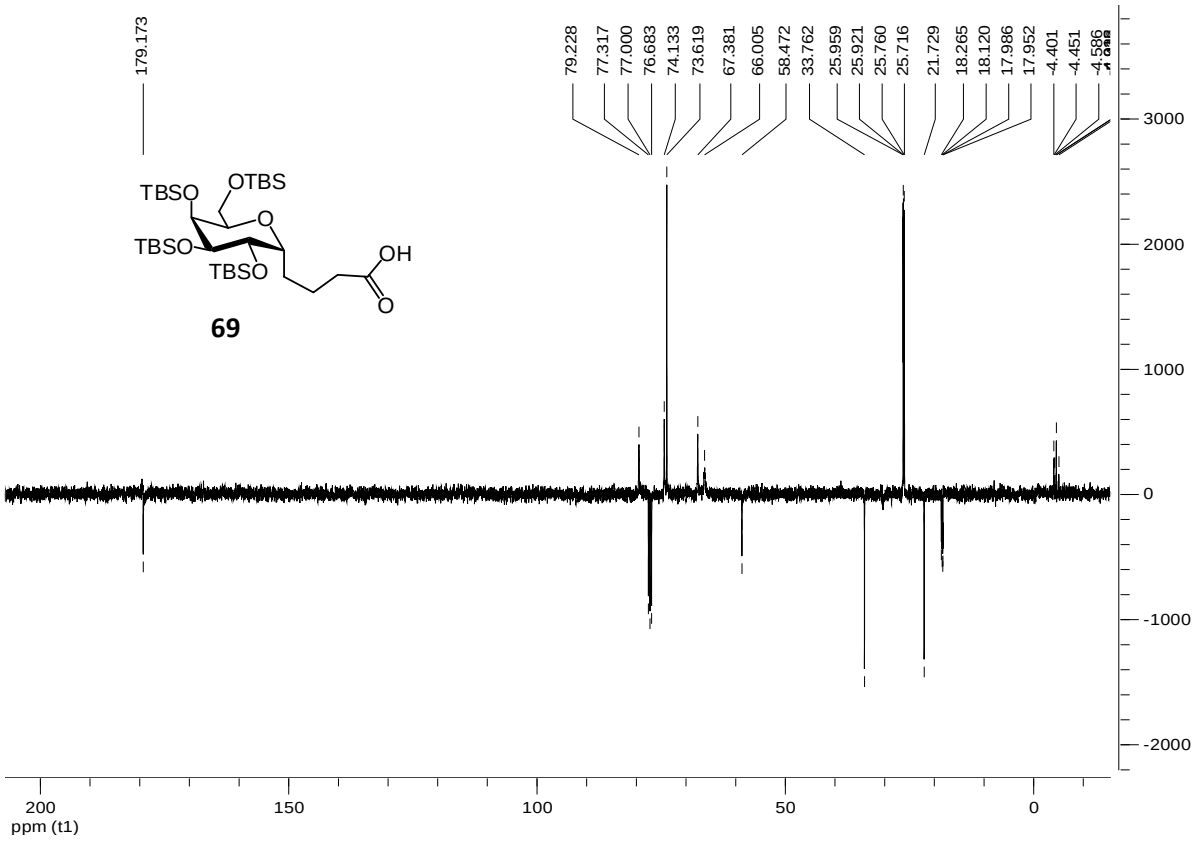

3`-(2,3,4,6-tetra-*O*-acetyl-α-D-galactopyran-1-yl)-1`-methoxyprop-1`-ene (70)

^{1}H NMR (500 MHz, $CDCl_3$)

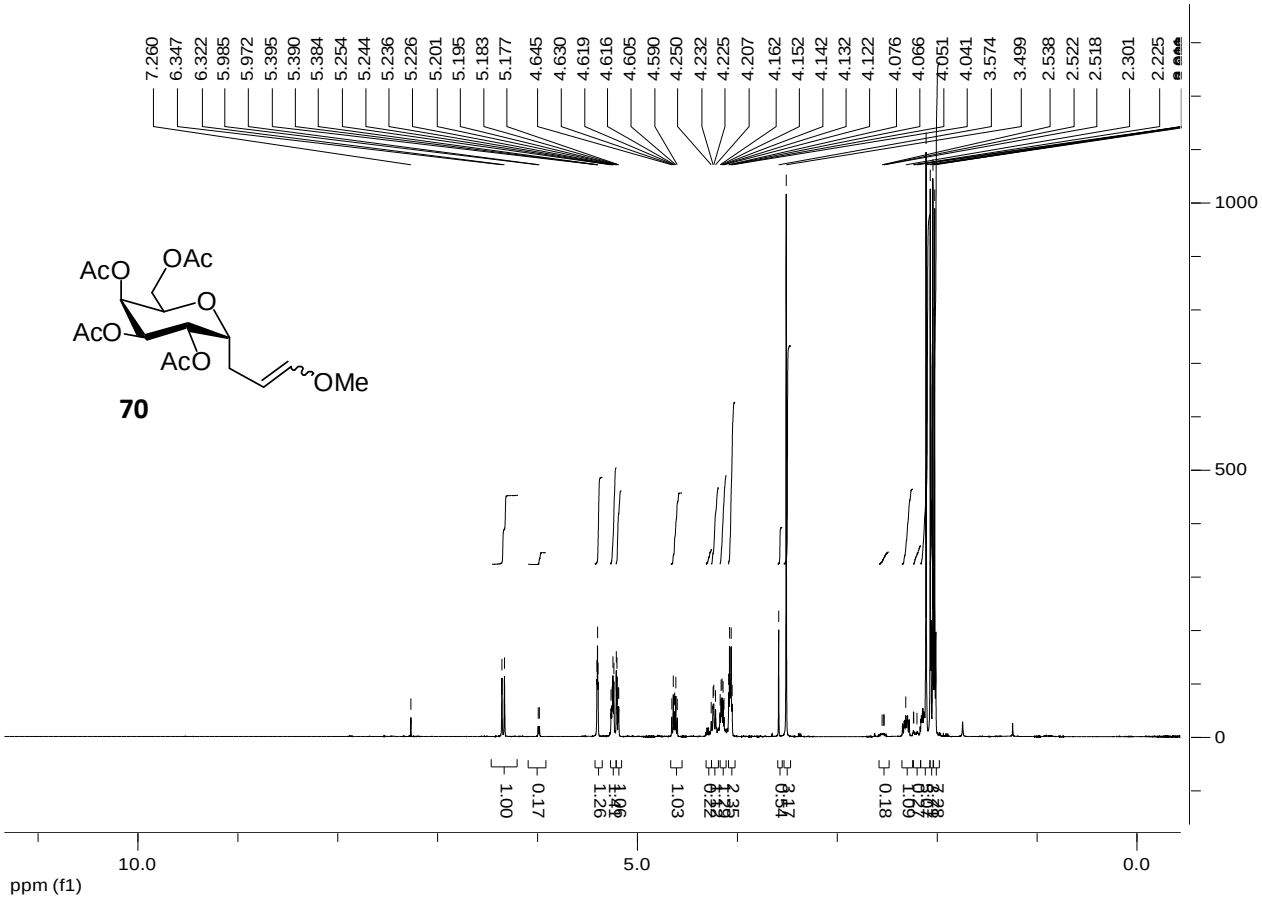

^{13}C NMR (101 MHz, $CDCl_3$)

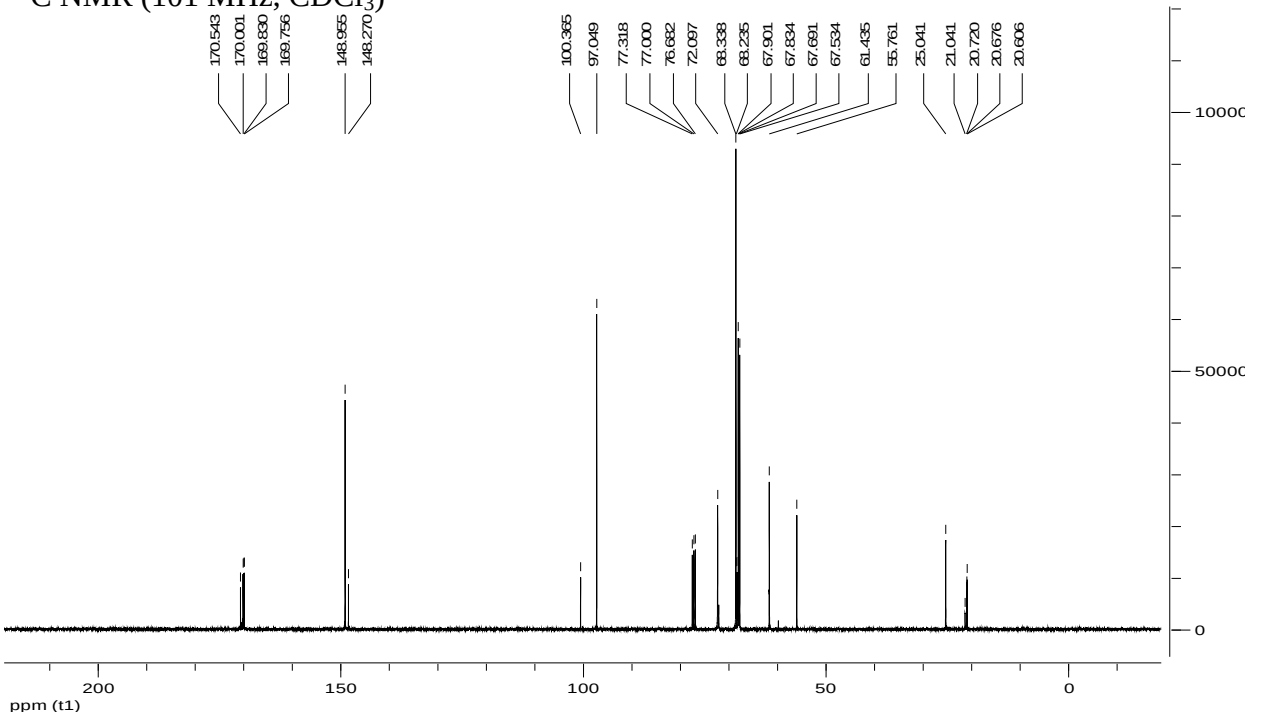

3`-(2,3,4,6-tetra-*O*-acetyl-α-D-galactopyran-1-yl)-propan-1`-al (71),

^{1}H NMR (500 MHz, $CDCl_3$)

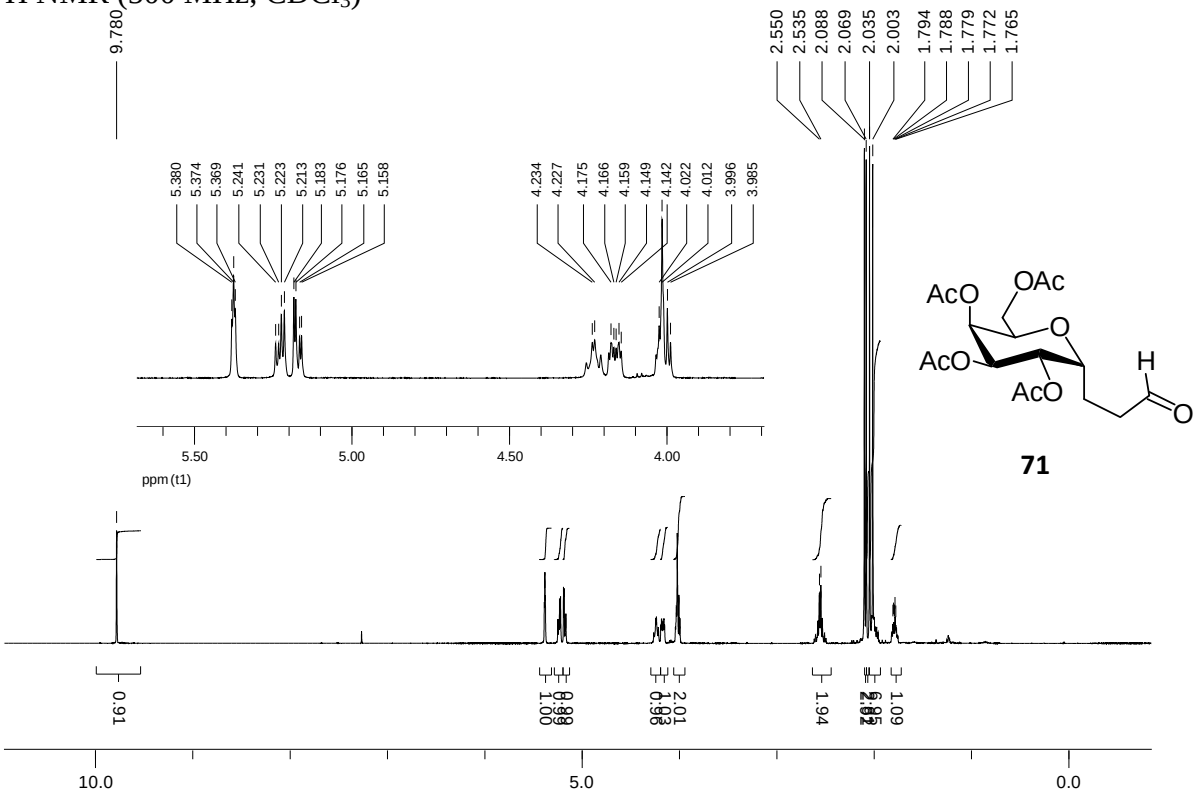

^{13}C DEPTQ 135 NMR (101 MHz, $CDCl_3$)

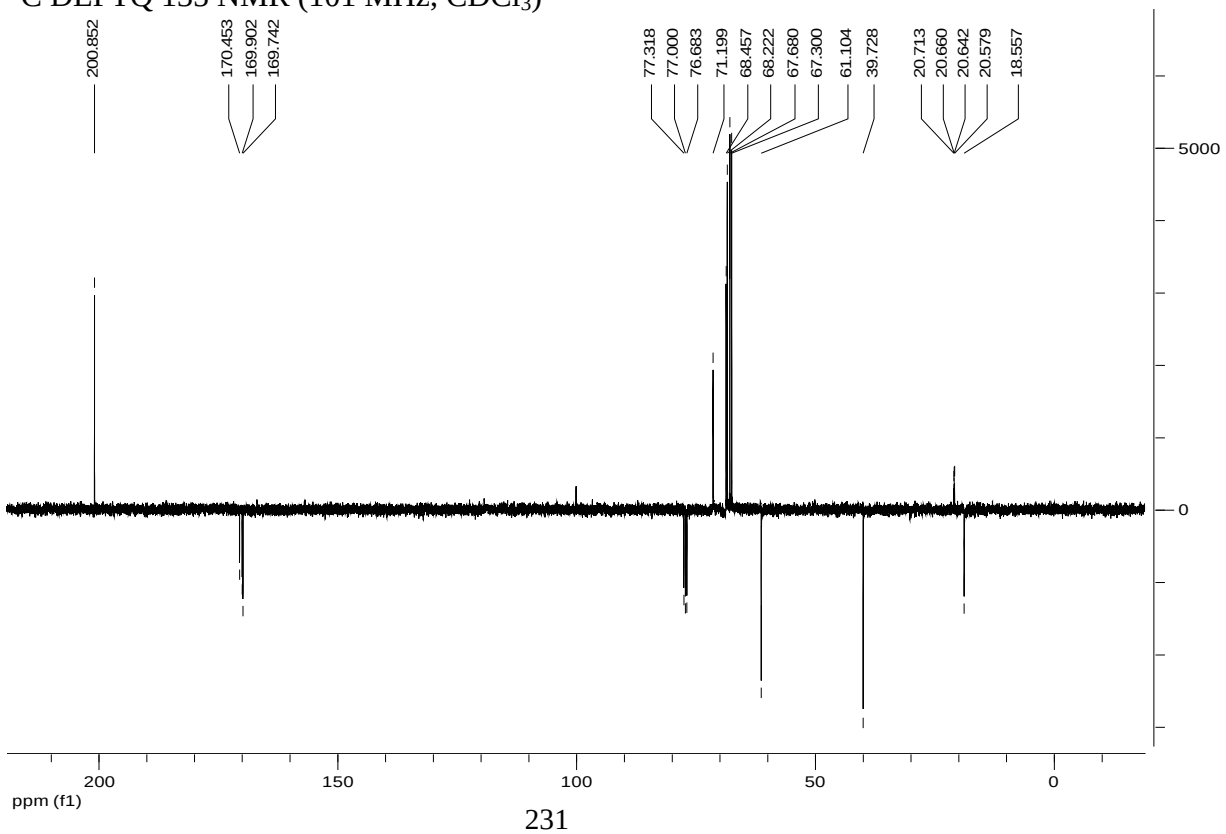

Benzyl *Nα*-(S)-[(9H-fluoren-9-ylmethoxy)carbonyl]-*Nγ*-[3`-(2,3,4,6-tetra-*O*-acetyl-α-D-galactopyran-1-yl) propan-1`-amido]-α,γ-diaminobutanoate (72),

^{1}H NMR (500 MHz, $CDCl_3$)

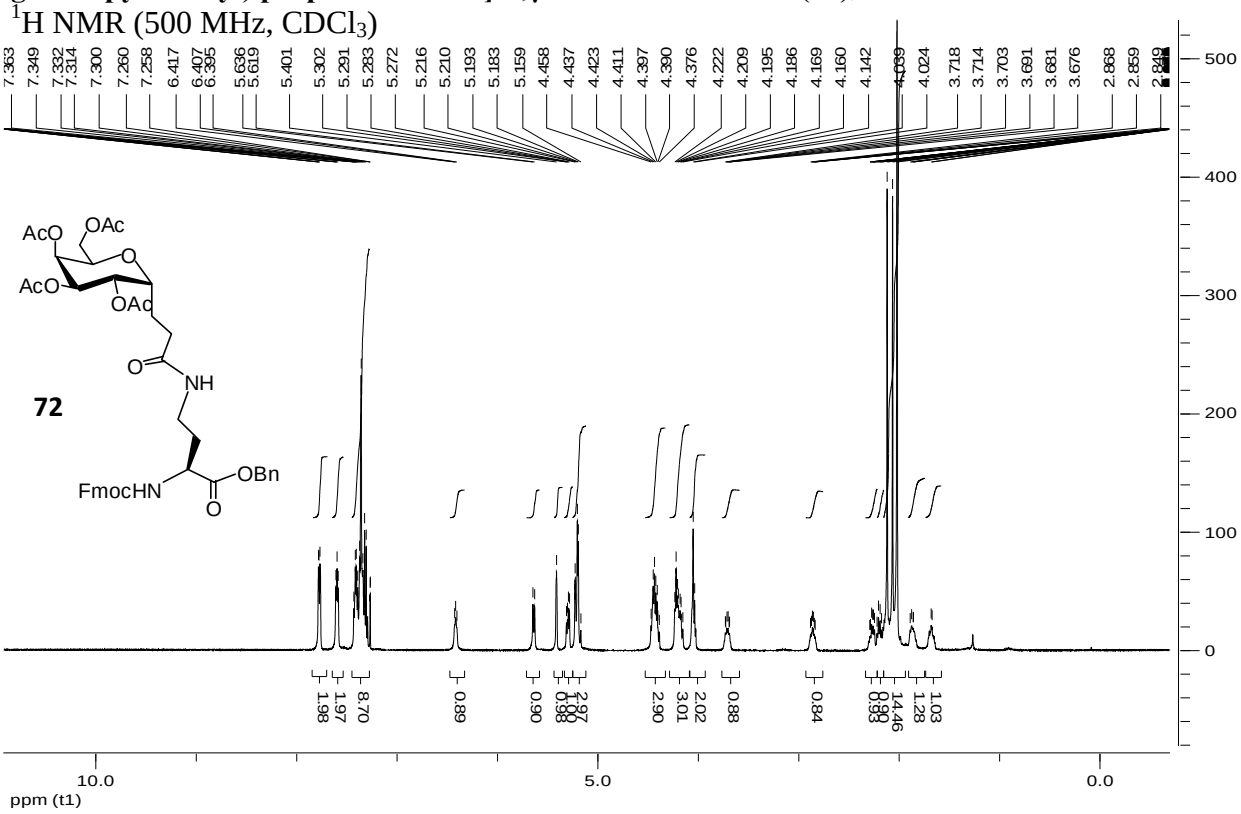

^{13}C NMR (101 MHz, $CDCl_3$)

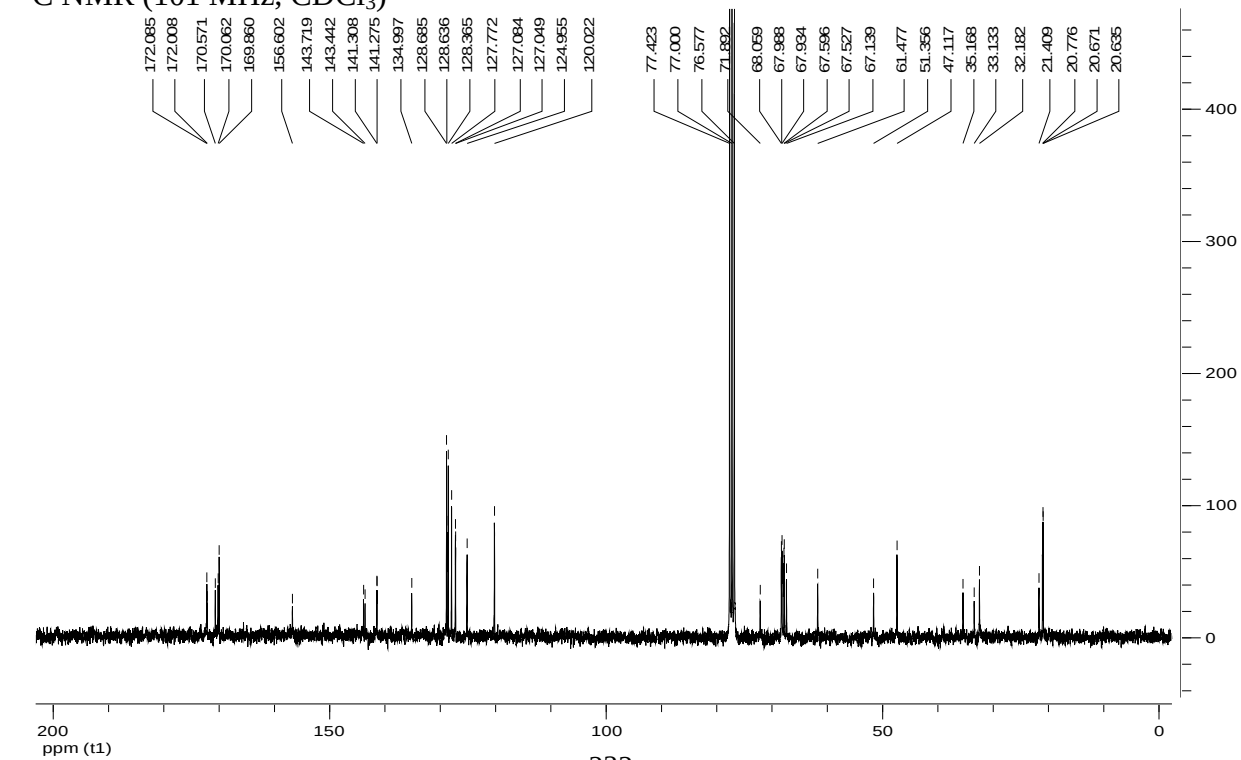

Methyl-4`-(2,3,4,6-tetra-*O*-acetyl-α-D-galactopyran-1-yl)-but-2`-en-1`-oate (74)

^{1}H NMR (500 MHz, $CDCl_3$)

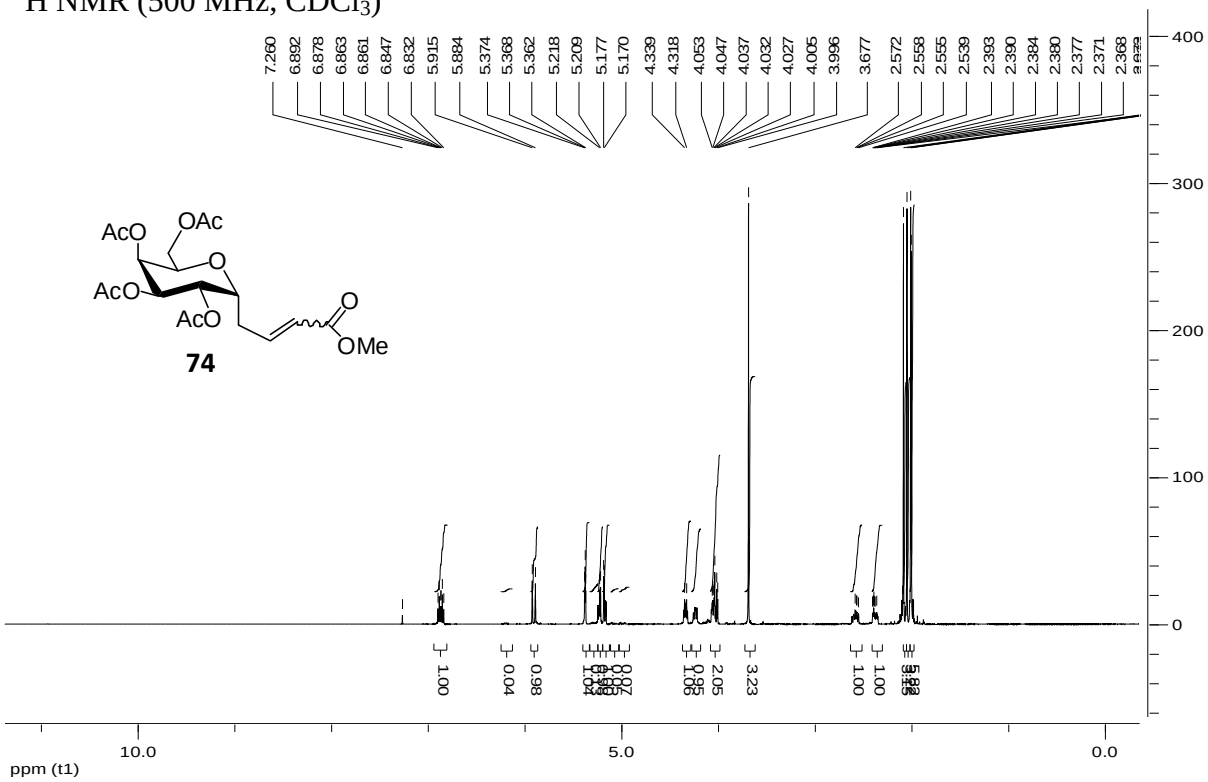

^{13}C NMR (101 MHz, $CDCl_3$)

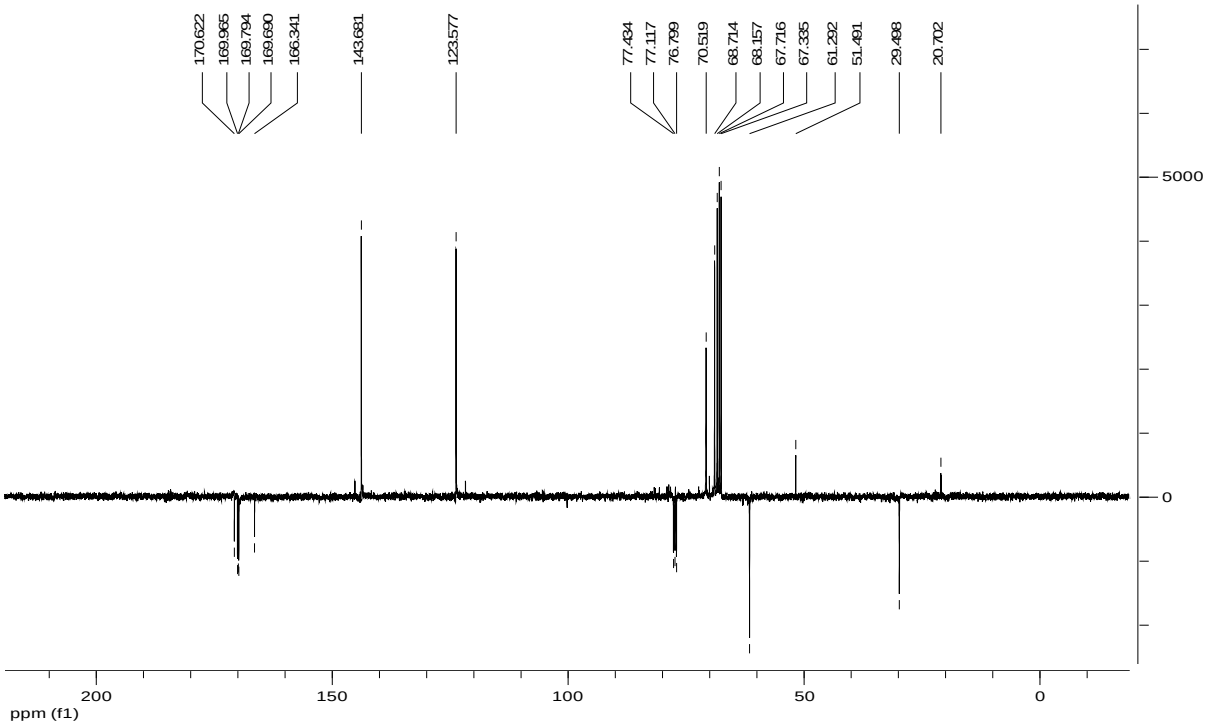

Methyl-4`-(2,3,4,6-tetra-*O*-acetyl-α-D-galactopyran-1-yl)-butan-1`-oate (75)

^{1}H NMR (500 MHz, $CDCl_3$)

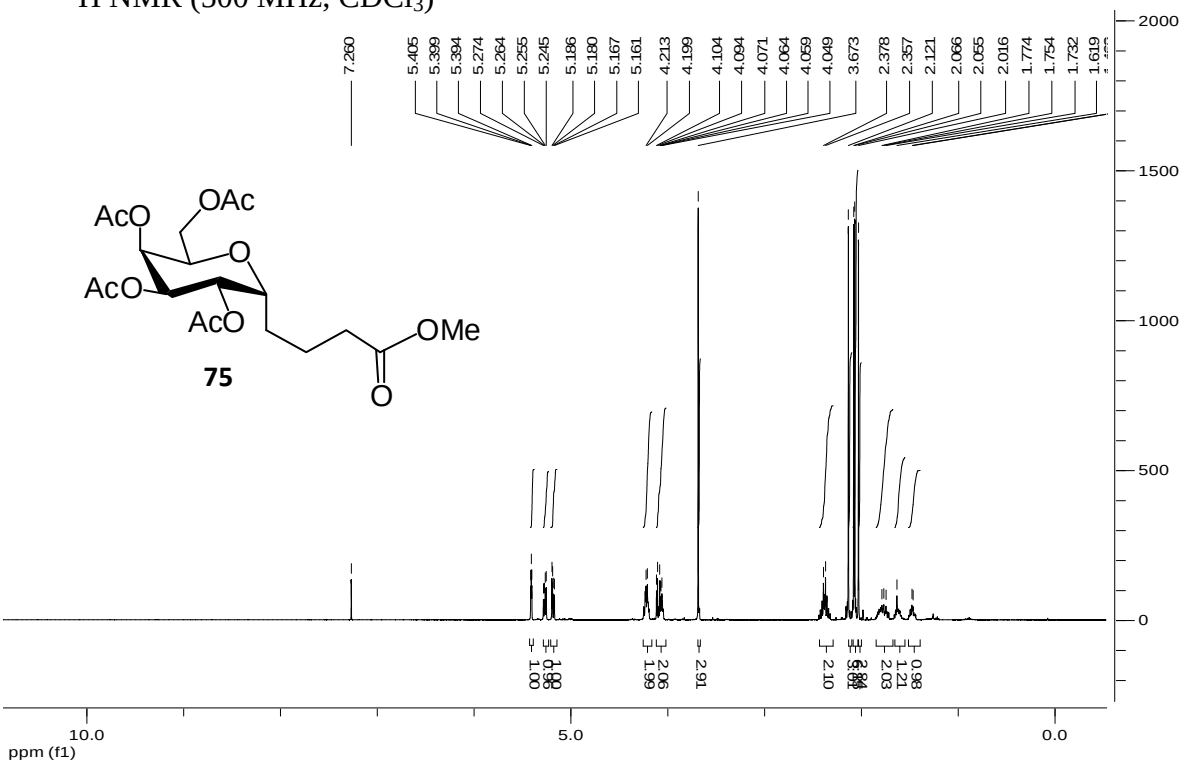

^{13}C DEPTQ 135NMR (101 MHz, $CDCl_3$)

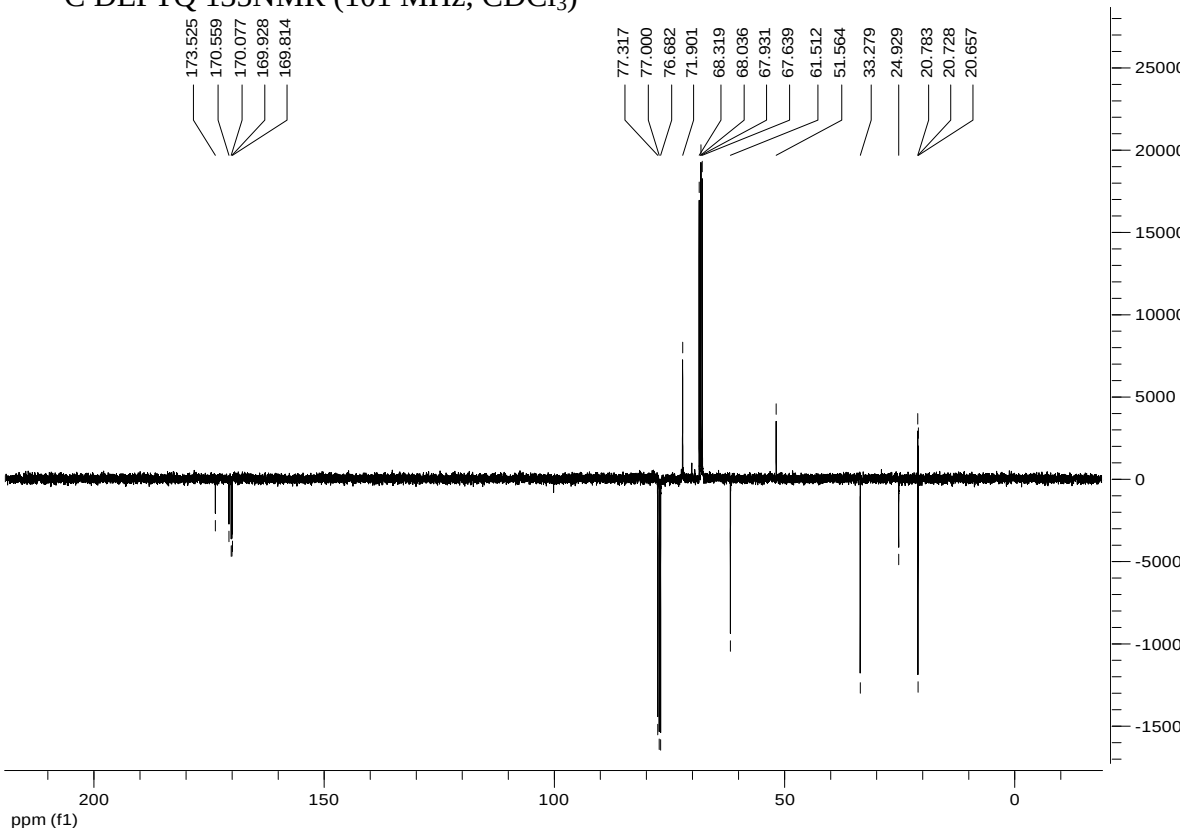

Methyl-4`-(2,3,4,6-tetra-*O-tert*-butyldimethylsilyl-α-D-galactopyran-1-yl)-butan-1`-oate (76),

^{1}H NMR (500 MHz, $CDCl_3$)

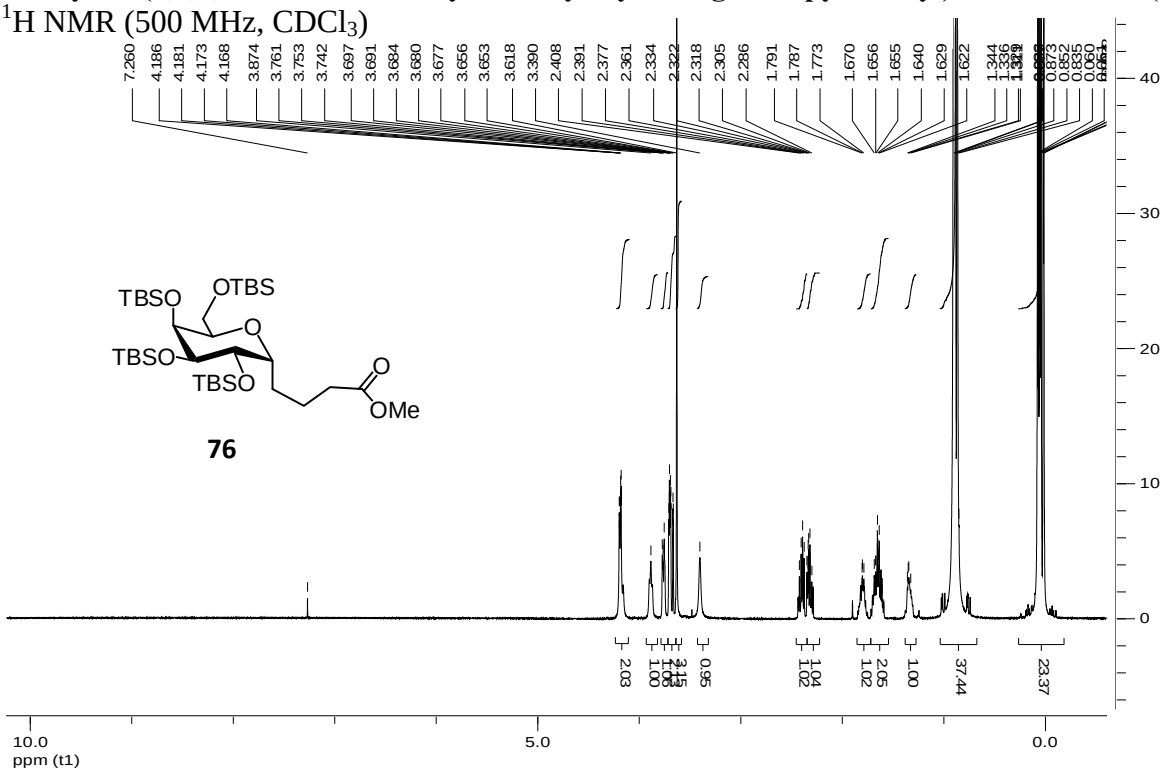

^{13}C DEPT Q135 NMR (101 MHz, $CDCl_3$)

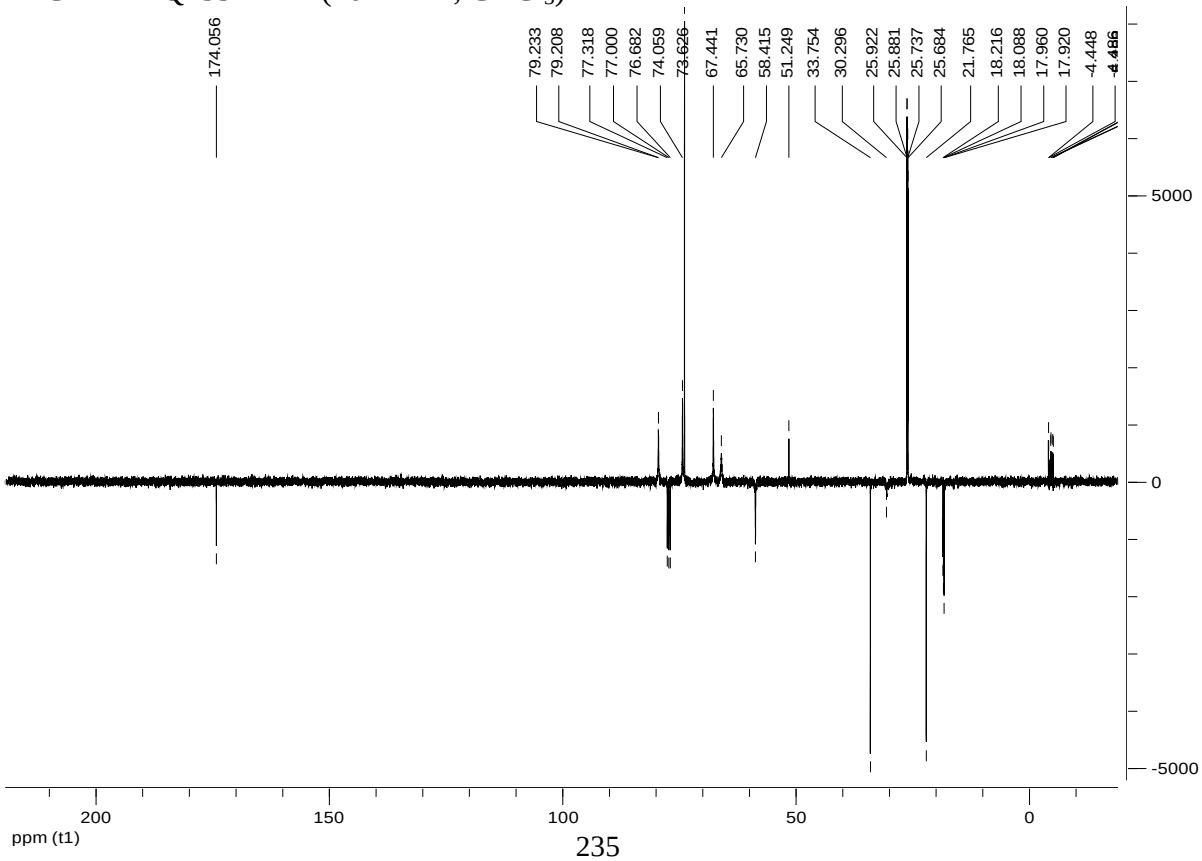

Benzyl *Nα*-(S)-[(9H-fluoren-9-ylmethoxy)carbonyl]-*Nβ*-[4`-(2,3,4,6-tetra-*O*-*tert*-butyl-dimethylsilyl)-α-D-galactopyran-1-yl)-butan-1`-amido)-α,β-diaminopropanoate (77),

^{1}H NMR (500 MHz, $CDCl_3$)

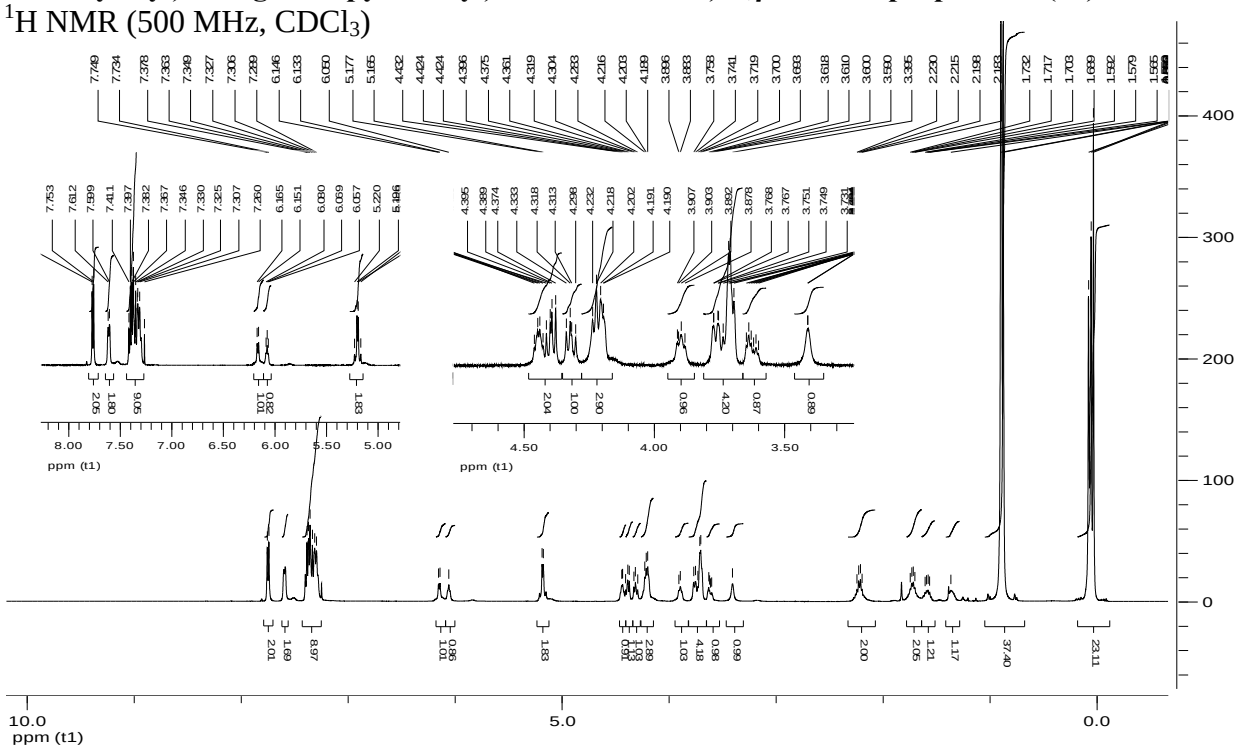

^{13}C DEPT Q135NMR (101 MHz, $CDCl_3$)

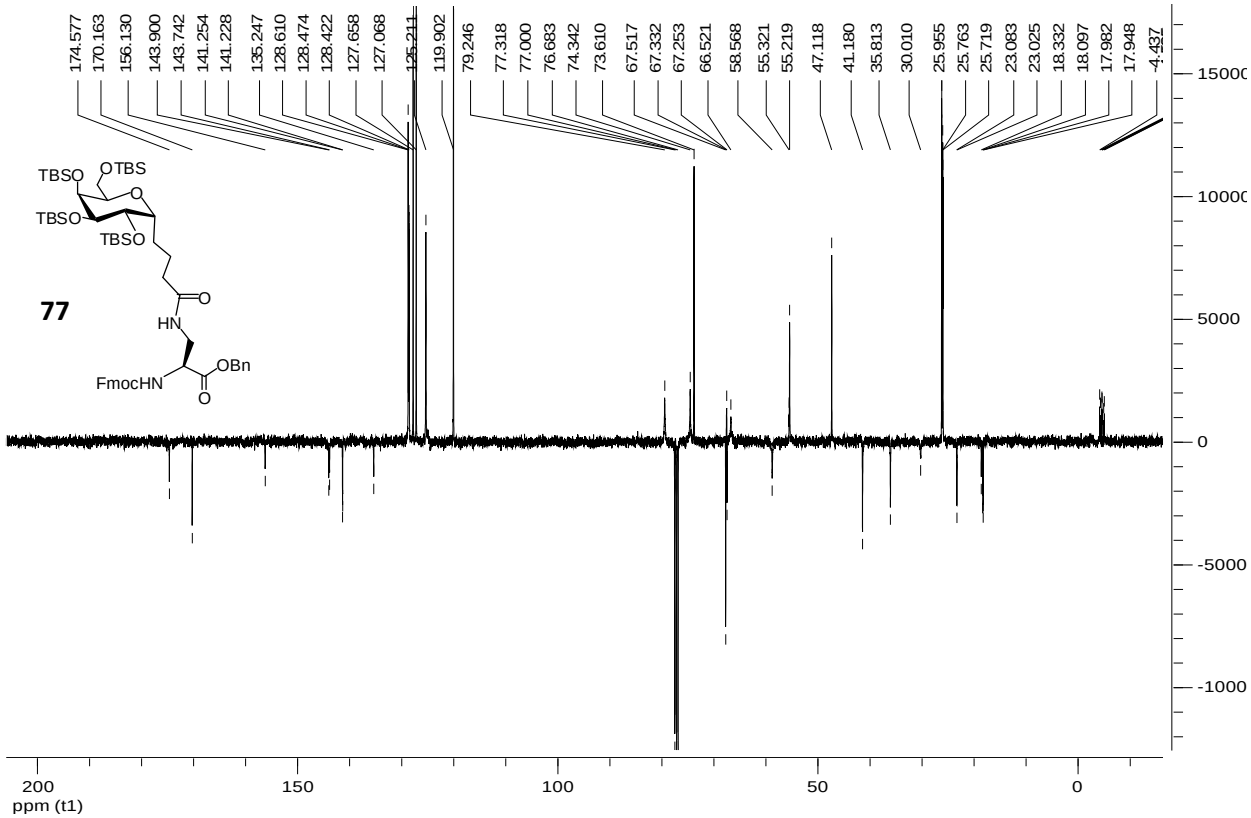

***Nα*-(S)-[(9H-fluoren-9-ylmethoxy)carbonyl]- *Nε*-[1`-( 2,3,4,6-tetra-*O*-benzyl-α-D-galactopyran-1-yl)-methyl-1`-amino]- homoglutamine (81)**,

^{1}H NMR (500 MHz, $CDCl_3$)

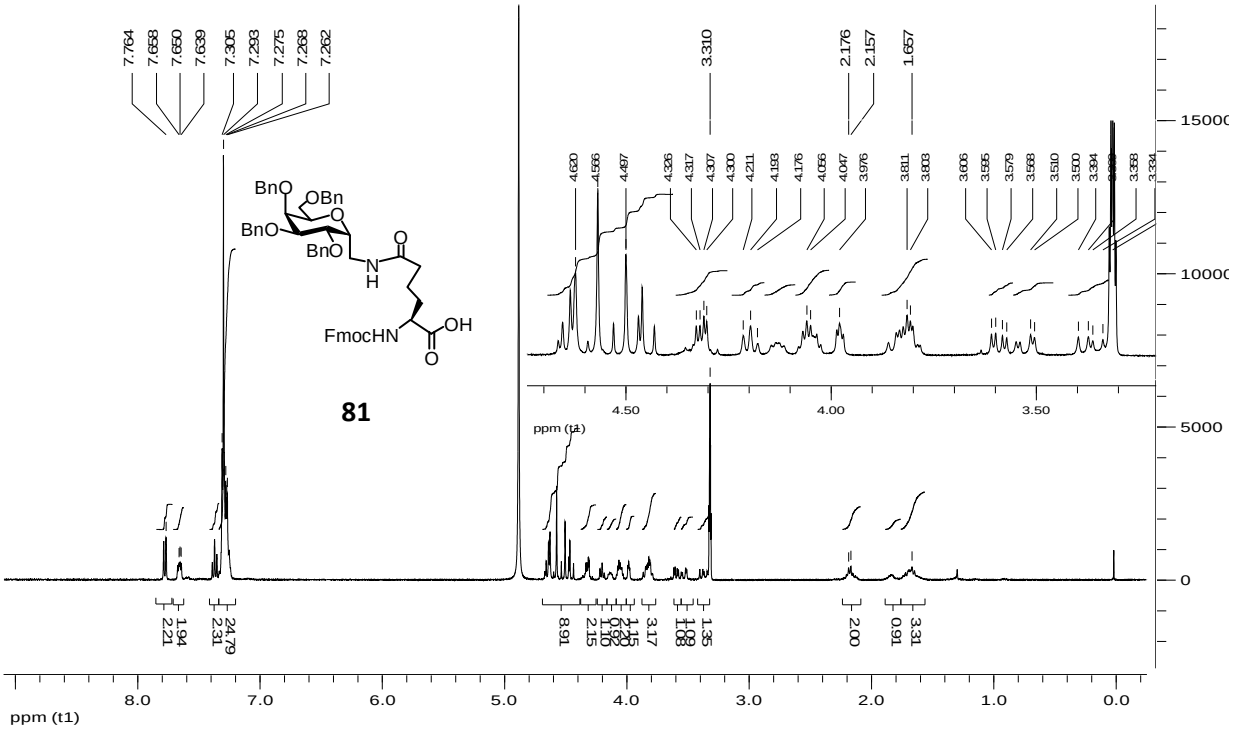

^{13}C DeptQ 135 NMR (101 MHz, $CDCl_3$)

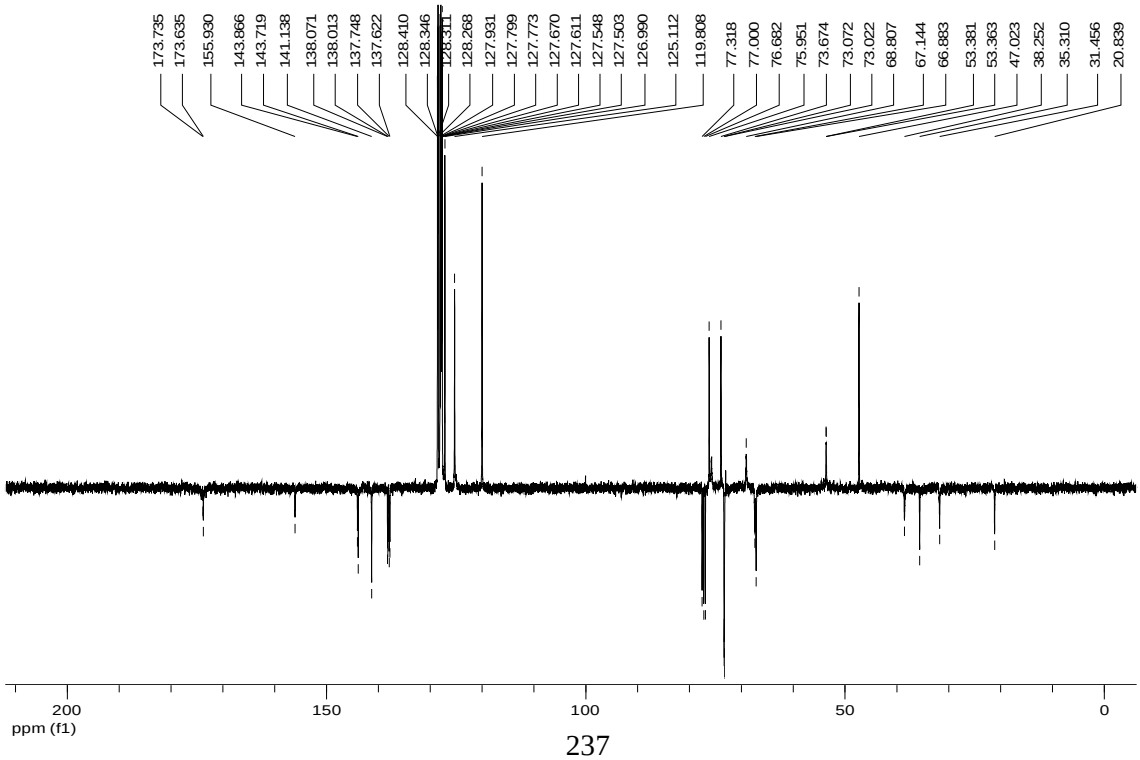

2,3,4,6-tetra-*O*-benzyl-α-D-galactopyranosyl cyanide (83), ^{1}H NMR (400 MHz, $CDCl_3$)

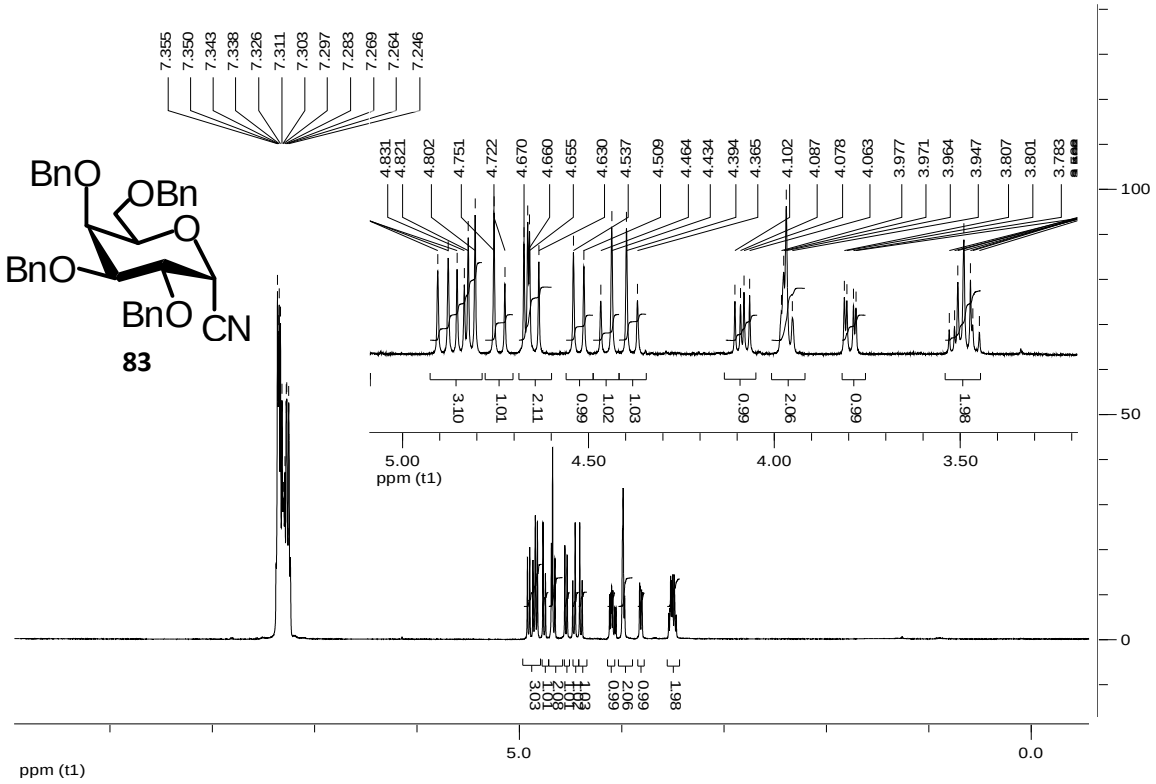

^{13}C NMR (101 MHz, $CDCl_3$)

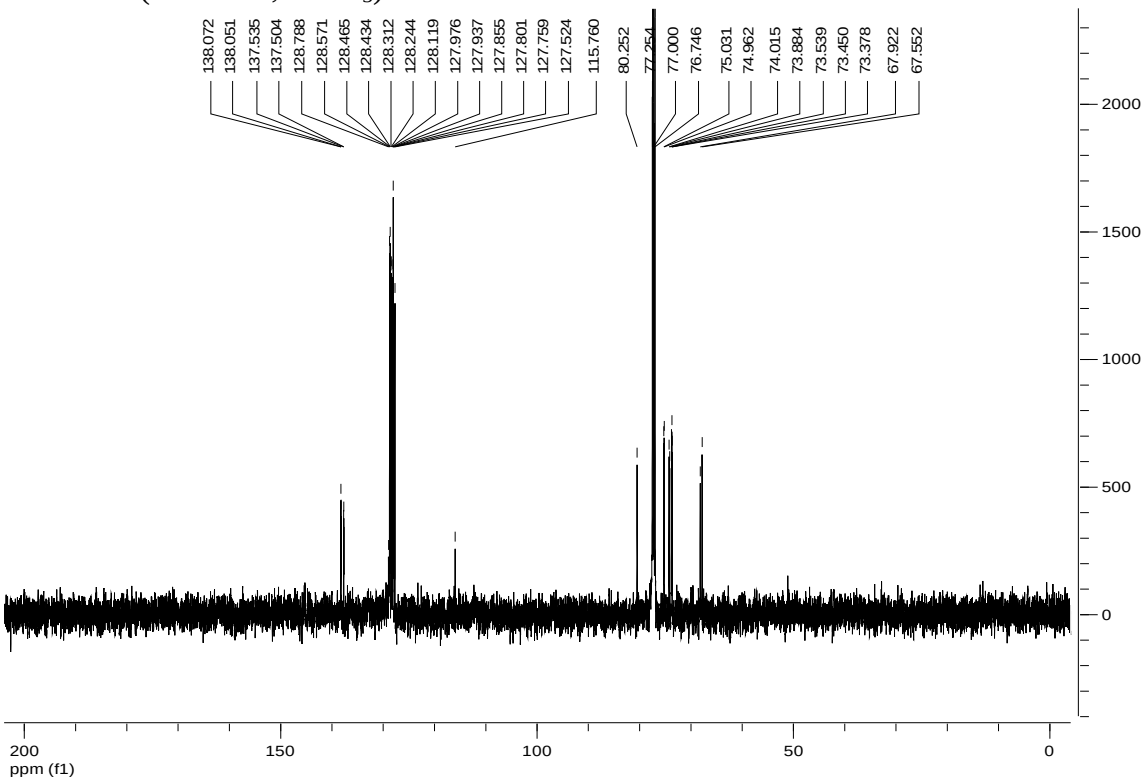

***Nα*-(S)-[(9H-fluoren-9-ylmethoxy)carbonyl]-homoglutam-1-yl methyl ester (84)**,
^{1}H NMR (500 MHz, CD_3OD)

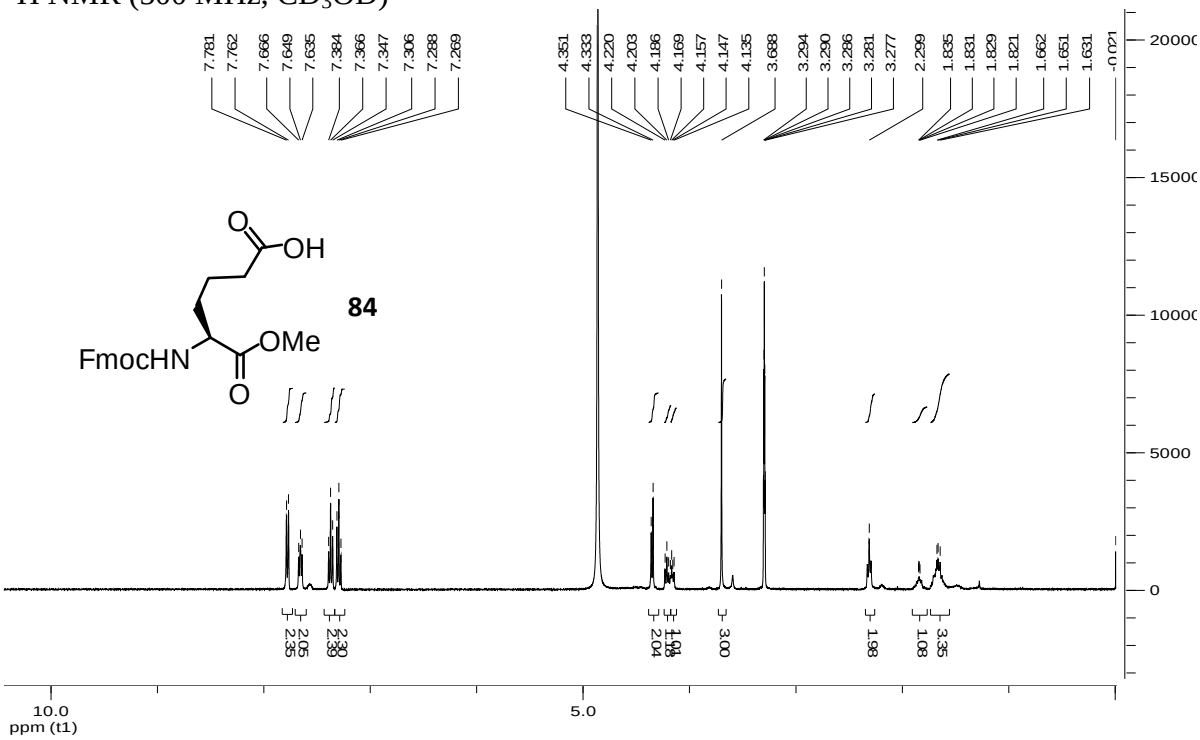

^{13}C NMR (101 MHz, CD_3OD)

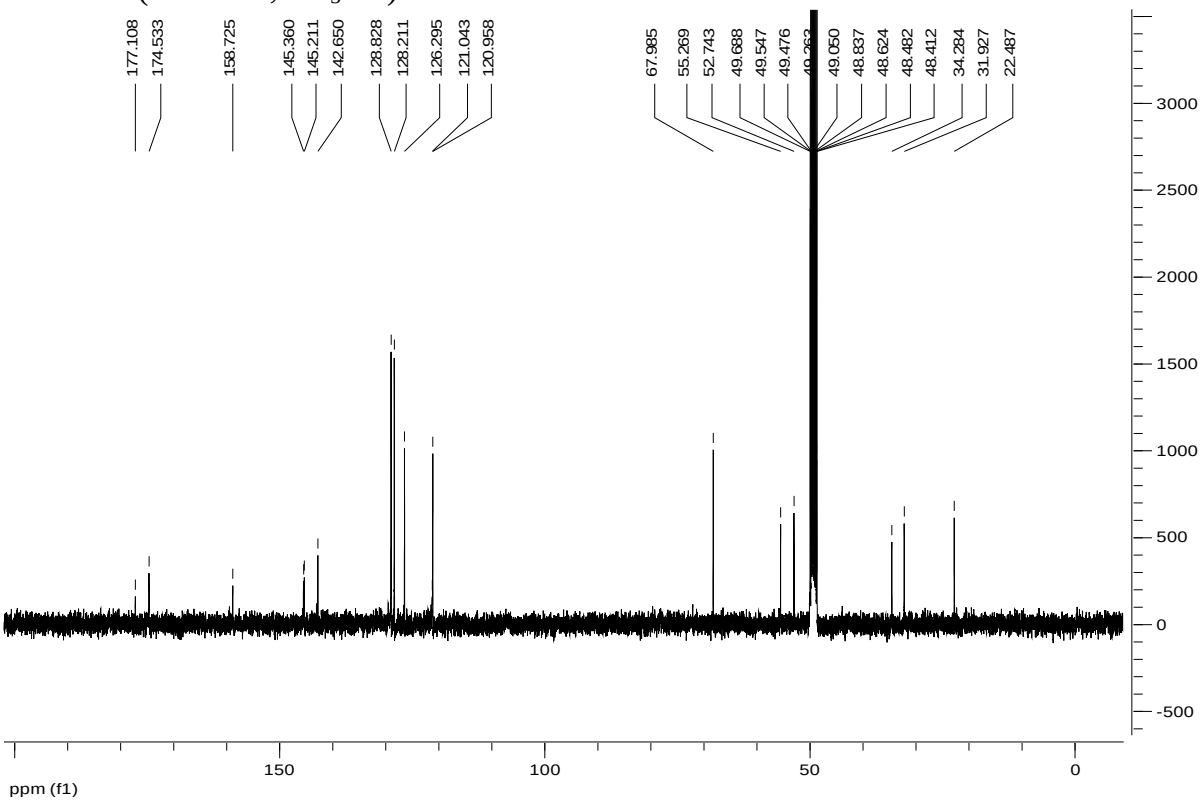

***Nα*-(S)-[(9H-fluoren-9-ylmethoxy)carbonyl]-glutam-1-yl methyl ester (85)**,

^{1}H NMR (500 MHz, CD_3OD)

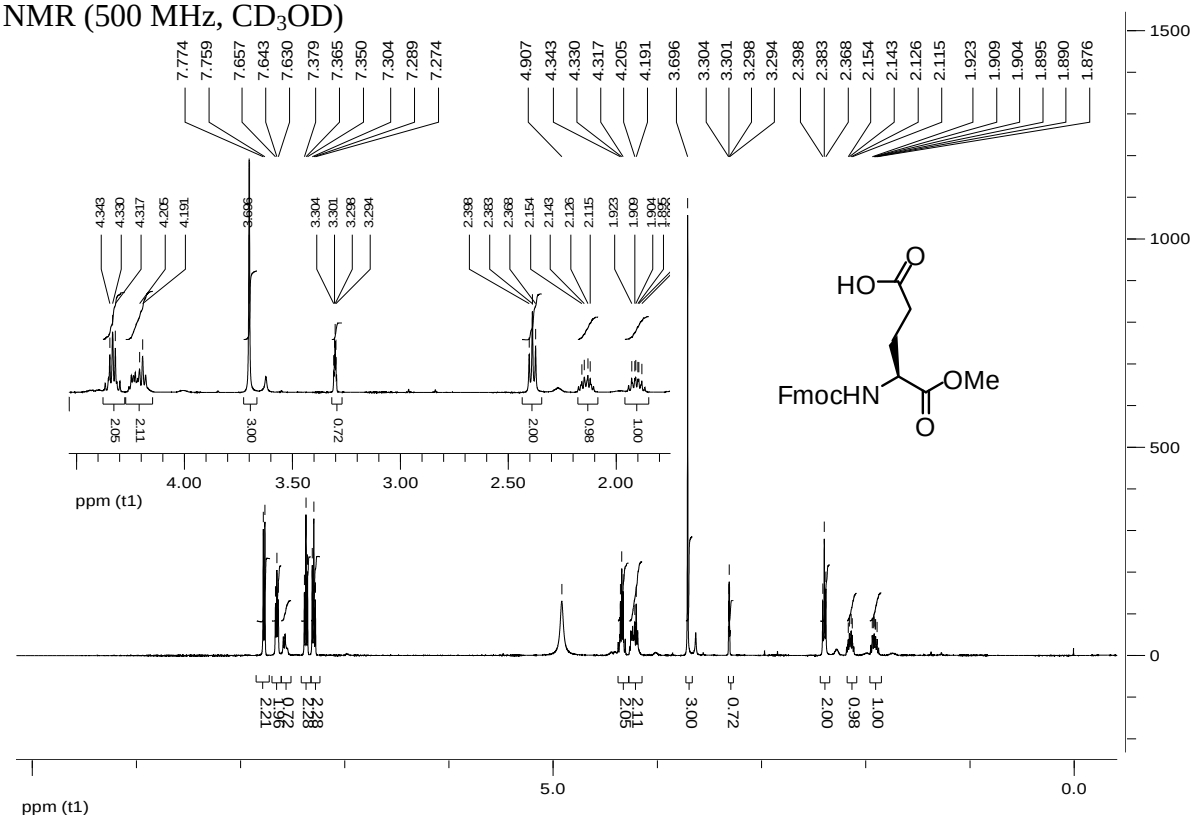

^{13}C DEPT Q135 NMR (101 MHz, CD_3OD)

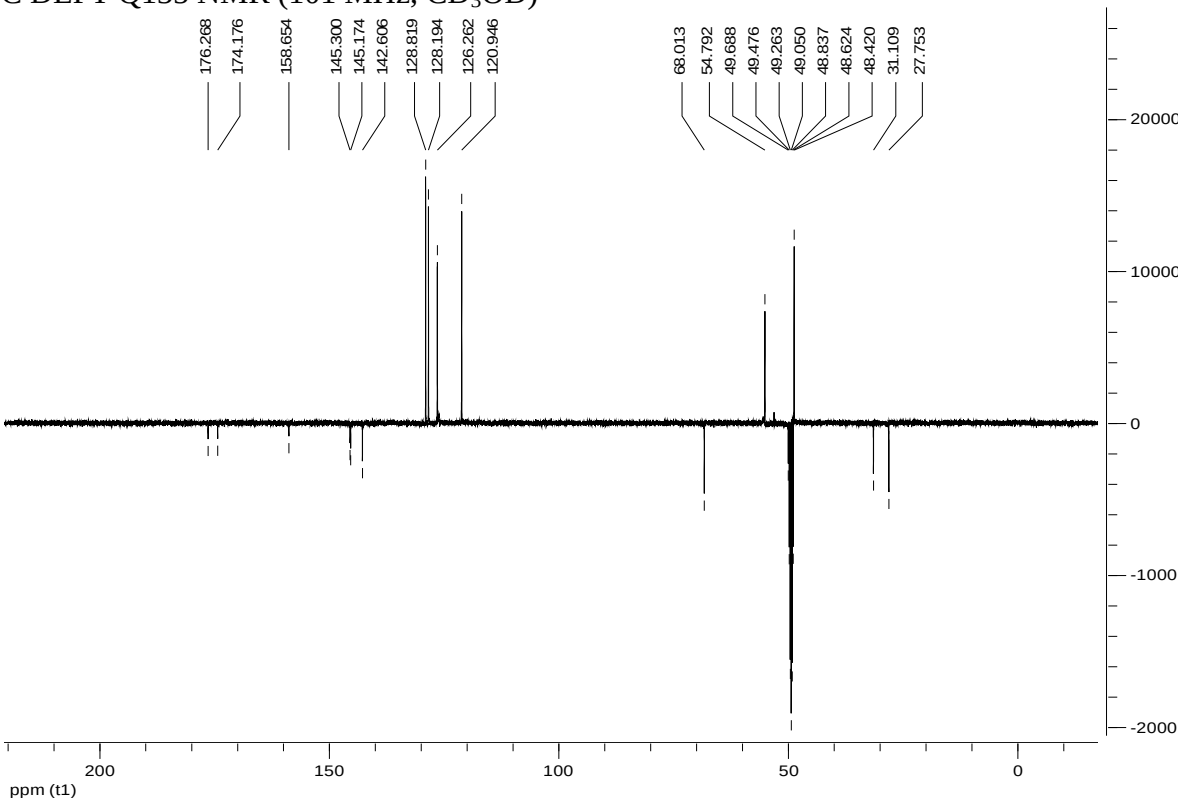

1-acetoxy-2,3,4,6-tetra-*O*-benzyl-D-galactopyranose (88), ^{1}H NMR (400 MHz, $CDCl_3$)

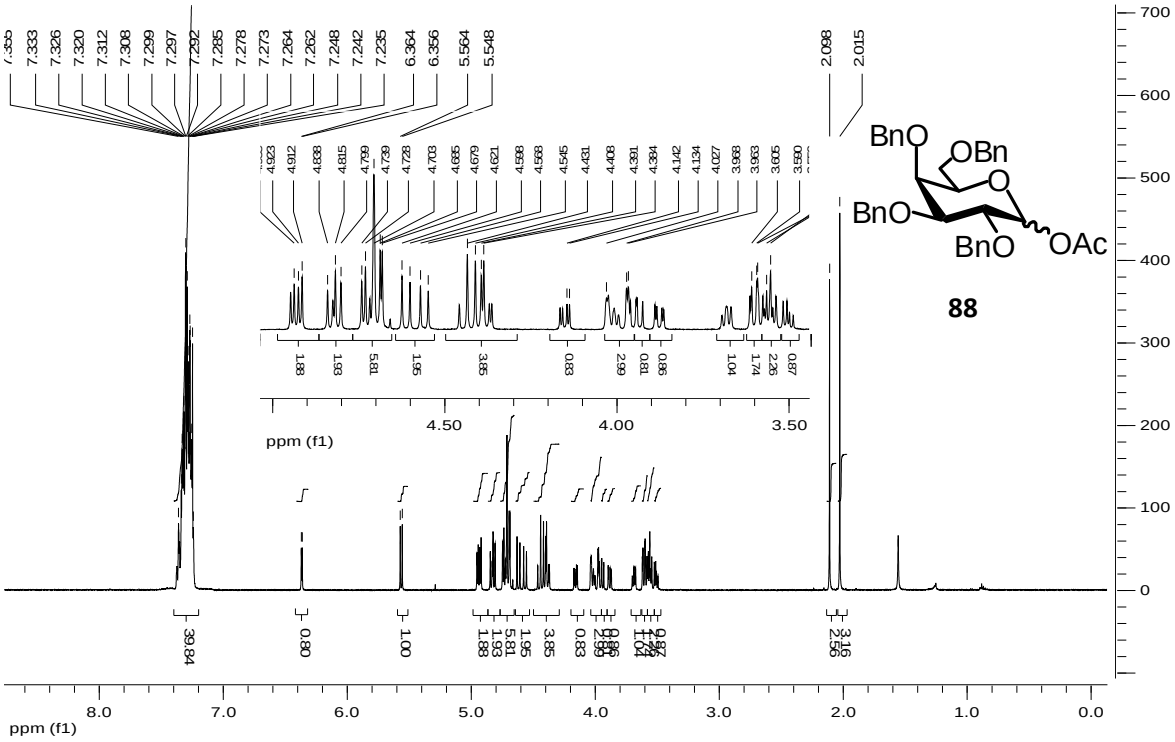

^{13}C NMR (101 MHz, $CDCl_3$)

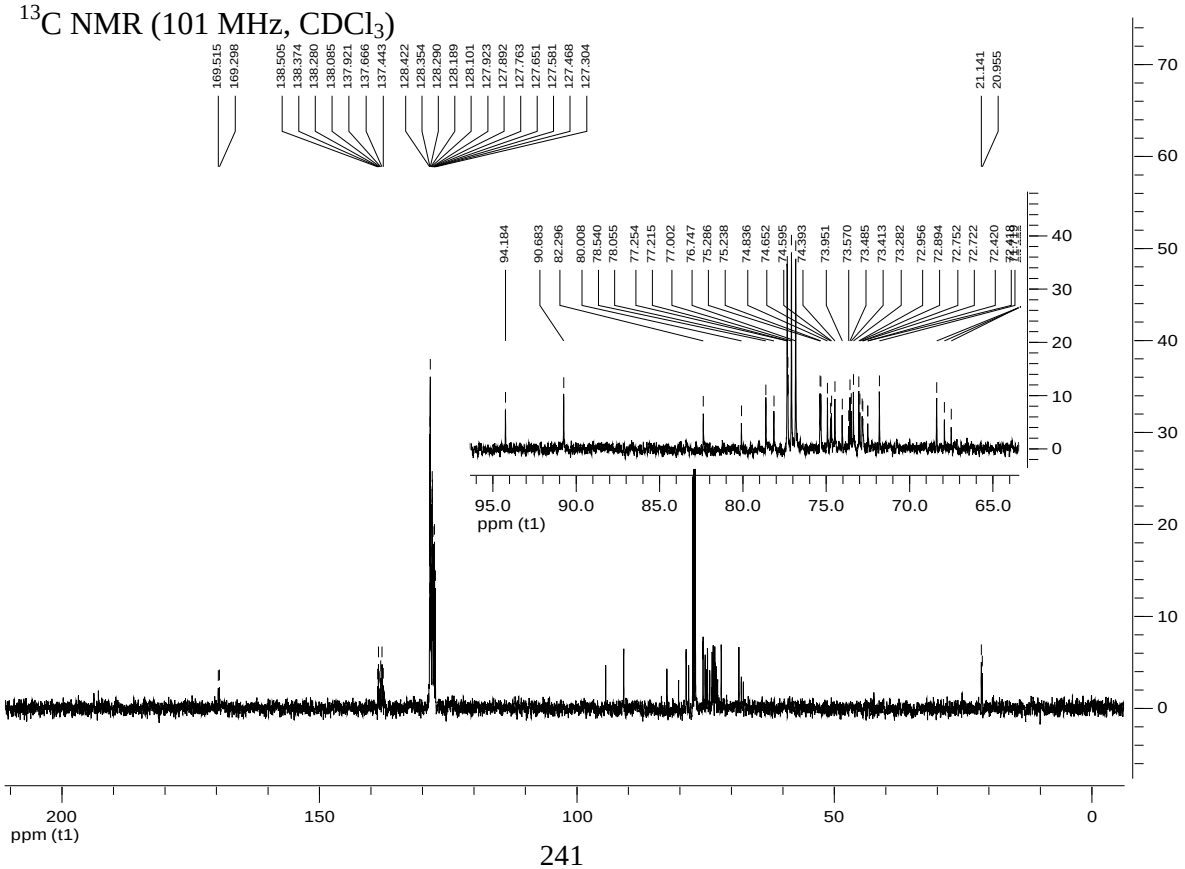

2,3,4,6-tetra-*O*-benzyl-β-D-galactopyranosyl cyanide (89), ^{1}H NMR (500 MHz, $CDCl_3$)

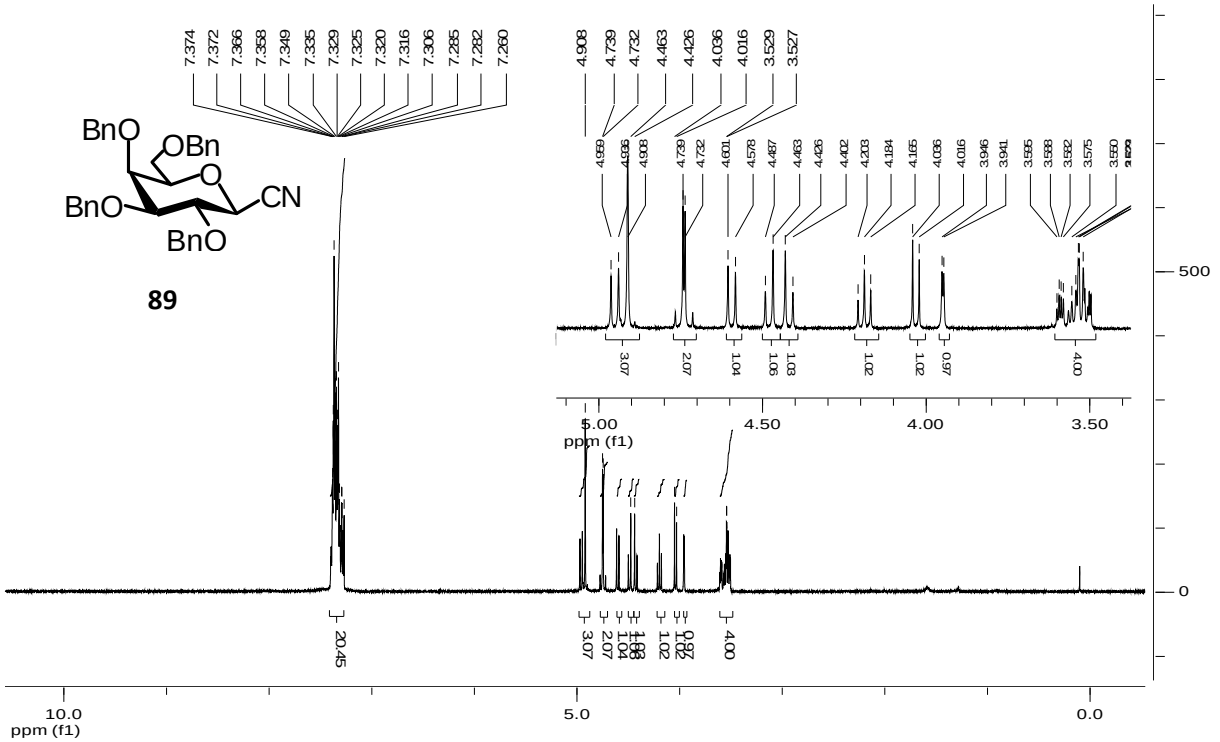

^{13}C NMR (126 MHz, $CDCl_3$)

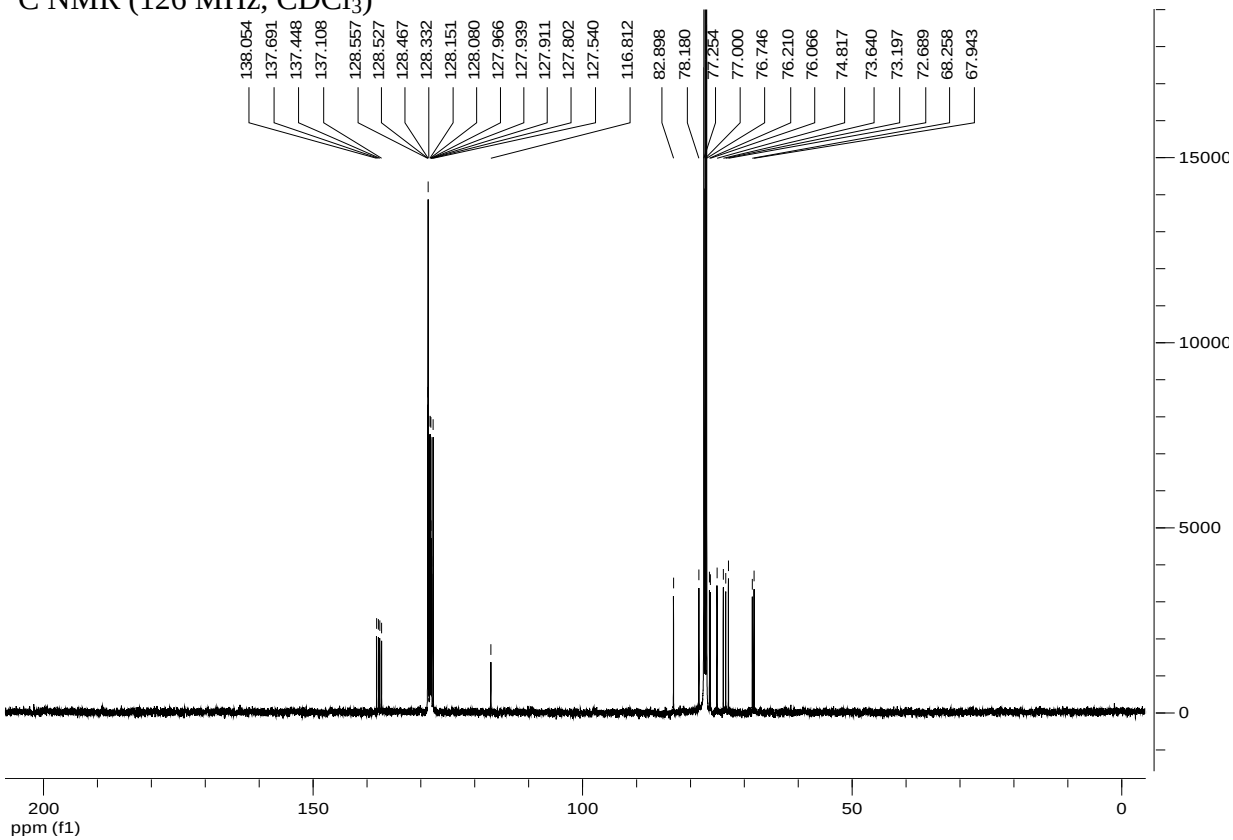

Methyl *Nα*-(S)-[(9H-fluoren-9-ylmethoxy)carbonyl]-*Cδ*-oxo-*C*ε-diazo-α-aminohexan-1-oate (90), ^{1}H NMR (500 MHz, $CDCl_3$)

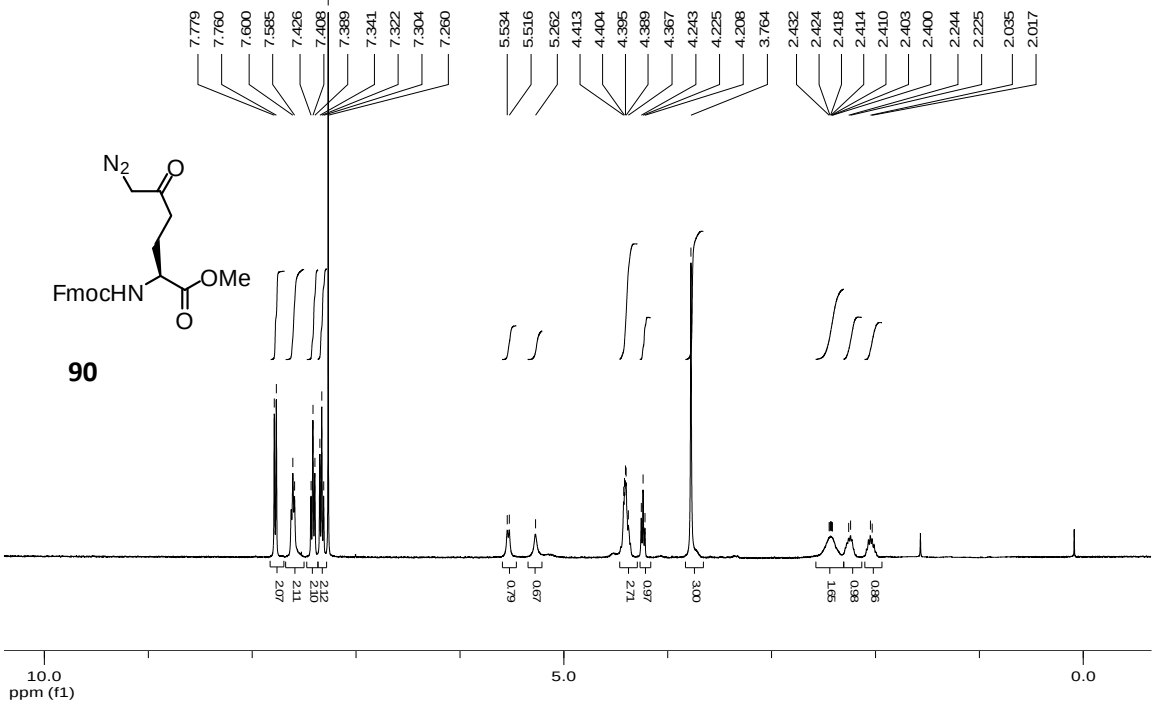

^{13}C DEPT Q135 NMR (101 MHz, $CDCl_3$)

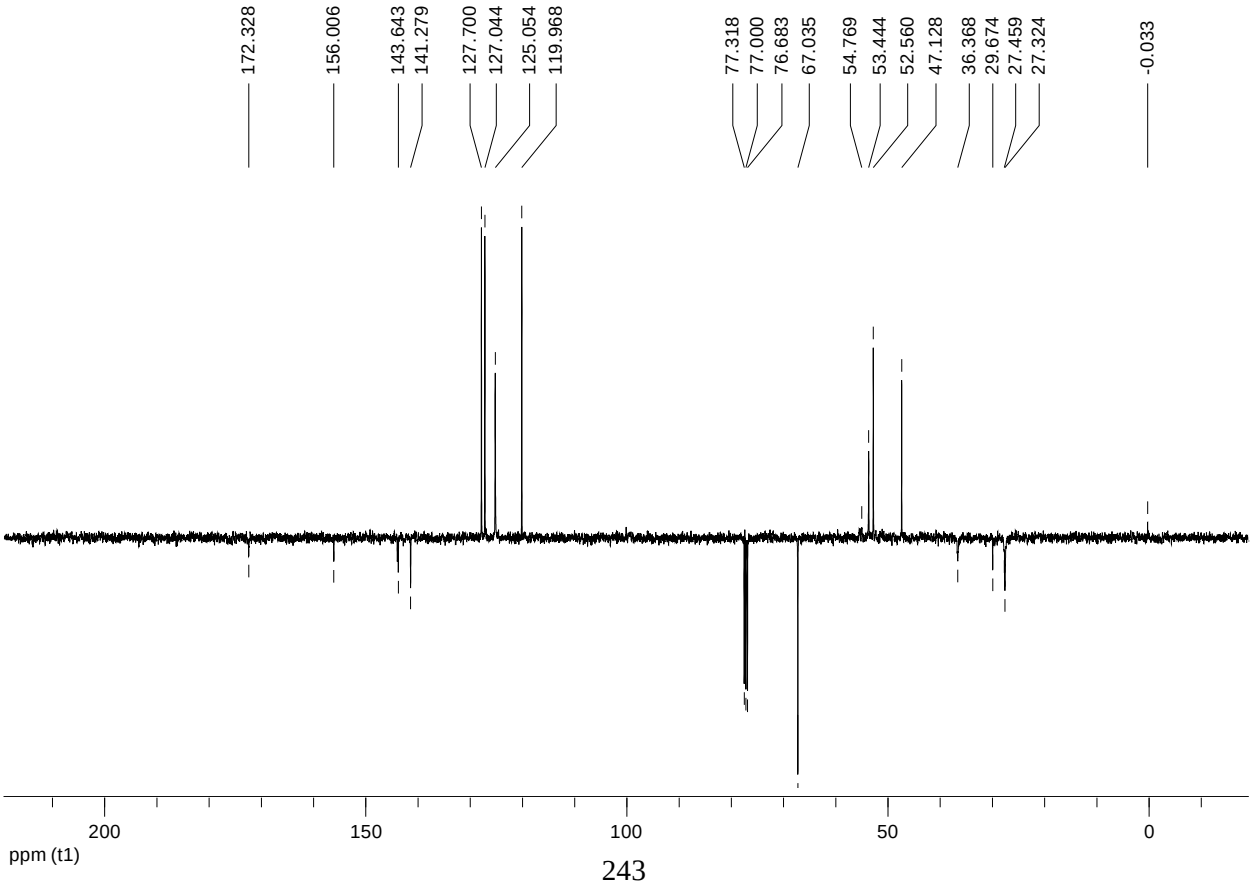

^{13}C NMR (101 MHz, $CDCl_3$)

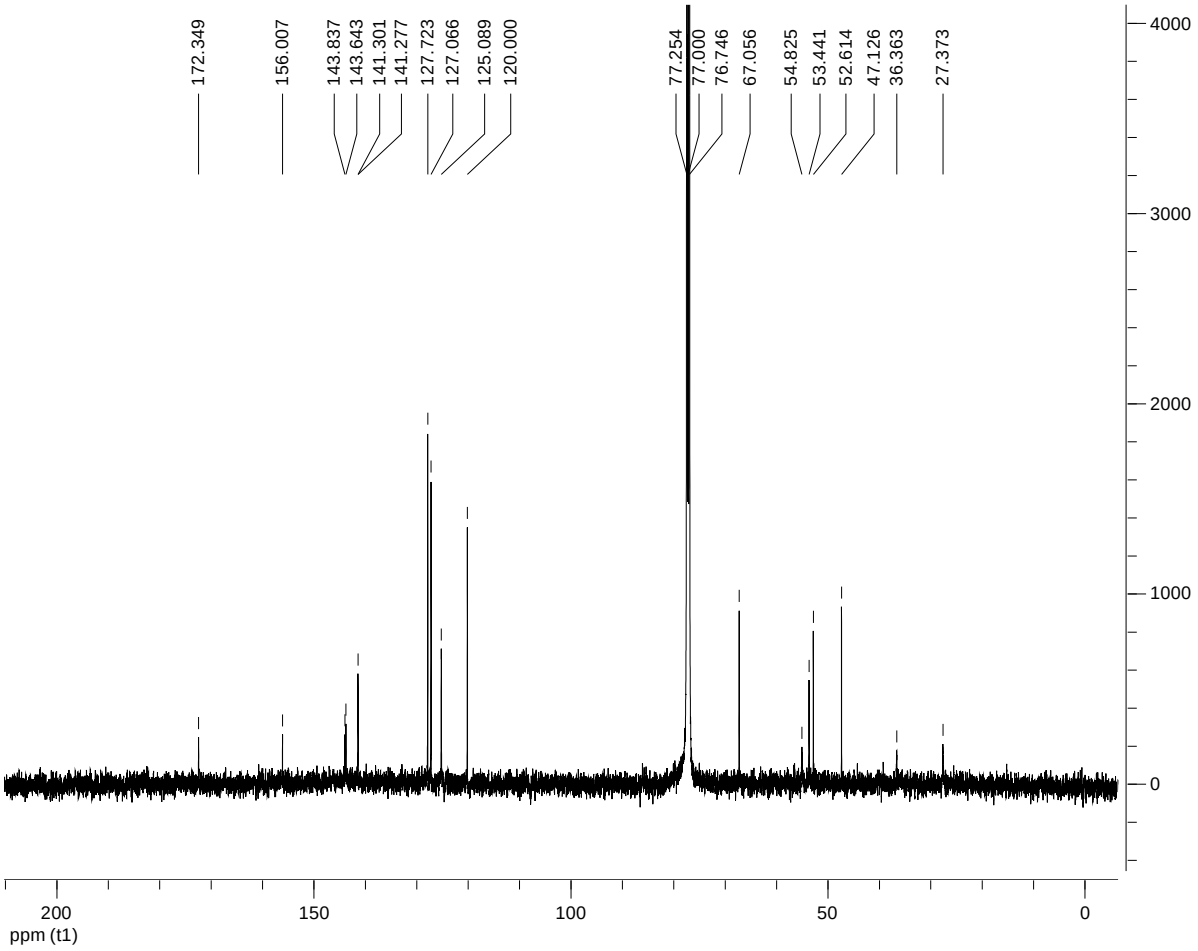

Methyl *Nα*-(S)-[(9H-fluoren-9-ylmethoxy)carbonyl]- *Nε*-[1`-( 2,3,4,6-tetra-*O*-benzyl-α-D-galactopyran-1-yl)-methyl-1`-amino]- homoglutam-ε-amido-1-ate (93),

^{1}H NMR (500 MHz, $CDCl_3$)

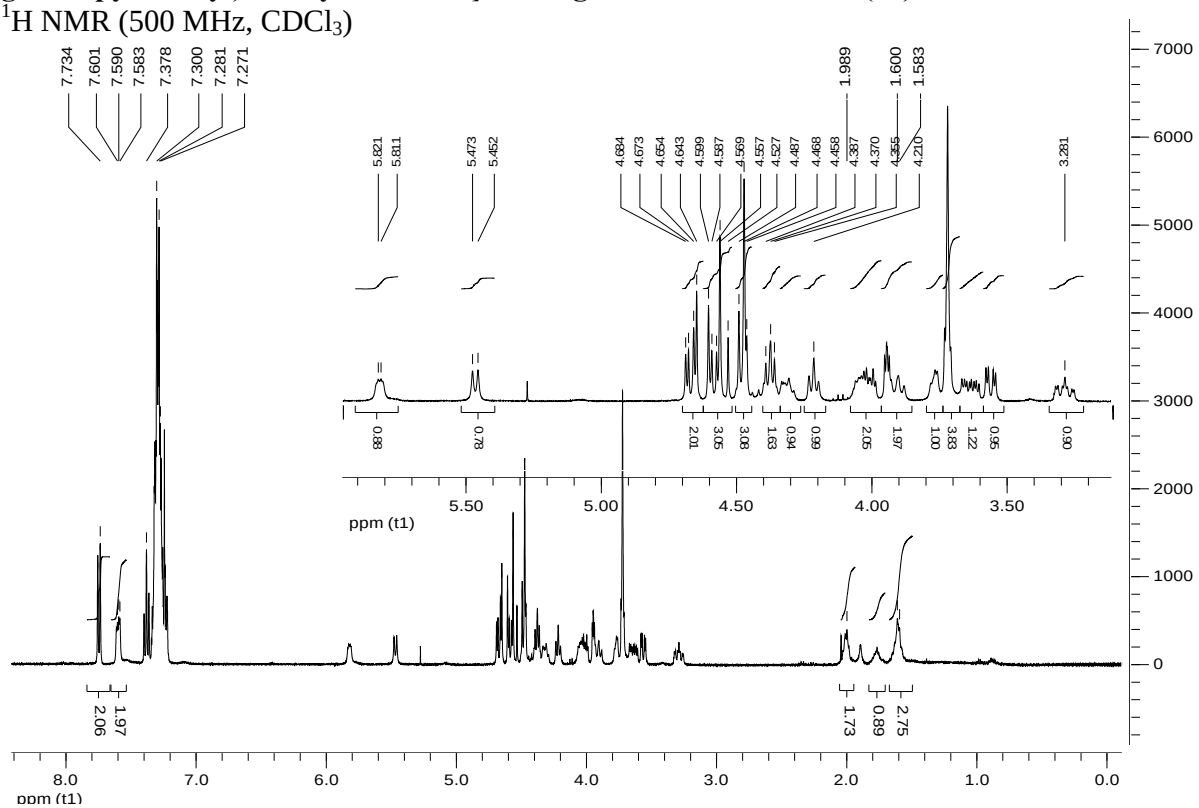

^{13}C DEPT Q135 NMR (101 MHz, $CDCl_3$)

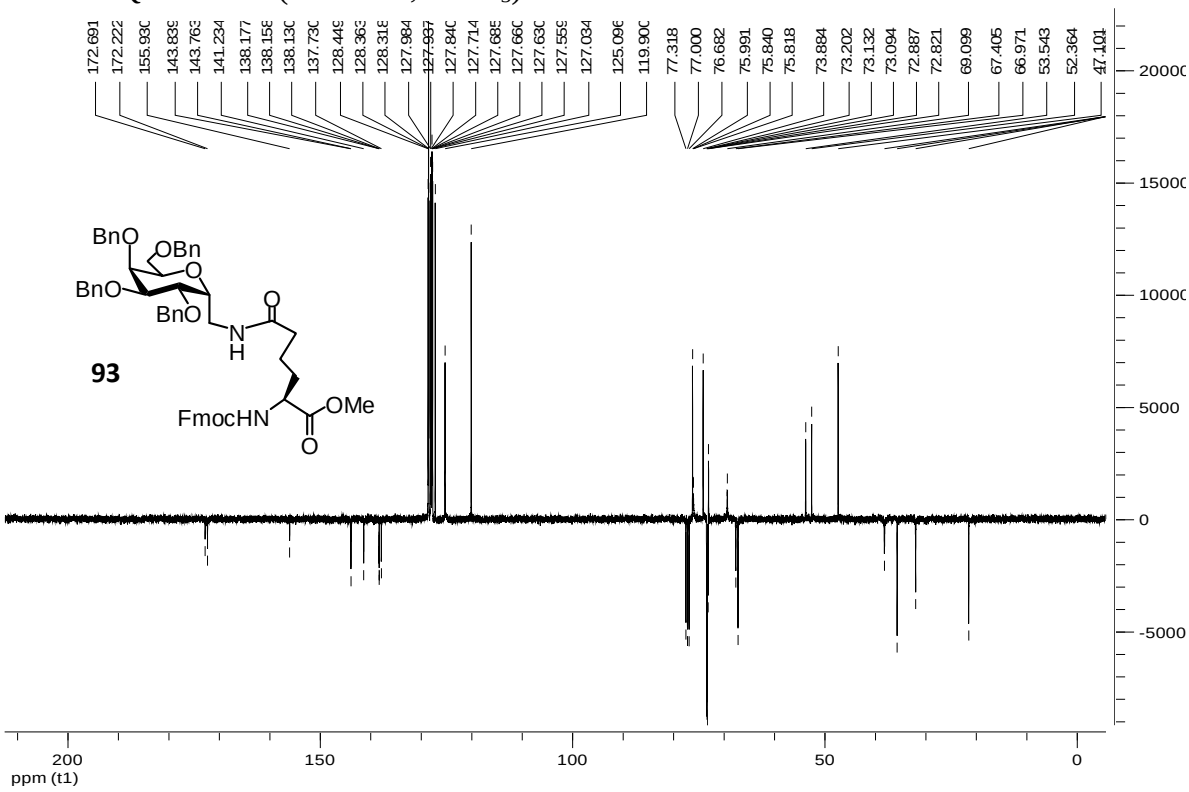

Methyl *Nα*-(S)-[(9H-fluoren-9-ylmethoxy)carbonyl]- *Nδ*-[1`-( 2,3,4,6-tetra-*O*-benzyl-α-D-galactopyran-1-yl)-methyl-1`-amino]- glutam-δ-amido-1-ate (94),

^{1}H NMR (400 MHz, $CDCl_3$)

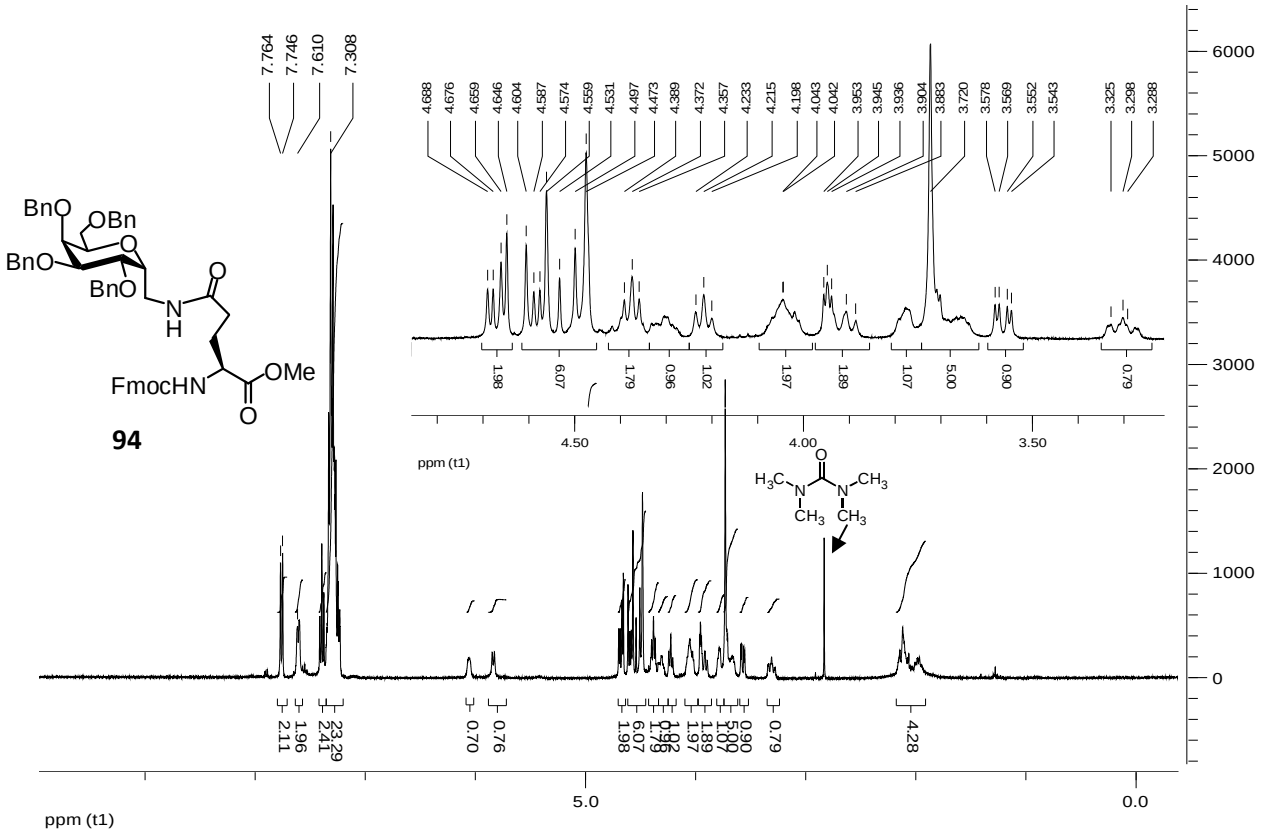

^{13}C NMR (101 MHz, $CDCl_3$)

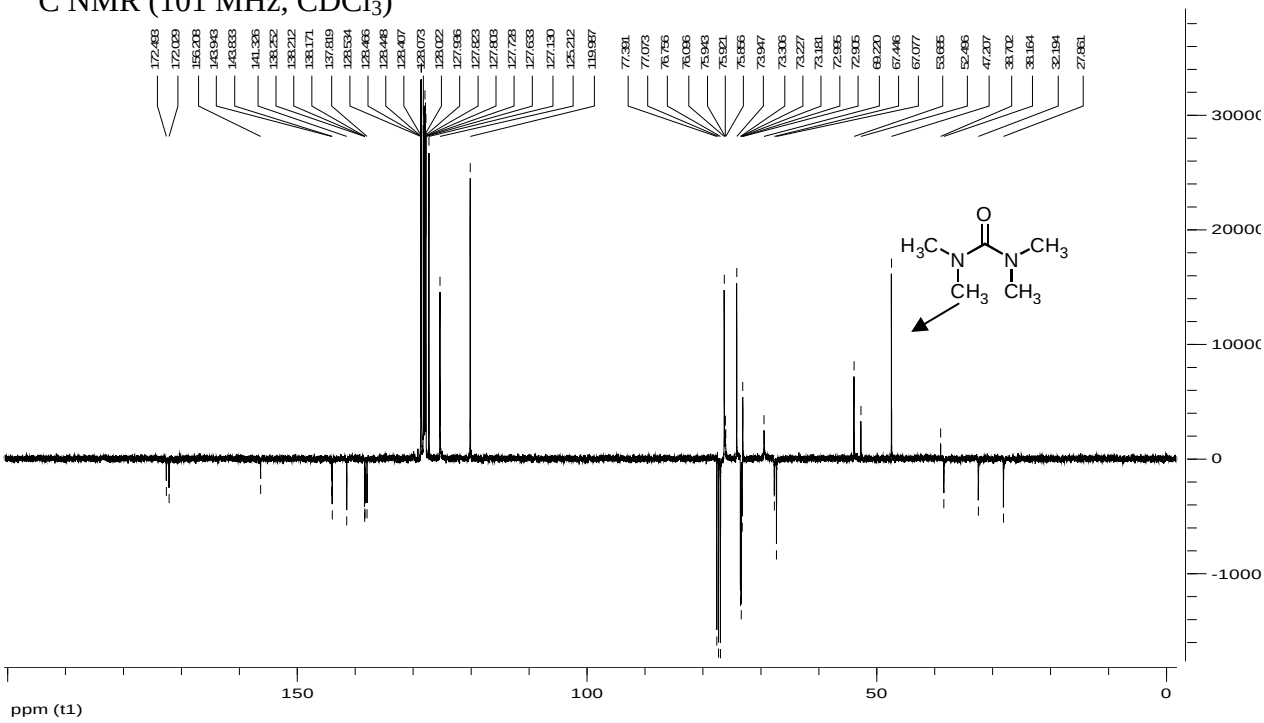

***Nα*-(S)-[(9H-fluoren-9-ylmethoxy)carbonyl]- *Nδ*-[1`-( 2,3,4,6-tetra-*O*-benzyl-α-D-galactopyran-1-yl)-methyl-1`-amino]- glutamine (95)**, ^{1}H NMR (500 MHz, $CDCl_3$)

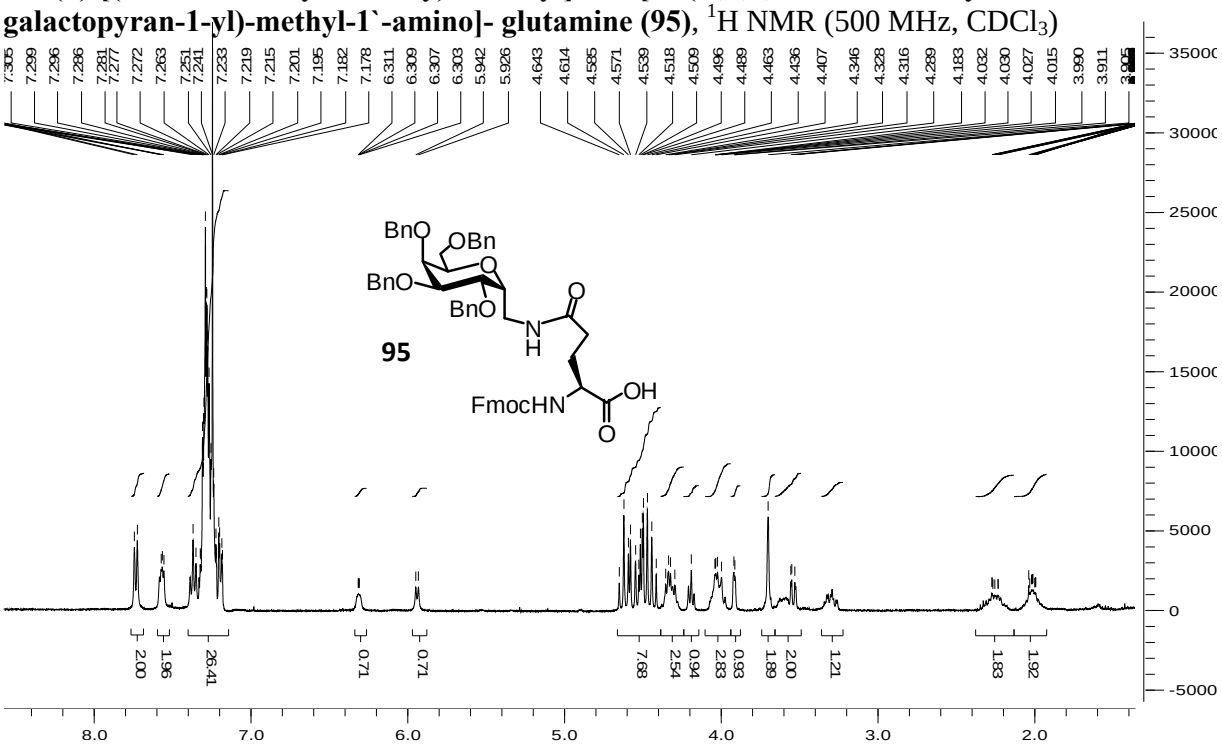

^{13}C NMR (101 MHz, $CDCl_3$)

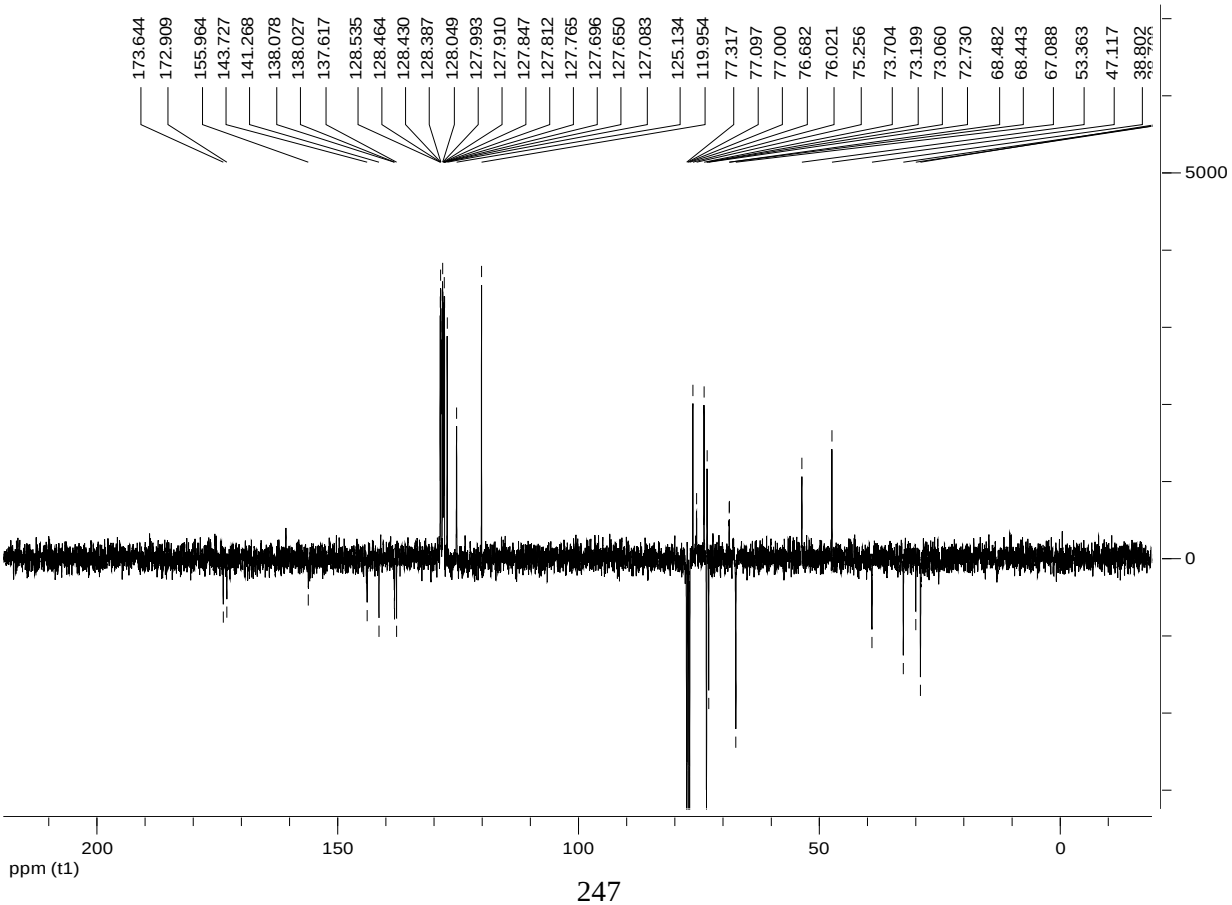

***Nα*-(S)-[(9H-fluoren-9-ylmethoxy)carbonyl]- *Nδ*-[1`-( 2,3,4,6-tetra-*O*-benzyl-β-D-galactopyran-1-yl)-methyl-1`-amino]- glutamine (97)** ^{1}H NMR (500 MHz, $CDCl_3$)

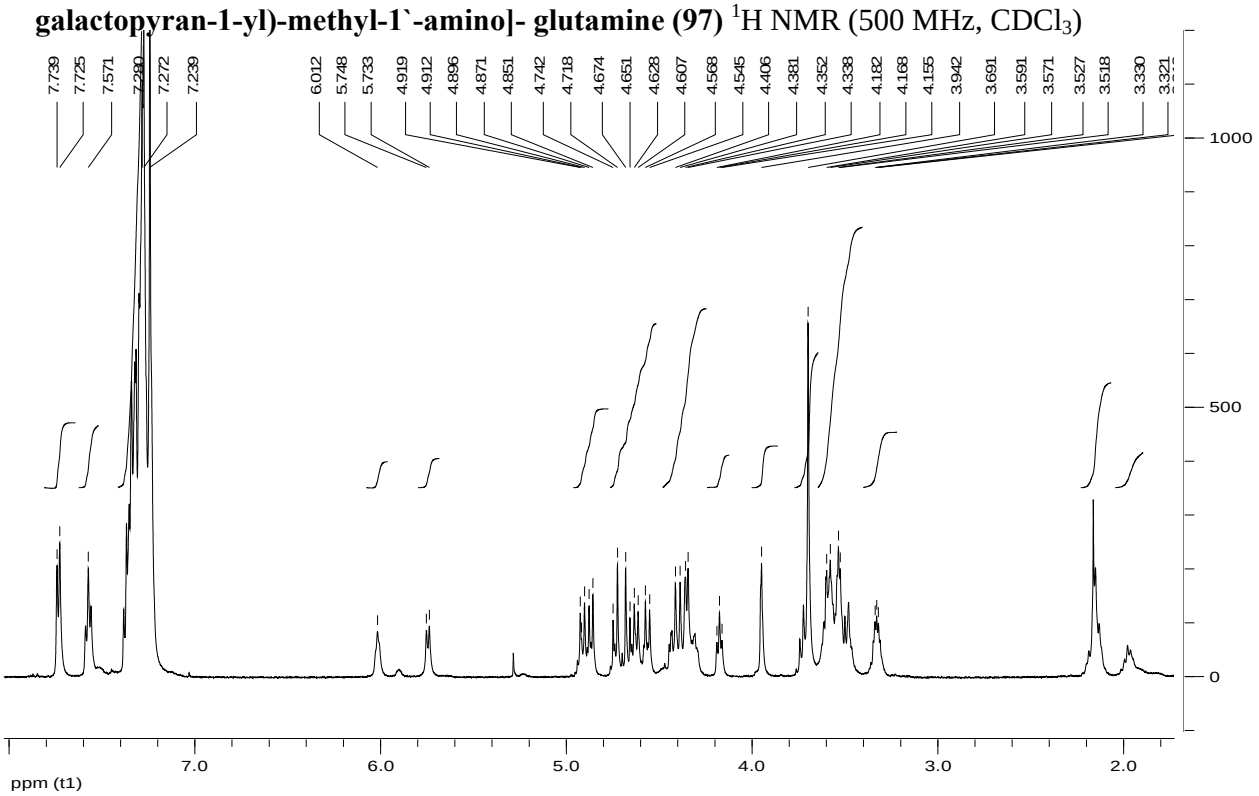

^{13}C NMR (101 MHz, $CDCl_3$)

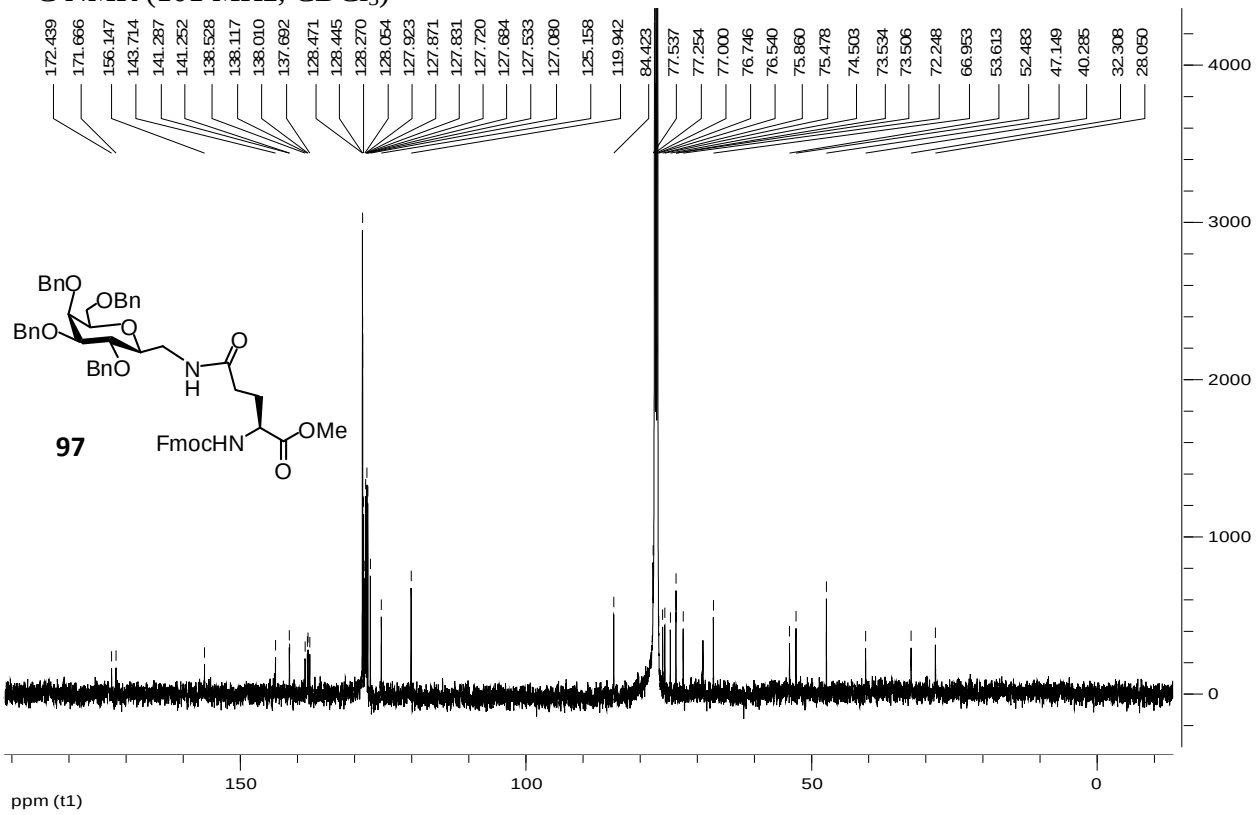

97

Thiophenyl 3,4-*O*-isopropylidene-6-*O*-*tert*-butyldimethylsilyl-β-D–*lyxo*-hexa-2-ulose (103), ^{1}H NMR (500 MHz, $CDCl_3$)

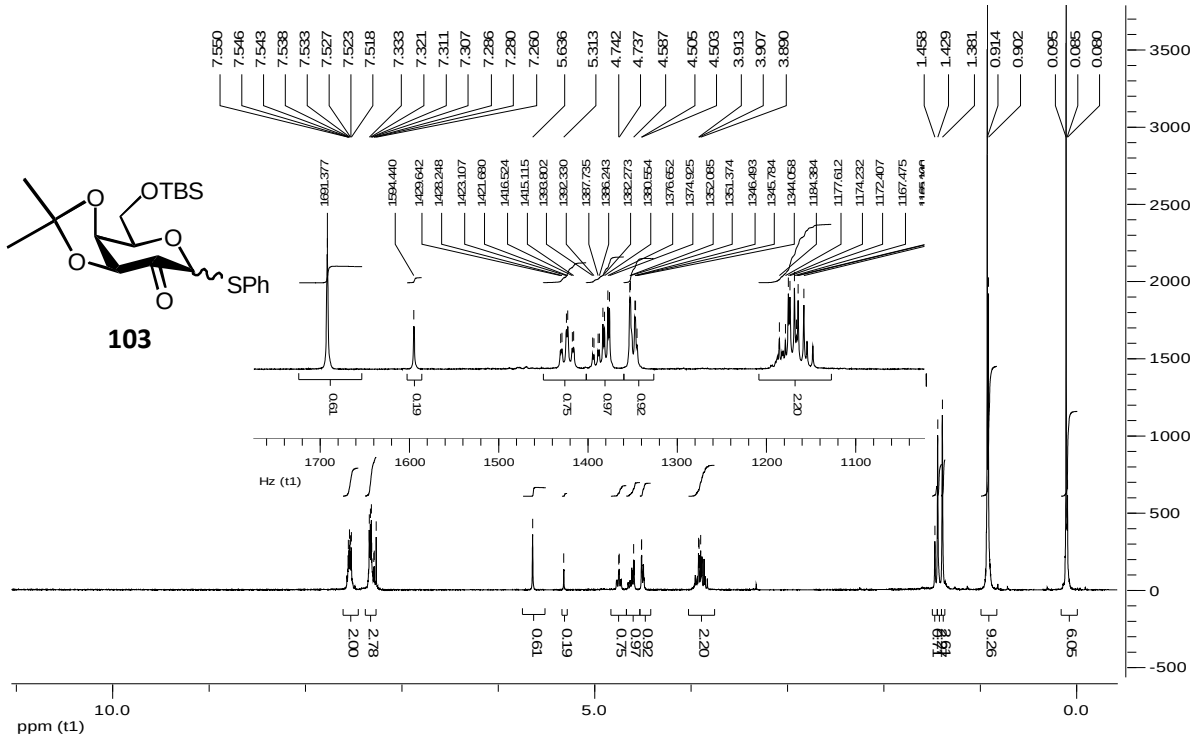

^{13}C NMR (101 MHz, $CDCl_3$)

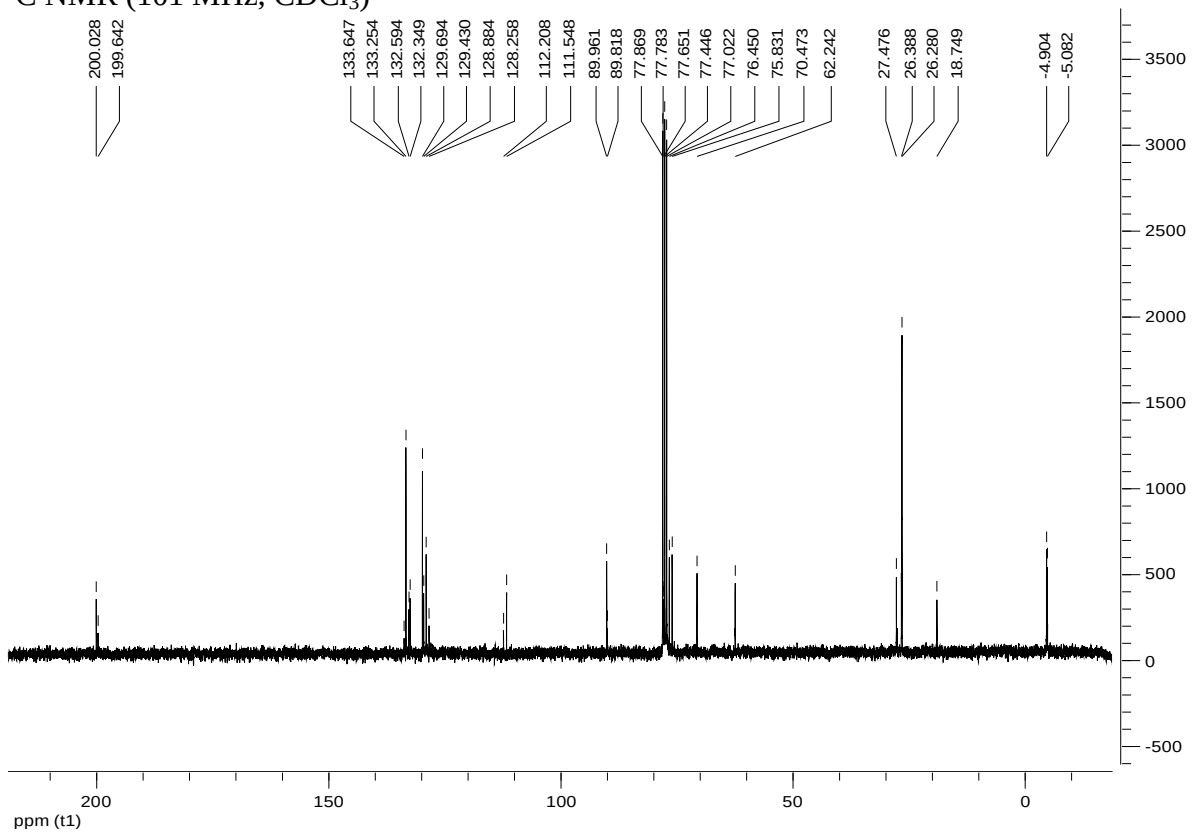

***tert*-butyl-4-(S)-[2`-(*E*)-1`-[(2-diphenylphosphino)-benzoyl]-oxy-prop-2`-en-3`-yl]-2,2-dimethyl-1,3-oxazolidine-3-carboxylate (104)**, ^{1}H NMR (300 MHz, $CDCl_3$)

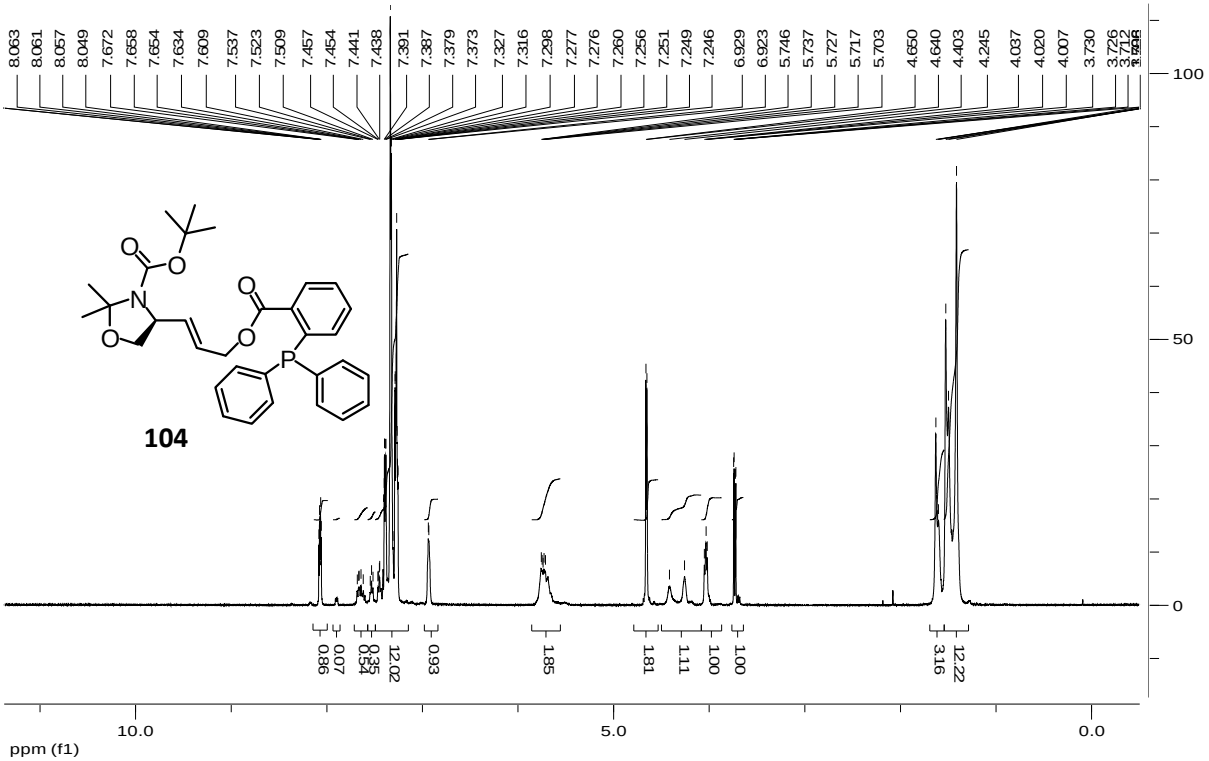

104

^{13}C NMR (101 MHz, $CDCl_3$)

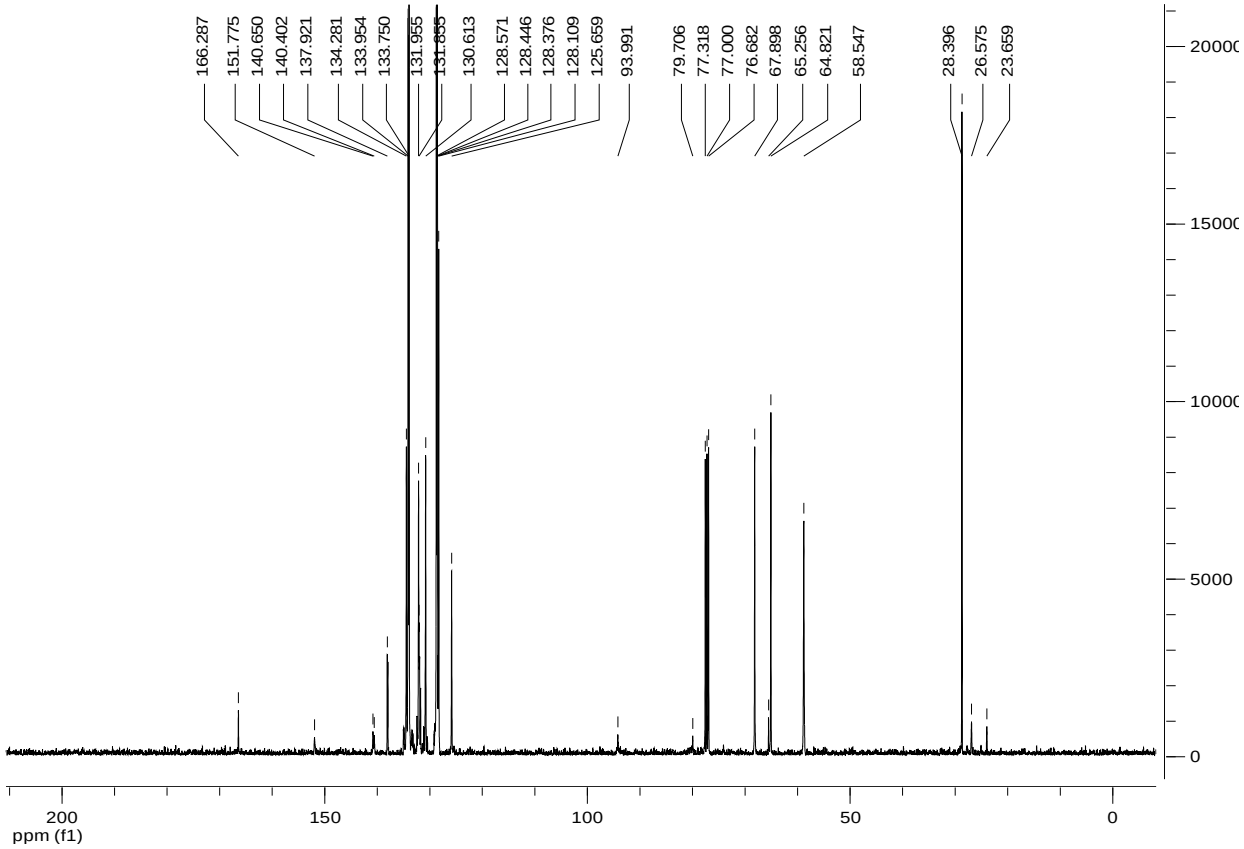

***tert*-butyl-4(S)-[3`-(*S*)-but-1`-en-3`-yl]-2,2-dimethyl-1,3-oxazolidine-3-carboxylate (major diastereromer, 105)**, ^{1}H NMR (500 MHz, 20 ^{o}C, $CDCl_3$)

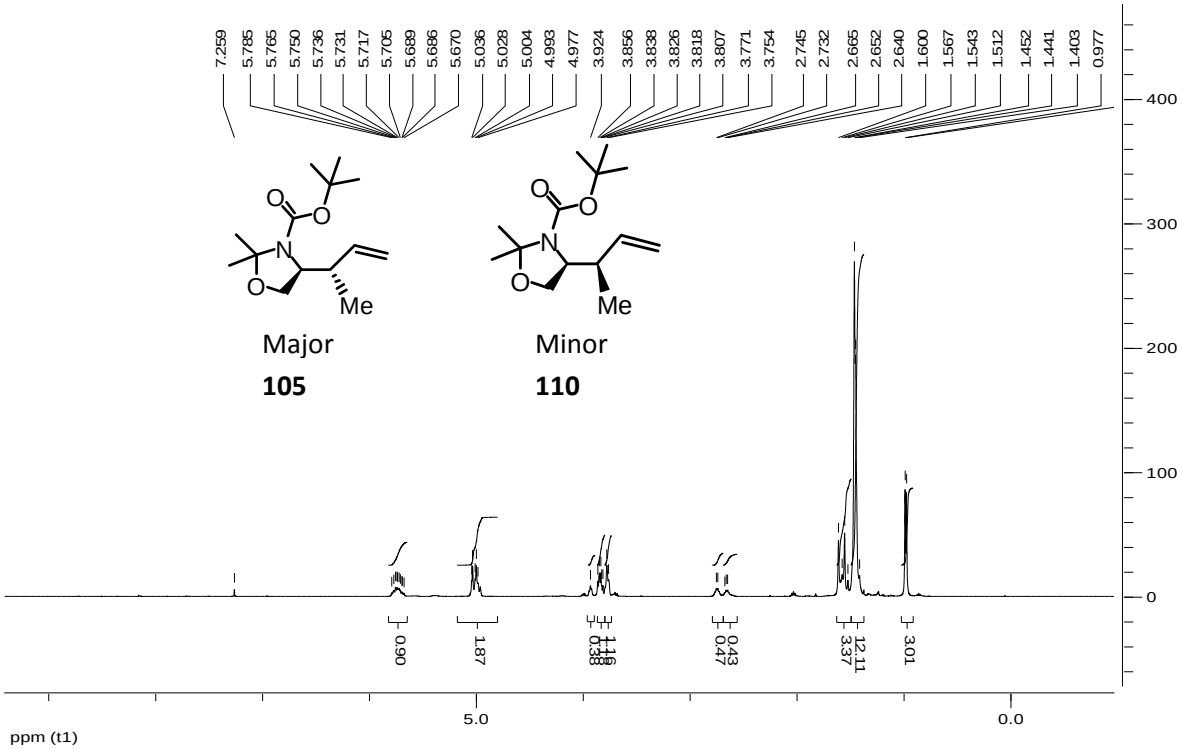

^{1}H NMR (500 MHz, 50 ^{o}C, $CDCl_3$)

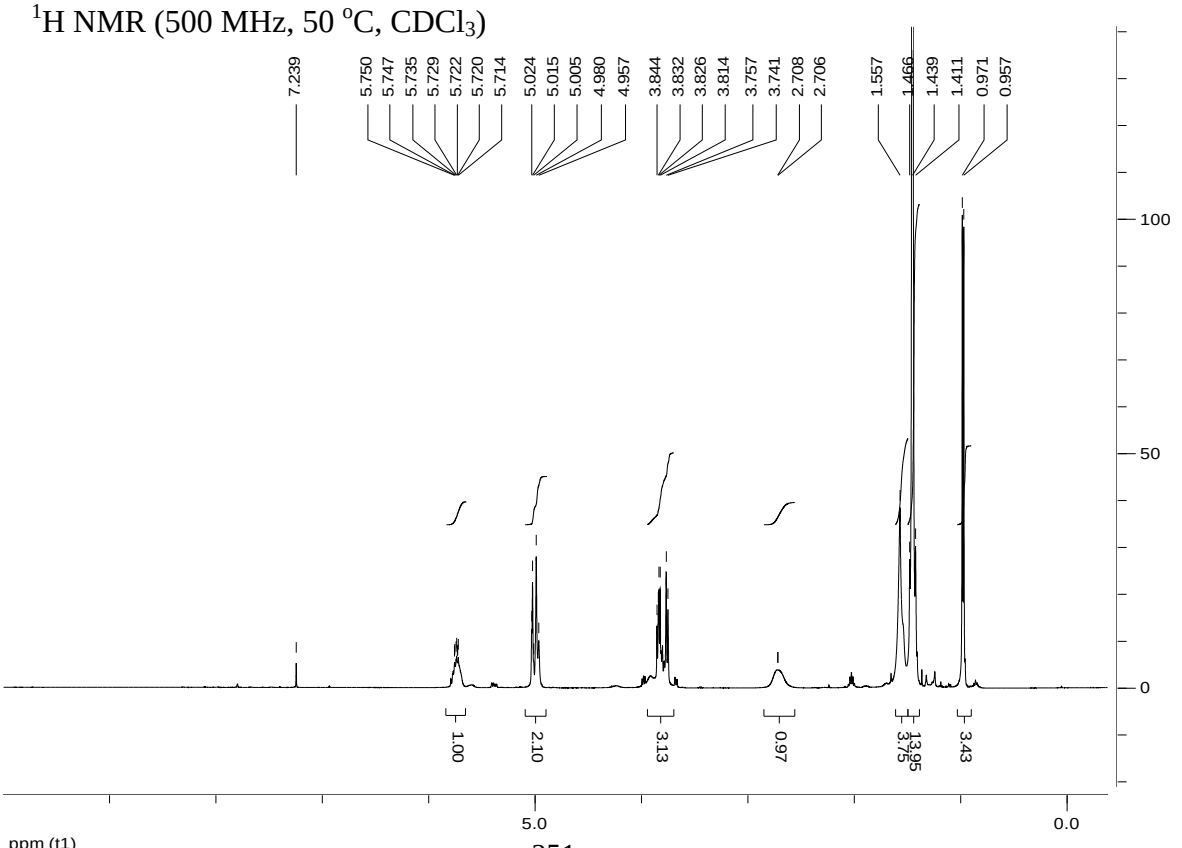

***tert*-butyl-4(S)-[3`-(*S*)-but-1`-en-3`-yl]-2,2-dimethyl-1,3-oxazolidine-3-carboxylate (major diastereromer, 105)**, ^{13}C NMR (101 MHz, 20 ^{o}C, $CDCl_3$)

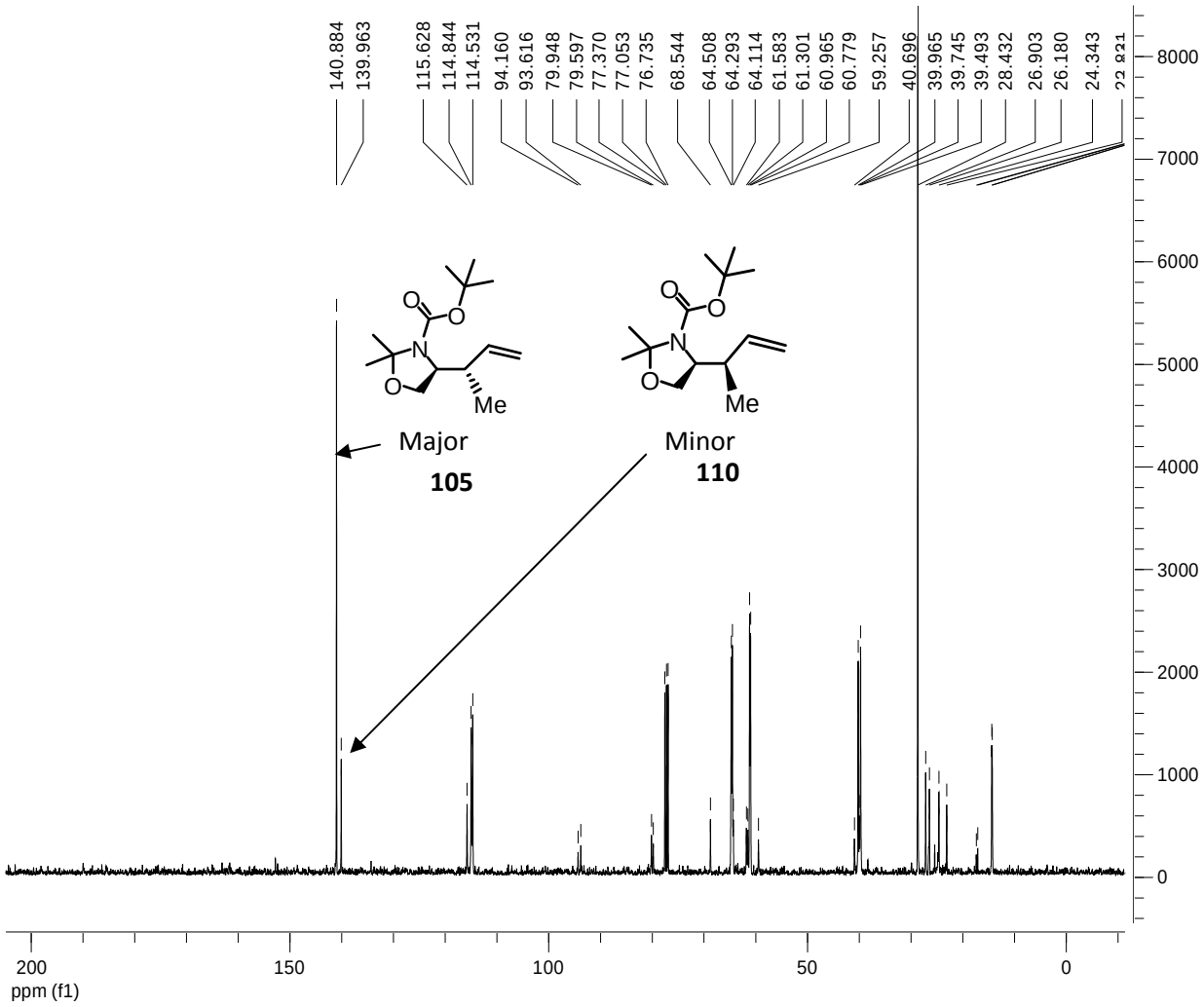

***tert*-butyl-4(S)-[2`-(Z)-1`-methoxy-1`-oxoprop-2`-en-3`-yl]-2,2-dimethyl-1,3-oxazolidine-3-carboxylate (107)**, ^{1}H NMR (300 MHz, $CDCl_3$)

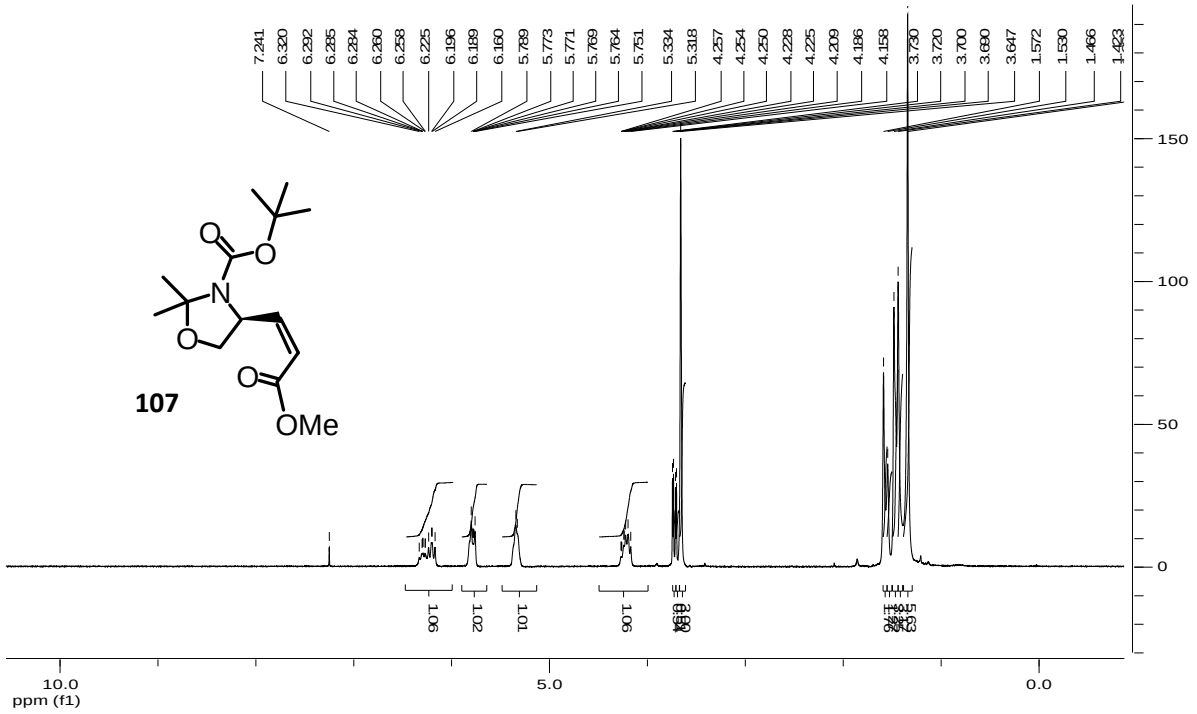

107

^{13}C NMR (75 MHz, $CDCl_3$)

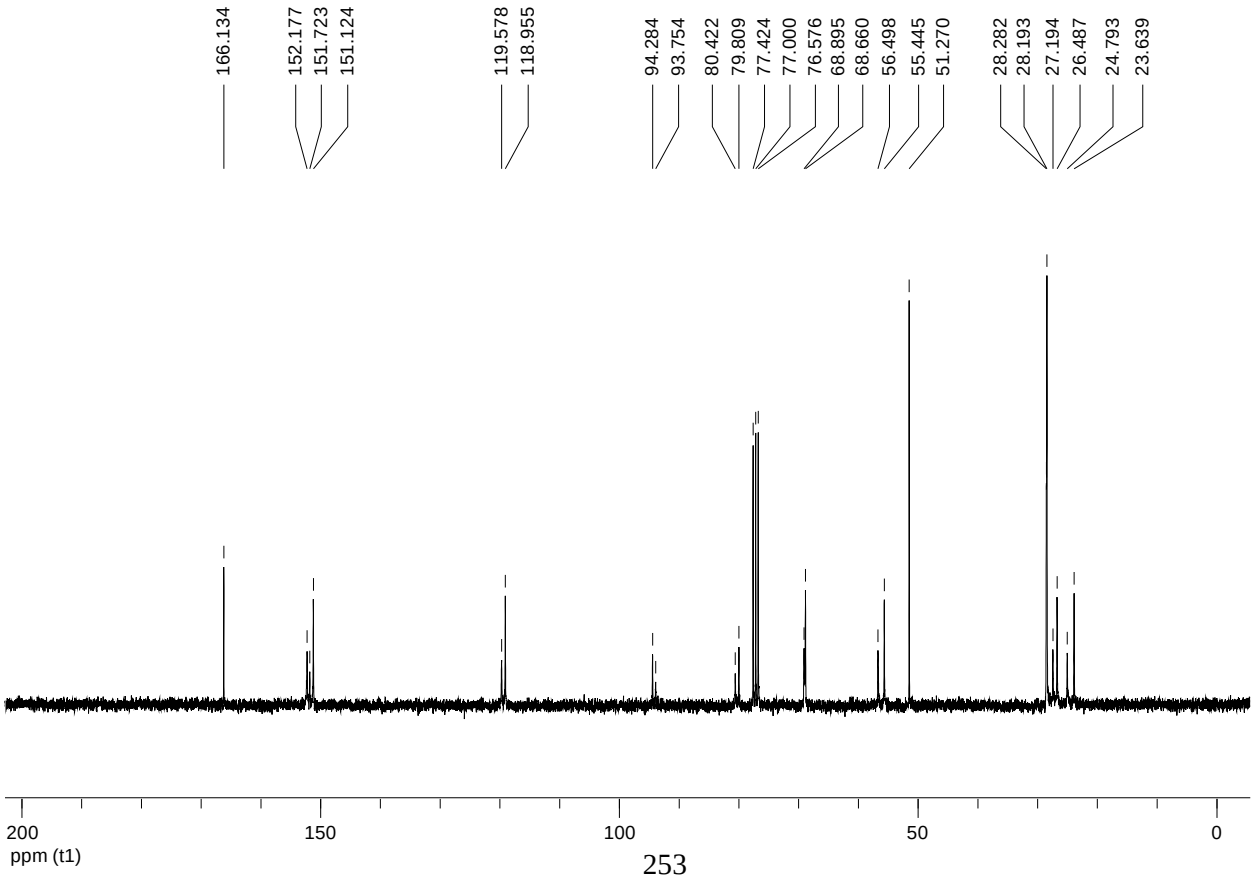

***tert*-butyl-4(S)-[2`-(E)-1`-methoxy-1`-oxoprop-2`-en-3`-yl]-2,2-dimethyl-1,3-oxazolidine-3-carboxylate (108)**, ^{1}H NMR (500 MHz, $CDCl_3$)

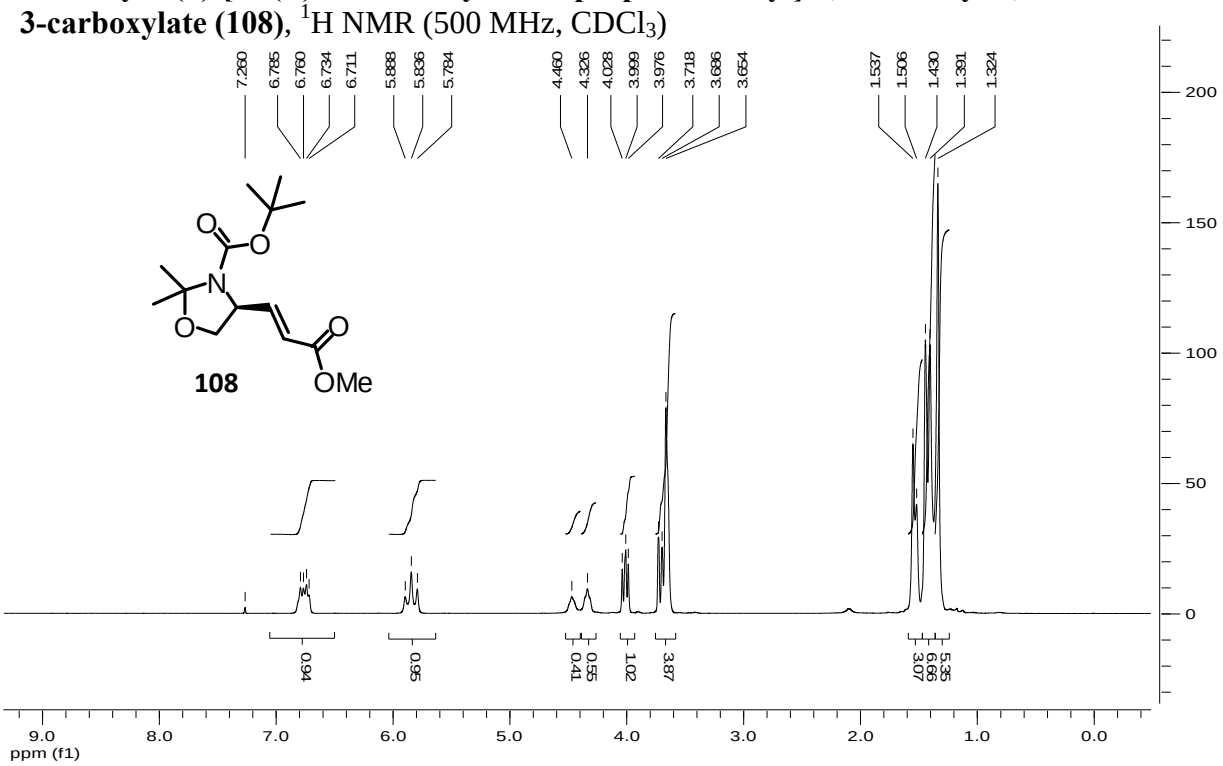

^{13}C NMR (101 MHz, $CDCl_3$)

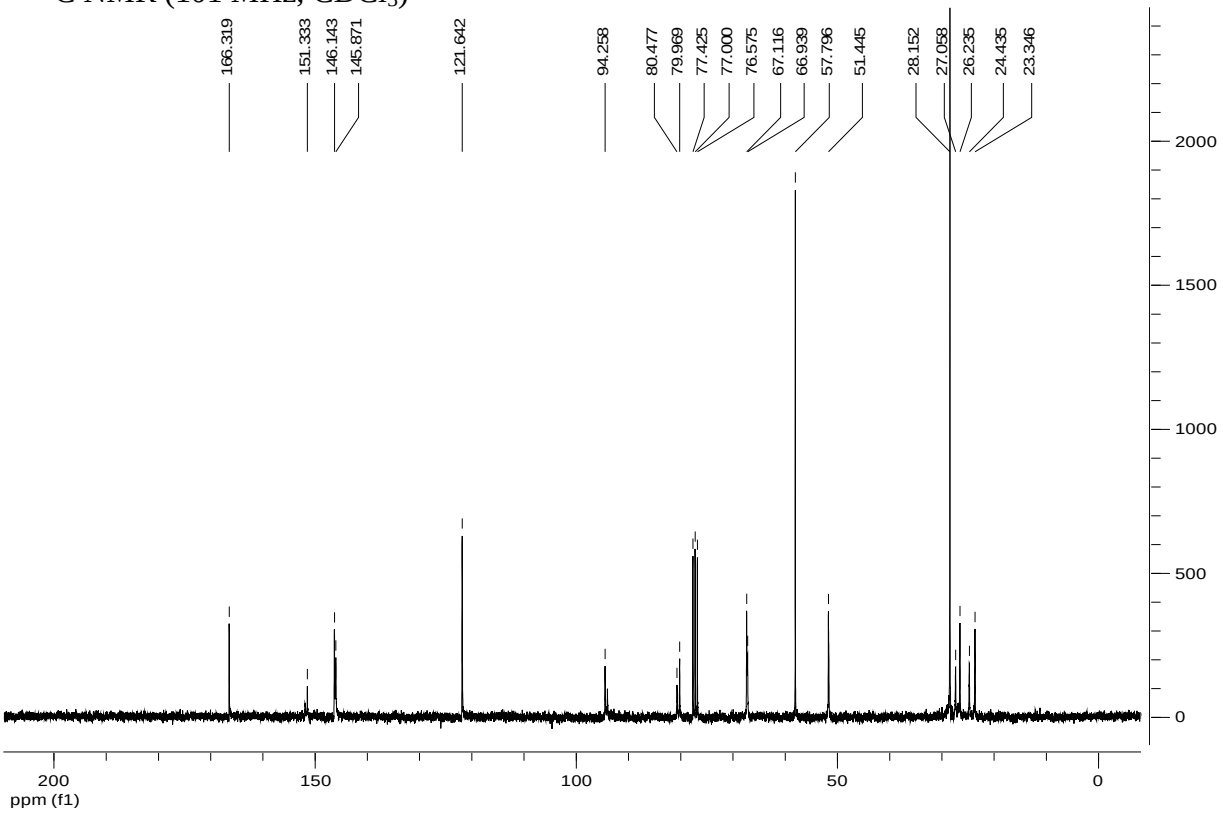

***tert*-butyl-4-(S)-[2`-(*E*)-1`-hydroxy-prop-2`-en-3`-yl]-2,2-dimethyl-1,3-oxazolidine-3-carboxylate (109)**, ^{1}H NMR (300 MHz, $CDCl_3$)

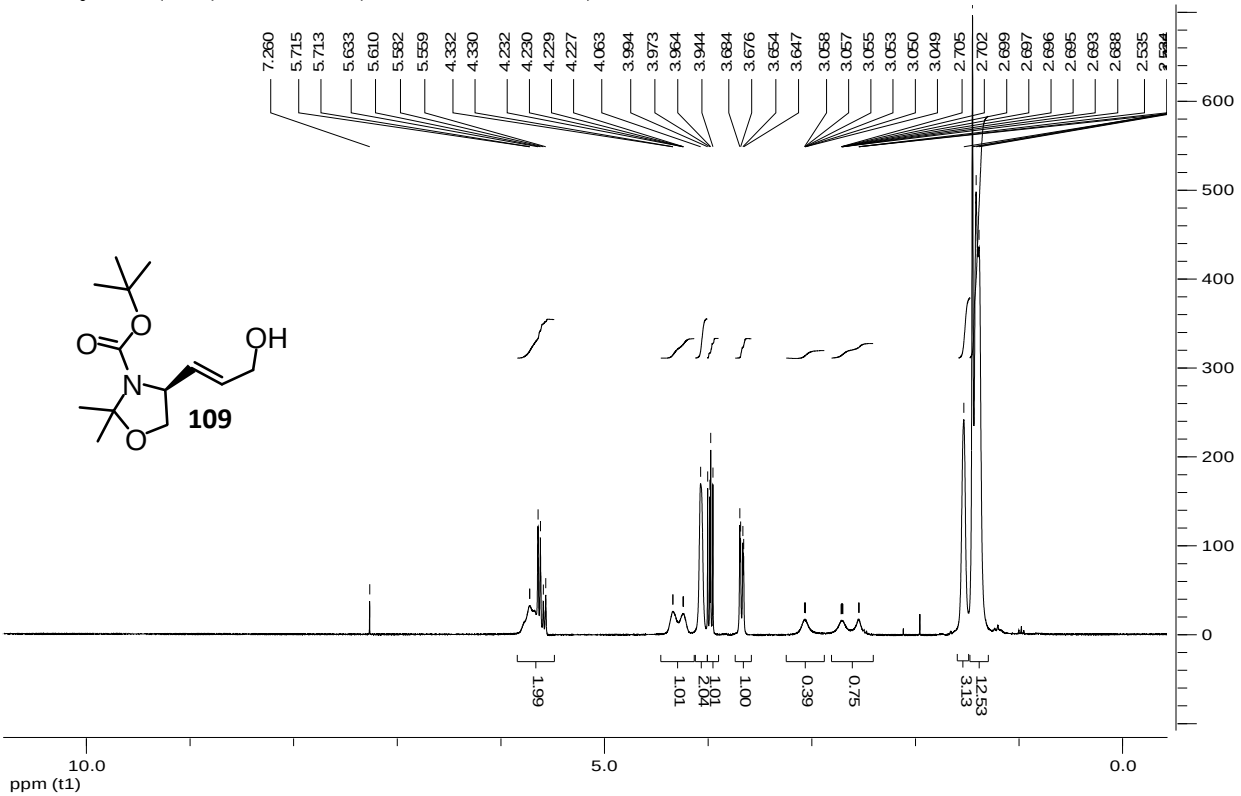

^{13}C NMR (101 MHz, $CDCl_3$)

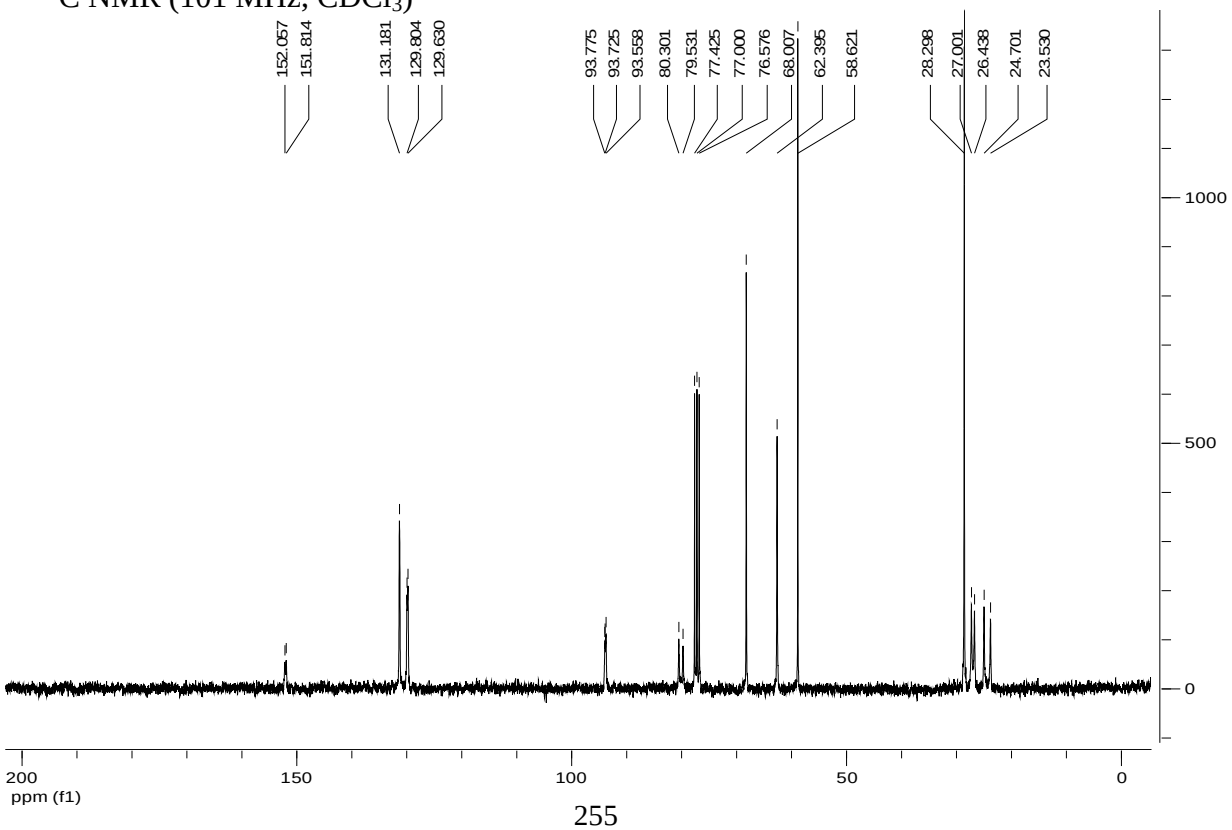

***tert*-butyl-4-(S)-[2`-(*Z*)-1`-hydroxy-prop-2`-en-3`-yl]-2,2-dimethyl-1,3-oxazolidine-3-carboxylate (112)**, ^{1}H NMR (300 MHz, $CDCl_3$)

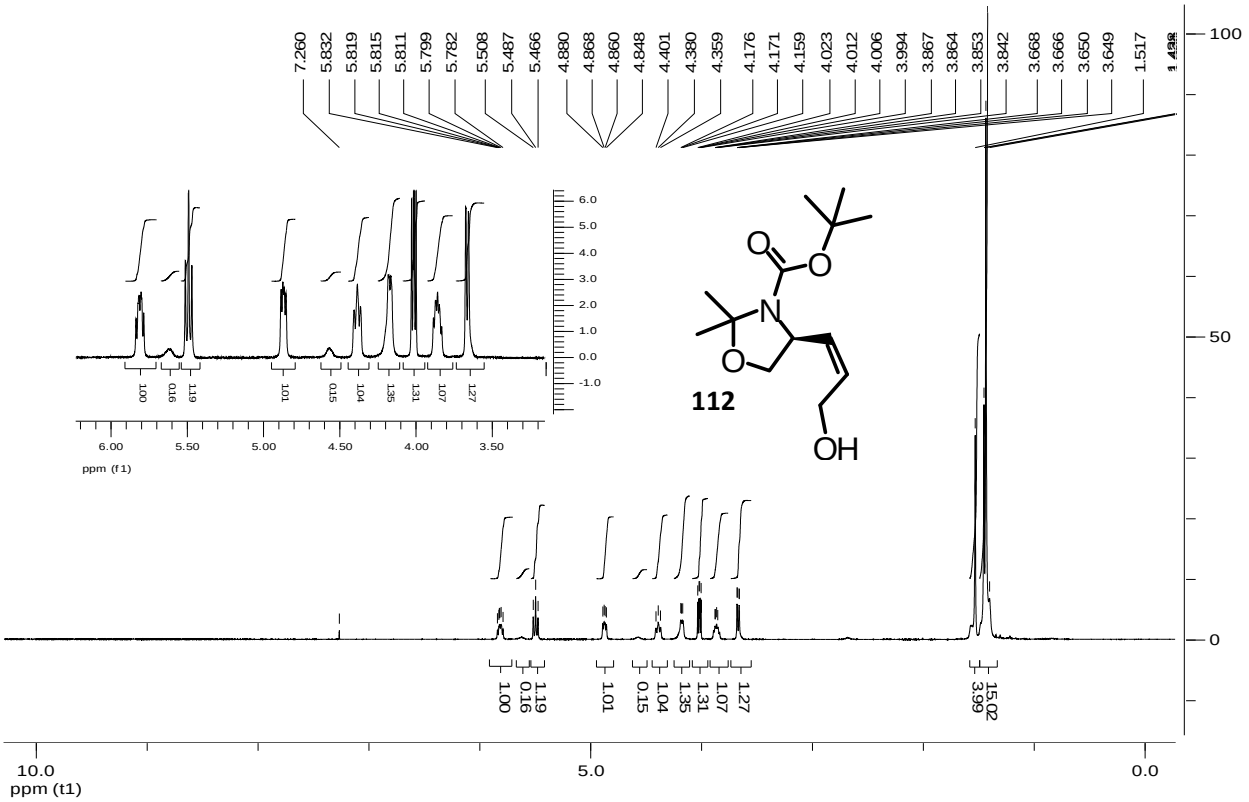

^{13}C DEPT Q135 NMR (101 MHz, $CDCl_3$)

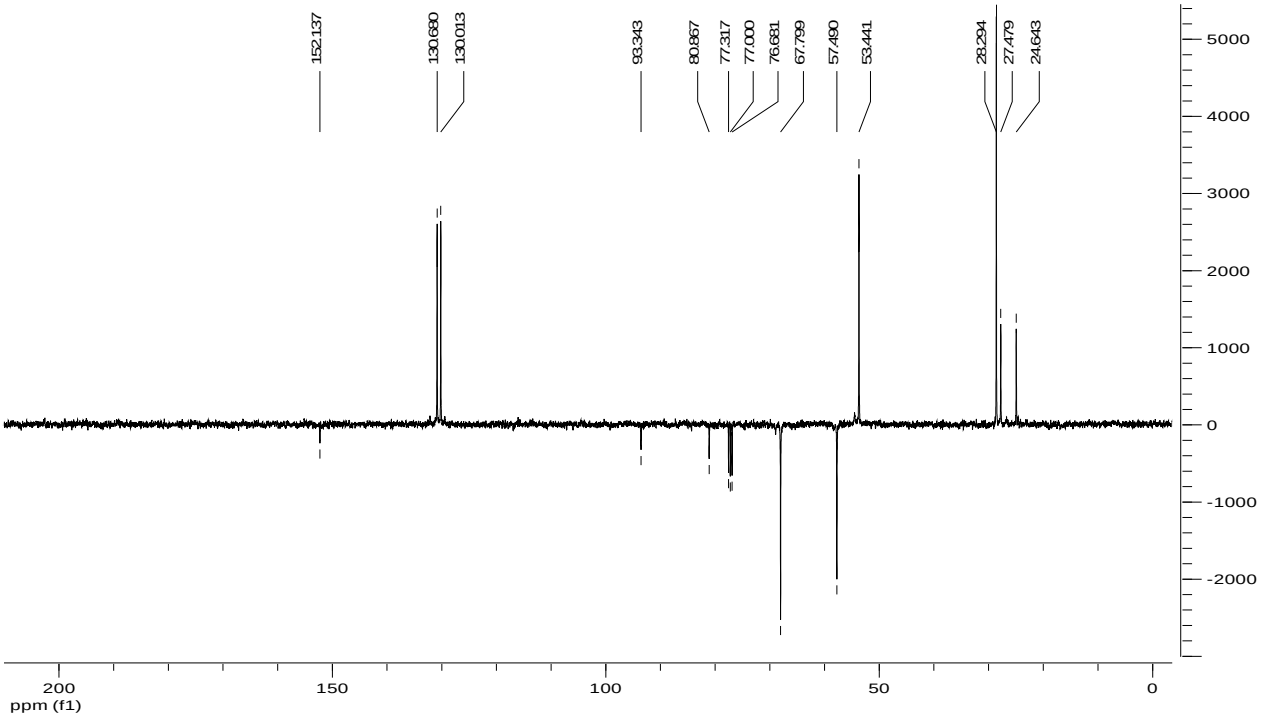

***tert*-butyl-4-(S)-[2`-(Z)-1`-[(2-diphenylphosphino)-benzoyl]-oxy-prop-2`-en-3`-yl]-2,2-dimethyl-1,3-oxazolidine-3-carboxylate (113)**, ^{1}H NMR (500 MHz, $CDCl_3$)

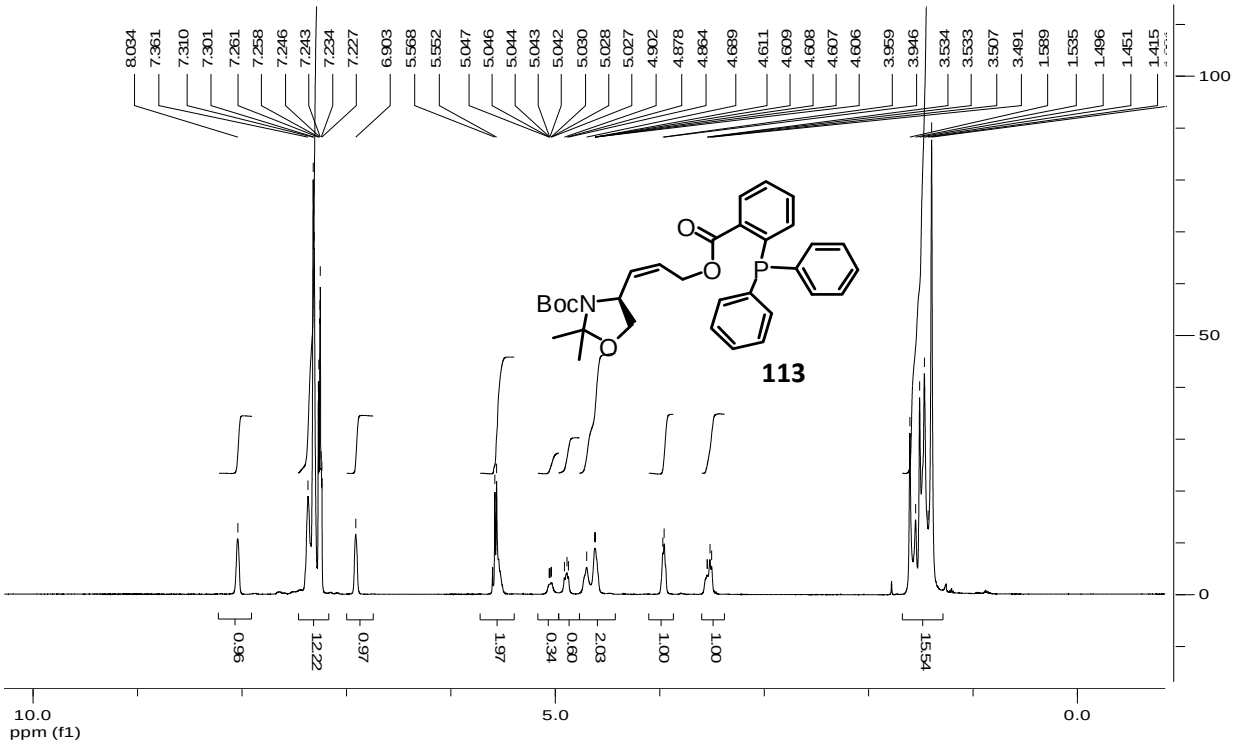

^{13}C NMR (101 MHz, $CDCl_3$)

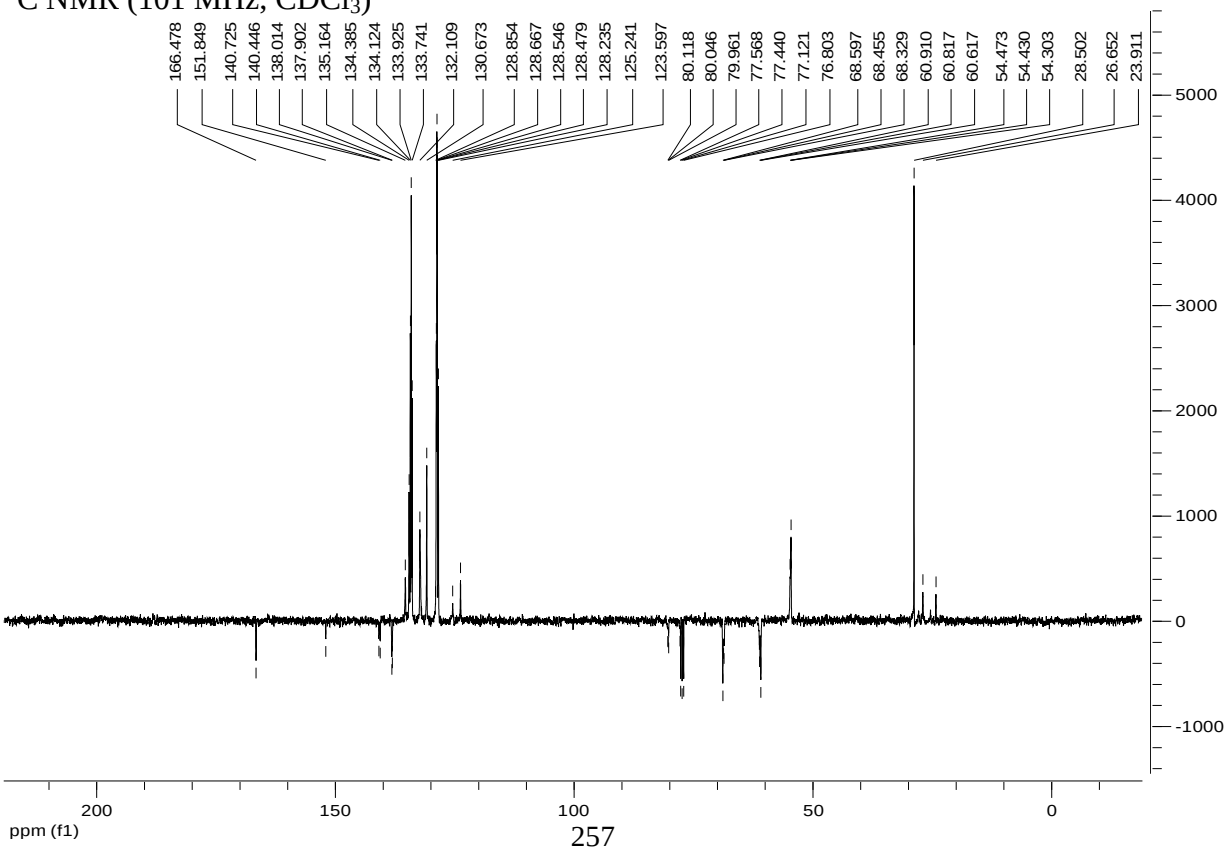

Thiophenyl 3,4-*O*-isopropylidene-β-D-galactopyranose (115),[1]H NMR (400 MHz, $CDCl_3$)

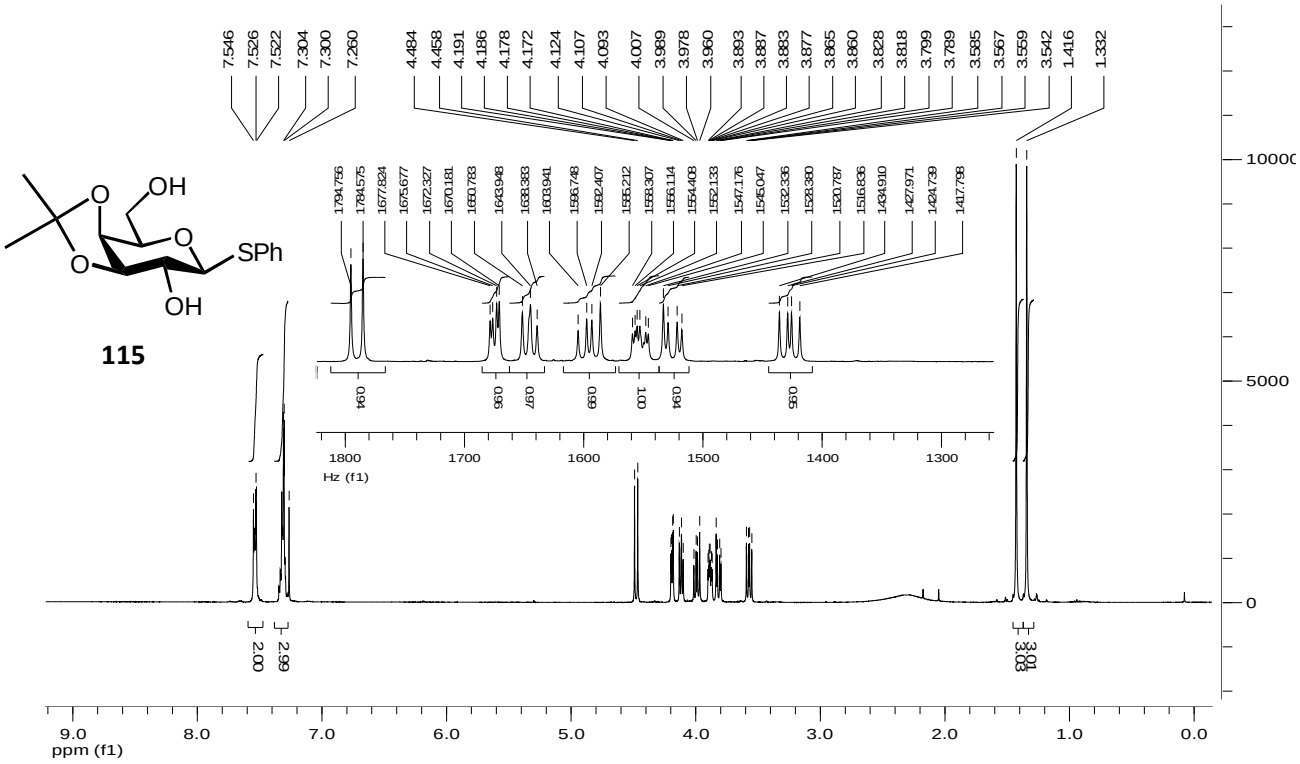

Thiophenyl 3,4-*O*-isopropylidene-6-*O*-*tert*-butyldimethylsilyl-β-D-galactopyranose (116),[1]H NMR (400 MHz, $CDCl_3$)

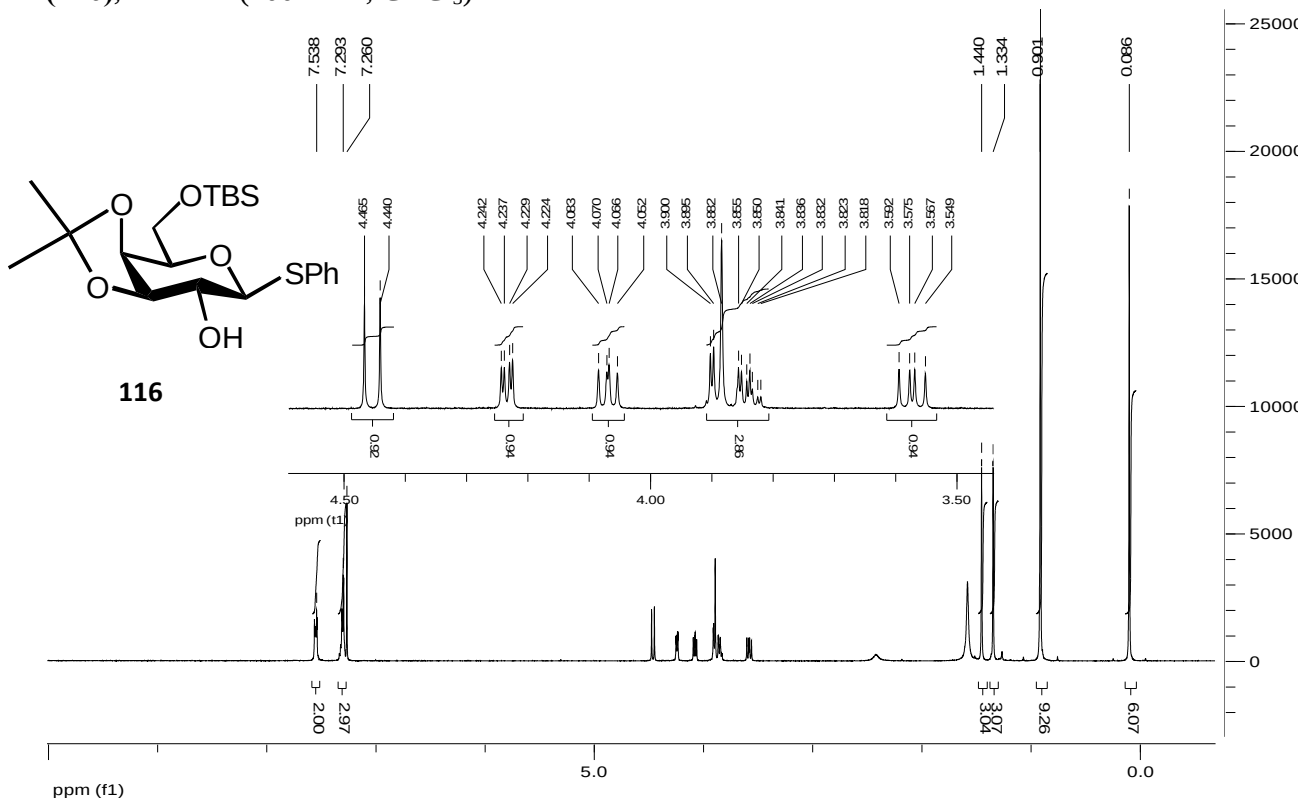

Thiophenyl 3,4-*O*-isopropylidene-6-*O*-triisopropylsilyl-β-D-galactopyranose (119),

^{1}H NMR (400 MHz, $CDCl_3$)

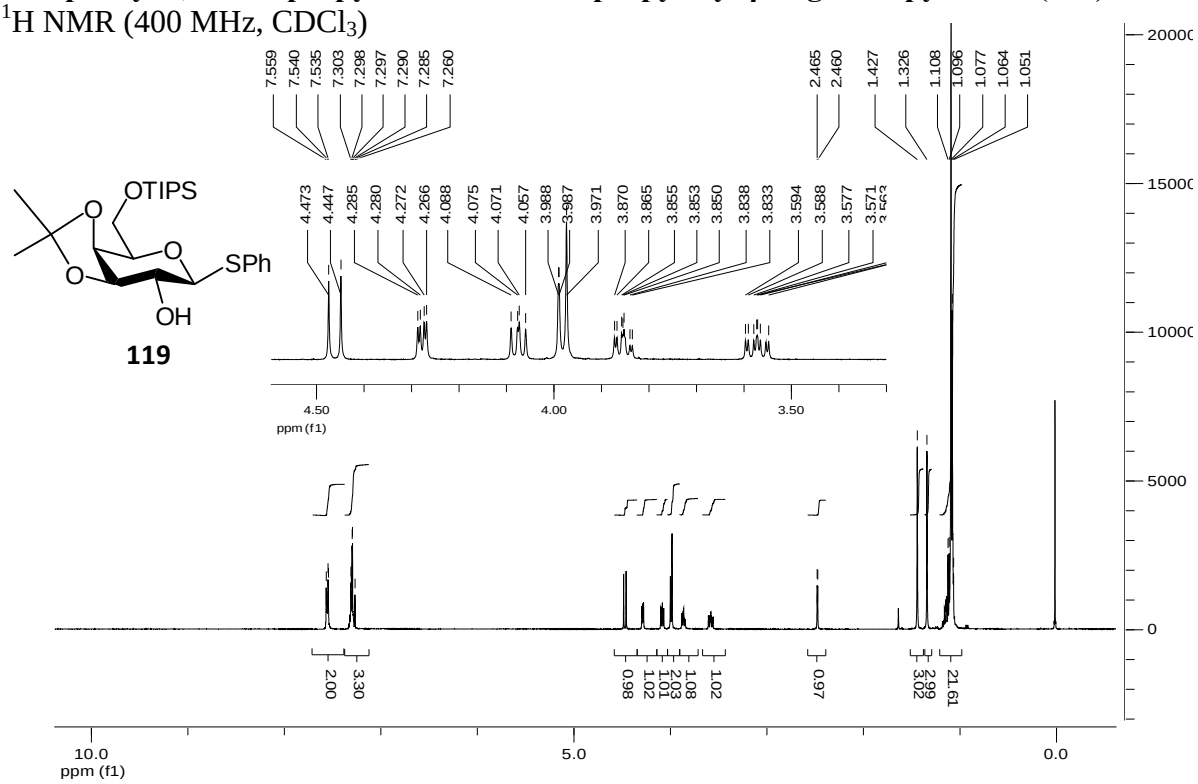

^{13}C NMR (101 MHz, $CDCl_3$)

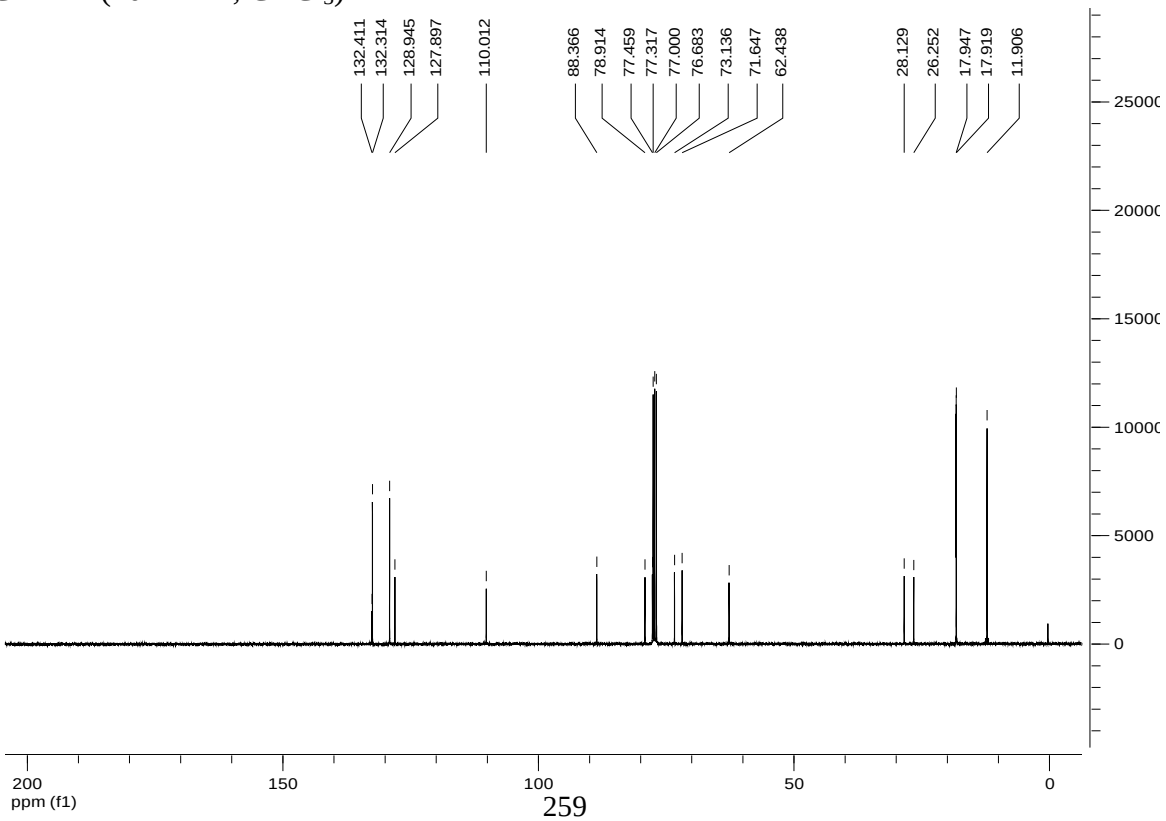

***tert*-butyl-4(S)-[2`-(*S*)-1`-hydroxy-1`-(3,4-*O*-isopropylidene-6-*O*-triisopropylsilyl-D–*lyxo*-hexa-2-ulos-1-yl)-prop-2`-yl]-2,2-dimethyl-1,3-oxazolidine-3-carboxylate (120)**

^{1}H NMR (500 MHz, $CDCl_3$)

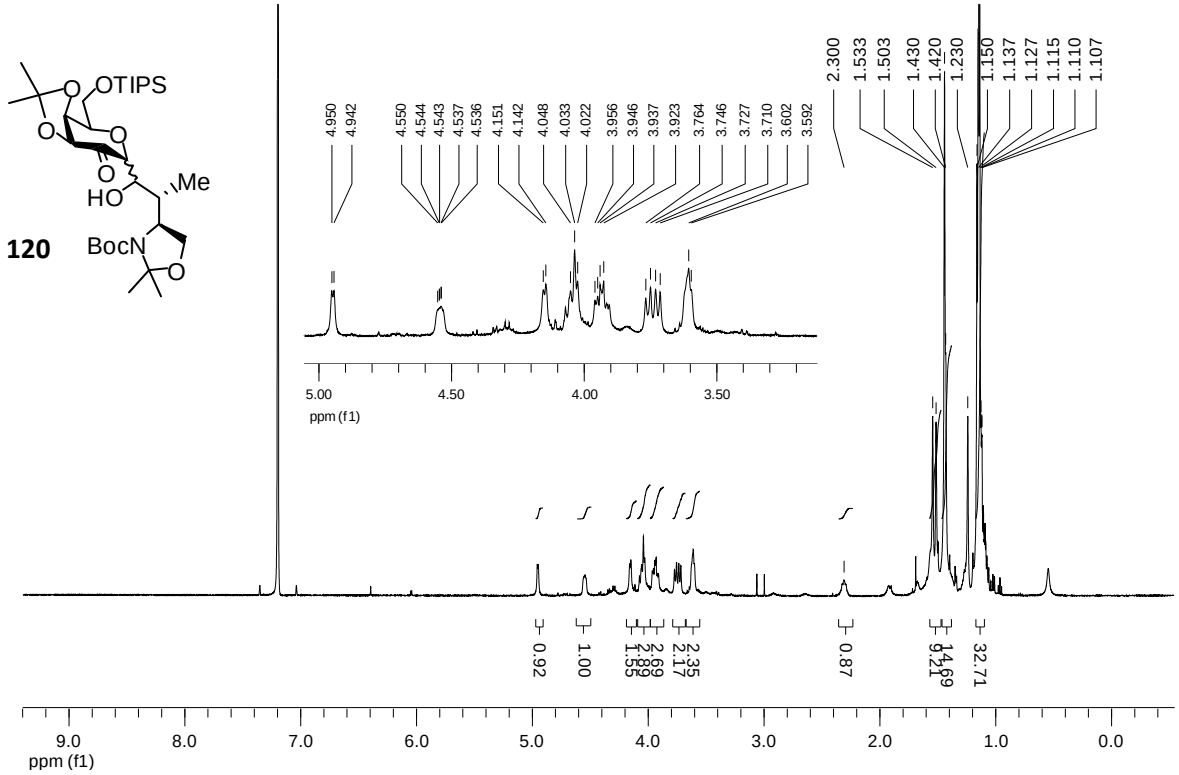

^{13}C NMR (126 MHz, $CDCl_3$)

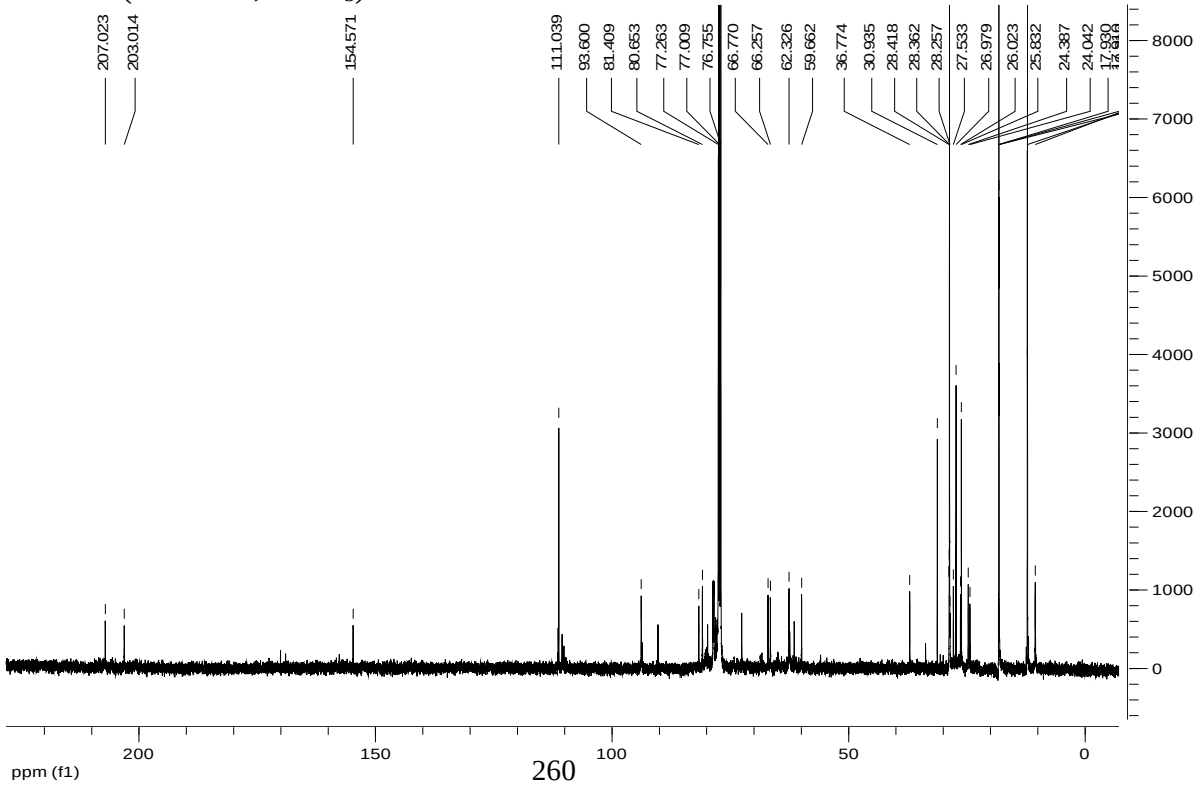

***tert*-butyl-4(S)-[2`-(*S*)-1`-hydroxy-1`-(3,4-*O*-isopropylidene-6-*O*-triisopropylsilyl-D–*lyxo*-hexa-2-ulos-1-yl)-prop-2`-yl]-2,2-dimethyl-1,3-oxazolidine-3-carboxylate (120)**

2D COSY NMR (500 MHz, $CDCl_3$)

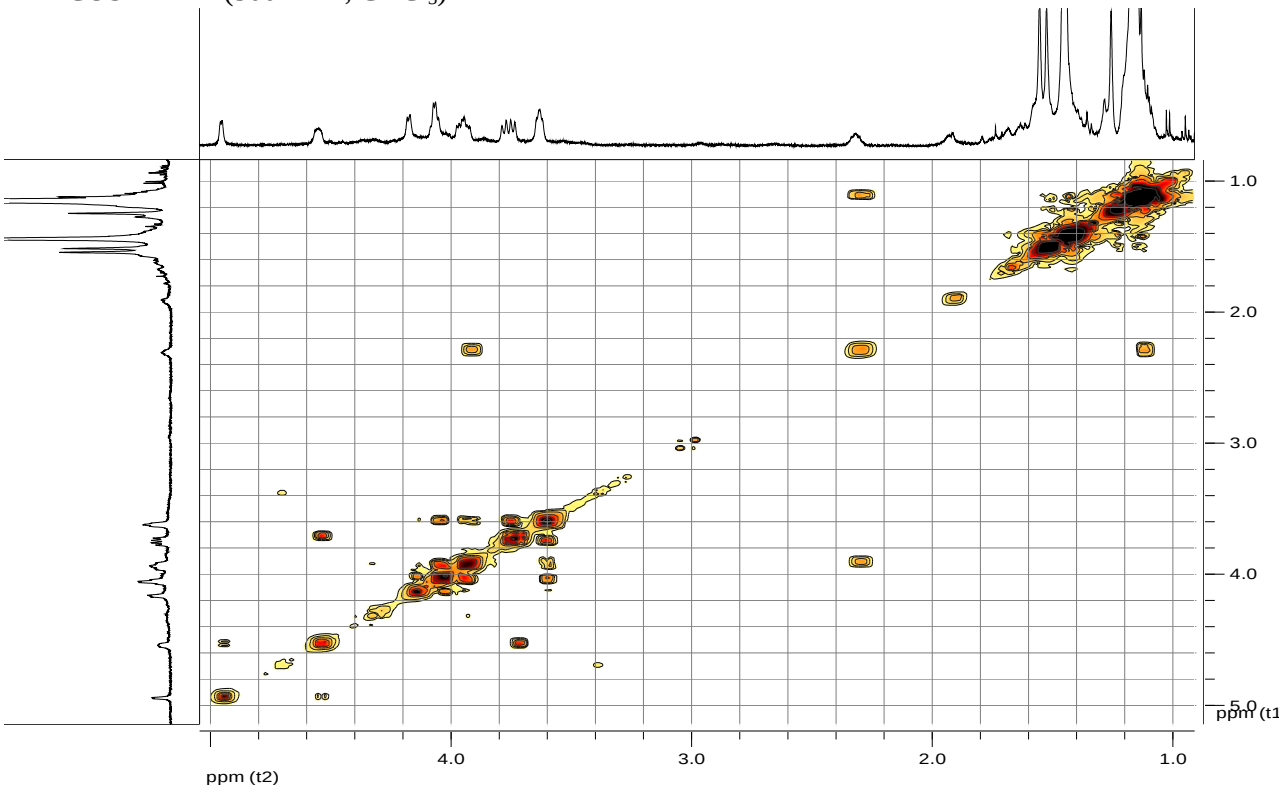

2D HMQC NMR